

**THE SYNTHESIS AND CHARACTERIZATION OF
1,1'-DISUBSTITUTED FERROCENE IMINE SCHIFF BASE LIGAND
SYSTEMS FOR USE AS POTENTIAL ENVIRONMENTAL HEAVY METAL
CATIONIC SENSORS**

A Dissertation

presented to

the Faculty of the Graduate School

at the University of Missouri-Columbia

In Partial Fulfillment

of the Requirements for the Degree

Doctor of Philosophy

by

CHAD LEROY MAGEE

Dr. Steven W. Keller, Dissertation Supervisor

MAY 2008

The undersigned appointed by the dean of the Graduate School, have examined the dissertation entitled

THE SYNTHESIS AND CHARACTERIZATION OF 1,1'-DISUBSTITUTED
FERROCENE IMINE SCHIFF BASE LIGAND SYSTEMS FOR USE AS POTENTIAL
ENVIRONMENTAL HEAVY METAL CATIONIC SENSORS

Presented by Chad Leroy Magee

a candidate for the degree of doctor of philosophy in inorganic chemistry,
and hereby certify that, in their opinion, it is worthy of acceptance,

Professor Steven Keller

Professor Silvia Jurisson

Professor Stanley Manahan

Professor Carol Deakne

Professor Mitch Schulte

I would like to dedicate this dissertation to my parents, the late Donald L. Magee, and Genevieve L. Magee, to whom I would not have completed this research project without their guidance in my life.....

ACKNOWLEDGEMENTS

I would like to personally thank Dr. Paul Duval, research supervisor; Dr. Steven Keller, Committee member and dissertation chair; Dr. Stanley Manahan, Committee member; Dr. Silvia Jurisson, Committee member; Dr. Mitch Shulte, Committee member; Dr. Carol Deakyne, Committee member; Dr. Charles Barnes, X-ray Crystallography help; Dr. Wei Wycoff, help with NMR techniques; Dr. Nathan Leigh, help with MS spectroscopy; Dr. David Robertson, help with X-ray Fluorescence spectroscopy; Steve Bockhold, help with Magnetic Susceptibility measurements; Former and Current Duval Group Members: Dr. S. Kannon, Joy Biswas, Levi Banks, Dr. Leah Arrigo, Shaquetta Stovall, Anthony Vaughn, Eric Weis, Morgan Moody; Dr. Tamas Szabo; Dr. Scott Dalgarno; Dr. Nicholas Power; Jochan Antesberger; Jim Guthry; Many friends that have helped me along the way here at MU and the University of Missouri- Columbia Chemistry Department for their support while working on my research project.

TABLE OF CONTENTS

Acknowledgements	ii
Table of Contents	iii
List of Illustrations	iv
List of Tables	viii
List of Illustrations and Tables for Appendix	ix
Abstract	xvii
Chapter One:	
Introduction.....	1
Background on heavy metals.....	1
Background on chemical sensors.....	4
Chapter Two: Synthesis of the Fc₂ Ligand System	
Introduction.....	29
Experimental.....	31
Results and Discussion.....	39
Conclusion.....	49
Chapter Three: Synthesis of the FcOH₂ Ligand System	
Introduction.....	53
Experimental.....	55
Results and Discussion.....	63
Conclusion.....	81
Chapter Four: Synthesis of the FcSH₂ Ligand System	
Introduction.....	83
Experimental.....	86
Results and Discussion.....	94
Conclusion.....	139
Chapter Five: Chemical Sensors and Selectivity Tests	
Introduction.....	142
Experimental.....	144
Results and Discussion.....	157
Conclusion.....	159
Experimental sampling in the real world.....	160
Current mercury detection technology for aqueous systems.....	161
Potential applications.....	162
Chapter Six: Conclusion	169
Appendix of Spectral Technique Definitions	174
Appendix of Spectral Properties	178
Vita	361

LIST OF ILLUSTRATIONS

Figure:	Page:
Figure 1.1: 4,4'-bipyridine-ferrocene sensor for anions in aqueous environments.....	5
Figure 1.2: 1,1'-disubstituted ferrocene amine derivative.....	6
Figures 1.3a and 1.3b: An example of a [3,3]-ferrocenophane and a [5]ferrocenophane.....	7
Figure 1.4: Li⁺ sensor containing both ferrocene and 9-anthracene units.....	7
Figure 1.5: 18-crown-6 ferrocene ligand for sensing first and second group metals in solution.....	8
Figure 1.6: Ferrocene derivatives as Ca²⁺ multi-detection sensors.....	8
Figure 1.7: An example of an alkaline earth sensor.....	9
Figure 1.8: Cu²⁺ sensor with multiple sites for chelation.....	10
Figure 1.9: Example of a ferrocene-anthracene ligand as a Zn²⁺ sensor.....	11
Figure 1.10: Bisferrocene amine derivative.....	13
Figure 1.11a and b: Multi-detectable ferrocene-Rhodamine B sensors for Hg²⁺.....	14
Figures 1.12 (a-c): examples of fluorescent aromatic molecules: (a) anthracene (non-sensor), (b) 1,5-anthracene derivative and (c) 9,10-anthracene derivative.....	15
Figures 1.13 (a-c): Structures of (a) ferrocene, (b) 1-monosubstituted ferrocene, and (c) 1,1'-disubstituted ferrocene.....	16
Figure 2.1: The Fc₂ ligand (1): FeN₂C₂₄H₂₀.....	29
Figure 2.2: The structure of Fc₂-NiBr₂.....	30
Figure 2.3: The proposed structure of the Fc₂-MCl₂ compounds.....	31
Figure 2.4: Synthesis scheme for producing 1,1'-disubstituted Schiff Base ferrocene ligands from ferrocene.....	40
Figure 2.5: ¹H NMR spectrum of Fc₂-ZnCl₂ in d₆-DMSO.....	43

Figure 2.6: The ^1H NMR peak locations for the Fc2 system in CDCl_3	44
Figure 2.7: The ^1H NMR peak locations for the Fc2 system in d_6 -DMSO.....	44
Figure 2.8: Molar absorptivity (UV-Vis) of Fc2 ligand in DMSO.....	46
Figure 2.9: Comparison between the molar absorptivity (UV-Vis) of Fc2- ZnCl_2 and the molar absorptivity of the combined starting materials (SM) in DMSO.....	47
Figure 2.10: CV scan of Fc2 ligand in DMSO, scan rate 100 mV/sec.....	49
Figure 3.1: The FcOH2 ligand: $\text{FeN}_2\text{O}_2\text{C}_{24}\text{H}_{20}$	53
Figure 3.2 (a) and (b): (a) the structure of the FcOH1 ligand and (b) the structure of the $[\text{FcO1}]_2\text{-Zn}$ complex.....	53
Figure 3.3 Proposed structure of the FcO2-Zn complex.....	54
Fig. 3.4 ^1H NMR spectrum of FcOH2 ligand in CDCl_3	72
Figure 3.5: ^1H NMR spectrum of FcO2-Pb in CDCl_3	73
Figure 3.6: ^1H NMR spectrum of FcO2-Pb in d_6 -DMSO.....	73
Figure 3.7: The ^1H NMR peak locations for the FcOH2 system in CDCl_3	74
Figure 3.8: The ^1H NMR peak locations for the FcOH2 system in d_6 -DMSO.....	74
Figure 3.9: Molar absorptivity (UV-Vis) of FcOH2 ligand in DMSO.....	76
Figure 3.10: Comparison between the molar absorptivity (UV-Vis) of FcO2-Pb and the molar absorptivity of the combined starting materials in DMSO.....	77
Figure 3.11: CV of FcOH2 ligand in DMSO, scan rate 100 mV/sec.....	80
Figure 3.12: Comparison between the CV of FcO2-Pb and the CV of FcOH2 in DMSO	80
Figure 4.1: The FcSH2 ligand (in DRCT form): $\text{FeN}_2\text{S}_2\text{C}_{24}\text{H}_{20}$	83
Figure 4.2: Scheme of DRCT of the FcSH2 ligand.....	84
Figures 4.3 (a) and (b): (a) the structure of the FcSH1 ligand and (b) the structure of the $[\text{FcS}_1]_2\text{-Hg}$ complex.....	85

Figure 4.4: Proposed potential use of Lawessons Reagent in conversion of dialcohol to dithiol ligands.....	85
Figure 4.5: ¹H NMR spectrum of FcS2-Hg in CDCl₃.....	95
Figure 4.6: ¹H NMR spectrum of FcS2-Hg in d₆-DMSO.....	96
Figure 4.7: The ¹H NMR peak locations for the FcSH2 system in CDCl₃.....	97
Figure 4.8: The ¹H NMR peak locations for the FcSH2 system in d₆-DMSO.....	98
Figure 4.9: Molar absorptivity (UV-Vis) of the FcSH2 ligand in DMSO. The bands at 470 and 317 nm correspond to d-d transitions.....	130
Figure 4.10: Comparison between the molar absorptivity (UV-Vis) of FcS2-Hg and the molar absorptivity of the combined starting materials in DMSO.....	131
Figure 4.11: CV of the FcSH2 ligand in DMSO, scan rate 100 mV/second.....	132
Figure 4.12: Comparison between the CV of FcS2-Hg and the CV of FcSH2 in DMSO, scan rate 100 mV/sec.....	133
Figure 4.13: Molar absorptivity (UV-Vis) of the three ligand systems in DMSO: Fc2 (yellow), FcOH2 (blue) and FcSH2 (purple).....	136
Figure 4.14: Combined CV scans of the three ligand systems: Fc2 (purple), FcOH2 (blue) and FcSH2 (yellow).....	138
Figure 5.1: ¹H NMR spectrum of FcOH2 mixed metal reaction (dried solution) in CDCl₃.....	145
Figure 5.2: ¹H NMR spectrum of FcOH2 mixed metal reaction (dried solution) in d₆-DMSO.....	146
Figure 5.3: UV-Vis. of FcOH2 mixed metal reaction product in DMSO.....	146
Figure 5.4: Cyclic voltammetry of FcOH2 mixed metal reaction product in 1x10⁻³ M TBAHFP/DMSO solution, scan rate 100 mV/sec.....	147
Figure 5.5: ¹H NMR spectrum of FcSH2 mixed metal reaction (dried solution) in CDCl₃.....	150
Figure 5.6: ¹H NMR spectrum of FcSH2 mixed metal reaction (dried solution) in d₆-DMSO. (1:1:2:1:4 H equivalency).....	151
Figure 5.7: FcSH2 mixed metal reaction product in DMSO.....	151

Figure 5.8: Cyclic voltammetry of FcSH2 (1:1) 1.37×10^{-3} M mixed metal reaction product in 1×10^{-3} M TBAHFP/DMSO solution.....152

Figure 5.9: ^1H NMR of FcSH2 mixed metal product in d_6 -DMSO.....155

Figure 5.10: a.) Proposed measuring probe for environmental samples with FcSH2 ligand in solution with a semi-permeable membrane at the bottom, b.) Color of probe solution after contact with Hg^{2+} from an aqueous source, compound 28 has formed, c.) CV probes inserted into testing probe for electrochemical measurement, d.) UV-Vis absorption testing on the probe solution.....163

Figure 5.11: Proposed test strip method with FcSH2 ligand coated paper.....164

LIST OF TABLES

Table:	Page:
Table 1: Melting points, Colors and Percent Yields of the Fc₂ ligand and metal complex products.....	39
Table 2: Elemental Analysis of the Fc₂ systems.....	39
Table 3: Melting Points, Colors and Percent Yields of the FcOH₂ ligand and metal complex reactions.....	62
Table 4: Elemental Analysis of the FcOH₂ systems.....	63
Table 5: Crystal Structure of the FCOH₂ ligand.....	64
Table 6: Melting points, Colors, and Percent Yields of the FcSH₂ ligand and metal complex products.....	93
Table 7: Elemental Analysis of the FcSH₂ system.....	94
Table 8: Crystal structure of the FcSH₂ ligand.....	99
Table 9: Crystal structure of FcS₂-Co.....	107
Table 10: Crystal structure of FcS₂-Zn.....	115
Table 11: Crystal structure of FcS₂-Hg.....	123
Table 12: CV data comparisons for FcSH₂ and metal complexes vs. ferrocene.....	134
Table 13: X-ray Fluorescence data of the FcO₂-M mixed metal reaction product.....	148
Table 14: X-ray Fluorescence data of the FcS₂-M mixed metal reaction product.....	153

LIST OF ILLUSTRATIONS AND TABLES FOR APPENDIX

Figure or Table:	Page:
Table A-1: Elemental Analysis of Fc2, FcOH2 and FcSH2 systems.....	178
Table A-2: Magnetic Susceptibility Measurements of the Fc2, FcOH2 and FcSH2 systems.....	179
Figure A.1: CV background scan of electrolyte (1.0×10^{-3} M TBAHFP) in DMSO, scan rate 100 mV/sec.....	180
Figure A.2: CV scan of ferrocene in DMSO (with 1.0×10^{-3} M TBAHFP), scan rate 100 mV/sec.....	180
Figure A.3: ^1H NMR spectrum of Fc2 in CDCl_3	181
Figure A.4: ^1H NMR spectrum of Fc2 in d_6 -DMSO.....	182
Figure A.5: Molar absorptivity (UV-Vis) of the Fc2 ligand in DMSO.....	182
Figure A.6: CV scan of the Fc2 ligand in DMSO, scan rate 100 mV/sec.....	183
Figure A.7: ^1H NMR spectrum of Fc2- FeCl_2 in CDCl_3	184
Figure A.8: ^1H NMR spectrum of Fc2- FeCl_2 in d_6 -DMSO.....	184
Figure A.9: Comparison between the molar absorptivity (UV-Vis) of Fc2- FeCl_2 and the molar absorptivity of the starting materials (269 nm peak) in DMSO.....	185
Figure A.10: ^1H NMR spectrum of Fc2- CoCl_2 in CDCl_3	186
Figure A.11: ^1H NMR spectrum of Fc2- CoCl_2 in d_6 -DMSO.....	186
Figure A.12: Comparison between the molar absorptivity (UV-Vis) of Fc2- CoCl_2 and the molar absorptivity of the starting materials (321m 470 nm peaks) in DMSO.....	187
Figure A.13: ^1H NMR spectrum of Fc2- NiCl_2 in CDCl_3	188
Figure A.14: ^1H NMR spectrum of Fc2- NiCl_2 in d_6 -DMSO.....	188
Figure A.15: Comparison between the molar absorptivity (UV-Vis) of Fc2- NiCl_2 and the molar absorptivity of the starting materials (319, 470 nm peaks) in DMSO....	189
Figure A.16: ^1H NMR spectrum of Fc2- CuCl_2 in CDCl_3	190

Figure A.17: ^1H NMR spectrum of Fc2-CuCl₂ in d₆-DMSO.....	190
Figure A.18: Comparison between the molar absorptivity (UV-Vis) of Fc2-CuCl₂ and the molar absorptivity of the starting materials (311, 470 nm peaks) in DMSO.....	191
Figure A.19: ^1H NMR spectrum of Fc2-ZnCl₂ in CDCl₃.....	192
Figure A.20: ^1H NMR spectrum of Fc2-ZnCl₂ in d₆-DMSO.....	192
Figure A.21: Comparison between the molar absorptivity (UV-Vis) of Fc2-ZnCl₂ and the molar absorptivity of the starting materials (319, 470 nm peaks) in DMSO.....	193
Figure A.22: ^1H NMR spectrum of Fc2-CdCl₂ in CDCl₃.....	194
Figure A.23: ^1H NMR spectrum of Fc2-CdCl₂ in d₆-DMSO.....	194
Figure A.24: Comparison between the molar absorptivity (UV-Vis) of Fc2-CdCl₂ and the molar absorptivity of the starting materials (319, 470 nm peaks) in DMSO.....	195
Figure A.25: ^1H NMR spectrum of Fc2-HgCl₂ in CDCl₃.....	196
Figure A.26: ^1H NMR spectrum of Fc2-HgCl₂ in d₆-DMSO.....	196
Figure A.27: Comparison between the molar absorptivity (UV-Vis) of Fc2-HgCl₂ and the molar absorptivity of the starting materials (319, 470 nm peaks) in DMSO.....	197
Figure A.28: ^1H NMR spectrum of Fc2-PbCl₂ in CDCl₃.....	198
Figure A.29: ^1H NMR spectrum of Fc2-PbCl₂ in d₆-DMSO.....	198
Figure A.30: Comparison between the molar absorptivity (UV-Vis) of Fc2-PbCl₂ and the molar absorptivity of the starting materials (319, 470 nm peaks) in DMSO.....	199
Figure A.31: ^1H NMR spectrum of FcOH₂ in CDCl₃.....	200
Figure A.32: ^1H NMR spectrum of FcOH₂ in d₆-DMSO.....	200
Figure A.33: Molar absorptivity (UV-Vis) of the FcOH₂ ligand in DMSO.....	201
Figure A.34: CV scan of the FcOH₂ ligand in DMSO, scan rate 100 mV/sec.....	202

Figure A.35: Crystal structure of the FcOH₂ ligand.....	202
Figure A.36: ¹H NMR spectrum of FcO₂-Fe in CDCl₃.....	213
Figure A.37: ¹H NMR spectrum of FcO₂-Fe in d₆-DMSO.....	214
Figure A.38: Comparison between the molar absorptivity (UV-Vis) of FcO₂-Fe and the molar absorptivity of the starting materials (351 nm peak) in DMSO.....	215
Figure A.39: ¹H NMR spectrum of FcO₂-Co in CDCl₃.....	216
Figure A.40: ¹H NMR spectrum of FcO₂-Co in d₆-DMSO.....	216
Figure A.41: Comparison between the molar absorptivity (UV-Vis) of FcO₂-Co and the molar absorptivity of the starting materials (351, 463 nm peaks) in DMSO....	217
Figure A.42: ¹H NMR spectrum of FcO₂-Ni in CDCl₃.....	218
Figure A.43: ¹H NMR spectrum of FcO₂-Ni in d-DMSO.....	218
Figure A.44: Comparison between the molar absorptivity (UV-Vis) of FcO₂-Ni and the molar absorptivity of the starting materials (351, 463 nm peaks) in DMSO....	219
Figure A.45: ¹H NMR spectrum of FcO₂-Cu in CDCl₃.....	220
Figure A.46: ¹H NMR spectrum of FcO₂-Cu in d₆-DMSO.....	220
Figure A.47: Comparison between the molar absorptivity (UV-Vis) of FcO₂-Cu and the molar absorptivity of the starting materials (351, 455 nm peaks) in DMSO....	221
Figure A.48: ¹H NMR spectrum of FcO₂-Zn in CDCl₃.....	222
Figure A.49: ¹H NMR spectrum of FcO₂-Zn in d₆-DMSO.....	222
Figure A.50: Comparison between the molar absorptivity (UV-Vis) of FcO₂-Zn and the molar absorptivity of the starting materials (351, 463 nm peaks) in DMSO....	223
Figure A.51: ¹H NMR spectrum of FcO₂-Cd in CDCl₃.....	224
Figure A.52: ¹H NMR spectrum of FcO₂-Cd in d₆-DMSO.....	224
Figure A.53: Comparison between the molar absorptivity (UV-Vis) of FcO₂-Cd and the molar absorptivity of the starting materials (351, 463 nm peaks) in DMSO... 	225
Figure A.54: ¹H NMR spectrum of FcO₂-Hg in CDCl₃.....	226

Figure A.55: ^1H NMR spectrum of FcO2-Hg in $\text{d}_6\text{-DMSO}$.....	226
Figure A.56: Comparison between the molar absorptivity (UV-Vis) of FcO2-Hg and the molar absorptivity of the starting materials (351, 463 nm peaks) in DMSO...227	227
Figure A.57: ^1H NMR spectrum of FcO2-Pb in CDCl_3.....	228
Figure A.58: ^1H NMR spectrum of FcO2-Pb in $\text{d}_6\text{-DMSO}$.....	229
Figure A.59: Comparison between the molar absorptivity (UV-Vis) of FcO2-Pb and the molar absorptivity of the starting materials (351, 463 nm peaks) in DMSO....	230
Figure A.60: ^1H NMR Spectrum of FcOH1 (4-<i>t</i> butyl) ligand in CDCl_3.....	230
Figure A.61: ^1H NMR Spectrum of FcOH1 (4-<i>t</i> butyl) ligand in $\text{d}_6\text{-DMSO}$.....	231
Figure A.62: ^1H NMR Spectrum of FcOH2 (4-<i>t</i> butyl) Ligand in CDCl_3.....	232
Figure A.63: ^1H NMR Spectrum of FcOH2 (4-<i>t</i> butyl) Ligand in d-DMSO.....	232
Figure A.64: ^1H NMR spectrum of FcSH2 in CDCl_3.....	233
Figure A.65: ^1H NMR spectrum of FcSH2 in $\text{d}_6\text{-DMSO}$.....	234
Figure A.66: Molar absorptivity (UV-Vis) of the FcSH2 ligand in DMSO.....	235
Figure A.67: CV scan of the FcSH2 ligand in DMSO, scan rate 100 mV/sec.....	235
Figure A.68: Emission fluorescence of the FcSH2 ligand in ethanol at 317 nm.....	236
Figure A.69: Emission fluorescence of the FcSH ligand in DMSO at 317 nm.....	236
Figure A.70: Crystal structure of the FcSH2 Ligand.....	237
Figure A.71: ^1H NMR spectrum of FcS2-Fe in CDCl_3.....	268
Figure A.72: ^1H NMR spectrum of FcS2-Fe in $\text{d}_6\text{-DMSO}$.....	269
Figure A.73: ^1H NMR spectrum of precipitate from reaction of 22 with $\text{Hg}(\text{CH}_3\text{COO})_2$ in CDCl_3.....	269
Figure A.74: ^1H NMR spectrum of dried liquid portion from reaction of 22 with $\text{Hg}(\text{CH}_3\text{COO})_2$ in CDCl_3.....	270

Figure A.75: Comparison between the molar absorptivity (UV-Vis) of FcS2-Fe and the molar absorptivity of the starting materials in DMSO.....	271
Figure A.76: Comparison between the CV scan of FcS2-Fe and the CV scan of FcSH2 in DMSO, scan rate 100 mV/sec.....	271
Figure A.77: Emission fluorescence of FcS2-Fe in ethanol at 317 nm.....	272
Figure A.78: Emission fluorescence of FcS2-Fe in DMSO at 317 nm.....	272
Figure A.79: ¹H NMR spectrum of FcS2-Co in CDCl₃.....	273
Figure A.80: ¹H NMR spectrum of FcS2-Co in d₆-DMSO.....	274
Figure A.81: ¹H NMR spectrum of precipitate from reaction of 23 with Hg(CH₃COO)₂ in CDCl₃.....	274
Figure A.82: ¹H NMR spectrum of dried liquid portion from reaction of 23 with Hg(CH₃COO)₂ in CDCl₃.....	275
Figure A.83: Comparison between the molar absorptivity (UV-Vis) of FcS2-Co and the molar absorptivity of the starting materials (317, 402 nm peaks) in DMSO....	275
Figure A.84: Comparison between the CV scan of FcS2-Co and the CV scan of FcSH2 in DMSO, scan rate 100 mV/sec.....	276
Figure A.85: Emission fluorescence of FcS2-Co in ethanol at 317 nm.....	276
Figure A.86: Emission fluorescence of FcS2-Co in DMSO at 317 nm.....	277
Figure A.97: Crystal Structure of FcS2-Co.....	277
Figure A.88: ¹H NMR spectrum of FcS2-Ni in CDCl₃.....	296
Figure A.89: ¹H NMR spectrum of FcS2-Ni in d₆-DMSO.....	296
Figure A.90: ¹H NMR spectrum of precipitate from reaction of 24 with Hg(CH₃COO)₂ in CDCl₃.....	297
Figure A.91: ¹H NMR spectrum of dried liquid portion from reaction of 24 with Hg(CH₃COO)₂ in CDCl₃.....	297
Figure A.92: Comparison between the molar absorptivity (UV-Vis) of FcS2-Ni and the molar absorptivity of the starting materials (317, 402 nm peaks) in DMSO....	298

Figure A.93: Comparison between the CV scan of FcS2-Ni and the CV scan of FcSH2 in DMSO, scan rate 100 mV/sec.....	298
Figure A.94: Emission fluorescence of FcS2-Ni in DMSO at 317 nm.....	299
Figure A.95: ¹H NMR spectrum of FcS2-Cu in CDCl₃.....	300
Figure A.96: ¹H NMR spectrum of FcS2-Cu in d₆-DMSO.....	300
Figure A.97: ¹H NMR spectrum of precipitate from reaction of 25 with Hg(CH₃COO)₂ in CDCl₃.....	301
Figure A.98: ¹H NMR spectrum of dried liquid portion from reaction of 25 with Hg(CH₃COO)₂ in CDCl₃.....	301
Figure A.99: Comparison between the molar absorptivity (UV-Vis) of Fcs2-Cu and the molar absorptivity of the starting materials (313, 398 nm peaks) in DMSO....	302
Figure A.100: Comparison between the CV scan of FcS2-Cu and the CV scan of FcSH2 in DMSO, scan rate 100 mV/sec.....	302
Figure A.101: Emission fluorescence of FcS2-Cu in ethanol at 317 nm.....	303
Figure A.102: Emission fluorescence of FcS2-Cu in DMSO at 317 nm.....	303
Figure A.103: ¹H NMR spectrum of FcS2-Zn in CDCl₃.....	304
Figure A.104: ¹H NMR spectrum of FcS2-Zn in d₆-DMSO.....	304
Figure A.105: ¹H NMR spectrum of precipitate from reaction of 26 with Hg(CH₃COO)₂ in CDCl₃.....	305
Figure A.106: ¹H NMR spectrum of dried liquid portion from reaction of 26 with Hg(CH₃COO)₂ in CDCl₃.....	305
Figure A.107: Comparison between the molar absorptivity (UV-Vis) of FcS2-Zn and the molar absorptivity of the starting materials (317, 402 nm peaks) in DMSO....	306
Figure A.108: Comparison between the CV scan of FcS2-Zn and the CV scan of FcSH2 in DMSO, scan rate 100 mV/sec.....	307
Figure A.109: Emission fluorescence of FcS2-Zn in ethanol at 317 nm.....	307
Figure A.110: Emission fluorescence of FcS2-Zn in DMSO at 317 nm.....	308
Figure A.111: Crystal Structure of FcS2-Zn.....	308

Figure A.112: ^1H NMR spectrum of FcS2-Cd in CDCl_3	327
Figure A.113: ^1H NMR spectrum of FcS2-Cd in d_6 -DMSO.....	328
Figure A.114: ^1H NMR spectrum of precipitate from reaction of 27 with $\text{Hg}(\text{CH}_3\text{COO})_2$ in CDCl_3	328
Figure A.115: ^1H NMR spectrum of dried liquid portion from reaction of 27 with $\text{Hg}(\text{CH}_3\text{COO})_2$ in CDCl_3	329
Figure A.116: Comparison between the molar absorptivity (UV-Vis) of FcS2-Cd and the molar absorptivity of the starting materials (317, 402 nm peaks) in DMSO....	330
Figure A.117: Comparison between the CV scan of FcS2- Cd and the CV scan of FcSH2 in DMSO, scan rate 100 mV/sec.....	330
Figure A.118: Emission fluorescence of FcS2-Cd in ethanol at 317 nm.....	331
Figure A.119: Emission fluorescence of FcS2-Cd in DMSO at 317 nm.....	331
Figure A.120: ^1H NMR spectrum of FcS2-Hg in CDCl_3	332
Figure A.121: ^1H NMR spectrum of FcS2-Hg in d_6 -DMSO.....	333
Figure A.122: Comparison between the molar absorptivity (UV-Vis) of FcS2-Hg and the molar absorptivity of the starting materials (317, 398 nm peaks) in DMSO....	334
Figure A.123: Comparison between the CV scan of FcS2-Hg and the CV scan of FcSH2 in DMSO, scan rate 100 mV/sec.....	335
Figure A.124: Emission fluorescence of FcS2-Hg in ethanol at 317 nm.....	335
Figure A.125: Emission fluorescence of FcS2-Hg in DMSO at 317 nm.....	336
Figure A-126: Crystal Structure of FcS2-Hg.....	336
Figure A.127: ^1H NMR spectrum of FcS2-Pb in CDCl_3	350
Figure A.128: ^1H NMR spectrum of FcS2-Pb in d_6 -DMSO.....	351
Figure A.129: ^1H NMR spectrum of precipitate from reaction of 29 with $\text{Hg}(\text{CH}_3\text{COO})_2$ in CDCl_3	351
Figure A.130: ^1H NMR spectrum of dried liquid portion from reaction of 29 with $\text{Hg}(\text{CH}_3\text{COO})_2$ in CDCl_3	352

Figure A.131: Comparison between the molar absorptivity (UV-Vis) of FcS2-Pb and the molar absorptivity of the starting materials (317, 403 nm peaks) in DMSO.....	352
Figure A.132: Comparison between the CV scan of FcS2-Pb and the CV scan of FcSH2 in DMSO, scan rate 100 mV/sec.....	353
Figure A.133: Emission fluorescence of FcS2-Pb in ethanol at 317 nm.....	353
Figure A.134: Emission fluorescence of FcS2-Pb in DMSO at 317 nm.....	354
Figure A.135: ¹H NMR spectrum of [FcS1]₂-Co in CDCl₃.....	354
Table 15: FcOH2 mixed metal reaction precipitate measured by X-ray.....	355
Table 16: FcSH2 mixed metal reaction precipitate measured by X-ray fluorescence.....	357

ABSTRACT

Heavy metals in the environment such as Cd, Hg and Pb are toxic to life forms. They can enter the ecological system through both natural and industrial sources. By developing chemical sensors that can detect these metals, scientists can identify problem areas and assist in the removal of the hazardous materials. Although sensors have been developed that can measure using one experimental method, the quest goes on to find sensors that have multiple routes to detection when a particular metal species becomes bound.

Ferrocene derivatives hold promise as a possible route to a multiple detector ion sensor. Since the iron center can undergo reversible oxidation, it is susceptible to the change in electron density that occurs when another metal center becomes bound to the ligand. Recently, some mono-substituted ferrocenes have been reported to have sensing abilities for heavy metals.^{1,2} The 1,1'-disubstituted ferrocene derivative chemistry has been less explored, but still holds promise as proven in the creation of a new Zn^{2+} sensor reported this year.³ By changing the functional groups on the ferrocene derivative, the selectivity of the ligand system can be modified towards a particular metal cation. One reported and two unreported 1,1'-disubstituted ferrocene systems have been tested with eight metals and their complexes characterized as a means to develop a spectroscopic database. The information can be used to determine the products formed during the selectivity experiments with each system. During this research project, one system was found to be very selective for chelating Hg^{2+} in the presence of other commonly found metal cations and could be detected from other complexes in the database through three

means: proton nuclear magnetic resonance (^1H NMR), ultraviolet-visible spectroscopy (UV-Vis) and cyclic voltammetry (CV). While a working universal heavy metal sensor was not achieved during this research project, it advanced the progress towards the formation of one.

¹ Caballero, A.; Martinez, R.; Lloveras, V.; Ratera, I.; Vidal-Gancedo, J.; Wurst, K.; Tarraga, A.; Molina, P.; Veciana, J., Highly Selective Chromogenic and Redox or Fluorescent Sensors of Hg²⁺ in Aqueous Environment Based on 1,4-Disubstituted Azines. *J. Am. Chem. Soc.* **2005**, 127, (45), 15666-15667.

² Yang, H.; Zhou, Z.; Huang, K.; Yu, M.; Li, F.; Yi, T.; Huang, C., Multisignaling Optical-Electrochemical Sensor for Hg²⁺ Based on a Rhodamine Derivative with a Ferrocene Unit. *Org. Lett.* **2007**, 9 (23), 4729-4732.

³ Zapata, F.; Caballero, A.; Espinosa, A.; Tarraga, A.; Molina, P., A Simple but Effective Ferrocene Derivative as a Redox, Colorimetric, and Fluorescent Receptor for Highly Selective Recognition of Zn²⁺ Ions. *Org. Lett.* **2007**, 9, (12), 2385-2388.

CHAPTER ONE

Brief overview of heavy metal pollution:

Heavy metal pollution remains a persistent problem facing our generation and generations to come. The toxic effects of exposure to high levels of heavy metals in the environment are varied, but range from liver/kidney damage⁴, developmental and reproductive problems⁵, mental disorders/damage⁶, and death⁷. The first step in the solution to this problem rests with the identification of the sources and the removal of the toxic materials from our environment⁸. The heavy metal cations that are most problematic due to toxicity in the environment are Cd^{2+} , Hg^{2+} , and Pb^{2+} .

Cadmium is found in many rechargeable NiCd batteries^{9,10}, soldering wire¹¹, older T.V. screens¹² and some protective coatings for automobile parts¹³. Soils that contain a high concentration of zinc usually have high amounts of cadmium that can be extracted by consumable plants as proven by tobacco grown in these soils.^{8,14} A growing source of cadmium pollution is the production and improper disposal of NiCd batteries by developing countries such as China. The optimal prevention technique to reduce NiCd battery pollution is replacing the batteries with suitable alternative non-Cd batteries such as Li ion and NiH while recycling the old batteries.¹⁵ Many years ago, the major industrial pollution sources of cadmium occurred near metal smelting and plating operations¹⁶, whereby the unwanted leftover solutions commonly were either dumped into the ground or nearby sources of water. This allowed for water soluble Cd^{2+} to infiltrate municipal water supplies creating major health problems from exposure¹⁷. The EPA has since set strict rules¹⁸ on this industry such that all unwanted solutions or solids

that contain cadmium (and other metals) must be handled in an environmentally friendly fashion.

A more serious threat to the population and the environment is due to mercury contamination. It can be found in older thermometers/barometers¹⁹, dental amalgams²⁰, some vapor lamp bulbs and switches²¹, old medicinal drugs²², and batteries²³ to name a few sources. It also has an important role in the mining industry as an extractant for precious metals²⁴. That is also a major source of mercury pollution in the environment as not all of the mercury is recovered from each extraction process²⁵. Elemental mercury can be oxidized into a water soluble Hg^{2+} form by the action of certain bacteria on Hg^0 as a means to produce methylmercury.²⁶ This organometallic compound is among the most toxic compounds found in the environment and bioaccumulates in larger marine species such as tuna.^{27,28,29} A major case of industrially caused methylmercury poisoning was discovered in Minamata, Japan in the mid-1950s³⁰, after a company was found disposing of their mercurial materials into a local sea. Marine life absorbed the toxic methylmercury, which was then subsequently eaten by the local population. The intake of methylmercury caused many birth defects, health disorders and deaths³¹. The effects of the mercury exposure can still be seen in the area even though it has been fifty years since the clean up process began³².

Another heavy metal pollutant, lead, is found in older paints³³, water pipes³⁴, batteries³⁵, older gas additives³⁶, bullets, fishing weights and in radioactive shields³⁷. It was once used to seal food cans, although this process has since been banned by the FDA due to health regulations.³⁸ Tetraethyl lead was used as an anti-knock additive in gasoline, but it was phased out after many studies indicated that it was a source of lead

pollution in the environment.³⁹ Microscopic lead particulates were formed during the combustion process and emitted from the exhaust system of vehicles that used leaded gasoline.⁴⁰ The effects of burning leaded gasoline can still be seen many years later in the soils near some major highways, which still have a very high lead content⁴¹. This particular pollutant is dangerous as it can be inhaled as well as leached into a water supply rather easily.

Recently, concerns over toys made in China containing excessive levels of lead have dominated the news.⁴² The lead can be consumed by children (and pets) when the toy is chewed and the paint flakes off. While that potential problem to consumers can easily be fixed by recalling the toys (thus removing the source of lead), not all of the problems associated with heavy metal pollution are quite so easy to fix. The real problem becomes compounded when taking into account that intake of heavy metals can be in the form of ingesting contaminated food (mostly fish) and older paint chips (house paint), drinking from contaminated water supplies, breathing in toxic dust, and even skin exposure to contaminated surfaces⁴³. With so many possible sources of heavy metal exposure, it is prudent to find new ways to remove toxic heavy metals from our environment.

One way to determine and prevent the accumulation of heavy metals is through the development of chemical sensors⁴⁴ that can react with specific heavy metal cations, making the contaminant easily identifiable through spectroscopic techniques. Chelation of particular species is a major idea used in the creation of chemical sensing materials⁴⁵. The cation becomes bound to two or more sites on the sensing molecule, leading to changes that occur in the electron density throughout the molecule. These differences can be used to identify the species by various spectroscopic techniques. Some molecules

undergo a geometric transition, charge transfer (CT) or a visible shift in the color that can also be measured to sense the presence of the toxin.⁴⁶

Brief overview on chemical sensors:

Ever since the synthesis of ferrocene⁴⁷ was first reported in 1951, derivatives of ferrocenes have been made for various reasons for chelating to metal centers. One way that an organic molecular sensor⁴⁸ can be improved is by the addition of a redox active group that could potentially interact with the bound metal cation. This would allow detection using cyclic voltammetry (CV). Ferrocene, $\text{Fe}(\text{C}_5\text{H}_5)_2$, is a logical choice for a redox active group as it undergoes a reversible oxidation at a known potential⁴⁹.

Interactions with metals that can cause charge transfer within the molecule will shift the CV peaks correspondingly and show that the electron density is being greatly shifted around on the molecule.⁵⁰ Further research in this area is important for developing new chemical sensors.

Recently, environmental sensing of specific compounds has become an important field in chemistry. An example of this is in the measurement of pollutant gases with chemical sensors.⁵¹ Various gas molecules (SO_2 , NH_3) can be sensed using a ferrocene polymer⁵² attached to a fiber optical array or semiconductor system. The ferrocene polymer undergoes an electrochemical interaction with the gases as they flow over the surface, while it undergoes a colorimetric change upon reaction with particular species. The change in color can be detected by the device giving real time concentration measurements. These systems might even be built into the faceplate of the masks to alert the user whether or not the mask can safely be removed after a chemical attack.

The sensing of both anions and cations is important in environmental chemistry. Excess concentrations of particular cations or anions (toxic metals, perchlorates, etc.) out in the environment could be a sign of a larger problem, for example industrial pollution.⁵³ While water sources will naturally contain levels of anions, levels that are too high can be detrimental to life. Many anions, such as halides, SO_4^{2-} , HPO_4^{2-} and ATP, can also be sensed using ferrocene derivatives^{54,55,56}. Gold surfaces layered with either a bisferrocene-rotaxane⁵⁷ or a ferrocene-cyclodecapeptide⁵⁸ can be used as electrodes for the sensing of anions in organic solutions. Ferrocene derivatives containing amide chelating groups⁵⁹ can be used to determine halide, PF_6^- , and BF_4^- ions due to the shifting in the ^1H NMR of the N-H proton. Ferrocene attached to 4,4'-bipyridine⁶⁰ (Figure 1.1) or pyrroles^{61,62} has proven to be effective as a molecular sensor for specific anions in water. Similarly, ferrocene-urea systems^{63,64,65} have been reported to sense electrochemically F^- , Cl^- , HPO_4^{2-} , CH_3CO_2^- and K^+ (even with competing cations)⁶⁶. Neutral molecules, such as diamines, can be sensed using macrocycles containing ferrocene pendants.⁶⁷

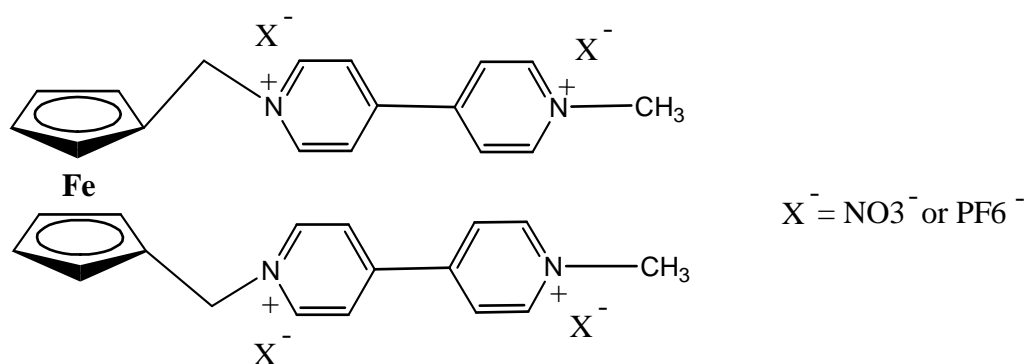


Figure 1.1: 4,4'-bipyridine-ferrocene sensor for anions in aqueous environments.⁶⁸

Modified dendrimers containing ferrocene groups^{69,70} have been designed to work as anionic sensors for both anions and cations via cyclic voltammetry (CV).

Calix[4]pyrroles containing attached ferrocene groups were reported^{71,72} to sense halides

using ^1H NMR, while H_2PO_4^- could be detected using both ^1H NMR and CV. The NMR shifting patterns induced by the interaction of the anion with protons was used to identify the halide⁷³. Similar derivatives containing ferrocene amines⁷⁴ (Figure 1.2) were found to be an effective carboxylate detector through both CV and NMR spectroscopic techniques. A Zn^{2+} -ferrocene metalloporphyrin⁷³ was reported to sense halide, nitrate and sulfate ions via NMR and CV. The zinc metal center plays an important role in the detection ability of this system as the free ligand does not sense these anions by itself⁷⁵. Another mixed metal sensor has been developed by attaching bipyridyl-bis(ferrocene)⁷⁵ to Ru^{II} . It undergoes luminescence when H_2PO_4^- becomes bound to the molecule⁷⁶.

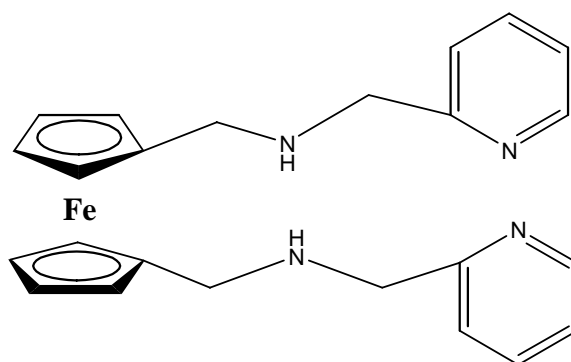
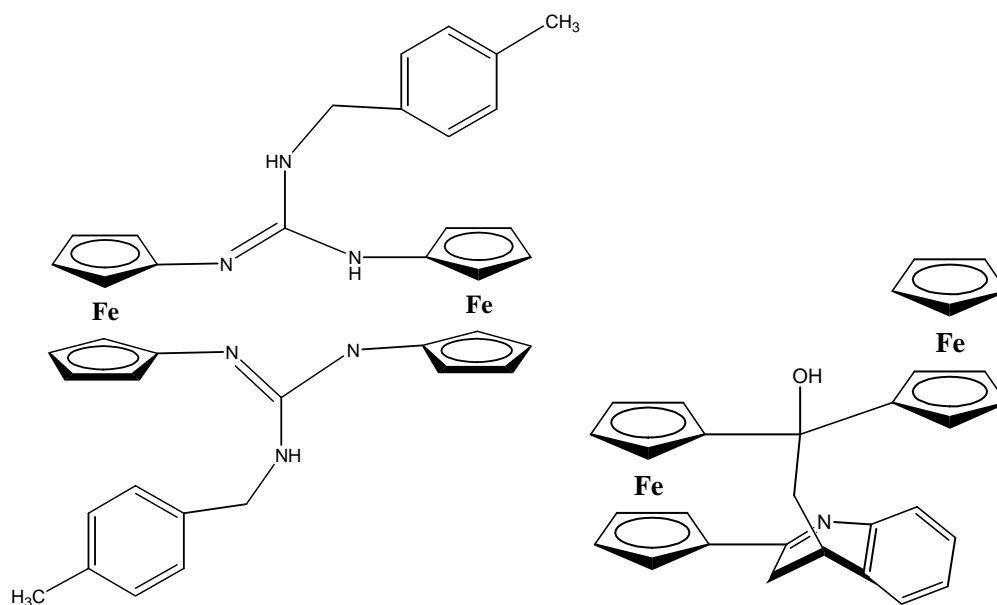


Figure 1.2: 1,1'-disubstituted ferrocene amine derivative.⁷⁷

Ferrocenophane derivatives (Figures 1.3a and 1.3b) are also known anion sensors. [3,3]Ferrocenophanes attached to guanidine form colorimetric and electrochemical sensors for many anions and cations⁷⁸. 1,n-Diaza[n]ferrocenophanes⁷⁹ can sense F^- and HPO_4^{2-} electrochemically. Ferrocenophane derivatives containing tin have also been developed as a sensor for anions⁸⁰. Polymers containing ferrocene-ammonium salts are reported to sense both sulfate and phosphate anions in solution electrochemically⁸¹. Thus, many different ferrocene systems have been and continue to be developed to sense anions.



Figures 1.3a and 1.3b: An example of a [3,3]-ferrocenophane⁷⁹ and a [5]ferrocenophane⁸², both are sensors for transition metal cations.

Ferrocene derivatives have been developed to detect concentrations of both anions and cations⁸³. Cations of the Group 1 metals are important to monitor as they are essential to biosystem health. A ferrocene derivative attached to anthracene⁸⁴ fluoresces when it interacts with Li⁺ (Figure 1.4). A similar system³ is used to sense heavier metal cations in aqueous environments.

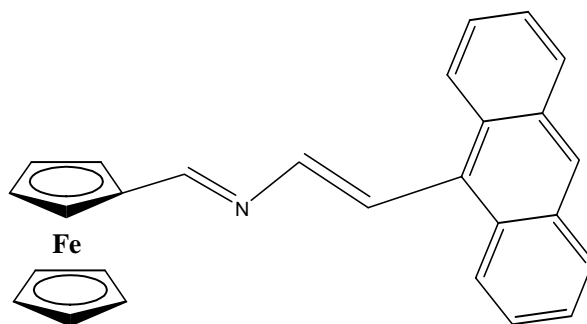


Figure 1.4: Li⁺ sensor containing both ferrocene and 9-anthracene units.⁸⁴

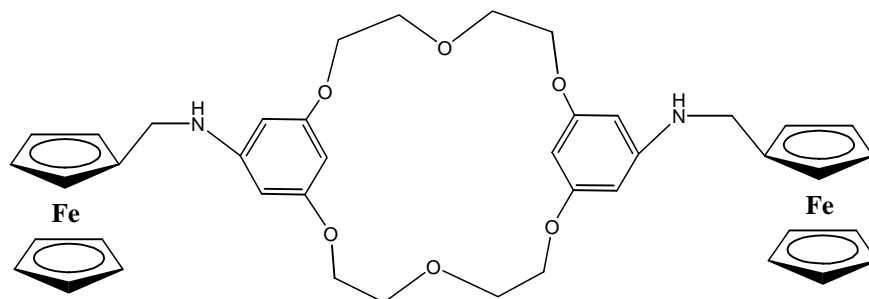


Figure 1.5: 18-crown-6 ferrocene ligand for sensing first and second group metals in solution.⁸⁵

A ferrocene-18-crown-6 derivative (Figure 1.5) contains a pocket that binds both Group 1 and 2 cations⁸⁵ Once bound, the redox properties and electronic spectrum can be used to identify a particular cation. Another type of ferrocene sensors can measure Ca^{2+} cations similarly.⁸⁶ (Figure 1.6). These particular ligands have very useful multipurpose detection properties in that they can be tested using fluorescence (phenyl ring makes this possible), UV-Vis, CV and ^1H NMR.

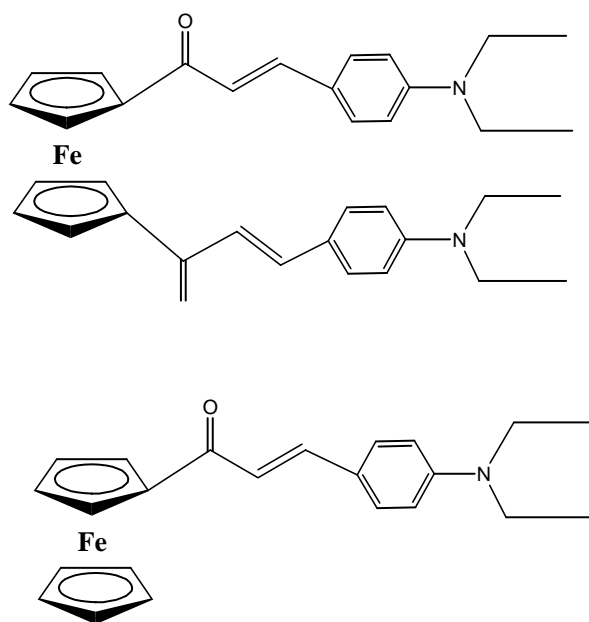


Figure 1.6: Ferrocene derivatives as Ca^{2+} multi-detection sensors.⁸⁶

A multi-detection sensor is one that can analyze by more than one technique to verify if a particular target has interacted with it. By having multiple ways that the reaction product can be detected, a sensor can be more versatile in the real world environment. An example of this would be in the addition of a fluorescent group to a sensor that normally does not fluoresce. This could potentially increase the detection ability for the ligand since it would need only a small amount of the product to be able to measure a sample accurately.

In another multi-detection system, a ferrocenophane derivative⁸² (Figure 1.7) has been developed that can sense Mg^{2+} cations in solution, although the complex does not undergo fluorescence. Octamethyl-1,1'-di(2-pyridyl) ferrocene⁸⁷ can sense Mg^{2+} , Ca^{2+} as well as Zn^{2+} and Cd^{2+} in acetonitrile via CV and UV-Vis even when competing alkali cations are present due to the hardness of the nitrogen groups present. An interesting side note is that a similar derivative octamethyl-1,1'-di(2-thiophenyl) ferrocene, a softer ligand due to the sulfur groups, does not sense these ions under the same conditions that the previous ligand system was tested with.⁸⁷

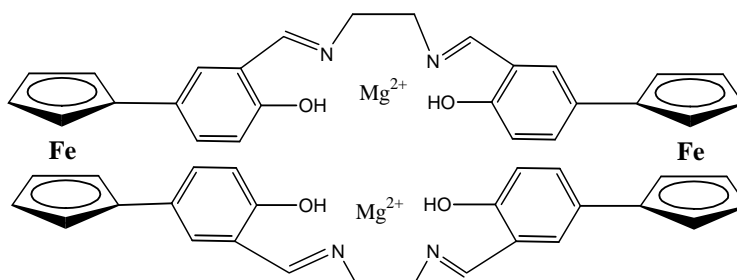


Figure 1.7: An example of an alkaline earth sensor.⁸⁸

Transition metal cations can be measured with ferrocene derivatives, particularly Cu^+

⁸⁸ and Cu^{2+} ⁸³ (Figure 1.8). This is useful in obtaining metal concentrations in water supplies as too much of a particular metal (even a useful one) can be harmful to living systems. Both transition and heavy metals can be measured using a particular ferrocene derivative⁸⁹ that undergoes a measurable change in the electrochemistry upon metal chelation. Similar properties have been reported for modified electrochemical probes^{90,91}. An interesting polyazaferrocene macrocyclic system⁵⁶ has dual sensing properties depending upon pH levels in solution. At low pH phosphate ions can be detected, while at a high pH, Cu^{2+} can be measured using CV.

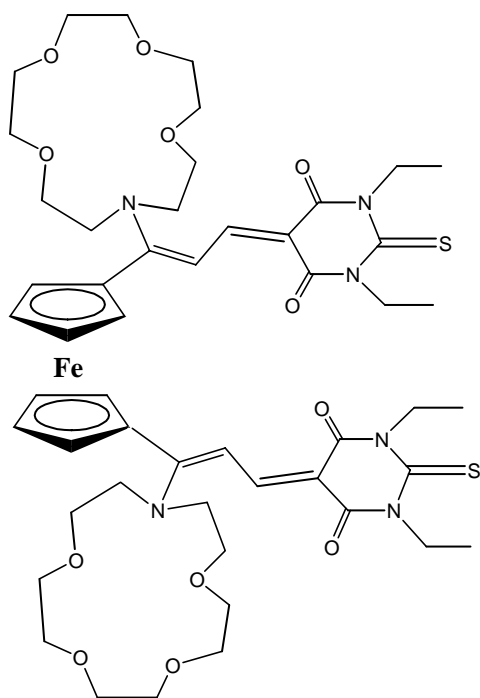


Figure 1.8: Cu^{2+} sensor with multiple sites for chelation.⁸³

Another cation of interest for detection with ferrocene sensors is Zn^{2+} . Zinc is an essential element used in most biological systems, while metals in the same group (cadmium, mercury) are not.^{92,93} Since d^{10} metals have no unpaired electrons, they do not undergo absorption in the UV-Vis range, causing their compounds to be typically white

in nature. Upon chelation of a d^{10} cation with a transition metal complex, the color of the new complex will be due to the transition metal present.

Organic molecules containing nitrogen groups can be used to detect Zn^{2+} .⁹⁴ A fluorescent oxa-sensor⁹⁵ shows a significant increase in fluorescence once a zinc cation binds to the molecule in two possible sites. *Bis-9-anthryldiamine*⁹⁶ undergoes a similar change. Some biological units have been employed to sense zinc, as in the case with the protein, *S. aureus czr A*.⁹⁷

Zinc cations (like many other cations) have an affinity towards porphyrin rings. One particular ring system attached to ferrocene has been used to determine electrochemically the concentration of zinc within a solution.⁹⁸ NMR spectroscopy can also be used to help measure cation concentrations. One particular porphyrin-ferrocene derivative⁹⁹ forms a supramolecular assembly with the cation that can be detected by both NMR and CV. Other ferrocene derivatives¹⁰⁰ can also sense the cation (and other heavy metals) through CV, UV-Vis, NMR, as well as fluorescence. By attaching anthracene units to a disubstituted ferrocene amine, a particularly useful zinc sensor is produced³ (Figure 1.9), since it can be detected using many different spectroscopic techniques.

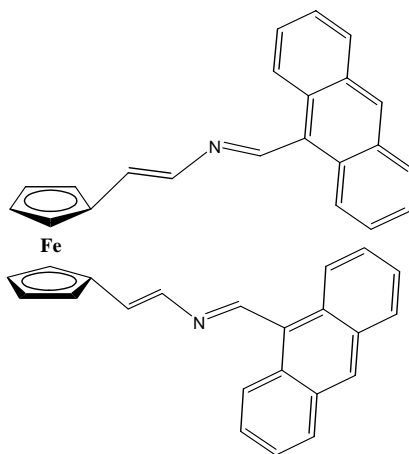


Figure 1.9: Example of a ferrocene-anthracene ligand as a Zn^{2+} sensor.³

Cd is a metal that needs to be closely monitored and removed from the environment due to possible human toxicity. Once a high concentration of Cd^{2+} is found, it can be removed via various methods. A means to absorb Cd cations has been reported using a mesoporous membrane,¹⁰¹ which captures the Cd^{2+} much like a sponge catches water. A similar effect is seen with some ferrocene derivatives that can cage Cd cations. While that is useful in cleaning up a contaminated site, it does not help detect the levels of the heavy metal (with the exception of dry weight). The sensing of Cd^{2+} can be done by a few reported chemical sensors. One example of a Cd^{2+} detection sensor is formed using a ferrocene derivative attached to an amino acid, cysteine.¹⁰² The change in the electrochemical properties can be detected once the cation becomes chelated to the molecule.

Because mercury compounds are very toxic, the development of new ways to detect the metal in the environment has increased during the past two decades. As used in measuring other metal systems, anthracene derivatives¹⁰³ can be used to measure Hg^{2+} through fluorescence, and Cu^{2+} through fluorescence quenching. The ring system undergoes a great increase in the intensity of the signal once the Hg^{2+} cation becomes chelated. Polyaniline¹⁰⁴ has a measurable electrochemical change upon exposure to the cation of interest. Phthalyltetrathioacetic acid (PTTA)¹⁰⁵ is useful in detecting mercury levels in water. Other organic thiols¹⁰⁶ have also been used to capture and detect mercury in solutions. Even lead bound to carboxymethylcellulose can be used to analyze mercury concentrations as it undergoes a decrease in its phosphorescence.¹⁰⁷ Calix[4]arene in a Schiff Base polymer¹⁰⁸ and a plastic material containing sulfur groups¹⁰⁹ have both been reported to remove mercury cations out of solutions. Another approach to mercury

removal is in the supramolecular assembly of 4,6-dimethylpyrimidine¹⁰⁶ around the cations.

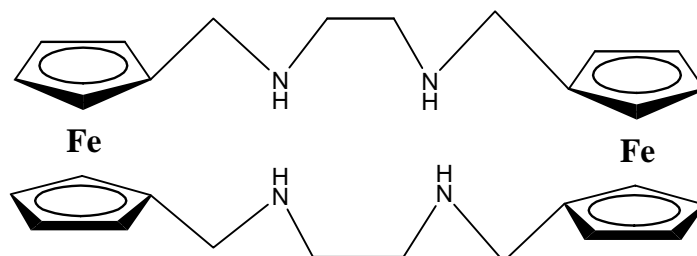


Figure 1.10: Bisferrocene amine derivative.¹¹⁰

Mercury levels can also be measured using ferrocene derivatives, such as ferrocene-cysteine¹⁰². A bisferrocene amine derivative (Figure 1.10) is a CV sensor for mercury while other heavy metal cations are present¹¹⁰. Monosubstituted ferrocenes attached together through an organic bridge containing chelating groups can sense mercury in water if a pyrene derivative is also used at the same time.¹ The mercury becomes bound to both the ferrocene derivative and the aromatic molecule. By attaching the two groups together between the metal cation of interest, the resulting system can be detected through fluorescence, UV-Vis and CV techniques. Another multi-detection system has been developed using a disubstituted ferrocene with diazabutadienes.¹¹¹ It can be measured using color, fluorescence and CV. A similar system has been reported with Rhodamine B² (Figure 1.11).

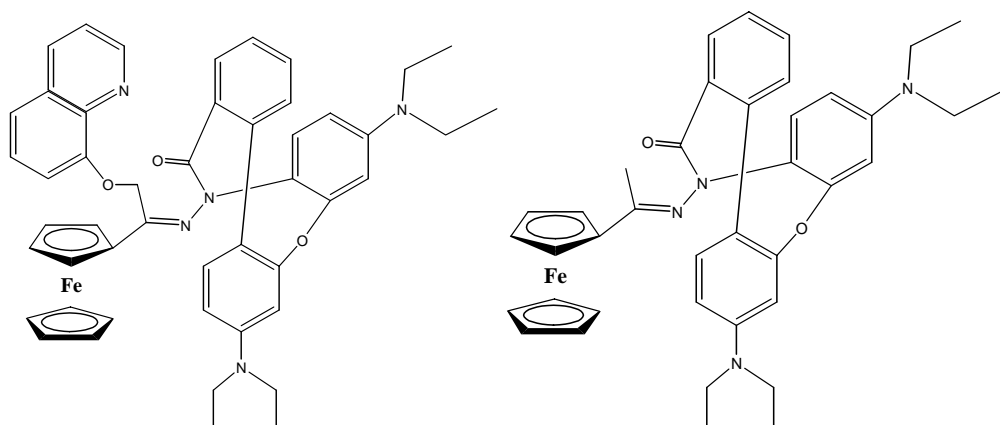
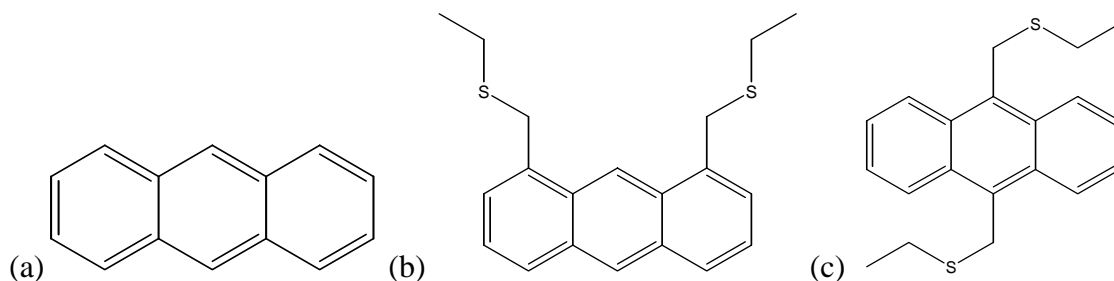


Figure 1.11a and b: Multi-detectable ferrocene-Rhodamine B sensors for Hg²⁺.

Lead is a particularly hazardous element for young children. Since it is so prevalent in the environment, major pollution sources need to be identified to prevent further toxification of living areas.¹¹² Many macrocyclic complexes have been formed with Pb²⁺.¹¹³ A calix[4]arene Schiff Base polymer⁶¹ has been reported in the literature that can absorb lead cations out of solution. Fiber optical arrays attached to a liquid membrane can be used to detect lead by means of a quenching of the fluorescent signal once the cation interacts with the membrane.¹¹⁴ Although the concentration of Pb²⁺ is not measured in lead acid batteries by ferrocene derivatives, the H⁺ concentration can be measured electrochemically¹¹⁵. This is of particular use in determining the lifetime of the battery and whether or not it needs to be replaced (and recycled). Sensors have been planned to be incorporated into the battery housing as a visible indicator for battery health.¹¹⁵ If the H⁺ levels become too low, the battery will not hold a charge and the system will soon fail. Biosensors have been developed using poly(pyrrole) containing ferrocenes with glucose oxidase as a glucose sensor¹¹⁶. This phenomenon holds great promise for potential further applications that may develop in the medical fields for ferrocene sensors.

Because some ferrocene compounds can be used as sensors, the development of new ferrocene ligand systems is an important part of environmental organometallic chemistry. Based upon the literature for known ferrocene sensors, four unreported ferrocene ligands were synthesized and characterized to determine their feasibility as potential heavy metal sensors.

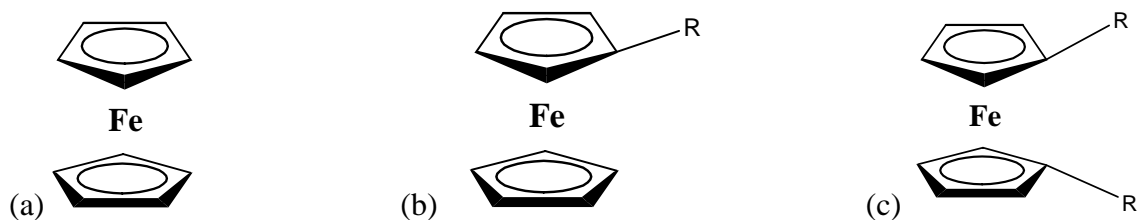


Figures 1.12 (a-c): examples of fluorescent aromatic molecules: (a) anthracene (non-sensor), (b) 1,5-anthracene derivative and (c) 9,10-anthracene derivative. Both (b) and (c) could be used as chemical sensors for fluorescent detection.¹⁰³

Organic molecules have been synthesized that act as chemical sensors through the addition of specific binding groups.^{117,118} Extensively conjugated systems (Figure 1.12a-c) are ideal for making sensors as they allow for delocalized electron density to be moved around on the molecule when a metal becomes bonded.¹¹⁹ This effect is usually seen in the UV-Vis spectrum as a shifting of the primary peaks to different wavelength. By modifying the ligand system, the shifts can be quite dramatic and the potential of a colorimetric sensor becomes possible¹²⁰. Ferrocene derivatives seem to be the ideal addition to allow for multi-detection with these systems.

Ferrocene derivatives do have drawbacks (low water solubility is one of them) that can possibly be corrected through further modification. Some of the ferrocene ligands can form polymers through supermolecular assembly with other species, such as cations.¹²¹ An electrode sensor could possibly be developed that could take advantage of

electronic communication from metal centers in the polymerized sensor for environmental testing out in the field. Colorimetric chemical sensors could also be developed to form single use test strips that would be easy to use.



Figures 1.13 (a-c): Structures of (a) ferrocene, (b) 1-monosubstituted ferrocene, and (c) 1,1'-disubstituted ferrocene. R = organic sidegroup

Most ferrocene derivatives (Figure 1.13a-c) are monosubstituted with only one pendant group off one of the cyclopentadienyl (Cp) rings¹²². The typical starting point in the Schiff base synthesis of these ligands is either formylferrocene or acetylferrocene. The 1,1'-disubstituted Schiff base ligands can be produced under similar conditions except that the 1,1'-diformylferrocene requires two equivalents of an organic amine to form the product. 1,1'-Disubstituted ferrocenes are rarer in the literature than their monosubstituted forms due to the purification steps for the required precursor. However, the 1,1'-disubstituted ferrocene ligands offer properties that the mono-substituted derivatives do not have (the possibility of co-polymerization being one of them). Some of these properties will be explored further in this work.

Most of the recent literature articles about disubstituted ferrocene imines involve unsymmetrical ligand pendant groups off the Cp rings.¹⁹ This can be obtained through the selective addition of one particular group to a Cp while protecting the other Cp ring, then the other (different) group can be added. This is different from what has been explored in this study, but does allow for the potential for a mixed ligand system that would have a

different chelating ability over the symmetric ligand systems. The ability of ferrocene derivatives to chelate different chemical groups becomes important in the potential application as environmental sensors.

This research project focused on the creation of a metal compound database and the selectivity experiments for the ligand systems: Fc2 (Fe[Cp-CH=N-C₆H₅]₂), FcOH2 (Fe[Cp-CH=N-C₆H₄-o-OH]₂), and FcSH2 (Fe[Cp-CH=N-C₆H₄-o-SH]₂). Five commonly found transition metal and three heavy metal cations were selected for the creation of the database: Fe²⁺, Co²⁺, Ni²⁺, Cu²⁺, Zn²⁺, Cd²⁺, Hg²⁺ and Pb²⁺. Each of these was chelated to each ligand system and then analyzed by melting point, elemental analysis, IR, UV-Vis spectroscopy, mass spectroscopy, cyclic voltammetry, magnetic susceptibility, and ¹H NMR spectroscopy. The identifying data were used to formulate the spectral database for the metal complexes (24 unreported complexes). Single crystal X-ray diffraction data were obtained for the samples that grew crystals, but the majority of the complexes did not form usable crystals after multiple attempts with various techniques (slow evaporation, solvent mixing, slow vapor diffusion - SVD, etc.). The resulting database was used for identifying the products formed during the selectivity measurements.

Much recent literature has focused on the discoveries of new chemical sensors based on ferrocene derivatives, some of which target heavy metals such as Cd²⁺, Hg²⁺ and Pb²⁺. Since ferrocene has the potential to interact electrochemically with the heavy metal cations, the resulting differences in the redox potentials can be used as a method to sense specific metal binding with the ligand. For example, mono-substituted ferrocene imine derivatives have been developed that chelate heavy metals in combination with an aromatic macrocycle to give a molecular sensor for Hg²⁺ in water.¹ While this system is

quite good at sensing Hg^{2+} , the potential is there to create a single molecule 1,1'-ferrocene diimine heavy metal cationic sensor that does not need another moiety to achieve the same detectability. Since the functional groups dictate the type of metal chelation, selectivity towards a particular heavy metal cation may be tunable within similar systems.

By choosing a disubstituted 1,1'-ferrocene ligand that only contains imine functional groups with attaching phenyl rings as the starting point, the differences in metal cation chelation was studied by adding different functional groups (such as OH and SH) ortho to the imine nitrogen. The bonding between the metal and the ligand (having either ionic or covalent character) helps dictate what metal cation might prefer a particular ligand system. The development of a heavy metal cationic sensor using these ideas is the major goal of this research project.

The following three chapters contain the synthesis and characterization of three disubstituted ferrocene ligands and their metal complexes as described above. Chapter five relates the selectivity experiments of each ligand system and their sensing abilities with metal cations. Chapter six concludes the discussion of the project.

⁴ Sarkar, B., *Heavy Metals in the Environment*. Marcel Dekker, Inc.: New York, 2002; p 242.

⁵ Final Report: Jasper County, Missouri Superfund Site Lead and Cadmium Exposure Study. In Services, U. S. D. O. H. H., Ed. 1995; p 3.

⁶ Tucker, A., *The Toxic Metals*. Ballantine Books: New York, 1972; p 36-40.

⁷ Luckey, T. D.; Venugopal, B.; Hutcheson, D.; Coulston, F., *Heavy Metal Toxicity, Safety and Hormology*. Academic Press: New York, 1975; Vol. Supplement Volume I, p 4-11.

⁸ Wennberg, M.; Lundh, T.; Bergdahl, I. A.; Hallmans, G.; Jansson, J.-H.; Stegmayr, B.; Custodio, H. M.; Skerfving, S., Time trends in burdens of cadmium, lead, and mercury in the population of northern Sweden. *Environ. Res.* **2006**, 100, (3), 330-338.

⁹ Greenwood, N. N.; Earnshaw, A., *Chemistry of the Elements*. 2nd. ed.; Butterworth-Heinemann: Oxford, 2001; p 1204.

¹⁰ Grey, H. B.; Simon, H. D.; Trogler, W. C., *Braving the Elements*. University Science Books: Sausalito, 1995; p 167.

¹¹ Lide, D. R., *CRC Handbook of Chemistry and Physics*. 71st ed.; CRC Press: Boca Raton, 1991, 4-7.

¹² Lide, D. R., *CRC Handbook of Chemistry and Physics*. 71st ed.; CRC Press: Boca Raton, 1991, 4-7.

¹³ Friberg, L.; Piscator, M.; Nordberg, G., *Cadmium in the Environment*. CRC Press: Cleveland, 1971; p 19.

¹⁴ Friberg, L.; Piscator, M.; Nordberg, G., *Cadmium in the Environment*. CRC Press: Cleveland, 1971; p 24.

¹⁵ Grey, H. B.; Simon, H. D.; Trogler, W. C., *Braving the Elements*. University Science Books: Sausalito, 1995; p 168.

¹⁶ Tucker, A., *The Toxic Metals*. Ballantine Books: New York, 1972; p 189.

¹⁷ Friberg, L.; Piscator, M.; Nordberg, G., *Cadmium in the Environment*. CRC Press: Cleveland, 1971; p. 22.

¹⁸ Pryde, L. T., *Environmental Chemistry: An Introduction*. Cummings Publishing Company: Menlo Park, 1973; p 223-225.

-
- ¹⁹ Lide, D. R., *CRC Handbook of Chemistry and Physics*. 71st ed.; CRC Press: Boca Raton, 1991, 4-20.
- ²⁰ Hartung, R.O; Dinman, B. D., *Environmental Mercury Contamination*. Ann Arbor Science Publishers Inc.: Ann Arbor, 1974; p 8.
- ²¹ Hartung, R.O; Dinman, B. D., *Environmental Mercury Contamination*. Ann Arbor Science Publishers Inc.: Ann Arbor, 1974; p 6.
- ²² McAuliffe, C. A., *The Chemistry of Mercury*. The Macmillan Press Ltd.: Toronto, 1977; p 25-31.
- ²³ Lide, D. R., *CRC Handbook of Chemistry and Physics*. 71st ed.; CRC Press: Boca Raton, 1991, 4-20.
- ²⁴ McAuliffe, C. A., *The Chemistry of Mercury*. The Macmillan Press Ltd.: Toronto, 1977; p 288.
- ²⁵ Sarkar, B., *Heavy Metals in the Environment*. Marcel Dekker, Inc.: New York, 2002; p 458.
- ²⁶ Friberg, L.; Vostal, J., *Mercury in the Environment*. CRC Press: Cleveland, 1972; p 17.
- ²⁷ Pryde, L. T., *Environmental Chemistry: An Introduction*. Cummings Publishing Company: Menlo Park, 1973; p 200-206.
- ²⁸ Palbus, A. C.; MacNeil, J., Heavy metal analysis of commercially purchased fish. *Abstracts of Papers, 229th ACS National Meeting, San Diego, CA 2005*, Ched-965.
- ²⁹ Eboh, L.; Mepba, H. D.; Ekpo, M. B., Heavy metal contaminants and processing effects on the composition, storage stability and fatty acid profiles of five common commercially available fish species in Oron Local Government, Nigeria. *Food Chem.* **2006**, 97, 490-497.
- ³⁰ Tucker, A., *The Toxic Metals*. Ballantine Books: New York, 1972; p 14-46.
- ³¹ Pryde, L. T., *Environmental Chemistry: An Introduction*. Cummings Publishing Company: Menlo Park, 1973; p 200.
- ³² Sarkar, B., *Heavy Metals in the Environment*. Marcel Dekker, Inc.: New York, 2002; p 457-501.

-
- ³³ Beard, M. E.; Iske, D. D. A., *Lead in Paint, Soil and Dust: Health Risks, Exposure Studies, Control Measures, Measurement Methods, and Quality Assurance*. ASTM: Philadelphia, 1995; p 175-187.
- ³⁴ Joesten, M. D.; Wood, J. L., *World of Chemistry Essentials*. 2nd. ed.; Harcourt Brace College Publishers: Fort Worth, 1999; p 402.
- ³⁵ Selim, H. M.; Iskandar, I. K., *Fate and Transport of Heavy Metals in the Vandose Zone*. Lewis Publishers: Boca Raton, 1999; p 1-3.
- ³⁶ Cotton, F. A.; Wilkinson, G., *Advanced Inorganic Chemistry: A Comprehensive Text*. 3rd. ed.; Interscience Publishers: New York, 1972; p 336.
- ³⁷ Lide, D. R., *CRC Handbook of Chemistry and Physics*. 71st ed.; CRC Press: Boca Raton, 1991, 4-19.
- ³⁸ Tucker, A., *The Toxic Metals*. Ballantine Books: New York, 1972; p 105.
- ³⁹ Castellino, N.; Castellino, P.; Sannolo, N., *Inorganic Lead Exposure, Metabolism and Intoxication*. CRC Press: Boca Raton, 1995; p 56-68.
- ⁴⁰ Tucker, A., *The Toxic Metals*. Ballantine Books: New York, 1972; p 106-109.
- ⁴¹ Sarkar, B., *Heavy Metals in the Environment*. Marcel Dekker, Inc.: New York, 2002; p 437-438.
- ⁴² O'Donnell, J., Feds focus on lead in kid's jewelry. *USA Today* September 6, 2007, pp 1B-2B.
- ⁴³ Castellino, N.; Castellino, P.; Sannolo, N., *Inorganic Lead Exposure, Metabolism and Intoxication*. CRC Press: Boca Raton, 1995; p 83-111.
- ⁴⁴ Cattrall, R. W., *Chem. Sens.* Oxford University Press: Oxford, 1997; p 11.
- ⁴⁵ Cattrall, R. W., *Chem. Sens.* Oxford University Press: Oxford, 1997; p 13-23.
- ⁴⁶ Cattrall, R. W., *Chem. Sens.* Oxford University Press: Oxford, 1997; p 2.
- ⁴⁷ Wilkinson, G.; Rosenblum, M.; Whiting, M. C.; Woodward, R. B., The Structure of Iron Bis-cyclopentadienyl. *J. Am. Chem. Soc.* **1952**, 2125-2126.
- ⁴⁸ Blake, D. A.; Jones, R. M.; II, Blake, R.C.; Pavlov, A. R.; Darwish, I. A.; Yu, H. N., Antibody-based sensors for heavy metal ions. *Biosens. Bioelectron.* **2001**, 16, (9-12), 799-809.

-
- ⁴⁹ Wang, H., *Analytical Electrochemistry*. 3rd. ed.; Wiley-VCH: Hoboken, 2006; p 250.
- ⁵⁰ Bosque, R.; Lopez, C.; Sales, J., Substituent effects on the electrochemical behaviour of iron(II) in Schiff bases derived from ferrocene and their cyclopalladated compounds. *Inorg. Chim. Acta* **1996**, 224, (1), 141-145.
- ⁵¹ Catrall, R. W., *Chemical Sensors*. Oxford University Press: Oxford, 1997; p 53-60.
- ⁵² Refaei, M.; Espada, L. I.; Shadaram, M., Application of ferrocene-based polymers in optical fiber gas sensing. *Proceedings of SPIE- The International Society for Optical Engineering* **2000**, 4036, 123-131.
- ⁵³ Joesten, M. D.; Wood, J. L., *World of Chemistry Essentials*. 2nd. ed.; Harcourt Brace College Publishers: Fort Worth, 1999; p 395-400.
- ⁵⁴ Martinez-Manez, R.; Soto, J.; Lloris, J. M.; Pardo, T., Receptors for the electrochemical sensing of transition metal ions and anions in aqueous environments. *Trends Inorg.Chem.* **1998**, 5, 183-203.
- ⁵⁵ Beer, P. D.; Szemes, F.; Balzani, V.; Sala, C. M.; Drew, M. G. B.; Dent, S. W.; Maestri, M., Anion Selective Recognition and Sensing by Novel Macrocyclic Transition Metal Receptor Systems, 1H NMR, Electrochemical, and Photophysical Investigations. *Inorg. Chem.* **1997**, 119, (49), 11864-11875.
- ⁵⁶ Beer, P. D.; Chen, Z.; Drew, M. G. B.; Johnson, A. O. M.; Smith, D. K.; Spencer, P., Transition metal cation and phosphate anion electrochemical recognition in water by new polyaza ferrocene macrocyclic ligands. *Inorg. Chim. Acta* **1996**, 246, (1-2), 143-150.
- ⁵⁷ Bayly, S. R.; Grey, T. M.; Chmielewski, M. J.; Davis, J. J.; Beer, P. D., Anion templated surface assembly of a redox-active sensory rotaxane. *Chem. Commun.* **2007**, 22, 2234-2236.
- ⁵⁸ Devillers, C. H.; Boturnyn, D.; Bucher, C.; Dumy, P.; Labbe, P.; Moutet, J.-C.; Royal, G.; Saint-Aman, E., Redox-Active Biomolecular Architectures and Self-Assembled Monolayers Based on a Cyclodecapeptide Regioselectivity Addressable Functional Template. *Langmuir* **2006**, 22, (19), 8134-8143.
- ⁵⁹ Vue, B.; Attar, S., Synthesis and characterization of new ferrocene-based anion sensors. *Abstracts of Papers, 229th ACS National Meeting, San Diego, CA 2005*, 320-Inorg. Part 1.
- ⁶⁰ Reynes, O.; Bucher, C.; Moutet, J.-C.; Royal, G.; Saint-Aman, R., Redox sensing of anions in pure aqueous environment by ferrocene-containing 4,4'-bipyridinium-based receptors and polymer films. *Chem. Commun.* **2004**, 4, 428-429.
- ⁶¹ Scherer, M.; Sessler, J. L.; Gebauer, A.; Lynch, V., A bridged pyrrolic ansa-ferrocene. A new type of anion receptor. *Chem. Commun.* **1998**, 1, 85-86.

-
- ⁶² Zimmerman, R. S.; Sessler, J. L.; Anrioletti, B.; Gebauer, A., Development and investigation of the electrochemical properties of anion-binding, pyrrole-substituted ferrocene systems. *Book of Abstracts, 218th ACS National Meeting, New Orleans 1999*, Inorg-176.
- ⁶³ Oton, F.; Tarraga, A.; Espinosa, A.; Velasco, M. D.; Molina, P., Ferrocene-Based Ureas as Multisignaling Receptors for Anions. *J. Org. Chem.* **2006**, 71 (12), 4590-4598.
- ⁶⁴ Oton, F.; Tarraga, A.; Espinosa, A.; Velasco, M. D.; Molina, P., Heteroditopic ferrocene-based ureas as receptors for anions and cations. *J. Chem. Soc., Dalton Trans.* **2006**, 30, 3685-3692.
- ⁶⁵ Kingston, J. E.; Ashford, L.; Beer, P. D.; Drew, M. G. B., Anion recognition and sensing by neutral and charged transition metal coordinated ferrocene phosphine amide receptors. *Dalton Trans.* **1999**, 2, 251-257.
- ⁶⁶ Oton, F.; Tarraga, A.; Velasco, M. D.; Molina, P., A ferrocene-based heteroditopic ligand for electrochemical sensing of cations and anions. *J. Chem. Soc., Dalton Trans.* **2005**, 7, 1159-1161.
- ⁶⁷ Li, C.; Medina, J. C.; Maguire, G. E. M.; Abel, E.; Atwood, J. L.; Gokel, G. W., Neutral Molecule Receptor Systems Using Ferrocene's "Atomic Ball Bearing Character as the Flexible Element. *J. Am. Chem. Soc.* **1997**, 119 (7), 1609-1618.
- ⁶⁸ Reynes, O.; Bucher, C.; Moutet, J.-C.; Royal, G.; Saint-Aman, R., Redox sensing of anions in pure aqueous environment by ferrocene-containing 4,4'-bipyridinium-based receptors and polymer films. *Chem. Commun.* **2004**, 4, 428-429.
- ⁶⁹ Yamamoto, K.; Higuchi, M.; Nakajima, R.; Suzuki, M.; Tsuruta, M., Ferrocene-modified phenylazomethine dendrimer and its use in ion sensor and ion detection and determination. *Jpn. Kokai Tokkyo Koho* **2005**, 9.
- ⁷⁰ Daniel, M.-C.; Ruiz, J.; Astruc, D., Supramolecular H-Bonded Assemblies of Redox-Active Metallodendrimers and Positive and Unusual Dendritic Effects on the Recognition of H_2PO_4^- . *J. Am. Chem. Soc.* **2003**, 125, (5), 1150-1151.
- ⁷¹ Evans, A. J.; Matthews, S. E.; Cowley, A. R.; Beer, P. D., Anion binding by calix[4]arene ferrocene ureas. *J. Chem. Soc., Dalton Trans.* **2003**, 24, 4644-4650.
- ⁷² Tomapatanaget, B.; Tuntulani, T.; Chailapakul, O., Calix[4]arenes Containing Ferrocene Amide as Carboxylate Anion Receptors and Sensors. *Org. Lett.* **2003**, 5, (9), 1539-1542.

-
- ⁷³ Beer, P. D.; Drew, M. G. B.; Jagessar, J., Selective anion recognition by novel 5,10,15,20-tetrakis(o-ferrocenylcarbonylamino)phenyl-substituted zinc metalloporphyrin receptors. *Dalton Trans.* **1997**, 5, 881-886.
- ⁷⁴ Tomapatanaget, B.; Tuntulani, T.; Chailapakul, O., Calix[4]arenes Containing Ferrocene Amide as Carboxylate Anion Receptors and Sensors. *Org. Lett.* **2003**, 5, (9), 1539-1542.
- ⁷⁵ Beer, P. D.; Graydon, A. R.; Sutton, L. R., Luminescent anion recognition: Selective induced emission by binding of dihydrogenphosphate. *Polyhedron* **1996**, 15, (14), 2457-2461.
- ⁷⁶ Beer, P. D.; Cadman, J., Electrochemical and optical sensing of anions by transition metal based receptors. *Coord. Chem. Rev.* **2000**, 205, 131-155.
- ⁷⁷ Cui, X. L.; Carapuca, H. M.; Delgado, R.; Drew, M. G. B.; Felix, V., Bis[1,1'-N,N'-(2-picolyl)aminomethyl]ferrocene as a redox sensor for transition metal ions. *J. Chem. Soc., Dalton Trans.* **2004**, 1743-1751.
- ⁷⁸ Oton, F.; Espinosa, A.; Tarraga, A.; de Arellano, C. R. d.; Molina, P., [3.3]Ferrocenophanes with guanidine bridging units as multisignalling receptor molecules for selective recognition of anions, cations, and amino acids. *Chem.-Eur. J.* **2007**, 13, (20), 5742-5752.
- ⁷⁹ Oton, F.; Tarraga, A.; Espinosa, A.; Velasco, M. D.; Bautista, D.; Molina, P., Preparation, Structure, and Anion Sensing Properties of 1,n-Diaza[n]ferrocenophanes. *J. Org. Chem.* **2005**, 70, (17), 6603-6608.
- ⁸⁰ Altmann, R.; Gausset, O.; Horn, D.; Jurkschat, K.; Schurmann, M.; Fontani, M.; Zanello, P., Novel Silicon- and Tin-Containing Ferrocenophanes and Related Compounds as Lewis Acids. *Organometallics* **2000**, 19, (4), 430-443.
- ⁸¹ Reynes, O.; Royal, G.; Chainet, E.; Moutet, J.-C.; Saint-Aman, E., Poly(ferrocenylalkylammonium): A molecular electrode material for dihydrogenphosphate sensing. *Electroanalysis* **2002**, 15, (1), 65-69.
- ⁸² Lopez, J. L.; Tarraga, A.; Espinosa, A.; Velasco, M. D.; Molina, P.; Lloveras, V.; Vidal-Gancedo, J.; Rovira, C.; Veciana, J.; Evans, D. J.; Wurst, K., A New Multifunctional Ferrocenyl-Substituted Ferrocenophane Derivative: Optical and Electronic Properties and Selective Recognition of Mg²⁺ Ions. *Chem. Eur. J.* **2004**, 10, 1815-1826.
- ⁸³ Basurto, S.; Riant, O.; Moreno, D.; Rojo, J.; Torroba, T., Colormetric Detection of Cu(II) Cation and Acetate, Benzoate, and Cyanide Anions by Cooperative Binding in

New alpha, alpha'-Bis-substituted Donor-Acceptor Ferrocene Sensors. *J. Org. Chem.* **2007**, 72, 4673-4688.

⁸⁴ Caballero, A.; Tormos, R.; Espinosa, A.; Velasco, M. D.; Tarraga, A.; Miranda, M. A.; Molina, P., Selective Fluorescence Sensing of Li⁺ in Aqueous Environment by a Ferrocene-Anthracene-Linked Dyad. *Org. Lett.* **2004**, 6, (24), 4599-4602.

⁸⁵ Beer, P. D.; Wild, K. Y., New Bis-ferrocenyl Dibenzo-18-crown-6 Ligands that can Electrochemically Sense Group 1 and 2 Metal Cations. *Polyhedron* **1996**, 15, (5-6), 775-780.

⁸⁶ Delavaux-Nicot, B.; Maynadie, J.; Lavabre, D.; Fery-Forgues, S., Ferrocenyl Compound as a Multiresponsive Calcium Chemosensor with Remarkable Fluorescent Properties in CH₃CN. *Inorg. Chem.* **2006**, 45 (14), 5691-5702.

⁸⁷ Siemeling, U.; Neumann, B.; Stammeler, H.-G.; Salmon, A., Octamethyl-1,1'-di(2-pyridyl)ferrocene: A redox-active ligand with a pronounced selectivity for divalent metal ions. *Z. Anorg. Allg. Chem.* **2002**, 628, (11), 2315-2320.

⁸⁸ Hall, C. D.; Sachsinger, N.; Nyburg, S. C.; Steed, J. W., Redox-active Schiff base ligands. *J. Organomet. Chem.* **1998**, 561 (1-2), 209-219.

⁸⁹ Caltagirone, C.; Bencini, A.; Demartin, F.; Devillanova, F. A.; Garan, A.; Isaia, F.; Lippolis, V.; Mariani, P.; Papke, U.; Tei, L.; Verani, G., Redox chemosensors: coordination chemistry towards Cu^{II}, Zn^{II}, Cd^{II}, Hg^{II}, and Pb^{II} of 1-aza-4,10-dithia-7-oxacyclododecane([12]aneNS₂O) and its N-ferrocenylmethyl derivative. *J. Chem. Soc., Dalton Trans.* **2003** (5), 901-909.

⁹⁰ Gooding, J. J.; Hibbert, D. B.; Yang, W., Electrochemical Metal Ions Sensors. Exploiting Amino Acids and Peptides as Recognition Elements. *Sensors* **2001**, 1, 75-90.

⁹¹ Singh, L. P.; Bhatnagar, J. M., PVC Based Selective Sensors for Ni²⁺ Ions Using Carboxylated and Methylated Porphine. *Sensors* **2003**, 3, (9), 393-403.

⁹² Garrett, R. H.; Grisham, C. M., *Biochemistry*. Saunders College Publishing: Fort Worth, 1995; p 356.

⁹³ Tucker, A., *The Toxic Metals*. Ballantine Books: New York, 1972; p 141-142.

⁹⁴ Wu, Z.; Zhung, Y.; Ma, J. S.; Yang, G., Ratiometric Zn²⁺ Sensor and Strategy for Hg²⁺ Selective Recognition by Central Metal Ion Replacement. *Inorg. Chem.* **2006**, 45, 3140-3142.

⁹⁵ Ohshima, A.; Momotake, A.; Arai, T., A new fluorescent metal sensor with two binding moieties. *Tetrahedron Lett.* **2004**, 45, (51), 9377-9381.

-
- ⁹⁶ Zhang, G.-Q.; Yang, G.-Q.; Zhu, L.-N.; Chen, Q.-Q.; Ma, J.-S., A potential fluorescent sensor for Zn²⁺ based on a selective bis-9-anthryldiamine ligand operating in buffer. *Sens. Actuators B* **2006**, 114, 995-1000.
- ⁹⁷ Lee, S.; Arunkumar, A. I.; Chen, X.H.; Giedroc, D. P., Structural Insights into Homo- and Heterotropic Allosteric Coupling in the Zinc Sensor *S. aureus* CzrA from Covalently Fused Dimers. *J. Am. Chem. Soc.* **2006**, 128, (6), 1937-1947.
- ⁹⁸ Gupta, V. K.; Chauhan, D. K.; Saini, V. K.; Agarwal, S.; Antonijevic, M. M.; Lang, H., A Porphyrin Based Potentiometric Sensor for Zn²⁺ Determination. *Sensors* **2003**, 3, (7), 223-235.
- ⁹⁹ Bucher, C.; Devillers, C. H.; Moutet, J.-C.; Royal, G.; Saint-Aman, E., Self-assembly of a ferrocene-substituted porphyrin capable of electrochemically sensing neutral molecules via a "tail on-tail off process. *Chem. Commun.* **2003**, 7, 888-889.
- ¹⁰⁰ Caballero, A.; Espinosa, A.; Tarraga, A.; Molina, P., Synthesis, electrochemical, and optical properties of linear homo- and heterometallocene triads. *J. Org. Chem.* **2007**, 72, (18), 6924-6937.
- ¹⁰¹ Lam, K. F.; Yeung, K. L.; McKay, G., Efficient Approach for Cd²⁺ and Ni²⁺ Removal and Recovery Using Mesoporous Adsorbent with Tunable Selectivity. *Environ. Sci. Technol.* **2007**, 41, (9), 3329-3334.
- ¹⁰² Scully, C.; Rutledge, P. J., Cysteine based ferrocenyl peptides as heavy metal sensors. *Abstracts of Papers, 232nd ACS National Meeting, San Francisco, CA* **2006**, Biol-205.
- ¹⁰³ Lee, Y. J.; Seo, D.; Kwon, J. Y.; Son, G.; Park, M. S.; Choi, Y.-H.; Soh, J. H.; Lee, H. N.; Lee, K. D.; Yoon, J., Anthracene derivatives bearing sulfur atoms or selenium atoms as fluorescent chemosensors for Cu²⁺ and Hg²⁺: different selectivity induced from ligand immobilization onto anthracene. *Tetrahedron* **2006**, 62, (52), 12340-12344.
- ¹⁰⁴ Singh, P. R.; Contractor, A. Q., Conductometric Hg sensor based on polyaniline as transducer. *Intern. J. Environ. Anal. Chem.* **2005**, 85, (12-13), 831-835.
- ¹⁰⁵ Jones, M. M.; Banks, A. J.; Brown, C. H., Stability constant studies on a new selective chelating agent for mercury(II). *J. Inorgan. Nucl. Chem.* **1974**, 36, (8), 1833-1836.
- ¹⁰⁶ Das, A. K.; Seth, S., The Crystal and Molecular Structure of (HgL₂)_n (L = 4,6-dimethylpyrimidine-2-thiolate) - An Unusual Helical Supramolecular Assembly in Solid Phase: In Search of a New Antidote to Mercury Poisoning. *J. Inorg. Biochem.* **1997**, 65, (3), 207-218.

- ¹⁰⁷ Liu, J.-M.; Wu, A.-H.; Xu, H.-H.; Wang, Q.-H.; Li, L.-D.; Zhu, G.-H., Determination of trace mercury by solid substrate room temperature phosphorescence quenching method based on lead carboxymethyl cellulose (Pb(CMC)₂) particles containing luminescent salicyl fluorones molecules. *Talanta* **2005**, 65, (2), 501-504.
- ¹⁰⁸ Karakucuk, A.; Kocabas, E.; Sirit, A.; Memon, S.; Yilmaz, M.; Roundhill, D. M., Polymer Supported Calix[4]arene Schiff Bases: A Novel Chelating Resin for Hg²⁺ and Dichromate Anions. *J. Macromol. Sci., Part A* **2005**, 42, (6), 691-704.
- ¹⁰⁹ Ji, C.; Qu, R.; Sun, C.; Wang, C.; Sun, Y.; Zhao, N.; Xie, H., Preparation and Adsorption Selectivity for Hg(II) and Ag(I) of Chelating Resin Immobilizing Benzothiazolyl Group on Crosslinked Polystyrene via Hydrophilic Sulfur-Containing PEG Spacer. *J. Appl. Polym. Sci.* **2005**, 100, 5034-5038.
- ¹¹⁰ Lloris, J. M.; Benito, A.; Martinez-Manez, R.; Padilla-Tosta, M. E., Pardo, T.,; Soto, J.; Tendero, M. J., Electrochemical Sensing of Mercury over Cadmium and Lead Cations by the Redox-Active Polyazacycloalkane Ligand 1,1':1'',1'''-Bis[ethane-1,2-diylbis(iminomethylene)]bis[ferrcoene]. *Helv. Chim. Acta* **1998**, 81, (11),2024-2030.
- ¹¹¹ Caballero, A.; Tarraga, A.; Velasco, M. D.; Molina, P., Ferrocene-thiophene dyads with azadiene spacers: electrochemical, electronic and cation sensing properties. *J. Chem. Soc., Dalton Trans.* **2005**, 1390-1398.
- ¹¹² Sarkar, B., *Heavy Metals in the Environment*. Marcel Dekker, Inc.: New York, 2002; p 409-455.
- ¹¹³ Parr, J., Some recent coordination chemistry of lead(II). *Polyhedron* **1997**, 16, (4), 551-556.
- ¹¹⁴ Ueberfeid, J.; Parthasarathy, N.; Zbinden, H.; Gisin, N.; Buffle, J., Coupling Fiber Optics to a Permeation Liquid Membrane for Heavy Metal Sensor Development. *Anal. Chem.* **2002**, 74, (3), 664-670.
- ¹¹⁵ Issa, T. B.; Singh, P.; Baker, M.; Verma, B. S., 1,1'-Bis(11-mercaptoundecyl)ferrocene for potentiometric sensing of H⁺ ion in sulfuric acid media simulating lead acid battery electrolyte. *J. Appl. Electrochem.* **2001**, 31, (8), 921-924.
- ¹¹⁶ Fiorito, P. A.; de Torresi, S. I. C. d., Glucose amperometric biosensor based on the co-immobilization of glucose oxidase (GOx) and ferrocene in poly(pyrrole) generated from ethanol/water mixtures. *J. Brazil. Chem. Soc.* **2001**, 12, (6), 729-733.
- ¹¹⁷ Klein, G.; Kaufmann, D.; Schurch, S.; Reymond, J.-L., A fluorescent metal sensor based on macrocyclic chelation. *Chem. Commun.* **2001**, (6), 561-562.

-
- ¹¹⁸ Ganjali, M. R.; Dodangeh, M.; Ghorbani, H.; Norouzi, P.; Adib, M., PPB Level Monitoring of Dy(III) Ions by a Highly Sensitive and Selective Dy(III) Sensor Based on a New Asymmetrical Schiff's Base. *Anal. Lett.* **2006**, 39, (3), 495-506.
- ¹¹⁹ Chen, Y.-G.; Zhao, D.; He, Z.-K.; Ai, X.-P., Fluorescence quenching of water-soluble conjugated polymer by metal cations and its application in sensor. *Spectrochim. Acta Part A* **2007**, 66, (2), 448-452.
- ¹²⁰ Lee, Y. J.; Kwon, J. Y.; Son, G.; Park, M. S.; Choi, Y.-H.; Soh, J. H.; Lee, H. N.; Lee, K. D.; Yoon, J., Anthracene derivatives bearing sulfur atoms or selenium atoms as fluorescent chemosensors for Cu²⁺ and Hg²⁺: different selectivity induced from ligand immobilization onto anthracene. *Tetrahedron* **2006**, 62, (52), 12340-12344.
- ¹²¹ Khan, I. M., *Synthetic Macromolecules with Higher Structural Order*. American Chemical Society: Washington, 2002; p 230.
- ¹²² Kettle, S. F. A., *Phys. Inorg. Chem.*. Oxford University Press: Oxford 1998; p 490.

CHAPTER TWO

Fc2 Ligand System: neutral donor

The imine groups that are produced during the Schiff base condensation between 1,1'-diformylferrocene and the appropriate aryl amine are important in the chelating ability for the ligand. The lone pair on the nitrogen can be donated to the metal center to form a bond. Three ligand systems have been studied during this research project: *Bis*[1,1'-(benzyl)iminomethyl]ferrocene (Fc2), *Bis*[1,1'-(2-phenol)iminomethyl]ferrocene (FcOH2) and *Bis*[1,1'-(2-thiolphenol)iminomethyl]ferrocene (FcSH2). Fc2 (Figure 2.1) contains only the two imine groups for metal chelation, with a phenyl ring attached directly to the imine nitrogens. In each ligand system, extensive conjugation in the backbones allows for delocalized electrons to move easily within the molecule. This allows for the greater possibility of fluorescence bands for detection of a metal complex product.

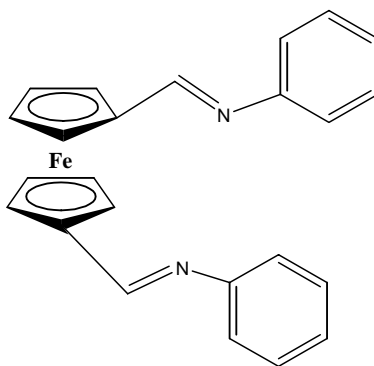


Figure 2.1: The Fc2 ligand (1): $\text{FeN}_2\text{C}_{24}\text{H}_{20}$ ¹²³

Previously, only the Fc2-NiBr₂ system has been reported.¹²³ It was used to obtain a group patent for its catalytic properties since Fc2-NiBr₂ (Figure 2.2) is a very effective ethylene polymerization catalyst.¹²³ By binding the Fc2 ligand to the NiBr₂ salt, the compound becomes very active in the polymerization of certain alkenes. The MCl₂

complexes have not been reported yet, so they were chosen as the starting point for studying the sensing ability of disubstituted ferrocene imines.

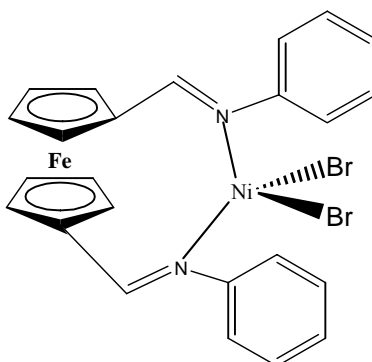


Figure 2.2: The structure of Fc2-NiBr₂.¹²³

This system is similar to a known Zn²⁺ sensor³, so this ligand will be tested to see if it too can selectively complex Zn²⁺, or potentially Cd²⁺. In addition, this ligand system may be used as a precursor for studying other mixed metal systems. The chlorides can be displaced with the proper reactions to form new complexes. Similar work has been done with other systems containing ML₂Cl₂ precursors, but not much is reported with 1,1'-disubstituted ferrocene. Due to the fact that the halogens can be accessed for removal, this system might allow for the creation of new mixed metal systems that could be used for various purposes (molecular switches for example).

The Fc2 ligand has been very sparsely studied since it was first reported a few years ago¹²⁴, with only a single metal bromide product listed. The metal chloride derivatives (Figure 2.3) were chosen in this study as a starting point to see the differences in selectivity and detection that can occur with varying the chelation groups, since this particular system does not have a functional group on the phenyl ring. The metal cation can only be bound to the ligand through the imine groups, which allows for a bit more steric freedom in the geometry around the metal center.

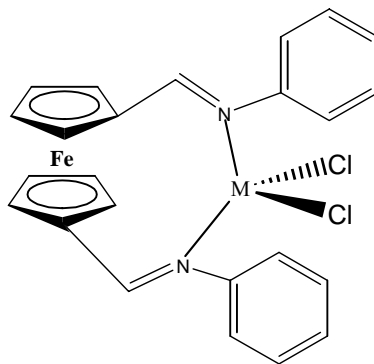


Figure 2.3: The proposed structure of the Fc2-MCl₂ compounds.

As mentioned previously, the Fc2 system has similarities to a reported Zn²⁺ sensor³. The imine nitrogens are closer to the Cp rings and the phenyl group has been replaced with an anthracene unit in the Zn²⁺ sensor. The larger aromatic ring system allows for greater potential fluorescent properties of the complexes¹²⁴. As a means to see if the Fc2 system might also be selective for Zn²⁺ cations, the Fc2 ligand was reacted with all eight metals separately and each product analytically characterized.

Experimental:

The Fc2 ligand was prepared according to the literature by means of a slightly modified Dean-Stark apparatus (containing a spigot) using diformylferrocene that was previously produced and purified¹²³. 1,1'-diformylferrocene was produced and purified prior to use according to the literature procedure.¹²⁵ Aniline was dried using CaH₂ then vacuum distilled prior to use. Benzene, absolute ethanol and all other solvents were used as obtained. ¹H NMR was measured using a Bruker spectrometer operating at 250 MHz using either CDCl₃ or d₆-DMSO as solvents with parts per million (ppm) spectral units. Infrared spectra were taken on a Thermo Nicolet spectrometer using emersion oil as a mull upon KBr salt plates. Molar absorptivity was measured on a HP 8453 UV-Vis

spectrophotometer using reagent grade DMSO as the solvent, with tungsten and deuterium lamps. Magnetic susceptibility measurements were taken on a Johnson Matthey magnetic susceptibility balance, type MSB, model NO MK1-8256 at room temperature. CVs were taken using a Bioanalytic Systems Epsilon EC-2000-Xp C3 cyclic voltammetry system in reagent grade DMSO with 0.1 M tetrabutylammonium hexafluorophosphate (TBAHFP) as the electrolyte, using a 0.01 M AgNO₃ silver reference electrode, platinum disk working electrode and a platinum wire auxiliary electrode. MS was done using a Finnigan TSQ7000 triple-quadrupole mass spectrometer with samples in methanol solutions, using the electrospray ionization method. The sheath gas was set to 80 psi during measurements. Melting point data were taken on a Fisher-Johns melting point apparatus.

Synthesis of Fc2 ligand: (1)

To a dried, N₂ flushed 250 mL side arm round bottom flask containing a stir bar, 600 mg of 1,1'-diformylferrocene (2.48×10^{-3} mol), 0.45 mL of aniline (5.0×10^{-3} mol) and 100 mL of benzene were added. The solution was allowed to undergo slow reflux for three hours (color darkened) and then the majority of the benzene was refluxed away via a modified Dean-Stark apparatus. Upon cooling, the deep red solution was filtered, washed with cold ethanol and dried to recover product. Amount recovered: 0.97 g of brownish-red solid. (2.47×10^{-3} mol, 99% yield, Table 1), mp 82-86 °C; ¹H NMR (CDCl₃): 8.33 ppm (2H, s, Cp-CH=N), 7.38-7.08 ppm (8H, m, phenyl), 4.90 ppm (4H, d, Cp), 4.55 ppm (4H, d, Cp); ¹H NMR (d₆-DMSO): 8.33 ppm (2H, s, Cp-CH=N), 7.39-7.00 ppm (6H, m, phenyl), 6.56-6.3 ppm (2H, d, phenyl), 4.94 ppm (4H, d, Cp), 4.62 ppm (4H, d,

Cp); Molar absorptivity (DMSO, Figure 2.8): 254 nm ($12700 \text{ M}^{-1}\text{cm}^{-1}$), 258 nm ($35700 \text{ M}^{-1}\text{cm}^{-1}$), 319 nm ($14600 \text{ M}^{-1}\text{cm}^{-1}$), 470 nm ($1930 \text{ M}^{-1}\text{cm}^{-1}$); MS: M+1: 392.94 amu, CV data (Figure 2.10) are shown below; see Appendix (Figures A.3-6) for spectra.

Synthesis of Fc2-FeCl₂: (2)

To a dried, N₂ flushed Schlenk flask containing a stir bar, 220 mg of **1** (5.61×10^{-4} mol), 110 mg of FeCl₂·4H₂O (5.53×10^{-4} mol), and 70 mL of ethanol were added. The solution was allowed to reflux for three hours, cooled to room temperature, filtered through a frit, washed with cold ethanol and dried under vacuum. The collected material (dried liquid portion) was washed with benzene to remove any free ligand, then dried again under vacuum. Amount recovered: 240 mg of black glass (191 mg, 3.68×10^{-4} mol, 66.8% yield, after correcting for starting material impurities, Table 1), mp >300 °C; ¹H NMR (CDCl₃): 7.4 ppm (H, broad m, phenyl), 6.7 ppm (H, broad m, phenyl), 4.7 ppm (H, broad m, Cp); ¹H NMR (d₆-DMSO): huge broad peak 8.5-6 ppm (H, m, phenyl), 7.04 ppm (H, broad s, phenyl), 6.64 ppm (H, broad s, phenyl), huge broad peak 5-3.5 ppm (H, m, Cp); Elemental analysis calculated for Fe₂Cl₂N₂C₂₄H₂₀ (actual), see Table 2: 52.77% C (52.77% C), 3.51% H (4.20% H), 5.42% N (5.25% N); Molar absorptivity (DMSO): 260 nm ($20300 \text{ M}^{-1}\text{cm}^{-1}$), 659 nm ($471 \text{ M}^{-1}\text{cm}^{-1}$); MS: three Fe containing peaks present, but none specific for the complex itself; see Appendix (Figures A.7-9) for spectra.

Synthesis of Fc2-CoCl₂: (3)

To a dried, N₂ flushed Schlenk flask containing a stir bar, 260 mg of **1** (6.63×10^{-4} mol), 160 mg of CoCl₂·6H₂O (6.72×10^{-4} mol) and 70 mL of ethanol were added. The

solution was allowed to reflux for three hours, cooled, filtered through a frit, and the dark solution dried under a vacuum. The deep reddish-purple solid (dried liquid portion) was rinsed with benzene to remove any free Fc₂ ligand, and then vacuum dried (product and CoCl₂ not soluble in benzene). Amount recovered: 230 mg (194 mg, 3.71×10^{-4} mol, 56.2% yield, after correcting for starting material impurities, Table 1) of deep reddish-purple glass-like powder, mp >300 °C; ¹H NMR (CDCl₃): 8.7-8.4 ppm (H, broad m); ¹H NMR (d₆-DMSO): 8.34 ppm (2H, s, Cp-CH=N), 7.28 ppm (2H, d, Phenyl), 7.08 ppm (2H, dd, phenyl), 6.97 ppm (2H, d, phenyl), 6.48 ppm (2H, t, phenyl), 4.86 ppm (4H, d, Cp), 4.58 ppm (4H, d, Cp); Elemental analysis calculated for FeCoCl₂N₂C₂₄H₂₀ (actual), see Table 2: 55.42% C (46.50% C), 3.49% H (4.06% H), 5.39% N (4.47% N); Molar absorptivity (DMSO): 433 nm ($2810 \text{ M}^{-1}\text{cm}^{-1}$), 655 nm ($292.0 \text{ M}^{-1}\text{cm}^{-1}$); MS: protonated ligand present; see Appendix (Figures A.10-12) for spectra.

Synthesis of Fc₂-NiCl₂: (4)

To a dried, N₂ flushed Schlenk flask containing a stir bar, 230 mg of **1** (5.86×10^{-4} mol), 140 mg of NiCl₂·6H₂O (5.89×10^{-4} mol) and 40 mL of ethanol were added. The solution was allowed to reflux for three hours, cooled, filtered through a frit, and dried under vacuum to obtain a reddish-brown solid. The dried liquid material was washed with benzene to remove any free Fc₂ ligand, then dried under a vacuum. Amount recovered: 200 mg of brown powder (142 mg, 2.72×10^{-4} mol, 46.5% yield, after correcting for starting material impurities, Table 1), mp >300 °C; ¹H NMR (CDCl₃): 7.2 ppm (H, t), 6.6 ppm (H, t), 4.5 ppm (H, broad m); ¹H NMR (d₆-DMSO): 7.34 ppm (2H, broad s, Cp-CH=N), 7.17 ppm (4H, broad s, phenyl), 6.99 ppm (4H, broad s, phenyl),

4.59 ppm (4H, broad s, Cp), 4.33 ppm (4H, broad s, Cp); Elemental analysis calculated for $\text{FeNiCl}_2\text{N}_2\text{C}_{24}\text{H}_{20}$ (actual), see Table 2: 55.45% C (39.17% C), 3.49% H (4.10% H), 5.39% N (4.05% N); Molar absorptivity (DMSO): 290 nm ($9600 \text{ M}^{-1}\text{cm}^{-1}$), 655 nm ($345.0 \text{ M}^{-1}\text{cm}^{-1}$); MS: free ligand observed; see Appendix (Figures A.13-15) for spectra.

Synthesis of $\text{Fc}_2\text{-CuCl}_2$: (5)

To a dried, N_2 flushed Schlenk flask containing a stir bar, 200 mg of **1** (5.10×10^{-4} mol), 70 mg of anhydrous CuCl_2 (5.021×10^{-4} mol), and 70 mL of ethanol were added. The solution was allowed to reflux for three hours, cooled, filtered through a frit, washed with cold ethanol and dried under a vacuum. The dried liquid fraction was washed with benzene to remove any free Fc_2 ligand, then dried under a vacuum. Amount recovered: 220 mg of black glass (199 mg, 3.77×10^{-4} mol, 74.2% yield, after correcting for starting material impurities, Table 1), mp >300 °C; ^1H NMR (CDCl_3): 7.68 ppm (2H, s, Cp- $\text{CH}=\text{N}$), 6.85 ppm (H, s, phenyl), 5.78 ppm (H, s), 4.71 ppm (H, s, Cp), 2.6 ppm (H, s); ^1H NMR ($d_6\text{-DMSO}$): 8.4 ppm (2H, s, Cp- $\text{CH}=\text{N}$), 7.36-7.31 ppm (2H, t, Phenyl), 7.28 ppm (2H, d, phenyl), 7.18-7.09 ppm (2H, d, phenyl), 6.7 ppm (2H, broad s, phenyl), 4.91 ppm (4H, s, Cp), 4.65 ppm (4H, s, Cp); Elemental analysis calculated for $\text{FeCuCl}_2\text{N}_2\text{C}_{24}\text{H}_{20}$ (actual), see Table 2: 54.94% C (49.41% C), 3.46% H (3.53% H), 5.34% N (4.77% N); Molar absorptivity (DMSO): 651 nm ($496.8 \text{ M}^{-1}\text{cm}^{-1}$); MS: observed free ligand; see Appendix (Figures A.16-18) for spectra.

Synthesis of $\text{Fc}_2\text{-ZnCl}_2$: (6)

To a dried, N₂ flushed Schlenk flask containing a stir bar, 230 mg of **1** (5.86×10^{-4} mol), 120 mg of ZnCl₂ (8.80×10^{-4} mol) and 70 mL of ethanol were added. The solution was allowed to reflux for three hours, cooled, filtered through a frit, washed with cold ethanol and dried under a vacuum. The dried liquid portion was washed with benzene to remove any free Fc2 ligand, then dried under a vacuum. Amount recovered: 260 mg of black glass (242 mg, 4.59×10^{-4} mol, 78.5% yield, after correcting for starting material impurities, Table 1), mp >300 °C; ¹H NMR (CDCl₃): no spectral peaks; ¹H NMR (d₆-DMSO, Fig. 2.5): 8.36 ppm (2H, s, Cp-CH=N), 7.35-7.31 ppm (H, q, phenyl), 7.28-7.19 ppm (H, d, phenyl), 7.16-7.10 ppm (H, d, phenyl), 7.01-6.95 ppm (H, t, phenyl), 4.88 ppm (H, s Cp), 4.57 ppm (H, s, Cp); Elemental analysis calculated for FeZnCl₂N₂C₂₄H₂₀ (actual), see Table 2: 54.74% C (50.82% C), 3.45% H (4.07% H), 5.32% N (4.70% N); Molar absorptivity (DMSO, Fig. 2.9): 584 nm ($165.6 \text{ M}^{-1}\text{cm}^{-1}$), 629 nm ($122.9 \text{ M}^{-1}\text{cm}^{-1}$), 655 nm ($217.3 \text{ M}^{-1}\text{cm}^{-1}$); MS: observed free ligand species; see appendix (Figures A.19-21) for spectra.

Synthesis of Fc2-CdCl₂: (**7**)

To a dried, N₂ flushed Schlenk flask containing a stir bar, 150 mg of **1** (3.82×10^{-4} mol), 80 mg of CdCl₂·2.5H₂O (3.50×10^{-4} mol), and 40 mL of ethanol were added. The solution was allowed to reflux overnight, cooled, filtered through a frit, washed with cold ethanol and dried under a vacuum. The dried liquid fraction was washed with benzene to remove any free Fc2 ligand, then dried under a vacuum. Amount recovered: 60 mg of deep red powder (36 mg, 6.32×10^{-5} mol, 18.1 % yield, after correcting for starting material impurities, Table 1), mp >300 °C; ¹H NMR (CDCl₃): 7.15 ppm (H, t), 6.8 ppm

(H, d), 6.7 ppm (H, d), Very broad peak 3.8-3.4 ppm (H); ^1H NMR (d_6 -DMSO): 8.37 ppm (2H, s, Cp-CH=N), 7.30 ppm (H, t, phenyl), 7.11-6.96 ppm (H, t, phenyl), 6.58-6.47 ppm (H, t, phenyl), Very broad peak at 5.22 ppm (H, s, Cp), 4.89 ppm (H, s, Cp), 4.61 ppm (H, s, Cp), Very broad peak 4.3-3.7 ppm (H, Cp); Elemental analysis calculated for $\text{FeCdCl}_2\text{N}_2\text{C}_{24}\text{H}_{20}$ (actual), see Table 2: 50.26% C (30.36% C), 3.16% H (2.26% H), 4.88% N (3.83% N); Molar absorptivity (DMSO): 296 nm ($12300 \text{ M}^{-1}\text{cm}^{-1}$), 362 nm ($10100 \text{ M}^{-1}\text{cm}^{-1}$), 655 nm ($413.6 \text{ M}^{-1}\text{cm}^{-1}$); MS: free ligand observed; see Appendix (Figures A.22-24) for spectra.

Synthesis of $\text{Fc}_2\text{-HgCl}_2$: (8)

To a dried, N_2 flushed Schlenk flask containing a stir bar, 230 mg of **1** (5.86×10^{-4} mol), 160 mg of HgCl_2 (5.89×10^{-4} mol), and 40 mL of ethanol were added. The solution was allowed to reflux for three hours, cooled, filtered through a frit, washed with cold ethanol and dried under a vacuum. The dried liquid portion was washed with benzene to remove any free Fc_2 ligand, then dried under a vacuum. Amount recovered: 260 mg of black powder (223 mg, 3.36×10^{-4} mol, 57.2 % yield, after correcting for starting material impurities, Table 1), mp >300 °C; ^1H NMR (CDCl_3): 7.70 ppm (2H, s, Cp-CH=N), 7.18 ppm (1H, d, phenyl), 6.86 ppm (1H, s, phenyl), 6.60 ppm (2H, d, phenyl), 4.9 ppm (4H, m, Cp), 4.7 ppm (2H, s, Cp), 4.5 ppm (2H, s, Cp); ^1H NMR (d_6 -DMSO): 8.83 ppm (H, broad s, Cp-CH=N), Very broad from 8.0-6.0 ppm (H, s), 7.37 ppm (H, s, phenyl), 7.25 ppm (H, s, phenyl), Very broad from 5.7-3.7 ppm (H, m), 4.81 ppm (H, s, Cp), 4.42 ppm (H, s, Cp); Elemental analysis calculated for $\text{FeHgCl}_2\text{N}_2\text{C}_{24}\text{H}_{20}$ (actual), see Table 2: 45.63% C (37.24% C), 2.87% H (2.64% H), 4.43% N (3.12% N); Molar absorptivity

(DMSO): 655 nm ($706.0 \text{ M}^{-1}\text{cm}^{-1}$); MS: complex not present but M+1 ligand peak was present; see Appendix (Figures A.25-27) for spectra.

Synthesis of Fc2-PbCl₂: (9)

To a dried, N₂ flushed Schlenk flask containing a stir bar, 150 mg of **1** (3.82×10^{-4} mol), 100 mg of PbCl₂ (3.16×10^{-4} mol, dissolved up into 50 mL DI water/ethanol) were added. The solution was allowed to reflux for three hours, cooled, filtered through a frit, washed with cold ethanol and dried under a vacuum. The dried liquid fraction was washed with benzene to remove any free Fc2 ligand, then dried under a vacuum.

Amount recovered: 80 mg of black powder (60 mg, 8.87×10^{-5} mol, 24.8 % yield, after correcting for starting material impurities, Table 1), mp >300 °C; ¹H NMR (CDCl₃): 8.0-7.4 ppm (H, s), 6.73 ppm (H, d), Very broad 5.0-4.0 ppm (H, m), Very broad 3.7-3.3 ppm (H, m); ¹H NMR (d₆-DMSO): 7.5 ppm (2H, broad s, phenyl), 7.06 ppm (2H, broad s, phenyl), 6.63 ppm (4H, broad d, phenyl), Very broad peak 6.0-5.0 ppm (H, m, Cp), Very broad peak 5.0-4.0 ppm (H, m, Cp); Elemental analysis calculated for FePbCl₂N₂C₂₄H₂₀ (actual), see Table 2: 43.13% C (32.01% C), 2.71% H (3.97% H), 4.19% N (2.76% N); Molar absorptivity (DMSO): 655 nm ($864.0 \text{ M}^{-1}\text{cm}^{-1}$); MS: complex not present but M+1 ligand peak was present; see Appendix (Figures A.28-30) for spectra.

Table 1: Melting points, Colors and Percent Yields of the Fc₂ ligand and metal complex products

Compound #	Formula	Color	Melting Point	Percent Yield of Reaction
1	FeN ₂ C ₂₄ H ₂₀	deep red	82-86 °C	99 %
2	Fe ₂ Cl ₂ N ₂ C ₂₄ H ₂₀	black (glass)	>300 °C	66.8 %
3	FeCoCl ₂ N ₂ C ₂₄ H ₂₀	black (glass)	>300 °C	56.2 %
4	FeNiCl ₂ N ₂ C ₂₄ H ₂₀	brown	>300 °C	46.5 %
5	FeCuCl ₂ N ₂ C ₂₄ H ₂₀	black (glass)	>300 °C	74.2 %
6	FeZnCl ₂ N ₂ C ₂₄ H ₂₀	black (glass)	>300 °C	78.5 %
7	FeCdCl ₂ N ₂ C ₂₄ H ₂₀	deep red	>300 °C	18.1 %
8	FeHgCl ₂ N ₂ C ₂₄ H ₂₀	black	>300 °C	57.2 %
9	FePbCl ₂ N ₂ C ₂₄ H ₂₀	black	>300 °C	24.8 %

Compounds **2-9** contained varying amounts of hydrated metal chloride starting materials according to the elemental analysis discrepancies. The amount of impurities was calculated by matching the actual value vs. values of the compound with differing amounts of impurities present.

Table 2: Elemental Analysis of the Fc₂ systems.

	Calc. C%	Actual C%	Calc. H%	Actual H%	Calc. N%	Actual N%	impurities %
2	52.77	52.77	3.51	4.20	5.42	5.25	20.42
3	55.42	46.50	3.49	4.06	5.39	4.47	15.74
4	55.45	39.17	3.49	4.10	5.39	4.05	29.07
5	54.94	49.41	3.46	3.53	5.34	4.77	9.65
6	54.74	50.82	3.45	4.07	5.32	4.70	6.73
7	50.26	30.36	3.16	2.26	4.88	3.83	39.42
8	45.63	37.24	2.87	2.64	4.43	3.12	14.36
9	43.13	32.01	2.71	3.97	4.19	2.76	25.61

Discussion Section for Fc₂-MCl₂ complexes:

The free ligand was prepared (Figure 2.4) via a modified Dean-Stark apparatus, such that the volume of benzene/water azeotrope could be continuously removed by a spigot (which, using Le Châtelier's principle, forces the reaction toward the formation of products). Fc₂ is very soluble in benzene, so much so that it does not precipitate out

when formed (much different from the FcOH_2 ligand system). Upon removal of the solvent, the deep reddish tar becomes waxy upon air drying overnight. (^1H NMR spectra of the tar and the waxy form of Fc_2 are identical.) The ligand is very soluble in aromatic solvents but only sparingly soluble in aliphatic solvents. It has a very high degree of solubility when compared to the other disubstituted ligands. Although many attempts were made to grow a crystal of this particular ligand, none of the attempted trials formed any usable crystals due to the high degree of solubility in mixed solvents.

Upon reaction with a metal cation, the ligand in solution undergoes a change in color, which can be quite dramatic in some reactions (dark red to black, dark red to orange). Upon filtering and drying of the ethanol portion, the products obtained were typically glass-like (possibly indicative that left over starting materials are present).

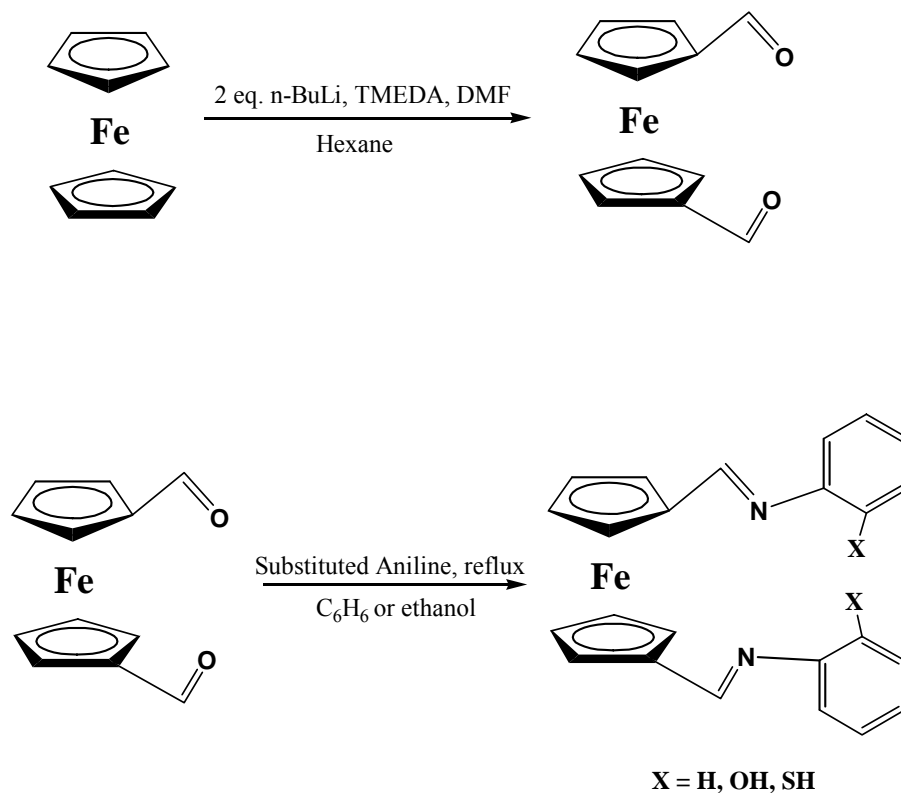


Figure 2.4: Synthesis scheme for producing 1,1'-disubstituted Schiff Base ferrocene ligands from ferrocene.

The metal complexes have many differences over the unbound Fc2 ligand. The melting points of all of the metal complexes (Fc2-MCl₂) are above 300 °C, whereby the free ligand melts at 82-86 °C. Unfortunately, some unreacted metal chloride starting materials were present in the product (the amount of impurities can be seen in the elemental analysis results for the complexes at the end of the experimental section). Later experimentation revealed that the starting MCl₂ could be removed through the use of methanol extractions. No free Fc2 ligand was present in the products. As previously mentioned, the free ligand is quite soluble in benzene and the products from each reaction were washed well with benzene to remove any unbound ligand that was present (the color of the benzene gave an indication on how much ligand was removed). In most instances, the benzene color was either colorless or only slightly colored, indicating a near completion of the reaction. The product would have started to melt (partially) at around 80-100 °C if any unbound Fc2 was present. To verify this, one of the metal chloride complexes with a small amount of Fc2 was mixed together and the free ligand started melting around the indicated range, while the product did not melt during the range of the melting point instrument.

Each metal product that was formed by the Fc2 system was analyzed to obtain a spectral database as a means for further identification of products in a selectivity experiment. All attempts to grow X-ray quality crystals failed despite many trials due to the presence of the MCl₂ impurities. The materials formed either glasses or powders when allowed to dry by evaporation.

Melting point, MS, and ¹H NMR:

Compound **1** (see Table 1) shows a melting point range between 82-86 °C after drying to a deep reddish solid. It has a low melting point and is somewhat waxy. The Fc₂-MCl₂ compounds undergo an increase in the melting points over **1** to over 300 °C (the limit of the melting point instrument). Since there are no clear distinct melting points that occur for the metal complexes using the melting point apparatus, identification of selectivity experiment products using this ligand system via melting point is pointless (if chosen as a method for identification).

The Electro Spray Ionization (ESI)-MS for the Fc₂-MCl₂ complexes does not show M+1 peaks that would be characteristic of an ionized complex that has held together long enough to reach the detector. MS gives no conformational data for any of the metal complexes, so it would not be of any use in identifying selectivity products.

The ¹H NMR spectrum of **1** (see Appendix, Figures A.3-4) showed characteristic peaks that could be attributed to protons on the ligand. The furthest downfield peak (8.33 ppm in either solvent) corresponds to the Cp-CH=N-R proton due to the influence of the imine. The phenyl ring protons show up around 7.40-7.00 ppm and the Cp peaks appear between 5-4.5 ppm. There are two Cp proton peaks since each Cp has one R group. The protons next to the R group are equivalent, as are the other two furthest away. The ¹H NMR spectra for some of the Fc₂-MCl₂ complexes are harder to define for some complexes, even after further purification. Complex **3** contains unpaired electrons due to the Co^{II} moiety (high spin tetrahedral, 3 unpaired e⁻s), which induces some paramagnetic behavior. ¹H NMR measurements can be distorted in paramagnetic samples. It causes broadening of spectral peaks, shifting of peak locations, decoupling of peaks and/or disappearance of peaks altogether. The type and amount of these effects are specific to

the material being measured. Since most of the $\text{Fc}_2\text{-MCl}_2$ compounds are diamagnetic (no unpaired electrons), the ^1H NMR spectrums can be determined. Based upon the NMR data, products formed during the sensing experiments might be characterizable using ^1H NMR, although some products might be very difficult to identify if a mixture of complexes is present. The ^1H NMR spectra of $\text{Fc}_2\text{-ZnCl}_2$, compound **7**, the target product for the selectivity of this ligand system is shown below (Figure 2.5)

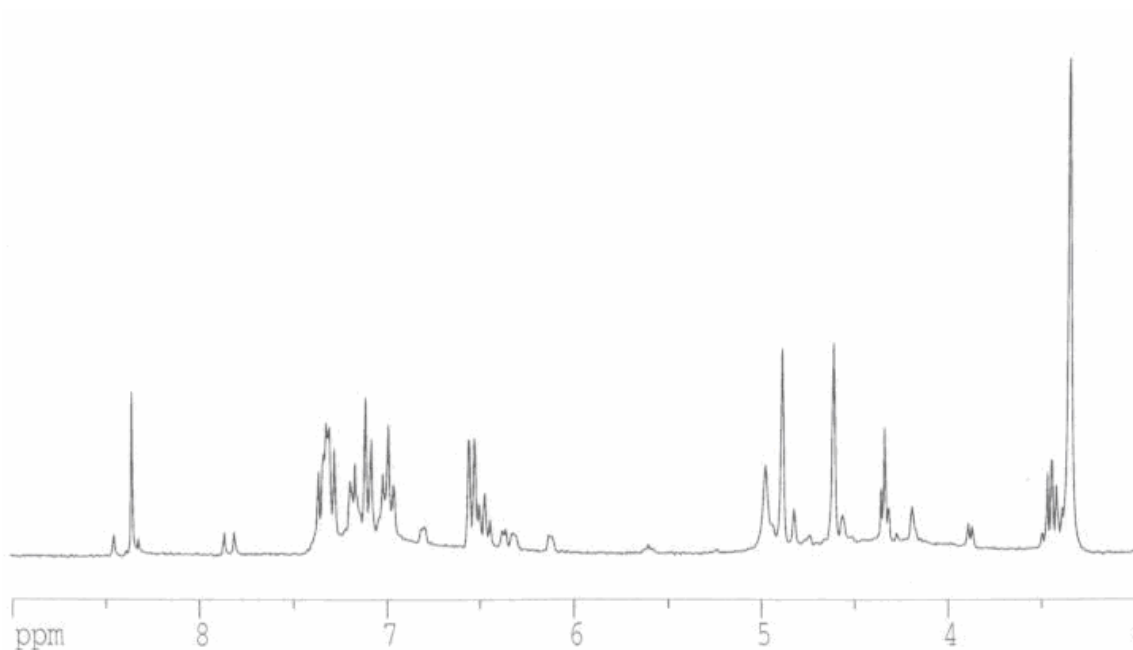


Figure 2.5: ^1H NMR spectrum of $\text{Fc}_2\text{-ZnCl}_2$ in $\text{d}_6\text{-DMSO}$. The peaks around 8-7ppm correspond to aromatic peaks from the phenyl hydrogens, while the two largest peaks between 5-4 ppm belong to the Cp ring protons. The Cp- $\underline{\text{C}}\text{H}=\text{N-R}$ peak is furthest upfield at 8.4 ppm. (1:4:2:2:2:2:2 H equivalency, no peak at 9.95 ppm present corresponding to leftover 1,1'-diformylferrocene)

^1H NMR spectral peak comparison graphs (Figures 2.6-7) are shown below.

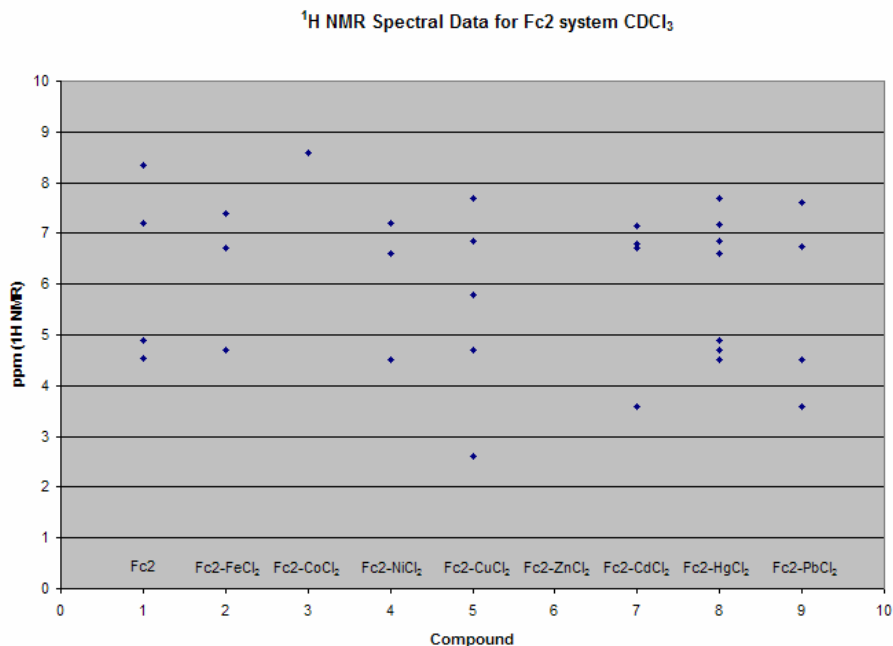


Figure 2.6: The ^1H NMR peak locations for the Fc2 system in CDCl_3

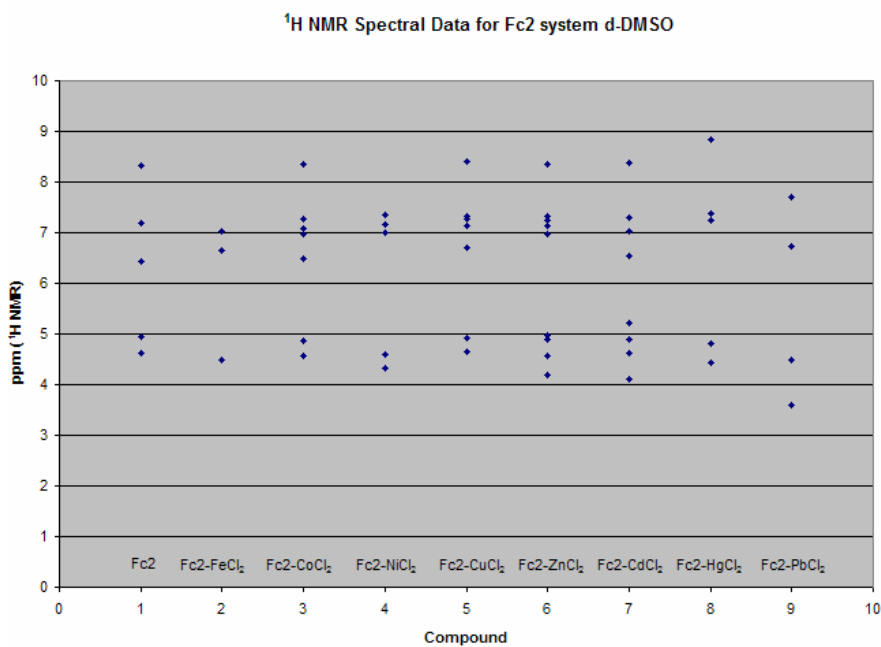


Figure 2.7: The ^1H NMR peak locations for the Fc2 system in $\text{d}_6\text{-DMSO}$

Colorimetric (IR, UV-Vis.):

The IR spectra for complexes **1-9** are identical in that the imine stretch and the ferrocene Cp (1643 cm^{-1} , 890 cm^{-1}) are the only noteworthy peaks. The spectra differ based upon the MCl_2 that is present, which do not show up in the IR readily. IR is an example of a technique that would not be useful in identifying individual complexes of this system.

Ferrocene contains a Fe^{II} octahedral d^6 metal center sandwiched between two Cp rings (see Appendix for MO diagram with further information) and will give a UV-Vis spectrum with two d-d transitional peaks when measured.¹²⁶ Some substituted ferrocene ligands showed two bands within the same ranges in the UV-Vis spectrum, (${}^1\text{E}_{2g} \leftarrow {}^1\text{A}_{1g}$) was assigned to the higher energy band and (${}^1\text{E}_{1g} \leftarrow {}^1\text{A}_{1g}$) to the lower one.¹²⁶ Other monosubstituted ferrocenes with conjugated bridges between aromatic ring systems show two transitions within the UV-Vis spectrum, corresponding to transitions between the metal orbitals and the π orbitals within the system.¹²⁷ DMSO solvent was chosen for this research project as all compounds and starting materials dissolve readily in it. The absorption spectrum for compound **1** in DMSO shows two primary peaks in the visible range, 319 nm ($\text{E}_2 \leftarrow \text{A}_1$) and 470 nm ($\text{E}_1 \leftarrow \text{A}_1$) due to a combination of d-d and d-ligand transitions within the complex (Figure 2.8), typical behavior of ferrocene derivatives. Ethanol might also be used to measure UV-Vis spectra for this system. Compounds **2-9** have less definition in the peaks when compared to the combined molar absorptivity of their respective starting materials (**1** + MCl_2). This absorbance behavior is expected to occur.

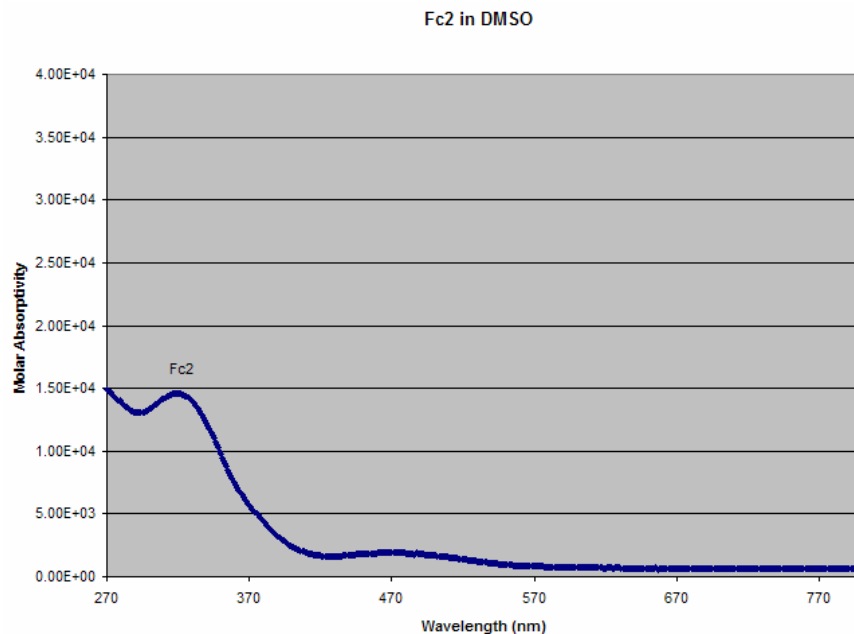


Figure 2.8: Molar absorptivity (UV-Vis) of Fc2 ligand in DMSO. The bands at 470 and 319 nm correspond to d-d transitions.

The molar absorptivity of **2** decreases greatly, although there is not much spectral detail, when compared to the combined starting materials. Compound **3** decreases (hypochromic shift) under the portion for the first peak, but is equal in intensity for the rest of the spectrum. It does not appear to have the first peak at 321 nm that the starting materials have. **4** decreases moderately when compared to the starting materials in the first peak (also blue shifted to 290 nm from 319 nm), while the other portion is almost as intense as the second peak. The molar absorptivity of **5** is very similar to **4**, except that there is no defined first peak. **6** is almost as intense as the starting materials, but the first (high energy) peak is less defined (and slightly lower), while the rest is equal in intensity (Figure 2.9). **7** has a spectrum that is lower in intensity than the starting materials, but shows three peaks (296 nm, 362 nm and the final peak that matches the second peak for the starting materials). Both **8** and **9** decrease in intensity with the first peak looking like a shoulder that is slightly red shifted (bathochromic shift), the second peak is slightly

greater than the starting material. Both complexes appear to have almost identical molar absorptivities, leading to a problem in identifying them separately. Based on the data measured, UV-Vis spectra would not be a good method for identification of the selectivity experiment products for this ligand system, since only **7** has a spectrum that is very different from the other metal complexes with the additional peak at 296 nm. Being able to identify only one product out of eight possible complexes is not very useful unless the ligand system has a high preference for that particular metal cation. Unfortunately, the Fc2 system does not look like it will be selective for either Cd^{2+} when other cations are present in solution.

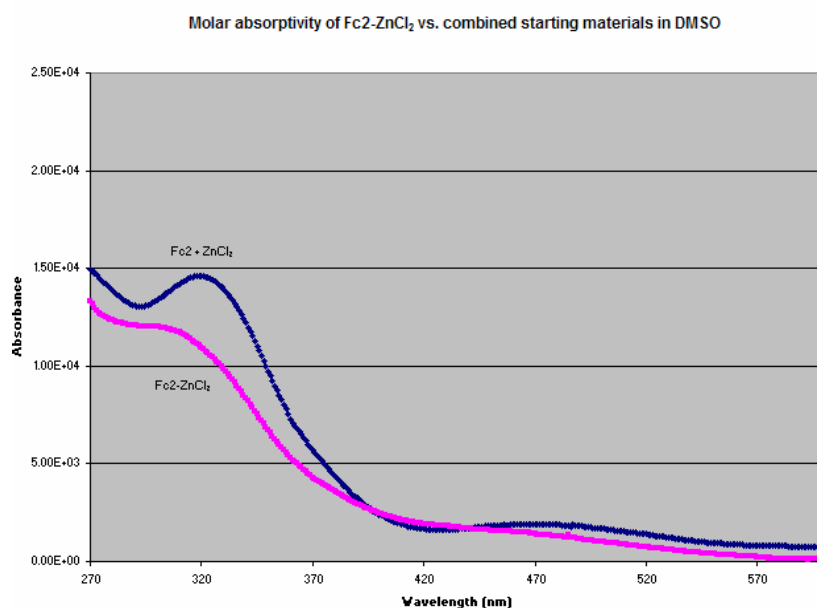


Figure 2.9: Comparison between the molar absorptivity (UV-Vis) of Fc2-ZnCl₂ and the molar absorptivity of the combined starting materials (SM) in DMSO. Starting materials spectrum contain peaks at 319 nm and 470 nm from the d-d transitions of the ligand, while the spectrum for Fc2-ZnCl₂ contains peaks with less intensity and slight blue shifting (hypsochromic) from the ferrocene moiety.

Electrochemistry:

The electrochemistry of **1** in 1×10^{-3} M tetrabutylammonium hexafluorophosphate (TBAHFP) electrolyte DMSO solution has a $\text{Fe}^{\text{II}}\text{-Fe}^{\text{III}}$ couple at 450 mV (vs. 0.01 M Ag/AgNO_3) and has a very subdued peak in the CV spectrum (Figure 2.10). This coupling will be used to analyze the electrochemistry of any metal complexes based on their shifting of potential vs. the starting ligand, **1**. DMSO electrochemical working range is between +1.5 V and -2.5 V. Unsubstituted ferrocene has $\text{Fe}^{\text{II}}\text{-Fe}^{\text{III}}$ oxidation at 388 mV in the same solvent/electrolyte when measured. Compound **2** has an $\text{Fe}^{\text{II}}\text{-Fe}^{\text{III}}$ peak at 936 mV, while **3** has a peak at 994 mV corresponding to the same oxidation. **4** has a peak at 886 mV, while **5** has multiple peaks present (221 mV, 545mV, and a large less defined (broad) peak near 1.1 V). **6** has a peak at 705 mV, but there also exists a less defined peak past 1.0 V. The heavy metal complexes have iron oxidations that allow for identification due to their relative differences in potential. **7** has a peak at 850 mV, **8** has a small peak at 731 mV and **9** has a peak at 950 mV. Because each metal complex for this ligand system has a particular $\text{Fe}^{\text{II}}\text{-Fe}^{\text{III}}$ potential, cyclic voltammetry can be used to determine the product formed during selectivity experiments.

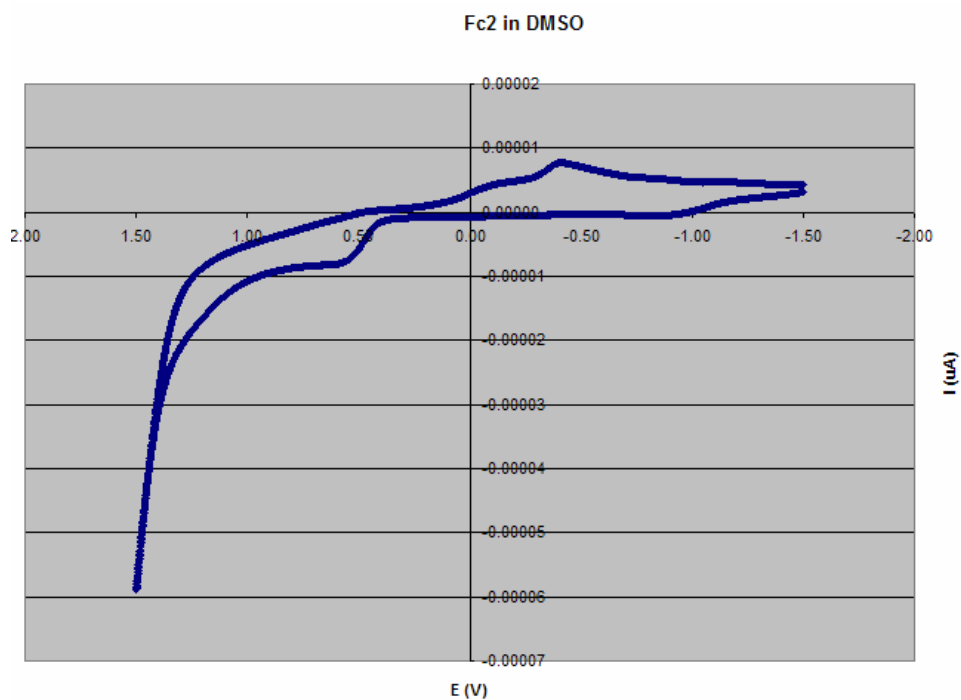


Figure 2.10: CV scan of Fc2 ligand in DMSO, scan rate 100 mV/sec. The peak near 450 V corresponds to the Fe^{II} oxidation to Fe^{III} within the ferrocene moiety.

Conclusion for the Fc2 system:

The complexation of **1** with MCl_2 salts in ethanolic solutions yielded no precipitates, but upon drying, the resulting dark glass-like material gave melting points that were significantly higher than the starting ligand. Unfortunately, unreacted MCl_2 salts were present in the products that could not be easily removed during synthesis. Methanol can be used to extract them from the product. This can account for the discrepancies that are seen in the elemental analysis for compounds **2** through **9**.

This ligand had promise of being a possible Zn^{2+} sensor, based upon the similarities with a known sensor for that cation. Unfortunately, this system will not be as versatile for detection of the cationic species due to the lack of differentiation in some of the spectroscopic data of the metal complexes. For example, ^1H NMR spectra do not have

spectral peaks that can be easily identifiable for all individual metal complexes due to the presence of starting material impurities that were not properly removed using methanol extraction. It is not completely useless as a technique and it can give hints on what possible products might be present.

Other detection techniques that fail to identify single metal complexes are IR, MS, and UV-Vis. IR only shows the imine stretch and the Cp ring stretch for each compound that are at the same locations regardless of the chelated metal center. MS can not define the M+1 peak for each metal complex, as it falls apart with ionization and cannot be detected as a cohesive molecule. UV-Vis spectra can only identify the metal compound containing Cd^{2+} , not the target Zn^{2+} . That leaves only electrochemistry as an identification technique for all the metal complexes of this ligand. The ligand cannot even use geometric steric hindrance as a differentiation between metal centers, as the heavy metal systems seem to bind just as well as the smaller transition metal centers. The phenyl rings would move if the bound metal chloride came into contact with them, so the system appears to be somewhat less ordered when it comes to the phenyl geometry.

This leads to the conclusion that it would be an ineffective Zn^{2+} multi-detection sensor as it only has one real mode for detection, CV. The selectivity of the ligand would not be expected to be great for one metal cation over others due to the imine bonds not differentiating between metal centers as they chelate. Since this ligand system has flaws, it becomes critical to design derivatives that might hold a better chance at doing their intended job. A much better way to sensor metals is by adding either hard donor or soft donor chelating groups to the phenyl rings, thereby holding the metal into a specific

(tetrahedral) geometry. Two ligand systems incorporating this idea are discussed in chapters three (FcOH₂) and four (FcSH₂).

-
- ¹²³ Wananabe, Makoto; Okada, Takashi, Ethylene/polar monomer copolymerization using (Aza)ferrocenyl(di)imine nickel(II) catalysts. *Toso Kenkyu, Gijutsu Hokoku* **2004**, 48, 15-22.
- ¹²⁴ Silverstein, R. M.; Webster, F. X., *Spectrometric Identification of Organic Compounds*. 6th. ed.; John Wiley & Sons, Inc.: New York, 1997; p 482.
- ¹²⁵ Balavoine, G. G. A.; Doisneau, G.; Fillebeen-Khan, T., An improved synthesis of ferrocene-1,1'-dicarbaldehyde. *J. Organomet. Chem.* **1991**, 412, (3), 381-382.
- ¹²⁶ Pal, S.K; Krishnan, A.; Das,P.K.; Samuelson, A.G; Schiff base linked ferrocenyl complexes for second-order nonlinear optics. *J. Organom. Chem.* **2000**, 604, 248-259.
- ¹²⁷ Barlow, S.; Bunting, H. E.; Ringham, C.; Green, J. C.; Bublitz, G. U.; Boxer, S. G.; Perry, J. W.; Marder, S. R., Studies of the Electronic Structure of Metallocene-Based Second-Order Nonlinear Optical Dyes. *J. Am. Chem. Soc.* **1999**, 121, 3715-3723.

CHAPTER THREE

The FcOH2 Ligand System: hard donor

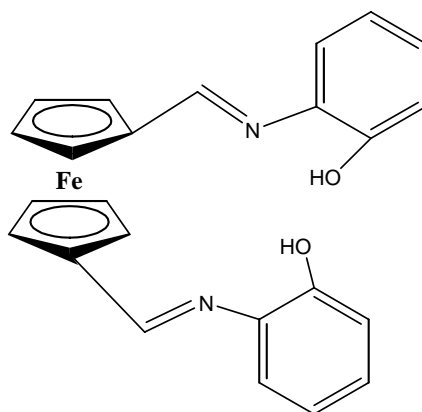


Figure 3.1: The FcOH2 ligand: $\text{FeN}_2\text{O}_2\text{C}_{24}\text{H}_{20}$.

The second system, FcOH2 (Figure 3.1), contains two imine groups as well as two alcohol groups on the ortho position of the pendant phenyl ring. This allows for bidentate chelation to a metal center per each ligand arm. Due to oxygen's high electronegativity, the bonds formed with the metal center were more ionic in character, a property that can be potentially exploited for chelating certain metals over others. A mono-substituted form of this ligand¹²⁸, FcOH1 (Figure 3.2a), and its corresponding metal complexes, $(\text{FcO1})_2\text{M}$ (Figure 3.2b), have been reported in the literature.

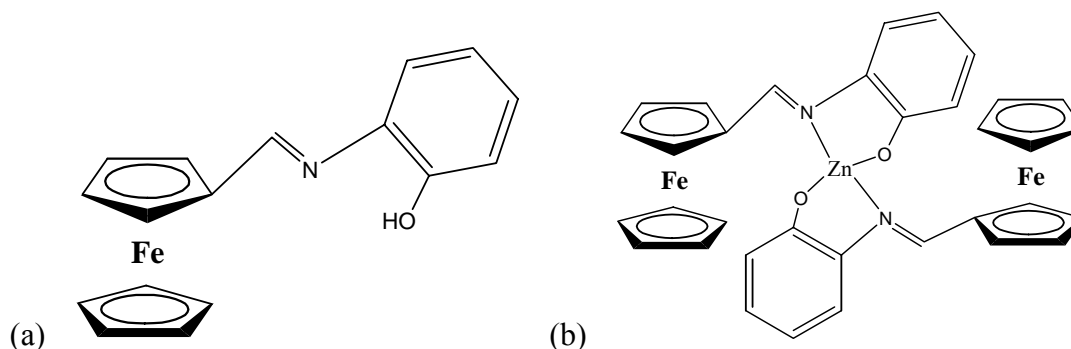


Figure 3.2 (a) and (b): (a) the structure of the FcOH1 ligand and (b) the structure of the $[\text{FcO1}]_2\text{-Zn}$ complex¹²⁸

Neither the mono or disubstituted forms undergo ring closing tautomerization, although the addition of a methylene group between the phenyl ring and the alcohol will allow for this to occur.¹²⁹

There is potential that FcOH2 could be a sensor for lead, but that rests in both the selectivity and ability to detect FcO2-Pb over other metal complexes that might form.

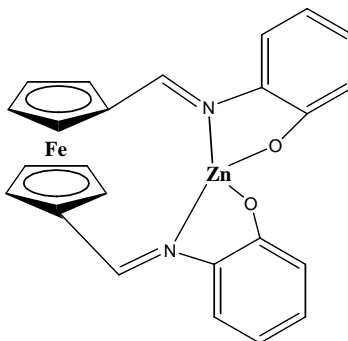


Figure 3.3 Proposed structure of the FcO2-Zn complex.

The FcOH2 system has not been reported in the literature, although the mono-substituted ligand form is well known.¹²⁸ FcOH1 forms (FcO1)₂-M complexes (Figure 3.2b) containing two ferrocene units per formed product. The FcO2-M complexes (see Figure 3.3 for an example) that are produced with the FcOH2 system contain only one ferrocene unit within the complex. Since the FcOH2 system contains two imine groups and two phenolic groups that are all used during chelation, the metal cations are typically held in a tetrahedral geometry (although other geometries are possible). The addition of the highly electronegative oxygen atoms in the alcoholic side groups greatly affects the chemistry over the Fc2 system that has no oxygen atoms present. The melting point of the free ligand increases by almost 90 °C. It is much less soluble in benzene than the Fc2 ligand.

Experimental:**Synthesis of FcOH₂ ligand: (10)**

To a dried, N₂ flushed 250 mL side arm round bottom flask containing a stir bar, 600 mg of 1,1'-diformylferrocene (2.48×10^{-3} mol), 540 mg of 2-aminophenol (4.96×10^{-3} mol) and 100 mL of benzene were added. The solution was allowed to undergo reflux for three hours (color darkened) and then the majority of the benzene was removed via a modified Dean-Stark apparatus. Upon cooling, the deep red solution was filtered, washed with ethanol and dried to recover the solid product precipitate. Amount recovered: 680 mg of deep red solid (1.60×10^{-3} mol, 60.1% yield, Table 3), mp 172-174 °C; ¹H NMR (CDCl₃): 8.50 ppm (2H, s, Cp-CH=N), 7.95 ppm (broad s, OH), 7.17-7.11 ppm (2H, t, Phenyl), 7.02-6.96 ppm (4H, q, Phenyl), 6.85-6.79 ppm (2H, t, Phenyl), 4.86 ppm (4H, d, Cp), 4.58 ppm (4H, d, Cp); ¹H NMR (d₆-DMSO): 8.78 ppm (2H, s, OH), 8.44 ppm (2H, s, Cp-CH=N), 7.03-6.97 ppm (4H, t, Phenyl), 6.90-6.84 ppm (2H, d, Phenyl), 6.75-6.69 ppm (2H, t, Phenyl), 4.92 ppm (4H, d, Cp), 4.59 ppm (4H, d, Cp); Elemental analysis calculated for FeN₂O₂C₂₄H₂₀ (actual): 67.94% C (67.81% C); 4.75% H (5.07% H); 6.60% N (6.63% N); 67.94% C (67.81% C), 4.75% H (5.07% H), 6.60% N (6.63% N); Elemental analysis calculated for FeN₂O₂C₂₄H₂₀ (actual), Table 4: Molar absorptivity (DMSO, Fig. 3.8): 254 nm (8510), 258 nm (26300 M⁻¹cm⁻¹), 351 nm (17000 M⁻¹cm⁻¹), 455 nm (1990 M⁻¹cm⁻¹), 463 nm (1990 M⁻¹cm⁻¹), 472 nm (1980 M⁻¹cm⁻¹); MS: M+1: 424.98 amu, CV (Fig. 3.10) and X-ray crystal structure data (Table 6); see Appendix (Figures A.31-35) for spectra.

Synthesis of FcO₂-Fe: (11)

To a dried, N₂ flushed Schlenk flask containing a stir bar, 260 mg of **10** (6.13×10^{-4} mol), 110 mg of Fe(CH₃COO)₂ (6.13×10^{-4} mol), 70 mL of ethanol and 3 mL of NH₄OH were added. The solution was allowed to reflux for three hours, cooled, filtered through a frit, washed with cold ethanol and the precipitate was dried under a vacuum. Amount recovered: 150 mg of deep red-black powder (133 mg, 2.78×10^{-4} mol, 45.6% yield, after correcting for starting material impurities, Table 3), mp >300 °C; ¹H NMR (CDCl₃): 8.47 ppm (2H, d, Cp-CH=N), 7.20 ppm (2H, m, phenyl), 7.02-6.96 ppm (4H, dd, phenyl), 6.8 ppm (2H, t, phenyl), 4.93-4.85 ppm (4H, t, Cp), 4.65-4.58 ppm (4H, t, Cp); ¹H NMR (d₆-DMSO): 8.79 ppm (2H, s, Cp-CH=N), 8.44 ppm (2H, d, phenyl), 7.09-7.02 ppm (2H, dd, phenyl), 6.85-6.82 ppm (4H, t, phenyl), 5.00-4.90 ppm (4H, t, Cp), 4.75 ppm (2H, d, Cp), 4.63 ppm (2H, d, Cp); Elemental analysis calculated for Fe₂N₂O₂C₂₄H₁₈ (actual), see Table 4: 60.29% C (55.69% C); 3.79% H (3.86% H); 5.86% N (5.15% N); Molar absorptivity (DMSO): 299 nm ($11500 \text{ M}^{-1} \text{ cm}^{-1}$), 321 nm ($11300 \text{ M}^{-1} \text{ m}^{-1}$), 364 nm ($13500 \text{ M}^{-1} \text{ m}^{-1}$); MS: Fe containing species present; see Appendix (Figures A.36-38) for spectra.

Synthesis of FcO2-Co: (12)

To a dried, N₂ flushed Schlenk flask containing a stir bar, 240 mg of **10** (5.66×10^{-4} mol), 140 mg of Co(CH₃COO)₂·4H₂O (5.62×10^{-4} mol), 70 mL of ethanol and 3 mL of NH₄OH were added. The solution was allowed to reflux for three hours, cooled, filtered through a frit, washed with cold ethanol and the precipitate was dried under a vacuum. Amount recovered: 120 mg of deep red-black powder (102 mg, 2.12×10^{-4} mol, 37.8% yield, after correcting for starting material impurities, Table 3), mp >300 °C; ¹H NMR (CDCl₃): no signal present; ¹H NMR (d₆-DMSO): 7.5-7.3 ppm (2H, broad d, Cp-CH=N),

6.8 ppm (2H, broad s, phenyl), 6.6-6.4 ppm (4H, broad d, phenyl), 6.3-5.2 ppm (2H, broad d, phenyl), 4.9 ppm (2H, s, Cp), 4.7 ppm (2H, s, Cp), 4.4 ppm (4H, s, Cp); Elemental analysis calculated for $\text{FeCoN}_2\text{O}_2\text{C}_{24}\text{H}_{18}$ (actual), see Table 4: 59.91% C (49.36% C); 3.77% H (4.00% H); 5.82% N (7.31% N); Molar absorptivity (DMSO): 334 nm ($7440 \text{ M}^{-1}\text{cm}^{-1}$), 448 nm ($4810 \text{ M}^{-1}\text{cm}^{-1}$); MS: free ligand, see Appendix (Figures A.39-41) for spectra.

Synthesis of FcO2-Ni: (13)

To a dried, N_2 flushed Schlenk flask containing a stir bar, 330 mg of **10** (7.78×10^{-4} mol), 200 mg of $\text{Ni}(\text{CH}_3\text{COO})_2 \cdot 4\text{H}_2\text{O}$ (8.04×10^{-4} mol), 70 mL of ethanol and 3 mL of NH_4OH were added. The solution was allowed to reflux for three hours, cooled, filtered through a frit, washed with cold ethanol and the precipitate was dried under a vacuum. Amount recovered: 40 mg of deep brown-red powder (32 mg, 6.65×10^{-5} mol, 8.5% yield, after correcting for starting material impurities, Table 3), mp >300 °C; ^1H NMR (CDCl_3): very broad from 5-4 ppm (m, Cps); ^1H NMR (d_6 -DMSO): 7.7-7.4 ppm (m, phenyls), very broad peak 5-4 ppm (m, Cps); Elemental analysis calculated for $\text{FeNiN}_2\text{O}_2\text{C}_{24}\text{H}_{18}$ (actual), see Table 4: 59.94% C (51.59% C); 3.77% H (4.15% H); 5.82% N (3.74% N); Molar absorptivity (DMSO): 651 nm ($2170 \text{ M}^{-1}\text{cm}^{-1}$); MS: protonated ligand; see Appendix (Figures A.42-44) for spectra.

Synthesis of FcO2-Cu: (14)

To a dried, N_2 flushed Schlenk flask containing a stir bar, 280 mg of **10** (6.60×10^{-4} mol), 140 mg of $\text{Cu}(\text{CH}_3\text{COO})_2 \cdot \text{H}_2\text{O}$ (7.01×10^{-4} mol), 70 mL of ethanol and 3 mL of

NH₄OH were added. The solution was allowed to reflux for three hours, cooled, filtered through a frit, washed with cold ethanol and the precipitate was dried under a vacuum. Amount recovered: 150 mg of deep red powder (139 mg, 2.86×10^{-4} mol, 43.5% yield, after correcting for starting material impurities, Table 3), mp >300 °C; ¹H NMR (CDCl₃): 4.6-4.4 ppm (broad m, Cps); ¹H NMR (d₆-DMSO): 6.36 ppm (s, phenyls), 4.92 ppm (s, Cps), 4.76 ppm (s, Cps), 4.33 ppm (s, Cps); Elemental analysis calculated for FeCuN₂O₂C₂₄H₁₈ (actual), see Table 4: 59.34% C (52.25% C); 3.73% H (3.69% H); 5.77% N (6.50% N); Molar absorptivity (DMSO): 480 nm ($3820 \text{ M}^{-1} \text{ cm}^{-1}$); MS: free ligand present; see Appendix Figures A.45-47) for spectra.

Synthesis of FcO₂-Zn: (15)

To a dried, N₂ flushed Schlenk flask containing a stir bar, 250 mg of **10** (5.89×10^{-4} mol), 130 mg of Zn(CH₃COO)₂·2H₂O (5.92×10^{-4} mol), 70 mL of ethanol and 3 mL of NH₄OH were added. The solution was allowed to reflux for three hours, cooled, filtered through a frit, washed with cold ethanol and the precipitate was dried under a vacuum. Amount recovered: 120 mg of deep red-black powder (63 mg, 1.29×10^{-4} mol, 22.0% yield, after correcting for starting material impurities, Table 3), mp >300 °C; ¹H NMR (CDCl₃): no spectral peaks; ¹H NMR (d₆-DMSO): very broad peak 7-6 ppm (m, phenyls), very broad peak 5-3.5 ppm (m, Cps); Elemental analysis calculated for FeZnN₂O₂C₂₄H₁₈ (actual), see Table 4: 59.11% C (41.45% C); 3.72% H (3.17% H); 5.74% N (2.51% N); Molar absorptivity (DMSO): no peaks; MS: protonated ligand present; see Appendix (Figures A.48-50) for spectra.

Synthesis of FcO2-Cd: (16)

To a dried, N₂ flushed Schlenk flask containing a stir bar, 160 mg of **10** (3.77×10^{-4} mol), 100 mg of Cd(CH₃COO)₂·2H₂O (3.75×10^{-4} mol), 50 mL of ethanol and 3 mL of NH₄OH were added. The solution was allowed to reflux overnight, cooled, filtered through a frit, washed with cold ethanol and the precipitate was dried under a vacuum. Amount recovered: 40 mg of deep red-orange powder (36 mg, 6.73×10^{-5} mol, 17.7% yield, after correcting for starting material impurities, Table 3), mp >300 °C; ¹H NMR (CDCl₃): 7.9 ppm (H, broad d, Cp-CH=N), 7.1-6.6 ppm (H, broad m, phenyl), 6.4-6.1 ppm (H, broad m, phenyl), 6.0-5.6 ppm (H, broad m, phenyl), 5.4 ppm (H, broad s, Cp), 4.8 ppm (H, broad s, Cp), very broad 4.6-3.8 ppm (H, m, Cp); ¹H NMR (d₆-DMSO): 8.2-7.8 ppm (2H, d, Cp-CH=N), 6.9 ppm (2H, d, phenyl), 6.55 ppm (4H, t, phenyl), 6.36 ppm (2H, d, phenyl), 4.93 ppm (2H, d, Cp), 4.72 ppm (4H, t, Cp), 4.44 ppm (2H, d, Cp); Elemental analysis calculated for FeCdN₂O₂C₂₄H₁₈ (actual), see Table 4: 53.91% C (49.89% C); 3.39% H (3.79% H); 5.23% N (3.94% N); Molar absorptivity (DMSO): 390 nm ($7670 \text{ M}^{-1} \text{ cm}^{-1}$), 655 nm ($816 \text{ M}^{-1} \text{ cm}^{-1}$); MS: free ligand present; see Appendix (Figures A.51-53) for spectra.

Synthesis of FcO2-Hg: (17)

To a dried, N₂ flushed Schlenk flask containing a stir bar, 160 mg of **10** (3.77×10^{-4} mol), 120 mg of Hg(CH₃COO)₂·H₂O (3.76×10^{-4} mol), 40 mL of ethanol and 3 mL of NH₄OH were added. The solution was allowed to reflux overnight, cooled, filtered through a frit, washed with cold ethanol and the precipitate was dried under a vacuum. Amount recovered: 90 mg of deep red powder (80 mg, 1.28×10^{-4} mol, 34.1% yield, after

correcting for starting material impurities, Table 3), mp >300 °C; ^1H NMR (CDCl_3): 4.90 ppm (4H, s, Cp), 4.68 ppm (4H, s, Cp), very broad 5.0-4.0 ppm; ^1H NMR (d_6 -DMSO): 8.0-6.0 ppm (H, m, phenyl), 4.9-4.7 ppm (H, s, Cp), 4.34 ppm (H, s, Cp); Elemental analysis calculated for $\text{FeHgN}_2\text{O}_2\text{C}_{24}\text{H}_{18}$ (actual), see Table 4: 46.28% C (42.82% C); 2.93% H (2.93% H); 4.50% N (3.62% N); Molar absorptivity (DMSO): 412 nm (2440 $\text{M}^{-1}\text{cm}^{-1}$); MS: mercury complex not observed; see Appendix (Figures A.54-56) for spectra.

Synthesis of **FcO2-Pb**: (18)

To a dried, N_2 flushed Schlenk flask containing a stir bar, 190 mg of **10** (4.48×10^{-4} mol), 170 mg of $\text{Pb}(\text{CH}_3\text{COO})_2 \cdot 3\text{H}_2\text{O}$ (6.11×10^{-4} mol), and 70 mL of ethanol were added. The solution was allowed to reflux for one hour (became metallic orange), cooled, filtered through a frit, washed with cold ethanol and the precipitate was dried under a vacuum. Amount recovered: 200 mg of copper-orange powder (192 mg, 3.05×10^{-4} mol, 68.0% yield, after correcting for starting material impurities, Table 3), decomposed at 250 °C; ^1H NMR (CDCl_3 , Figure 3.5): 8.5 ppm (2H, d, Cp- $\text{CH}=\text{N}$), 7.6 ppm (2H, d, phenyl), 7.4 ppm (2H, m, phenyl), 7.0 ppm (2H, broad s, phenyl), 6.8 ppm (2H, s, phenyl), 4.82 ppm (4H, s, Cp), 4.58 ppm (4H, s, Cp); ^1H NMR (d_6 -DMSO, Fig. 3.6): 8.54 ppm (2H, s, Cp- $\text{CH}=\text{N}$), 6.98 ppm (2H, d, phenyl), 6.87 ppm (2H, d, phenyl), 6.55 ppm (2H, d, phenyl), 6.28 ppm (2H, d, phenyl), 5.01 ppm (4H, d, Cp), 4.67 ppm (4H, d, Cp); Elemental analysis calculated for $\text{FePbN}_2\text{O}_2\text{C}_{24}\text{H}_{18}$ (actual), see Table 4: 45.79% C (44.48% C); 2.88% H (3.15% H); 4.45% N (4.14% N); Molar absorptivity (DMSO, Fig. 3.9): 438 nm ($16300 \text{ M}^{-1}\text{cm}^{-1}$); MS: lead complex not observed, CV data (Fig. 3.11); see Appendix (Figures 57-59) for spectra.

New Substituted FcOH1 and FcOH2 Ligands:

Two unreported ferrocene ligand systems were derived from the FcOH1 and FcOH2 systems as a means to improve solubility in aliphatic solvents. Both formed air stable ligands. Unfortunately, the products that were formed were oils that would bubble upon vacuum drying to form a glass-like solid. This solid was used for metal reactions with $M(PPh_3)_2$ precursors, but failed to form precipitates due to the increased solubility in the solvent used. An X-ray crystal structure was obtained with the FcOH2 (4-*t*-butyl) ligand, but was unfortunately of low quality and did not refine well due to disordered solvent molecules within the crystal matrix.

Synthesis of FcOH1(4-*t*-butyl) ligand: (19)

To a dried, N_2 flushed 250 mL side arm round bottom flask containing a stir bar, 600 mg of 1-formylferrocene (2.80×10^{-3} mol), 410 mg of 4-*t*-butyl,2-aminophenol (2.75×10^{-3} mol) and 100 mL of benzene were added. The solution was refluxed for three hours (color darkened) and then the majority of the benzene was removed via a modified Dean-Stark apparatus. Upon cooling, the deep red solution was filtered, washed and dried to recover product. Amount recovered: 870 mg (89.9 % yield); 1H NMR ($CDCl_3$): 8.59 ppm (s, 1H, Cp-CH=N), 7.37 (s, 1H, Phenyl), 7.23 (s, 2H, Phenyl), 7.20 (s, 1H, Phenyl), 6.93 (d, 1H, OH), 4.83 (s, 2H, Cp), 4.53 (s, 2H Cp), 4.27 (s, 5H, Cp unsubstituted), 1.37 (s, 9H, *t*-butyl Hs); 91-92°C; see appendix (Figures A.60-61) for spectra.

Synthesis of FcOH2(4-*t*-butyl) ligand: (20)

To a dried, N₂ flushed 250 mL side arm round bottom flask containing a stir bar, 600 mg of 1,1'-diformylferrocene (2.48×10^{-3} mol), 800 mg of 4-*t*-butyl,2-aminophenol (5.36×10^{-3} mol) and 100 mL of benzene were added together. The solution was allowed to undergo reflux for three hours (color darkened) and then the majority of the benzene was removed via a modified Dean-Stark apparatus. Upon cooling, the deep red solution was filtered, washed with more benzene and dried to recover a red oil that formed a glass-like solid upon vacuum drying overnight. Amount recovered: 1.20 g (96.0 % yield); ¹H NMR (CDCl₃): 8.50 (s, 2H, CpCH=N), 7.38 (s, 4H, Phenyl), 7.19 (m, 2H, Phenyl), 6.99 (s, 2H, Phenyl), 6.89 (d, 2H, OH), 4.74 (s, 4H, Cp), 4.58 (s, 4H, Cp), 1.33 (s, 18H, *t*-butyl Hs); mp 101-104°C; see Appendix (Figures A.62-63) for spectra.

Table 3: Melting Points, Colors and Percent Yields of the FcOH₂ ligand and metal complex reactions

Compound #	Formula	Color	Melting Point	Percent Yield of Reaction
10	FeN ₂ O ₂ C ₂₄ H ₂₀	deep red	172-174 °C	60.1 %
11	Fe ₂ N ₂ O ₂ C ₂₄ H ₁₈	deep red-black	>300 °C	45.6 %
12	FeCoN ₂ O ₂ C ₂₄ H ₁₈	deep red-black	>300 °C	37.8 %
13	FeNiN ₂ O ₂ C ₂₄ H ₁₈	deep brown-red	>300 °C	8.5 %
14	FeCuN ₂ O ₂ C ₂₄ H ₁₈	deep red	>300 °C	43.5 %
15	FeZnN ₂ O ₂ C ₂₄ H ₁₈	deep red-black	>300 °C	22.0 %
16	FeCdN ₂ O ₂ C ₂₄ H ₁₈	deep red-orange	>300 °C	17.7 %
17	FeHgN ₂ O ₂ C ₂₄ H ₁₈	deep red	>300 °C	34.1 %
18	FePbN ₂ O ₂ C ₂₄ H ₁₈	copper-orange	decomp. 250 °C	68.0 %
19	FeNOC ₂₁ H ₂₃	deep red tar	91-92 °C	89.9 %
20	FeN ₂ O ₂ C ₃₂ H ₃₆	deep red tar	101-104 °C	96.0 %

Table 4: Elemental Analysis of the FcOH₂ systems.

Compound #	Calc. C%	Actual C%	Calc. H%	Actual H%	Calc. N%	Actual N%	%I
10	67.94	67.81	4.75	5.07	6.60	6.63	
11	60.29	55.69	3.79	3.86	5.86	5.15	10.95
12	59.91	49.36	3.77	4.00	5.82	7.31	14.84
13	59.94	51.59	3.77	4.15	5.82	3.74	20.55
14	59.34	52.25	3.73	3.69	5.77	6.50	7.07
15	59.11	41.45	3.72	3.17	5.74	2.51	47.37
16	53.91	49.89	3.39	3.79	5.23	3.94	11.08
17	46.28	42.82	2.93	2.93	4.50	3.62	11.34
18	45.79	44.48	2.88	3.15	4.45	4.14	4.05

The last column in the preceding table (Table 4) corresponds to percentage of starting materials present in measured sample complex. These were calculated by matching the actual elemental analysis values with ones calculated for complexes with certain amounts of impurities present. For each metal complex listed in the experimental section, the percent yield was adjusted based upon the amount of impurities present by finding the actual amount of pure complex that was recovered from the product precipitate. The metal acetate hydrates can be removed via through extraction with methanol.

Results and Discussion:

FcOH₂ was formed by Schiff base addition of 2-aminophenol to 1,1'-diformylferrocene in benzene via a modified Dean-Stark apparatus (as was done with Fc₂). The formation of FcOH₂ precipitate upon cooling to room temperature is markedly different from the Fc₂ ligand, which is highly soluble in benzene. Dark reddish powder of FcOH₂ was recovered with a frit and washed with cold ethyl ether before vacuum drying. The mother liquor was further reduced in volume to obtain another crop of product.

The reactions to form the metal complexes with the FcOH2 ligand were similar to the Fc2 reactions, except for the addition of a small amount (1-2 mL) of conc. base (NH₄OH) to help catalyze the reaction. Without added base, either no product formed or very poor yields were obtained (with one exception, FcO2-Pb). The base is needed to help in the abstraction of the phenolic proton. Accidentally, base addition was not done on the Pb²⁺ reaction and it progressed rapidly to form FcO2-Pb (reaction was done in a few minutes rather than hours compared to the other metals). This result gave the potential that the FcOH2 ligand might be selective for Pb²⁺ if no base was present in the solution.

X-ray Crystal Structure:

Crystals of FcOH2 (Table 5) were obtained through evaporation of CDCl₃ overnight. The FcO2-M complexes did not form crystals in this manner, nor any other method that was tried due to starting material impurities. The FcOH2 system forms metal complexes that typically are less defined in the ¹H NMR measurements than the FcS2-M system that will soon be discussed.

Table 5: Crystal Structure of the FcOH2 ligand

<i>Crystal data</i>	
C ₂₄ H ₂₀ FeN ₂ O ₂	$D_x = 1.458 \text{ Mg m}^{-3}$
$M_r = 424.27$	Melting point: 445-447 K
Monoclinic, C2/c	Mo $K\alpha$ radiation
	$\lambda = 0.71073 \text{ \AA}$
	Cell parameters from 1908 reflections
$a = 16.6115 (13) \text{ \AA}$	$\theta = 2.6\text{--}27.0^\circ$
$b = 9.2151 (7) \text{ \AA}$	$\mu = 0.80 \text{ mm}^{-1}$
$c = 14.1716 (11) \text{ \AA}$	$T = 173 (2) \text{ K}$
$\beta = 117.017 (2)^\circ$	
$V = 1932.6 (3) \text{ \AA}^3$	Prism, red
$Z = 4$	$0.25 \times 0.25 \times 0.15 \text{ mm}$
$F_{000} = 880$	

Data collection

Bruker SMART CCD area detector
diffractometer

3887 measured reflections

Radiation source: Mo $\text{K}\alpha$

1935 independent reflections

Monochromator: graphite

1597 reflections with $I > 2\sigma(I)$

$R_{\text{int}} = 0.021$

$T = 173(2)$ K

$\theta_{\text{max}} = 27.1^\circ$

$P = ?$ kPa

$\theta_{\text{min}} = 2.6^\circ$

ω scans

$-18 \leq h \leq 20$

Absorption correction: multi-scan

Data were corrected for decay and absorption using
the program SADABS (Sheldrick, G. M. (2003).
SADABS. Version 2.10. University of Göttingen,
Germany).

$-11 \leq k \leq 8$

$T_{\text{min}} = 0.55$, $T_{\text{max}} = 0.89$

$-18 \leq l \leq 11$

Refinement

Refinement on F^2

Secondary atom site location: difference Fourier map

Least-squares matrix: full

Hydrogen site location: inferred from neighbouring
sites

$R[F^2 > 2\sigma(F^2)] = 0.037$

H-atom parameters not refined

$wR(F^2) = 0.098$

$w = 1/[\sigma^2(F_o^2) + (0.0487P)^2 + 1.4759P]$
where $P = (F_o^2 + 2F_c^2)/3$

$S = 1.06$

$(\Delta/\sigma)_{\text{max}} < 0.001$

1935 reflections

$\Delta\rho_{\text{max}} = 0.51 \text{ e}\text{\AA}^{-3}$

133 parameters

$\Delta\rho_{\text{min}} = -0.30 \text{ e}\text{\AA}^{-3}$

Extinction correction: none

Primary atom site location: structure-invariant direct
methods

Color code for the FcOH2 crystal structure:

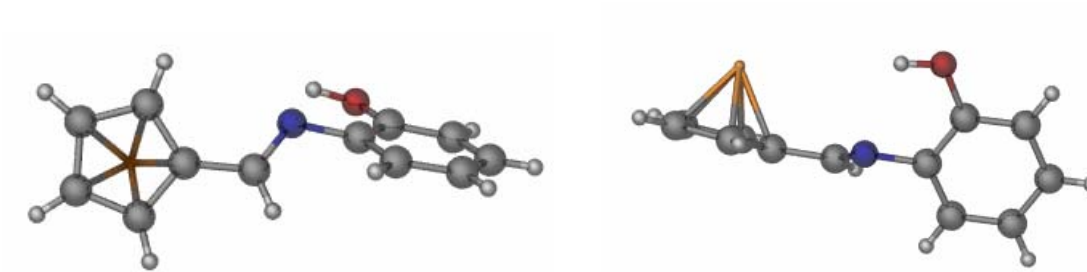
Orange (small): Fe atom

Dark grey: C atom

Light grey (small): H atom

Dark Blue: N atom

Red: Oxygen atom

Asymmetric unit structure:

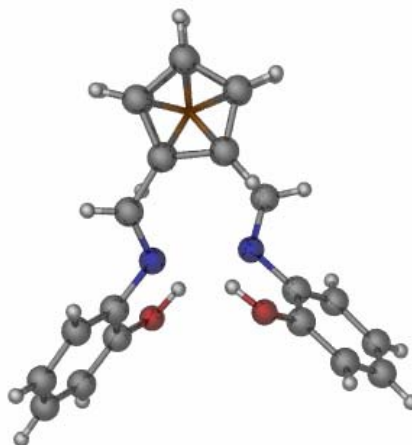
The asymmetric unit cell for the FcOH₂ complex is one half of the complex, with the Fe^{II} sitting upon a rotation axis.

Bond Lengths:

Cp C1-C2: 1.43(9) Å	Cp C2-C3: 1.41(1) Å	Cp C3-C4: 1.41(5) Å	Cp C4-C5: 1.42(1) Å
C1-C5: 1.42(4) Å	C1-C6: 1.45(3) Å	C6=N1: 1.27(9) Å	N1-C7: 1.42(5) Å
C7-C8: 1.40(4) Å	C8-C9: 1.38(3) Å	C9-C10: 1.39(4) Å	C10-C11: 1.37(8) Å
C11-C12: 1.38(8) Å	C7-C12: 1.39(1) Å	C8-O1: 1.36(4) Å	H1...H2: 2.42(2) Å

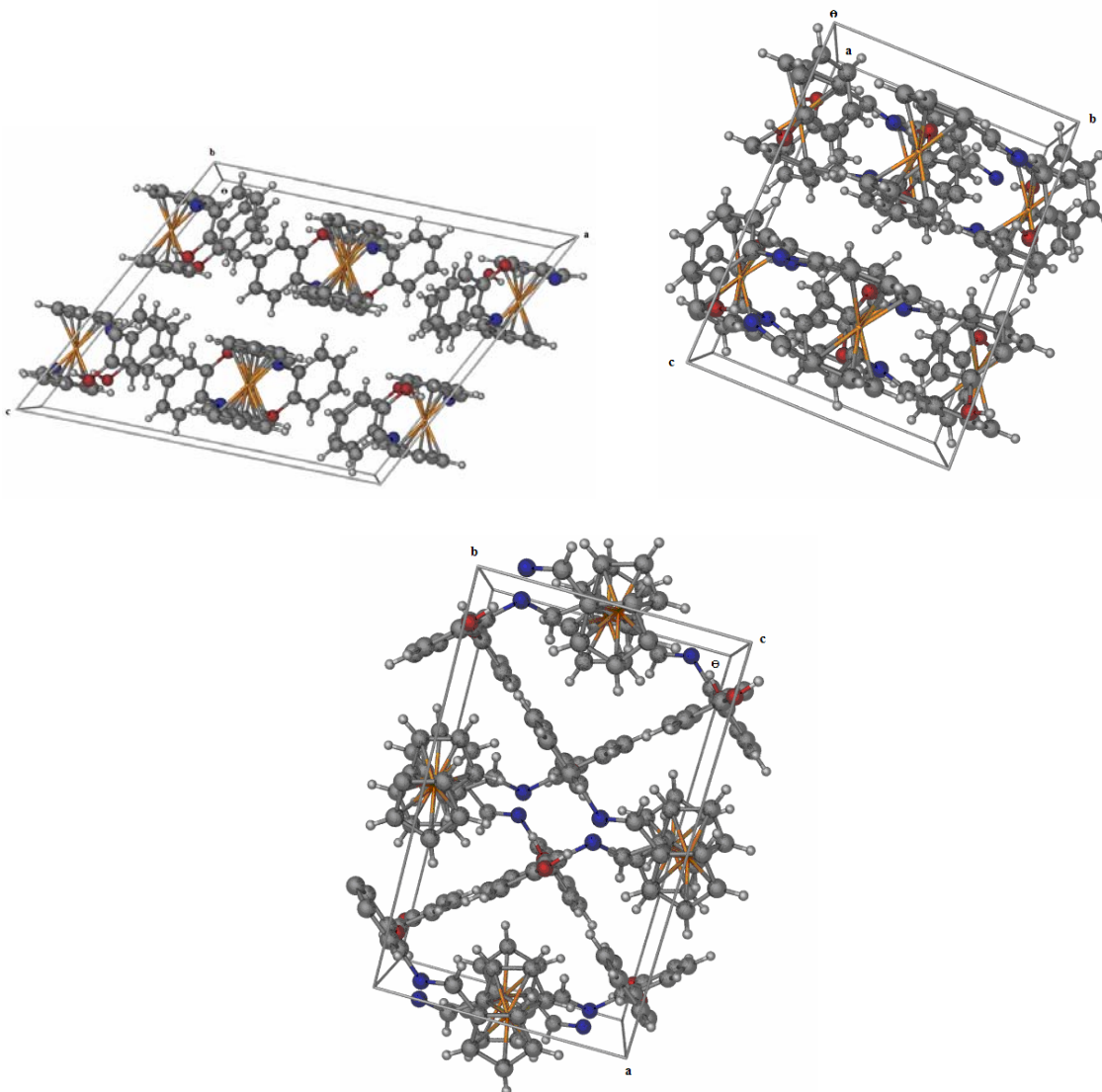
Bond Angles:

C1-C6=N1: 123.6(5)^o C6=N1-C7: 117.5(0)^o N1-C7-C8: 117.6(4)^o C7-C8-O1: 122.1(5)^o
 C8-O1-H: 114.3(7)^o

Cp ring overlap:

The Cp rings are completely eclipsed in the FcOH_2 crystal structure. This may be due to the substitution group upon each Cp ring being sterically hindered if they are placed parallel to each other.

Unit cell:

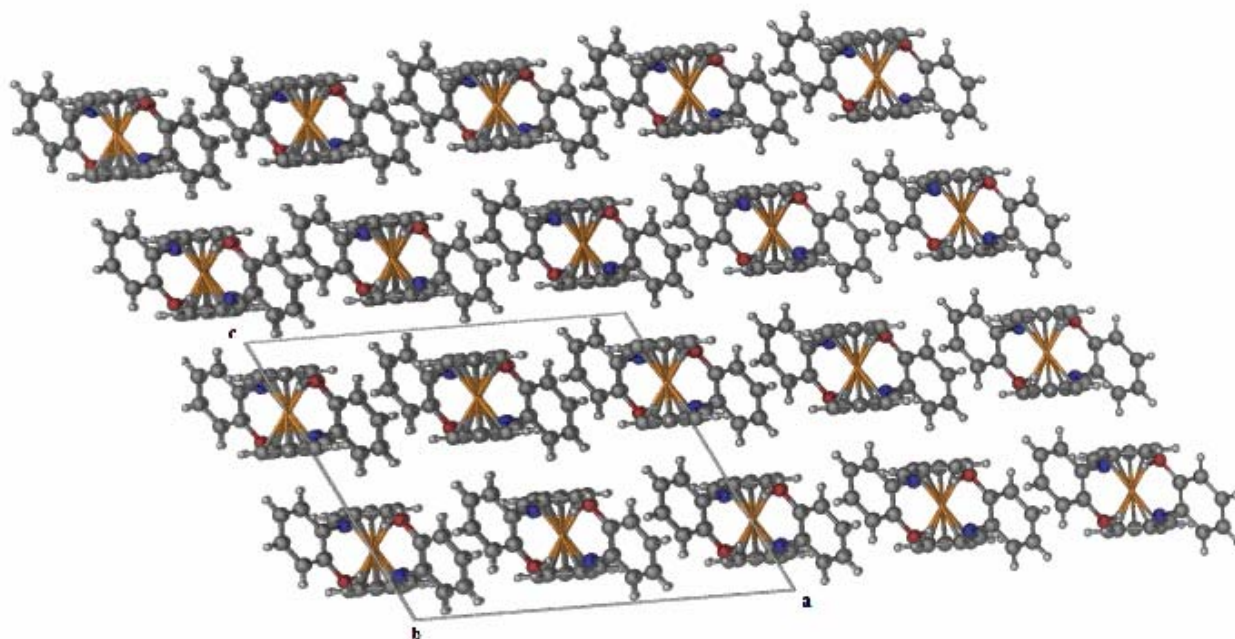


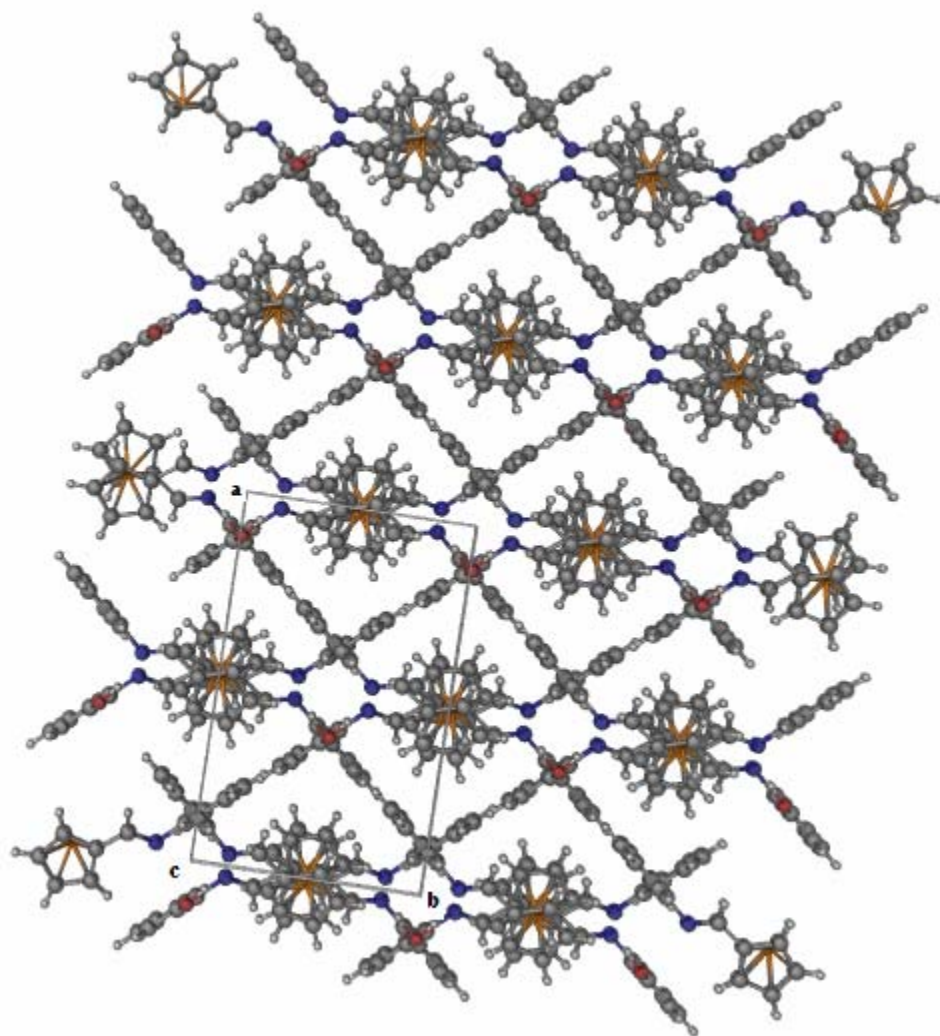
Crystal packing in three directions:

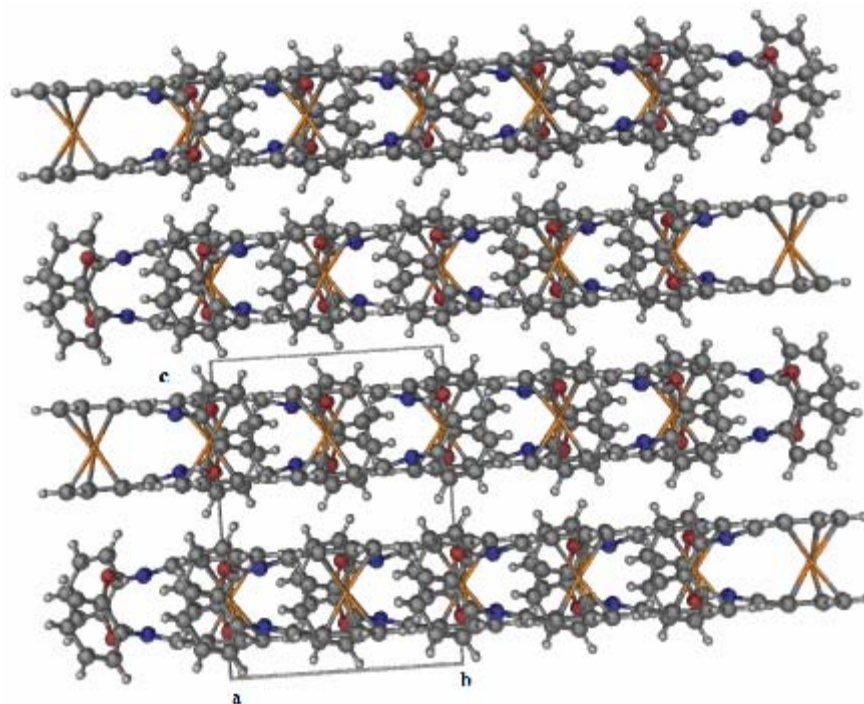
1: Θ along a

2: Θ along b

3: Θ along c







Discussion of the FcOH2 crystal structure:

The FcOH2 ligand forms dark reddish crystals that crystallize in the monoclinic space group C2/c. The FcOH1 ligand crystallizes from slow evaporation of benzene in the same configuration according to the literature.¹²⁷ The asymmetric unit is one half of the molecule, since the Fe²⁺ atom lies on a 2-fold rotation axis, so the Cp rings are completely eclipsed. No evidence of ring closing tautomerization has occurred for this compound. The molecules pack in with the phenyl rings stacking on top of each other, creating layers in one direction, while the functional groups form a network in the other direction. No free space for further packing of other materials is evident in this crystal system. The molecular units pack in a layering orientation (see unit cell), whereby each layer is staggered in respect to each other. There are two layers present within each unit cell.

Melting point, MS, ¹H NMR, Magnetic Susceptibility:

The melting point for **10** is almost 90 °C higher (Tables 1 and 3) than compound **1** due to the aryl alkoxide groups hydrogen bonding between molecules. Since all metal complexes for this ligand system (with the exception of **18**) do not melt below 300 °C, identification by melting point of the product formed during the selectivity experiments would only be useful in identifying the presence of **18**. It cannot be used to determine any of the other seven complexes that may be present.

The MS data for **10** show the M+1 peak at 424.88. The metal complexes of this system did not show M+1 peaks. Free ligand M+1 peaks commonly occurred in the MS data, indicating that the metal cations were removed from the complex before they could be detected, thus implying that impurities were present. This is unusual behavior as most reported Schiff-base ferrocene compounds have M+1 peaks when measured. Identification by MS of any selectivity products for this ligand system would not be fruitful.

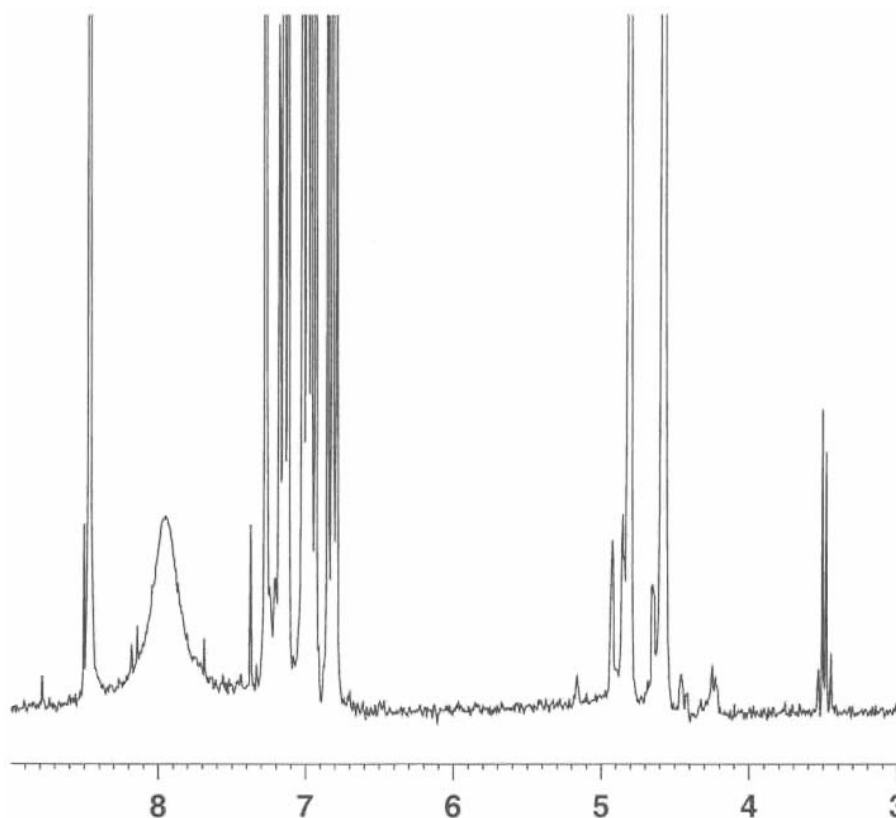


Fig. 3.4 ^1H NMR spectrum of FcOH2 ligand in CDCl_3 (CHCl_3 solvent peak at 7.27 ppm), with the broad peak between 8.3-7.7 ppm corresponding to the alcoholic proton. (1:1:1:2:1:2:2 H equivalency)

The ^1H NMR of compound **10** (Figure 3.4) shows a Cp- $\text{CH}=\text{N-R}$ proton chemical shift further downfield than in **1**. The hydroxyl proton is nearby in the 9-8 ppm range. This broad peak disappears upon metal complexation, as it becomes extracted to the side product acetic acid. The phenyl protons of **10** have peaks in the 7.2-6.5 ppm range, slightly shifted downfield in comparison to **1**. The two Cp peaks show up in the 4.9-4.5 ppm range, which is very similar to **1**. Measurements taken in CDCl_3 of **11-18** were less telling than ones taken in d_6 -DMSO due to lack of clearly defined peaks (see Figures 3.5-6 for examples). Many of the spectra in either solvent gave peak patterns that were difficult to assign. Based upon the differences seen in the d_6 -DMSO spectra of **11-18** (Figure 3.8), it can be used as an identification technique for any selectivity products that

might form from this system. The location of the methylene peak (Cp-CH=N-R) varies depending upon the resulting metals contained within the complex.

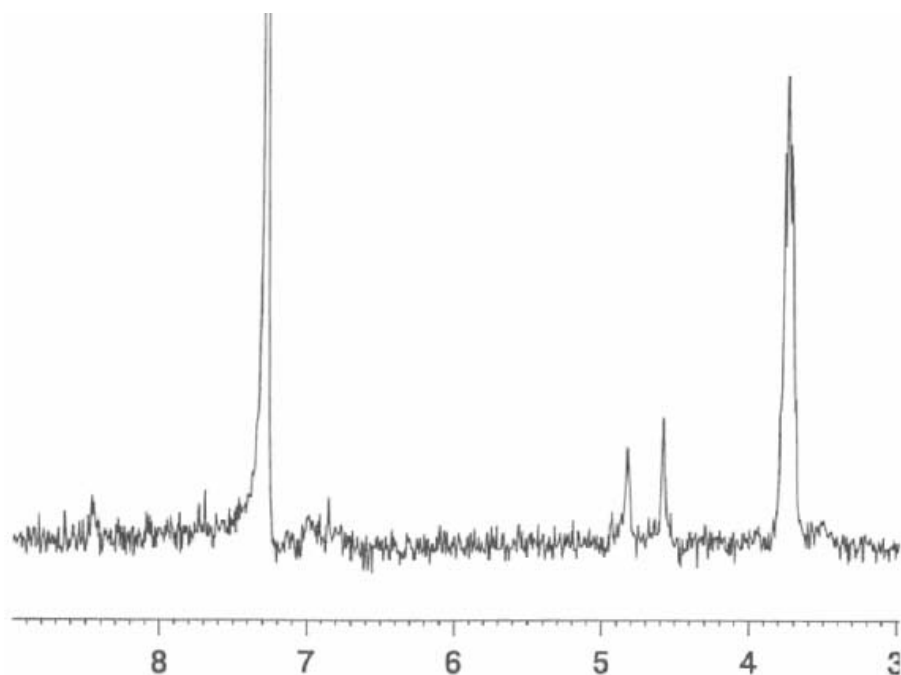


Figure 3.5: ^1H NMR spectrum of $\text{FcO}_2\text{-Pb}$ in CDCl_3 . Peaks between 5-4.5 ppm belong to the Cp ring protons (2 eq. H each), while the peak at 8.5 ppm (1 eq. H) indicates the presence of Cp-CH=N-R . (1:2:2 H equivalency, phenyl peaks hard to resolve)

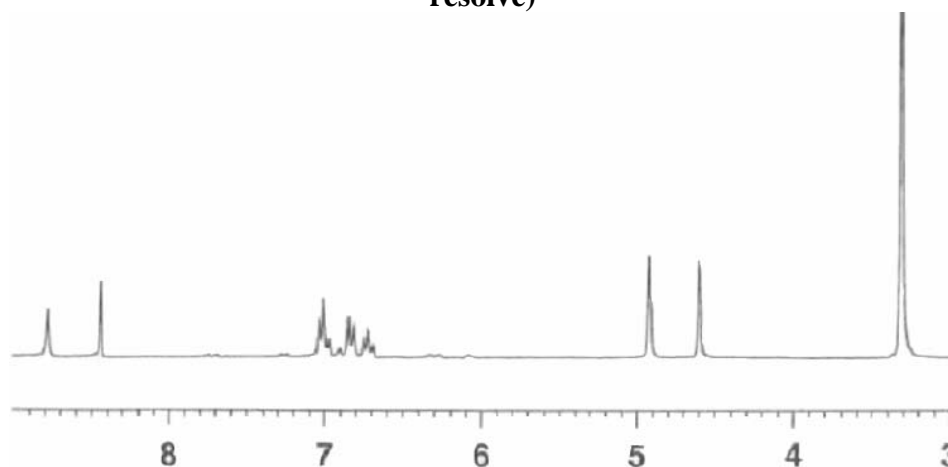


Figure 3.6: ^1H NMR spectrum of $\text{FcO}_2\text{-Pb}$ in $d_6\text{-DMSO}$. The peak at 8.6 ppm belongs to the Cp-CH=N-R protons, peaks between 7-6 ppm correspond to the phenyl protons, while the large peaks at 5-4.5 ppm are due to Cp protons. (1:1:2:1:1:2:2 H equivalency)

^1H NMR spectral peak location comparisons (Figures 3.7-8) are listed below.

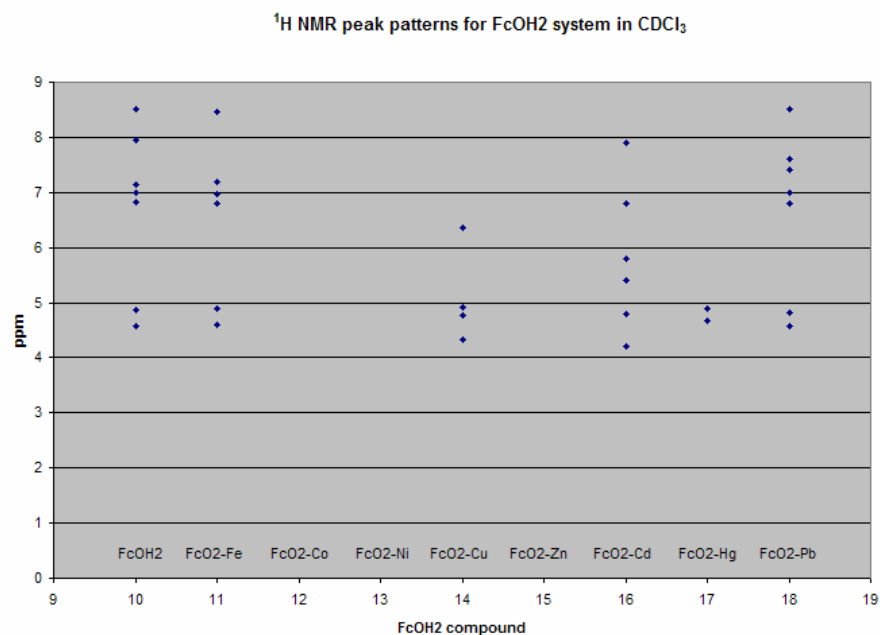


Figure 3.7: The ^1H NMR peak locations for the FcOH2 system in CDCl_3 , spectra for complexes 12, 13 and 15 did not give characterizable peaks.

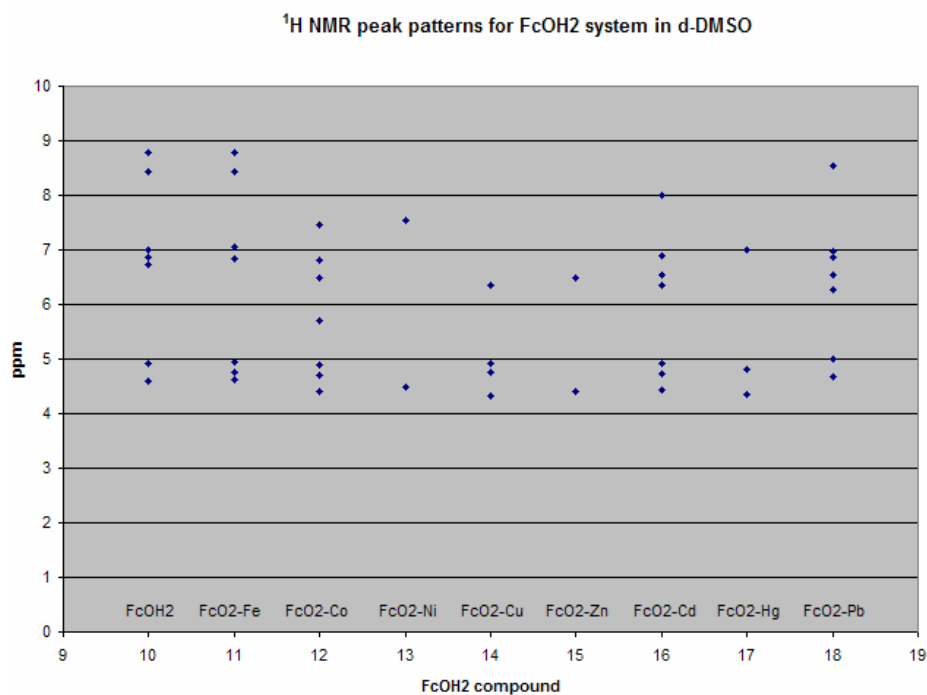


Figure 3.8: The ^1H NMR peak locations for the FcOH2 system in $\text{d}_6\text{-DMSO}$, spectra for complexes 13, 15 and 17 gave only a few recognizable peaks.

Magnetic susceptibility of **10** indicates that there are no unpaired electrons within the free ligand, which is to be expected based upon the molecular structure. All FcO₂-M complexes contained M(CH₃COO)₂ impurities that affected their calculated magnetic susceptibilities. Accurate measurements could not be taken of **13** and **16** due to the small amounts recovered during their synthesis. The metal complexes are for the most part diamagnetic, although **11** (FcS₂-Fe) and **12** (FcS₂-Co) tend to have larger calculated magnetic susceptibility values which would indicate more paramagnetic character within the complexes. This is indicative of metal centers with octahedral geometry, rather than tetrahedral, based on the number of unpaired electrons present.

Discussion of complexes 19 and 20:

The complexes **19** and **20** were synthesized to determine the differences in solubility versus ligand systems that did not contain *t*-butyl groups in the para position on the phenyl ring. They are soluble in aliphatic solvents, but the non *t*-butyl forms are not. Both ligands formed oils that upon drying under vacuum form a glass-like solid. After many attempts with different techniques, no single crystals could be formed of **19**. Although diffraction data was collected on **20**, much disorder was noticed in the lattice that prevented a good structure from being resolved. Neither form undergoes ring closing tautomerization based upon the ¹H NMR data for each ligand. Metal complexation studies were planned for these ligands, but time constraints prevented the testing of said materials.

Colorimetric (IR, UV-Vis.):

The IR spectra for **10-18** contain the 1643 cm^{-1} imine stretch and the 890 cm^{-1} ferrocene Cp as almost identical patterns, which is not useful in determining mixtures of complexes. Since **10-18** all show the same peaks, IR spectroscopy is not a preferred identification technique for future selectivity experiments with this particular ligand system.

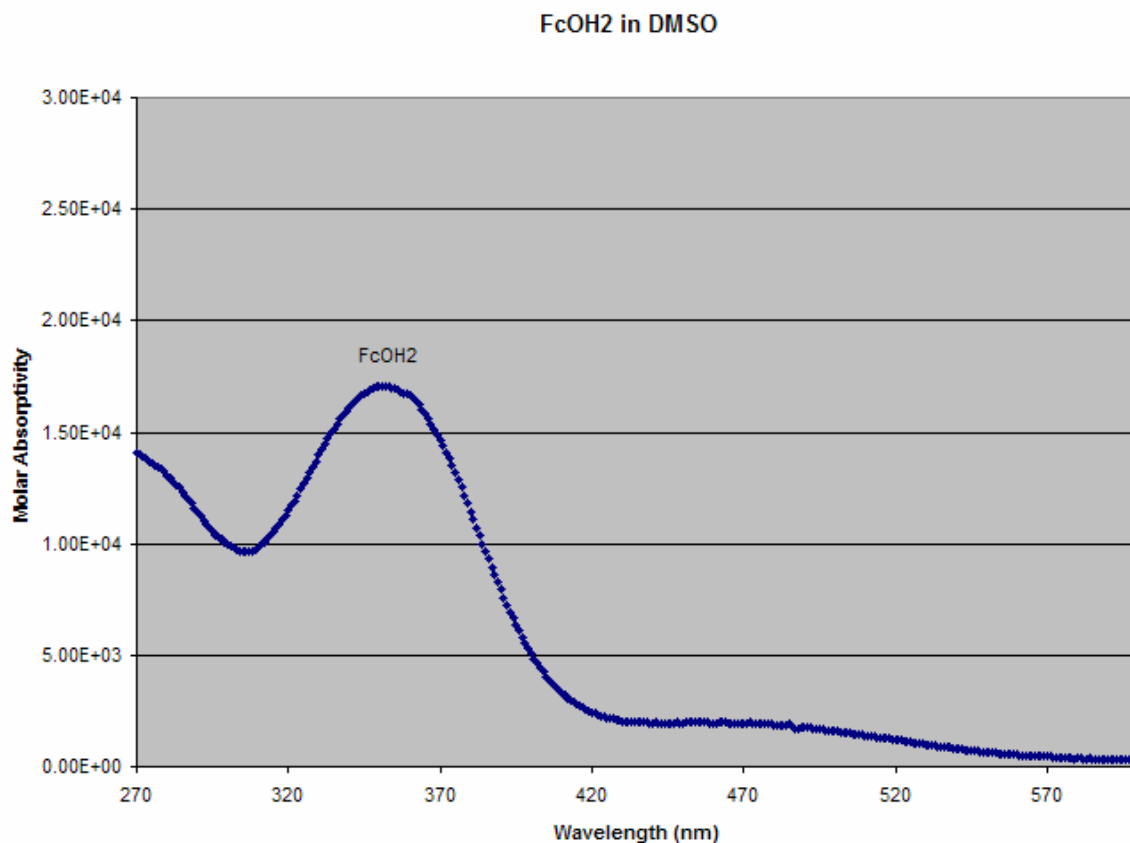


Figure 3.9: Molar absorptivity (UV-Vis) of FcOH2 ligand in DMSO. The bands at 463 and 351 nm correspond to d-d and d-ligand transitions.

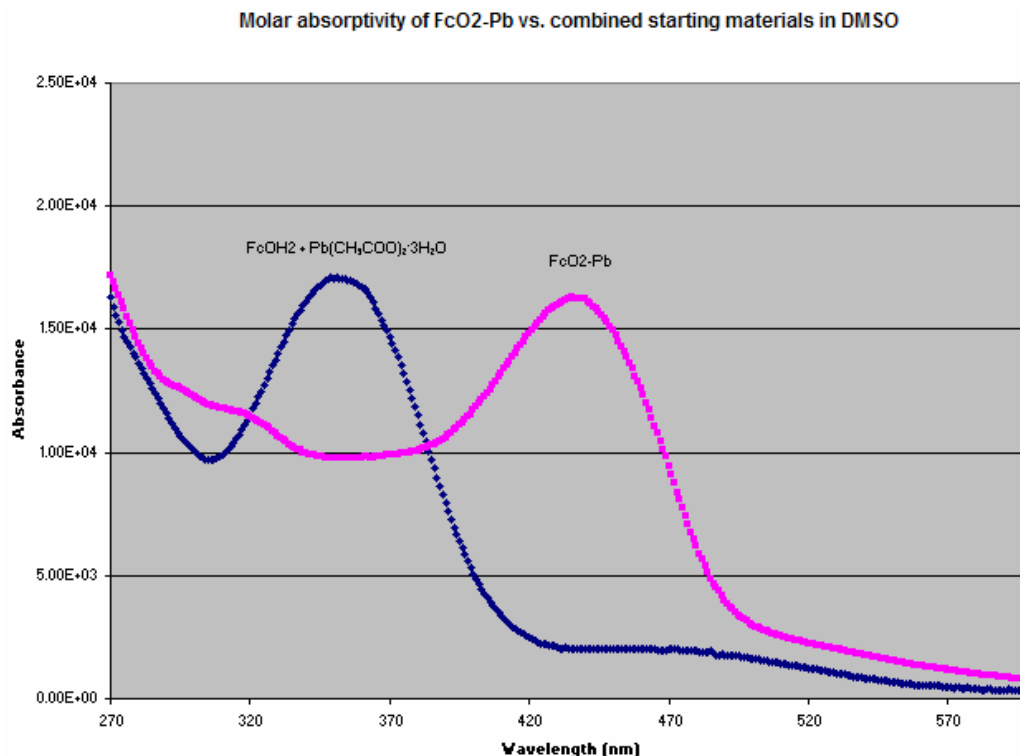


Figure 3.10: Comparison between the molar absorptivity (UV-Vis) of FcO₂-Pb and the molar absorptivity of the combined starting materials in DMSO (peak red shifted from 351 to 438 nm).

The UV-Vis spectrum for **10** shows two primary peaks in the visible range, 351 nm and 463 nm due to both d-d and d-ligand transitions (Figure 3.9). Many of the metal complexes of this system do not have defined peaks corresponding to the FcOH₂ ligand peak at 351 nm. The transition metal acetates used to produce the FcO₂-M complexes are colored, but the heavy metal acetates are not (full d e⁻ shells). The molar absorptivity of compound **11** becomes greater (hyperchromic shift) than the starting materials at longer wavelengths, while the lower energy peak is not defined. **12** is less intense on the first peak (high energy, much smaller and blue shifted to 334 nm), but the intensity becomes more than the starting materials on the blue shifted (hypsochromic shift) second

peak. The molar absorptivity of **13** is less intense (hypochromic shift) than the combined starting materials but with no first peak present, it gains in intensity above the starting materials on the second peak. The spectra of compounds **14**, **15** and **17** are almost identical to the spectrum of **13**, so this method would not be useful in identifying these in a mixture. **16** has a molar absorptivity that is initially less intense but it gains intensity over the blue-shifted (390 nm) peak then shortly decays into equal intensity when compared to the starting materials. The molar absorptivity of compound **18** is much different from the other metal complexes for this ligand system. It has the first peak of high energy red shifted (bathochromic shift) from 351 nm to 438 nm in equal intensity, while the second peak is much more broadened and lower in intensity, almost matching in intensity of the starting material (Figure 3.10). Due to it having a strong signal red shifted first peak, this can be used as a potential identification for the presence of **18** in a product formed in a selectivity experiment with the FcOH₂ ligand. This is of great potential use as this ligand has been sought as a potential Pb²⁺ sensor. Even though the other metals would not be easily identifiable, UV-Vis could still be used in conjunction with other spectroscopic methods to determine the selectivity towards Pb²⁺. If the selectivity product can be shown to contain no other metals than Pb²⁺ (and the Fe²⁺ from the ligand) through X-ray fluorescence, then the UV-Vis spectrum should match that of complex **18**.

Electrochemistry:

Compound **10** has a $\text{Fe}^{\text{II}}\text{-Fe}^{\text{III}}$ oxidation at 716 mV (vs. 0.01 M Ag/AgNO₃) in 1×10^{-3} M TBAHF/ DMSO solution (Figure 3.11), appearing as a rather distinct peak in the CV spectra when compared to the other two ligands. The iron couple is at a more positive potential than ferrocene at 388 mV because of the strong electronegative aryl alkoxide groups disturbing the electron delocalization in the ligand backbone. Metal complexes formed from **10** have a varied electrochemistry. Compounds **11**, **13**, **14**, **15** and **17** do not show a $\text{Fe}^{\text{II}}\text{-Fe}^{\text{III}}$ coupling peak with a positive potential due to the presence of starting material impurities. Compound **12** has a peak at 752 mV, **16** has a peak at 701 mV and **18** has a very small peak occurring at 646 mV (Figure 3.12). The electrochemistry of the compound changes upon ligand chelation to a transition or heavy metal cation because the electron density around the iron center in the ferrocene unit becomes perturbed, which affects the oxidation potential of the Fe^{II} center. Based upon the fact that only some of the complexes show ferrocene oxidation in DMSO and the primary target metal complex for the selectivity of this ligand is Pb^{2+} , CV would not be a preferred method for identification. It could be used as a backup test if **12**, **16** and/or **18** have been detected within the selectivity product.

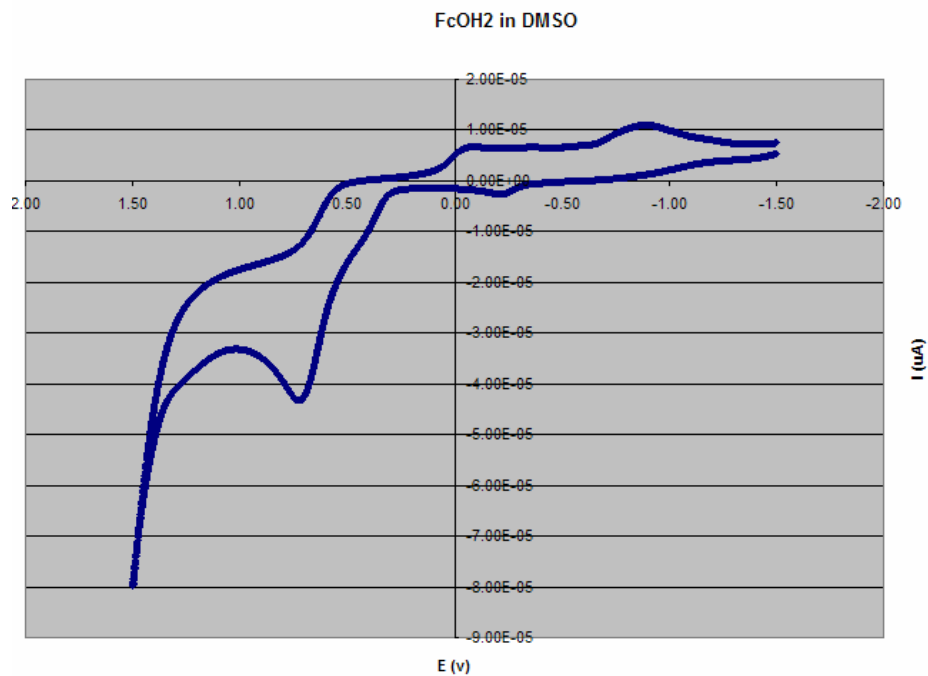


Figure 3.11: CV of FcOH2 ligand in DMSO, scan rate 100 mV/sec. The peak at 716 mV corresponds to the Fe^{II} to Fe^{III} oxidation.

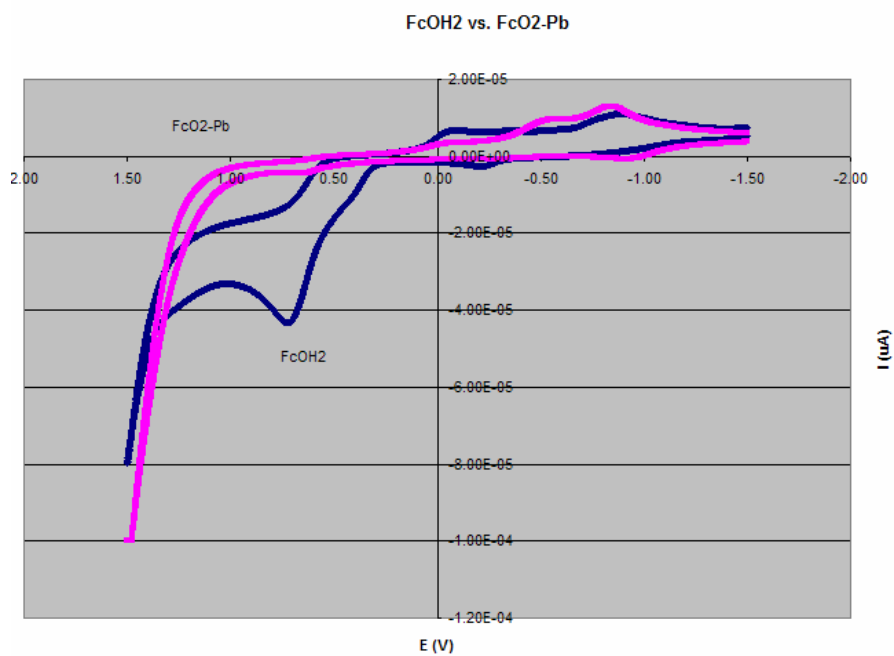


Figure 3.12: Comparison between the CV of FcO2-Pb and the CV of FcOH2 in DMSO, scan rate 100 mV/sec. The peak for FcO2-Pb is shifted to 646 mV for the oxidation of Fe^{II} to Fe^{III}.

Conclusion for the FcOH₂ system:

The incorporation of strongly electronegative OH groups para to the phenyl rings in Fc₂ greatly changes the possibility for cationic sensing as it forms the FcOH₂ ligand system. In this case, Pb²⁺ is the intended target species for detection. Some techniques cannot be used to determine the complex identity. IR does not differentiate between metal complexes and electrochemistry is only useful for the identification of three of the eight possible metal complexes. On the other hand, ¹H NMR can be used to sort out which product is formed, although with some difficulties due to the spectral peaks being broad. The best mode of selectivity product detection for this system is by using UV-Vis, as a very specific red shift that is fairly intense can be seen at 438 nm. No other metal complexes have peaks that have that level of intensity, so this is useful for identifying compound **18**, which just happens to be the target metal complex. UV-Vis spectroscopy will not determine the amount of other metal complexes that might have formed during a selectivity experiment, so other techniques such as ¹H NMR, X-ray fluorescence and possibly CV can be used to check for this.

The FcOH₂ ligand system might be an effective cationic sensor for Pb²⁺ based upon the possible multiple methods of detection that could be employed to analyze selectivity products. The highly electronegative OH groups will tend to form ionic bonds with metals and Pb²⁺ is known to form such bonds. Whether or not it can form exclusively compound **18** with other metal cations that are present will be explored later in chapter four.

¹²⁸ Lopez, C.; Bosque, R.; Perez, A.; Riog, A.; Molins, E.; Solans, X.; Font-Bardia, M., Relationships between Fe-57 NMR, Mossbauer parameters, electrochemical properties and the structures of ferrocenylketimines. *J. Organomet. Chem.* **2006**, 691, (3), 475-484.

¹²⁹ Perez, S.; Lopez, C.; Caubet, A.; Roig, A.; Molins, E., Ring-Chain Tautomerism of the Novel 2-Ferrocenyl-2,4-dihydro1H-3,1-benzoxazine. *J. Org. Chem.* **2005**, 70, (12), 4857-4860.

CHAPTER FOUR

The FcSH₂ Ligand System: soft donor

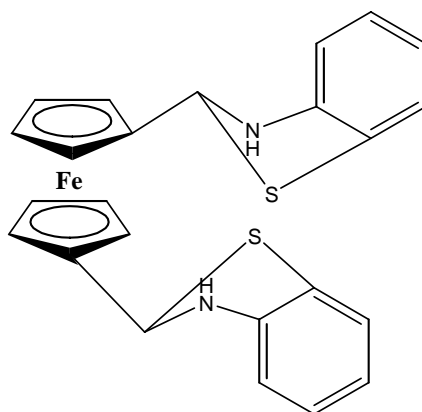


Figure 4.1: The FcSH₂ ligand (in DRCT form): FeN₂S₂C₂₄H₂₀

The third system, FcSH₂ (Figure 4.1), differs from the previous system by a pair of thiols replacing the alcohol groups. This system is rather unique in that it undergoes double ring closing tautomerization, DRCT (see Figure 4.2 for mechanism scheme)¹³⁰. The lone pair electrons on sulfur atoms on FcSH₂ donate to the carbon directly next to of the Cp ring, whereby the π -bond electrons in the imine bond shift to the nitrogen atom, along with the proton off of the sulfur atom to form the closed ring form on the right of the figure. The mono-substituted form¹³¹ undergoes ring closing tautomerization, RCT, whereby the lone pair on the sulfur donates to the carbon adjacent to the Cp, which shifts one pair of electrons over to the nitrogen, along with the proton off the sulfur. This can readily be seen in the IR spectrum of the solid, as only the N-H stretch is apparent (no S-H peak present).

The FcSH₂ system should have a preference for making strong bonds with heavy metals. This is due to the low Lewis acidity of Cd, Hg and Pb. Since the sulfur has a lower electronegativity value than oxygen, the bonding to the metal center in FcS₂-M

should be more covalent in nature than the same bonds in $\text{FcO}_2\text{-M}$, due to the smaller difference in electronegativity between the metals and the chelating groups. A hint on the potential selectivity for this ligand system can be seen in the reported monosubstituted version (FcSH1), as Hg^{2+} metal cations were able to replace other metal centers that were already chelated (such as Zn^{2+} and Pd^{2+})¹³². Mercury forms very strong covalent bonds with sulfur, so the FcSH2 ligand has a good chance of being selective for mercury in the presence of other competing cations. Whether or not it can be detected over other $\text{FcS}_2\text{-M}$ complexes was explored during this project and the results will be discussed later.

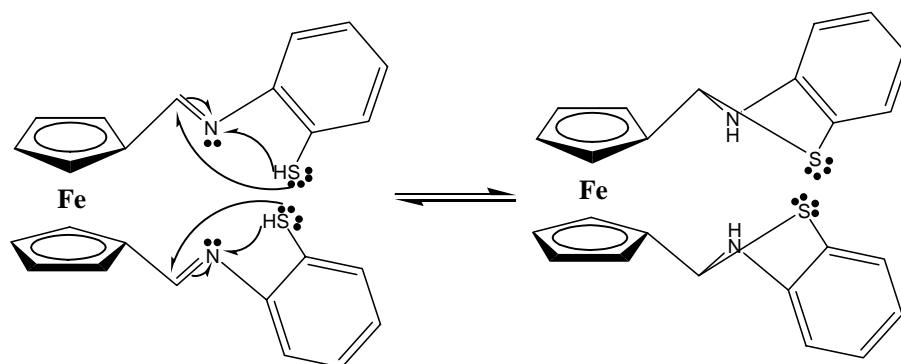
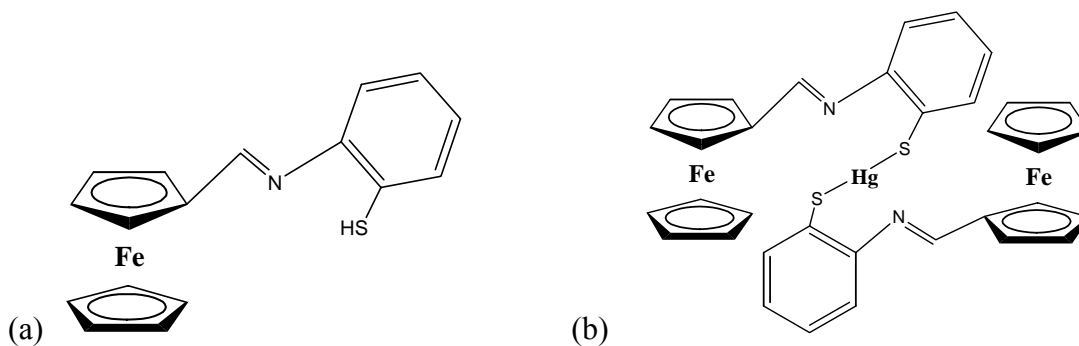


Figure 4.2: Scheme of DRCT of the FcSH_2 ligand.

The FcSH_2 ligand system has not been reported in the literature, but the monosubstituted derivative ligand (Figure 4.3a) has been reported with various divalent metals^{131,133,134,135}. FcSH1 metal products form compounds containing three metal centers, $(\text{FcS1})_2\text{-M}$ (Figure 4.3b) usually in the trans geometry, whereas FcSH_2 forms di-metal center compounds that are exclusively trans. While that may not seem like much of a difference, the metal cation is potentially held in a much more constrained geometry (usually tetrahedral) when compared to the $(\text{FcS1})_2\text{-M}$ products.



Figures 4.3 (a) and (b): (a) the structure of the FcSH1 ligand (fab)¹³¹ and (b) the structure of the [FcS₁]₂-Hg complex¹³¹

The FcSH2 ligand was formed via Schiff base addition of 2-aminothiophenol to 1,1'-diformylferrocene in an ethanolic solution. Upon stirring the heated solution, the color changes rapidly from dark red to a golden yellow, with pale yellow precipitate forming within 5 minutes of the addition. Upon cooling, the precipitate was filtered and washed with cold ethyl ether before vacuum drying to obtain the pale yellow product.

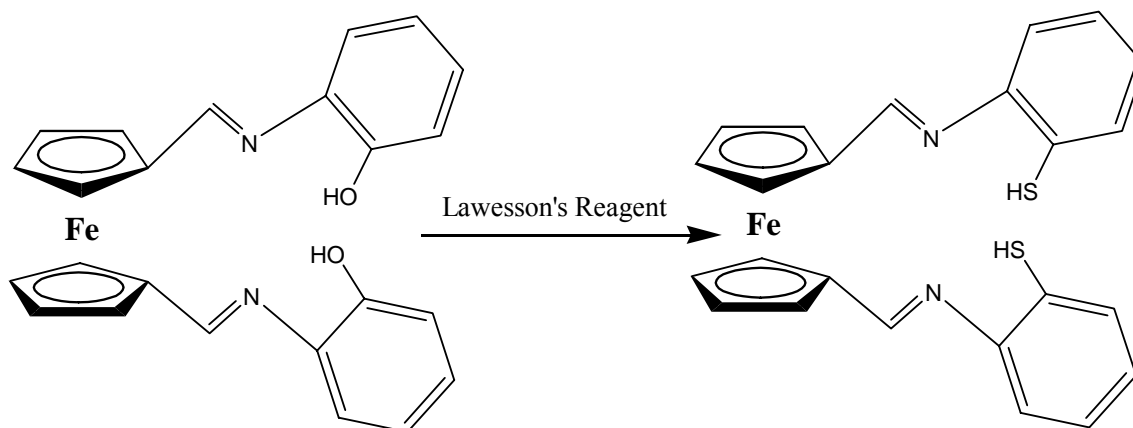


Figure 4.4: Proposed potential use of Lawessons Reagent in conversion of dialcohol to dithiol ligands, may have to convert to the aryl enolate form first, react with LR, and then reduce back to the thiol form.

There exists a possible route (Figure 4.4) to producing FcSH2 from the FcOH2 ligand through the use of Lawessons Reagent¹³⁶, whereby the alcoholic group becomes replaced by a thiol group, although this reaction has not been tested. Lawessons Reagent (2,4-

bis(4-methoxyphenyl)-1,3,2,4-dithiadiphosphetane 2,4-disulphide) is commonly used in organic chemistry to convert aryl ketones and ethers into aryl thiols, but can also be used on aryl alcohols. Since most aryl alcohols can be converted to aryl thiols using this compound, this method might allow for the potential creation of many new ligand groups based on commercially available materials (aryl alkoxides), even though the aryl thiol starting material is not commercially available.

Experimental:

Synthesis of FcSH₂ ligand: (21)

To a dried, N₂ flushed Schlenk flask containing a stir bar, 600 mg of 1,1'-diformylferrocene (2.40×10^{-3} moles), 1.0 mL of 2-aminothiophenol (9.34×10^{-3} mol, in 0.88x excess), and 40 mL of ethanol were added. A yellow precipitate formed almost immediately upon stirring. The solution was allowed to reflux for three hours, cooled, filtered through a frit, washed with cold ethanol and the precipitate was dried under a vacuum. Amount recovered of pale yellow product: 690 mg (1.51×10^{-3} moles, 63.0 %, Table 6), mp 121-123 °C, ¹H NMR (CDCl₃): 7.08-7.05 ppm (2H, d, phenyl), 6.95-6.92 ppm (4H, t, phenyl), 6.81-6.64 ppm (2H, t, phenyl), 6.17 ppm (2H, d, Cp-CH-N), 4.54 ppm (2H, s, N-H), 4.42 ppm (4H, d, Cp), 4.28 ppm (4H, d, Cp); ¹H NMR (d₆-DMSO): 7.04 ppm (2H, d, phenyl), 6.84 ppm (2H, t, phenyl), 6.71 ppm (4H, d, phenyl), 6.57 ppm (2H, d, N-H), 6.27 ppm (2H, d, Cp-CH-N), 4.35 ppm (2H, s, Cp), 4.25 ppm (6H, s, Cp); Elemental analysis calculated for FeN₂S₂C₂₄H₂₀ (actual), see Table 7: 63.16 % C (62.59% C), 4.42% H (4.24% H), 6.14% N (6.12% N); IR: 3346.515 cm⁻¹ (N-H stretch), 1640 cm⁻¹ (C=N stretch), 890 cm⁻¹ (Fc stretch); Molar absorptivity (DMSO, Figure 4.9): 250 nm (41400 M⁻¹cm⁻¹), 254 nm (24000 M⁻¹cm⁻¹), 317 nm (8130 M⁻¹cm⁻¹), 402 nm (1490 M⁻¹cm⁻¹)

¹); MS: M+1: 457.00 and internal protonated disulfide peak at 454.98 amu; CV scan (Figure 4.11) and X-ray crystal structure data (Table 9) is listed below; see Appendix (Figures A.64-70) for further spectra.

Synthesis of FcS₂-Fe: (22)

To a dried, N₂ flushed Schlenk flask containing a stir bar, 240 mg of **21** (5.76×10^{-4} mol), 80 mg of Fe(CH₃COO)₂ (4.60×10^{-4} mol), and 70 mL of ethanol were added. The solution was allowed to reflux for three hours, cooled, filtered through a frit, washed with cold ethanol and the precipitate was dried under a vacuum. Amount recovered: 50 mg (26 mg, 5.14×10^{-5} mol, 11.2 % yield, corrected for impurities, Table 6), mp >300 °C, ¹H NMR (CDCl₃): 8.0-7.5 ppm, q, 7.4-7.15 ppm, t, 6.7-6.4 ppm, q, 5.30 ppm, s, 5.09 ppm, d, 4.6-4.5 ppm, d, 4.2-4.10 ppm, d; ¹H NMR (d₆-DMSO): Broad 8.0 ppm (2H, Cp-CH=N), Broad 7.3 ppm (2H, phenyl), Broad 7.1 ppm (4H, phenyl), Broad 6.7 ppm (2H, phenyl), Very broad 5-4 ppm (8H, Cp); Elemental analysis calculated for Fe₂N₂S₂C₂₄H₁₈ (actual), see Table 7: 56.50% C (40.49% C), 3.56% H (3.86% H), 5.49% N (3.09% N) 52.5% pure/47.5% starting material; Molar absorptivity (DMSO): 260 nm (28900 M⁻¹cm⁻¹), 308 nm (23100 M⁻¹cm⁻¹); MS: Fe species present (ligand), but not expected M+1 product; see Appendix (Figures A.71-78) for spectra.

Synthesis of FcS₂-Co: (23)

To a dried, N₂ flushed Schlenk flask containing a stir bar, 200mg of **21** (4.38×10^{-4} mol), 110 mg of Co(CH₃COO)₂·4H₂O (4.42×10^{-4} mol), and 70 mL of ethanol were added. The solution was allowed to reflux for three hours, cooled, filtered through a frit, washed

with cold ethanol and the precipitate was dried under a vacuum. Amount recovered: 170 mg (3.31×10^{-4} mol, 75.6 % yield, Table 6), mp >300 °C, $^1\text{H NMR}$ (CDCl_3): 13.81 ppm (s, H), 8.94 ppm (s, H), -1.27 ppm (s, H), -3.11 ppm (s, H), -18.42 ppm (s, H); $^1\text{H NMR}$ (d_6 -DMSO): 15.67 ppm (s, H), 13-12 ppm (broad s, H), 4.35 ppm (s, H), 3.36 ppm (s, H), 1.07 ppm (s, H), -1.5 ppm (s, H), -3.00 ppm (s, H), -5.82 ppm (s, H), -18.65 ppm (s, H); Elemental analysis calculated for $\text{FeCoN}_2\text{S}_2\text{C}_{24}\text{H}_{18}$ (actual), see Table 7: 56.16% C (54.15% C), 3.53% H (3.61% H), 5.46% N (5.19% N); Molar absorptivity (DMSO): 257 nm ($50300 \text{ M}^{-1}\text{cm}^{-1}$), 266 nm ($47700 \text{ M}^{-1}\text{cm}^{-1}$), 392 nm ($34300 \text{ M}^{-1}\text{cm}^{-1}$); MS: M+1: 513.92 amu; X-ray crystal structure data (Table 10) is listed below; see Appendix (Figure A.79-87) for spectra.

Synthesis of **FcS2-Ni: (24)**

To a dried, N_2 flushed Schlenk flask containing a stir bar, 220 mg of **21** (4.82×10^{-4} mol), 120 mg of $\text{Ni}(\text{CH}_3\text{COO})_2 \cdot 4\text{H}_2\text{O}$, (4.82×10^{-4} mol) and 70 mL of ethanol were added. The solution was allowed to reflux for three hours, cooled, filtered through a frit, washed with cold ethanol and the precipitate was dried under a vacuum. Amount recovered: 220 mg (2.14×10^{-4} mol, 88.7 % yield, Table 6), mp >300 °C, $^1\text{H NMR}$ (CDCl_3): 7.7 ppm (2H, broad s, Cp- $\underline{\text{CH}}=\text{N}$), 7.2-6.9 ppm (4H, broad m, phenyl), 6.7-6.58 ppm (4H, broad m, phenyl), 4.5-4.41 ppm (4H, broad d, Cp), 4.29-4.14 ppm (4H, broad d, Cp); $^1\text{H NMR}$ (d_6 -DMSO): 8.96 ppm (2H, broad d, Cp- $\underline{\text{CH}}=\text{N}$), 7.38 ppm (2H, broad d, phenyl), 7.30 ppm (2H, broad d, phenyl), 7.14 ppm (2H, broad m, phenyl), 7.01 ppm (2H, broad m, phenyl), 5.23 ppm (2H, broad d, Cp), 5.17 ppm (2H, broad d, Cp), 4.77 ppm (4H, broad d, Cp); Elemental analysis calculated for $\text{FeNiN}_2\text{S}_2\text{C}_{24}\text{H}_{18}$ (actual), see Table 7: 56.18% C

(56.47% C), 3.54% H (3.58% H), 5.46% N (5.54% N); Molar absorptivity (DMSO): 260 nm ($77400 \text{ M}^{-1}\text{cm}^{-1}$), 495 nm ($11400 \text{ M}^{-1}\text{cm}^{-1}$); MS: M+1: 512.93 amu; see Appendix (Figures A.88-94) for spectra.

Synthesis of FcS2-Cu: (25)

To a dried, N₂ flushed Schlenk flask containing a stir bar, 200 mg of **21** (4.38×10^{-4} mol), 90 mg of Cu(CH₃COO)₂·H₂O (4.51×10^{-4} mol), and 70 mL of ethanol were added. The solution was allowed to reflux for three hours, cooled, filtered through a frit, washed with cold ethanol and the precipitate was dried under a vacuum. Amount recovered: 160 mg (3.09×10^{-4} mol, 70.5 % yield, Table 6), mp 232-234 °C, ¹H NMR (CDCl₃): 8.16 ppm (2H, s, Cp-CH=N), 7.69 ppm (4H, s, phenyl), 6.85 ppm (4H, s, phenyl), 5.01 ppm (4H, s, Cp), 4.55 ppm (4H, s, Cp); ¹H NMR (d₆-DMSO): 8.1 ppm (1H, s, Cp-CH=N), 7.3 ppm (2H, broad d, phenyl), 7.0 ppm (4H, broad s, phenyl), 6.8 ppm (2H, s, phenyl), 4.8 ppm (4H, s, Cp), 4.5 ppm (4H, s, Cp); Elemental analysis calculated for FeCuN₂S₂C₂₄H₁₈ (actual), see Table 7: 55.66% C (53.63% C), 3.50% H (3.52% H), 5.41% N 5.34% N); Molar absorptivity (DMSO): 257 nm ($18700 \text{ M}^{-1}\text{cm}^{-1}$); MS: protonated disulfide form of ligand present; see Appendix (Figures A.95-102) for spectra.

Synthesis of FcS2-Zn: (26)

To a dried, N₂ flushed Schlenk flask containing a stir bar, 100 mg of **21** (2.19×10^{-4} mol), 50 mg of Zn(CH₃COO)₂·2H₂O (2.28×10^{-4} mol), and 70 mL of ethanol were added. The solution was allowed to reflux for three hours, cooled, filtered through a frit, washed with cold ethanol and the precipitate was dried under a vacuum. Amount recovered: 70

mg (1.35×10^{-4} mol, 61.4 % yield, Table 6), mp >300 °C, ^1H NMR (CDCl_3): 8.61 ppm (2H, s, Cp-CH=N), 7.60 ppm (2H, d, phenyl), 7.17-7.12 ppm (2H, t, phenyl), 6.98 ppm (4H, d, phenyl), 5.50 ppm (2H, s, Cp), 5.03 ppm (2H, s, Cp), 4.58 ppm (2H, s, Cp), 4.48 ppm (2H, s, Cp); ^1H NMR (d_6 -DMSO): 8.96 ppm (2H, s, Cp-CH=N), 7.38 ppm (2H, d, phenyl), 7.30 ppm (2H, d, phenyl), 7.13 ppm (2H, t, phenyl), 7.01 ppm (2H, d, phenyl), 5.22-5.16 ppm (4H, d, Cp), 4.77 ppm (4H, s, Cp); Elemental analysis calculated for $\text{FeZnN}_2\text{S}_2\text{C}_{24}\text{H}_{18}$ (actual), see Table 7: 55.46% C (54.91% C), 3.49% H (3.42% H), 5.39% N (5.50% N); Molar absorptivity (DMSO): 299 nm ($1760 \text{ M}^{-1}\text{cm}^{-1}$), 335 nm ($1600 \text{ M}^{-1}\text{cm}^{-1}$), 409 nm ($2760 \text{ M}^{-1}\text{cm}^{-1}$); MS: M+1: 518.92 amu, X-ray crystal structure data (Table 11) is listed below; see Appendix (Figures A.103-111) for spectra.

Synthesis of FcS2-Cd: (27)

To a dried, N_2 flushed Schlenk flask containing a stir bar, 170 mg of **21** (3.72×10^{-4} mol), 100 mg of $\text{Cd}(\text{CH}_3\text{COO})_2 \cdot 2\text{H}_2\text{O}$ (3.75×10^{-4} mol), and 40 mL of ethanol were added. The solution was allowed to reflux for one hour, cooled, filtered through a frit, washed with cold ethanol and the precipitate was dried under a vacuum. Amount recovered: 150 mg (2.64×10^{-4} mol, 71.0 % yield, Table 6), mp >300 °C, ^1H NMR (CDCl_3): 8.48 ppm (2H, t, Cp-CH=N), 7.66 ppm (2H, d, phenyl), 7.16 ppm (2H, t, phenyl), 7.02 ppm (2H, t, phenyl), 6.86 ppm (2H, d, phenyl), 5.69 ppm (2H, broad s, Cp), 5.01 ppm (2H, broad s, Cp), 4.63 ppm (2H, broad s, Cp), 4.46 ppm (2H, broad s, Cp); ^1H NMR (d_6 -DMSO): 8.63 ppm (2H, s, Cp-CH=N), 7.42 ppm (2H, d, phenyl), 7.09-6.96 ppm (6H, m, phenyl), 5.06 ppm (4H, broad s, Cp), 4.91 ppm (4H, s, Cp); Elemental analysis calculated for $\text{FeCdN}_2\text{S}_2\text{C}_{24}\text{H}_{18}$ (actual), see Table 7: 50.86% C (50.77% C), 3.20% H (3.23% H),

4.94% N (5.13% N); Molar absorptivity (DMSO): 259 nm ($45500 \text{ M}^{-1}\text{cm}^{-1}$), 392 nm ($14400 \text{ M}^{-1}\text{cm}^{-1}$); MS: M+1: 569.1 amu; see Appendix (Figures A.112-119) for spectra.

Synthesis of FcS2-Hg: (28)

To a dried, N₂ flushed Schlenk flask containing a stir bar, 140 mg of **21** (3.07×10^{-4} mol), 100 mg of Hg(CH₃COO)₂ (3.14×10^{-4} mol), and 40 mL of ethanol were added. The solution was allowed to reflux for one hour, cooled, filtered through a frit, washed with cold ethanol and the precipitate was dried under a vacuum. Amount recovered: 190 mg (2.90×10^{-4} moles, 94.6 % yield, Table 6), decomposes at 245 °C, ¹H NMR (CDCl₃, Fig. 4.11): 8.34 ppm (2H, s, Cp-CH=N), 7.61 ppm (2H, s, phenyl), 7.14 ppm (2H, s, phenyl), 6.80 ppm (2H, s, phenyl), 5.77 ppm (2H, broad s, Cp), 4.80 ppm (2H, broad s, Cp), 4.53 ppm (2H, broad s, Cp), 4.42 ppm (2H, broad s, Cp); ¹H NMR (d₆-DMSO, Fig. 4.12): 8.48 ppm (2H, s, Cp-CH=N), 7.49 ppm (2H, t, phenyl), 7.14 ppm (4H, m, phenyl), 6.97 ppm (2H, t, phenyl), 6.0-5.0 ppm (4H, Cp), 4.85 ppm (4H, very broad s, Cp); Elemental analysis calculated for FeHgN₂S₂C₂₄H₁₈ (actual), see Table 7: 44.01% C (43.30% C), 2.77% H (2.82% H), 4.28% N (4.32% N); Molar absorptivity (DMSO, Fig. 4.10): 251 nm ($2260 \text{ M}^{-1}\text{cm}^{-1}$), 285 nm ($35100 \text{ M}^{-1}\text{cm}^{-1}$), 376 nm ($19000 \text{ M}^{-1}\text{cm}^{-1}$); MS: M+1: 657.2 amu; CV (Figure 4.12) and X-ray crystal structure data (Table 12) is listed below; see Appendix (Figures A.120-126) for spectra.

Synthesis of FcS2-Pb: (29)

To a dried, N₂ flushed Schlenk flask containing a stir bar, 240 mg of **21** (5.26×10^{-4} mol), 20 mg of Pb(CH₃COO)₂·3H₂O (5.27×10^{-4} mol), and 70 mL of ethanol were added.

The solution was allowed to reflux for three hours, cooled, filtered through a frit, washed with cold ethanol and the precipitate was dried under a vacuum. Amount recovered: 150 mg (2.27×10^{-4} mol, 42.7 % yield, Table 6), mp 200 °C, $^1\text{H NMR}$ (CDCl_3): 8.75 ppm (H, s), 7.16-6.93 ppm (H, d), 6.85-6.07 ppm (H, t), 6.57 ppm (H, t), 6.07 ppm (H, m), 4.69 ppm (H, d), 4.41 ppm (H, d), 4.25 ppm (H, t); $^1\text{H NMR}$ (d_6 -DMSO): 7.07-6.98 ppm (H, d, phenyl), 6.72 ppm (H, d, phenyl), 6.72 ppm (H, d, phenyl), 6.1 ppm (H, d, phenyl), 5.42 ppm (H, s, Cp- $\text{CH}=\text{N}$), 5.3-5.0 ppm (H, m, Cp), 4.5-3.8 ppm (H, m, Cp); Elemental analysis calculated for $\text{FePbN}_2\text{S}_2\text{C}_{24}\text{H}_{18}$ (actual), see Table 7: 43.57% C (45.04% C), 2.74% H (2.90% H), 4.23% N (4.32% N); Molar absorptivity (DMSO): 257 nm ($23600 \text{ M}^{-1}\text{cm}^{-1}$), 430 nm ($11500 \text{ M}^{-1}\text{cm}^{-1}$); MS: lead complex not observed; see Appendix (Figures A.127-134) for spectra.

The melting point of FcSH2 is midway between the melting points of the Fc2 and FcOH2 ligand systems. After many attempts to grow single crystals, the slow vapor diffusion (SVD) method with benzene/ethyl ether gave a crystal suitable for X-ray analysis and the data proved the double ring closed structure is preferred in the solid state. Crystals were also obtained using SVD with benzene/hexane and benzene/heptane, but they were not of as high quality as those formed by the previously mentioned procedure.

The reactions to form the metal complexes gave color changes that ranged from very dark red, to black, to even a metallic orange from the initial pale yellow solution. This color change is of particular interest, since colorimetric changes can be used to identify bound targets in some chemical sensors. The FcS2-M products precipitated out upon

cooling, whereby they were recovered upon filtering, washing with cold ethanol/ethyl ether and vacuum dried. As expected, the FcS2-Hg reaction produced a very high yield (94.6%), much greater than the percent yields of other FcS2-M complexes. This result gave a good indication that the FcSH2 ligand would be potentially selective for Hg²⁺ cations. All of the FcS2-M products were analyzed to form a spectral database.

After many failed attempts, single crystals were obtained of three of the FcS2-M complexes (M=Co, Zn, Hg). Not surprisingly, two of these crystals were obtained using the same method/solution combination as the free ligand. The FcS2-Hg system was quite different in that it grew crystals in all methods and solution combinations that were tried. The crystals grown using CDCl₃ evaporation were used for the X-ray measurement and gave a very ordered data set. Many of the other crystal trials (such as FcS2-Cd) grew microcrystals that were not useable or, in the specific case of FcS2-Ni, were precipitates.

Table 6: Melting points, Colors, and Percent Yields of the FcSH2 ligand and metal complex products

Compound #	Formula	Color	Melting Point	Percent Yield
21	FeN ₂ S ₂ C ₂₄ H ₂₀	pale yellow	121-123 °C	63.0 %
22	Fe ₂ N ₂ S ₂ C ₂₄ H ₁₈	orange-red	>300 °C	21.3 %
23	FeCoN ₂ S ₂ C ₂₄ H ₁₈	deep red-black	>300 °C	75.6 %
24	FeNiN ₂ S ₂ C ₂₄ H ₁₈	deep red-black	>300 °C	88.7 %
25	FeCuN ₂ S ₂ C ₂₄ H ₁₈	deep red-black	232-234 °C	70.5 %
26	FeZnN ₂ S ₂ C ₂₄ H ₁₈	deep red-black	>300 °C	61.4 %
27	FeCdN ₂ S ₂ C ₂₄ H ₁₈	deep red	>300 °C	71.0 %
28	FeHgN ₂ S ₂ C ₂₄ H ₁₈	red	decomp. 245 °C	94.6 %
29	FePbN ₂ S ₂ C ₂₄ H ₁₈	orange	200 °C	42.7 %

Table 7: Elemental Analysis of the FcSH2 system.

Compound #	Calc. C%	Actual C%	Calc. H%	Actual H%	Calc. N%	Actual N%
21	63.16	62.59	4.42	4.24	6.14	6.12
22	56.50	40.49	3.56	3.86	5.49	3.09
23	56.16	54.15	3.53	3.61	5.46	5.19
24	56.18	56.47	3.54	3.58	5.46	5.54
25	55.66	53.63	3.50	3.52	5.41	5.34
26	55.46	54.91	3.49	3.42	5.39	5.50
27	50.86	50.77	3.20	3.23	4.94	5.13
28	44.01	43.30	2.77	2.82	4.28	4.32
29	43.57	45.04	2.74	2.90	4.23	4.32

*Compound 22 contained a starting material impurity of 47.5%, calculated with amounts of starting material added to product.

Results and Discussion:

Melting point, MS, ¹H NMR, and Magnetic Susceptibility:

The melting point for compound **21** (Table 6) is between the melting points of compounds **1** and **10**. Compounds **22-29** have melting points that range from 200 °C to above 300 °C (Table 6), all increasing over the starting ligand. Compound **28** undergoes decomposition at 245 °C as indicated by a color change from cherry red to deep black. This change is a potential way of seeing if that particular compound is present within a sample product. Due to the material decomposing and possible mercury vapor becoming present, this determination would best be made in a sealed heated probe. A bit of **21** was mixed with a small portion of **23** and the melting point showed a vapor present among the solid at around 124 °C. Thus, melting point testing can determine the presence of a free ligand that was not removed from the product. While this will not help strictly identify all possible products in the selectivity experiments for this ligand system, it may be of use if the product happens to be either **25**, **28** or **29** since they have distinct melting (or

decomposing) ranges that differ from the other complexes. Since this particular ligand system is targeted for sensing Hg^{2+} , melting point measurements will be used to determine if **28** is formed in a pure form when other metal cations are present in solution.

The MS data for **21** do show the M+1 peak at 454.98 amu. Most of the metal complexes of this system showed M+1 peaks that were discernable (with the exception of **22**, **25**, and **29**). Since three of the complexes cannot be determined by MS, the utility in identifying products from a selectivity experiment with this ligand system is limited to only five possible metals. Since **28** is measurable by MS, it can be used in identifying the potential presence of Hg^{2+} in selectivity products, but use of MS for identification is limited in potential real world applications for chemical sensors.

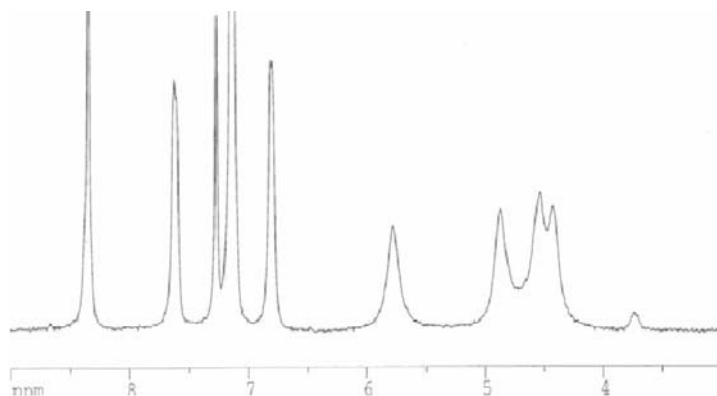


Figure 4.5: ^1H NMR spectrum of FcS2-Hg in CDCl_3 (CHCl_3 solvent peak at 7.27 ppm). The peak at 8.4 ppm is due to the Cp- $\underline{\text{C}}\text{H}=\text{N}-\text{R}$ protons, while the three broad peaks between 7.5-6.5 ppm correspond to the phenyl protons and the peaks between 6-4.5 are from the Cp protons. (1:1:2:1:2:2:2:2 H equivalency)

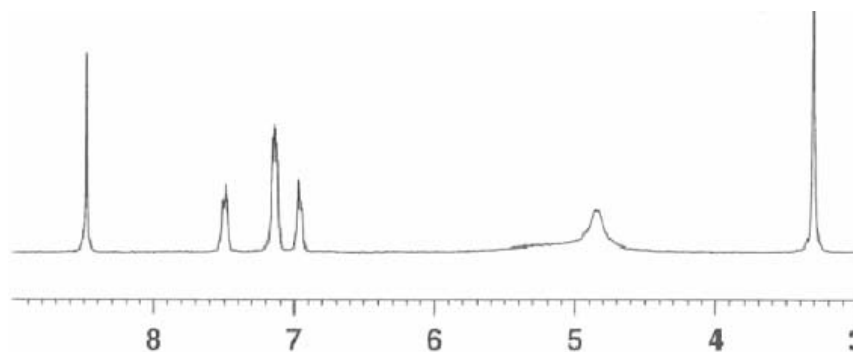


Figure 4.6: ^1H NMR spectrum of $\text{FcS}_2\text{-Hg}$ in $d_6\text{-DMSO}$. The peak at 8.5 ppm is due to Cp-CH=N-R protons, the three peaks at 8-56.5 ppm are due to phenyl protons, while the Cp protons appear as a very broad, shallow peak from 5.5-4 ppm. (1:1:2:1:4 H equivalency)

The ^1H NMR spectra of compound **21** is quite different than the spectra of **1** and **10**, as there is no Cp-CH=N-R peak due to the DRCT effect. The amine proton peaks are shifted upfield to near the Cp proton peak range. The phenyl protons appear between 7.1-6.6 ppm, which is slightly downfield from those in **1** and **10**. The amine proton does appear as a broad peak, and disappears once a metal becomes chelated. The ^1H NMR spectra of **22-29** are characterizable to most protons on each complex. **25-29** show four peaks for the Cp protons due to an inequivalency that exists between the Cp rings. The Cp splitting can be used to differentiate between the metals, since there is at least one peak difference between each of them. The Cp-CH=N-R proton is the key to identifying selectivity products using ^1H NMR. Since **21** is being targeted as a Hg^{2+} sensor, any product that shows a sharp peak at 8.34 ppm has a strong indication of the presence of **28** (Figures 4.5-6), since the nearest corresponding Cp-CH=N-R peak for another complex is for **27** at 8.48 ppm (a 0.14 ppm difference which can be used to differentiate a mixed solution of the two).

^1H NMR spectral peak locations are compared below (Figures 4.7-8). ^1H NMR spectra of FcS2-Co is greatly influenced by the paramagnetic behavior of the Co^{2+} metal center within the molecule (three unpaired electrons present). FcS2-Ni has some paramagenetic behavior due to the possible presence of two unpaired electrons on Ni^{2+} (tetrahedral geometry).

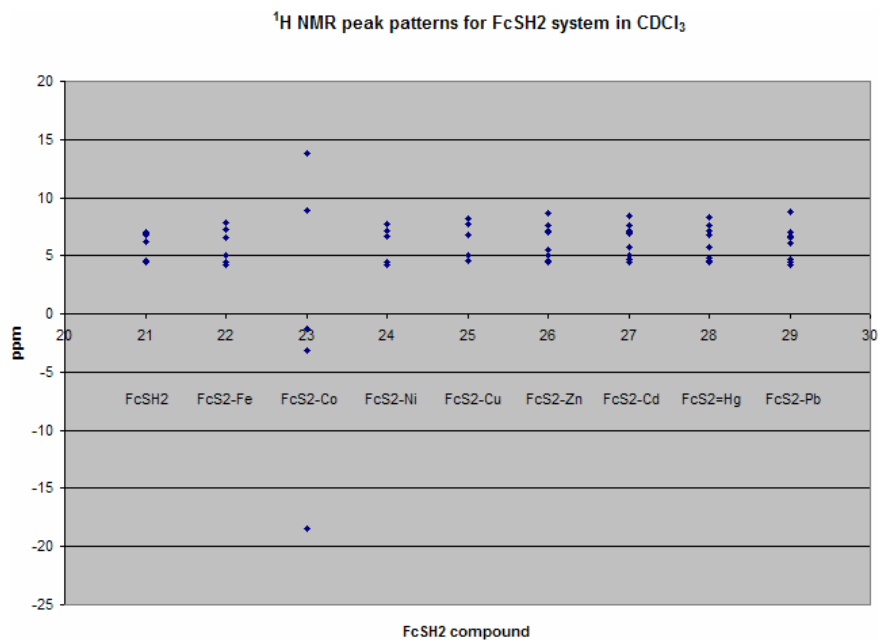


Figure 4.7: The ^1H NMR peak locations for the FcSH2 system in CDCl_3 . Compound 23 has paramagnetic shifting of the spectral peaks.

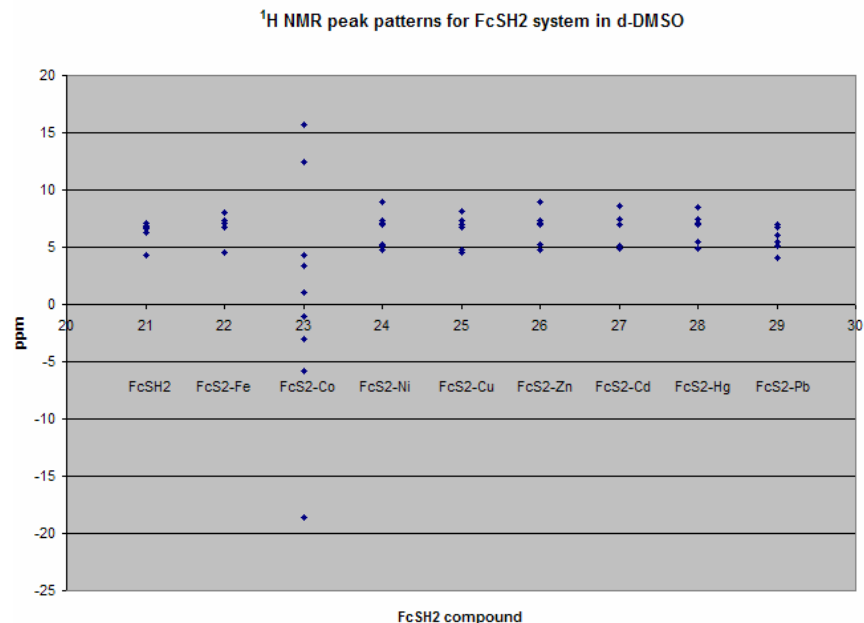


Figure 4.8: The ¹H NMR peak locations for the FcSH2 system in d₆-DMSO

Magnetic susceptibility of **21** indicates no unpaired electrons within the free ligand. Complexes of FcS₂-M show paramagnetism in **22** and **23**, while the rest of the series are diamagnetic. The results indicate fewer unpaired electrons than expected for compounds **22-25**, as they all should be paramagnetic (if the cation is in high spin tetrahedral geometry). Complexes **26-29** do not contain unpaired electrons, which are expected because the target cations contain full electron shells.

Discussion of Crystal Structures:

X-ray quality single crystals of compounds **21** (table 8), **23** (table 9), **26** (table 10), and **28** (table 11) were grown by either slow vapor diffusion (SVD) using benzene/heptane or benzene/ethyl ether combinations. Complex **28** also gave X-ray quality single crystals via CDCl₃ evaporation. The crystal structure of **21** showed only

the DRCT form (triclinic $P\bar{1}$ unit cell). Crystal structure data tables can be found in the attached appendix along with a comparison between the known $[\text{FcS1}]_2\text{-Zn}$ and $[\text{FcS1}]_2\text{-Hg}$ complexes for **26** and **28** (Orthorhombic, $C222_1$). Not surprisingly, the distances for **23** (Monoclinic, $P2_1/n$ unit cell) and **26** (Monoclinic, $P2_1/n$ unit cell) between the two metal centers were almost identical at 3.96 Å and 3.98 Å with a tetrahedral geometry for the chelated metal center. The metal to metal distances for **28** were longer (4.50 Å) due to the strong bonding occurring between the Hg-S groups, although there was a slight interaction between the Hg center and the imine nitrogens based on the S-Hg-S bond angle not being strictly linear (166.10°).

Table 8: Crystal structure of the FcSH2 ligand

Crystal data	
$\text{C}_{24}\text{H}_{18}\text{FeN}_2\text{S}_2$	$F_{000} = 936$
$M_r = 454.37$	$D_x = 1.510 \text{ Mg m}^{-3}$
Triclinic, $P\bar{1}$	Melting point: 394-396 K
	Mo $K\alpha$ radiation
	$\lambda = 0.71073 \text{ \AA}$
$a = 10.0682 (16) \text{ \AA}$	Cell parameters from 4139 reflections
$b = 12.0464 (19) \text{ \AA}$	$\Theta = 2.2\text{--}27.1^\circ$
$c = 18.983 (3) \text{ \AA}$	$\mu = 0.98 \text{ mm}^{-1}$
$\alpha = 71.793 (3)^\circ$	$T = 173 (2) \text{ K}$
$\beta = 85.700 (3)^\circ$	
$\Gamma = 66.279 (3)^\circ$	Needle, yellow
$V = 1998.9 (6) \text{ \AA}^3$	$0.55 \times 0.02 \times 0.02 \text{ mm}$
$Z = 4$	

Data collection

Bruker SMART CCD area detector diffractometer	14017 measured reflections
Radiation source: Mo $K\alpha$	8545 independent reflections
Monochromator: graphite	4806 reflections with $I > 2\sigma(I)$
	$R_{\text{int}} = 0.055$
$T = 173(2)$ K	$\theta_{\text{max}} = 27.1^\circ$
	$\theta_{\text{min}} = 1.1^\circ$
ω scans	$-11 \leq h \leq 12$
Absorption correction: multi-scan	
Data were corrected for decay and absorption using the program SADABS (Sheldrick, G. M. (2003). SADABS. Version 2.10. University of Göttingen, Germany).	$-10 \leq k \leq 15$
$T_{\text{min}} = 0.67$, $T_{\text{max}} = 0.98$	$-24 \leq l \leq 24$

Refinement

Refinement on F^2	Secondary atom site location: difference Fourier map
Least-squares matrix: full	Hydrogen site location: inferred from neighbouring sites
$R[F^2 > 2\sigma(F^2)] = 0.073$	H-atom parameters constrained
$wR(F^2) = 0.206$	$w = 1/[\sigma^2(F_o^2) + (0.1092P)^2]$
$S = 0.99$	where $P = (F_o^2 + 2F_c^2)/3$
8545 reflections	$(\Delta/\sigma)_{\text{max}} < 0.001$
518 parameters	$\Delta\rho_{\text{max}} = 2.91 \text{ e}\text{\AA}^{-3}$
	$\Delta\rho_{\text{min}} = -0.99 \text{ e}\text{\AA}^{-3}$
	Extinction correction: none
Primary atom site location: structure-invariant direct methods	

Color code for the FcSH2 crystal structure:

Orange: Fe atom

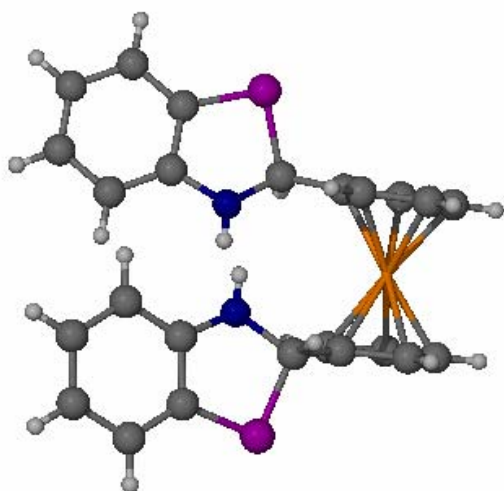
Dark grey: C atom

Light grey: H atom

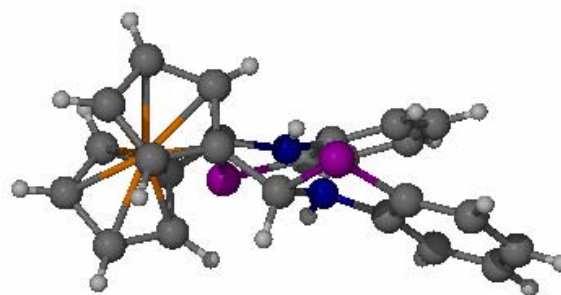
Dark Blue: N atom

Purple: S atom

Asymmetric unit structure: (two molecules)



A



B

Bond Lengths (Å):

C1-C2: 1.42(9) Å	C2-C3: 1.42(0) Å	C3-C4: 1.42(3) Å	C4-C5: 1.42(9) Å
C1-C5: 1.43(0) Å	C1-C6: 1.49(4) Å	C6-N1: 1.46(4) Å	C6-S1: 1.85(5) Å
N1-C7: 1.40(8) Å	C7-C8: 1.39(5) Å	C8-S1: 1.77(1) Å	C8-C9: 1.37(9) Å
C9-C10: 1.40(2) Å	C10-C11: 1.37(9) Å	C11-C12: 1.40(0) Å	C7-C12: 1.39(1) Å
C13-C14: 1.43(1) Å	C14-C15: 1.43(2) Å	C15-C16: 1.41(8) Å	C16-C17: 1.42(1) Å
C13-C17: 1.42(8) Å	C13-C18: 1.49(1) Å	C18-N2: 1.45(8) Å	C18-S2: 1.86(1) Å
N2-C18: 1.41(0) Å	C19-S2: 1.76(4) Å	C19-C20: 1.39(9) Å	C20-C21: 1.38(7) Å
C21-C22: 1.38(8) Å	C22-C23: 1.38(5) Å	C23-C24: 1.39(7) Å	C18-C24: 1.38(3) Å
H1...H2: 2.34(2) Å			

Bond Angles (°):

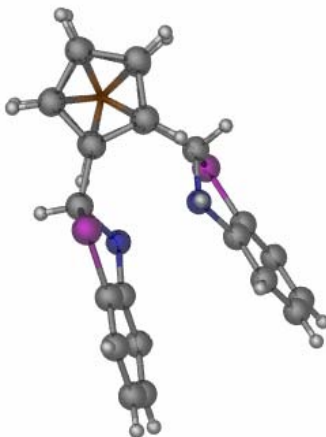
C1-C6-N1: 113.9(4)°	C6-N1-C7: 110.5(1)°	N1-C7-C8: 113.4(1)°
C7-C8-S1: 110.7(9)°	C1-C6-S1: 111.0(7)°	N1-C6-S1: 102.9(8)°
C13-C18-N2: 113.8(5)°	C18-N2-C19: 110.2(4)°	N2-C19-C20: 112.8(3)°
C19-C20-S2: 110.9(2)°	C13-C18-S2: 111.8(9)°	N2-C18-S2: 102.4(6)°

Bond Lengths (B):

C1-C2: 1.42(3) Å	C2-C3: 1.42(9) Å	C3-C4: 1.42(3) Å	C4-C5: 1.42(5) Å
C1-C5: 1.43(3) Å	C1-C6: 1.49(3) Å	C6-N1: 1.45(7) Å	C6-S1: 1.85(3) Å
N1-C7: 1.40(7) Å	C7-C8: 1.40(5) Å	C8-S1: 1.78(5) Å	C8-C9: 1.38(9) Å
C9-C10: 1.38(4) Å	C10-C11: 1.39(2) Å	C11-C12: 1.39(1) Å	C7-C12: 1.38(3) Å
C13-C14: 1.42(8) Å	C14-C15: 1.41(6) Å	C15-C16: 1.42(7) Å	C16-C17: 1.42(6) Å
C13-C17: 1.43(2) Å	C13-C18: 1.49(2) Å	C18-N2: 1.46(9) Å	C18-S2: 1.85(1) Å
N2-C18: 1.39(9) Å	C19-S2: 1.76(3) Å	C19-C20: 1.39(9) Å	C20-C21: 1.38(6) Å
C21-C22: 1.39(3) Å	C22-C23: 1.38(6) Å	C23-C24: 1.40(1) Å	C19-C24: 1.38(8) Å
H1...H2: 2.38(4) Å			

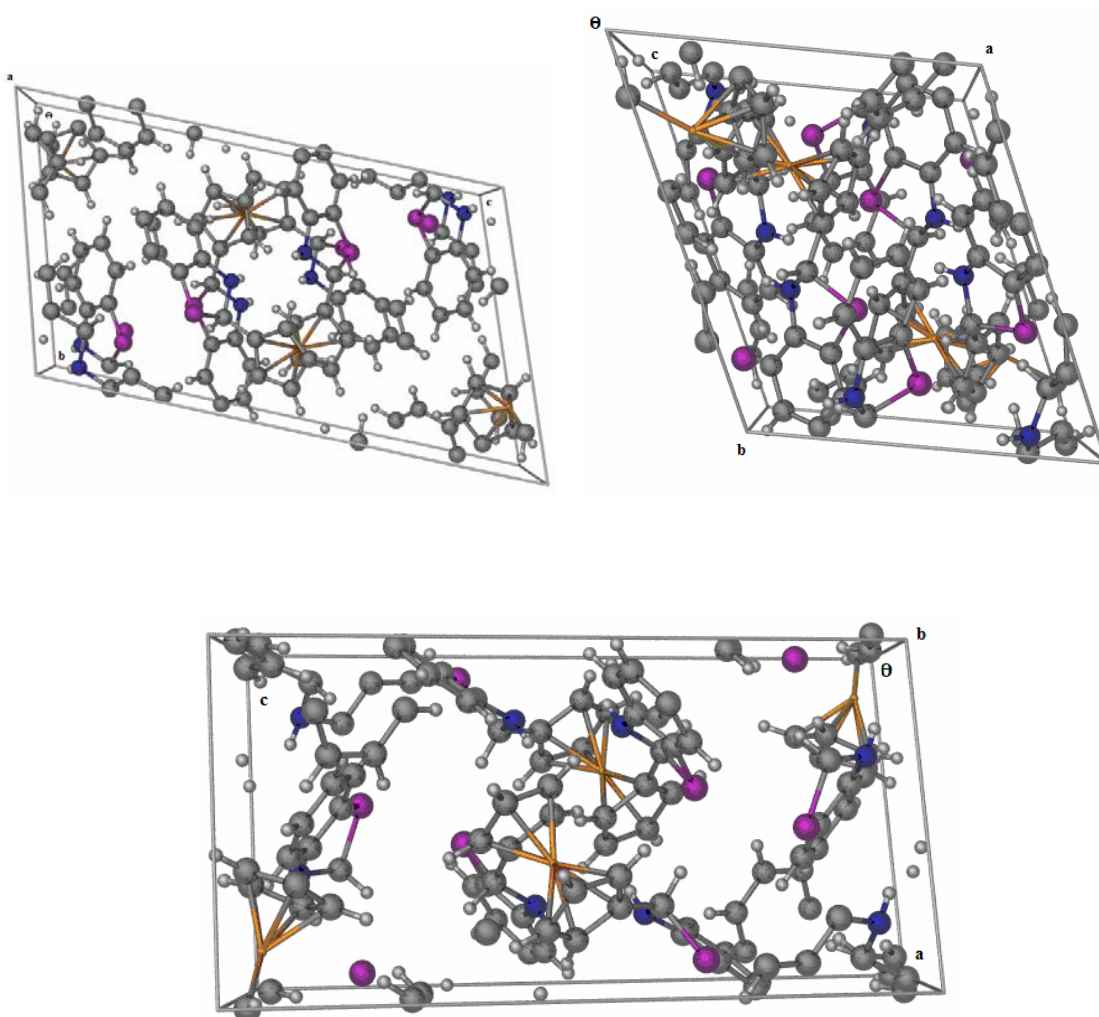
Bond Angles (B):

C1-C6-N1: 114.8(4)°	C6-N1-C7: 111.6(6)°	N1-C7-C8: 112.4(8)°
C7-C8-S1: 111.3(9)°	C1-C6-S1: 109.7(6)°	N1-C6-S1: 103.3(3)°
C13-C18-N2: 114.3(8)°	C18-N2-C19: 111.9(1)°	N2-C19-C20: 112.9(6)°
C19-C20-S2: 111.2(4)°	C13-C18-S2: 109.6(8)°	N2-C18-S2: 103.0(8)°

Cp ring overlap:

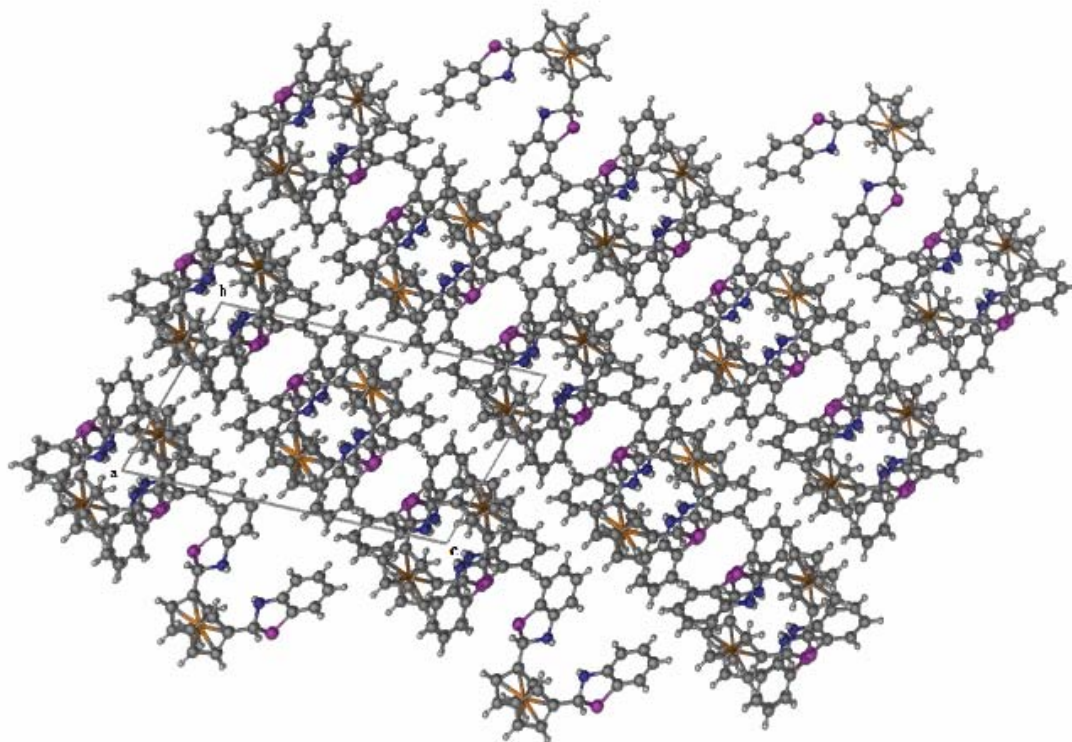
The Cp rings are almost completely eclipsed in the FcSH₂ crystal structure.

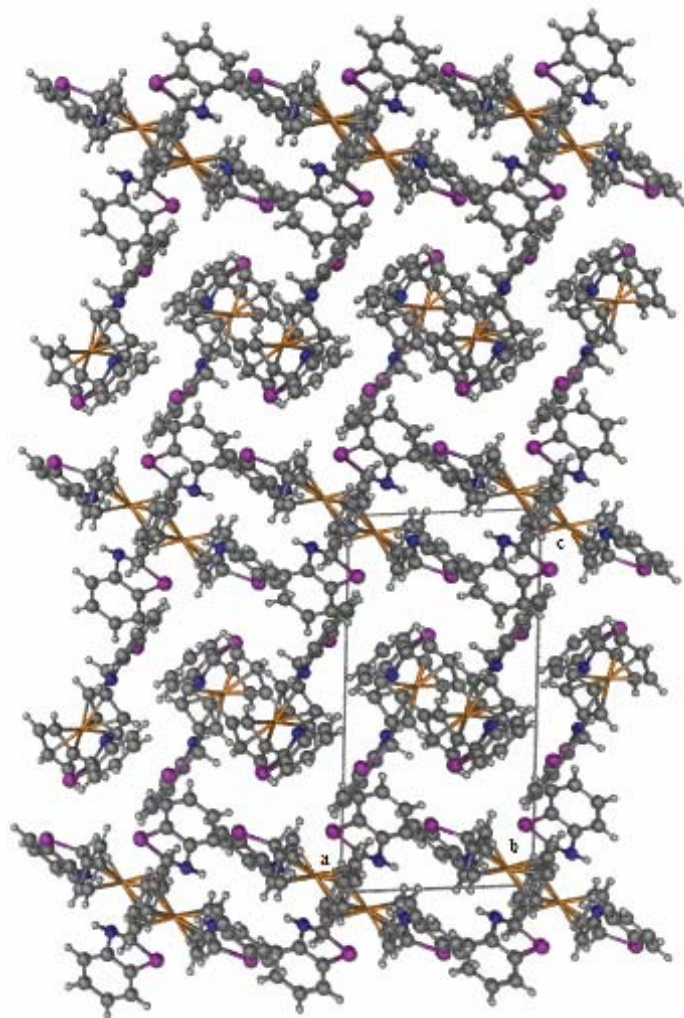
Unit cell:

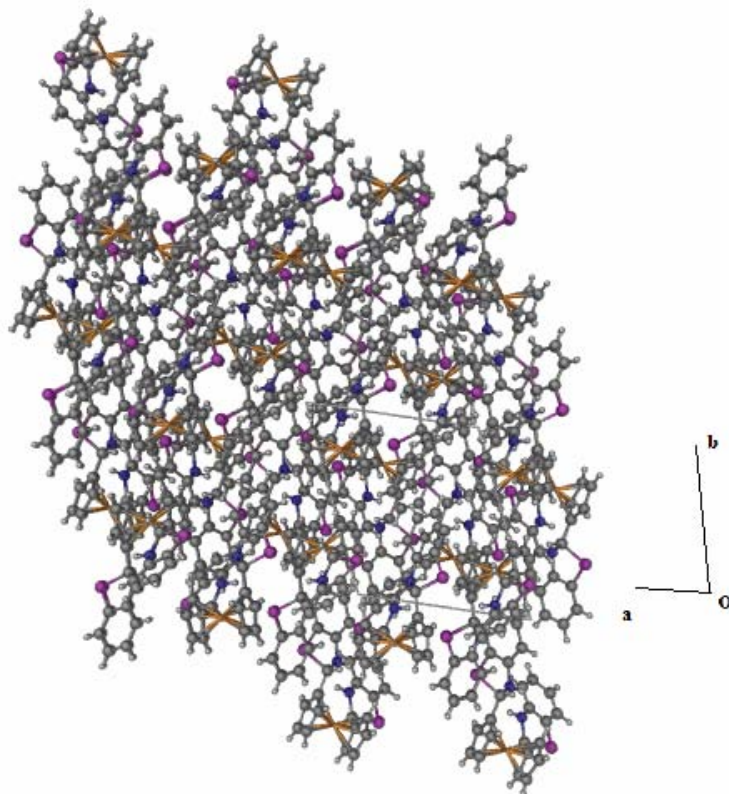


Crystal packing in three directions:

- 1: Θ along a
- 2: Θ along b
- 3: Θ along c







Discussion of the FcSH2 crystal structure:

The FcSH2 ligand forms dark reddish crystals that crystallize in the triclinic space group $P\bar{1}$. Although the synthesis and characterization of the FcSH1 ligand system (and some tri-metal complexes)¹³² has been reported, the crystal structure for this molecule has not. The asymmetric unit is the full molecule. The Cp rings are completely eclipsed in the solid state and both of the side groups are in the RCT form. Crystal packing is much different than the FcOH2 ligand because of the DRCT effect with FcSH2.

Table 9: Crystal structure of FcS2-Co*Crystal data* $C_{24}H_{18}CoFeN_2S_2$ $M_r = 513.30$ Monoclinic, $P2_1/n$ $a = 7.1861 (6) \text{ \AA}$ $b = 19.2478 (17) \text{ \AA}$ $c = 15.2958 (13) \text{ \AA}$ $\beta = 100.209 (2)^\circ$ $V = 2082.2 (3) \text{ \AA}^3$ $Z = 4$ $F_{000} = 1044$ $D_x = 1.637 \text{ Mg m}^{-3}$ Melting point: $>573 \text{ K}$ Mo $K\alpha$ radiation $\lambda = 0.71073 \text{ \AA}$

Cell parameters from 5446 reflections

 $\theta = 2.5\text{--}27.0^\circ$ $\mu = 1.71 \text{ mm}^{-1}$ $T = 173 (2) \text{ K}$

Plate, red

 $0.35 \times 0.20 \times 0.05 \text{ mm}$ *Data collection*Bruker SMART CCD area detector
diffractometerRadiation source: Mo $K\alpha$

Monochromator: graphite

 $T = 173(2) \text{ K}$ ω scans

Absorption correction: multi-scan

Data were corrected for decay and absorption using
the program SADABS (Sheldrick, G. M. (2003).
SADABS. Version 2.10. University of Göttingen,
Germany). $T_{\min} = 0.68, T_{\max} = 0.92$

14375 measured reflections

4577 independent reflections

3431 reflections with $I > 2\sigma(I)$ $R_{\text{int}} = 0.043$ $\theta_{\text{max}} = 27.1^\circ$ $\theta_{\text{min}} = 1.7^\circ$ $-9 \leq h \leq 9$ $-24 \leq k \leq 24$ $-17 \leq l \leq 19$ *Refinement*Refinement on F^2

Least-squares matrix: full

 $R[F^2 > 2\sigma(F^2)] = 0.044$ $wR(F^2) = 0.093$ $S = 1.09$

4577 reflections

271 parameters

Secondary atom site location: difference Fourier map

Hydrogen site location: inferred from neighbouring
sites

H-atom parameters constrained

 $w = 1/[\sigma^2(F_o^2) + (0.0327P)^2 + 2.616P]$ where $P = (F_o^2 + 2F_c^2)/3$ $(\Delta/\sigma)_{\text{max}} = 0.001$ $\Delta\rho_{\text{max}} = 0.62 \text{ e \AA}^{-3}$ $\Delta\rho_{\text{min}} = -0.48 \text{ e \AA}^{-3}$

Extinction correction: none

Primary atom site location: structure-invariant direct methods

Color code for the FcS2-Co crystal structure:

Orange: Fe atom

Dark grey: C atom

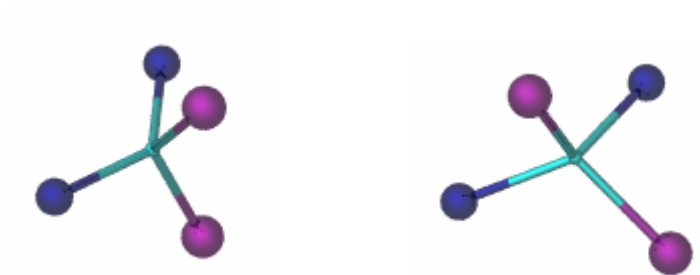
Light grey: H atom

Dark Blue: N atom

Purple: S atom

Light Blue: Co atom

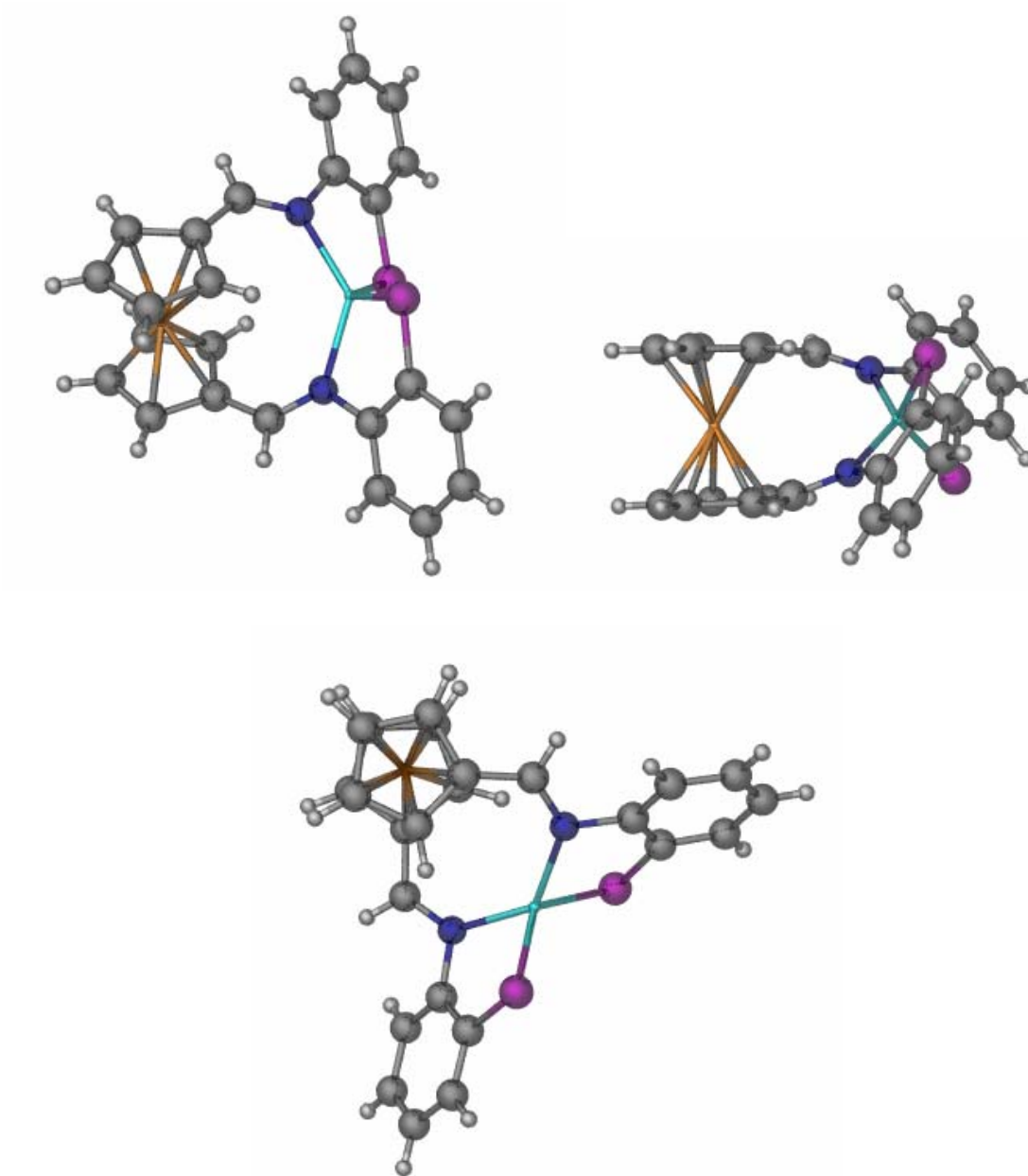
Metal geometry:



The Co^{2+} metal center has distorted tetrahedral geometry in the FcS2-Co complex.

The angles between the nitrogen atoms in the complex are 133.29° and between the sulfur atoms are 129.82° . The angles between nitrogen and sulfur atoms ranged from 87.09° - 87.20° for those on the same attaching group and 112.65° - 112.76° for those on different attaching groups.

Asymmetric unit structure:



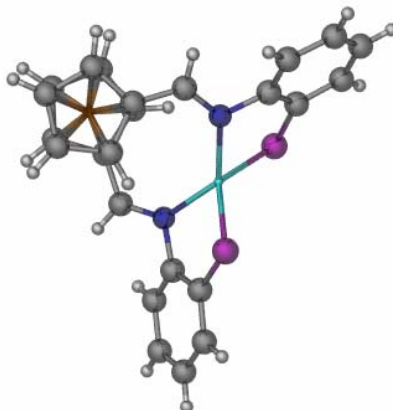
The asymmetric unit for the FcS₂-Co complex is its whole structure.

Bond Lengths:

C1-C2: 1.44(0) Å	C2-C3: 1.41(4) Å	C3-C4: 1.42(0) Å	C4-C5: 1.41(0) Å
C1-C5: 1.43(6) Å	C1-C6: 1.44(5) Å	C6-N1: 1.29(4) Å	N1-Co: 2.06(5) Å
N1-C7: 1.44(1) Å	C7-C8: 1.40(4) Å	C8-S1: 1.76(4) Å	S1-Co: 2.26(0) Å
C8-C9: 1.39(3) Å	C9-C10: 1.38(9) Å	C10-C11: 1.38(5) Å	C11-C12: 1.39(1) Å
C7-C12: 1.38(8) Å	C13-C14: 1.43(0) Å	C14-C15: 1.41(8) Å	C15-C16: 1.41(1) Å
C16-C17: 1.41(7) Å	C13-C17: 1.43(1) Å	C13-C18: 1.44(2) Å	C18-N2: 1.29(1) Å
N2-Co: 2.06(9) Å	N2-C19: 1.44(6) Å	C19-C20: 1.41(0) Å	C20-S2: 1.76(2) Å
S2-Co: 2.26(5) Å	C20-C21: 1.39(0) Å	C21-C22: 1.39(1) Å	C22-C23: 1.38(5) Å
C23-C24: 1.38(3) Å	C19-C24: 1.39(7) Å		

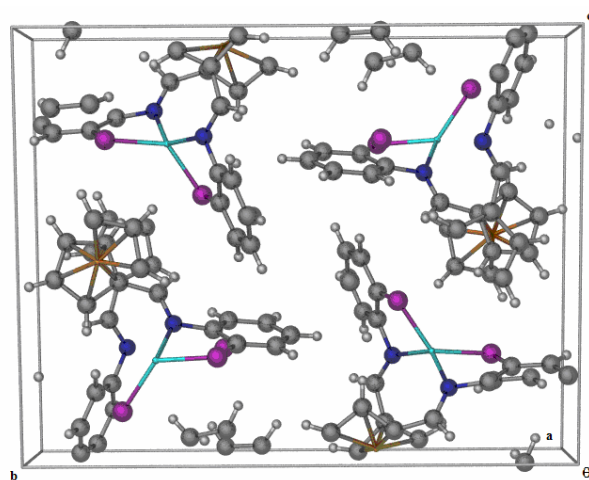
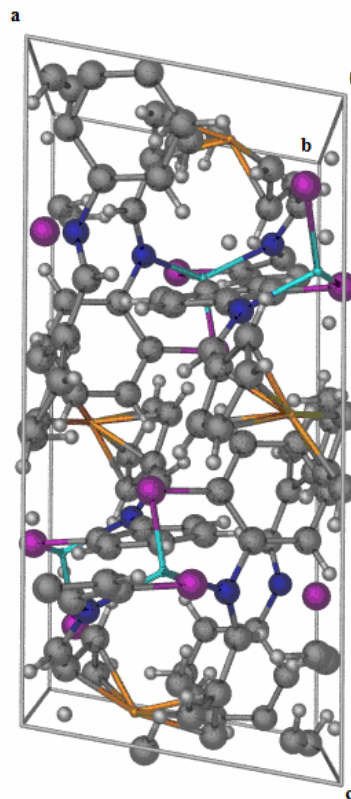
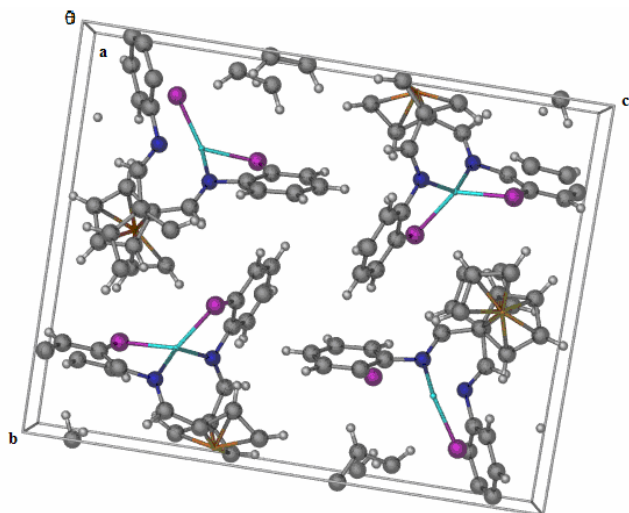
Bond Angles:

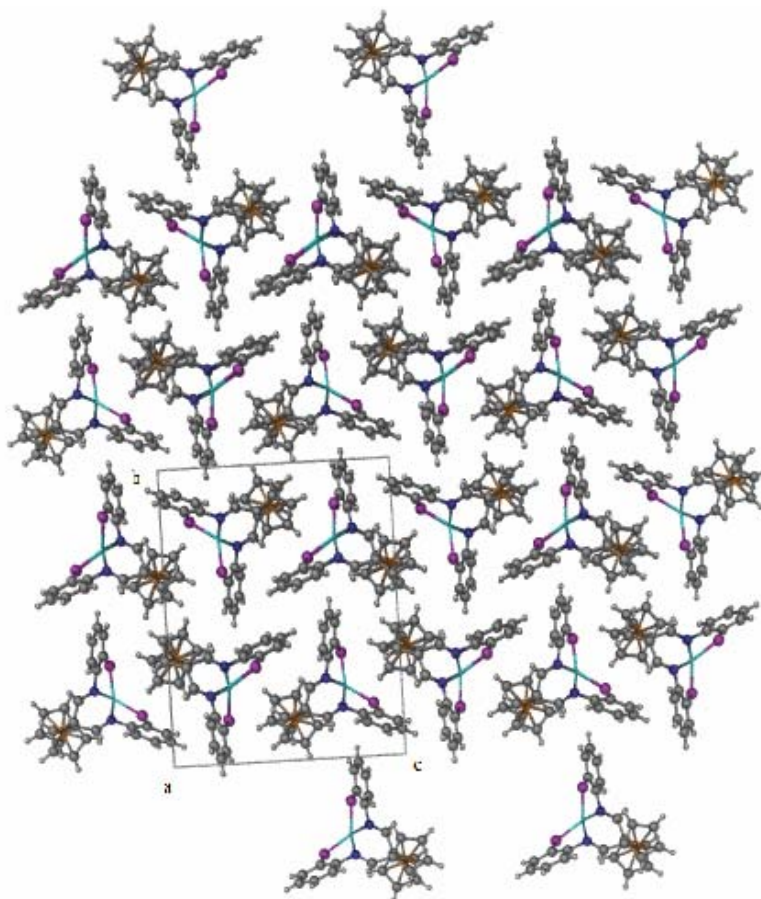
C1-C6-N1: 125.0(7)°	C6-N1-Co: 131.2(2)°	C6-N1-C7: 116.4(9)°
N1-C7-C8: 117.2(8)°	C7-C8-S1: 121.1(1)°	C8-S1-Co: 94.0(3)°
N1-Co-S1: 87.2(0)°	C13-C18-N2: 126.1(7)°	C18-N2-Co: 131.6(9)°
C18-N2-C19: 116.1(3)°	N2-C19-C20: 117.2(1)°	C18-C19-S2: 121.0(7)°
C19-S2-Co: 94.2(7)°	N2-Co-S2: 87.0(9)°	N1-Co-S2: 112.7(6)°
N2-Co-S1: 112.6(5)°	N1-Co-N2: 133.2(9)°	S1-Co-S2: 129.8(2)°

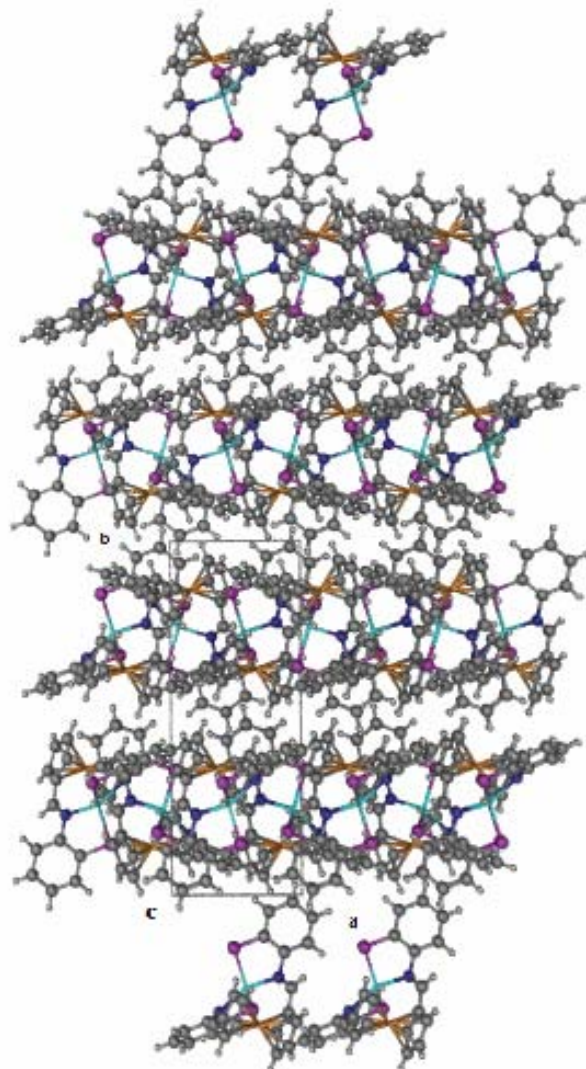
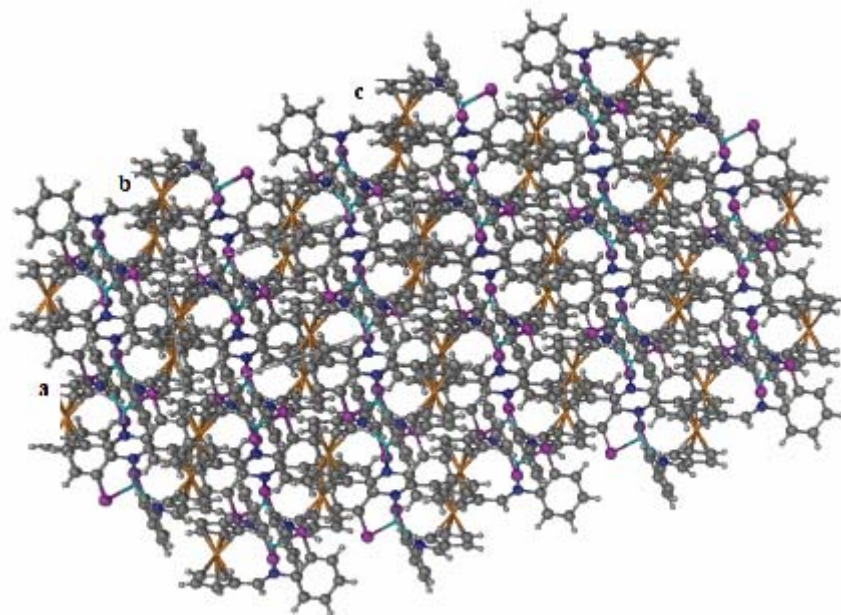
Cp ring overlap:

The Cp rings of the ferrocene unit of the FcS2-Co complex have been shifted 5° from being eclipsed (from the FcSH2 ligand structure).

Unit cell:



Crystal packing in three directions:1: Θ along a2: Θ along b3: Θ along c



Discussion of the FcS2-Co crystal structure:

The FcS2-Co forms dark reddish crystals that crystallize in the monoclinic space group $P2_1/n$. The corresponding $[\text{FcS1}]_2\text{-Co}$ complex crystal structure has not been reported in the literature as of yet, so no comparison can be done. The asymmetric unit is the full molecule. The Cp rings are mostly eclipsed in the solid state, with only a slight offset (5°). Metal-to-metal distance from the Fe^{2+} atom to the Co^{2+} atom was 3.969 \AA . The Co^{2+} atom has a distorted tetrahedral geometry containing an N1-Co-N2 angle of 133.29° and an S1-Co-S2 angle of 129.82° .

Comparisons:

Cobalt complex¹³⁷: $[\text{CoL}^4(\text{mim})]$, where $\text{H}_2\text{L}^4 = N,N'$ -bis(5-mercapto-3-methyl-1-phenylpyrazol-4-ylmethylene)-*o*-phenylenediamine and mim = *N*-methylimidazole

$[\text{CoL}^4(\text{mim})]^*$:

No metal to metal distance
 N-Co distance: $1.984(8)$, $1.966(7) \text{ \AA}$
 S-Co distance: $2.255(3)$, $2.277(4) \text{ \AA}$
 N-Co-N angle: $81.9(3)^\circ$
 S-Co-S angle: $82.2(1)^\circ$
 S(1)-Co-N(1): $97.5(3)^\circ$
 S(2)-Co-N(2): $97.2(3)^\circ$

FcS2-Co:

Metal to Metal distance: 3.969 \AA
 N-Co distance: 2.069 , 2.065 \AA
 S-Co distance: 2.265 , 2.260 \AA
 N-Co-N angle: 133.290°
 S-Co-S angle: 129.82°
 S(1)-Co-N(1): 87.09°
 S(2)-Co-N(2): 87.20°

* five coordinate Co^{2+} complex.

The Co-N bonds became slightly longer and Co-S bonds stayed almost the same in the FcS2-Co complex. A much larger difference was seen in the N1-Co-N2 angle as it increased by 51.36° over the same angle in the $[\text{CoL}^4(\text{mim})]$, but that can be partially attributed to the five coordinate geometry of the Co^{II} atom in $[\text{CoL}^4(\text{mim})]$, as it has smaller angles due to more bonds around the Co center. The S1-Co-S2 angle also increased by 47.61° , while the S-Co-N angles decreased by 10° . The differences can be attributed to the more confined structure of the FcS2-Co complex, since the chelating

groups are both being held in place by the same ferrocene moiety while the [CoL⁴(mim)] complex contains an extra group attached to the Co metal center. Since [FcS1]₂-Co has not yet been reported in the literature, it was synthesized for comparison (listed further on in this section). Unfortunately, no crystals could be grown of this compound suitable for X-ray crystallography. It should have a structure similar to [FcS1]₂-Zn, giving expected distances and angles between those of FcS2-Co and [CoL₄(mim)].

Table 10: Crystal structure of FcS2-Zn

<i>Crystal data</i>	
C ₂₄ H ₁₈ FeN ₂ S ₂ Zn	$D_x = 1.653 \text{ Mg m}^{-3}$
$M_r = 519.74$	Melting point: >573 K
Monoclinic, $P2_1/n$	Mo $K\alpha$ radiation
	$\lambda = 0.71073 \text{ \AA}$
	Cell parameters from 6068 reflections
$a = 7.2002 (5) \text{ \AA}$	$\theta = 2.5\text{--}27.1^\circ$
$b = 19.2667 (12) \text{ \AA}$	$\mu = 2.06 \text{ mm}^{-1}$
$c = 15.2798 (10) \text{ \AA}$	$T = 173 (2) \text{ K}$
$\beta = 99.7670 (10)^\circ$	
$V = 2089.0 (2) \text{ \AA}^3$	Plate, red
$Z = 4$	$0.35 \times 0.20 \times 0.05 \text{ mm}$
$F_{000} = 1056$	
<i>Data collection</i>	
Bruker SMART CCD area detector diffractometer	14762 measured reflections
Radiation source: Mo $K\alpha$	4600 independent reflections
Monochromator: graphite	3688 reflections with $I > 2\sigma(I)$
	$R_{\text{int}} = 0.037$
$T = 173(2) \text{ K}$	$\theta_{\text{max}} = 27.1^\circ$
	$\theta_{\text{min}} = 1.7^\circ$
ω scans	$-7 \leq h \leq 9$
Absorption correction: multi-scan	
Data were corrected for decay and absorption using the program SADABS (Sheldrick, G. M. (2003). SADABS. Version 2.10. University of Göttingen, Germany).	$-24 \leq k \leq 24$
$T_{\text{min}} = 0.63, T_{\text{max}} = 0.90$	$-19 \leq l \leq 19$

*Refinement*Refinement on F^2

Least-squares matrix: full

$$R[F^2 > 2\sigma(F^2)] = 0.032$$

$$wR(F^2) = 0.071$$

$$S = 1.02$$

4600 reflections

271 parameters

Primary atom site location: structure-invariant direct methods

Secondary atom site location: difference Fourier map

Hydrogen site location: inferred from neighbouring sites

H-atom parameters constrained

$$w = 1/[\sigma^2(F_o^2) + (0.0285P)^2 + 0.9836P]$$

$$\text{where } P = (F_o^2 + 2F_c^2)/3$$

$$(\Delta/\sigma)_{\max} = 0.001$$

$$\Delta\rho_{\max} = 0.40 \text{ e} \cdot \text{\AA}^{-3}$$

$$\Delta\rho_{\min} = -0.28 \text{ e} \cdot \text{\AA}^{-3}$$

Extinction correction: none

Color code for the FcS2-Zn crystal structure:

Orange: Fe atom

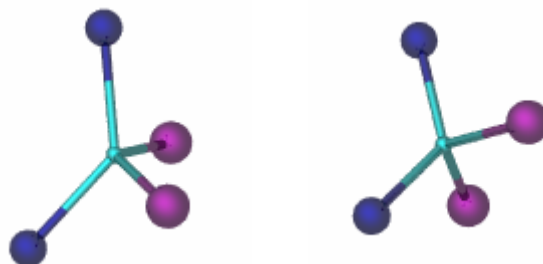
Dark grey: C atom

Light grey: H atom

Dark Blue: N atom

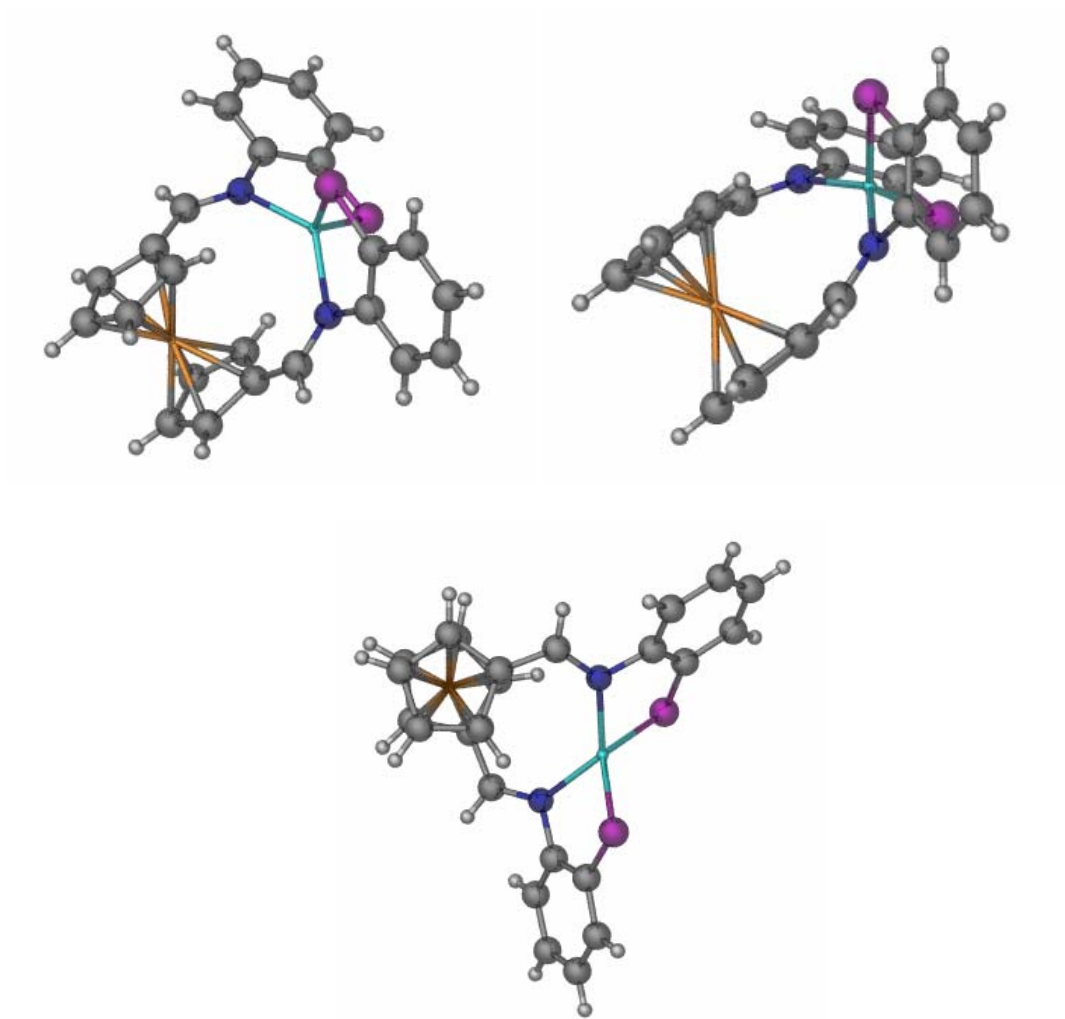
Purple: S atom

Light Blue: Zn atom

Metal geometry:

The Zn^{2+} metal center has distorted tetrahedral geometry in the FcS2-Zn complex.

The angles between the nitrogen atoms in the complex are 132.19° and between the sulfur atoms are 130.15° . The angles between nitrogen and sulfur atoms ranged from 86.65° - 87.35° for those on the same branch and 113.12° - 113.27° for those on different branches.

Asymmetric unit structure:

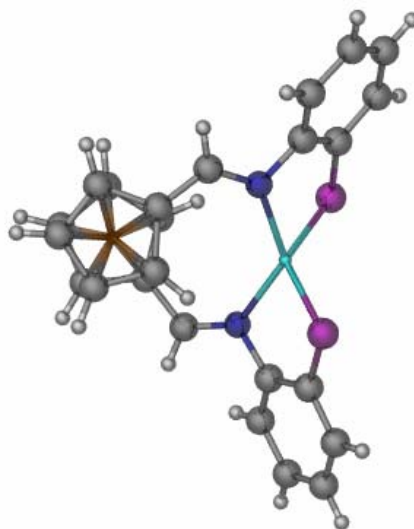
The asymmetric unit for the FcS₂-Zn complex is its whole structure.

Bond Lengths:

C1-C2: 1.43(5) Å	C2-C3: 1.41(1) Å	C3-C4: 1.41(5) Å	C4-C5: 1.41(3) Å
C1-C5: 1.43(4) Å	C1-C6: 1.44(5) Å	C6-N1: 1.28(5) Å	N1-Zn: 2.11(9) Å
N1-C7: 1.43(4) Å	C7-C8: 1.40(8) Å	C8-S1: 1.76(3) Å	S1-Zn: 2.28(3) Å
C8-C9: 1.39(8) Å	C9-C10: 1.38(7) Å	C10-C11: 1.38(2) Å	C11-C12: 1.38(1) Å
C7-C12: 1.39(7) Å	C13-C14: 1.43(4) Å	C14-C15: 1.41(4) Å	C15-C16: 1.42(0) Å
C16-C17: 1.41(2) Å	C13-C17: 1.43(5) Å	C13-C18: 1.44(6) Å	C18-N2: 1.28(5) Å
N2-Zn: 2.11(1) Å	N2-C19: 1.43(7) Å	C19-C20: 1.40(8) Å	C20-S2: 1.76(2) Å
S2-Zn: 2.27(8) Å	C20-C21: 1.39(6) Å	C21-C22: 1.38(5) Å	C22-C23: 1.38(1) Å
C23-C24: 1.38(5) Å	C19-C24: 1.39(0) Å		

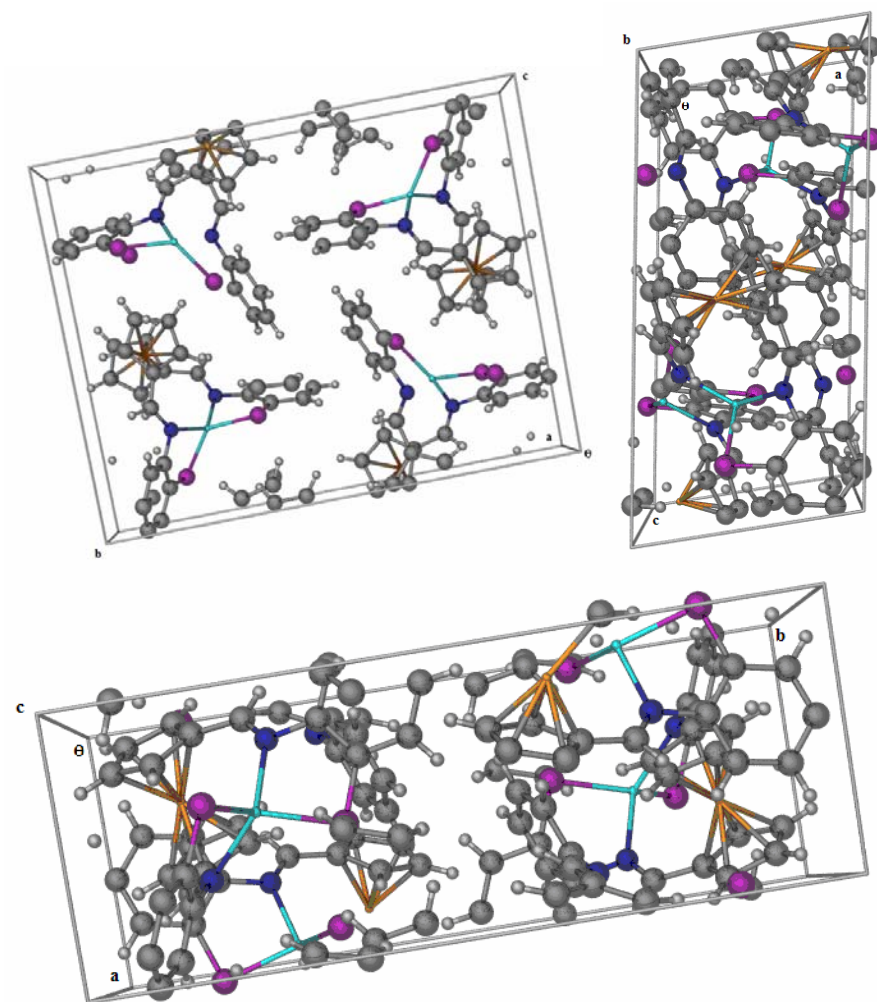
Bond Angles:

C1-C6-N1: 126.2(9) ^o	C6-N1-Zn: 131.3(2) ^o	C6-N1-C7: 117.0(9) ^o
N1-C7-C8: 117.6(9) ^o	C7-C8-S1: 122.2(3) ^o	C8-S1-Zn: 93.7(0) ^o
N1-Zn-S1: 86.6(5) ^o	C13-C18-N2: 124.9(2) ^o	C18-N2-Zn: 131.2(8) ^o
C18-N2-C19: 117.3(2) ^o	N2-C19-C20: 117.9(2) ^o	C18-C19-S2: 122.3(7) ^o
C19-S2-Zn: 93.4(5) ^o	N2-Zn-S2: 87.3(5) ^o	N1-Zn-S2: 113.2(7) ^o
N2-Zn-S1: 113.1(2) ^o	N1-Zn-N2: 132.1(9) ^o	S1-Zn-S2: 130.1(5) ^o

Cp ring overlap:

The Cp rings of the ferrocene unit of the FcS2-Zn complex have been shifted 8^o from being eclipsed (from the FcSH2 ligand structure). This is slightly greater than the FcS2-Co complex (by 3^o).

Unit cell:

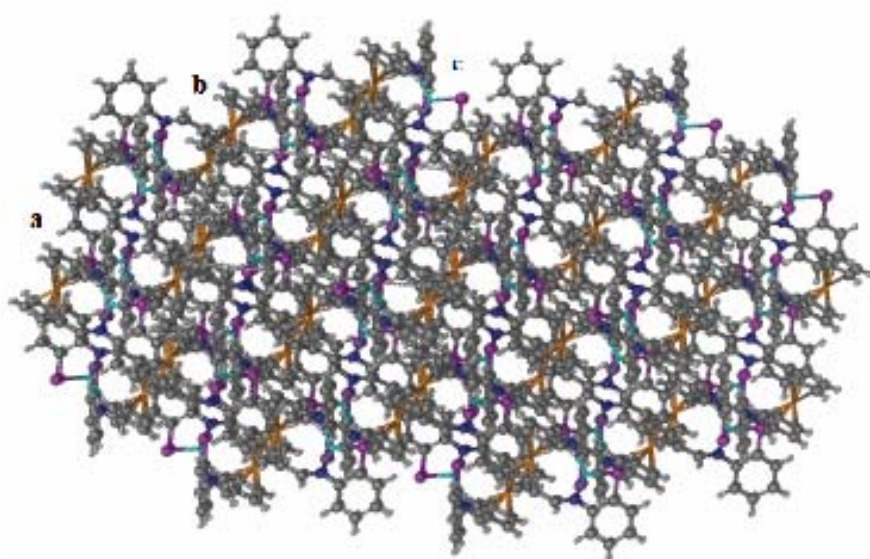
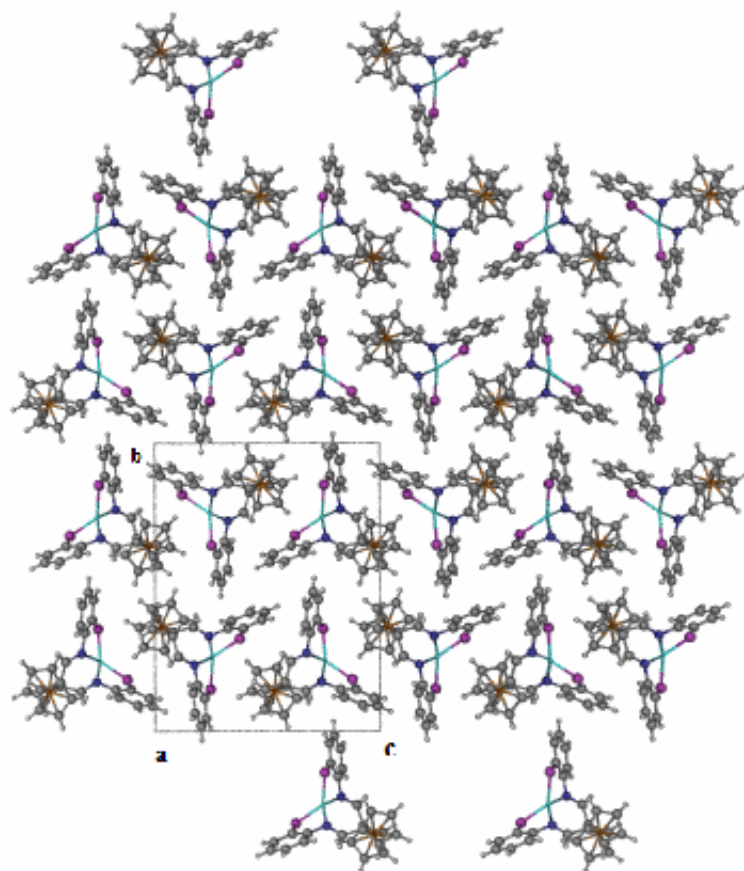


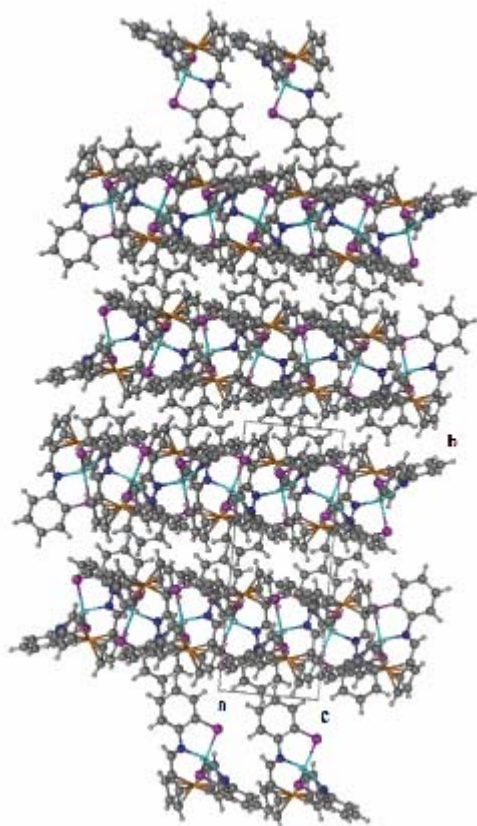
Crystal packing in three directions:

1: Θ along a

2: Θ along b

3: Θ along c





Discussion of the FcS2-Zn crystal structure:

The FcS2-Zn forms dark reddish crystals that crystallize in the monoclinic space group $P2_1/n$. The [FcS1]₂-Zn complex crystallizes in the same group via evaporation of CHCl₃/ethanol according to the literature.¹³² The asymmetric unit is the full molecule. The Cp rings are mostly eclipsed in the solid state, much like in FcS2-Co. Metal to metal distance from the Fe²⁺ atom to the Zn²⁺ atom was 3.984 Å. The Zn²⁺ atom has a tetrahedral geometry containing an N-Zn-N angle of 132.19° and an S-Zn-S angle of 130.15°.

Comparisons:**[FcS1]₂-Zn**¹³²:

Metal to Metal distance: not reported
 N-Zn distance: 2.089(5), 2.062(5) Å
 S-Zn distance: 2.266(2), 2.264(2) Å
 N-Zn-N angle: 106.9(2)^o
 S-Zn-S angle: 123.4(1)^o
 S(1)-Zn-N(1): 88.7(2)^o
 S(2)-Zn-N(2): 89.7(2)^o

FcS2-Zn:

Metal to Metal distance: 3.984 Å
 N-Zn distance: 2.111, 2.119 Å
 S-Zn distance: 2.278, 2.283 Å
 N-Zn-N angle: 132.19^o
 S-Zn-S angle: 130.15^o
 S(1)-Zn-N(1): 87.35^o
 S(2)-Zn-N(2): 86.65^o

The distance for the Zn-N and Zn-S bonds became slightly longer in the FcS2-Zn complex. A much larger difference was seen in the N-Zn-N angle as it increased by 25.27^o over the same angle in [FcS1]₂-Zn. The S-Zn-S angle also increased by 6.74^o, while the S-Zn-N angles decreased slightly by 1-2^o. The differences can be attributed to the more confined structure of the FcS2-Zn complex, since the chelating groups are both being held in place by the same ferrocene moiety.

Table 11: Crystal structure of FcS2-Hg*Crystal data*C₂₄H₁₈FeHgN₂S₂M_r = 654.96Orthorhombic, C222₁

A = 7.7926 (4) Å

B = 17.5924 (8) Å

C = 15.7168 (7) Å

V = 2154.62 (18) Å³

Z = 4

F₀₀₀ = 1256D_x = 2.019 Mg m⁻³

Melting point: 517 K

Mo Kα radiation

λ = 0.71073 Å

Cell parameters from 5902 reflections

θ = 2.3–27.1^oμ = 8.00 mm⁻¹

T = 173 (2) K

Plate, red

0.50 × 0.15 × 0.05 mm

Data collection

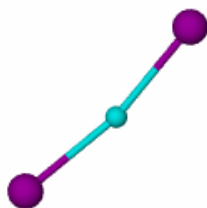
Bruker SMART CCD area detector diffractometer	7762 measured reflections
Radiation source: Mo $K\alpha$	2400 independent reflections
Monochromator: graphite	2261 reflections with $I > 2\sigma(I)$
	$R_{\text{int}} = 0.028$
$T = 173(2)$ K	$\theta_{\text{max}} = 27.1^\circ$
	$\theta_{\text{min}} = 2.3^\circ$
Ω scans	$-10 \leq h \leq 9$
Absorption correction: multi-scan	
Data were corrected for decay and absorption using the program SADABS (Sheldrick, G. M. (2003). SADABS. Version 2.10. University of Göttingen, Germany).	$-22 \leq k \leq 17$
$T_{\text{min}} = 0.36$, $T_{\text{max}} = 0.69$	$-20 \leq l \leq 20$

Refinement

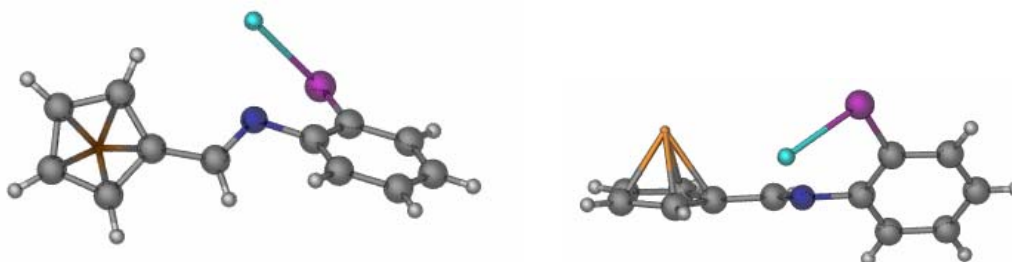
Refinement on F^2	Hydrogen site location: inferred from neighbouring sites
Least-squares matrix: full	H atoms treated by a mixture of independent and constrained refinement
$R[F^2 > 2\sigma(F^2)] = 0.019$	$w = 1/[\sigma^2(F_o^2) + (0.0076P)^2 + 1.6112P]$
$wR(F^2) = 0.039$	where $P = (F_o^2 + 2F_c^2)/3$
$S = 1.09$	$(\Delta/\sigma)_{\text{max}} = 0.001$
2400 reflections	$\Delta\rho_{\text{max}} = 0.99 \text{ e} \cdot \text{\AA}^{-3}$
138 parameters	$\Delta\rho_{\text{min}} = -0.65 \text{ e} \cdot \text{\AA}^{-3}$
	Extinction correction: none
	Absolute structure: Flack H D (1983), Acta Cryst. A39, 876-881
Primary atom site location: structure-invariant direct methods	Flack parameter: 0.351 (8)
Secondary atom site location: difference Fourier map	

Color code for the FcS2-Hg crystal structure:

Orange: Fe atom
 Dark grey: C atom
 Light grey: H atom
 Dark Blue: N atom
 Purple: S atom
 Light Blue: Hg atom

Metal geometry:

The Hg^{2+} metal center has a nearly linear geometry in the $\text{FcS}_2\text{-Hg}$ complex. The bond angle between sulfur groups is 166.10° .

Asymmetric unit structure:

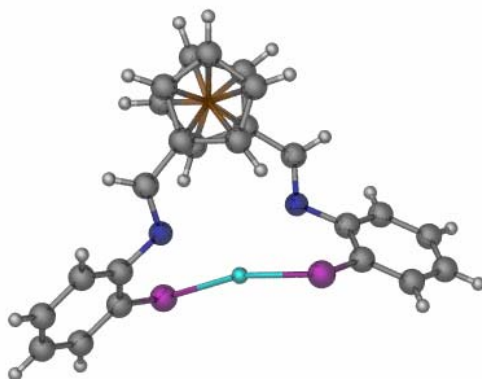
The asymmetric unit for the $\text{FcS}_2\text{-Hg}$ complex is one half of the whole structure, since both the Fe^{2+} and the Hg^{2+} atoms lay on a 2-fold rotation axis. The rest of the complex can be produced using operations.

Bond Lengths:

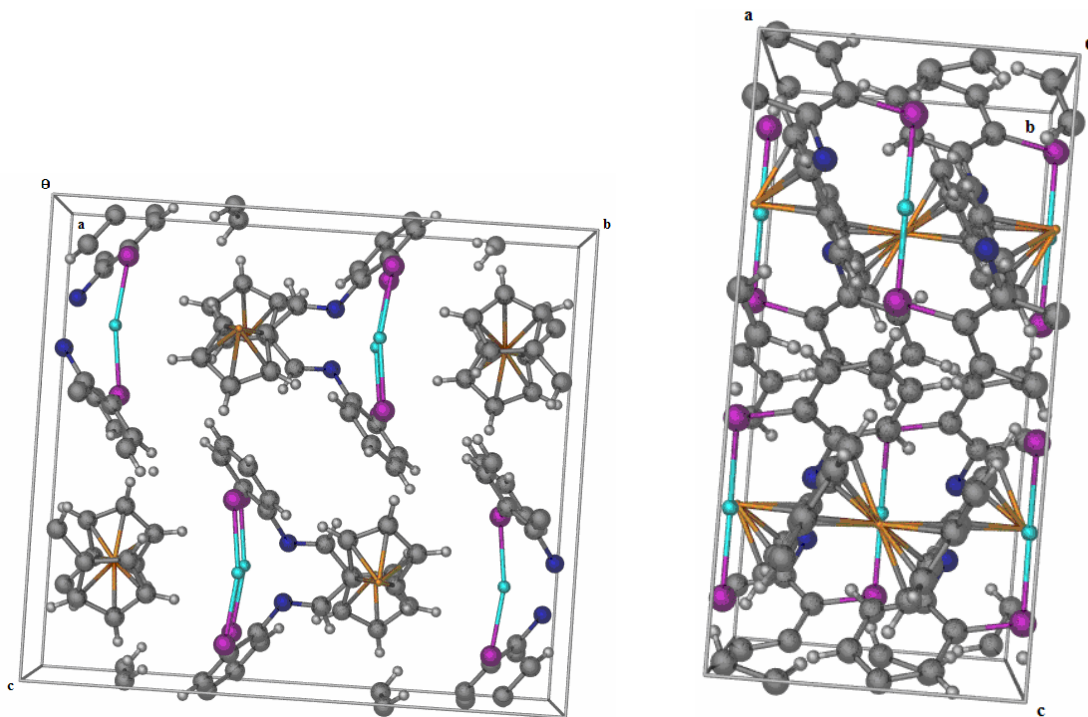
C1-C2: 1.42(7) Å	C2-C3: 1.41(3) Å	C3-C4: 1.41(6) Å	C4-C5: 1.40(1) Å
C1-C5: 1.43(6) Å	C1-C6: 1.46(1) Å	C6-N1: 1.27(9) Å	N1-Hg: 2.70(9) Å
N1-C7: 1.42(7) Å	C7-C8: 1.40(2) Å	C8-S1: 1.76(8) Å	S1-Hg: 2.35(1) Å
C8-C9: 1.40(8) Å	C9-C10: 1.38(3) Å	C10-C11: 1.37(3) Å	C11-C12: 1.39(6) Å
C7-C12: 1.38(3) Å			

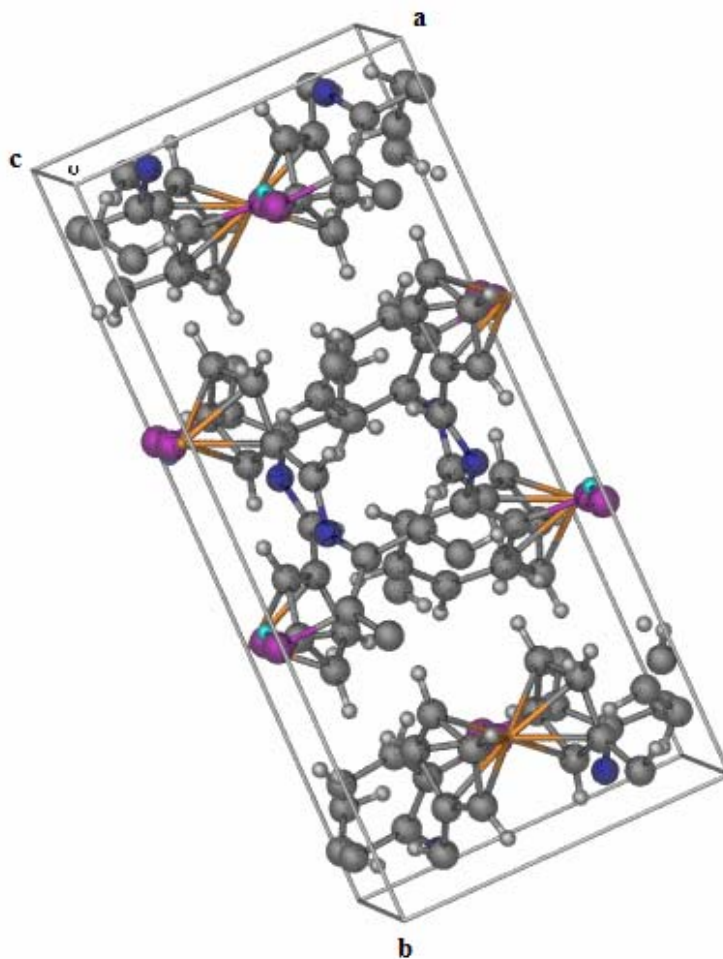
Bond Angles:

C1-C6-N1: 124.1(7) $^\circ$	C6-N1-C7: 116.1(5) $^\circ$	N1-C7-C8: 119.1(2) $^\circ$
C7-C8-S1: 122.7(4) $^\circ$	C8-S1-Hg: 100.7(6) $^\circ$	S1-Hg-S2: 166.1(0) $^\circ$

Cp ring overlap:

The Cp rings of the ferrocene unit of the FcS2-Hg complex has been shifted 12° from being eclipsed (from the FcSH2 ligand structure). This is greater than both FcS2-Co and FcS2-Zn. One reason why this is occurring might be due to the preferred linear geometry around the Hg²⁺ center causing the chelating side groups to spread further out than they normally would to accommodate the Hg²⁺ cation.

Unit cell:

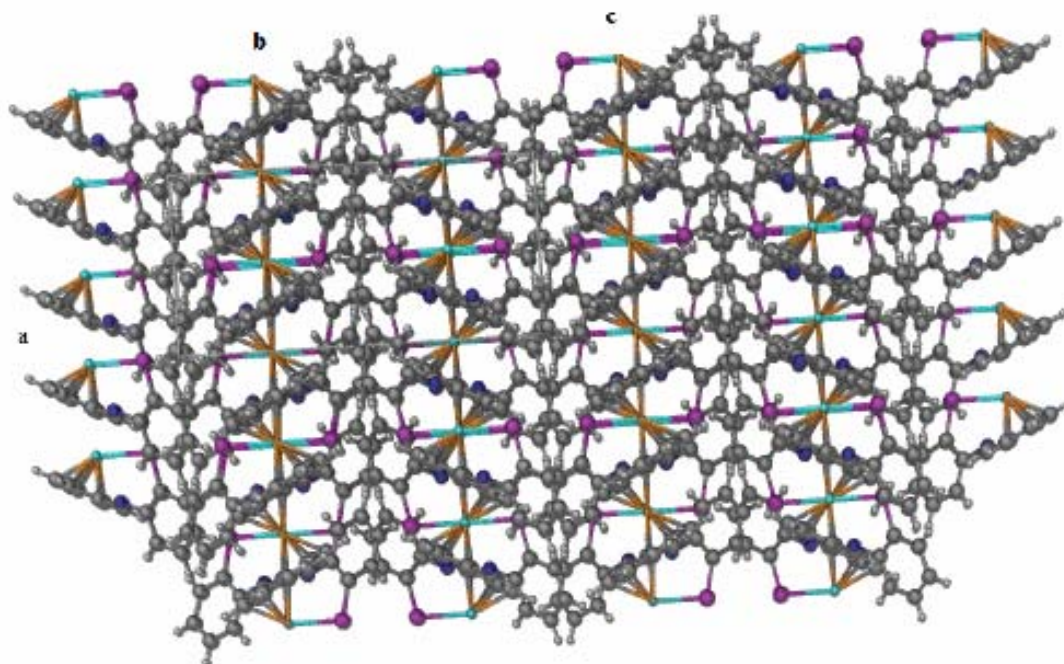
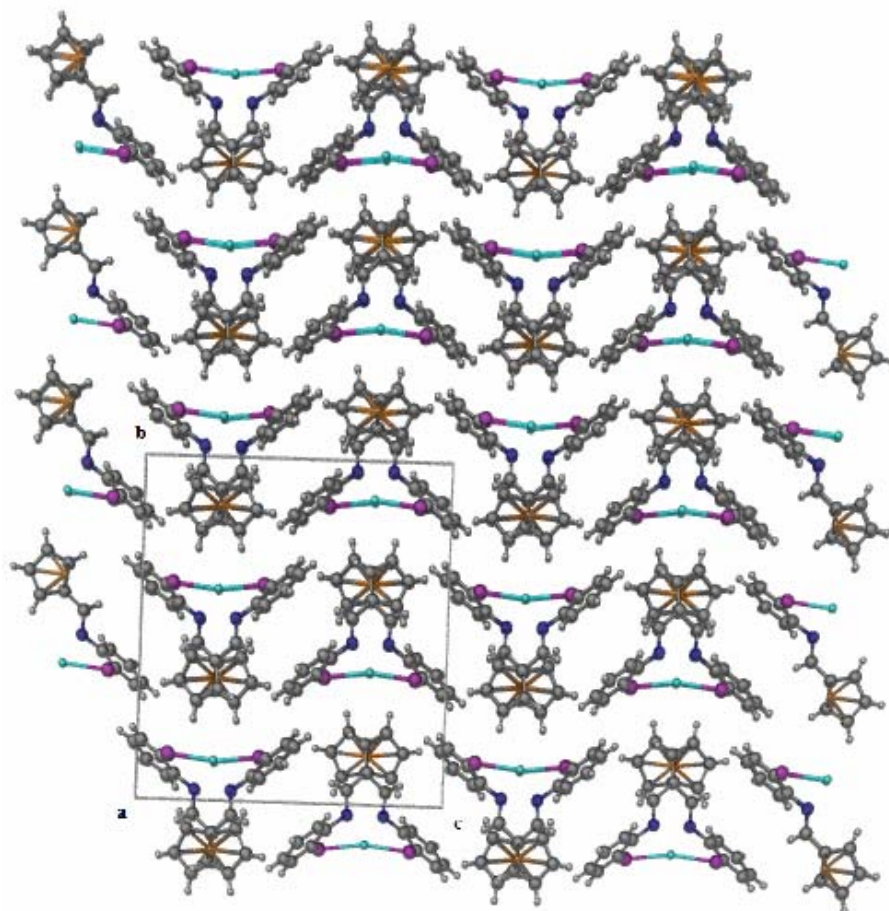


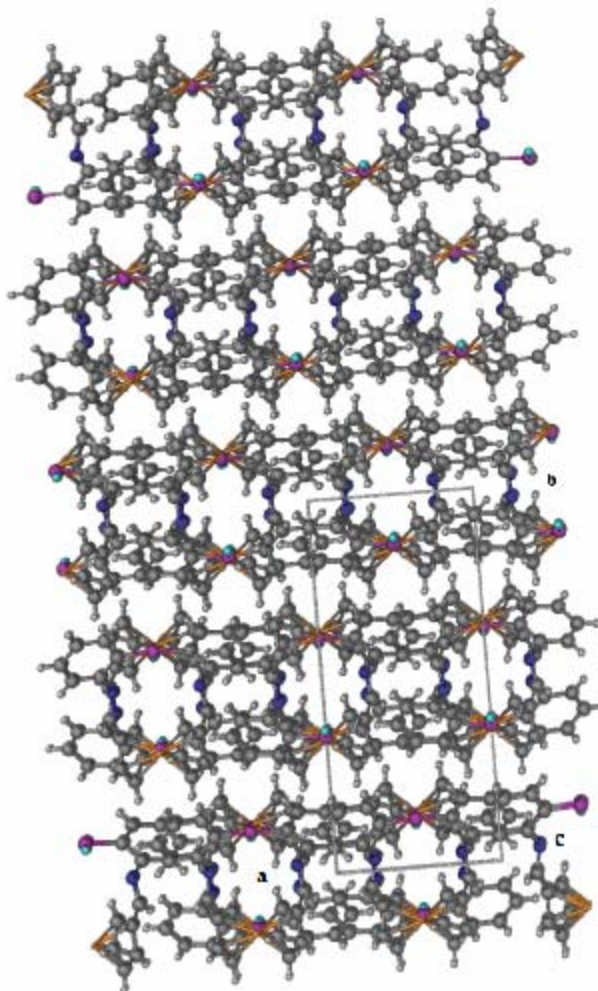
Crystal packing in three directions:

1: Θ along a

2: Θ along b

3: Θ along c





Discussion section for the FcS2-Hg crystal structure:

The FcS2-Hg forms dark reddish crystals that crystallize in the orthorhombic space group $C222_1$. The $[\text{FcS1}]_2\text{-Hg}$ complex crystallizes out of CHCl_3 /ethanol in the triclinic space group $P\bar{1}$ (same as the FcSH2 ligand) according to the literature.¹³² The asymmetric unit is one half of the molecule, since both Fe^{2+} and Hg^{2+} lie on a two-fold rotation axis. The Cp rings are partially staggered in the solid state (12°), more than in either FcS2-Co or FcS2-Zn. This could be the reason why there are four Cp peaks occurring in the ^1H NMR rather than the typical two spectral peaks for 1,1'-disubstituted ferrocenes, since each set of protons on the Cps are no longer equivalent to the protons on

the other Cp ring. The metal to metal distance between the Fe²⁺ atom and the Hg²⁺ atom was 4.539 Å, half a Å longer than in either FcS2-Co or FcS2-Zn. This can be attributed to the very slight imine interactions with the Hg^{II} center and the much stronger Hg-S binding within the molecule. The geometry around the Hg^{II} metal center is a slightly bent-linear, with an S1-Hg-S2 angle of 166.10°. That is much greater than in either FcS2-Co or FcS2-Zn, both containing distorted tetrahedral geometries around the Co²⁺ and Zn²⁺ atoms.

Comparisons:

[FcS1]₂-Hg¹³²:

Metal to Metal distance: not reported
 N-Hg distance: 2.808(13), 2.860(14) Å
 S-Hg distance: 2.345(4), 2.329(4) Å
 N-Hg-N angle: 131.6(3)°
 S-Hg-S angle: 174.0(1)°
 S(1)-Hg-N(1): 73.2(2)°
 S(2)-Hg-N(2): 72.2(2)°

FcS2-Hg:

Metal to Metal distance: 4.539 Å
 N-Hg distance: 2.709, 2.709 Å
 S-Hg distance: 2.351, 2.351 Å
 N-Hg-N angle: 113.41°
 S-Hg-S angle: 166.10°
 S(1)-Hg-N(1): 74.21°
 S(2)-Hg-N(2): 74.21°

The distance for the Hg-N bonds became slightly shorter in the FcS2-Hg complex, while the Hg-S bond distances stayed almost the same. A much larger difference was seen in the N1-Hg-N2 angle as it decreased by 18.19° over the same angle in [FcS1]₂-Hg. It is important to note that in both complexes, the imine nitrogens have an intermolecular interaction with the Hg²⁺, although a formal bond does not seem to be present (indicated by the very large S1-Hg-S2 bond angle in both complexes). The S1-Hg-S2 angle also decreased by 7.91°, while the S-Hg-N angles increased slightly by 1-2° in FcS2-Hg. The resulting differences are opposite than the comparative results for the [FcS1]₂-Zn/FcS2-Zn complex comparisons.

Colorimetric (IR, UV-Vis):

The IR spectra for complexes **21-29** all contain the imine stretch and the ferrocene Cp ring stretch that occur at 1643 cm^{-1} and 890 cm^{-1} , respectively. One major difference is in the N-H stretch that occurs at 3346 cm^{-1} in **21** due to the ring closed tautomerized form in the solid state. If the open form had occurred in the solid state, an S-H stretch should have been visible in the range of $2800\text{-}2900\text{ cm}^{-1}$, but this was not present in the IR spectrum for **21**. The N-H stretch can be used as an identification technique to determine the presence (and concentration based on size of peak) of free ligands within a product. None of the measured complexes for FcS2-M showed this particular peak in their IR spectra. Based upon this result, IR will not be a useful identification technique for selectivity experiments, since the presence of free ligand can also be readily seen via melting point changes.

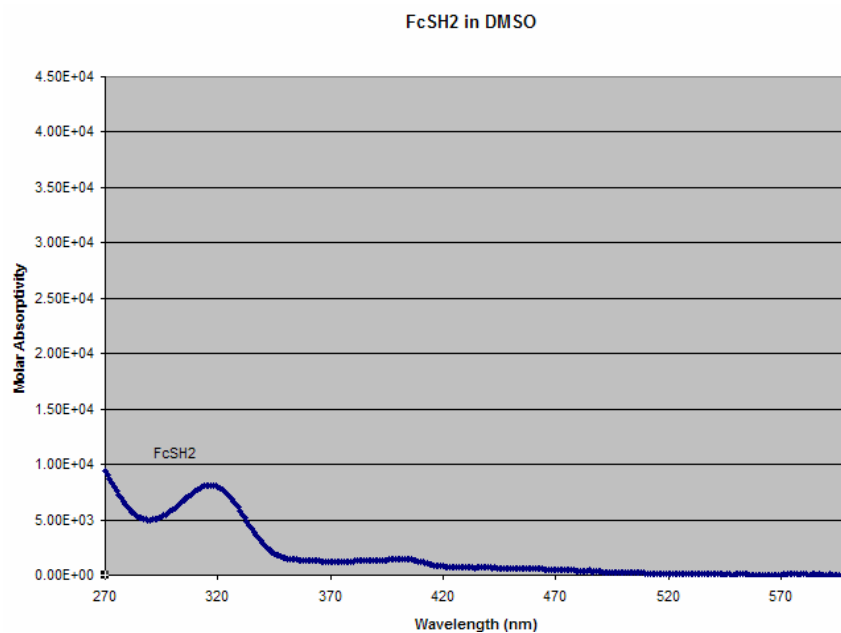


Figure 4.9: Molar absorptivity (UV-Vis) of the FcSH2 ligand in DMSO. The bands at 470 and 317 nm correspond to d-d transitions.

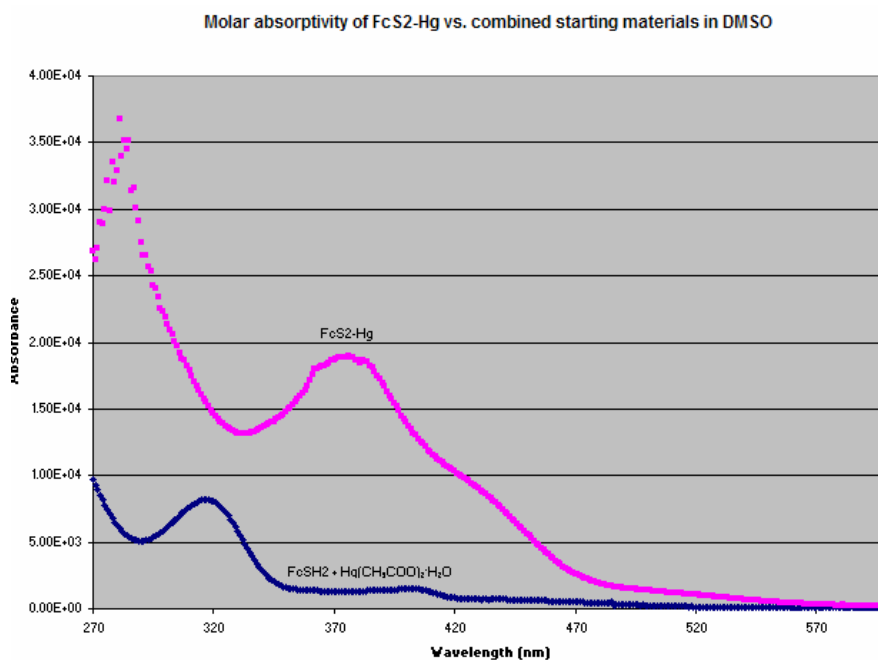


Figure 4.10: Comparison between the molar absorptivity (UV-Vis) of FcS2-Hg and the molar absorptivity of the combined starting materials in DMSO. The FcS2-Hg complex has undergone a red shift from 317 nm to 376 nm upon Hg^{2+} complexation, whereby the intensity greatly increased due to more p characterization within the electron orbitals.

The molar absorptivity spectrum for **21** shows two primary peaks, 317 nm and 402 nm due to d-d and d-ligand transitions (Figure 4.9). These transitions typically occur in ferrocene derivatives, although the wavelenths of the two peaks are shifted depending upon the attached groups.¹²⁶ All of the FcS2-M complexes (with the exception of **26**) showed an increase in the molar absorptivity over the starting materials (hyperchromic shift). This could be due to the potential influence of an intensity stealing mechanism¹³⁸, whereby the orbitals become lowered enough in energy upon metal chelation that some normally forbidden transitions are easily accessed. This causes the absorption to increase over what would normally be expected. The FcS2-M complexes are very dark in color, with the exception of **28**. The molar absorptivity of compound **28** can be used as a means

to identify it over the other complexes due to the red shifting (bathochromic shift) of the 317 nm FcSH₂ peak to 376 nm (Figure 4.10). Other complexes shift this peak to 309 nm (**22**), 392 nm (**23**), 406 nm (**24**), 409 nm (**26**), 392 nm (**27**), and 361 nm (**29**). **25** does not have a distinctive peak within the range of the instrument. Thus, UV-Vis spectroscopy can be used to determine the formation of **28** within a sample even if other FcS₂-M complexes are present. It can also be used to determine if any other metals are present in moderate concentrations when testing selectivity products.

Electrochemistry:

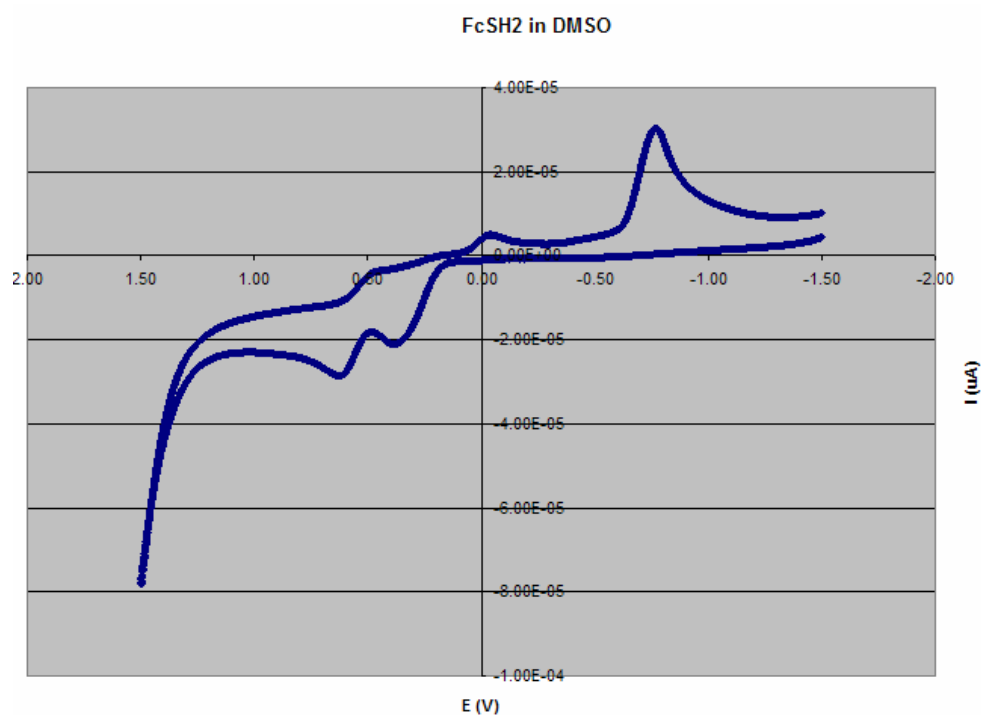


Figure 4.11: CV of the FcSH₂ ligand in DMSO, scan rate 100 mV/second. The oxidation peak at 400 mV is due to an irreversible oxidation of the ligand (R-SH moiety quite possibly), while the peak at 600 mV is due to the Fe^{II} to Fe^{III} oxidation of the ligand.

Compound **21** has two main oxidative peaks in the positive voltage range when measured in 1×10^{-3} M TBAHFP/DMSO solution (Figure 4.11). One is due to the $\text{Fe}^{\text{II}}-\text{Fe}^{\text{III}}$ couple around 627 mV (vs. 0.01 M Ag/AgNO₃ in DMSO) and the other is an irreversible oxidation that is occurring within the complex (more than likely due to the thiol groups) at 389 mV. Upon metal chelation, the irreversible oxidation disappears and each metal product shifts the $\text{Fe}^{\text{II}}-\text{Fe}^{\text{III}}$ couple to differing degrees. This shifting is a common occurrence with ferrocene derivatives in the literature.

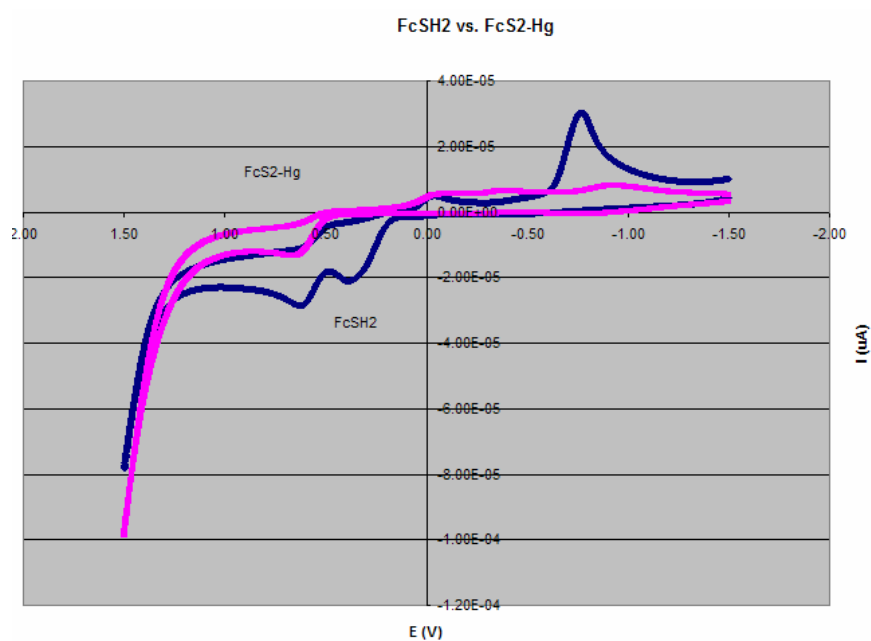


Figure 4.12: Comparison between the CV of FcS2-Hg and the CV of FcSH2 in DMSO, scan rate 100 mV/sec. The FcS2-Hg complex has shifted the Fe^{II} oxidation to 663 mV (furthest positive potential of all FcS2-M complexes).

Compound **28** has the greatest positive potential shift for this couple at 663 mV (Figure 4.12), which can be used as an identification marker for the electrochemical sensing for the presence of this compound in solution. The shifting of the $\text{Fe}^{\text{II}}-\text{Fe}^{\text{III}}$ potential occurs because the electron density around the molecule changes upon metal chelation. In this case, it causes the Fe^{2+} moiety to become harder to oxidize (anodic

shift). The Fe^{2+} metal center has a more electropositive metal atom neighbor when chelated, so more potential is needed to remove an electron from the metal center which translates to a leftward movement of the $\text{Fe}^{\text{II}}\text{-Fe}^{\text{III}}$ peak. **28**, contains a very electropositive metal center and shows this positive potential shifting the most, while **29** has a lesser shifting effect (602 mV) since it has two more valence electrons. **27** shows a similar shifting as **29** for that coupling (602 mV), but it also undergoes an irreversible oxidation at (445 mV). **26** has only a single coupling (495 mV) due to less electron density around the iron center compared to the heavier members of the same group. The transition metal complexes of **22**, **23** and **24** show potential in the range of 585-598 mV (see Table 8 and Table 12 for specifics), while **25** does not appear to show a $\text{Fe}^{\text{II}}\text{-Fe}^{\text{III}}$ coupling potential in the CV spectrum. Since the transition metals have a narrow coupling range that is less positive in potential than Hg^{2+} , their concentration does not inhibit the detection of compound **28** that will form in the presence of Hg^{2+} . Based upon these findings, CV is a useful tool for identifying selectivity products from the FcSH2 ligand system.

Table 12: CV data comparisons for FcSH2 and metal complexes vs. ferrocene.

<u>Compound</u>	<u>$\text{Fe}^{\text{II}}\text{-Fe}^{\text{III}}$ couple (mV)</u>	<u>Difference (mV)</u>
Ferrocene	388	
FcSH2	389, 627	1, 239
FcS2-Fe	585	197
FcS2-Co	599	211
FcS2-Ni	592	204
FcS2-Cu	none	-----
FcS2-Zn	495	107
FcS2-Cd	(445), 602	(57), 214
FcS2-Hg	663	275
FcS2-Pb	602	214

A New Unreported [FcS1]₂-M Complex:**Synthesis of [FcS1]₂-Co: (30)**

To a dried, N₂ flushed Schlenk flask containing a stir bar, 200 mg of FcSH1 (4.38×10^{-4} mol), 80 mg of Co(CH₃COO)₂·4H₂O (3.21×10^{-4} mol), and 70 mL of ethanol were added. The solution was allowed to reflux for three hours, cooled, filtered through a frit, washed with cold ethanol and dried under a vacuum. Amount recovered: 180 mg (2.57×10^{-4} mol, 82.7 % yield), mp >300°C, ¹H NMR (CDCl₃): 58.48 ppm (1H, broad s), 41.92 ppm (1H, s), 34.59 ppm (1H, broad s), 16.82 ppm (1H, s), 6.25 ppm (1H, s), 4.28 ppm (3H, s), -7.96 ppm (1H, s), -9.99 ppm (5H, s), -21.51 ppm (1H, broad s), see Appendix (Figure A35) for spectra., paramagnetic compound.

Spectral Database Comparisons of Disubstituted Ligand Systems:

The three 1,1'-disubstituted ferrocene ligand systems can be used to study the electronic, magnetic and other changes that occur when metal cations become chelated to the imines and any other possible chelating groups that are present on the ortho position on the phenyl ring. The spectroscopic data are important in the potential designing of better ferrocene chemical sensors in the future. For example, changing the chelating groups or modifying the phenyl system to one that has better fluorescence might improve the desired spectral properties. The ¹H NMR data are particularly useful in obtaining structural information about each complex. Since the signal peaks are directly related to both the coupling of nearby protons and other groups, peaks that are shifted from a previously measured position can indicate changes occurring within the molecule. For

instance, 1,1'-dicarbaldehyde ferrocene has a singlet peak at 9.95 ppm that can be attributed to the carbaldehyde protons (the two peaks corresponding to the Cp protons lie in the 4.5-4 ppm range). Once the 1,1'-dicarbaldehyde ferrocene is reacted with aryl amines, the product formed no longer contains a carbaldehyde proton off of the Cp rings. Instead, the previously carbaldehyde proton is now next to an imine nitrogen, which shifts the location of the corresponding NMR peak into the 8-9 ppm range (with the exception of the FcSH2 ligand due to the DRCT effect).

The crystal structure data from FcSH2, FcS2-Co, FcS2-Zn and FcS2-Hg can be used to understand the geometric changes that occur in the system upon metal chelation. If a great conformational change occurs during the formation of the product, the resulting spectral data can be used to help further signal the creation of that complex.

UV-Vis Molar Absorptivity (DMSO):

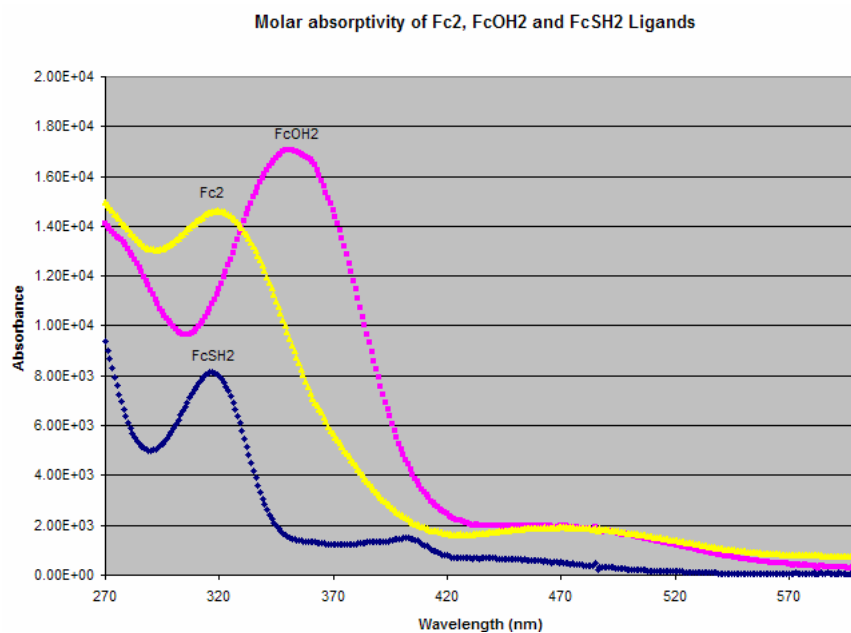


Figure 4.13: Molar absorptivity (UV-Vis) of the three ligand systems in DMSO: Fc2 (yellow), FcOH2 (blue) and FcSH2 (purple)

Peak locations:

Fc2: 319 nm, 470 nm

FcOH2: 351 nm, 463 nm

FcSH2: 317 nm, 402 nm

UV-Vis molar absorptivity spectra (Figure 4.13) can give insight into what is occurring within the electron orbitals of each complex. Red-shifting of peaks in the spectra of metal complexes indicate that the system has undergone a lowering in the energy of one of the electron orbitals, leading to a lower energy band (longer wavelength) in the spectrum.¹²⁶ Based upon the molar absorptivity data for the Fc2 ligand system, the metal complexes undergo a decrease in absorptivity when compared to the combined starting materials. By binding a metal chloride to the Fc2 ligand, the absorption signal decreases (an expected result).

Most of the metal complexes of the FcOH2 system undergo a decrease in molar absorbance over the starting materials for the 351 nm peak (high energy) of the ligand. While many of the spectra are similar for this ligand system, there is one large exception that allows UV-Vis spectroscopy to be used in identifying some of the selectivity products. The FcO2-Pb complex has a molar absorptivity spectrum that is almost as intense as the combined starting materials and the first peak (high energy) is red shifted to 436 nm. Since Pb^{2+} is the target metal for the selectivity experiments for this ligand system, UV-Vis can be used to determine if **18** forms in the presence of other metal cations. If other metal complexes are present, the first peak should be less intense and possibly shifted to a shorter wavelength.

The metal complexes of the FcSH2 ligand system undergo a great increase in molar absorptivity over the starting materials with the exception of FcS2-Zn. This could be a sign of an intensity stealing mechanism occurring within the complexes. In most cases, the 317 nm band undergoes a red shift, indicating a lowering of the energy in some orbitals. The Hg²⁺ target has a very specific red shift that is located at a different wavelength from any other metal complex, allowing for a means of detection of the presence of **28**. UV-Vis spectroscopy can be used to determine the products that are formed during a selectivity test using the FcSH2 ligand.

Cyclic Voltammetry (DMSO) of Fc, FcOH2 and FcSH2:

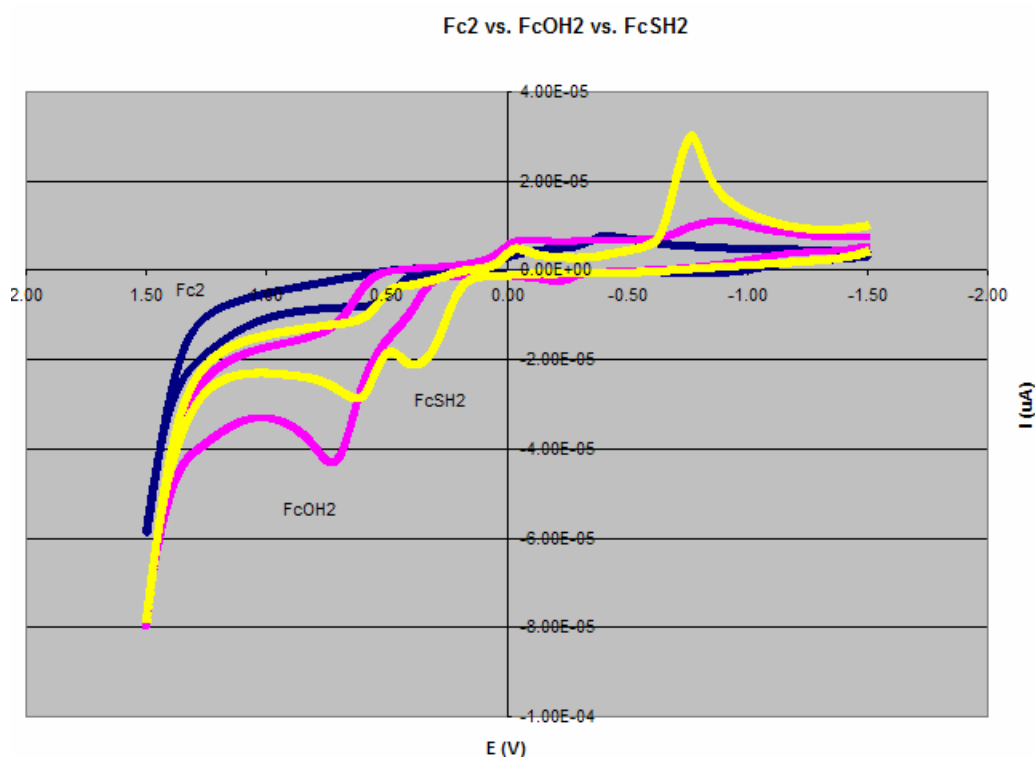


Figure 4.14: Combined CV scans of the three ligand systems: Fc2 (purple), FcOH2 (blue) and FcSH2 (yellow)

Peak locations, bold font is for Fe^{2+/3+} couple within ligand:

Fc2 ligand: **412 mV**

FcOH2 ligand: -816 mV, **725 mV**, -102 mV, -888 mV

FcSH2 ligand: 389 mV, **627 mV**, -42 mV, -788 mV

The CVs of each metal compound (Figure 4.14) show a change over the free ligands due to possible metal-to-metal or metal-to-ligand electronic communication that can occur and the possible change in the redox potential due to the presence of another metal center. The Fc2 ligand system undergoes a positive shift for each of the metal complexes that can be used to identify species, although some mixtures might be hard to quantify. The FcOH2 system had only a few metal complexes that gave measurable Fe^{II}-Fe^{III} couples, so CV would not be very useful for identification purposes, including the target Pb²⁺. The FcSH2 system gave electrochemical spectra that can be used to measure each metal compound, with the target Hg²⁺ complex having the most positive potential for the iron coupling.

Conclusion for the FcSH2 system:

The addition of soft donor thiol groups to some of the ortho positions on the phenyl ring of the Fc2 ligand formed the DRCT system, FcSH2. This ligand system is a good candidate for a potential multidetection sensor for Hg²⁺ based upon well known chemistry of Hg²⁺ and thiol groups. This can also explain the high yield for compound **28**, since the Hg will form a strong covalent bond with the sulfur atoms quite rapidly.

Another reason why the FcSH2 ligand system is a good candidate for possible Hg²⁺ sensing is because it has at least four possible modes of detection for complex **28**, even if other metal compounds are present. Although it decomposes at around 245 °C, which is much different from the other melting points for the same system when measured using the same melting point apparatus, this method is not used to identify products out in the field. ¹H NMR (either CDCl₃ or d₆-DMSO) can be used to identify the presence of the mercury complex based upon the location of the Cp-CH=N-R peak and one of the Cp peaks that have unique chemical shifts. The MS data for complex 28 gave a strong M+1 peak that can be identified. The electrochemical detection of the mercury complex can be done since it changes the Fe^{II}-Fe^{III} coupling to the highest positive potential of all of the metal complexes that formed from this system.

The most important detection technique for the metal complexes is UV-Vis spectrophotometry. Upon metal chelation, the 317 nm band (in DMSO) shifts depending upon the metal center and the intensity of the absorption increases greatly. Complex **28** undergoes a red shift to 376 nm, which is not close to other metal complex peaks. Since UV-Vis is a non-intrusive technique, clear glass (or quartz) probes might be used with a solution of this ligand for measurements out in the field. Since the FcSH2 ligand system has multiple detection possibilities with the target cation, the selectivity of the system will dictate whether or not it can be actually used as a heavy metal sensor for Hg²⁺.

-
- ¹³⁰ Szatmari, I.; Martinek, T. A.; Lazar, L.; Koch, A.; Kleinpeter, E.; Neuvonen, K.; Fulop, F., Stereoelectronic Effects in Ring-Chain Tautomerization of 1,3-Diarylnaphth[1.2-e][1,3]oxazines and 3-Alkyl-1-arylnaphth[1,2-e][1,3]oxazines. *J. Org. Chem.* **2004**, 69, (11), 3645-3653.
- ¹³¹ Palmer, P. J.; Trigg, R. B.; Warrington, J. V., Benzothiazolines as Antituberculous Agents. *J. M. Chem.* **1971**, 14, (3), 248-251.
- ¹³² Kawamoto, T.; Kushi, Y., Helical Bis[2-(ferrocenylmethyleneamino)benzenethiolato] Metal(II) Complexes (M = Ni, Zn or Pd) and a Related Mercury(II) Complex. *J. Chem. Soc. Dalton Trans.* **1992**, (2), 3137-3143.
- ¹³³ Nagasawa, I.; Kawamoto, T.; Kuma, H.; Kushi, Y., A Pair of Trans and Cis-Isomers of Platinum(II) Schiff Base Complex with N, S Chelate Containing Ferrocenyl Pendent Groups. *Bull. Chem. Soc. Jpn.* **1998**, 71, 1337-1342.
- ¹³⁴ Nagasawa, I.; Kawamoto, T.; Kuma, H.; Kushi, Y., A Novel Trinuclear Platinum(II) Complex with C, N, S Donor Ligands Containing Ferrocenyl Groups. *Chemistry Letters* **1996**, 921-922.
- ¹³⁵ Kawamoto, T.; Kushi, Y., Synthesis and Characterization of Trinuclear Metal-Complex Showing Helical Chirality. *Chem. Lett.* **1992**, (2), 297-300.
- ¹³⁶ Nishio, T., Direct Conversion of Alcohols into Thiols. *J. Chem. Soc. Perkin Trans.* **1993**, 1 (10), 1113-1117.
- ¹³⁷ Nivorozhkin, A.; Toftlund, H.; Nielsen, M., Spin Equilibrium in Five-co-ordinate Lewis-base Adducts of Cobalt(II) Schiff-base Complexes with a S₂N₃ Ligand Environment. Molecular and Crystal Structure of [CoL⁴(mim)] at 293 and 103 K [H₂L⁴ = N,N'-bis(5-mercapto-3-methyl-1-phenylpyrazol-4-ylmethylene)-o-phenylenediamine, mim = N-methylimidazole] *J. Chem Soc. Dalton Trans.* **1994**, 361-367.
- ¹³⁸ Decurtins, S.; Guelel, H.U.; Pfeuti, A.; Optical spectroscopy of [(NH₃)₄Cr(OH)₂Cr(NH₃)₄]⁴⁺ and [(en)₂Cr(OH)₂Cr(en)₂]⁴⁺. *Inorg. Chem.*, **1982**, 12, (3), 1101-6.

Chapter Five

Cationic Selectivity of Fc2, FcOH2 and FcSH2 Ligand Systems:

Chemical sensors have an important role in protecting the environment. By designing chemical sensors that interact with specific chemical species in a way that can be detected, the sensor becomes selective in function. The selectivity of a ligand can be proven by testing potential chemical sensors with a mixture of species with which it may interact. In some cases, this will lead to competition between products, which are an indication that the ligand cannot be used as a specific chemical sensor without modification. Furthermore, the chelating ability of the potential sensor can be compared with a known sensor for a particular species through a competition reaction. If one system forms the only product, then it has a stronger binding ability than the other system for species at that concentration.

In the case with the Fc2, FcOH2, and FcSH2 systems, solutions that contain a known concentration of all eight metal cations (Fe^{2+} , Co^{2+} , Ni^{2+} , Cu^{2+} , Zn^{2+} , Cd^{2+} , Hg^{2+} , and Pb^{2+}) were reacted with each of the respective ligands. The reactions were carried out under the same conditions that were used to form the metal complexes for the database (at ppm levels). The spectral database of compounds **1-18**, **20-28** (see appendix) was used to determine any potential metal complexes that formed during the mixed metal reactions.

In the case of the Fc2 ligand system, no obvious selectivity was noticed in the liquid portion, upon drying, after the reaction (although the color became quite dark). The ^1H NMR and UV-Vis spectra were taken for comparison with the database. Both showed that there was no clear single metal product formed during the reaction, leading to the

conclusion that it is not specific for one metal cation over the others in a (1:1) mixed solution.

In the case of the FcOH₂ ligand system, the dark precipitate formed during the mixed metal reaction did not show one particular product when analyzed by ¹H NMR as the spectral peaks did not match the database of any of the metal complexes. Since both the FcOH₂ ligand and the metal acetates are soluble in the solvent, leftover starting materials could be removed from the product upon washing with ethanol. UV-Vis spectra obtained in ethanol indicate that the major product is FcO₂-Pb due to the red shifting of the major ligand peak from 317 nm to 330 nm (although it would have shifted completely to 338 nm if only FcO₂-Pb was present).

In the case of the FcSH₂ ligand system, only the FcS₂-Hg product was formed during the mixed metal reaction at two different concentrations. This product was identified by color, ¹H NMR and UV-Vis (red shift from 317 nm to 376 nm) with no indication that any other metal complex (or FcSH₂) was present. X-ray fluorescence showed that the major product is **28**. The possibility of unbound Hg²⁺ was tested by reacting the filtered liquid solution of the 1.37x10⁻³ M mixed metal solution with 2-aminothiophenol. 2-aminothiophenol forms an *Bis*[organothiolato] mercury complex, Hg(H₂N-Ph-o-S)₂, when exposed to Hg²⁺ under reflux conditions in ethanol. An amount of this product was prepared and analyzed by both ¹H NMR and UV-Vis spectroscopy for use in identifying any unreacted Hg²⁺ that was in the 3.5x10⁻⁵ M mixed metal solution. After reviewing the data, no free Hg²⁺ was present in the solution, which means that the FcSH₂ ligand is very selective for Hg²⁺ and does not form other metal complexes in the presence of Hg²⁺. This

result was expected based upon the literature of the mono-substituted form of this system.¹³²

The three 1,1'-disubstituted ferrocene diimine systems were tested for metal selectivity using the following eight metal cations: Fe²⁺, Co²⁺, Ni²⁺, Cu²⁺, Zn²⁺, Cd²⁺, Hg²⁺ and Pb²⁺ using the spectral database as a means to identify the product(s) formed.

Selectivity experiments:

Mixed metal reaction involving Fc2 ligand: (3.19 x10⁻³ M solution)

An ethanolic solution containing one equivalent of each of the metal acetate hydrates (100 mg FeCl₂·4H₂O, 120 mg CoCl₂·6H₂O, 120 mg NiCl₂·6H₂O, 90 mg CuCl₂·2H₂O, 70 mg ZnCl₂·H₂O, 120 mg CdCl₂·2.5H₂O, 140 mg HgCl₂·H₂O, and 190 mg PbCl₂·H₂O) was prepared using 120 mL ethanol. After stirring for thirty minutes, 200 mg of Fc2 ligand was added along with 40 mL ethanol and refluxed overnight (heating increases rate of formation of products). The solution was then cooled, filtered (no precipitate formed) and dried to a black powder. ¹H NMRs and UV-Vis spectra indicated multiple metal products present, along with unreacted metal chloride starting materials, but no unreacted Fc2 ligand. CV spectrum is not definable to a single product, multiple products present. Amount of black powder recovered: 790 mg.

Mixed metal reaction involving FcOH2 ligand: (1.47x10⁻³ M solution)

A solution containing one equivalent (2.36x10⁻⁴ mol) of the eight metal acetate hydrates (41.0 mg Fe(CH₃COO)₂, 58.7 mg Co(CH₃COO)₂·4H₂O, 58.7 mg Ni(CH₃COO)₂·4H₂O, 47.1 mg Cu(CH₃COO)₂·H₂O, 51.7 mg Zn(CH₃COO)₂·2H₂O, 62.8

mg $\text{Cd}(\text{CH}_3\text{COO})_2 \cdot 2\text{H}_2\text{O}$, 75.1 mg $\text{Hg}(\text{CH}_3\text{COO})_2$, and 65.6 mg $\text{Pb}(\text{CH}_3\text{COO})_2 \cdot 3\text{H}_2\text{O}$ was prepared using 120 mL absolute ethanol. Products will form in the absence of heating, but under a slower rate of formation. After stirring for thirty minutes, 100.0 mg of FcOH2 ligand was added and the brownish solution was refluxed for three hours, whereby it turned red. Upon filtering, a blackish precipitate was collected. Amount recovered: 47.5 mg. ^1H NMR spectra (Figures 5.1-2), UV-Vis spectra (Figure 5.3) and X-ray fluorescence of the precipitate proved multiple metal products were present, although compound **18** ($\text{M} = \text{Pb}^{2+}$) had a higher concentration. CV spectrum (Figure 5.4) of the product material is missing the expected $\text{Fe}^{\text{II}}\text{-Fe}^{\text{III}}$ couple, possibly due to both multiple products and starting metal chloride salts being present.

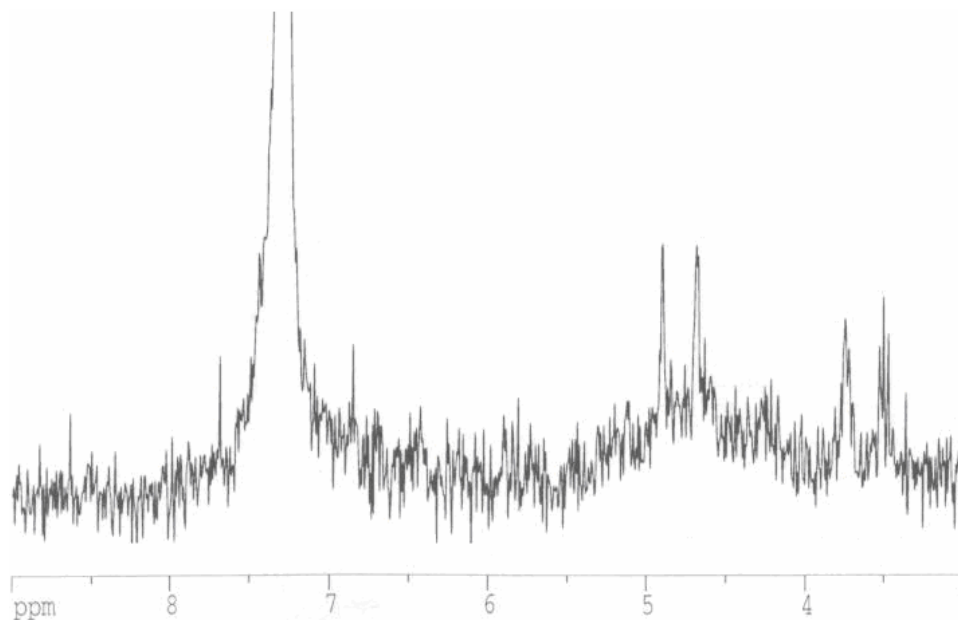


Figure 5.1: ^1H NMR spectrum of FcOH2 mixed metal reaction (dried solution) in CDCl_3 . The two peaks between 5 and 4.5 ppm (1:1 H) correspond to Cp peaks that are consistent with compound **18**, although other products are present indicating only partial selectivity may be occurring.

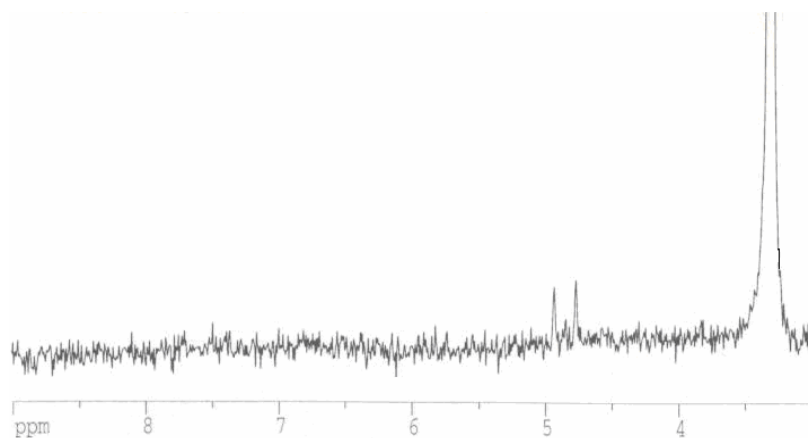


Figure 5.2: ¹H NMR spectrum of FcOH₂ mixed metal reaction (dried solution) in d₆-DMSO. The two peaks between 5 and 4.5 ppm (1:1 H) are consistent with Cp protons on FcO₂-M complexes, although peaks for other protons do not appear to be present, leading to a conclusion that the ligand is not selective for a particular metal cation.

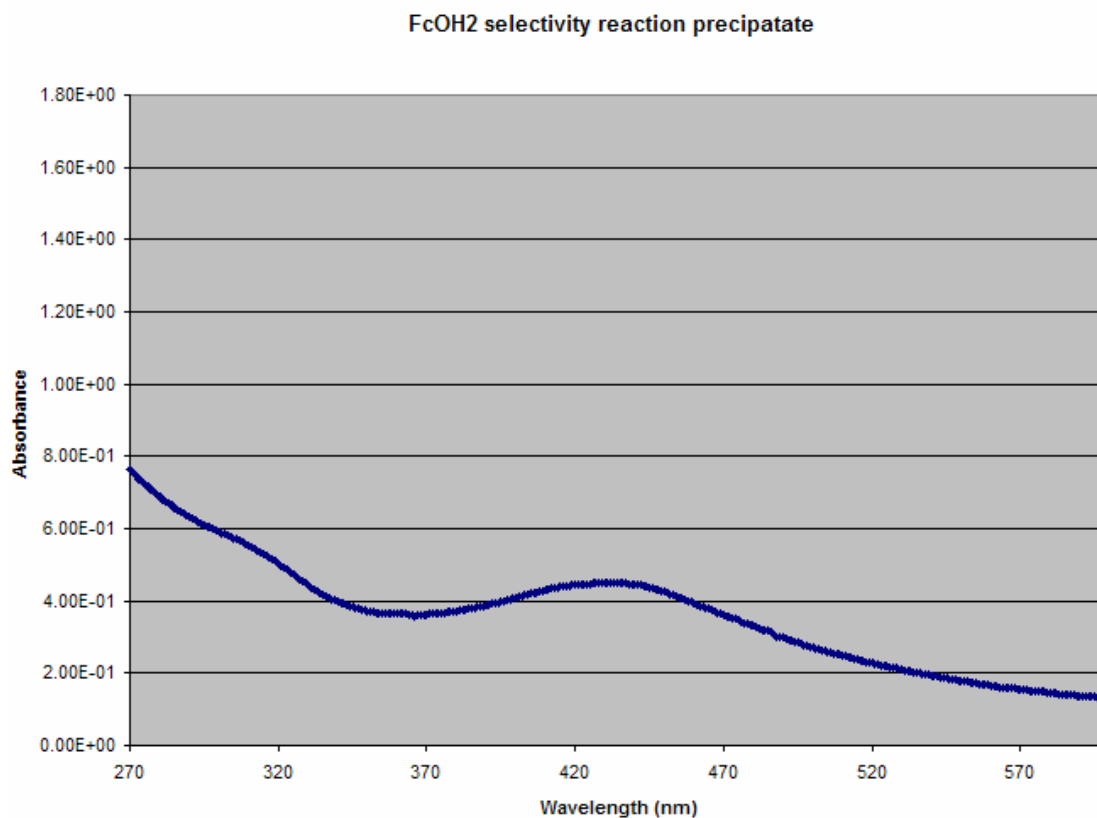


Figure 5.3: UV-Vis. of FcOH₂ mixed metal reaction product in DMSO. The peak of the mixed metal reaction is at 430 nm, while compound 18 has a peak at 438 nm. This indicates that more than one metal product may be present in the precipitate.

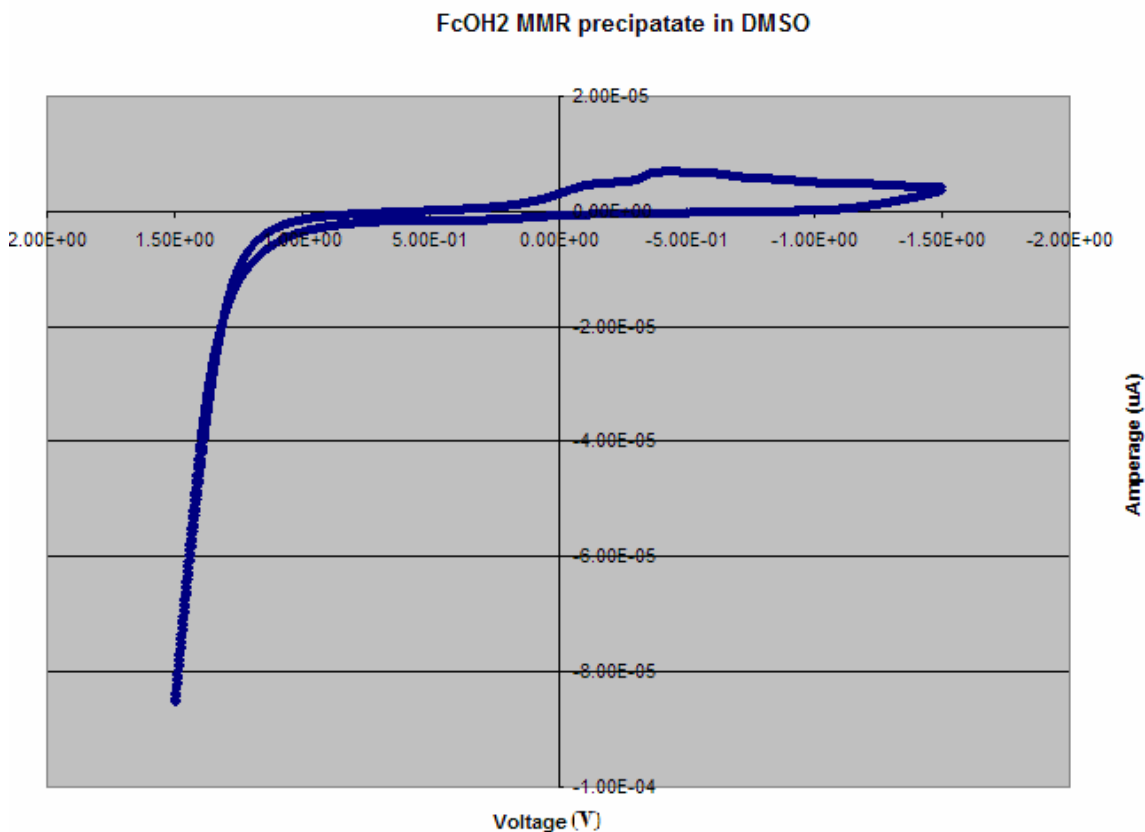


Figure 5.4: Cyclic voltammety of FcOH2 mixed metal reaction product in 1×10^{-3} M TBAHFP/DMSO solution, scan rate 100 mV/sec.

X-ray Fluorescence data of FcOH2 Mixed Metal Reaction:

Four samples were prepared by dripping a concentrated solution (benzene) of the FcOH2 mixed metal reaction precipitate (from reaction above that had been rinsed with methanol to remove starting materials) onto four weighed paper filters. They were then transported to MURR and tested with help from Dr. Robertson's research group. Each filter was tested four times in two different directions during the measurements, whereby the fluorescent signals were recorded by a detector. Unfortunately, the Hg standard was missing for the calibration of the detector, so Tl was used in its place. This leads to the test being slightly less accurate, but still usable for this study. Based upon the data (see

Appendix Table 15 for specifics), the majority of the metals present in this product were the heavy metals, with exception of the iron present in the ligand. The fluorescent signals for an element that the detector measures are directly proportional to the concentration of that element within a sample. If an element contains a high signal ratio vs. other elements, then the sample contains a higher amount of that particular specie than other elements. Heavy metals gave consistent fluorescent numbers greater than the majority of the transition metals. Unfortunately, none of the metals that were tested for selectivity with this ligand system had a concentration that was much greater than the other metals, which would have been an indication of a particular metal selectivity for that ligand. See Table 13 below (or appendix Table 15) for further information on product composition, units are in impulses.

Table 13: X-ray Fluorescence data of the FcO₂-M mixed metal reaction product.

FcO₂-M Mixed Metal Reaction Precipitate:
Counts/sample run (F = filter, T = trial)

	F#1 T#1	F#1 T#2	F#2 T#1	F#2 T#2	F#3 T#1	F#3 T#2	F#4 T#1	F#4 T#1
Fe	2.6805	3.7753	2.8937	2.8185	2.6393	2.8319	2.7226	2.822
Co	0.03081	0.02697	0	0.01336	0	0.0897	0	0.02475
Ni	0	0	0	0	0	0	0	0
Cu	0	0.41798	0	0	0	0	0	0
Zn	0.44675	0.39101	0.38583	0.32059	0.49682	0.21784	0	0.70551
Cd	0.01555	0.0048	0.01	0.01347	0.00472	0.00869	0.00973	0
Hg	0.23108	0.4854	0	0	0	0	0	1.2006
Pb	0.06162	0.22922	0.14468	0.10686	0.17078	0.11533	0.10022	0.23517

	Total	Ave	
Fe	23.1838	2.897975	ligand
Co	0.18559	0.023199	
Ni	0	0	
Cu	0.41798	0.052248	
Zn	2.96435	0.370544	Zn
Cd	0.06696	0.00837	
Hg	1.91708	0.239635	Hg
Pb	1.16388	0.145485	Pb

Mixed metal reaction involving FcSH2 ligand: (1.37×10^{-3} M solution)

A solution containing one equivalent (2.19×10^{-4} mol) of each of the metal acetates was made with 120 mL of absolute ethanol (38.1 mg $\text{Fe}(\text{CH}_3\text{COO})_2$, 54.6 mg $\text{Co}(\text{CH}_3\text{COO})_2 \cdot 4\text{H}_2\text{O}$, 54.5 mg $\text{Ni}(\text{CH}_3\text{COO})_2 \cdot 4\text{H}_2\text{O}$, 43.7 mg $\text{Cu}(\text{CH}_3\text{COO})_2 \cdot \text{H}_2\text{O}$, 48.1 mg $\text{Zn}(\text{CH}_3\text{COO})_2 \cdot 2\text{H}_2\text{O}$, 58.4 mg $\text{Cd}(\text{CH}_3\text{COO})_2 \cdot 2\text{H}_2\text{O}$, 69.8 mg $\text{Hg}(\text{CH}_3\text{COO})_2$, and 60.9 mg $\text{Pb}(\text{CH}_3\text{COO})_2 \cdot 3\text{H}_2\text{O}$). Products will form at a much slower rate if allowed to stir at room temperature. After stirring for thirty minutes, 100.0 mg of the FcSH2 ligand was added along with 40 mL ethanol and the solution quickly turned from brownish to red. It was refluxed for three hours under N_2 , cooled to room temperature and the red precipitate collected. The product was washed with cold ethanol, then ethyl ether, before drying under vacuum. Amount of product collected: 101.2 mg (70.5 % yield). ^1H NMR (CDCl_3) spectrum (Figure 5.5) showed only FcS2-Hg present. (Second batch yielded 97.0 mg of **28** ($\text{M} = \text{Hg}^{2+}$), a sample decomposed upon heating at 244°C after washing with methanol and drying). ^1H NMR spectrum (Figure 5.6) in d_6 -DMSO of product was also correlated to only contain FcS2-Hg, although the peaks were less defined than in CDCl_3 . Both UV-Vis. (Figure 5.7) and CV (Figure 5.8) spectrums matched those of FcS2-Hg. Melting point of product precipitate was 244°C and MS data contained the M+1 peak of **28**.

Repeating on a 1.37×10^{-4} M scale (20.0 mg ligand/320 mL ethanol, with 5 fold decrease in concentration of the metal acetates) gave no precipitate, but upon drying the

reddish solution under a vacuum, a red solid appeared that only contained the FcS2-Hg product by ^1H NMR.

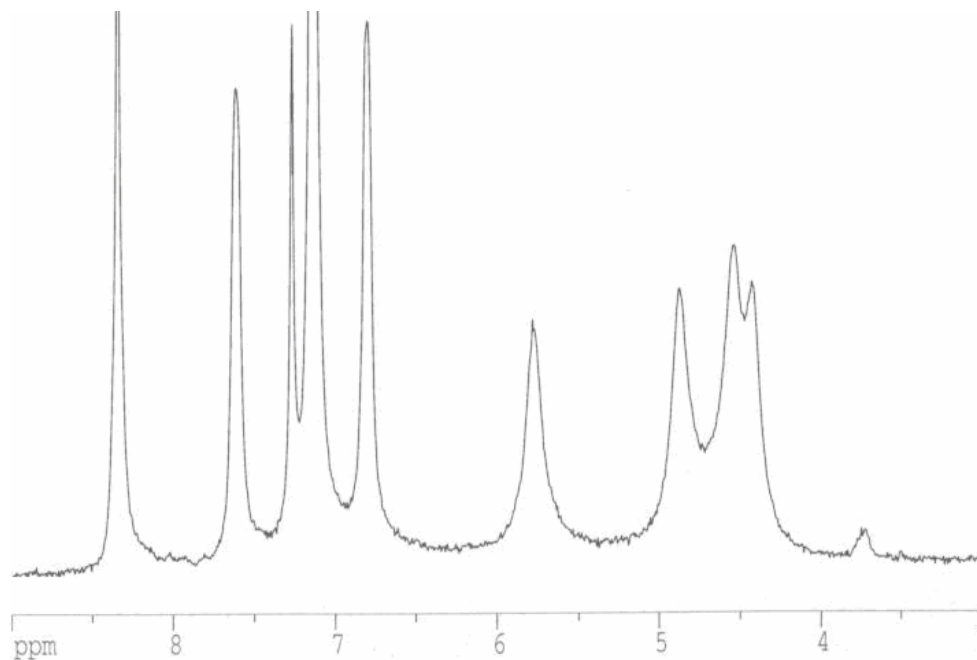


Figure 5.5: ^1H NMR spectrum of FcSH2 mixed metal reaction (dried solution) in CDCl_3 . The peak at 8.35 ppm corresponds to $\text{Cp}-\underline{\text{C}}\text{H}=\text{N}-\text{R}$ of complex 28, the three peaks between 7.5 to 6.8 ppm correspond to the $-\text{C}_6\underline{\text{H}}_4-$ moiety, and the four peaks between 5.7 to 4.5 ppm correspond to the Cp protons from complex 28. (1:1:2:1:1:1:1:1 H equivalency)

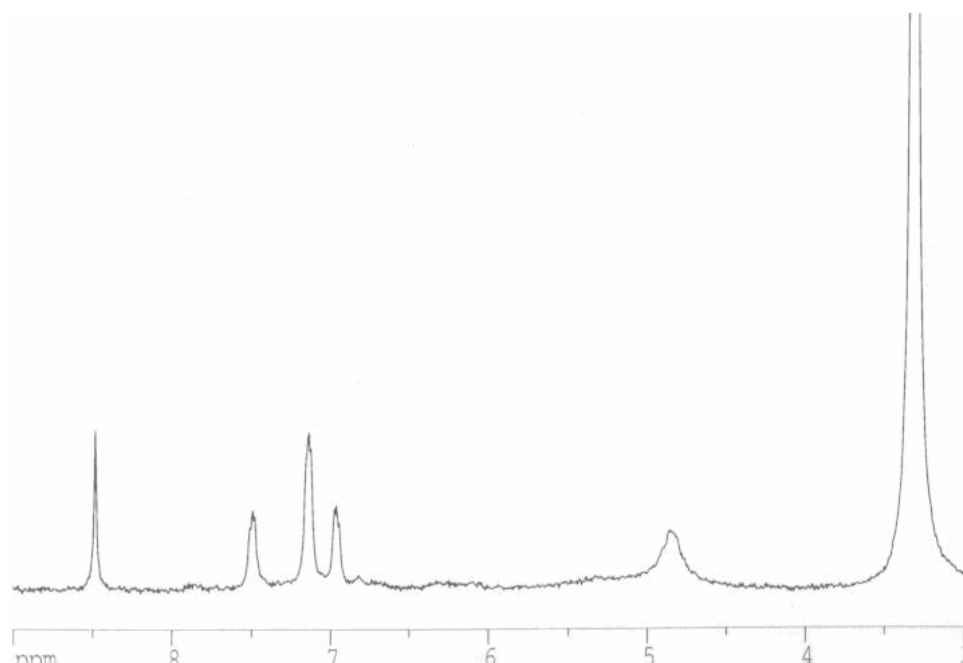


Figure 5.6: ^1H NMR spectrum of FcSH2 mixed metal reaction (dried solution) in d_6 -DMSO. (1:1:2:1:4 H equivalency)

FcSH2 selectivity reaction precipitate

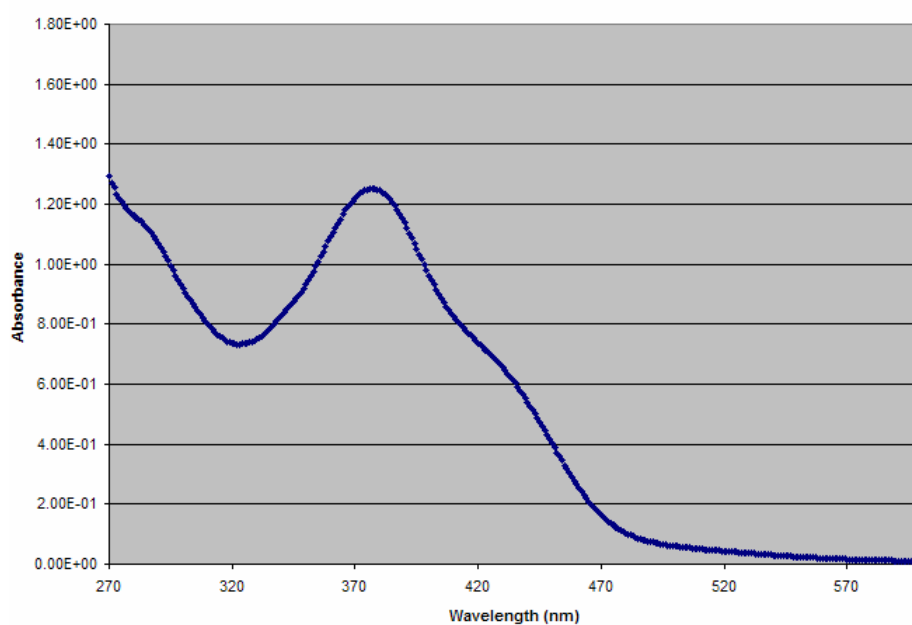


Figure 5.7: FcSH2 mixed metal reaction product in DMSO: The large peak at 376 nm for the FcSH2 (1:1) mixed metal reaction matches with the expected product peak for FcS2-Hg (376 nm).

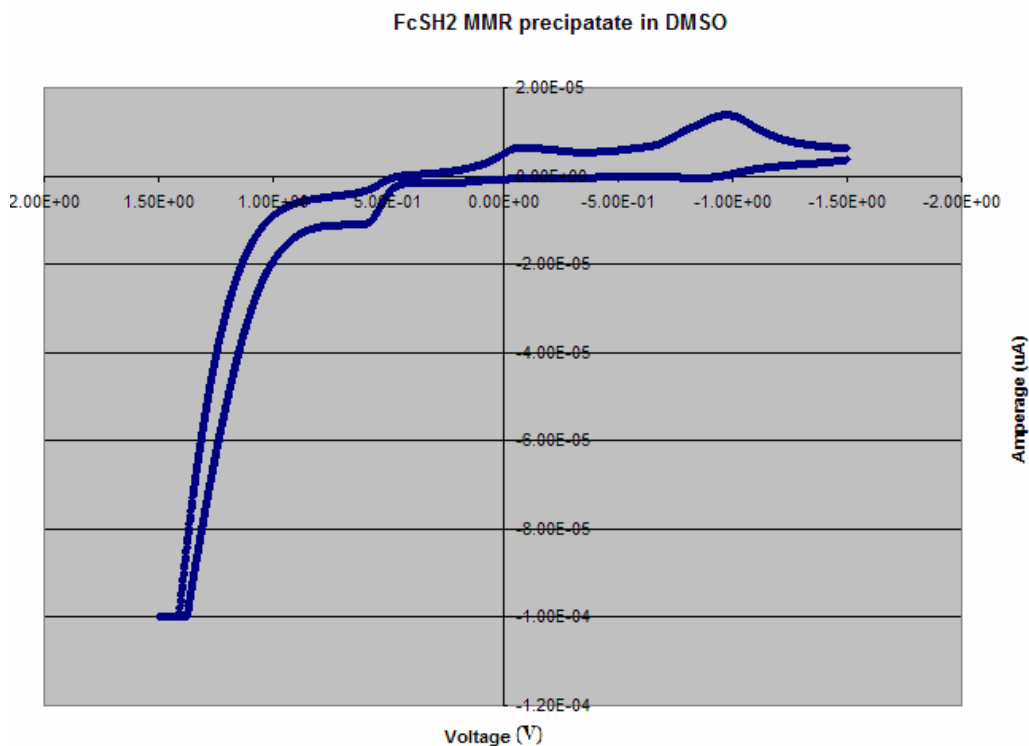


Figure 5.8: Cyclic voltammetry of FcSH2 (1:1) 1.37×10^{-3} M mixed metal reaction product in 1×10^{-3} M TBAHFP/DMSO solution.

X-ray Fluorescence data for FcSH2 mixed metal reaction product

Four samples were prepared by dissolving the FcSH2 selectivity precipitate product (after a methanol wash to remove starting materials) in benzene and adding it to pre-weighed filter papers. Each sample was scanned in two directions, in the same way the FcOH2 mixed metal reaction product was tested at MURR with help of Dr. Robertson's research group. Based upon the data obtained (see Appendix for specifics), **28** is the primary product formed during the selectivity experiment. Trace amounts of other metals are present, most noticeably zinc and lead. The concentration and error values for mercury could not be calculated due to a missing standard (see appendix Table 16). A Tl standard was used to quantify the measurements for the presence Hg due to a missing Hg standard. This experiment would be more analytically correct if the Hg standard was

used, but it still gives valuable information about the selectivity of the FcSH2 ligand when competing cations are present in solution. The reason why Tl can be used as a substitute for Hg is because it is the element most similar in atomic weight to Hg. The results indicate that the FcSH2 system has a great preference in chelating Hg^{2+} when other metal cations are present. See Table 14 below (or appendix Table 16) for further information about concentration of elements in the precipitate, units are in impulses.

Table 14: X-ray Fluorescence data of the FcS2-M mixed metal reaction product.

FcS2-M Mixed Metal Reaction Precipitate:
Counts/Sample run (F = filter, T = trial)

	F#1 T#1	F#1 T#2	F#2 T#1	F#2 T#2	F#3 T#1	F#3 T#2	F#4 T#1	F#4 T#1
Fe	13.152	13.131	27.405	28.112	26.569	27.156	23.1	26.263
Co	0	0.02555	0.08705	0.0821	0.0737	0	0.18247	0.04673
Ni	0	0	0	0	0	0	0	0
Cu	0	0.22992	0.38304	0.37767	0.47906	0.27268	0.74811	0
Zn	2.1024	1.9543	3.2036	3.6782	2.6532	3.4326	3.4121	2.2431
Cd	0.01492	0	0	0	0	0	0	0
Hg	37.371	37.131	94.384	100.66	91.629	94.283	84.208	87.7
Pb	0.3532	0.3321	0.81831	0.77176	0.47906	0.68972	0.63863	0.43616

	Total	Ave	
Fe	184.888	23.111	ligand
Co	0.4976	0.0622	
Ni	0	0	
Cu	2.49048	0.31131	
Zn	22.6795	2.834938	Zn
Cd	0.01492	0.001865	
Hg	627.366	78.42075	Hg
Pb	4.51894	0.564868	Pb

Method for testing filtered FcSH2 mixed metal solution for the presence of unbound

Hg^{2+}

To the ethanolic solution (recovered from the 1.37×10^{-3} M FcSH2 mixed metal reaction after filtering) was added 5 mL of 2-aminothiophenol. It was then refluxed

under N_2 for four hours, whereby a darkish red precipitate formed. The product was filtered, washed with ethanol and dried under vacuum. 1H NMR spectra showed various metal products formed, but the specific peaks for $Hg(H_2N-C_6H_4-o-S)_2$ were not present (spectral data was compared with NMR taken from a previously prepared sample of $Hg(H_2N-C_6H_4-o-S)_2$).

Test for Hg^{2+} binding conditions (water/ethanol stir-no heat)

A solution containing 14.0 mg of $Hg(CH_3COO)_2$ was dissolved in 25 mL of deionized (DI) water. 20.0 mg of FcSH2 in 25 mL absolute ethanol was then added to the solution while stirring to obtain a clear yellow solution that was allowed to stir for two hours. It was then set aside for one week. The red precipitate was filtered from the resulting solution (the filtering liquid was clear) and rinsed with cold ethanol, before drying under vacuum. 1H NMR showed an 80/20% mixture of FcS2-Hg/FcSH2 was present in the 23.0 mg of reddish precipitate that formed (80.1% yield).

The results of this test indicate that both the free ligand and the FcS2-Hg product do not decompose in the presence of water, as no 1,1'-diformylferrocene peaks were present in the 1H NMR spectrum. The reaction did not go to completion so the reaction must require some heat of activation to allow it to proceed to total product formation within the time frame given for this test (one week).

Test for Hg^{2+} selectivity with excess metals present

FcSH2 (1:1) with $Hg(CH_3COO)_2$, (1:5) other metal acetates

A solution containing 190.5 mg $\text{Fe}(\text{CH}_3\text{COO})_2$, 273.0 mg $\text{Co}(\text{CH}_3\text{COO})_2 \cdot 4\text{H}_2\text{O}$, 272.5 mg $\text{Ni}(\text{CH}_3\text{COO})_2 \cdot 4\text{H}_2\text{O}$, 218.5 mg $\text{Cu}(\text{CH}_3\text{COO})_2 \cdot \text{H}_2\text{O}$, 240.5 mg $\text{Zn}(\text{CH}_3\text{COO})_2 \cdot 2\text{H}_2\text{O}$, 292.0 mg $\text{Cd}(\text{CH}_3\text{COO})_2 \cdot 2\text{H}_2\text{O}$, 69.8 mg $\text{Hg}(\text{CH}_3\text{COO})_2$, and 304.5 mg $\text{Pb}(\text{CH}_3\text{COO})_2 \cdot 3\text{H}_2\text{O}$ in 300 mL ethanol was stirred for one hour (color: brown). 100.0 mg of FcSH2 dissolved in 50 mL of ethanol was added before refluxing under N_2 for three hours. The color became a dark cherry red. Upon cooling, it was filtered, washed with cold ethanol and vacuum dried. ^1H NMR spectrum (Figure 5.9) of the product showed the peak pattern characteristic for **28** ($\text{M} = \text{Hg}^{2+}$).

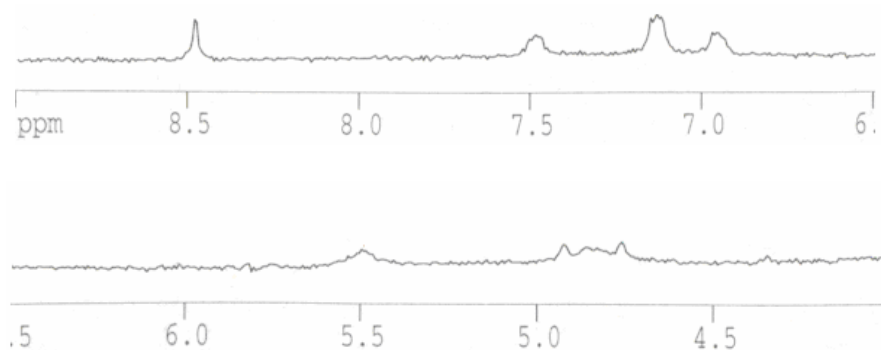


Figure 5.9: ^1H NMR of FcSH2 mixed metal product in $\text{d}_6\text{-DMSO}$ (after ethanol wash), only the FcS2-Hg spectrum matches the peak pattern

FcSH2 (1:1) with $\text{Hg}(\text{CH}_3\text{COO})_2$, (1:10) other metal acetates

A solution containing 76.2 mg $\text{Fe}(\text{CH}_3\text{COO})_2$, 109.2 mg $\text{Co}(\text{CH}_3\text{COO})_2 \cdot 4\text{H}_2\text{O}$, 109.0 mg $\text{Ni}(\text{CH}_3\text{COO})_2 \cdot 4\text{H}_2\text{O}$, 87.4 mg $\text{Cu}(\text{CH}_3\text{COO})_2 \cdot \text{H}_2\text{O}$, 96.2 mg $\text{Zn}(\text{CH}_3\text{COO})_2 \cdot 2\text{H}_2\text{O}$, 116.8 mg $\text{Cd}(\text{CH}_3\text{COO})_2 \cdot 2\text{H}_2\text{O}$, 14.0 mg $\text{Hg}(\text{CH}_3\text{COO})_2$, and 121.8 mg $\text{Pb}(\text{CH}_3\text{COO})_2 \cdot 3\text{H}_2\text{O}$ in 280 mL of ethanol was stirred for thirty minutes (brown). 20.0 mg of FcSH2 dissolved in 40 mL of ethanol was added and the mixture was refluxed for three hours under N_2 . No precipitate formed in the reddish solution, so the liquid was dried for a ^1H NMR study. The spectrum showed a very small peak at 8.34 ppm

corresponding to the FcS2-Hg Cp-CH=N-R proton, with no FcS2-M Cp-CH=N-R peaks present in that area. The rest of the spectrum was obscured due to the large amount of acetate and water present, so ^1H NMR would not be the best method of detection at this concentration of excess competing cations (10 times excess vs. Hg^{2+} at ppm levels).

FcSH2 ligand reaction with an *Bis*[organothiolato] mercury complex: $\text{Hg}(\text{H}_2\text{N}-\text{C}_6\text{H}_4-\text{o}-\text{S})_2$

2-aminothiophenol was chosen for this experiment, as it forms $\text{Hg}(\text{NH}_2\text{-Ph-o-SH})_2$ upon reaction with Hg^{2+} .¹³⁹ A small amount of this complex was prepared for spectral identification (^1H NMR). 10.0 mg of previously prepared $\text{Hg}(\text{H}_2\text{N}-\text{C}_6\text{H}_4-\text{o}-\text{S})_2$, 10.3 mg FcSH2 and 10 mL ethanol were stirred together for one day. The precipitate was filtered, washed with ethanol and dried. The ^1H NMR spectrum of the reddish precipitate only showed **28** and no spectral peaks corresponding to $\text{Hg}(\text{H}_2\text{N}-\text{C}_6\text{H}_4-\text{o}-\text{S})_2$ were present. Amount of precipitate recovered: 10.1 mg. The reverse reaction (**28** + $\text{H}_2\text{N}-\text{C}_6\text{H}_4-\text{SH}$) resulted in no reaction per ^1H NMR.

Method for testing reversibility of the FcSH2 ligand system with Hg^{2+} :

10.0 mg of **28**, 40 equivalents of KI and 10 mL of ethanol were stirred together one day. Upon filtering, no reaction could be detected by ^1H NMR, so the system is not reversible using KI. This result indicates that the binding between the Hg^{2+} and the thiol groups is quite strong, which prevents the formation of free ligand via removal of the Hg^{2+} from the complex.

Method for testing chelating ability of each FcS-M complex with Hg(CH₃COO)₂:

In separate vials were placed 4.0 mg of each of the FcS₂-M compounds except **28** along with 10 mL ethanol and a stir bar. One equivalent of Hg(CH₃COO)₂ was added to each before stirring them for two days. They were then filtered and washed with methanol to remove any starting materials present in the precipitate. Each precipitate was dissolved with CHCl₃ and then dried to remove them from the pipette filter. ¹H NMR spectra (see appendix) were taken of each precipitate and the corresponding dried liquid fraction. All FcS₂-M complexes showed either partial (**25**, **27**) or full (**23**, **24**, **26**, **29**) conversion to **28**, with the exception of **22** (Fe²⁺).

Discussion section of heavy metal selectivity:**Fc₂ and FcOH₂ ligand systems:**

Compound **1** showed no noticeable metal selectivity over the metals chosen for this study. The precipitate formed was tested by ¹H NMR, UV-Vis and CV, but no one metal product could be diagnosed from the results. The Fc₂ ligand system, although it bears some similarities to a known Zn²⁺ sensor, is not a sensor for any of the eight metal cations. Although this is not a positive result, the data gained in the creation of the Fc₂-MCl₂ database may be of use in redesigning the ligand to allow for selectivity.

Compound **10** showed potential selectivity towards Pb²⁺ based upon the UV-Vis spectrum, although there were other products present. Since the ¹H NMR and CV did not clearly define a specific product but more of a mixture, the FcOH₂ system seems to have poor selectivity for heavy metal cations in the presence of transition metal cations.

FcSH₂ ligand system

Compound **21** does show selectivity towards Hg^{2+} over Fe^{2+} , Co^{2+} , Ni^{2+} , Cu^{2+} , Zn^{2+} , Cd^{2+} and Pb^{2+} . The complex that forms, **28**, can be identified using ^1H NMR, UV-Vis, CV, melting point and X-ray fluorescence. Fluorescence in ethanol is not an effective means of detection for **28**, but that could be possible with further derivatization of **21**. Reactions were run in the $10^{-(3,4)}$ M range (ppm in ethanol), although it was tried at a ppb concentration (in ethanol) whereby the color did slightly change, but the product was not detectable by ^1H NMR due to the large concentration of starting materials that were present vs. the product concentration. Reactions involving 5 and 10 times excess of Fe^{2+} , Co^{2+} , Ni^{2+} , Cu^{2+} , Zn^{2+} , Cd^{2+} and Pb^{2+} with one equivalent of Hg^{2+} and FcSH₂ gave precipitates that are exclusively **28** via ^1H NMR. Mixed solutions of metal products containing **28** can be distinguished by ^1H NMR by the 8.35 ppm Cp-CH=N-R peak and one of the Cp peaks of **28** that do not show up in the spectra of **22-27** and **29**.

Reactions of **22-27**, and **29** with $\text{Hg}(\text{CH}_3\text{COO})_2$ confirm that even if some metal products form before a Hg^{2+} comes into contact with the ligand, the metal center can be replaced by the Hg^{2+} to form **28** for most of the metals studied via ^1H NMR of the precipitates. Three exceptions were noted: Fe^{2+} , Cu^{2+} and Cd^{2+} . Hg^{2+} has a very strong affinity for thiol groups, as proven by the FcS1 ligand system. The formation of **22** ($\text{M} = \text{Fe}^{2+}$) is very low when no other metals are present.

On the other hand, Cu^{2+} does show a preference for binding with **21**, although it would be more likely in an square planer geometry around the Cu^{2+} , which puts a strain upon the chelating areas of the ligand system. Cu^{2+} , like Ni^{2+} , would prefer a square planar geometry over tetrahedral. Cd^{2+} is partially (25%) replaced to form **21**, but the replacement may go to completion if enough time is given. Reports in the literature¹³¹

that indicate that Cd^{2+} has a lower preference for thiols than Hg^{2+} , are consistent with the difference in the formation of **27** (71.0%) vs. **28** (94.6%). Compounds **23** (Ni^{2+}), **24** (Cu^{2+}), **26** (Zn^{2+}) and **29** (Pb^{2+}) all undergo replacement to form the precipitate **28** (Hg^{2+}). The data confirm that even if some excess metal complexes form initially, the majority will be converted to **28** when exposed to free Hg^{2+} in solution. That result is important to show that the FcSH2 ligand is effective in determining Hg^{2+} concentration even if the FcSH2 ligand is bound to other metal cations initially. It demonstrates that even though other metals might bind with the FcSH2 ligand before Hg^{2+} , it will still form compound **28** when the Hg^{2+} comes into contact with the other complexes.

Conclusion for metal selectivity of the Fc2, FcOH2 and FcSH2 systems:

While the Fc2 and FcOH2 ligands were not multiple detection sensors for their heavy metal targets, the FcSH2 ligand was found to be a sensor for Hg^{2+} . The Fc2 system failed to be a sensor because it only has imine groups with which it can chelate metals. This result means that the Fc2 ligand does not target one particular metal out of the eight chosen in this study, since they will all tend to bind in the same manner. The FcOH system failed only because it has a lower selectivity for the target than needed. It does form complex **18** upon reaction with Pb^{2+} and can be detected by more than one method, but it does not form complex 18 exclusively if the other seven cations are present in solution.

The complex that forms upon reaction with FcSH2 and Hg^{2+} , **28**, can be detected by at least five methods and is exclusively formed as a bright red precipitate in 70 % yield with

other metal cations present. Since **28** is stable to 245°C, it can be used to sequester mercury from solutions after testing for environmental cleanup.

Environmental sampling in the real world:

Most water samples are tested for Hg^{2+} in the laboratory using atomic absorption or emission spectroscopy, which takes time to do properly. Although environmental testing instruments can be brought into the field, they remain quite bulky and expensive (both to buy and repair). A goal for researchers has been the creation of much cheaper, smaller and still effective means to measure the quantity of Hg^{2+} present in a water sample without polluting the environment further.

Water samples from a suspect source are typically sent into the laboratory where they are tested to determine metal concentration. Different elements give off different spectral band spectra, so the amounts of each element present within the sample can be calculated. HPLC can also be used to separate other impurities in water samples for further testing. While the accuracy of laboratory testing is quite high, it takes time to get the analysis data and the samples must be transported/stored properly before analysis. Delays in receiving concentration data can mean that polluted water becomes used (drinking, showers, etc) in manners that they should not before being purified. A technique that can accurately measure heavy metal concentration in the field has been a long standing goal for environmental chemists.

The eight metal cations that were tested during this study will not normally be found as simple hydrated chloride or hydrated acetate salts in nature. Most will be found as metal oxides, sulfates, hydroxides or halide salts (or combinations of those mentioned

above) and that can greatly affect the potential reactivity with the three ligand systems. The metal oxides would tend to prevent any complexes forming with the Fc2 and FcOH2 (since some M-O bonds would have to be broken to form the complexes), while the FcSH2 ligand should still react with Hg^{2+} (based upon a stronger affinity towards thiol over oxo groups). A real test of this particular ligand is if it can extract Hg^{2+} from HgS_2 . Further testing must be done in this area before a real world application as a heavy metal sensor can be fully realized.

Current Mercury Detection Technology for Aqueous Samples:

Many promising chemical sensors have been reported in the literature in the past decade. Recent aqueous Hg^{2+} sensor development has focused upon four main areas: gold nanoparticles, conjugated carbon chains connected to aromatic compounds, biological derived peptides and lipids and inorganic (Ru^{2+} , Fe^{2+}) complexes. Gold nanoparticles can abstract Hg^{2+} from water based upon chelation with thiol groups¹⁴⁰ or amalgamation¹⁴¹. Most gold nanoparticle sensors use either UV-Vis spectroscopy¹⁴² and/or fluorescence^{143, 144} from attached groups for the detection process of Hg^{2+} interactions, but fluorescence quenching can also be used¹⁴⁵. A gold electrode was reported for the electrochemical detection of Hg^{2+} in water, but other analytes can interfere with the signaling¹⁴⁶. The downside of such systems is that the gold-mercury interaction is hard to reverse and can be expensive to produce.

Self-assembled organic molecules containing conjugated ring systems such as anthracenes¹⁴⁷, porphyrins^{148, 149}, and calixarenes¹⁵⁰ can be used to chelate Hg^{2+} ions. Once bound, the concentration of bound Hg^{2+} is measured via UV-Vis or fluorescence

spectroscopy. They can be quite cheap to produce and can be incorporated into plastics for testing equipment. Some of these sensors have a lot of production steps and most are not capable of multi-detection methods.

Biological based sensors can be used to detect Hg^{2+} based upon the thiol groups present. Most are fluorescent indicators¹⁵¹, although a recent example¹⁵² undergoes fluorescent quenching upon interaction with Hg^{2+} . The drawbacks of such sensors are the interactions are not usually reversible and some are not very selective.

Inorganic complexes containing transition metals, such as Ru^{2+} or Fe^{2+} , can be used to detect Hg^{2+} in aqueous conditions. A Ru^{2+} sensor can detect Hg^{2+} concentrations via UV-Vis and fluorescence spectroscopy once the Hg^{2+} becomes reversibly bound to the molecule.¹⁵³ Ferrocene sensors have been reported to measure aqueous Hg^{2+} using multiple detection modes (CV, UV-Vis, fluorescence, etc.). This is the type of Hg^{2+} sensor system that was studied during this research project.

Potential Applications to Environmental Sampling and Analysis:

A preferred system of detecting materials is for the sensing material to be reuseable after detection. Since the FcSH2 ligand does not easily release the Hg^{2+} once it is chelated, it is a single use sensor/sequestering agent. But, since it can be produced in bulk rather cheaply from ferrocene, the cost effectiveness allows for it to still be a potentially useful sensor. The FcSH2 ligand system can be used in multiple ways for environmental sensing of mercury.

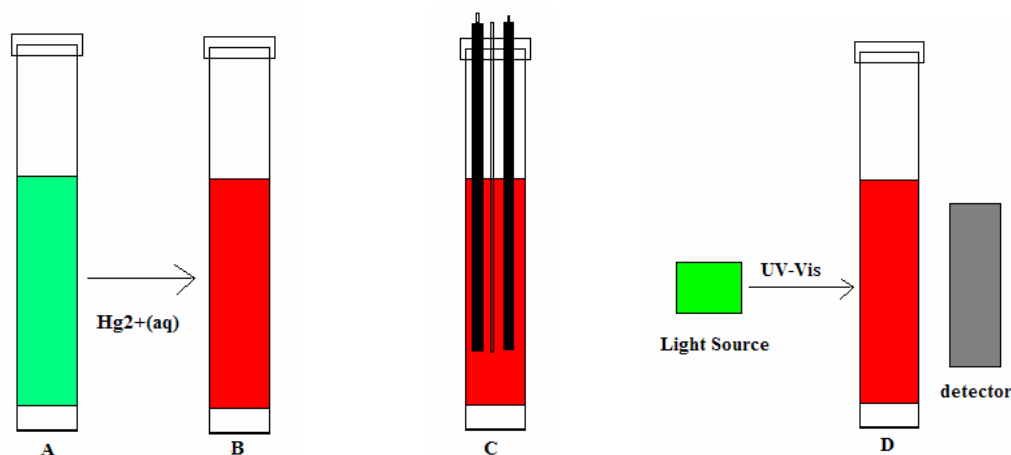


Figure 5.10: a.) Proposed measuring probe for environmental samples with FcSH2 ligand in solution with a semi-permeable membrane at the bottom, b.) Color of probe solution after contact with Hg^{2+} from an aqueous source, compound 28 has formed, c.) CV probes inserted into testing probe for electrochemical measurement, d.) UV-Vis absorption testing on the probe solution.

One method of using the FcSH2 ligand is in the creation of a probe containing an ethanolic (or other) solution of the ligand contained within a glass or quartz tube (Figure 5.10). At one end of the tube is a cap and at the other end is a membrane that allows only metal cations to be allowed to enter into the probe. The major drawback to this probe is the membrane of the probe, since the flow rate of the metal cations will have to be carefully measured to ensure that all cations are allowed to permeate through and not just selective ones. Since the reactions with the ligand need some energy of activation to force the reaction forward, a warming tube can either be inserted into the probe or around it for a period of time to allow the reaction to occur. Upon reaction, the probe might be analyzed using UV-Vis spectrometry (light absorbed through the sample cell), fluorescence of a particular wavelength (light emitted 90° from source) and cyclic voltammetry (via electrochemical probes placed into the cell). These tests will give a signal if mercury is present in appreciable levels and possibly the exact concentration within the sample size. After testing, the solution can be disposed of as an unwanted

material containing a mercury compound (the mercury can be reclaimed upon heating to a high temperature).

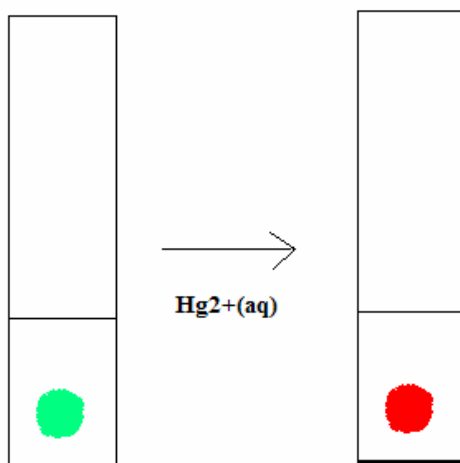


Figure 5.11: Proposed test strip method with FcSH2 ligand coated paper. Upon exposure to Hg^{2+} , the color should turn bright red upon reaction.

Another potential way to use the FcSH2 ligand as a mercury sensor in the real world is its use in a test strip (Figure 5.11) that can be dipped into a slightly warmed sample (or a heating apparatus can be applied to the test strip) in a sample holder. This will not affect the concentration of the metals present in the sample or the free ligand, but will allow for a much faster rate of reaction to occur. The ligand would be attached to a polymer-based sheet (by glue or incorporating it into the polymer design) or coated onto a glass slide. Upon reaction, the slight color change that occurs can be monitored using UV-Vis absorption down to the ppm level. Fluorescence might be possible with modification of the ligand to reach detection limits in the ppb level. The spectroscopic data would indicate if mercury is present in the sample and at approximately what concentration. A major influence on this method of detection is that it would be cheap to produce and can be easily done on a large amount of samples out in the field using only a small amount of

ligand. Similar sensing techniques have been reported for a ferrocene-rhodamine system with Hg^{2+} .² Unfortunately, a trial run of a fabricated test strip using this ligand system failed to show a color change after one day of submersion within a concentrated Hg^{2+} aquatic solution, showing more research work is needed in this area.

If a test strip can be made to work, then a dip test sensor (glass) could be designed and analyzed through heating the product to determine the exact product formed. Since the FcSH2 ligand has a much lower melting point than any of the metal complexes that form, it can be determined if a reaction has taken place and if the product decomposes at 245°C , then Hg^{2+} was present in the solution tested. After the testing, the strips can be disposed similarly as the probe solution. A potential future research goal would be to incorporate the ferrocene ligand system into a polymeric form such that the entire strip could be used for testing rather than just an attached spot on the surface. Since plastic sheet can be made very, very thin, the test strip potentially could be used as a membrane if water can be passed through (or over) the strip (but that is dependent upon quite a few factors that need to be explored, such as how porous is the material to begin with).

A third potential way that the FcSH2 ligand system might be used as a sensor is in the formation of water-soluble derivatives that then can be added directly to samples in vials. Upon reaction, they can be tested to see the concentration of mercury that is present if a precipitate forms. This method may be of use in the strip testing process as it would allow for more interaction with the solution.

Potential Water Treatment Applications:

There exists the potential of polymerizing the Cp rings on the FcSH₂ system for use as a porous filter for water treatment systems. It might be useful as a testing device for outflow pipes in sewer systems to prevent industrial contamination by mercury. This may become a means to both detect and sequester mercury from water sources before they are consumed by the population.

The ligands do not appear to be toxic to the environment, but this was not tested experimentally. The detection limits for these ligand systems appears to be in the parts per million (ppm) ranges, but could be potentially lowered into the parts per billion (ppb) ranges if the right fluorescent aromatic ring system would be substituted in for the phenyl rings. The form of the heavy metals does affect greatly the potential selectivity and binding ability of the ligands, although this was not explored much during this study. Future work in this area might solve those potentially complicating problems.

-
- ¹³⁹ Habibi, M. H.; Tangestantnejad, S.; Montazerozohori, M.; Tayari, S. F., Synthesis and Characterization of Bis(organothiolato)Mercury(II) Complexes by Disproportionation of Hg_2Cl_2 in the Presence of Thiols. *J. Coord. Chem.* **2004**, *57*, (16), 1387-1392.
- ¹⁴⁰ Huang, C-C; Chang, H-T; Selective Gold-Nanoparticle-Based “Turn-On” Fluorescent Sensors for Detector of Mercury(II) in Aqueous Solution. *Anal. Chem.*, **2006**, *78*, 8332-8338.
- ¹⁴¹ Rex, M.; Hernandez, F.E.; Campiglia, A.D.; Pushing the Limits of Mercury Sensors with Gold Nanorods. *Anal. Chem.*, **2006**, *78*, 445-451.
- ¹⁴² Si, S.; Kotal, A.; Mandal, T.K.; One-Dimensional Assembly of Peptide-Functionalized Gold Nanoparticles: An Approach Toward Mercury Ion Sensing. *J. Phys. Chem. C*; **2007**, *111*, 1248-1255.
- ¹⁴³ Huang, C-C; Yang, Z.; Lee, K-L; Chang, H-T; Synthesis of Highly Fluorescent Gold Nanoparticles for Sensing Mercury(II). *Angew. Chem. Int. Ed.*, **2007**, *46*, 6824-6828.
- ¹⁴⁴ Chen, J.; Zheng, A.; Chen, A.; Gao, Y.; He, C.; Kai, X.; Wu, G.; Chen, Y.; A functionalized gold nanoparticles and Rhodamine 6G based fluorescent sensor for high sensitive and selective detection of mercury(II) in environmental water samples. *Anal. Chem. Acta*, **2007**, *599*, 134-142.
- ¹⁴⁵ Darbha, G.K.; Ray, A.; Ray, P.C.; Gold Nanoparticle-Based Miniaturized Nonmaterials Surface Energy Transfer Probe for Rapid and Ultrasensitive Detection of Mercury in Soil, Water, and Fish *ACS NANO*, **2007**, *1*, (3), 208-214.
- ¹⁴⁶ Wang, J.; Tian, B.; Lu, J.; Wang, J.; Luo, D.; MacDonald, D.; Remote Electrochemical Sensor for Monitoring Trace Mercury *Electroanalysis*, **1998**, *10*, (6), 399-402.
- ¹⁴⁷ Cheung, S-M; Chan, W-H; Hg^{2+} sensing in aqueous solutions: and intramolecular charge transfer emission quenching fluorescent chemosensors. *Tetrahed.*, **2006**, *62*, 8379-8383.
- ¹⁴⁸ Zhang, X-B; Guo, C-C; Li, Z-Z; Shen, G-L; Yu, R-Q; An Optical Fiber Chemical Sensor for Mercury Ions Based on a Porphyrin Dimer. *Anal. Chem.*, **2002**, *74*, 821-825.
- ¹⁴⁹ Chan, W.H.; Yang, R.H.; Wang, K.M.; Development of a mercury ion-selective optical sensor based on fluorescence quenching of 5, 10, 15, 20-tetraphenylporphyrin. *Anal. Chim. Acta*, **2001**, 261-269.
- ¹⁵⁰ Metivier, R.; Leray, I.; Lebeau, B.; Valeur, B.; A mesoporous silica functionalized by a covalently bound calixarene-based fluoroionophore for selective optical sensing of mercury(II) in water. *J. Mater. Chem.*, **2005**, *15*, 2965-2973.

-
- ¹⁵¹ Ivask, A.; Virta, M.; Kahru, A.; Construction and use of specific luminescent recombinant bacterial sensors for the assessment of bioavailable fraction of cadmium, zinc, mercury and chromium in the soil. *Soil Biol. & Biochem.*, **2002**, 34, 1439-1447.
- ¹⁵² Kim, I-B; Bunz, U.H.F.; Modulating the Sensing Response of a Conjugated Polymer by Proteins: An Agglutination Assay for Mercury Ions in Water. *J. Am. Chem. Soc.*, **2006**, 128, 2818-2819.
- ¹⁵³ Coronado, E.; Galan-Mascaros, J.R.; Marti-Gastaldo, C.; Palomares, E.; Durrant, J.R.; Vilar, R.; Gratzel, M.; Nazeeruddin, M.K.; Reversible Colorimetric Probes for Mercury Sensing. *J. Am. Chem. Soc.* **2005**, 127, 12351-12356.

Chapter Six

Conclusion

Chemical sensors are an important tool for locating and measuring toxic materials in the environment. The sensors can be tailored for a specific detection mode, such as fluorescence or electrochemistry, based upon the molecule to which the chelation groups are attached. Most chemical sensors have only one method of detection when it is selectively reacted with a particular target. While that description basically fills the requirements on what is needed to make a chemical sensor, there exists a major push to make the chemical sensors better by allowing multiple detection modes.

Although a working universal heavy metal sensor was not produced in this research project, the new ligand systems increased the general chemical knowledge base on ferrocene sensors. The differences between each system gave insights on how to develop future multi-detection sensors for many potential targets, not just heavy metals. By adjusting the chelation groups, the sensor can be tailored for a particular target, such as a cation or anion. There is potential in forming many other ferrocene sensors based upon the Schiff Base synthesis method that may someday be the key to forming a commercial universal sensor for environmental testing.

One possible route to accomplishing this goal is in the incorporation of other molecules that have known detection properties with molecules that can selectively chelate to target species. For example, ferrocene has a well known electrochemical redox couple based upon the Fe^{II} center sandwiched between the Cp rings. When the ferrocene is derivatized, the attaching groups shift the $\text{Fe}^{\text{II}}\text{-Fe}^{\text{III}}$ redox couple based upon the amount of electron density that is perturbed due to the functionalization. If another metal

center is bound to the derivative, the electrochemistry will change in a measurable manner that can potentially be used as a method of detection.

While mono-substituted ferrocenes have been incorporated into chemical sensors on a large scale, chemical sensors using di-substituted ferrocenes have not been explored as much. Di-substituted ferrocenes have the potential of being more selective than the mono-substituted forms. Complexes such as $[\text{FcS1}]_2\text{-M}$ formed using mono-substituted ferrocene ligands have complexation centers that are not as sterically demanding as those formed with their di-substituted forms. The 1,1'-ferrocene complexes have functional groups that can only distort a specific amount, since the target is being held by groups attached to both Cp rings. This limits the amount of flexing that the groups can do when a target becomes chelated. Mono-substituted ferrocene ligands do not have that limitation since the bottom Cp ring is not used in the chelation process.

The area that is used to chelate a target within a di-substituted ferrocene sensor is constricted to particular geometries based primarily upon the modes of binding. If multiple chelation groups are present, the geometry around the target depends upon which groups it binds. This can be used to invoke a measure of selectivity to the ligand since the chelating groups can be tailored for use with a particular target. For example, cations that prefer an octahedral geometry would be less likely to bind with a ligand that contains a chelation center that has a constricted tetrahedral geometry.

It is with these ideas that 1,1'-ferrocene ligand systems were explored as heavy metal cationic sensors during this research project. Three Schiff Base ligands (Fc_2 , FcOH_2 , and FcSH_2) differing only in the ortho substituents off their attached phenyl rings were studied in their effectiveness to selectively bind both late transition and toxic heavy metal

cations. The Fc2 system was not selective since it only had a pair of imine groups to allow chelation with cations. The FcOH2 system showed some promise as being a Pb²⁺ sensor based upon the characteristic UV-Vis spectrum, but unfortunately, it was not fully selective to only the target cation after removing any possible starting materials from the product via a methanol wash. ¹H NMR, UV-Vis, CV and X-ray fluorescence data confirm this result. Although both systems failed to yield a selective heavy metal sensor, the spectroscopic data might be of use in designing further ligand systems.

The creation of a spectroscopic database for the Fc2 and FcOH2 ligand systems has provided information that is potentially very useful to the design of new ferrocene heavy metal sensors. Although neither system gave a positive result in the selectivity reactions with the chosen metals, the information gained from them allow for the refinement of future derivatives that might be more selective. The potential for using the three ligand systems as precursors for other inorganic complexes exists and hopefully will be explored by other researchers in the future.

The FcSH2 ligand system was determined to be an effective, although irreversible Hg²⁺ sensor. The reversibility of the ligand was tested with KI, whereby no reaction occurred. It has multiple means for detection, as the complex **28** can be identified via thermal decomposition (occurring at 245 °C), ¹H NMR, MS, CV and UV-Vis. Both ¹H NMR and MS would not be typically useful for environmental analysis out in the field. That still leaves three possible methods of detection as a one-shot chemical sensor. The best method for an application of this ligand system would be in the combination with a heated probe containing a membrane. UV-Vis spectroscopy could be done through a

clear portion of the probe, although the detection limit of the technique will have to be taken into account. CV can be tested upon the precipitate that forms in another solution.

There are drawbacks to this ligand system such as low water solubility and irreversibility that may be overcome through further derivatization. The low solubility in water might be corrected through the addition of carboxylate groups to the phenyl (or Cp) rings. The irreversibility of the FcSH₂ system will be harder to change, but since the ligand can be made relatively cheaply in bulk from ferrocene, it might be better suited as is. Other cations (or even anions) might be sensed by these systems if the chelating groups are changed.

Another design change that can be explored in these systems is in the substitution of larger aromatic ring systems in place of the phenyl group. This should greatly enhance the fluorescence capabilities of the ligands when bound to a metal center. A larger ring system might allow for multiple metal cations to be chelated to the same ligand if more chelating groups are attached to the aromatic rings.

As there has been a recent progression in the design of disubstituted ferrocene ligands for various applications, the chemical sensing abilities of said ligands needs further exploration. With the creation of a new potential Hg²⁺ cationic sensor, more interest may be developed in the designing of environmentally useful ferrocene ligand systems.

The main purpose of this research project has been achieved in the formation of a new ferrocene sensor that selectively binds Hg²⁺ over other metal cations that are present in solution. This was done through a buildup of a known ferrocene ligand system to form two new systems for testing. By studying these systems, further ferrocene sensors can be

designed for detecting toxins in the environment before they can become much larger problems.

The potential application of ferrocene sensors in the future is almost limitless. They could be incorporated into food packaging to detect exposure to toxins before they become consumed. Water supplies might be tested through an outflow sensor that would detect heavy metals (and other toxic materials) before the water can be distributed out into a municipality. The concentration of heavy metal particulates in the air might also be monitored by ferrocene sensors in air filters.

Appendix of Spectroscopic Techniques: How does it work and why is it important?

Melting points- Used to determine the cohesive molecular forces used to hold molecules in place within a solid. This can give an indication of purity in samples. The samples are placed between two clear glass slides, heated with a melting point apparatus and carefully watched via an eyepiece for evidence of melting/decomposition of the sample.

Mass Spectroscopy- Used to determine the molecular weight of the largest ion (and subsequent ions) when a sample is passed through a source of ionization and through a coil of tubing to a detector. The existence of the M+1 peak (compound weight minus an electron) is used to prove the compound was present in the sample.

Infrared Spectroscopy- Used to determine many of the motions of the bonds within a molecule. Since some bonds (such as C-H, O-H, C-N, etc.) can absorb energy within the IR range, the change in the absorbance (or % transmittance) is used to determine the groups presence within the spectrum. During this technique, a sample (either in the form of a KBr pellet, KBr salt plate, or liquid in a KBr holder) is held in the IR beam between the source and the detector.

Ultraviolet-Visible Spectroscopy- Used to determine the molar absorptivity of a compound based upon the absorbance of light within a solution of the compound of known concentration in a quartz cuvette. The sample is held between the light source and the detector, whereby the difference in the light emitted by the source and the amount of

light that reaches the detector is measured. A spectrum will show the light energy needed to excite electrons from certain parts of the molecule (as bands), since the absorbed energy is used in this process.

Emission Fluorescence- Used to determine the fluorescent light emitted from a sample when light of a certain wavelength is passed through. The detector is placed at 90° from the source of the light to prevent detection of incident light from the source. Also, light of the particular wavelength is not typically measured by the detector. As the sample absorbs the light, electrons become promoted into excited states, whereby they can go through a series of processes to return to ground state (depending upon allowed and forbidden transitions). Since energy can be lost during the process, the emitted light when the electron returns back to the ground state will be at a higher wavelength (lower energy) than the initial wavelength needed to excite the electron. If a highly aromatic compound is measured, it may give a very strong fluorescent signal, such as the case with anthracene.

^1H Nuclear Magnetic Resonance- Used to determine the structural identity of molecules that are organic or contain organic parts. A radiowave is used to flip the direction of the magnetic moment within the molecule. As the nuclei relax back to the ground state, the signal emitted is detected and FT is used to convert the signal into a coherent form. Peaks give an indication of coupling between protons, type of proton (based upon position in spectrum) and amount of protons present. Paramagnetic (unpaired electrons) samples can greatly affect NMR spectrums as they can either spread out or become quite

broad as they lose their fine structure (appear as singlets rather than a series of multiple peaks).

Elemental Analysis- Used to determine the concentration of C, H, N content within a sample. It is done by burning the sample in presence of excess oxygen and collecting the exhaust gases for analysis. It gives an indication of the purity of the sample as impurities tend to lead to actual values deviating from the calculated values.

X-ray Fluorescence- Used to determine the concentration of each element that is present within a sample. A sample is prepared via soaking filter paper with a concentrated solution of the compound. Upon drying, it is then placed into the instrument, whereby x-ray radiation strikes the sample and the signal emitted by the atoms is detected.

Single Crystal X-ray Diffraction- Used to determine the molecular structure of single crystals by detection of incident x-rays scattered from the crystal. A beam of x-ray radiation hits the crystal and the nucleus scatters them in many directions. A detector is used to measure the scattered x-ray radiation and computer programs are used to help determine the concentration of electron density within a unit cell parameter. Different programs are used to determine the actual structure of the compound and the crystal packing of the unit cell.

Magnetic Susceptibility- Used to measure the amount of unpaired electrons by suspending a sample in a premeasured tube between magnets in a balance. Samples

Appendix of Spectral Properties:

Table A-1: Elemental Analysis of Fc2, FcOH2 and FcSH2 systems.

	Calc. C%	Actual C%	Calc. H%	Actual H%	Calc. N%	Actual N%
2	52.77	52.77	3.51	4.20	5.42	5.25
3	55.42	46.50	3.49	4.06	5.39	4.47
4	55.45	39.17	3.49	4.10	5.39	4.05
5	54.94	49.41	3.46	3.53	5.34	4.77
6	54.74	50.82	3.45	4.07	5.32	4.70
7	50.26	30.36	3.16	2.26	4.88	3.83
8	45.63	37.24	2.87	2.64	4.43	3.12
9	43.13	32.01	2.71	3.97	4.19	2.76
10	67.94	67.81	4.75	5.07	6.60	6.63
11	60.29	55.69	3.79	3.86	5.86	5.15
12	59.91	49.36	3.77	4.00	5.82	7.31
13	59.94	51.59	3.77	4.15	5.82	3.74
14	59.34	52.25	3.73	3.69	5.77	6.50
15	59.11	41.45	3.72	3.17	5.74	2.51
16	53.91	49.89	3.39	3.79	5.23	3.94
17	46.28	42.82	2.93	2.93	4.50	3.62
18	45.79	44.48	2.88	3.15	4.45	4.14
21	63.16	62.59	4.42	4.24	6.14	6.12
22	56.50	40.49	3.56	3.86	5.49	3.09
23	56.16	54.15	3.53	3.61	5.46	5.19
24	56.18	56.47	3.54	3.58	5.46	5.54
25	55.66	53.63	3.50	3.52	5.41	5.34
26	55.46	54.91	3.49	3.42	5.39	5.50
27	50.86	50.77	3.20	3.23	4.94	5.13
28	44.01	43.30	2.77	2.82	4.28	4.32
29	43.57	45.04	2.74	2.90	4.23	4.32

Table A-2: Magnetic Susceptibility Measurements of the Fc2, FcOH2 and FcSH2 systems:

Compound	$\chi_a(\text{corrected})$	μ_{eff}	Number of unpaired electrons
Fe(acetate) ₂	-0.000368	0	0
Co(acetate) ₂ ·4H ₂ O	0.00251	2.43	2
Ni(acetate) ₂ ·4H ₂ O	0.000778	1.35	1
Cu(acetate) ₂ ·1H ₂ O	0.000305	0.848	0
Zn(acetate) ₂ ·2H ₂ O	6.37E-05	0.388	0
Cd(acetate) ₂ ·2H ₂ O	6.91E-05	0.404	0
Hg(acetate) ₂	8.32E-05	0.443	0
Pb(acetate) ₂ ·3H ₂ O	6.99E-05	0.406	0
FeCl ₂ ·4H ₂ O	0.00245	2.41	2
CoCl ₂ ·6H ₂ O	0.00188	2.11	2
NiCl ₂ ·6H ₂ O	0.000848	1.41	1
CuCl ₂ ·2H ₂ O	0.000526	1.11	1
ZnCl ₂	3.64E-05	0.293	0
CdCl ₂ ·2.5H ₂ O	5.83E-05	0.371	0
HgCl ₂	4.64E-05	0.331	0
PbCl ₂	1.89E-05	0.211	0
1	-5.00E-06	0	0
10	9.02E-06	0.146	0
21	7.014E-06	0.129	0
23	0.000717	1.30	1
24	3.75E-05	0.297	0
25	2.37E-05	0.237	0
26	5.44E-05	0.358	0
27	1.59E-05	0.194	0
28	3.78E-05	0.296	0
29	3.68E-06	0.0932	0

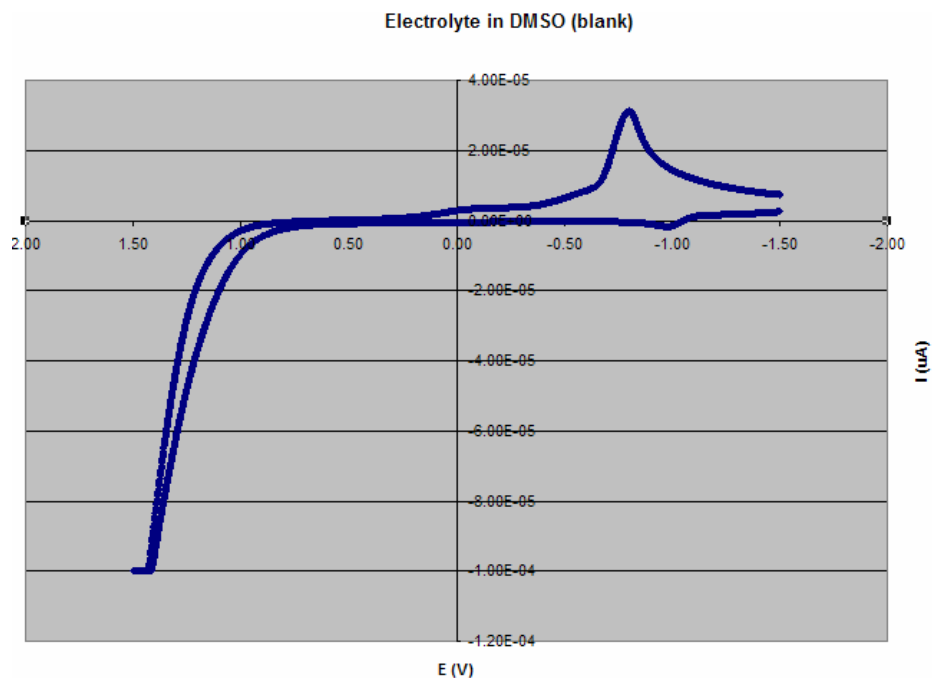


Figure A.1: CV background scan of electrolyte (1.0×10^{-3} M TBAHFP) in DMSO, scan rate 100 mV/sec.

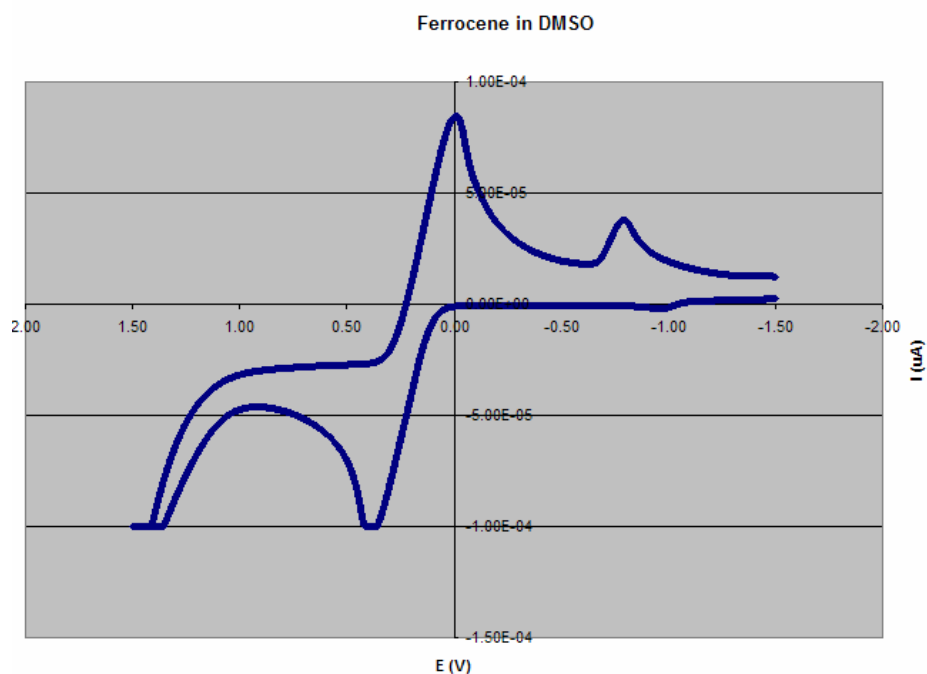


Figure A.2: CV scan of ferrocene in DMSO (with 1.0×10^{-3} M TBAHFP), scan rate 100 mV/sec. Fe^{II} to Fe^{III} ferrocene oxidation peak is at 388 mV (vs. 0.01 M Ag/AgNO_3 in DMSO).

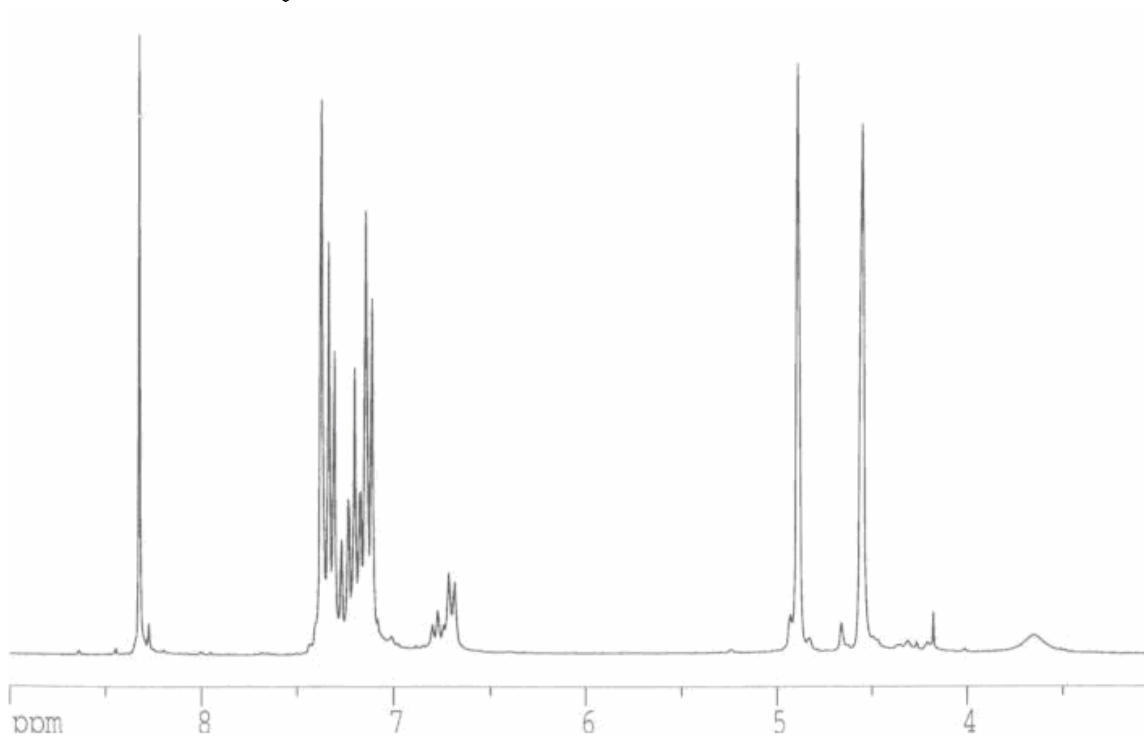
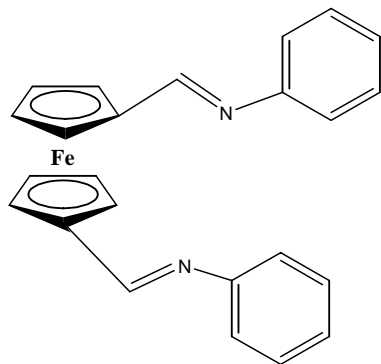
Compound 1:

Figure A.3: ^1H NMR spectrum of Fc2 in CDCl_3 : 8.33 ppm (2H, s, Cp-CH=N), 7.38-7.08 ppm (8H, m, phenyl), 4.90 ppm (4H, d, Cp), 4.55 ppm (4H, d, Cp);

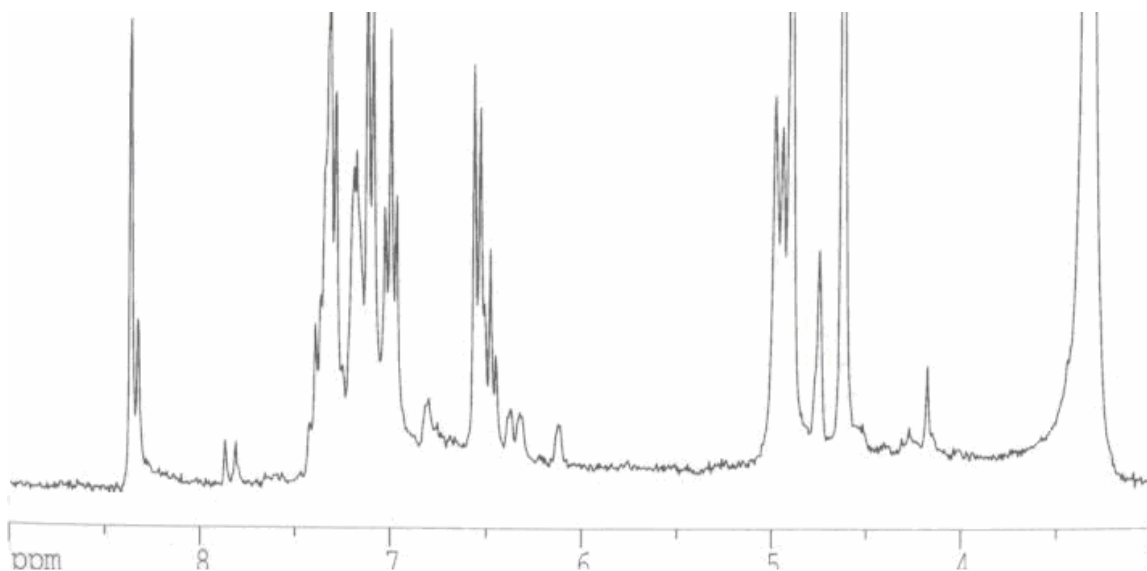


Figure A.4: ^1H NMR spectrum of Fc2 in d_6 -DMSO: 8.33 ppm (2H, s, Cp- $\underline{\text{C}}\text{H}=\text{N}$), 7.39-7.00 ppm (6H, m, phenyl), 6.56-6.3 ppm (2H, d, phenyl), 4.94 ppm (4H, d, Cp), 4.62 ppm (4H, d, Cp);

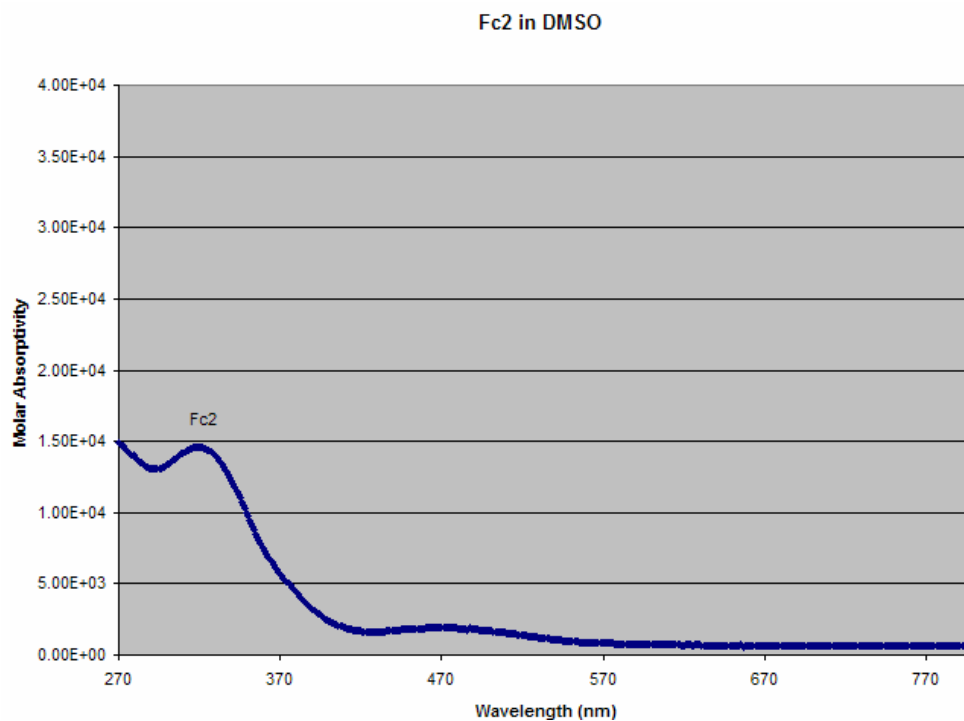


Figure A.5: Molar absorptivity (UV-Vis) of the Fc2 ligand in DMSO: 319 nm ($14600 \text{ M}^{-1}\text{cm}^{-1}$), 470 nm ($1930 \text{ M}^{-1}\text{cm}^{-1}$).

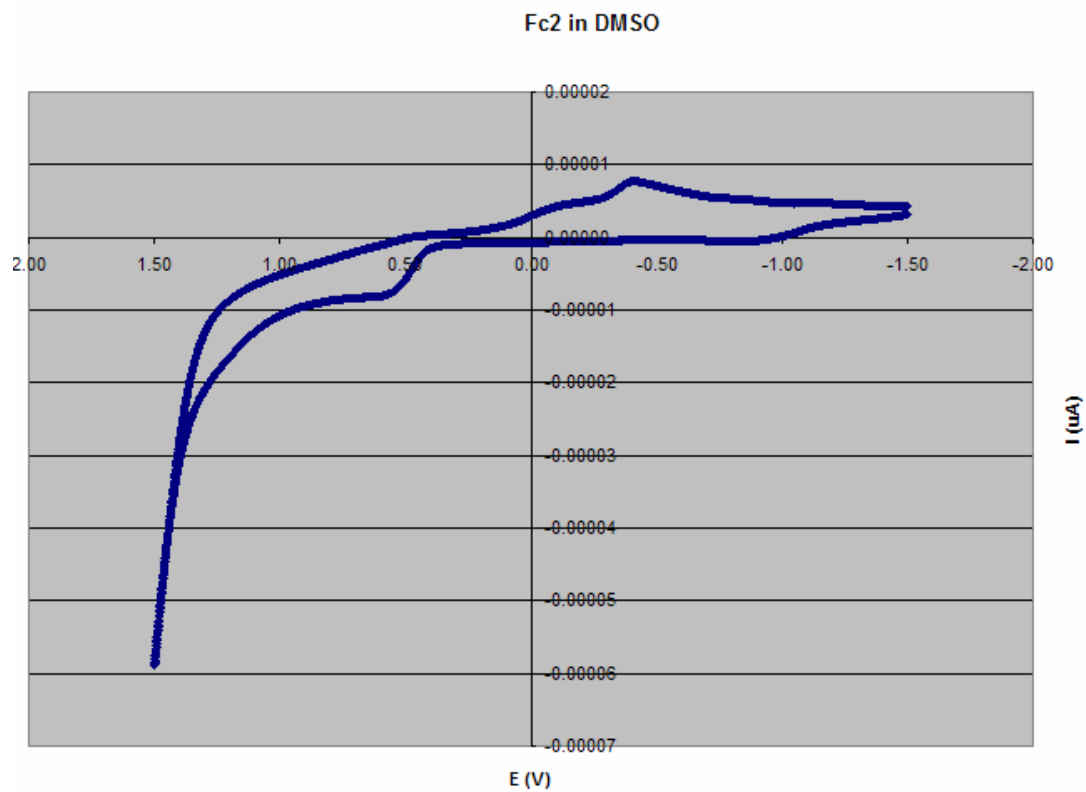
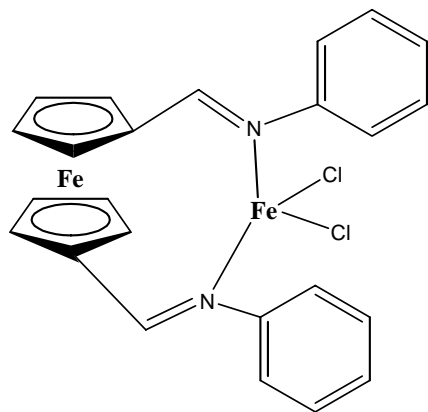


Figure A.6: CV scan of the Fc2 ligand in DMSO, scan rate 100 mV/sec. Fe^{II} to Fe^{III} oxidation peak is at 450 mV.

Compound 2:



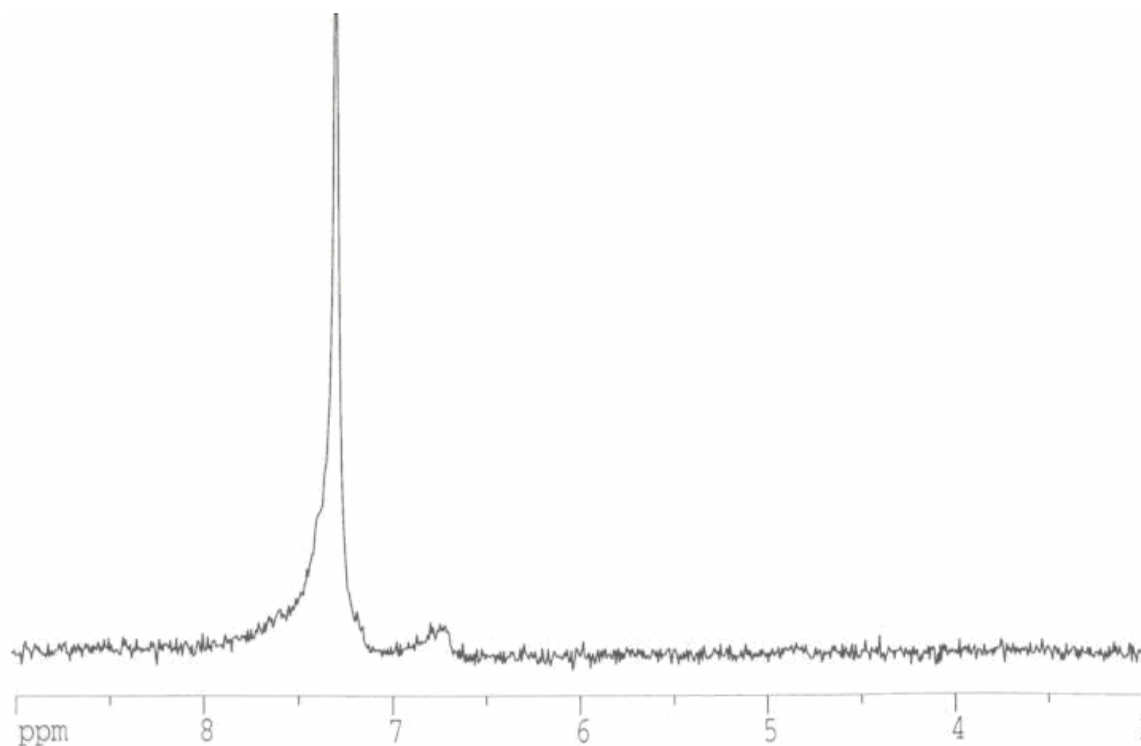


Figure A.7: ^1H NMR spectrum of $\text{Fc}_2\text{-FeCl}_2$ in CDCl_3 : 7.4 ppm (H, broad m, phenyl), 6.7 ppm (H, broad m, phenyl), 4.7 ppm (H, broad m, Cp);

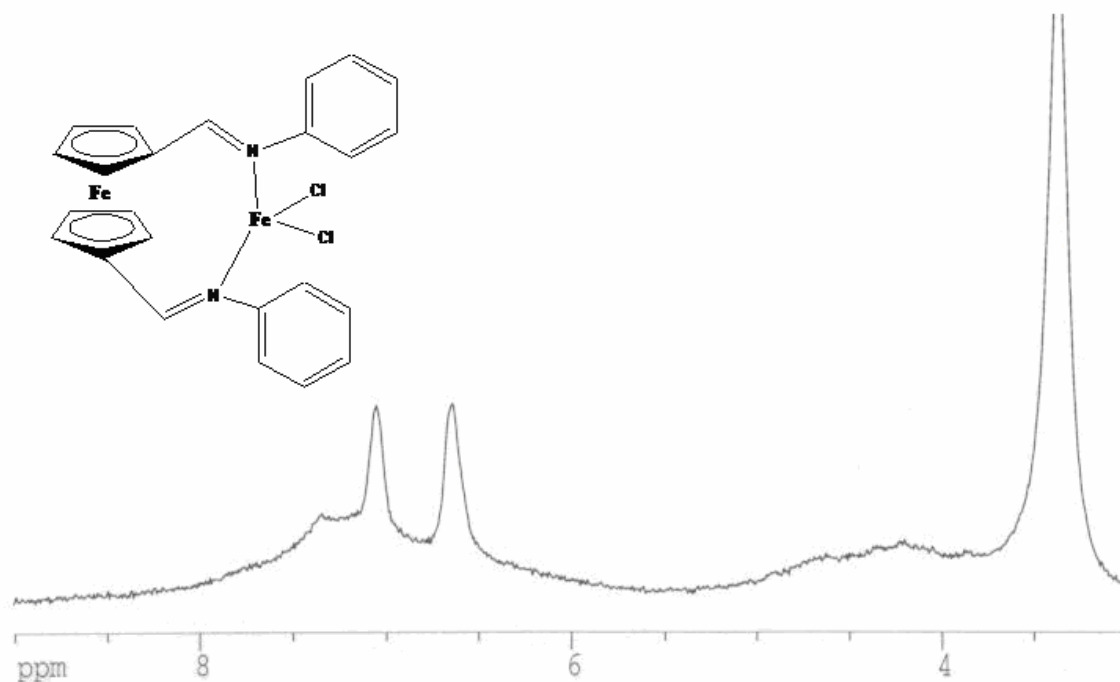


Figure A.8: ^1H NMR spectrum of $\text{Fc}_2\text{-FeCl}_2$ in $d_6\text{-DMSO}$: huge broad peak 8.5-6 ppm (H, m, phenyl), 7.04 ppm (H, broad s, phenyl), 6.64 ppm (H, broad s, phenyl), huge broad peak 5-3.5 ppm (H, m, Cp);

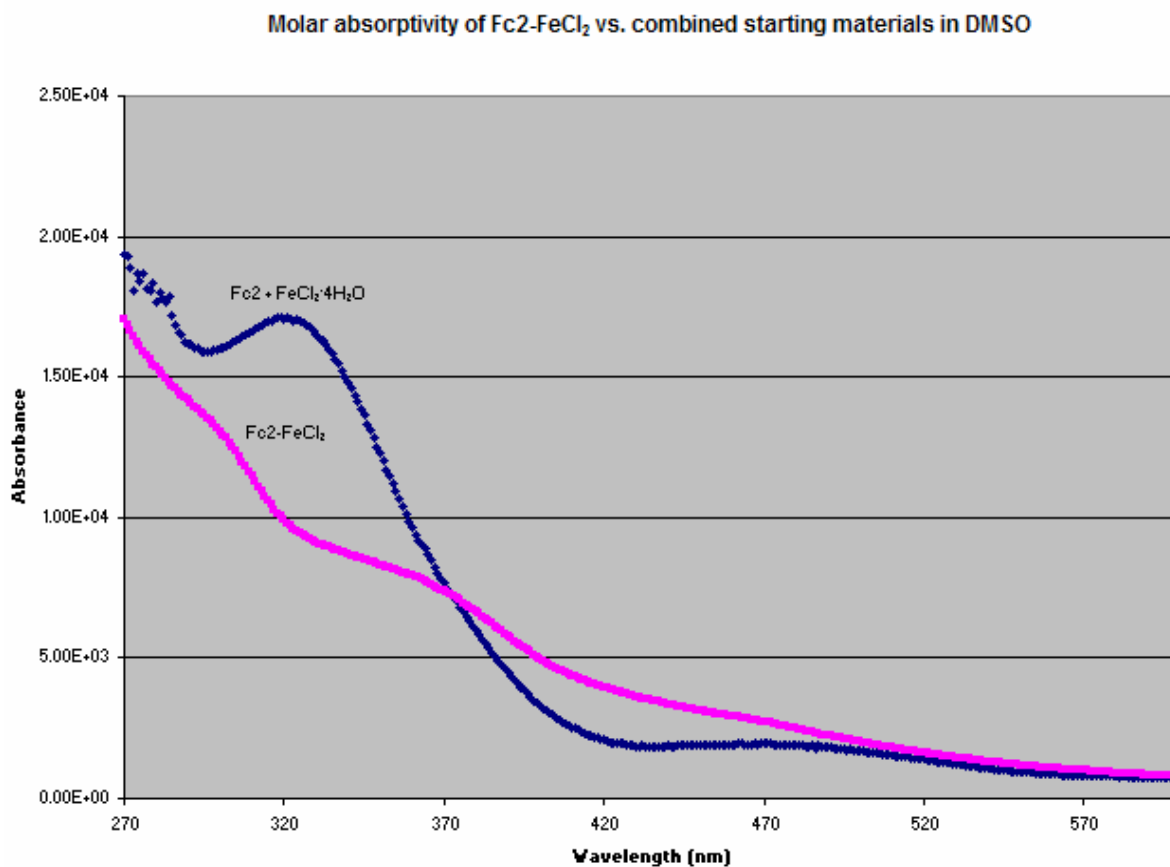
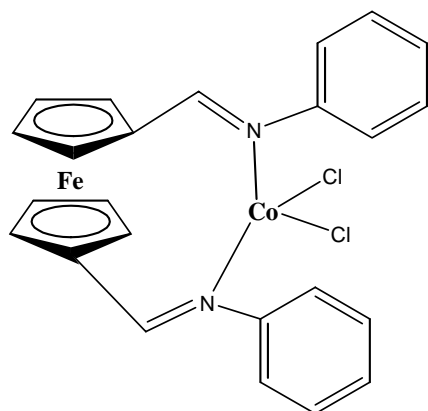


Figure A.9: Comparison between the molar absorptivity (UV-Vis) of $\text{Fc}_2\text{-FeCl}_2$ and the molar absorptivity of the starting materials (269 nm peak) in DMSO.

Compound 3:



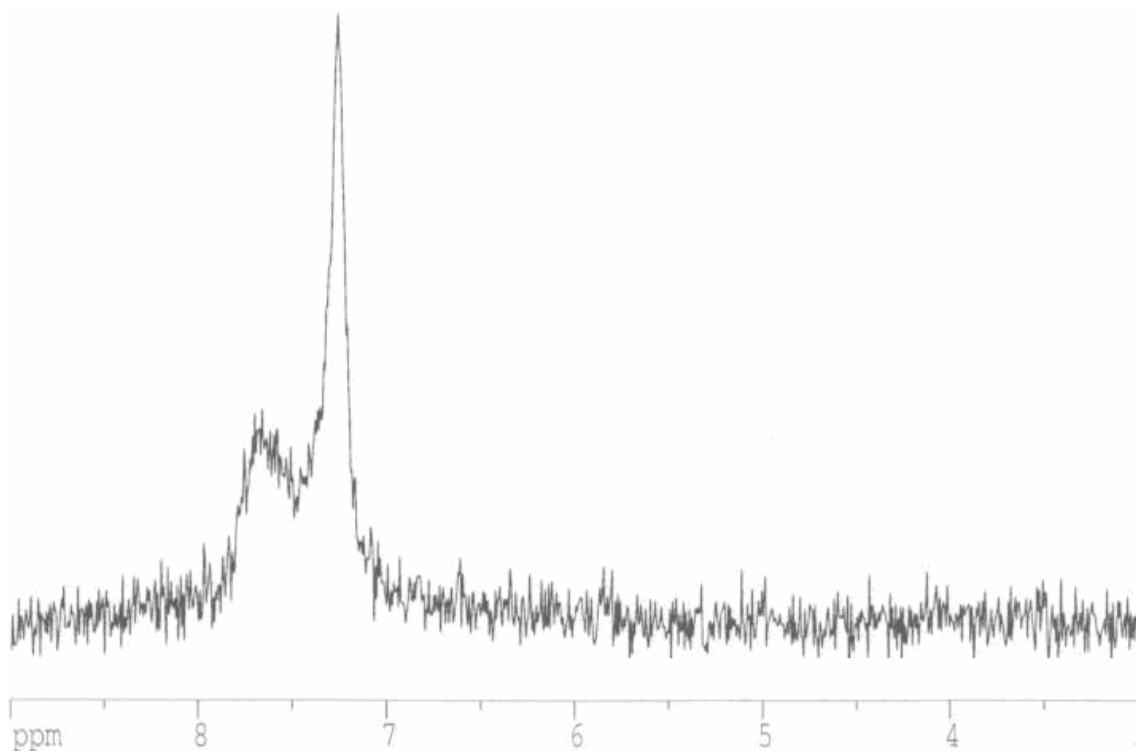


Figure A.10: ¹H NMR spectrum of Fc₂-CoCl₂ in CDCl₃: 8.7-8.4 ppm (H, broad m);

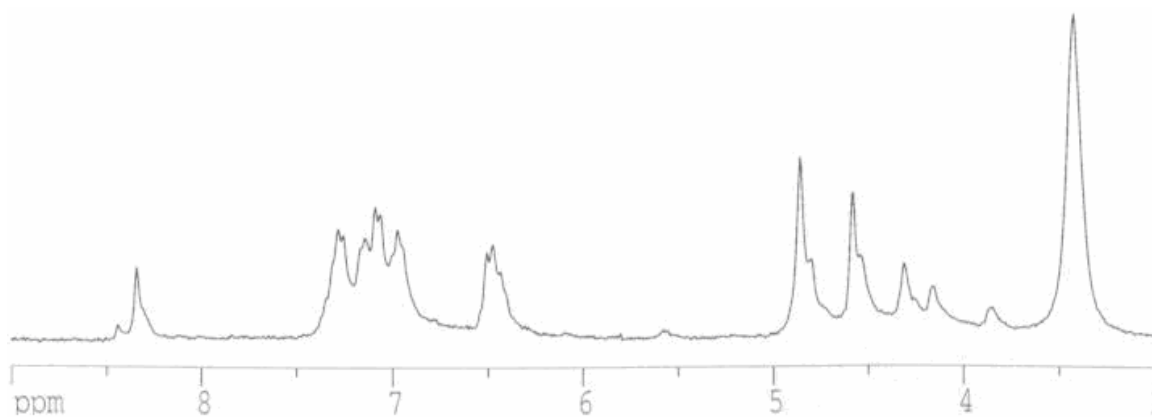


Figure A.11: ¹H NMR spectrum of Fc₂-CoCl₂ in d₆-DMSO: 8.34 ppm (2H, s, Cp-CH=N), 7.28 ppm (2H, d, Phenyl), 7.08 ppm (2H, dd, phenyl), 6.97 ppm (2H, d, phenyl), 6.48 ppm (2H, t, phenyl), 4.86 ppm (4H, d, Cp), 4.58 ppm (4H, d, Cp);

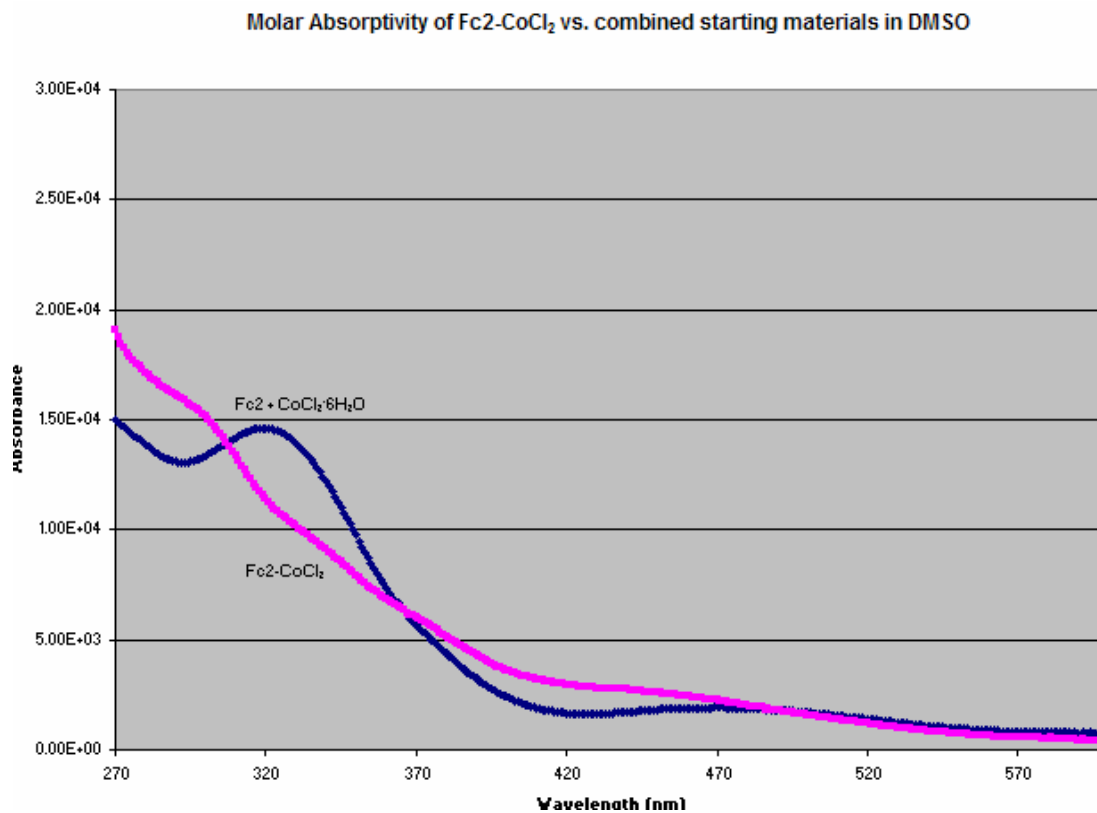
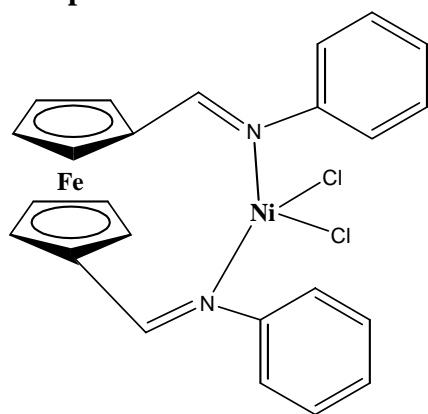


Figure A.12: Comparison between the molar absorptivity (UV-Vis) of Fe₂-CoCl₂ and the molar absorptivity of the starting materials (321m 470 nm peaks) in DMSO.

Compound 4:



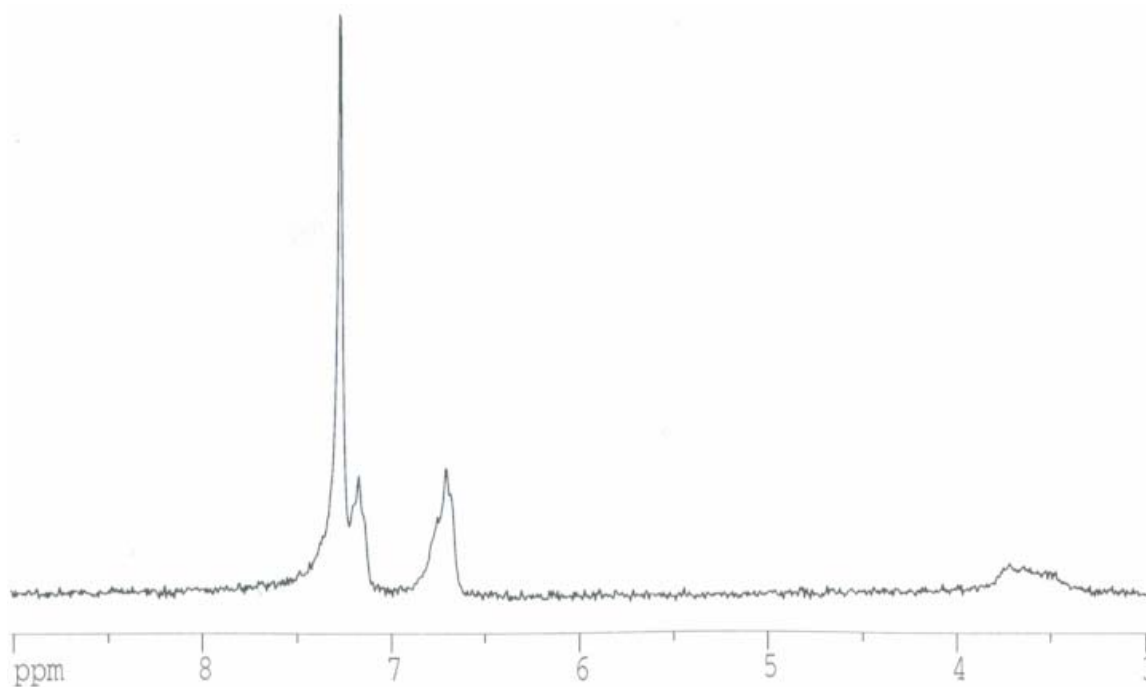


Figure A.13: ^1H NMR spectrum of $\text{Fc}_2\text{-NiCl}_2$ in CDCl_3 : 7.2 ppm (H, t), 6.6 ppm (H, t), 4.5 ppm (H, broad m);

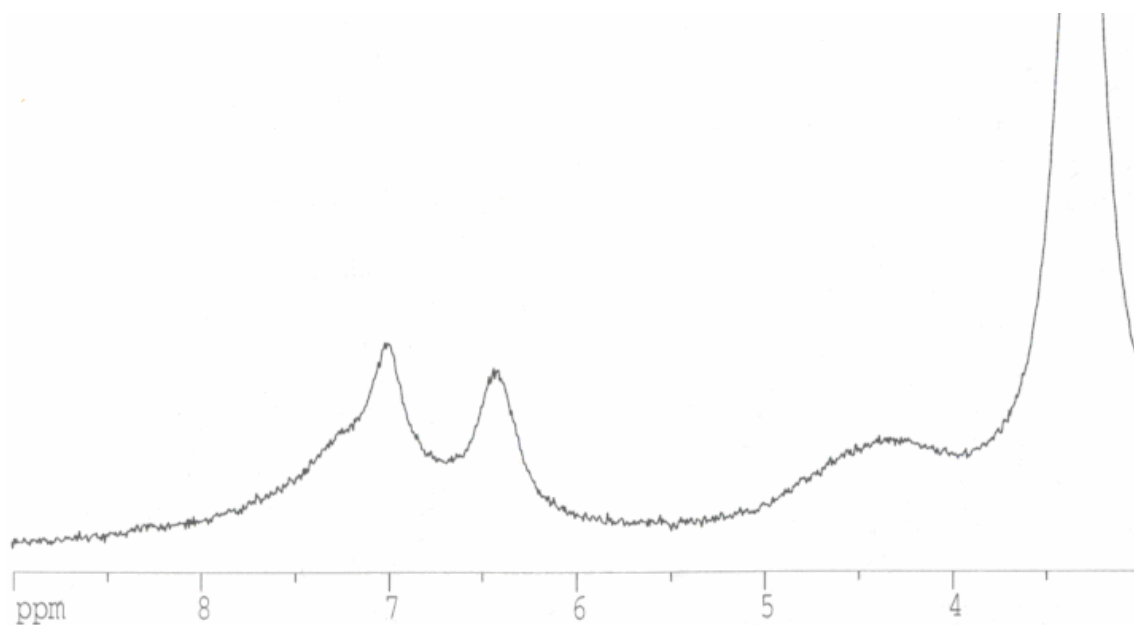


Figure A.14: ^1H NMR spectrum of $\text{Fc}_2\text{-NiCl}_2$ in $d_6\text{-DMSO}$: 7.34 ppm (2H, broad s, Cp- $\underline{\text{C}}\text{H}=\text{N}$), 7.17 ppm (4H, broad s, phenyl), 6.99 ppm (4H, broad s, phenyl), 4.59 ppm (4H, broad s, Cp), 4.33 ppm (4H, broad s, Cp);

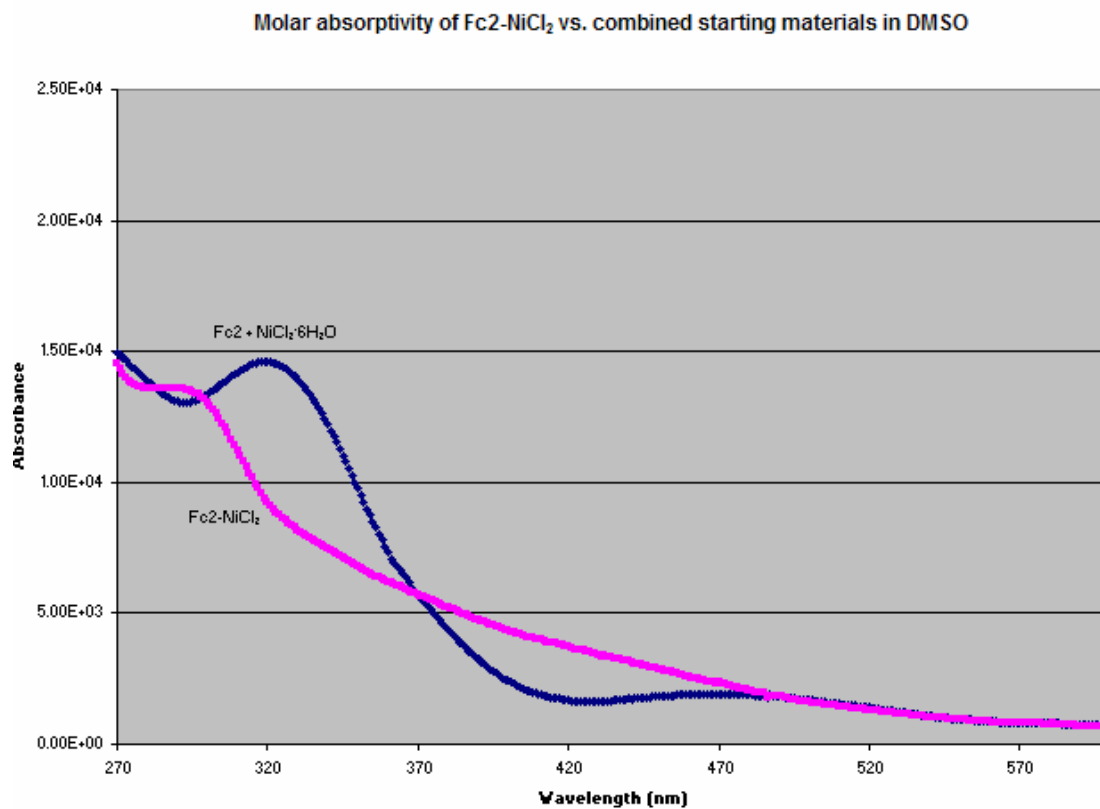
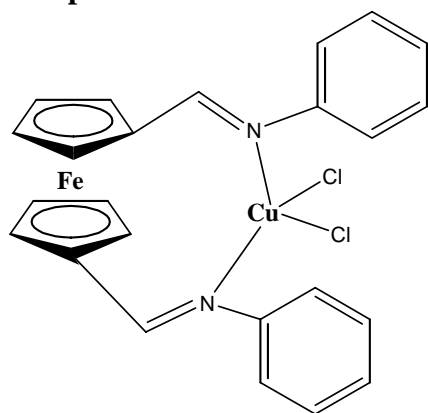


Figure A.15: Comparison between the molar absorptivity (UV-Vis) of $\text{Fc}_2\text{-NiCl}_2$ and the molar absorptivity of the starting materials (319, 470 nm peaks) in DMSO: 290 nm ($9600 \text{ M}^{-1}\text{cm}^{-1}$)

Compound 5:



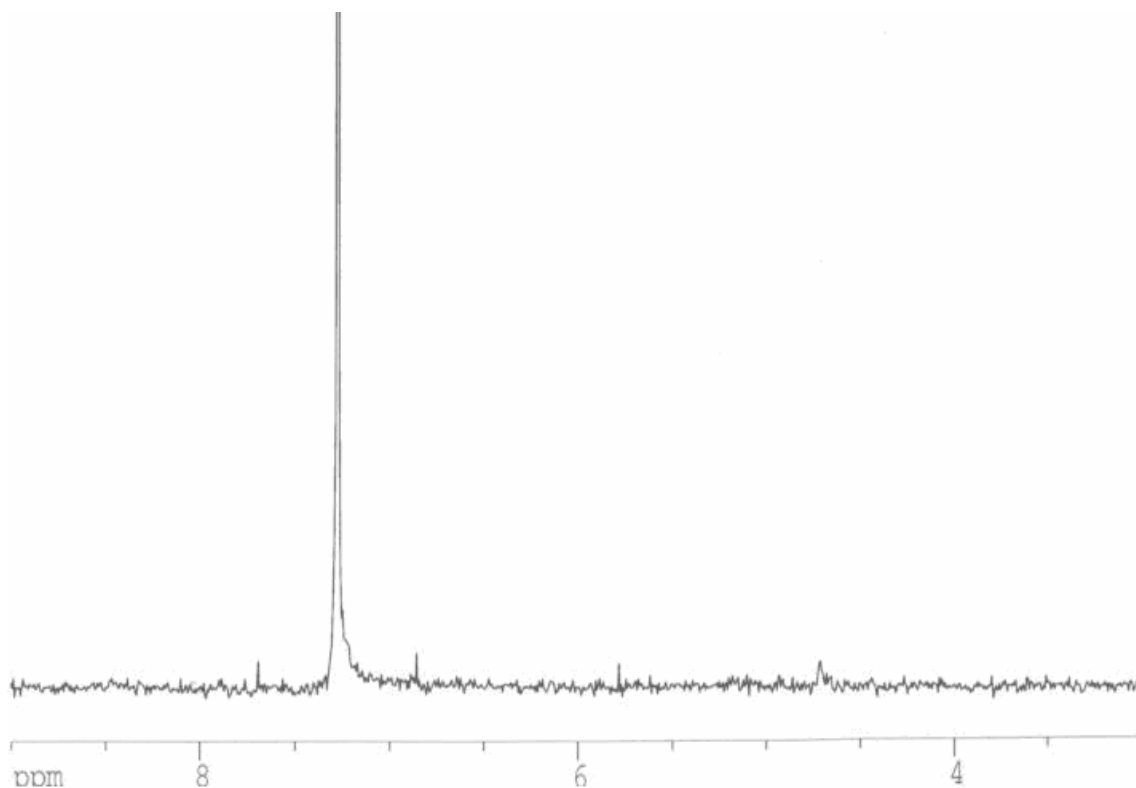


Figure A.16: ^1H NMR spectrum of $\text{Fc}_2\text{-CuCl}_2$ in CDCl_3 : 7.68 ppm (2H, s, Cp- $\underline{\text{C}}\text{H}=\text{N}$), 6.85 ppm (H, s, phenyl), 5.78 ppm (H, s), 4.71 ppm (H, s, Cp), 2.6 ppm (H, s);

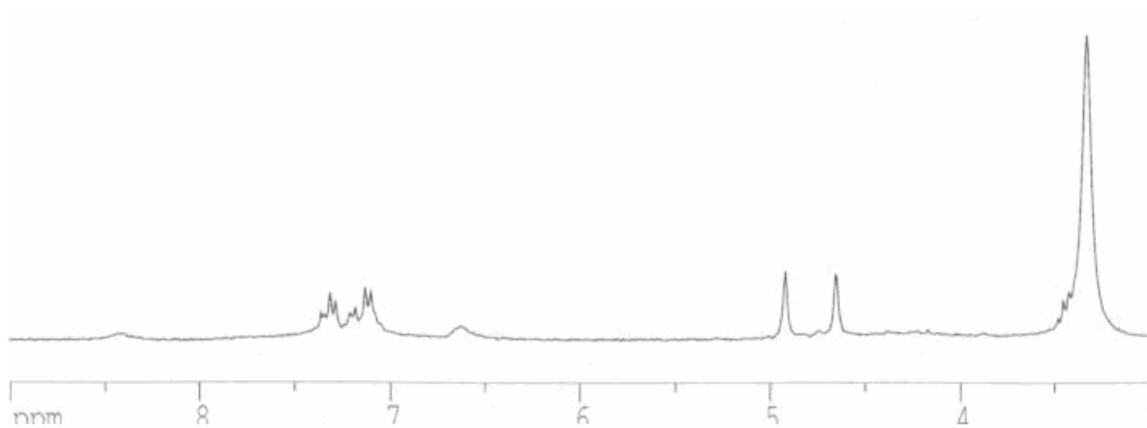


Figure A.17: ^1H NMR spectrum of $\text{Fc}_2\text{-CuCl}_2$ in $d_6\text{-DMSO}$: 8.4 ppm (2H, s, Cp- $\underline{\text{C}}\text{H}=\text{N}$), 7.36-7.31 ppm (2H, t, Phenyl), 7.28 ppm (2H, d, phenyl), 7.18-7.09 ppm (2H, d, phenyl), 6.7 ppm (2H, broad s, phenyl), 4.91 ppm (4H, s, Cp), 4.65 ppm (4H, s, Cp);

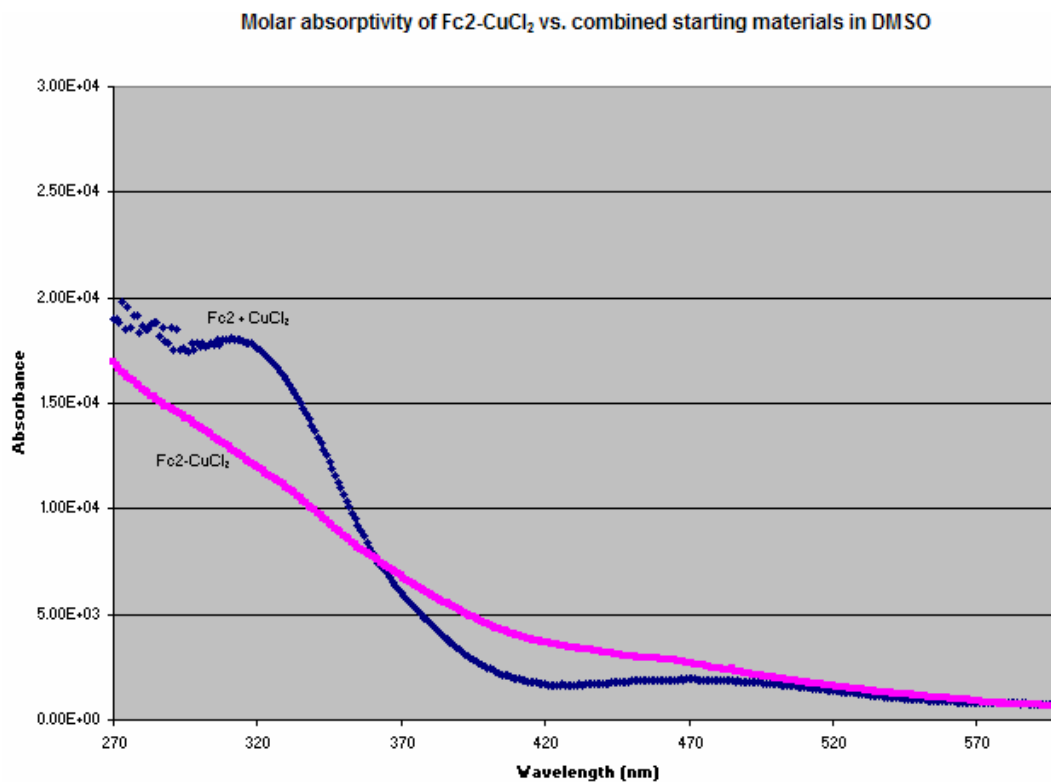
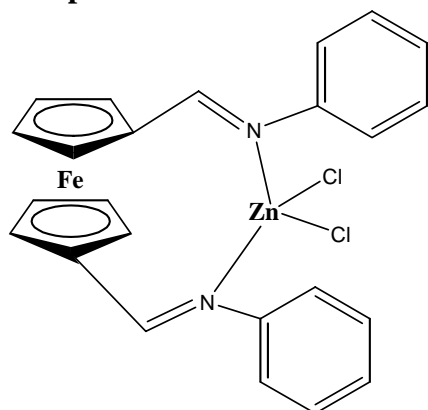


Figure A.18: Comparison between the molar absorptivity (UV-Vis) of $\text{Fc}_2\text{-CuCl}_2$ and the molar absorptivity of the starting materials (311, 470 nm peaks) in DMSO: 461 nm ($2590 \text{ M}^{-1}\text{cm}^{-1}$), 463 nm ($2580 \text{ M}^{-1}\text{cm}^{-1}$);

Compound 6:



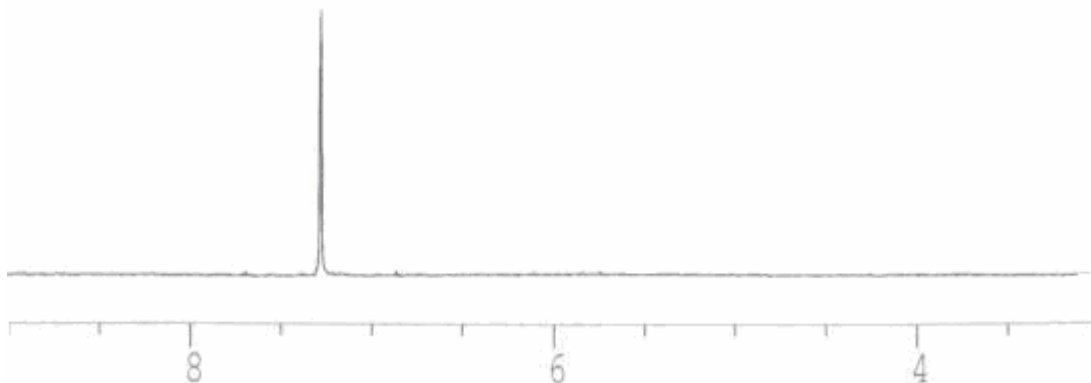


Figure A.19: ^1H NMR spectrum of $\text{Fc}_2\text{-ZnCl}_2$ in CDCl_3 : no peaks

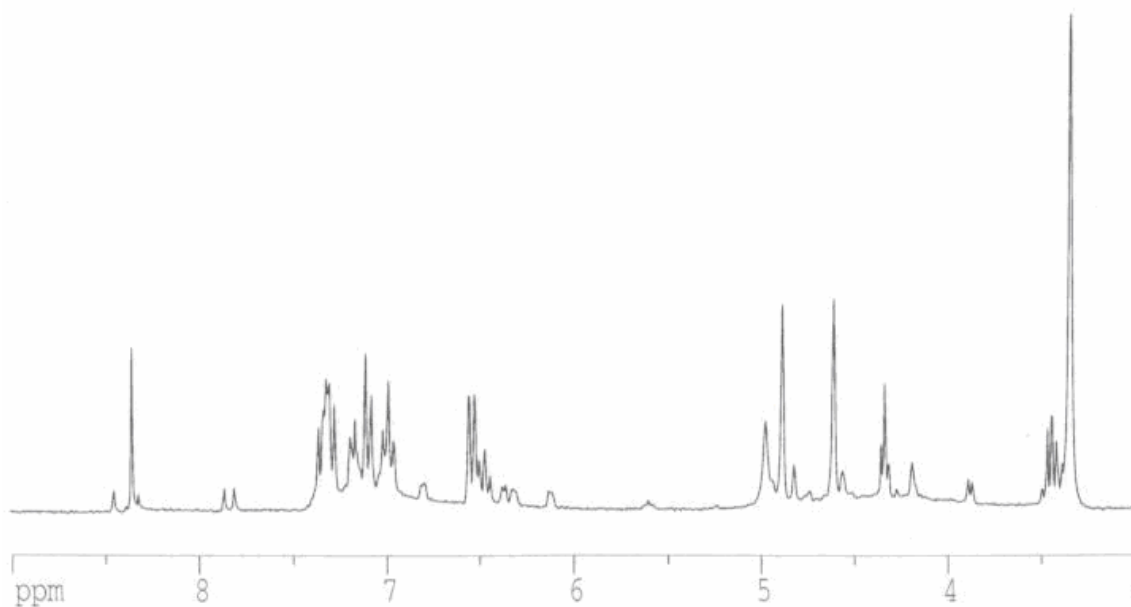


Figure A.20: ^1H NMR spectrum of $\text{Fc}_2\text{-ZnCl}_2$ in $d_6\text{-DMSO}$: 8.36 ppm (2H, s, Cp- $\underline{\text{C}}\text{H}=\text{N}$), 7.35-7.31 ppm (H, q, phenyl), 7.28-7.19 ppm (H, d, phenyl), 7.16-7.10 ppm (H, d, phenyl), 7.01-6.95 ppm (H, t, phenyl), 4.88 ppm (H, s Cp), 4.57 ppm (H, s, Cp);

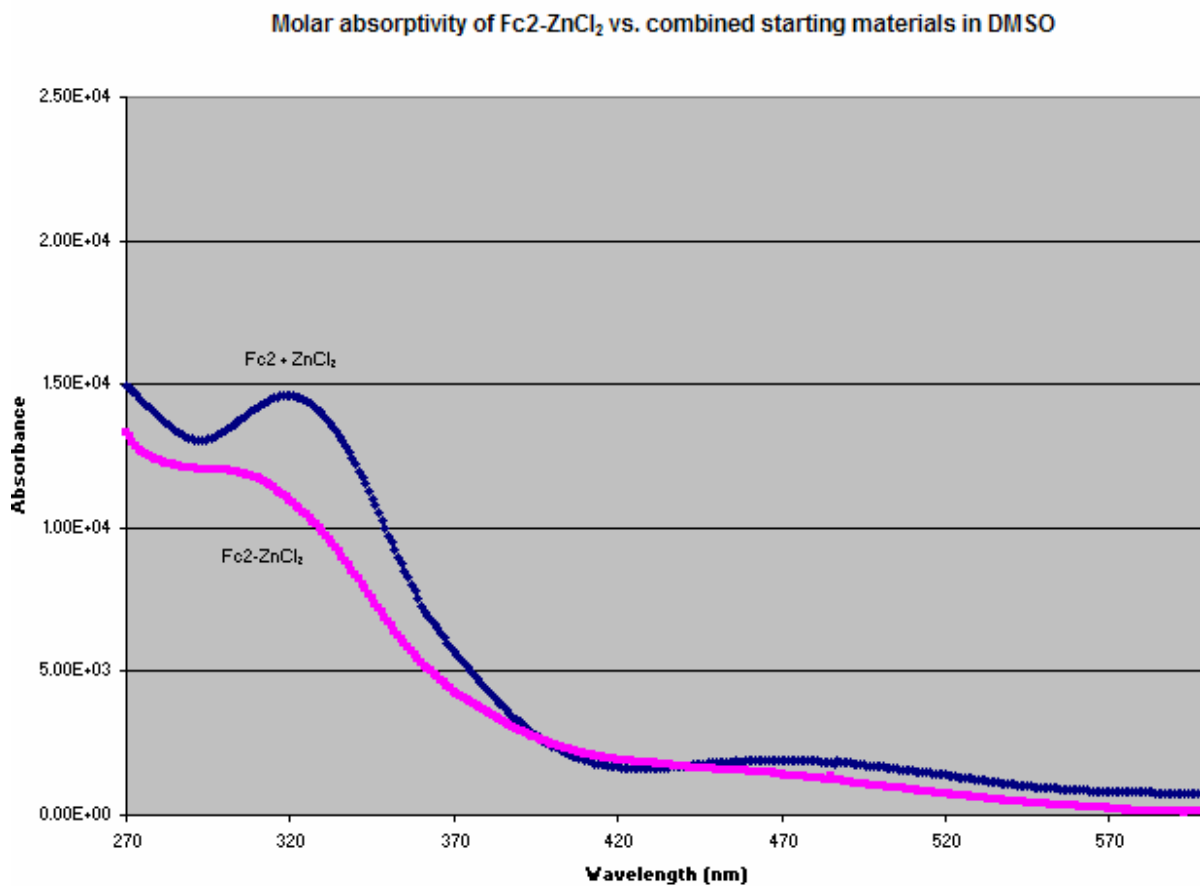
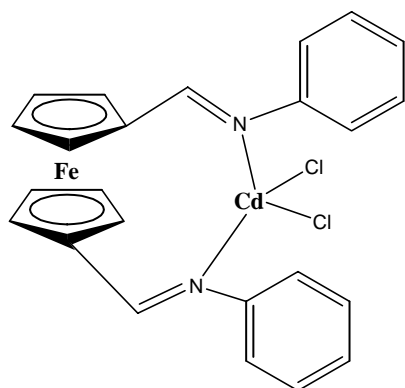


Figure A.21: Comparison between the molar absorptivity (UV-Vis) of $\text{Fc}_2\text{-ZnCl}_2$ and the molar absorptivity of the starting materials (319, 470 nm peaks) in DMSO: 295 nm ($11200 \text{ M}^{-1}\text{cm}^{-1}$)

Compound 7:



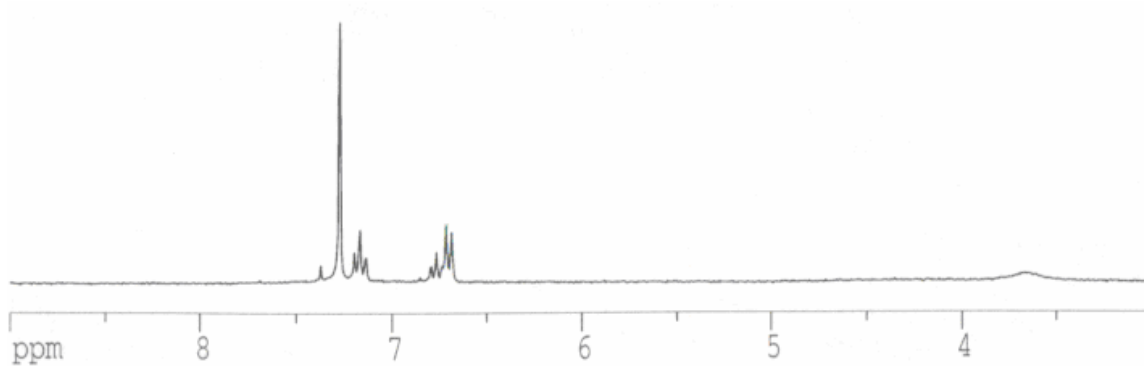


Figure A.22: ^1H NMR spectrum of $\text{Fc}_2\text{-CdCl}_2$ in CDCl_3 : 7.15 ppm (H, t), 6.8 ppm (H, d), 6.7 ppm (H, d), Very broad peak 3.8-3.4 ppm (H);

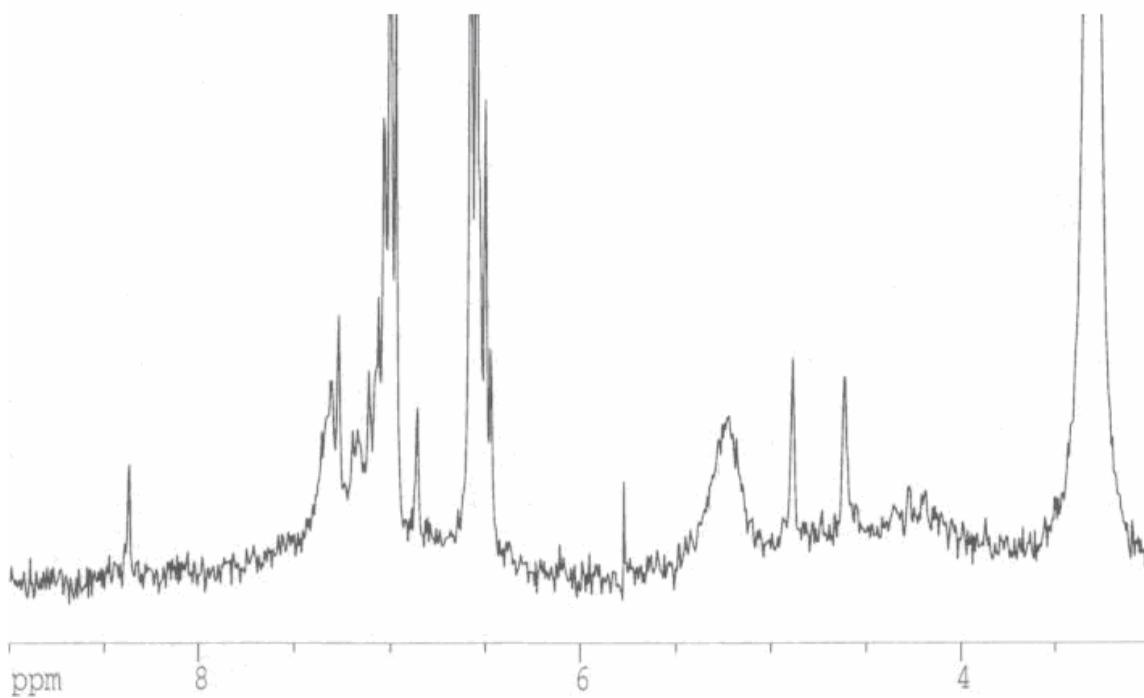


Figure A.23: ^1H NMR spectrum of $\text{Fc}_2\text{-CdCl}_2$ in $d_6\text{-DMSO}$: 8.37 ppm (2H, s, Cp- $\text{CH}=\text{N}$), 7.30 ppm (H, t, phenyl), 7.11-6.96 ppm (H, t, phenyl), 6.58-6.47 ppm (H, t, phenyl), Very broad peak at 5.22 ppm (H, s, Cp), 4.89 ppm (H, s, Cp), 4.61 ppm (H, s, Cp), Very broad peak 4.3-3.7 ppm (H, Cp);

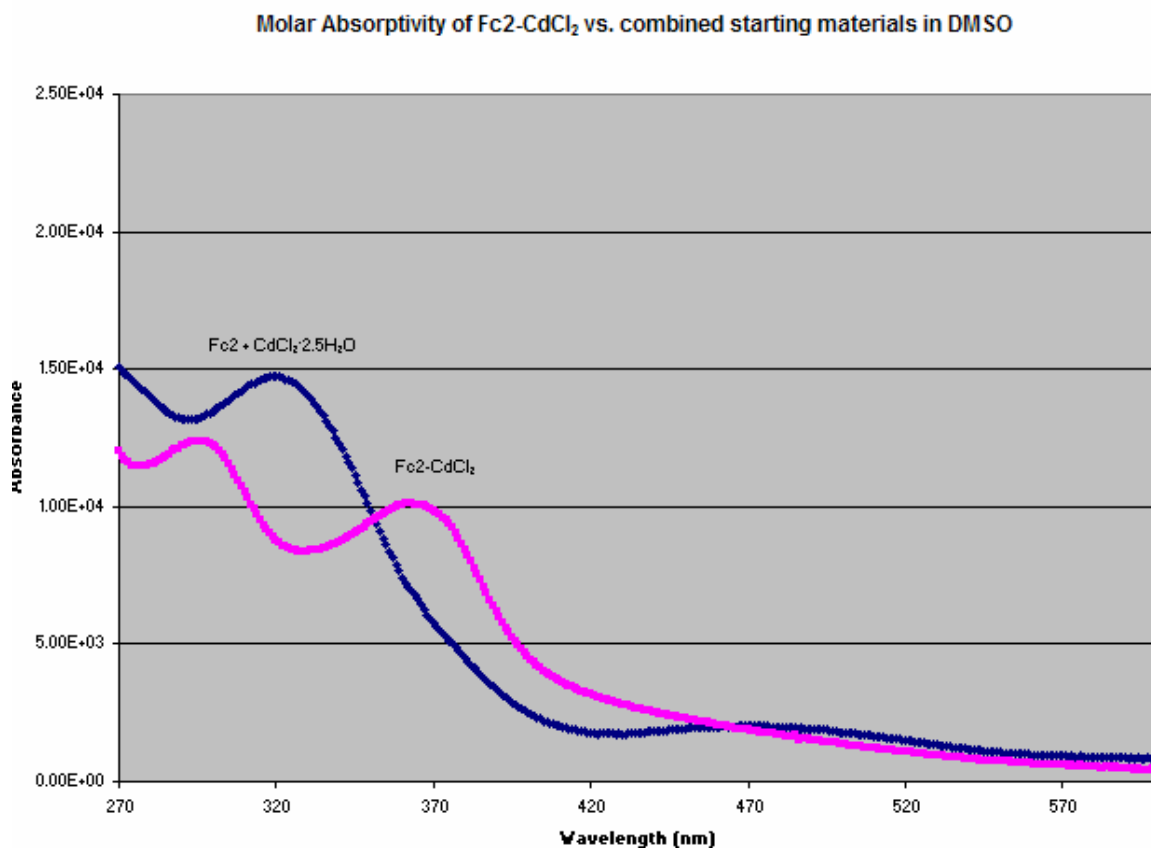
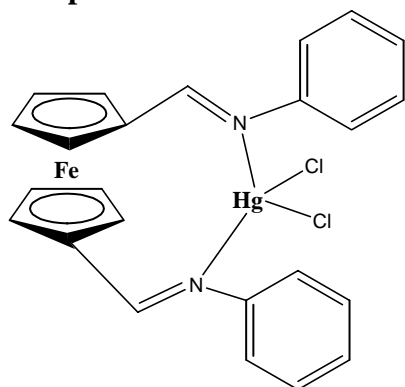


Figure A.24: Comparison between the molar absorptivity (UV-Vis) of $\text{Fc}_2\text{-CdCl}_2$ and the molar absorptivity of the starting materials (319, 470 nm peaks) in DMSO: 296 nm ($7510 \text{ M}^{-1}\text{cm}^{-1}$), 362 nm ($6140 \text{ M}^{-1}\text{cm}^{-1}$)

Compound 8:



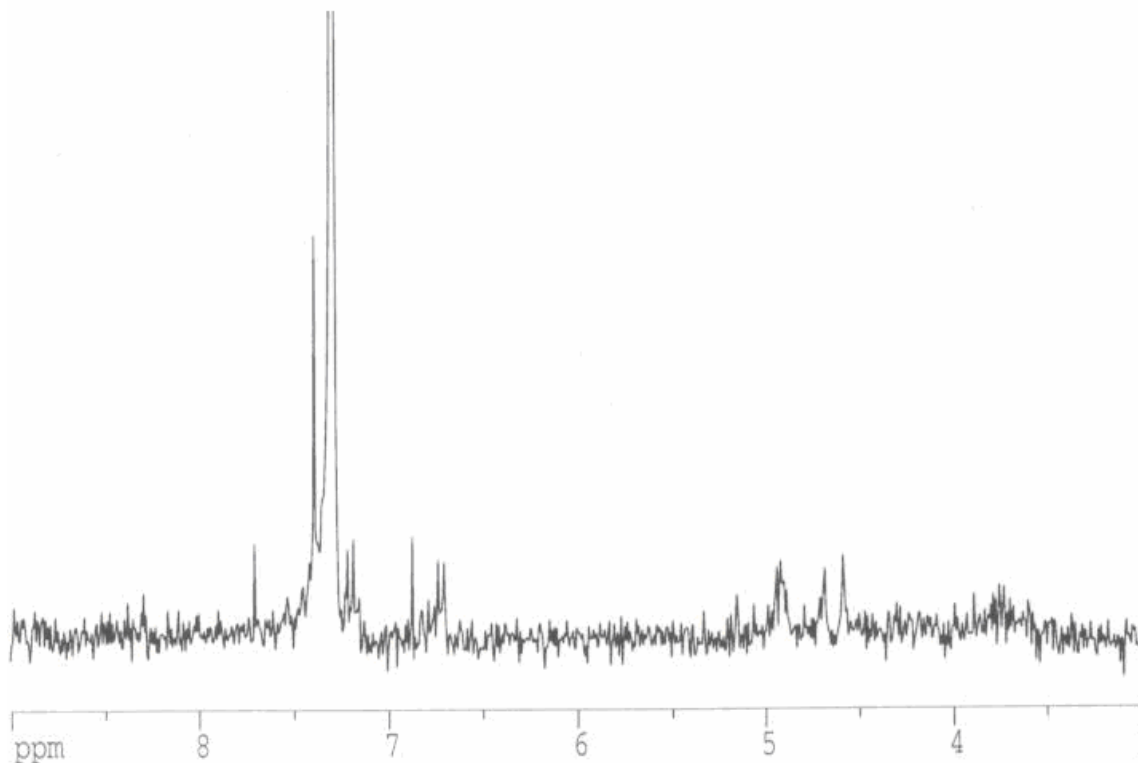


Figure A.25: ^1H NMR spectrum of $\text{Fc}_2\text{-HgCl}_2$ in CDCl_3 : 7.70 ppm (2H, s, Cp- $\underline{\text{C}}\text{H}=\text{N}$), 7.18 ppm (1H, d, phenyl), 6.86 ppm (1H, s, phenyl), 6.60 ppm (2H, d, phenyl), 4.9 ppm (4H, m, Cp), 4.7 ppm (2H, s, Cp), 4.5 ppm (2H, s, Cp);

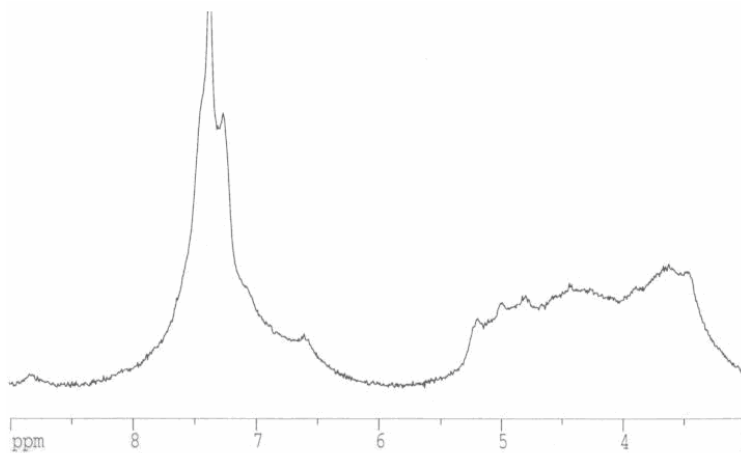


Figure A.26: ^1H NMR spectrum of $\text{Fc}_2\text{-HgCl}_2$ in $d_6\text{-DMSO}$: 8.83 ppm (H, broad s, Cp- $\underline{\text{C}}\text{H}=\text{N}$), Very broad from 8.0-6.0 ppm (H, s), 7.37 ppm (H, s, phenyl), 7.25 ppm (H, s, phenyl), Very broad from 5.7-3.7 ppm (H, m), 4.81 ppm (H, s, Cp), 4.42 ppm (H, s, Cp);

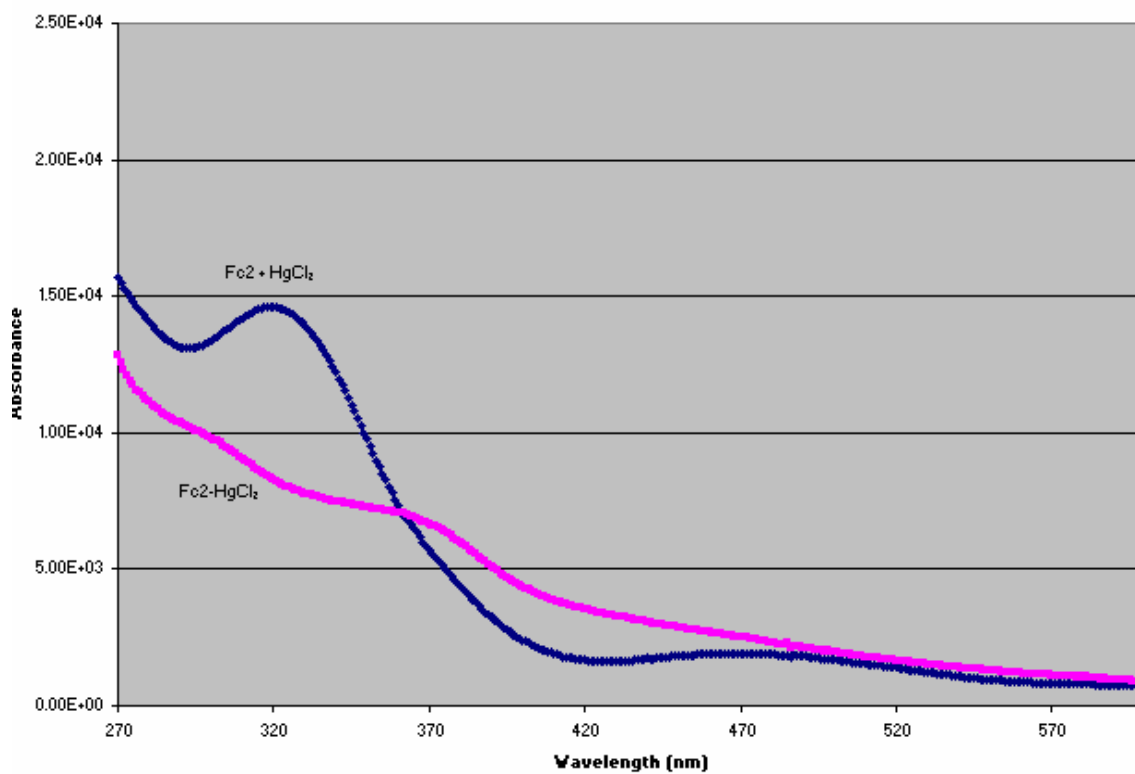
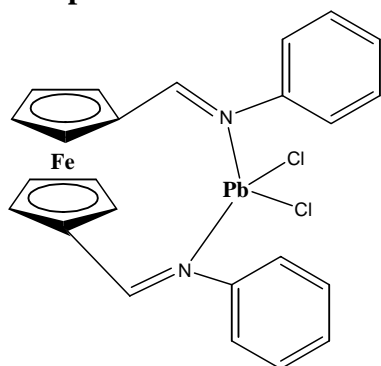
Molar absorptivity of $\text{Fc}_2\text{-HgCl}_2$ vs. combined starting materials in DMSO

Figure A.27: Comparison between the molar absorptivity (UV-Vis) of $\text{Fc}_2\text{-HgCl}_2$ and the molar absorptivity of the starting materials (319, 470 nm peaks) in DMSO.

Compound 9:



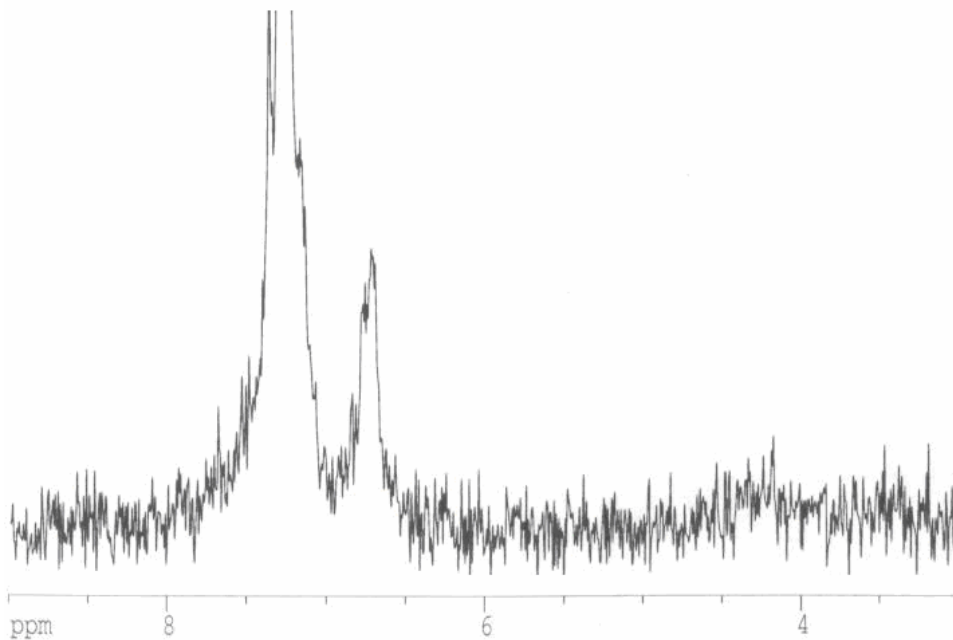


Figure A.28: ^1H NMR spectrum of $\text{Fc}_2\text{-PbCl}_2$ in CDCl_3 : 8.0-7.4 ppm (H, s), 6.73 ppm (H, d), Very broad 5.0-4.0 ppm (H, m), Very broad 3.7-3.3 ppm (H, m);

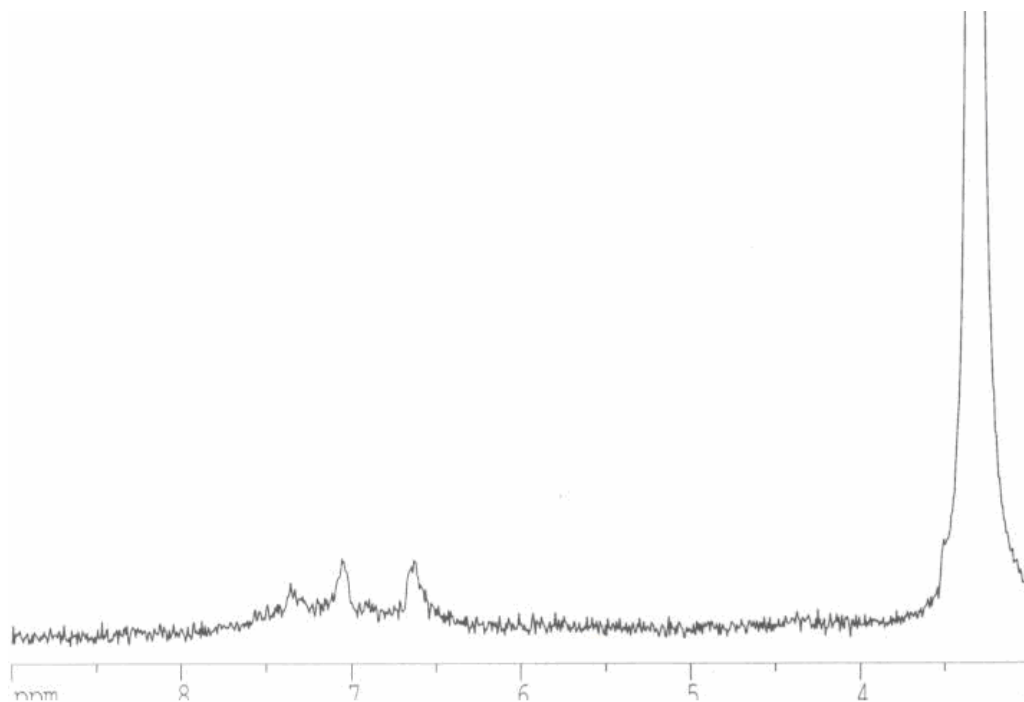


Figure A.29: ^1H NMR spectrum of $\text{Fc}_2\text{-PbCl}_2$ in $\text{d}_6\text{-DMSO}$: 7.5 ppm (2H, broad s, phenyl), 7.06 ppm (2H, broad s, phenyl), 6.63 ppm (4H, broad d, phenyl), Very broad peak 6.0-5.0 ppm (H, m, Cp), Very broad peak 5.0-4.0 ppm (H, m, Cp);

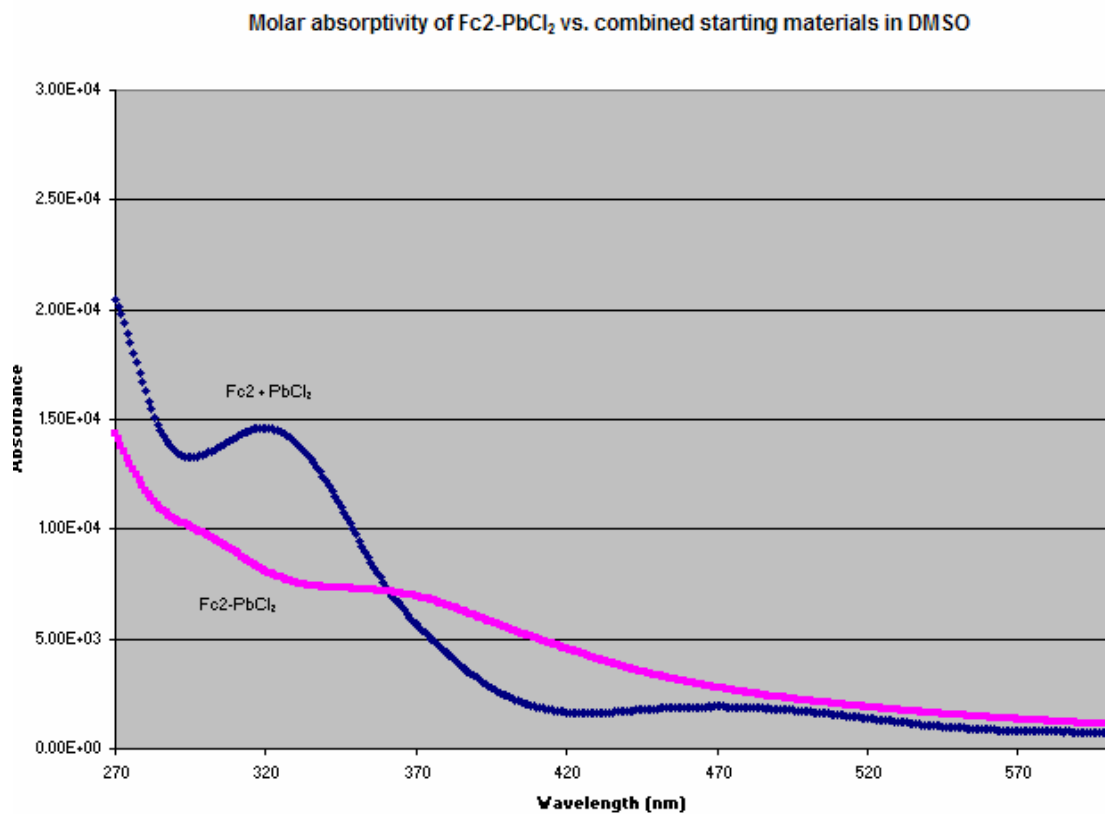
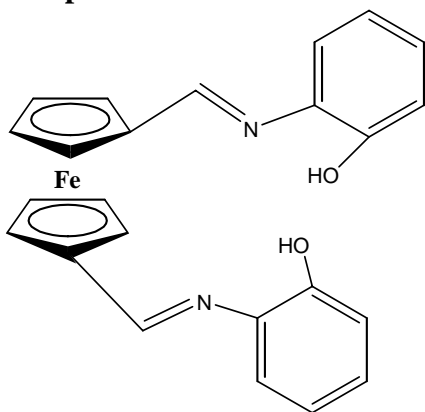


Figure A.30: Comparison between the molar absorptivity (UV-Vis) of Fc2-PbCl_2 and the molar absorptivity of the starting materials (319, 470 nm peaks) in DMSO: 340 nm ($5480 \text{ M}^{-1}\text{cm}^{-1}$);

Compound 10:



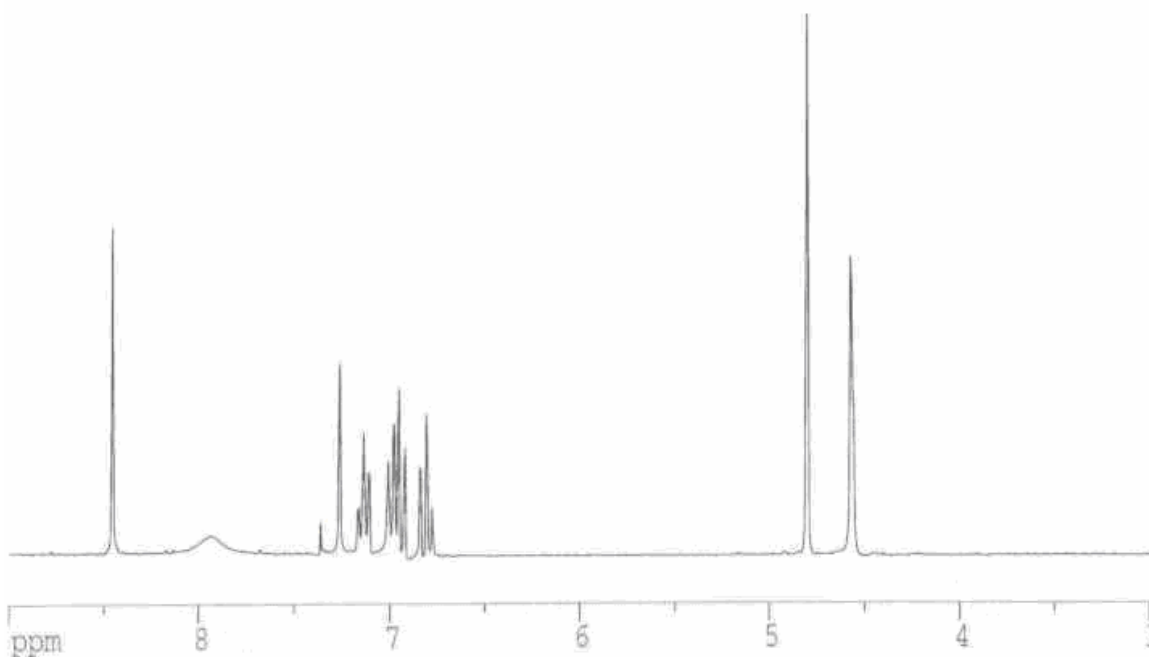


Figure A.31: ^1H NMR spectrum of FcOH2 in CDCl_3 : 8.50 ppm (2H, s, Cp- $\underline{\text{C}}\text{H}=\text{N}$), 7.95 ppm (broad s, OH), 7.17-7.11 ppm (2H, t, Phenyl), 7.02-6.96 ppm (4H, q, Phenyl), 6.85-6.79 ppm (2H, t, Phenyl), 4.86 ppm (4H, d, Cp), 4.58 ppm (4H, d, Cp);

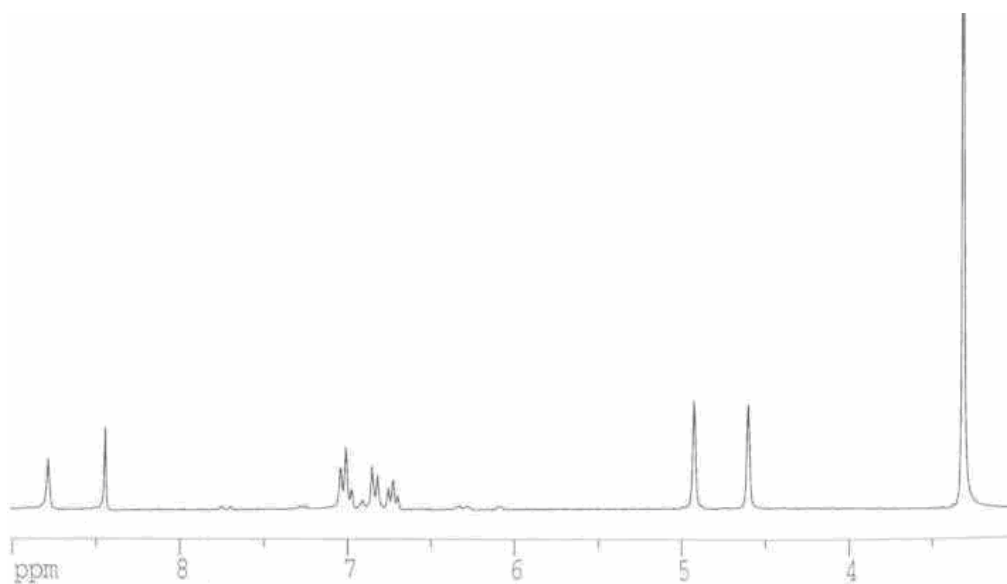


Figure A.32: ^1H NMR spectrum of FcOH2 in $\text{d}_6\text{-DMSO}$: 8.78 ppm (2H, s, OH), 8.44 ppm (2H, s, Cp- $\underline{\text{C}}\text{H}=\text{N}$), 7.03-6.97 ppm (4H, t, Phenyl), 6.90-6.84 ppm (2H, d, Phenyl), 6.75-6.69 ppm (2H, t, Phenyl), 4.92 ppm (4H, d, Cp), 4.59 ppm (4H, d, Cp);

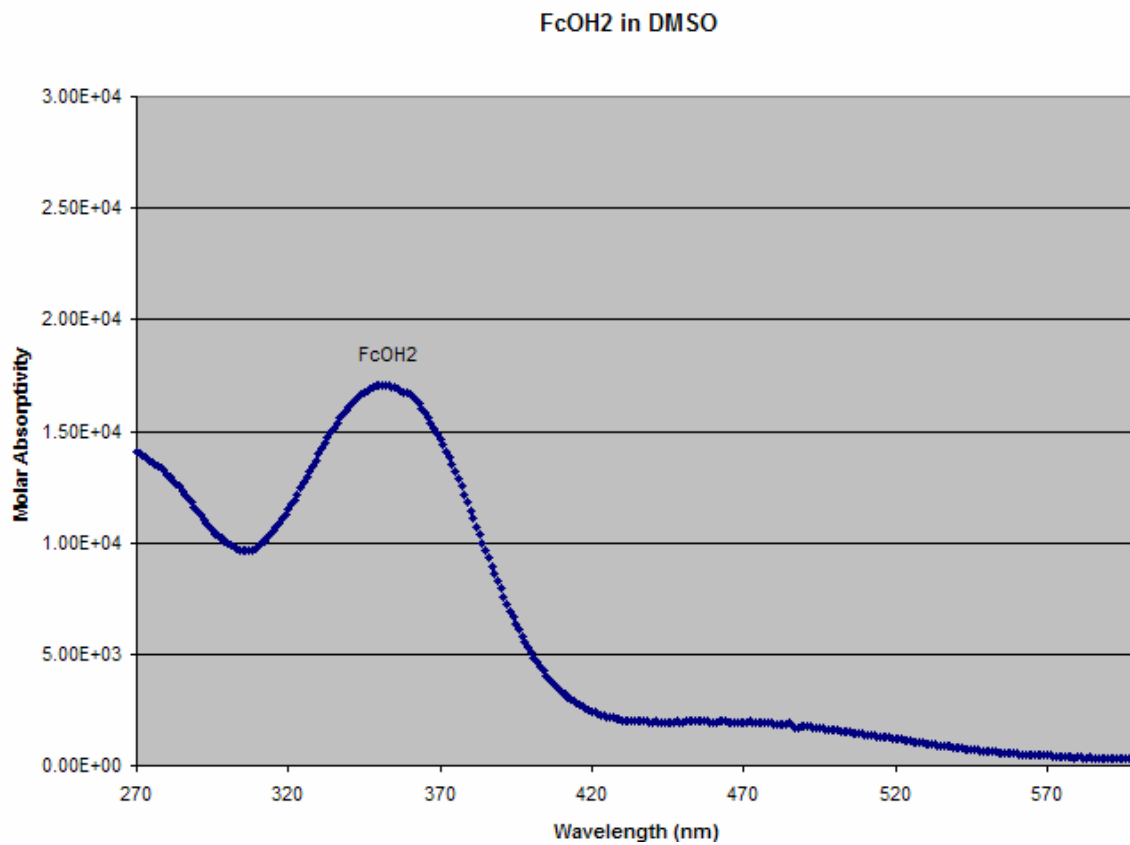


Figure A.33: Molar absorptivity (UV-Vis) of the FcOH2 ligand in DMSO: 351 nm ($17000 M^{-1}cm^{-1}$), 455 nm ($1990 M^{-1}cm^{-1}$), 463 nm ($1990 M^{-1}cm^{-1}$), 472 nm ($1980 M^{-1}cm^{-1}$);

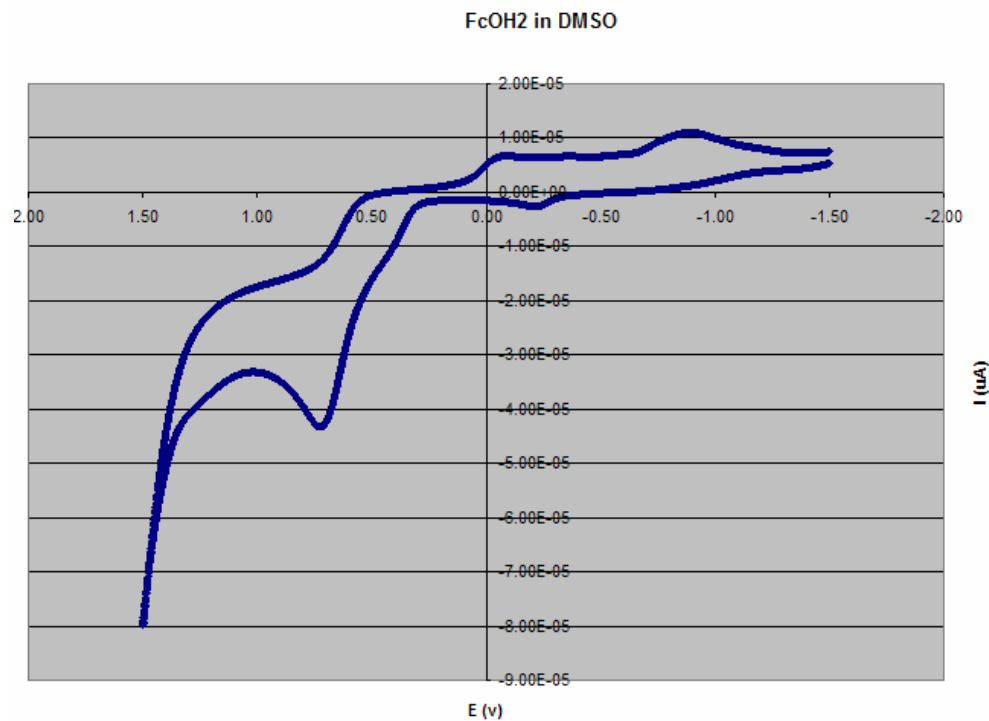


Figure A.34: CV scan of the FcOH2 ligand in DMSO, scan rate 100 mV/sec. Fe^{II} to Fe^{III} oxidation peak is at 716 mV.

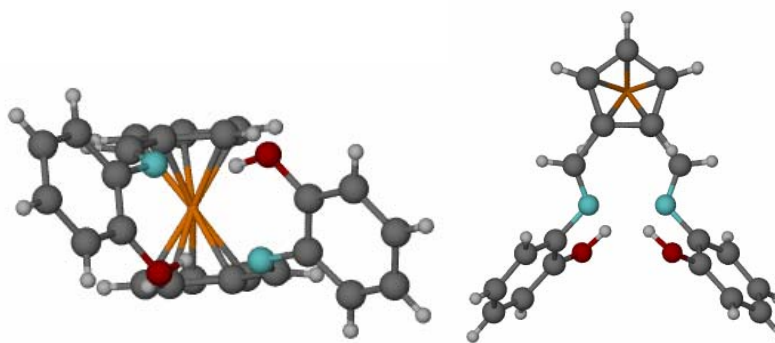


Figure A.35: Crystal structure of the FcOH2 ligand

Crystal data

$C_{24}H_{20}FeN_2O_2$

$M_r = 424.27$

Monoclinic, $C2/c$

$a = 16.6115 (13) \text{ \AA}$

$b = 9.2151 (7) \text{ \AA}$

$c = 14.1716 (11) \text{ \AA}$

$\beta = 117.017 (2)^\circ$

$D_x = 1.458 \text{ Mg m}^{-3}$

Mo $K\alpha$ radiation

$\lambda = 0.71073 \text{ \AA}$

Cell parameters from 1908 reflections

$\theta = 2.6\text{--}27.0^\circ$

$\mu = 0.80 \text{ mm}^{-1}$

$T = 173 (2) \text{ K}$

$V = 1932.6 (3) \text{ \AA}^3$
 $Z = 4$
 $F_{000} = 880$

Prism, red
 $0.25 \times 0.25 \times 0.15 \text{ mm}$

Data collection

Bruker SMART CCD area detector
 diffractometer

3887 measured reflections

1935 independent reflections

Monochromator: graphite

1597 reflections with $I > 2\sigma(I)$

$R_{\text{int}} = 0.021$

$T = 173(2) \text{ K}$

$\theta_{\text{max}} = 27.1^\circ$

$\theta_{\text{min}} = 2.6^\circ$

ω scans

$h = -18 \rightarrow 20$

Absorption correction: multi-scan

Data were corrected for decay and absorption using the program SADABS (Sheldrick, G. M. (2003). SADABS. Version 2.10. University of Göttingen, Germany).

$k = -11 \rightarrow 8$

$T_{\text{min}} = 0.55, T_{\text{max}} = 0.89$

$l = -18 \rightarrow 11$

Refinement

Refinement on F^2

Secondary atom site location: difference Fourier map

Least-squares matrix: full

Hydrogen site location: inferred from neighbouring sites

$R[F^2 > 2\sigma(F^2)] = 0.037$

H-atom parameters not refined

$wR(F^2) = 0.098$

$w = 1/[\sigma^2(F_o^2) + (0.0487P)^2 + 1.4759P]$
 where $P = (F_o^2 + 2F_c^2)/3$

$S = 1.06$

$(\Delta/\sigma)_{\text{max}} < 0.001$

1935 reflections

$\Delta\rho_{\text{max}} = 0.51 \text{ e \AA}^{-3}$

133 parameters

$\Delta\rho_{\text{min}} = -0.30 \text{ e \AA}^{-3}$

Extinction correction: none

Primary atom site location: structure-invariant direct methods

Refinement of F^2 against ALL reflections. The weighted R-factor wR and goodness of fit S are based on F^2 , conventional R-factors R are based on F , with F set to zero for negative F^2 . The threshold expression of $F^2 > 2\sigma(F^2)$ is used only for calculating R-factors(gt) etc. and is not relevant to the choice of reflections for refinement. R-factors based on F^2 are statistically about twice as large as those based on F , and R-factors based on ALL data will be even larger.

Fractional atomic coordinates and isotropic or equivalent isotropic displacement parameters (\AA^2)

	<i>x</i>	<i>Y</i>	<i>Z</i>	$U_{\text{iso}}^*/U_{\text{eq}}$
Fe1	0.5000	0.01895 (4)	0.2500	0.03697 (18)
O1	0.38235 (12)	-0.49145 (17)	0.15133 (12)	0.0406 (4)
C6	0.45224 (15)	-0.2143 (2)	0.36774 (15)	0.0316 (5)
H6	0.4006	-0.2020	0.3792	0.038*
C1	0.50883 (16)	-0.0886 (2)	0.37960 (15)	0.0337 (5)
C2	0.4819 (2)	0.0597 (2)	0.38043 (17)	0.0447 (6)
H2	0.4275	0.0914	0.3804	0.054*
C3	0.5510 (2)	0.1495 (2)	0.38127 (18)	0.0533 (7)
H3	0.5507	0.2526	0.3815	0.064*
C4	0.6209 (2)	0.0611 (3)	0.38175 (18)	0.0486 (7)
H4	0.6754	0.0943	0.3828	0.058*
C5	0.59484 (16)	-0.0861 (2)	0.38031 (16)	0.0373 (5)
H5	0.6289	-0.1686	0.3799	0.045*
N1	0.46809 (12)	-0.34068 (18)	0.34266 (13)	0.0299 (4)
C7	0.40530 (15)	-0.4531 (2)	0.33095 (16)	0.0297 (4)
C8	0.36533 (15)	-0.5274 (2)	0.23390 (17)	0.0317 (5)
C9	0.30416 (15)	-0.6374 (2)	0.21929 (18)	0.0383 (5)
H9	0.2748	-0.6850	0.1527	0.046*
C10	0.28535 (16)	-0.6789 (3)	0.30183 (19)	0.0415 (5)
H10	0.2447	-0.7566	0.2919	0.050*
C11	0.32542 (16)	-0.6076 (3)	0.39767 (18)	0.0415 (6)
H11	0.3128	-0.6365	0.4539	0.050*
C12	0.38436 (15)	-0.4935 (2)	0.41178 (17)	0.0354 (5)
H12	0.4106	-0.4427	0.4772	0.043*
H1O	0.4299	-0.4236	0.1685	0.067 (9)*

Atomic displacement parameters (\AA^2)

	U^{11}	U^{22}	U^{33}	U^{12}	U^{13}	U^{23}
Fe1	0.0630 (4)	0.0233 (2)	0.0258 (2)	0.000	0.0211 (2)	0.000
O1	0.0489 (10)	0.0460 (9)	0.0325 (8)	-0.0106 (8)	0.0234 (7)	-0.0082 (6)
C6	0.0405 (13)	0.0324 (11)	0.0227 (9)	0.0031 (9)	0.0151 (9)	0.0014 (8)
C1	0.0517 (14)	0.0280 (10)	0.0221 (9)	0.0002 (10)	0.0172 (9)	-0.0004 (8)
C2	0.0758 (19)	0.0319 (12)	0.0298 (11)	0.0069 (11)	0.0269 (12)	-0.0022 (9)
C3	0.100 (2)	0.0270 (12)	0.0320 (12)	-0.0110 (13)	0.0293 (13)	-0.0047 (9)
C4	0.0692 (18)	0.0362 (12)	0.0355 (12)	-0.0170 (12)	0.0193 (12)	-0.0014 (10)
C5	0.0493 (15)	0.0323 (11)	0.0270 (10)	-0.0064 (10)	0.0144 (9)	0.0012 (8)
N1	0.0366 (10)	0.0283 (9)	0.0278 (9)	-0.0013 (7)	0.0172 (7)	0.0003 (7)
C7	0.0301 (11)	0.0279 (10)	0.0312 (10)	0.0033 (8)	0.0141 (8)	0.0027 (8)
C8	0.0334 (12)	0.0301 (10)	0.0338 (11)	0.0047 (9)	0.0172 (9)	-0.0002 (8)
C9	0.0382 (13)	0.0355 (12)	0.0413 (12)	-0.0028 (10)	0.0182 (10)	-0.0086 (9)
C10	0.0353 (13)	0.0363 (12)	0.0527 (14)	-0.0046 (10)	0.0197 (11)	0.0014 (10)
C11	0.0393 (14)	0.0483 (13)	0.0382 (12)	-0.0028 (11)	0.0188 (10)	0.0090 (10)
C12	0.0373 (13)	0.0403 (12)	0.0292 (10)	-0.0008 (10)	0.0156 (9)	0.0012 (8)

Table 1

Geometric parameters (Å, °)

Fe1—C1 ⁱ	2.0326 (19)	C2—H2	0.9500
Fe1—C1	2.0326 (19)	C3—C4	1.415 (4)
Fe1—C2	2.038 (2)	C3—H3	0.9500
Fe1—C2 ⁱ	2.038 (2)	C4—C5	1.421 (3)
Fe1—C5 ⁱ	2.046 (2)	C4—H4	0.9500
Fe1—C5	2.046 (2)	C5—H5	0.9500
Fe1—C3	2.048 (2)	N1—C7	1.425 (3)
Fe1—C3 ⁱ	2.048 (2)	C7—C12	1.391 (3)
Fe1—C4	2.065 (3)	C7—C8	1.404 (3)

Fe1—C4 ⁱ	2.065 (3)	C8—C9	1.383 (3)
O1—C8	1.364 (3)	C9—C10	1.394 (3)
O1—H1O	0.9488	C9—H9	0.9500
C6—N1	1.279 (3)	C10—C11	1.378 (3)
C6—C1	1.453 (3)	C10—H10	0.9500
C6—H6	0.9500	C11—C12	1.388 (3)
C1—C5	1.424 (3)	C11—H11	0.9500
C1—C2	1.439 (3)	C12—H12	0.9500
C2—C3	1.411 (4)		
C1 ⁱ —Fe1—C1	121.66 (11)	C5—C1—C2	107.4 (2)
C1 ⁱ —Fe1—C2	158.37 (10)	C5—C1—C6	127.42 (19)
C1—Fe1—C2	41.42 (8)	C2—C1—C6	124.8 (2)
C1 ⁱ —Fe1—C2 ⁱ	41.42 (8)	C5—C1—Fe1	70.06 (12)
C1—Fe1—C2 ⁱ	158.37 (10)	C2—C1—Fe1	69.49 (11)
C2—Fe1—C2 ⁱ	158.75 (13)	C6—C1—Fe1	120.45 (14)
C1 ⁱ —Fe1—C5 ⁱ	40.88 (9)	C3—C2—C1	107.6 (2)
C1—Fe1—C5 ⁱ	107.15 (9)	C3—C2—Fe1	70.18 (13)
C2—Fe1—C5 ⁱ	122.38 (10)	C1—C2—Fe1	69.10 (11)
C2 ⁱ —Fe1—C5 ⁱ	68.83 (10)	C3—C2—H2	126.2
C1 ⁱ —Fe1—C5	107.15 (9)	C1—C2—H2	126.2
C1—Fe1—C5	40.88 (9)	Fe1—C2—H2	126.1
C2—Fe1—C5	68.83 (10)	C2—C3—C4	109.0 (2)
C2 ⁱ —Fe1—C5	122.38 (10)	C2—C3—Fe1	69.43 (13)
C5 ⁱ —Fe1—C5	123.53 (12)	C4—C3—Fe1	70.51 (13)
C1 ⁱ —Fe1—C3	159.62 (10)	C2—C3—H3	125.5
C1—Fe1—C3	68.60 (8)	C4—C3—H3	125.5
C2—Fe1—C3	40.39 (10)	Fe1—C3—H3	126.1
C2 ⁱ —Fe1—C3	123.03 (10)	C3—C4—C5	107.8 (2)
C5 ⁱ —Fe1—C3	158.29 (11)	C3—C4—Fe1	69.24 (15)
C5—Fe1—C3	68.08 (10)	C5—C4—Fe1	69.07 (13)
C1 ⁱ —Fe1—C3 ⁱ	68.60 (8)	C3—C4—H4	126.1

C1—Fe1—C3 ⁱ	159.62 (10)	C5—C4—H4	126.1
C2—Fe1—C3 ⁱ	123.03 (10)	Fe1—C4—H4	127.2
C2 ⁱ —Fe1—C3 ⁱ	40.39 (10)	C4—C5—C1	108.2 (2)
C5 ⁱ —Fe1—C3 ⁱ	68.08 (10)	C4—C5—Fe1	70.48 (14)
C5—Fe1—C3 ⁱ	158.29 (11)	C1—C5—Fe1	69.06 (12)
C3—Fe1—C3 ⁱ	108.06 (13)	C4—C5—H5	125.9
C1 ⁱ —Fe1—C4	123.39 (10)	C1—C5—H5	125.9
C1—Fe1—C4	68.48 (9)	Fe1—C5—H5	126.2
C2—Fe1—C4	68.20 (11)	C6—N1—C7	117.50 (18)
C2 ⁱ —Fe1—C4	107.58 (11)	C12—C7—C8	119.47 (19)
C5 ⁱ —Fe1—C4	159.90 (10)	C12—C7—N1	122.87 (18)
C5—Fe1—C4	40.45 (9)	C8—C7—N1	117.64 (18)
C3—Fe1—C4	40.25 (11)	O1—C8—C9	118.30 (19)
C3 ⁱ —Fe1—C4	122.83 (11)	O1—C8—C7	122.15 (19)
C1 ⁱ —Fe1—C4 ⁱ	68.48 (9)	C9—C8—C7	119.51 (19)
C1—Fe1—C4 ⁱ	123.39 (10)	C8—C9—C10	120.3 (2)
C2—Fe1—C4 ⁱ	107.58 (11)	C8—C9—H9	119.8
C2 ⁱ —Fe1—C4 ⁱ	68.20 (11)	C10—C9—H9	119.8
C5 ⁱ —Fe1—C4 ⁱ	40.45 (9)	C11—C10—C9	120.3 (2)
C5—Fe1—C4 ⁱ	159.90 (10)	C11—C10—H10	119.9
C3—Fe1—C4 ⁱ	122.83 (11)	C9—C10—H10	119.9
C3 ⁱ —Fe1—C4 ⁱ	40.25 (11)	C10—C11—C12	119.8 (2)
C4—Fe1—C4 ⁱ	158.30 (14)	C10—C11—H11	120.1
C8—O1—H10	114.4	C12—C11—H11	120.1
N1—C6—C1	123.7 (2)	C11—C12—C7	120.6 (2)
N1—C6—H6	118.2	C11—C12—H12	119.7
C1—C6—H6	118.2	C7—C12—H12	119.7
N1—C6—C1—C5	-9.2 (3)	C2 ⁱ —Fe1—C3—C4	-77.85 (17)
N1—C6—C1—C2	163.1 (2)	C5 ⁱ —Fe1—C3—C4	164.2 (2)
N1—C6—C1—Fe1	78.0 (2)	C5—Fe1—C3—C4	37.42 (13)
C1 ⁱ —Fe1—C1—C5	79.46 (12)	C3 ⁱ —Fe1—C3—C4	-119.82 (16)

C2—Fe1—C1—C5	-118.40 (19)	C4 ⁱ —Fe1—C3—C4	-161.67 (13)
C2 ⁱ —Fe1—C1—C5	46.1 (3)	C2—C3—C4—C5	0.5 (3)
C5 ⁱ —Fe1—C1—C5	121.78 (15)	Fe1—C3—C4—C5	-58.47 (15)
C3—Fe1—C1—C5	-80.80 (15)	C2—C3—C4—Fe1	58.95 (16)
C3 ⁱ —Fe1—C1—C5	-165.1 (2)	C1 ⁱ —Fe1—C4—C3	163.55 (13)
C4—Fe1—C1—C5	-37.40 (14)	C1—Fe1—C4—C3	-81.88 (14)
C4 ⁱ —Fe1—C1—C5	163.16 (13)	C2—Fe1—C4—C3	-37.15 (13)
C1 ⁱ —Fe1—C1—C2	-162.15 (16)	C2 ⁱ —Fe1—C4—C3	120.71 (15)
C2 ⁱ —Fe1—C1—C2	164.47 (16)	C5 ⁱ —Fe1—C4—C3	-163.0 (2)
C5 ⁱ —Fe1—C1—C2	-119.82 (15)	C5—Fe1—C4—C3	-119.7 (2)
C5—Fe1—C1—C2	118.40 (19)	C3 ⁱ —Fe1—C4—C3	79.0 (2)
C3—Fe1—C1—C2	37.60 (16)	C4 ⁱ —Fe1—C4—C3	45.64 (12)
C3 ⁱ —Fe1—C1—C2	-46.7 (3)	C1 ⁱ —Fe1—C4—C5	-76.78 (16)
C4—Fe1—C1—C2	80.99 (16)	C1—Fe1—C4—C5	37.79 (13)
C4 ⁱ —Fe1—C1—C2	-78.45 (17)	C2—Fe1—C4—C5	82.52 (15)
C1 ⁱ —Fe1—C1—C6	-42.99 (15)	C2 ⁱ —Fe1—C4—C5	-119.62 (14)
C2—Fe1—C1—C6	119.2 (2)	C5 ⁱ —Fe1—C4—C5	-43.3 (4)
C2 ⁱ —Fe1—C1—C6	-76.4 (3)	C3—Fe1—C4—C5	119.7 (2)
C5 ⁱ —Fe1—C1—C6	-0.66 (19)	C3 ⁱ —Fe1—C4—C5	-161.34 (14)
C5—Fe1—C1—C6	-122.4 (2)	C4 ⁱ —Fe1—C4—C5	165.31 (14)
C3—Fe1—C1—C6	156.8 (2)	C3—C4—C5—C1	-0.4 (2)
C3 ⁱ —Fe1—C1—C6	72.4 (3)	Fe1—C4—C5—C1	-58.93 (14)
C4—Fe1—C1—C6	-159.9 (2)	C3—C4—C5—Fe1	58.57 (16)
C4 ⁱ —Fe1—C1—C6	40.7 (2)	C2—C1—C5—C4	0.1 (2)
C5—C1—C2—C3	0.2 (2)	C6—C1—C5—C4	173.47 (19)
C6—C1—C2—C3	-173.40 (19)	Fe1—C1—C5—C4	59.82 (15)
Fe1—C1—C2—C3	-59.89 (15)	C2—C1—C5—Fe1	-59.71 (13)
C5—C1—C2—Fe1	60.07 (14)	C6—C1—C5—Fe1	113.7 (2)
C6—C1—C2—Fe1	-113.51 (19)	C1 ⁱ —Fe1—C5—C4	121.71 (15)
C1 ⁱ —Fe1—C2—C3	163.8 (2)	C1—Fe1—C5—C4	-119.4 (2)
C1—Fe1—C2—C3	118.8 (2)	C2—Fe1—C5—C4	-80.81 (16)

C2 ⁱ —Fe1—C2—C3	-45.43 (14)	C2 ⁱ —Fe1—C5—C4	78.90 (17)
C5 ⁱ —Fe1—C2—C3	-162.24 (15)	C5 ⁱ —Fe1—C5—C4	163.58 (16)
C5—Fe1—C2—C3	80.64 (16)	C3—Fe1—C5—C4	-37.24 (15)
C3 ⁱ —Fe1—C2—C3	-78.8 (2)	C3 ⁱ —Fe1—C5—C4	46.6 (3)
C4—Fe1—C2—C3	37.03 (15)	C4 ⁱ —Fe1—C5—C4	-164.17 (17)
C4 ⁱ —Fe1—C2—C3	-120.34 (17)	C1 ⁱ —Fe1—C5—C1	-118.87 (15)
C1 ⁱ —Fe1—C2—C1	45.1 (4)	C2—Fe1—C5—C1	38.61 (13)
C2 ⁱ —Fe1—C2—C1	-164.20 (14)	C2 ⁱ —Fe1—C5—C1	-161.68 (13)
C5 ⁱ —Fe1—C2—C1	79.00 (16)	C5 ⁱ —Fe1—C5—C1	-77.00 (11)
C5—Fe1—C2—C1	-38.13 (14)	C3—Fe1—C5—C1	82.18 (14)
C3—Fe1—C2—C1	-118.8 (2)	C3 ⁱ —Fe1—C5—C1	166.0 (2)
C3 ⁱ —Fe1—C2—C1	162.39 (15)	C4—Fe1—C5—C1	119.4 (2)
C4—Fe1—C2—C1	-81.74 (15)	C4 ⁱ —Fe1—C5—C1	-44.7 (3)
C4 ⁱ —Fe1—C2—C1	120.89 (15)	C1—C6—N1—C7	-178.28 (18)
C1—C2—C3—C4	-0.4 (2)	C6—N1—C7—C12	-58.0 (3)
Fe1—C2—C3—C4	-59.61 (16)	C6—N1—C7—C8	123.7 (2)
C1—C2—C3—Fe1	59.20 (14)	C12—C7—C8—O1	179.17 (19)
C1 ⁱ —Fe1—C3—C2	-162.9 (2)	N1—C7—C8—O1	-2.5 (3)
C1—Fe1—C3—C2	-38.53 (14)	C12—C7—C8—C9	1.5 (3)
C2 ⁱ —Fe1—C3—C2	162.07 (12)	N1—C7—C8—C9	179.86 (19)
C5 ⁱ —Fe1—C3—C2	44.1 (3)	O1—C8—C9—C10	179.3 (2)
C5—Fe1—C3—C2	-82.66 (15)	C7—C8—C9—C10	-2.9 (3)
C3 ⁱ —Fe1—C3—C2	120.10 (18)	C8—C9—C10—C11	2.0 (4)
C4—Fe1—C3—C2	-120.1 (2)	C9—C10—C11—C12	0.4 (4)
C4 ⁱ —Fe1—C3—C2	78.25 (18)	C10—C11—C12—C7	-1.8 (3)
C1 ⁱ —Fe1—C3—C4	-42.8 (3)	C8—C7—C12—C11	0.9 (3)
C1—Fe1—C3—C4	81.55 (15)	N1—C7—C12—C11	-177.4 (2)
C2—Fe1—C3—C4	120.1 (2)		

Symmetry codes: (i) $-x+1, y, -z+1/2$.

All esds (except the esd in the dihedral angle between two l.s. planes) are estimated using the full covariance matrix. The cell esds are taken into account individually in the estimation of esds in distances, angles and torsion angles; correlations between esds in cell parameters are only used when they are defined by crystal symmetry. An approximate (isotropic) treatment of cell esds is used for estimating esds involving l.s. planes.

Data collection: *SMART* (Bruker, 1998); cell refinement: *SAINTE* (Bruker, 1998); data reduction: *SAINTE* (Bruker, 1998); program(s) used to solve structure: *SHELXS97* (Sheldrick, 1997); program(s) used to refine structure: *SHELXL97* (Sheldrick, 1997); molecular graphics: *ORTEP*III (Burnett & Johnson, 1996); software used to prepare material for publication: *CIFTAB* (Sheldrick, 1997).

Color code for FcOH_2 crystal structure:

Orange: Fe atom

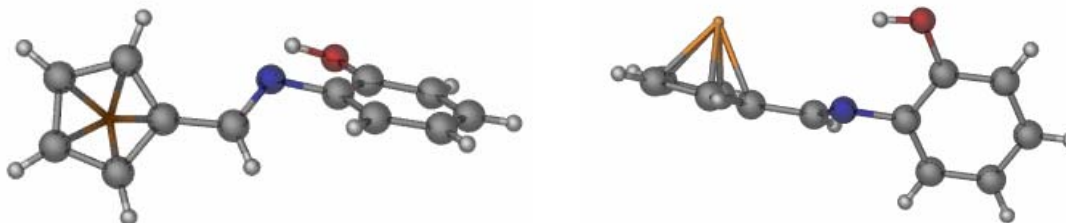
Dark grey: C atom

Light grey: H atom

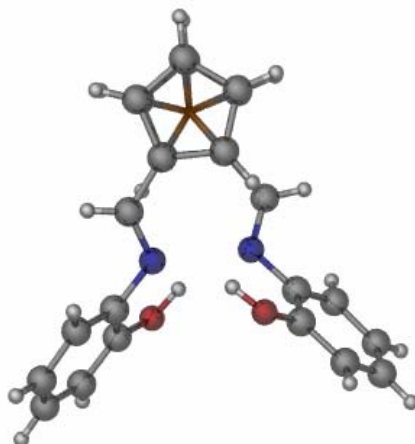
Dark Blue: N atom

Red: Oxygen atom

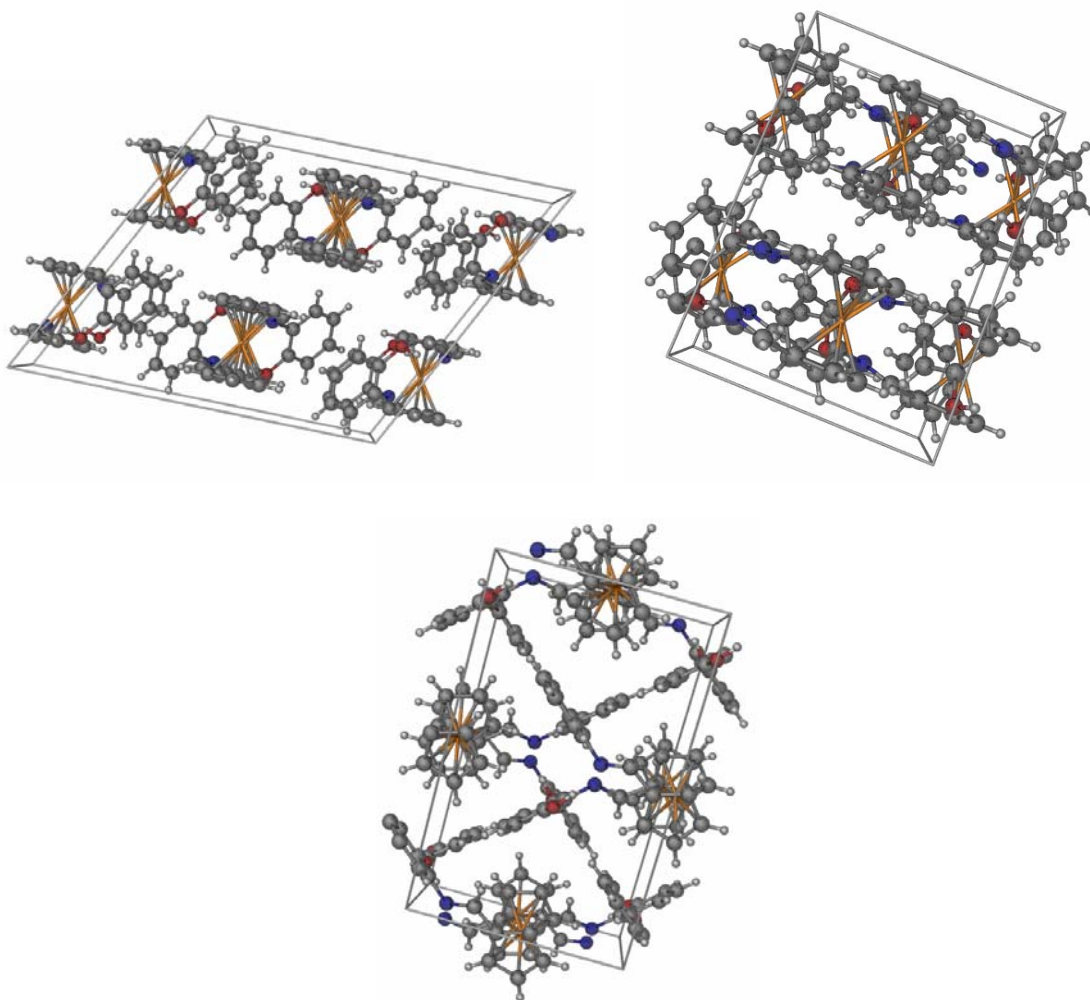
Asymmetric unit structure:



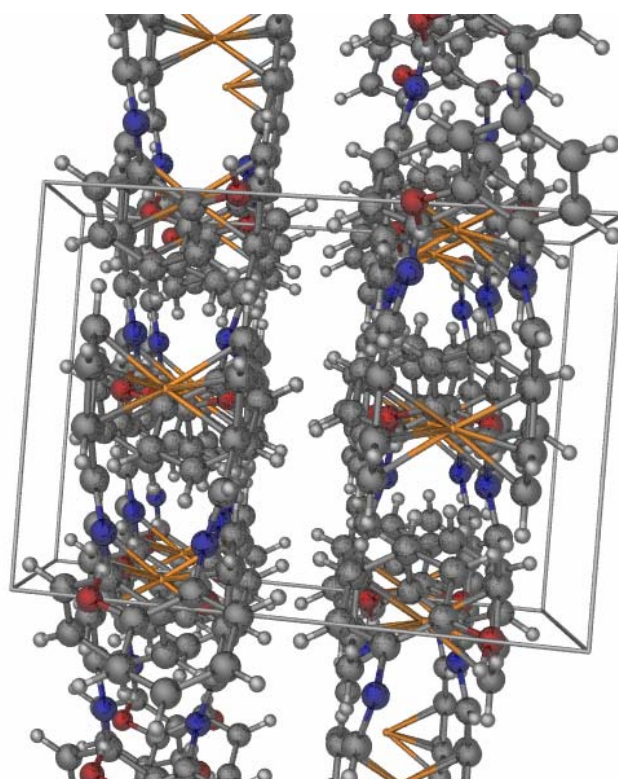
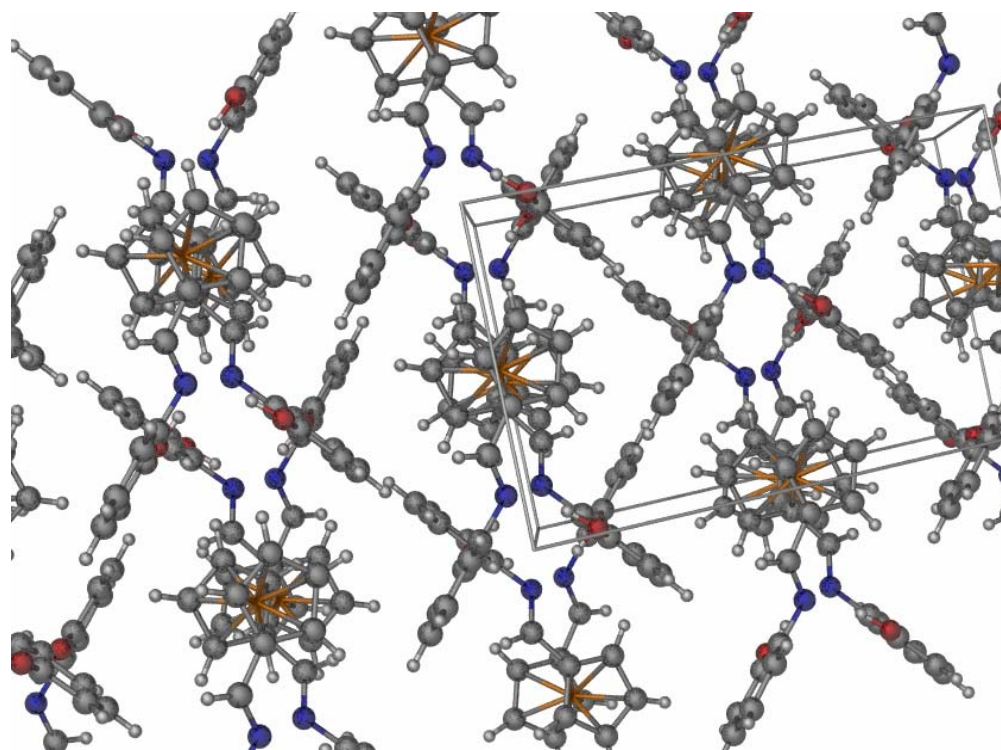
Cp ring overlap:



Unit cell:



Mass crystal packing:



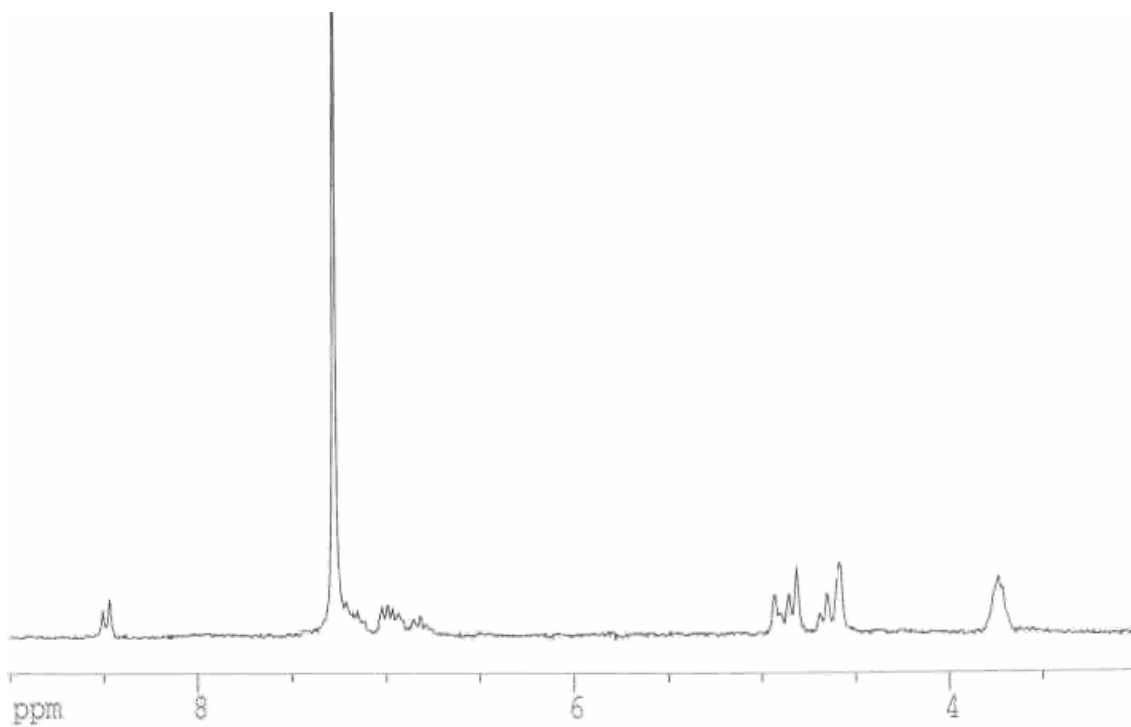
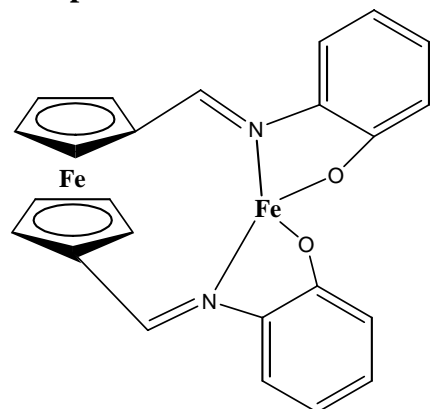
Compound 11:

Figure A.36: ^1H NMR spectrum of $\text{FcO}_2\text{-Fe}$ in CDCl_3 : 8.47 ppm (2H, d, Cp- $\underline{\text{C}}\text{H}=\text{N}$), 7.20 ppm (2H, m, phenyl), 7.02-6.96 ppm (4H, dd, phenyl), 6.8 ppm (2H, t, phenyl), 4.93-4.85 ppm (4H, t, Cp), 4.65-4.58 ppm (4H, t, Cp);

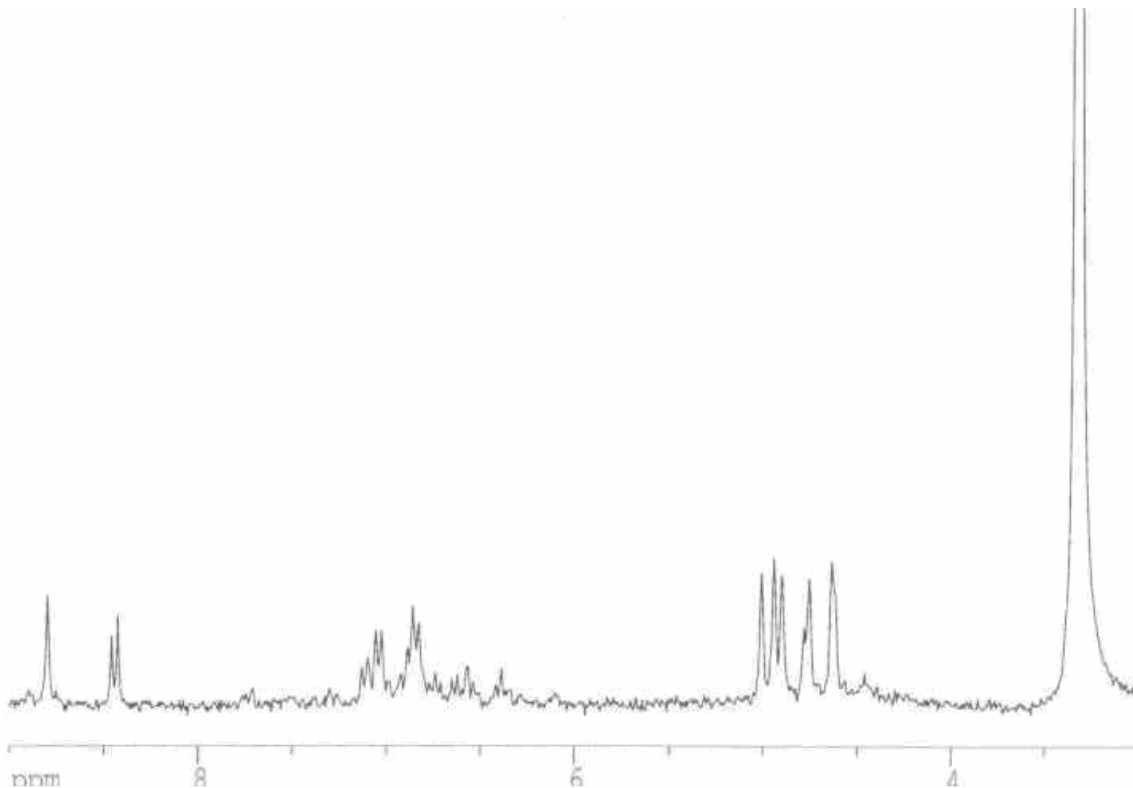


Figure A.37: ^1H NMR spectrum of $\text{FcO}_2\text{-Fe}$ in $d_6\text{-DMSO}$: 8.79 ppm (2H, s, Cp- $\text{CH}=\text{N}$), 8.44 ppm (2H, d, phenyl), 7.09-7.02 ppm (2H, dd, phenyl), 6.85-6.82 ppm (4H, t, phenyl), 5.00-4.90 ppm (4H, t, Cp), 4.75 ppm (2H, d, Cp), 4.63 ppm (2H, d, Cp);

Molar absorptivity of FeO2-Fe vs. combined starting materials in DMSO

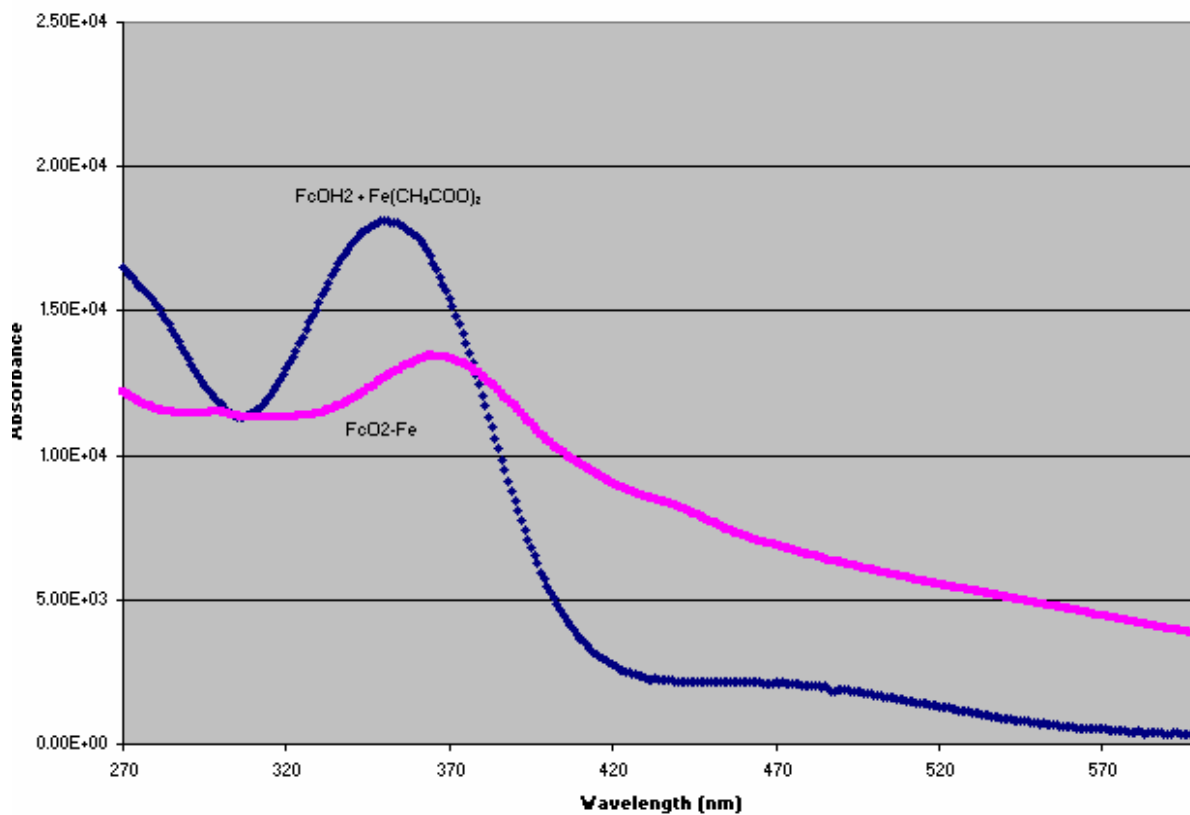
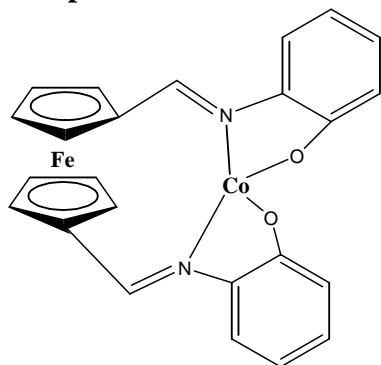


Figure A.38: Comparison between the molar absorptivity (UV-Vis) of FeO2-Fe and the molar absorptivity of the starting materials (351 nm peak) in DMSO: 299 nm ($11500 \text{ M}^{-1}\text{cm}^{-1}$), 321 nm ($11300 \text{ M}^{-1}\text{m}^{-1}$), 364 nm ($13500 \text{ M}^{-1}\text{m}^{-1}$);

Compound 12:



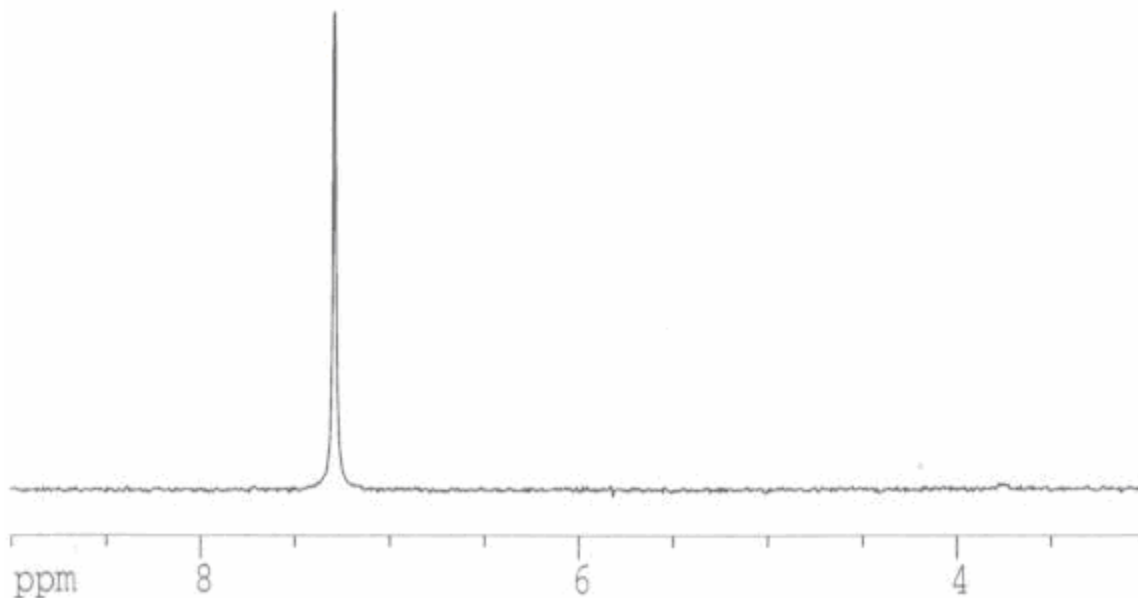


Figure A.39: ¹H NMR spectrum of FcO₂-Co in CDCl₃: no spectral peaks.

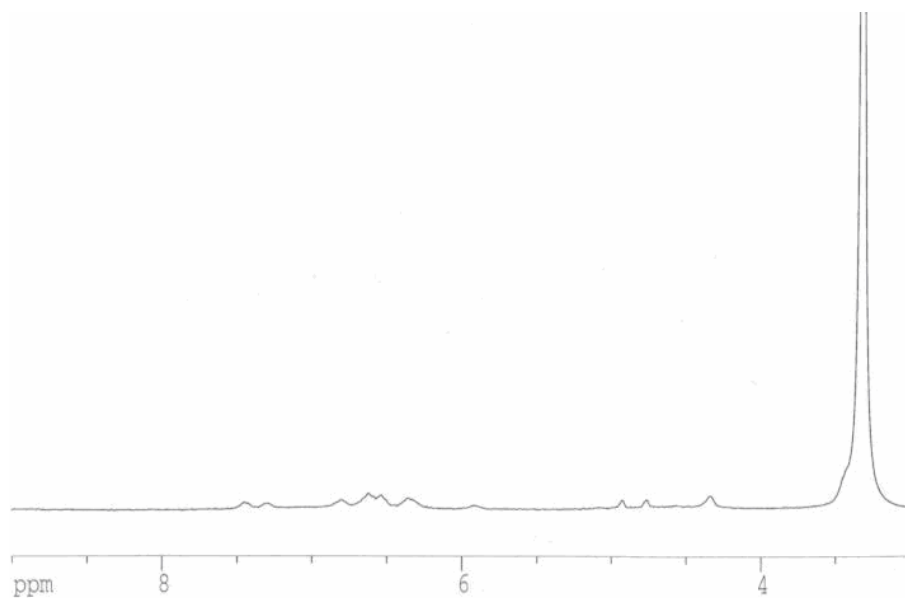


Figure A.40: ¹H NMR spectrum of FcO₂-Co in d₆-DMSO: .5-7.3 ppm (2H, broad d, Cp-CH=N), 6.8 ppm (2H, broad s, phenyl), 6.6-6.4 ppm (4H, broad d, phenyl), 6.3-5.2 ppm (2H, broad d, phenyl), 4.9 ppm (2H, s, Cp), 4.7 ppm (2H, s, Cp), 4.4 ppm (4H, s, Cp);

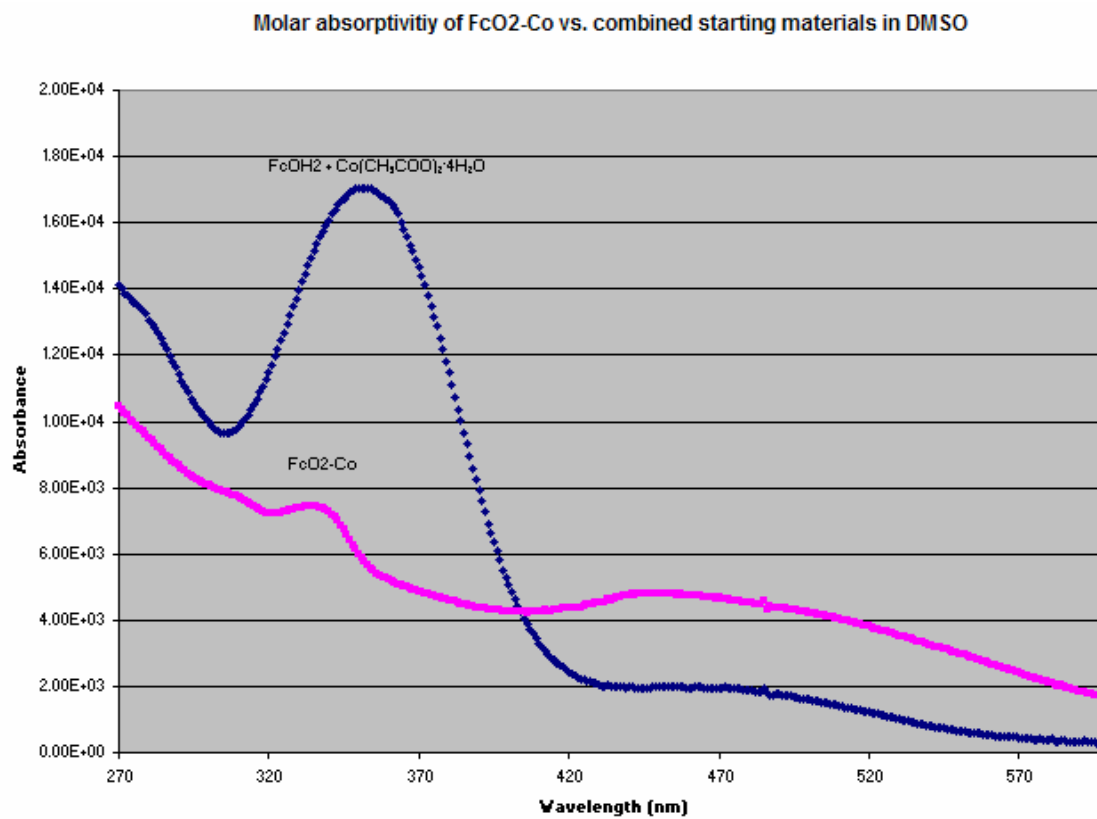
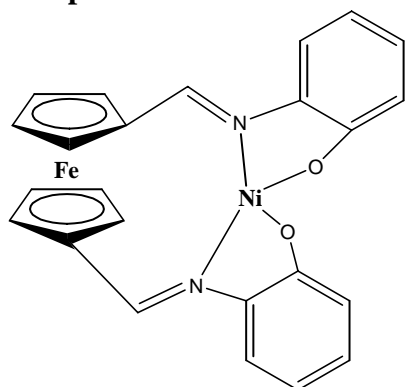


Figure A.41: Comparison between the molar absorptivity (UV-Vis) of FeO2-Co and the molar absorptivity of the starting materials (351, 463 nm peaks) in DMSO: 334 nm ($7440 \text{ M}^{-1}\text{cm}^{-1}$), 448 nm ($4810 \text{ M}^{-1}\text{cm}^{-1}$);

Compound 13:



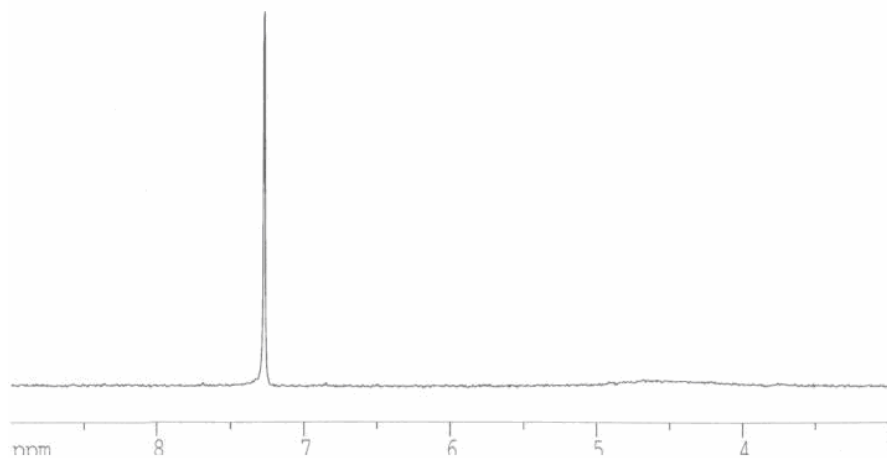


Figure A.42: ¹H NMR spectrum of FcO₂-Ni in CDCl₃: very broad from 5-4 ppm (m, Cps);

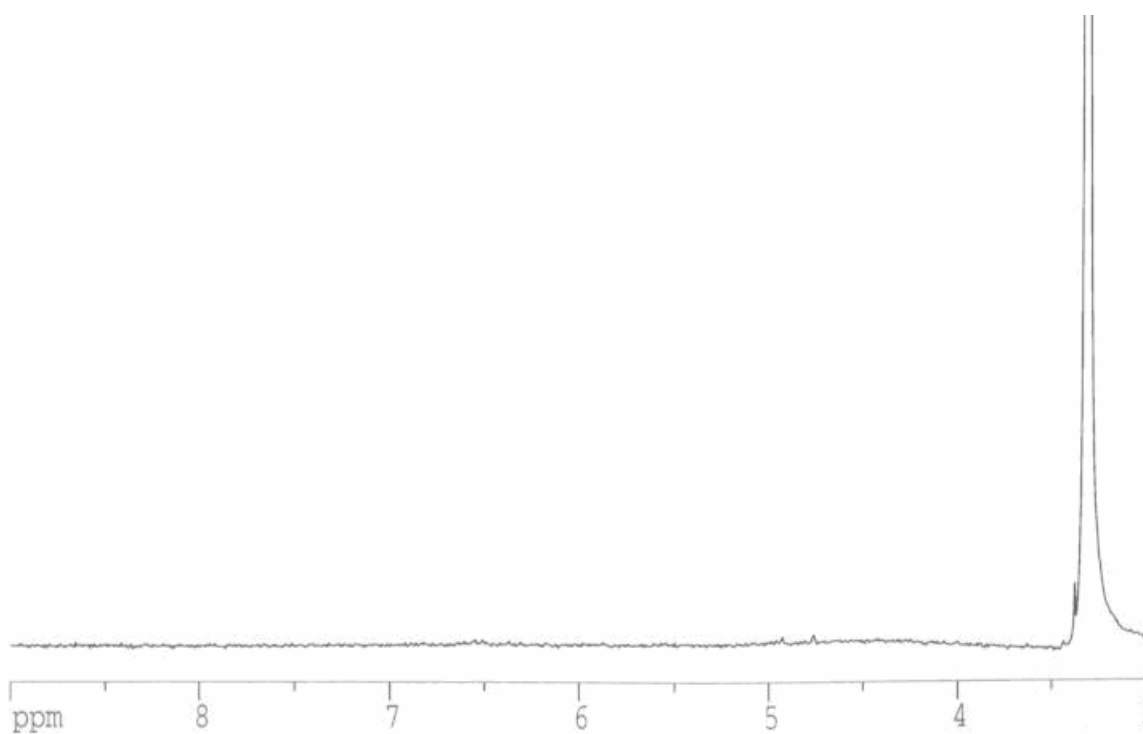


Figure A.43: ¹H NMR spectrum of FcO₂-Ni in d-DMSO: 7.7-7.4 ppm (m, phenyls), very broad peak 5-4 ppm (m, Cps);

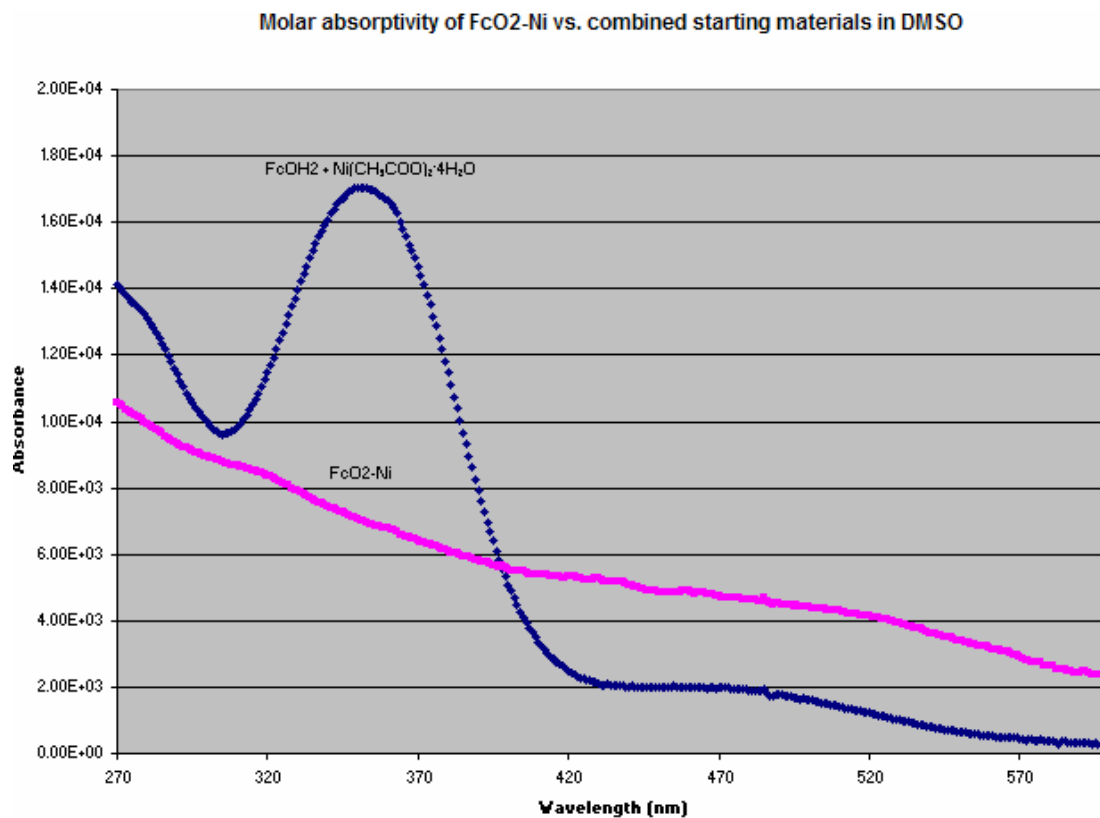
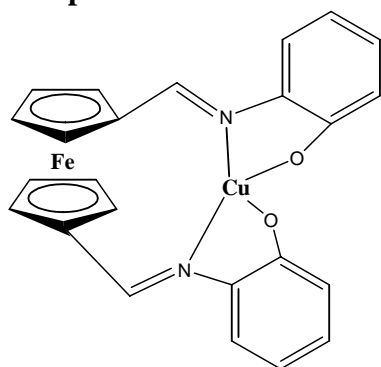


Figure A.44: Comparison between the molar absorptivity (UV-Vis) of FcO₂-Ni and the molar absorptivity of the starting materials (351, 463 nm peaks) in DMSO: 651 nm (2170 M⁻¹cm⁻¹);

Compound 14:



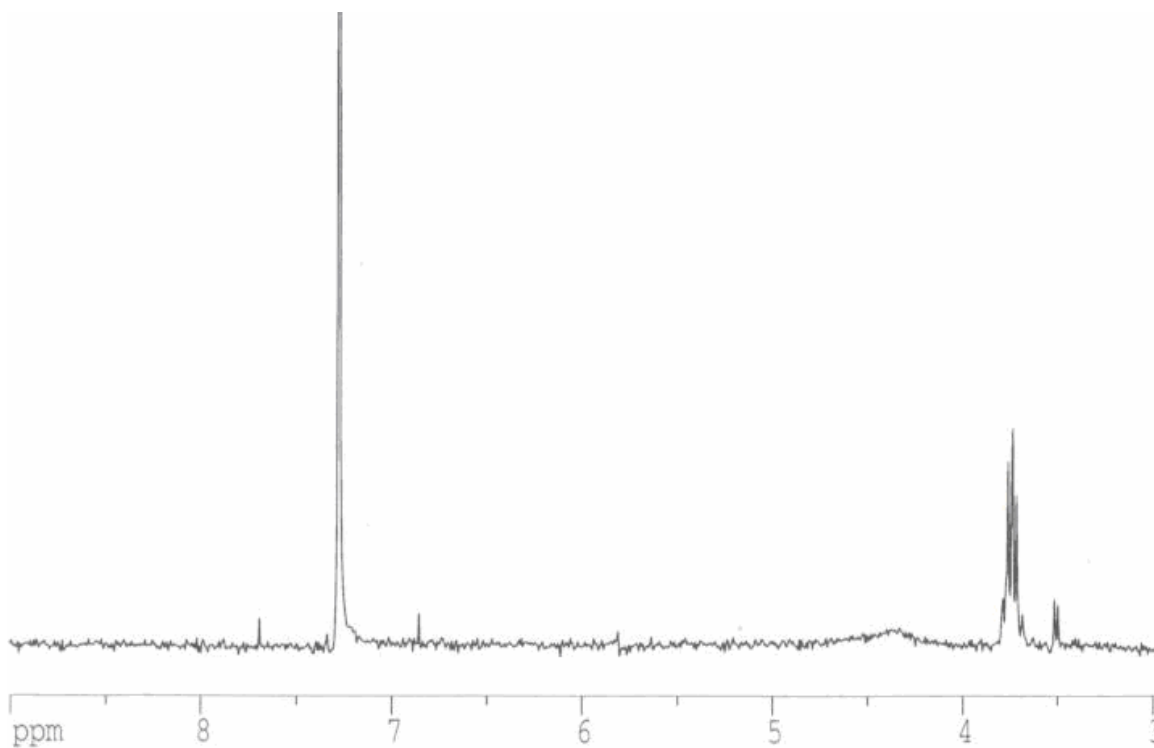


Figure A.45: ¹H NMR spectrum of FcO₂-Cu in CDCl₃: 4.6-4.4 ppm (broad m, Cps);

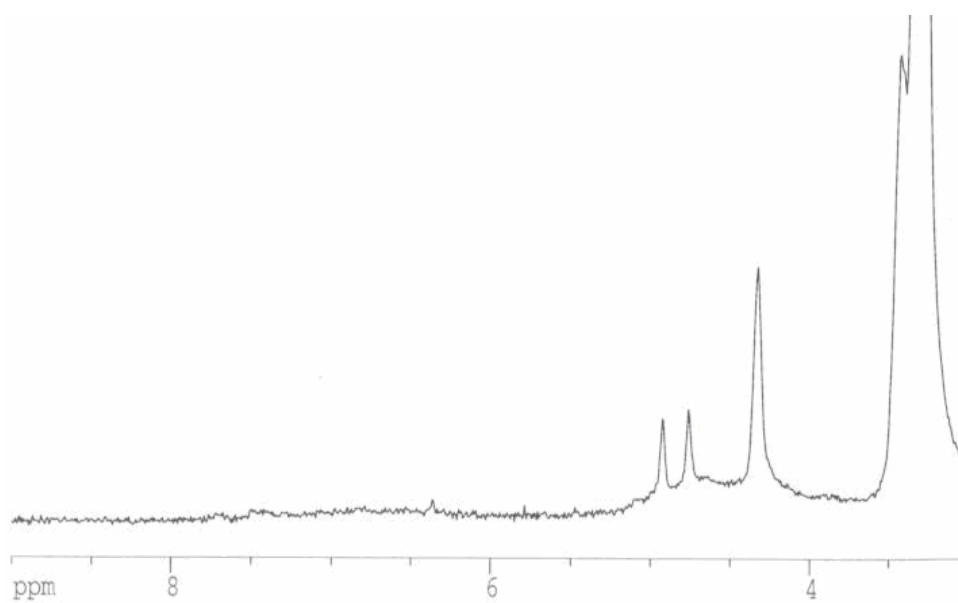


Figure A.46: ¹H NMR spectrum of FcO₂-Cu in d₆-DMSO: 6.36 ppm (s, phenyls), 4.92 ppm (s, Cps), 4.76 ppm (s, Cps), 4.33 ppm (s, Cps);

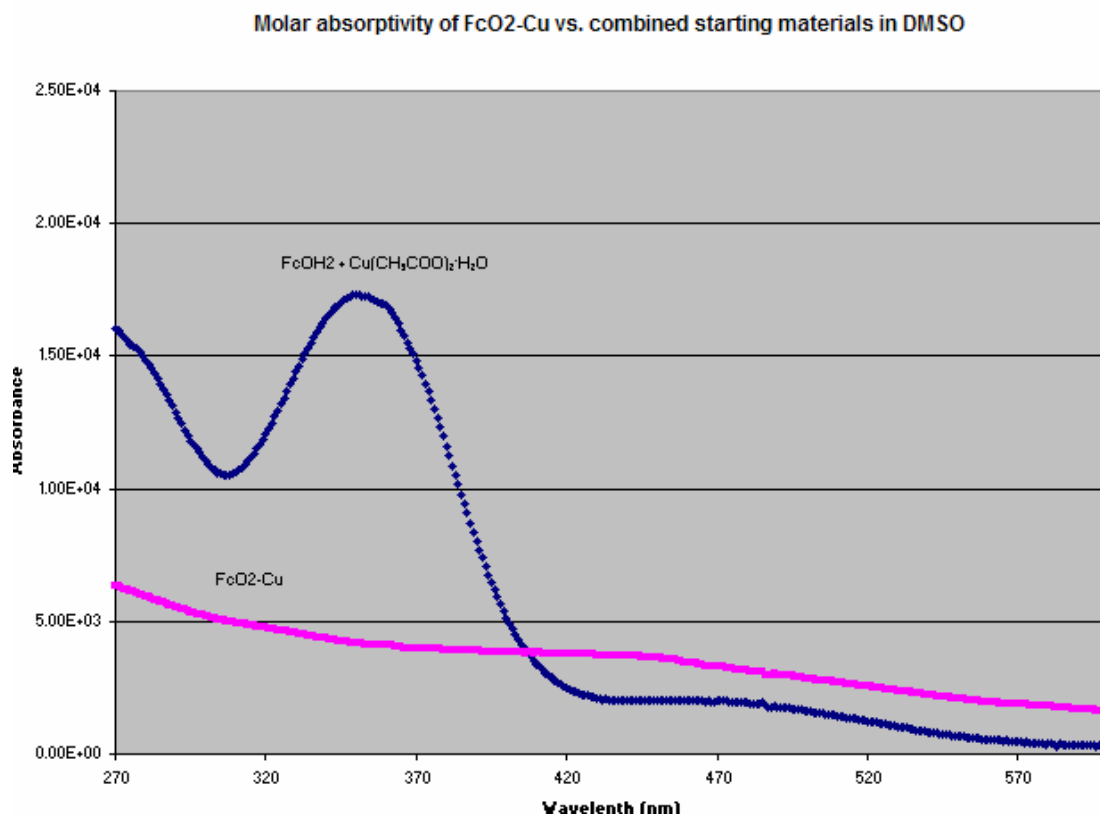
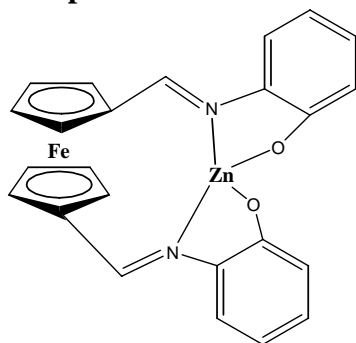


Figure A.47: Comparison between the molar absorptivity (UV-Vis) of FeO2-Cu and the molar absorptivity of the starting materials (351, 455 nm peaks) in DMSO: 480 nm ($3820 \text{ M}^{-1}\text{cm}^{-1}$);

Compound 15:



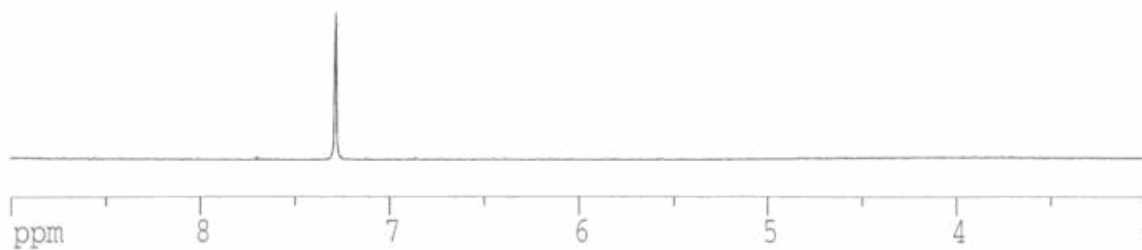


Figure A.48: ¹H NMR spectrum of FcO₂-Zn in CDCl₃: no spectral peaks.

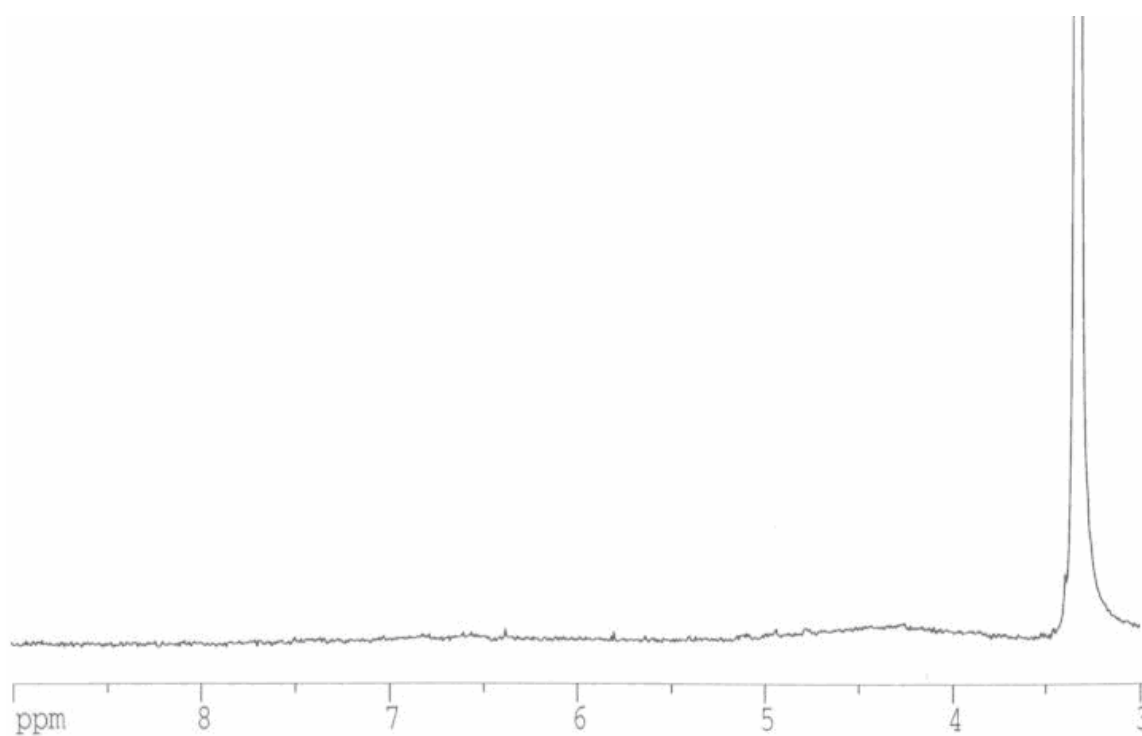


Figure A.49: ¹H NMR spectrum of FcO₂-Zn in d₆-DMSO: very broad peak 7-6 ppm (m, phenyls), very broad peak 5-3.5 ppm (m, Cps);

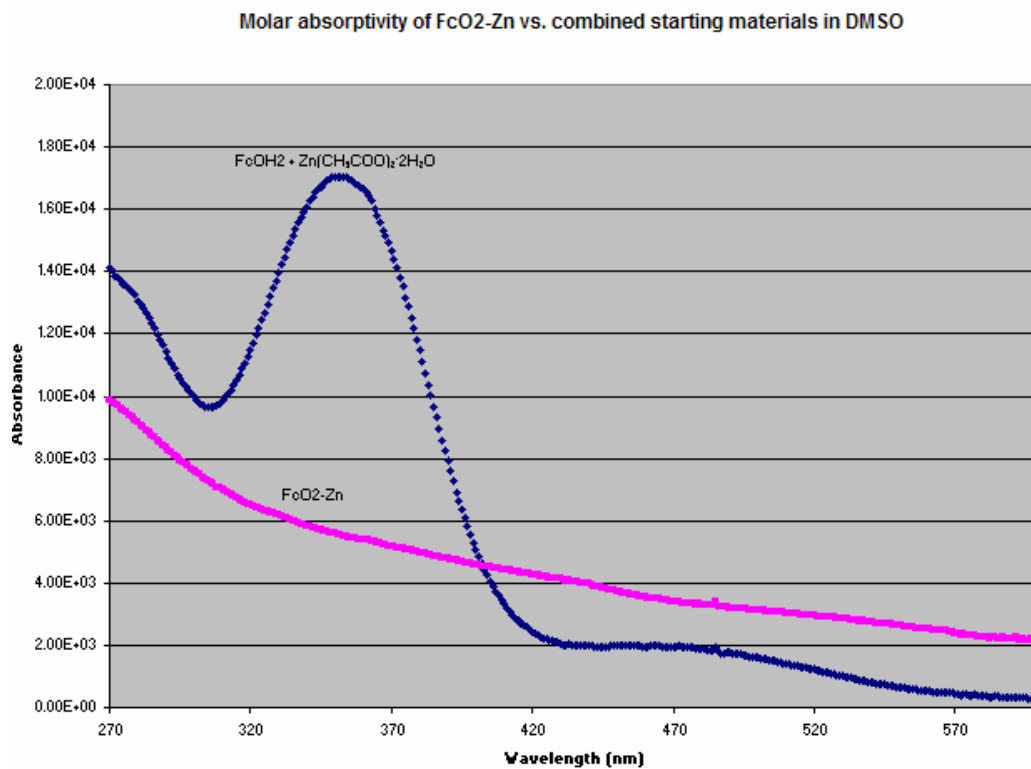
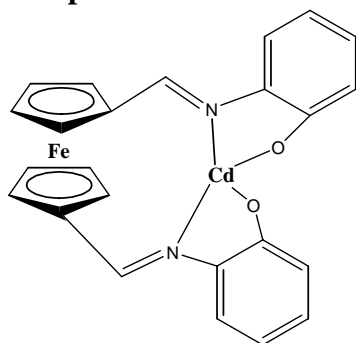


Figure A.50: Comparison between the molar absorptivity (UV-Vis) of FcO₂-Zn and the molar absorptivity of the starting materials (351, 463 nm peaks) in DMSO.

Compound 16:



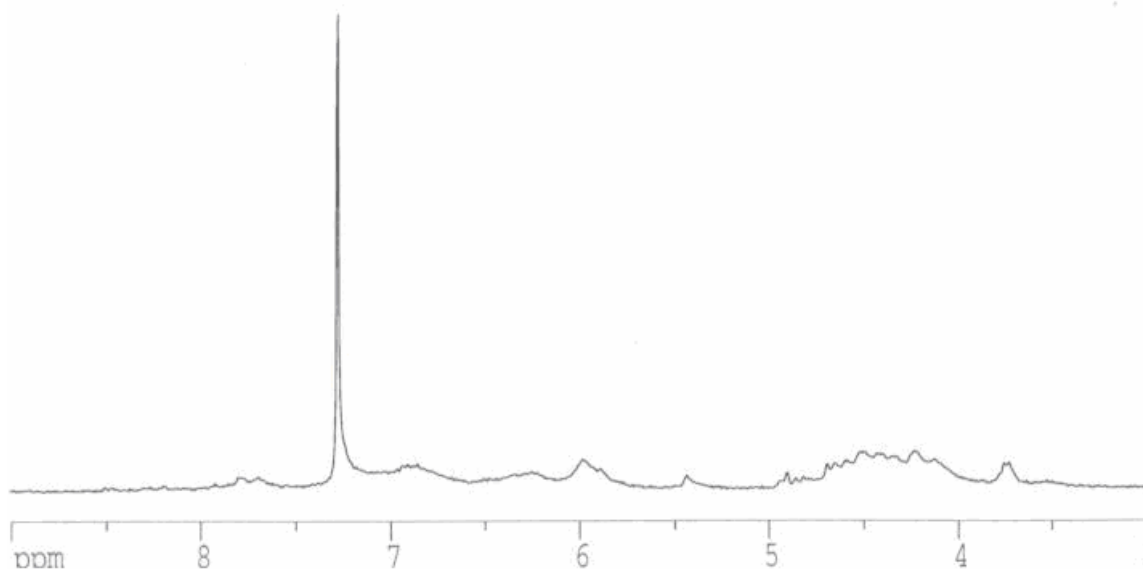


Figure A.51: ^1H NMR spectrum of FcO₂-Cd in CDCl₃: 7.9 ppm (H, broad d, Cp- $\underline{\text{C}}\text{H}=\text{N}$), 7.1-6.6 ppm (H, broad m, phenyl), 6.4-6.1 ppm (H, broad m, phenyl), 6.0-5.6 ppm (H, broad m, phenyl), 5.4 ppm (H, broad s, Cp), 4.8 ppm (H, broad s, Cp), very broad 4.6-3.8 ppm (H, m, Cp);

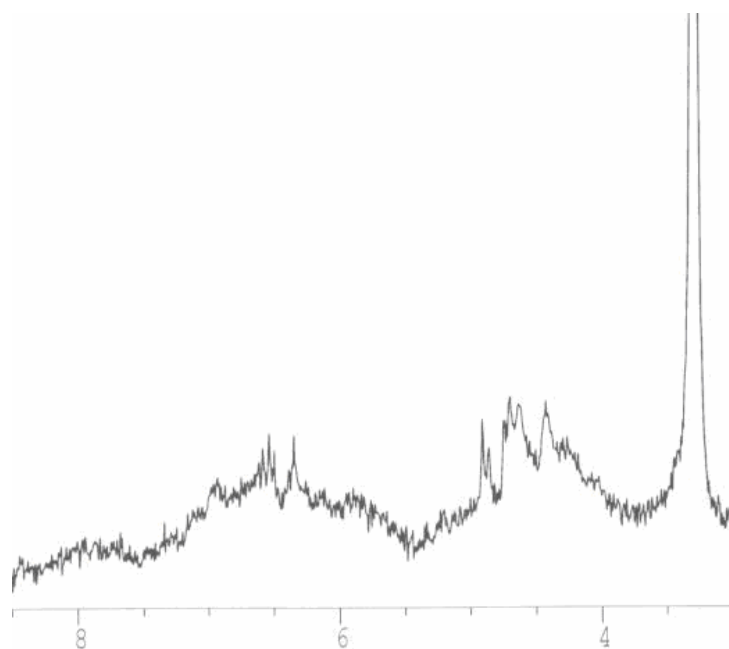


Figure A.52: ^1H NMR spectrum of FcO₂-Cd in d₆-DMSO: 8.2-7.8 ppm (2H, d, Cp- $\underline{\text{C}}\text{H}=\text{N}$), 6.9 ppm (2H, d, phenyl), 6.55 ppm (4H, t, phenyl), 6.36 ppm (2H, d, phenyl), 4.93 ppm (2H, d, Cp), 4.72 ppm (4H, t, Cp), 4.44 ppm (2H, d, Cp);

Molar absorptivity of FcO2-Cd vs. combined starting materials in DMSO

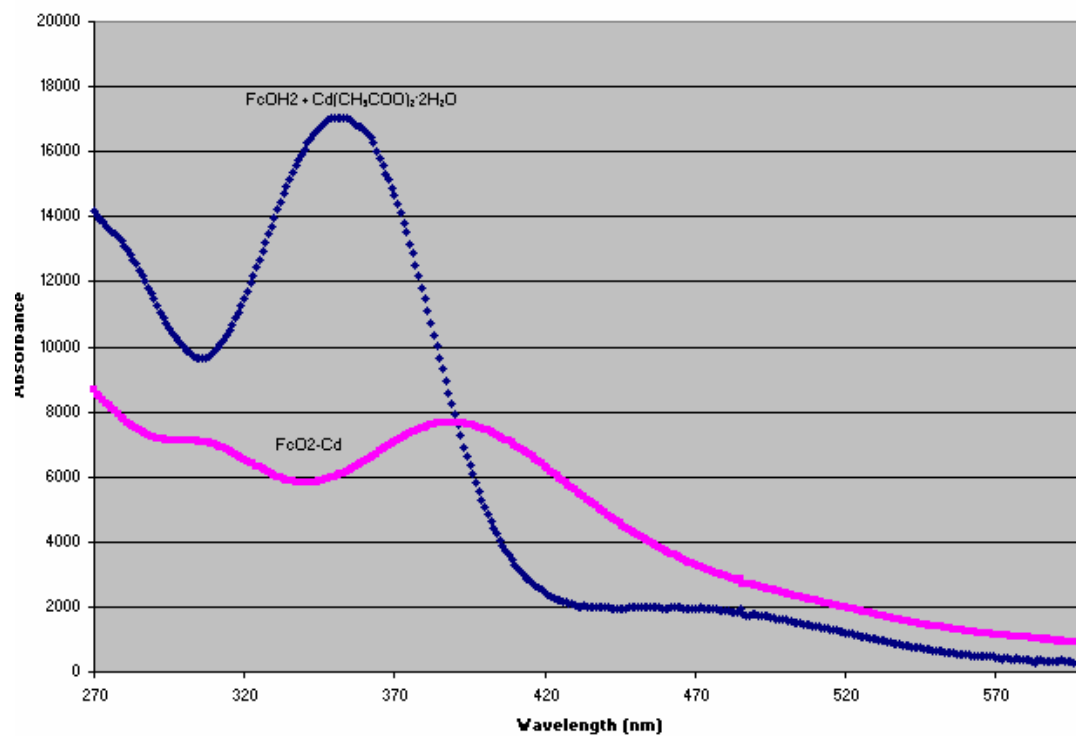
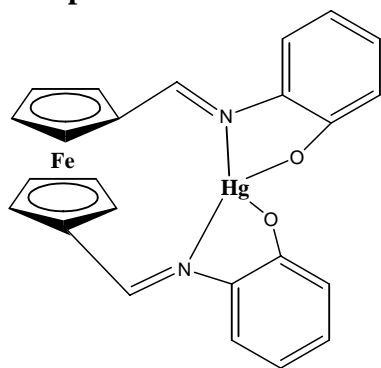


Figure A.53: Comparison between the molar absorptivity (UV-Vis) of FcO₂-Cd and the molar absorptivity of the starting materials (351, 463 nm peaks) in DMSO: 390 nm (7670 M⁻¹cm⁻¹), 655 nm (816 M⁻¹cm⁻¹);

Compound 17:



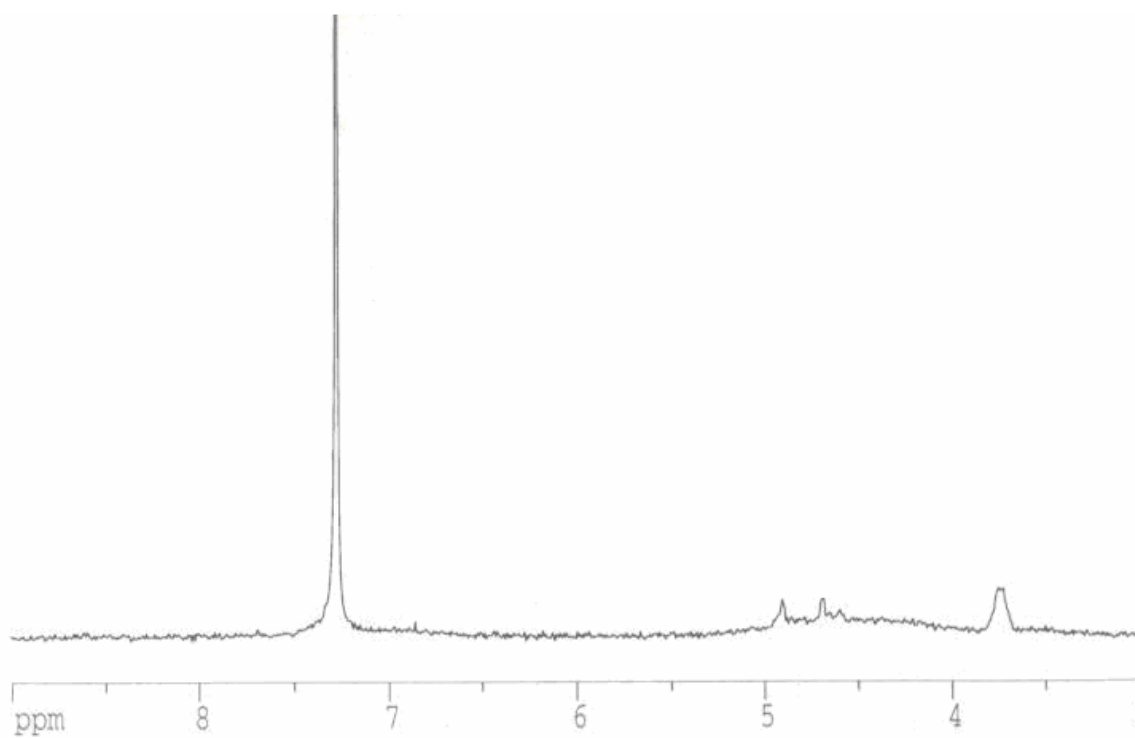


Figure A.54: ^1H NMR spectrum of $\text{FcO}_2\text{-Hg}$ in CDCl_3 : 4.90 ppm (4H, s, Cp), 4.68 ppm (4H, s, Cp), very broad 5.0-4.0 ppm;

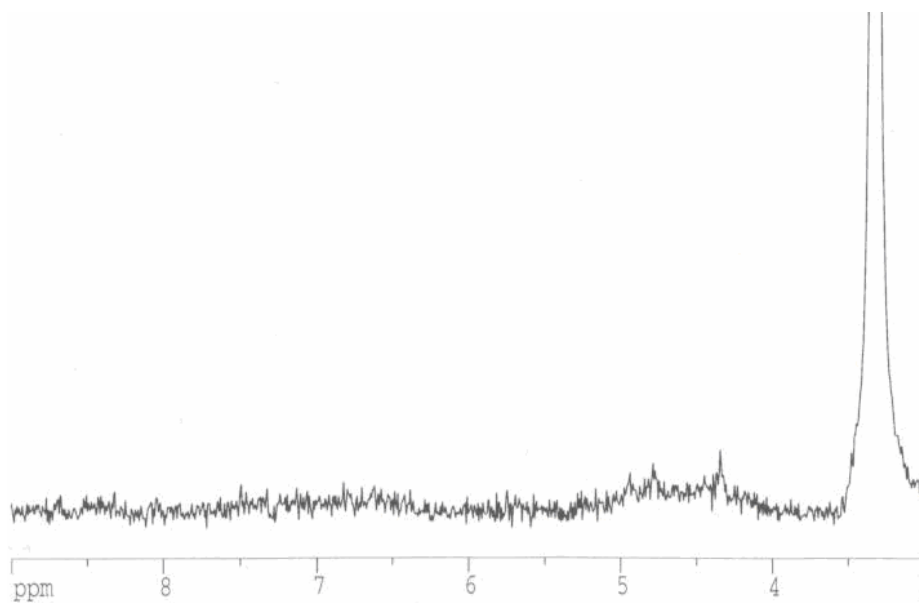


Figure A.55: ^1H NMR spectrum of $\text{FcO}_2\text{-Hg}$ in $d_6\text{-DMSO}$: 8.0-6.0 ppm (H, m, phenyl), 4.9-4.7 ppm (H, s, Cp), 4.34 ppm (H, s, Cp);

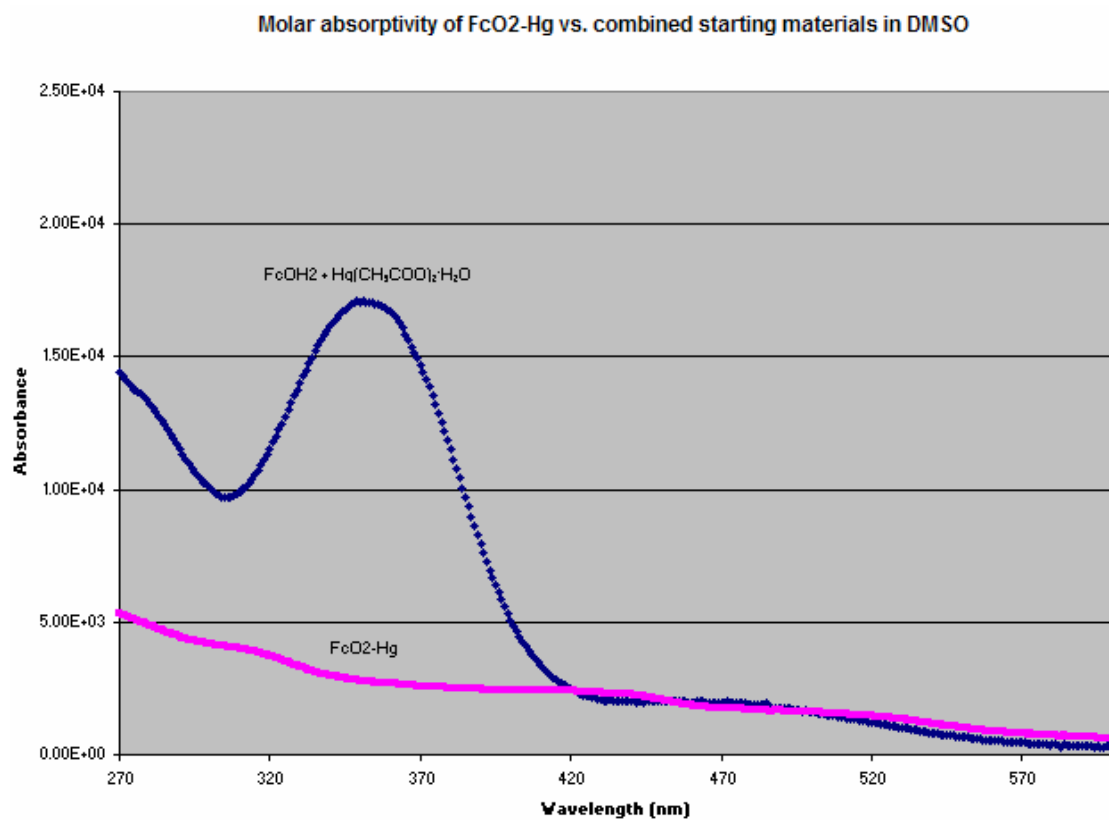
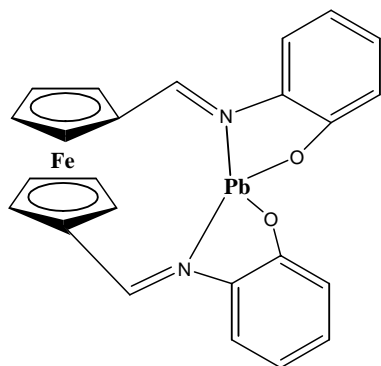


Figure A.56: Comparison between the molar absorptivity (UV-Vis) of FcO2-Hg and the molar absorptivity of the starting materials (351, 463 nm peaks) in DMSO: 412 nm ($2440 \text{ M}^{-1} \text{ cm}^{-1}$);

Compound 18:



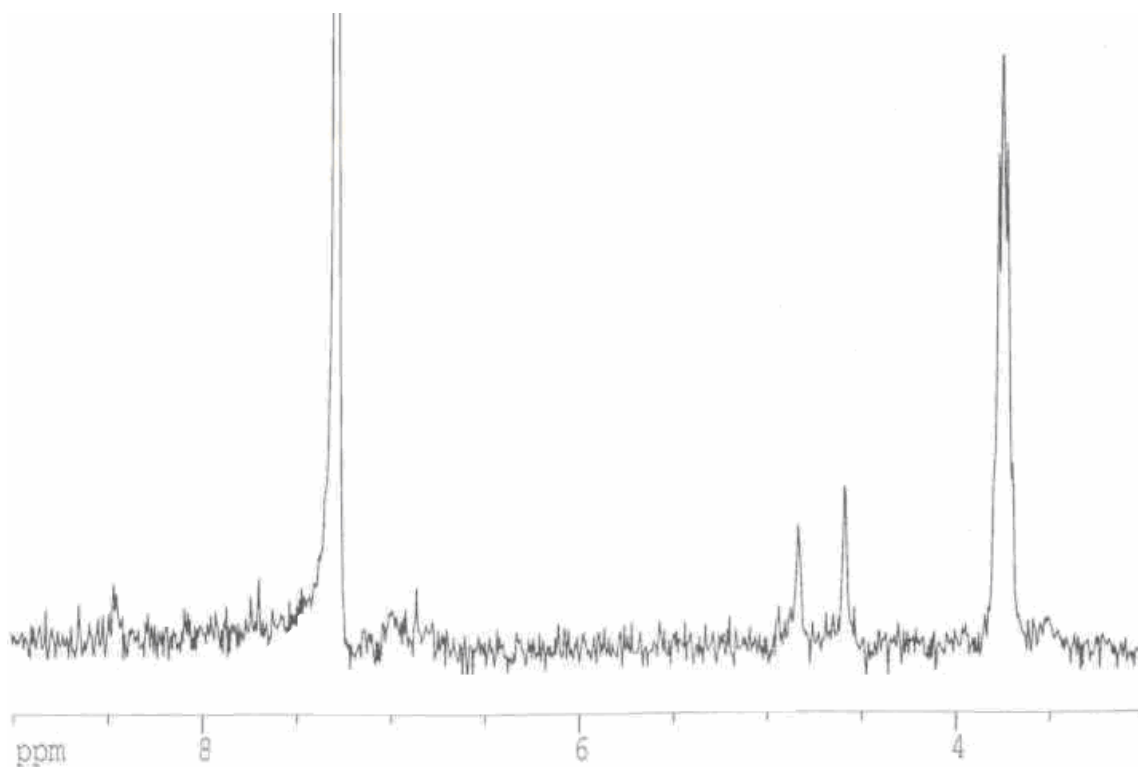


Figure A.57: ^1H NMR spectrum of $\text{FcO}_2\text{-Pb}$ in CDCl_3 : 8.5 ppm (2H, d, Cp-CH=N), 7.6 ppm (2H, d, phenyl), 7.4 ppm (2H, m, phenyl), 7.0 ppm (2H, broad s, phenyl), 6.8 ppm (2H, s, phenyl), 4.82 ppm (4H, s, Cp), 4.58 ppm (4H, s, Cp);

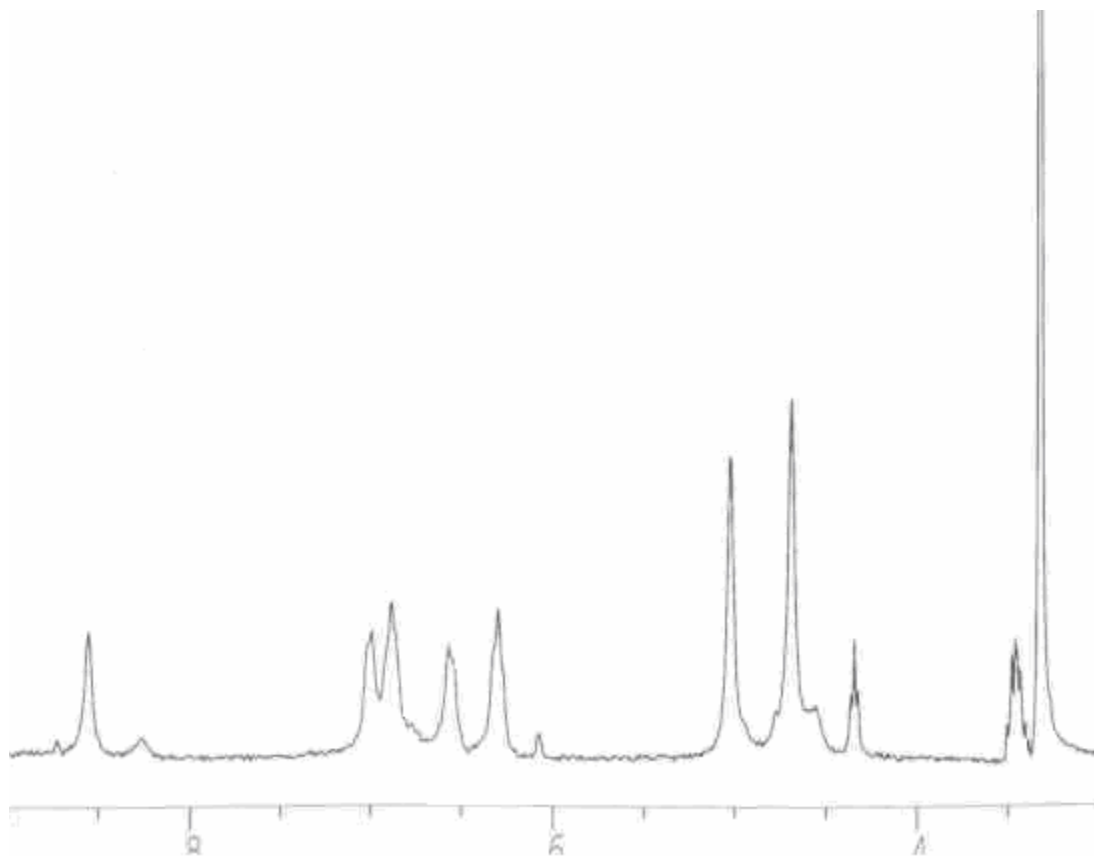


Figure A.58: ^1H NMR spectrum of FcO₂-Pb in d₆-DMSO: 8.54 ppm (2H, s, Cp- $\text{CH}=\text{N}$), 6.98 ppm (2H, d, phenyl), 6.87 ppm (2H, d, phenyl), 6.55 ppm (2H, d, phenyl), 6.28 ppm (2H, d, phenyl), 5.01 ppm (4H, d, Cp), 4.67 ppm (4H, d, Cp);

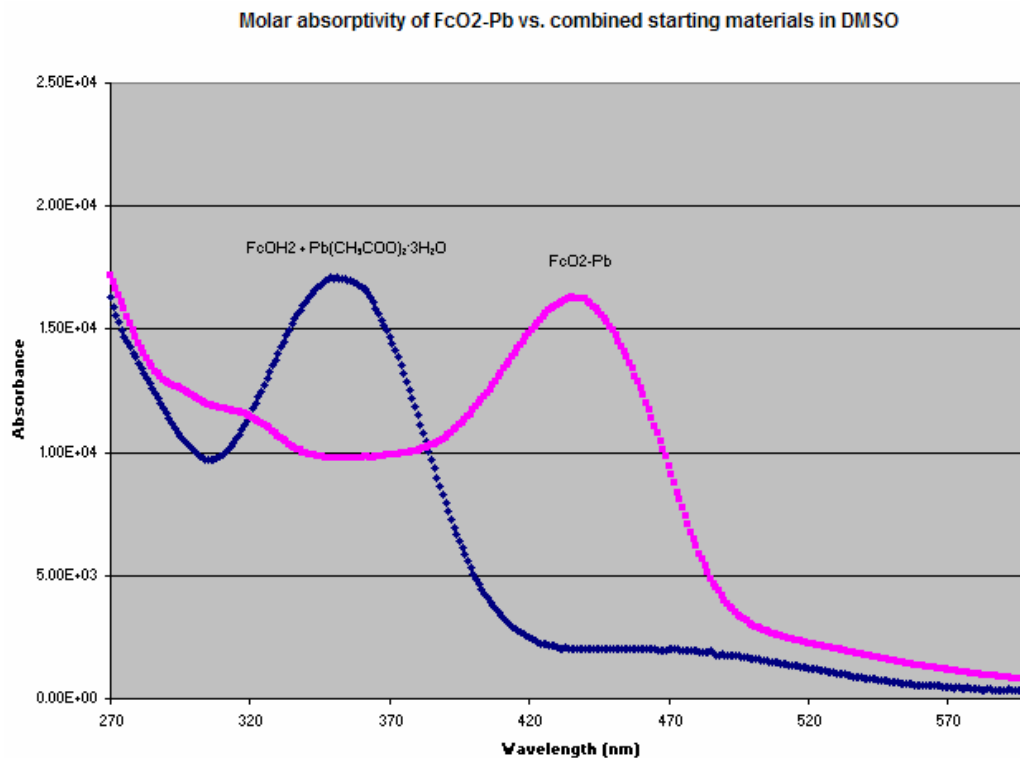


Figure A.59: Comparison between the molar absorptivity (UV-Vis) of FcO2-Pb and the molar absorptivity of the starting materials (351, 463 nm peaks) in DMSO: 438 nm ($16300 \text{ M}^{-1}\text{cm}^{-1}$);

Compound 19:

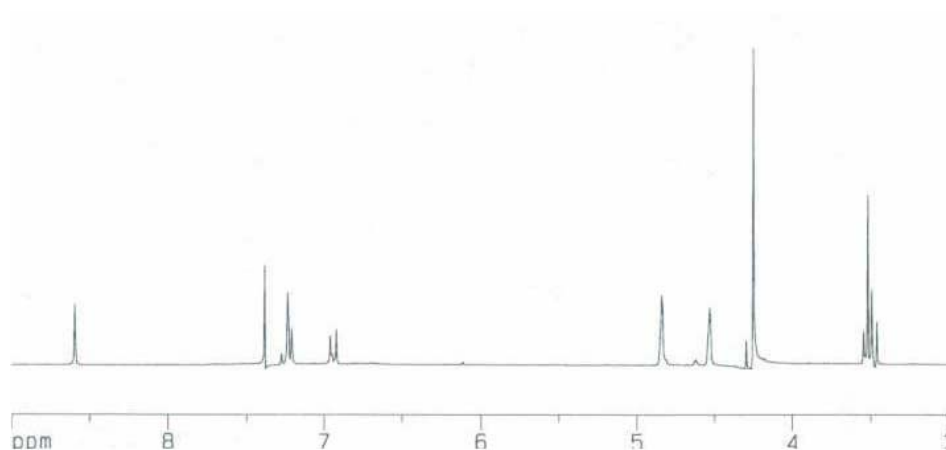


Figure A.60: ^1H NMR Spectrum of FcOH1 (4-*t* butyl) ligand in CDCl_3 : 8.59 ppm (s, 1H, Cp- $\text{CH}=\text{N}$), 7.37 (s, 1H, Phenyl), 7.23 (s, 2H, Phenyl), 7.20 (s, 1H, Phenyl), 6.93

(d, 1H, OH), 4.83 (s, 2H, Cp), 4.53 (s, 2H Cp), 4.27 (s, 5H, Cp unsubstituted), 1.37 (s, 9H, *t*-butyl Hs);

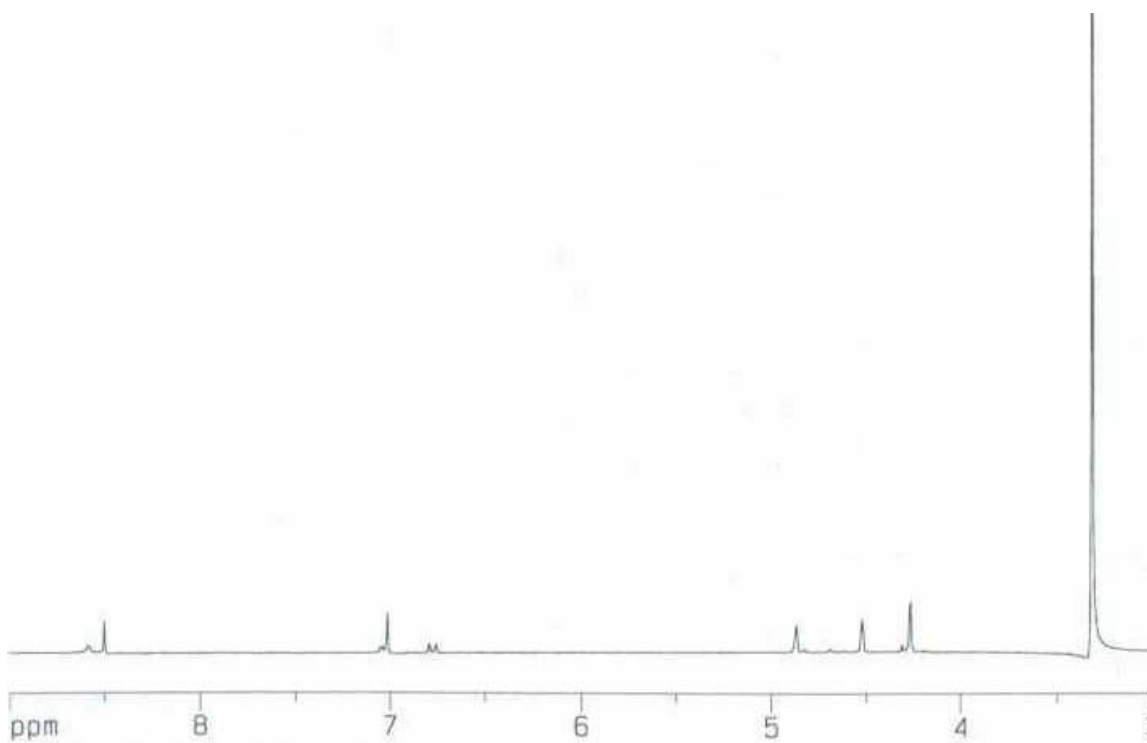


Figure A.61: ^1H NMR Spectrum of FcOH1 (4-*t* butyl) ligand in d_6 -DMSO:

Compound 20:

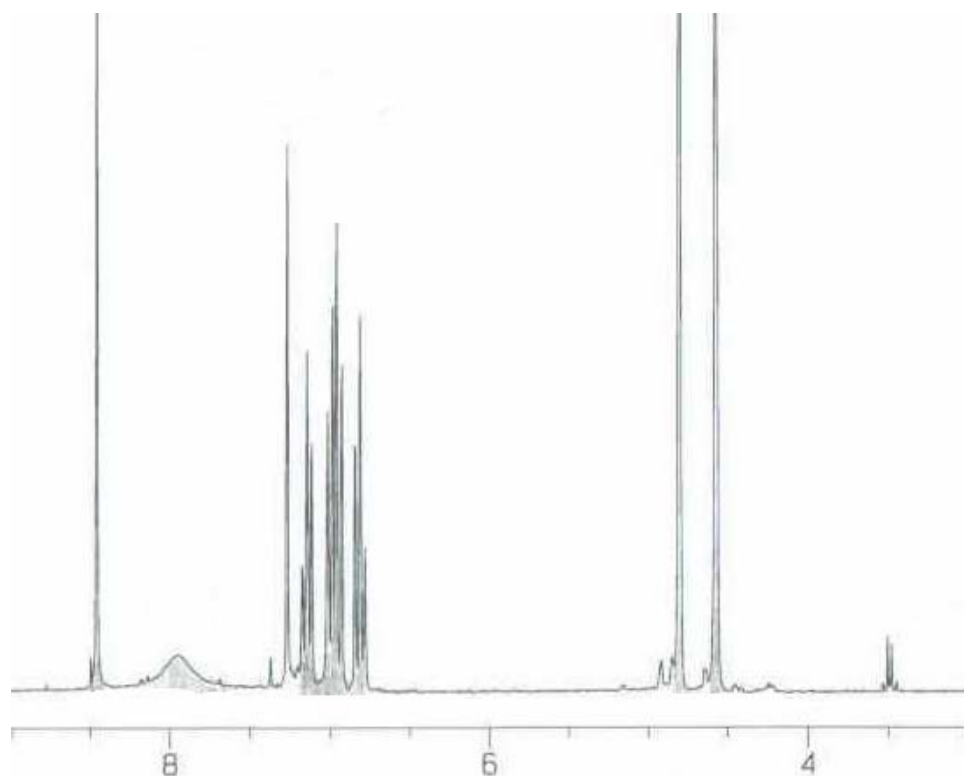


Figure A.62: ^1H NMR Spectrum of FcOH2 (4-*t* butyl) Ligand in CDCl_3 : 8.50 (s, 2H, $\text{CpCH}=\text{N}$), 7.38 (s, 4H, Phenyl), 7.19 (m, 2H, Phenyl), 6.99 (s, 2H, Phenyl), 6.89 (d, 2H, OH), 4.74 (s, 4H, Cp), 4.58 (s, 4H, Cp), 1.33 (s, 18H, *t*-butyl Hs);

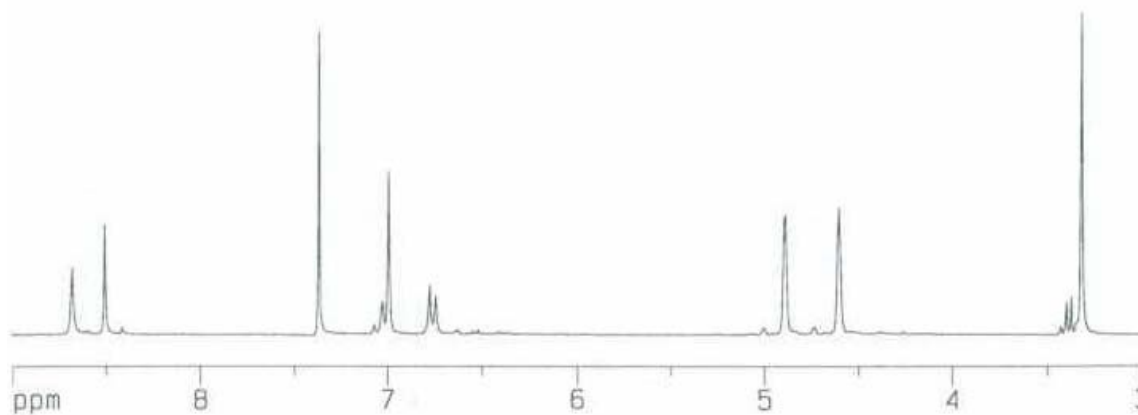


Figure A.63: ^1H NMR Spectrum of FcOH2 (4-*t* butyl) Ligand in d-DMSO:

Compound 21:

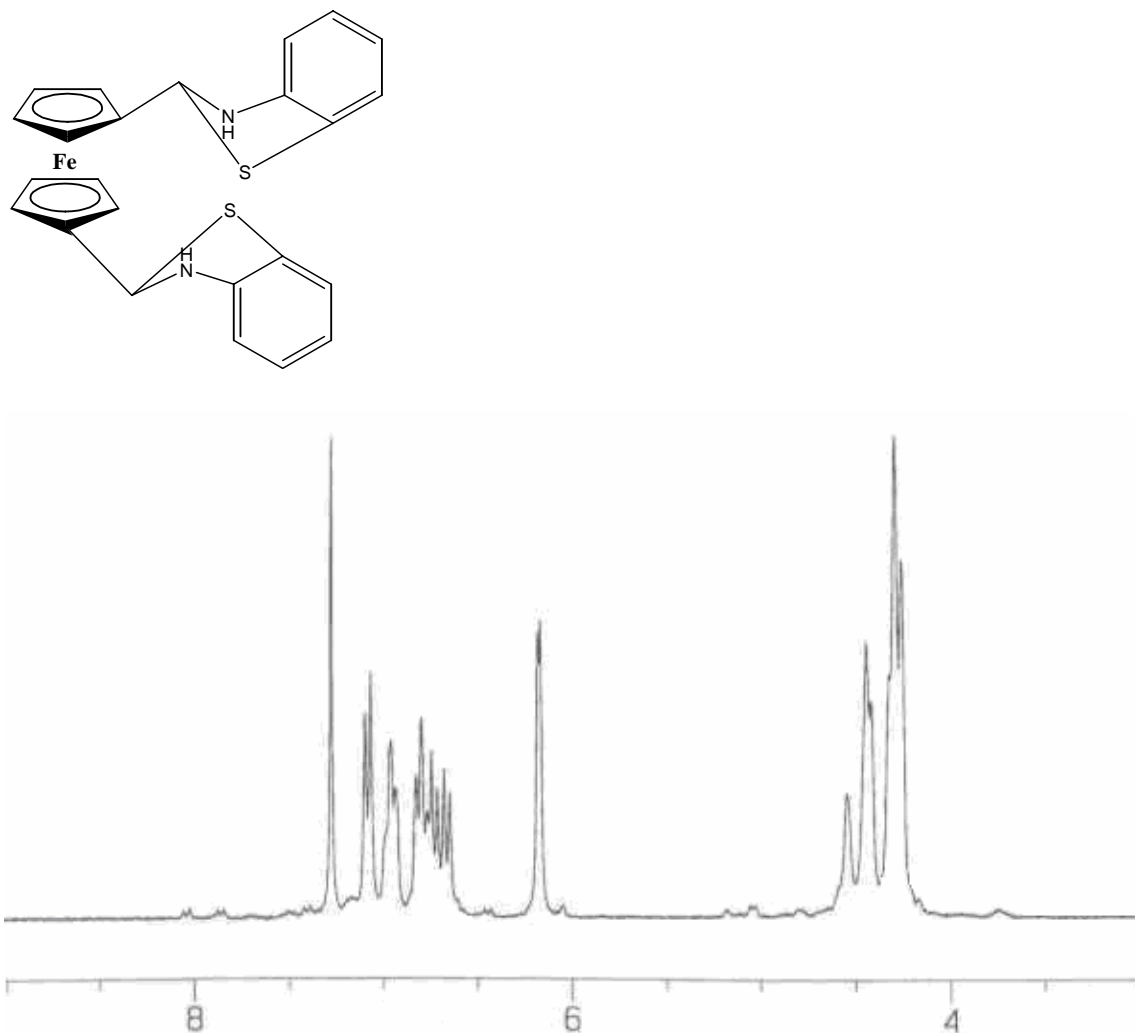


Figure A.64: ¹H NMR spectrum of FcSH₂ in CDCl₃: 7.08-7.05 ppm (2H, d, phenyl), 6.95-6.92 ppm (4H, t, phenyl), 6.81-6.64 ppm (2H, t, phenyl), 6.17 ppm (2H, d, Cp-CH-N), 4.54 ppm (2H, s, N-H), 4.42 ppm (4H, d, Cp), 4.28 ppm (4H, d, Cp);

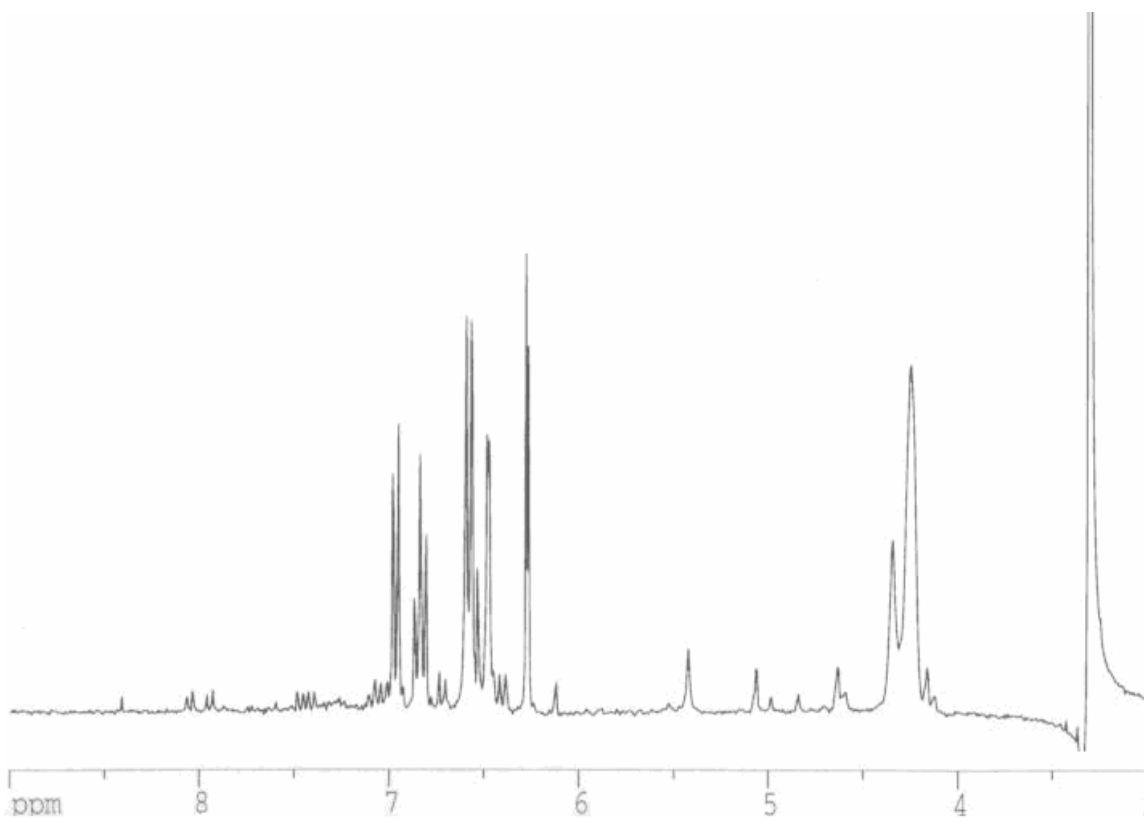


Figure A.65: ^1H NMR spectrum of FcSH₂ in d_6 -DMSO: 7.04 ppm (2H, d, phenyl), 6.84 ppm (2H, t, phenyl), 6.71 ppm (4H, d, phenyl), 6.57 ppm (2H, d, N-H), 6.27 ppm (2H, d, Cp-CH-N), 4.35 ppm (2H, s, Cp), 4.25 ppm (6H, s, Cp);

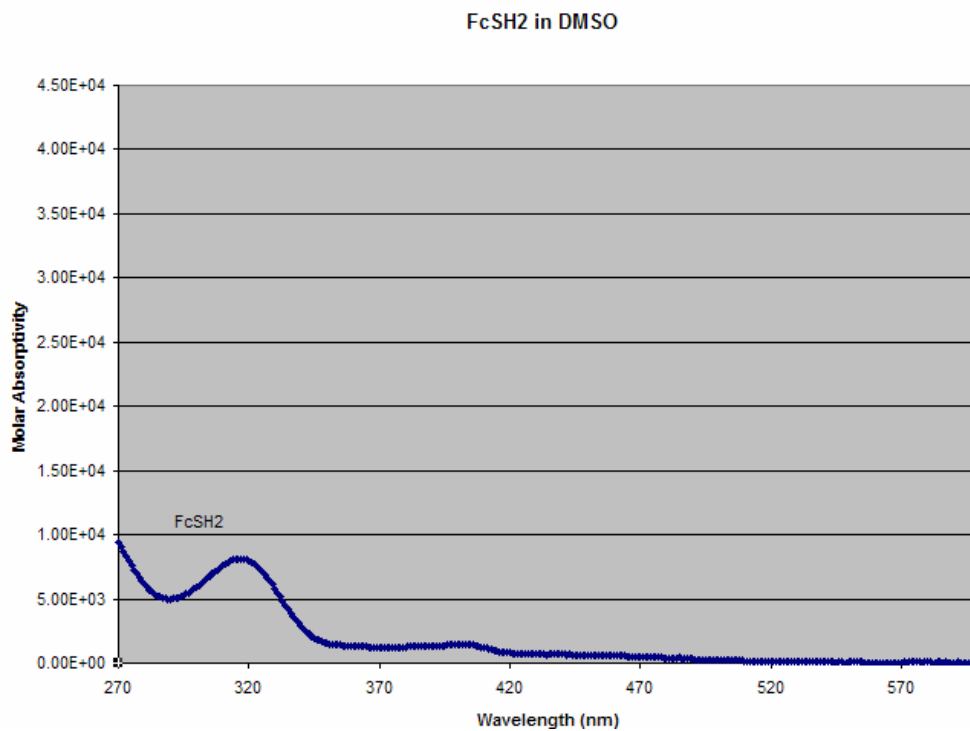


Figure A.66: Molar absorptivity (UV-Vis) of the FcSH2 ligand in DMSO: 317 nm ($8130 \text{ M}^{-1}\text{cm}^{-1}$), 402 nm ($1490 \text{ M}^{-1}\text{cm}^{-1}$);

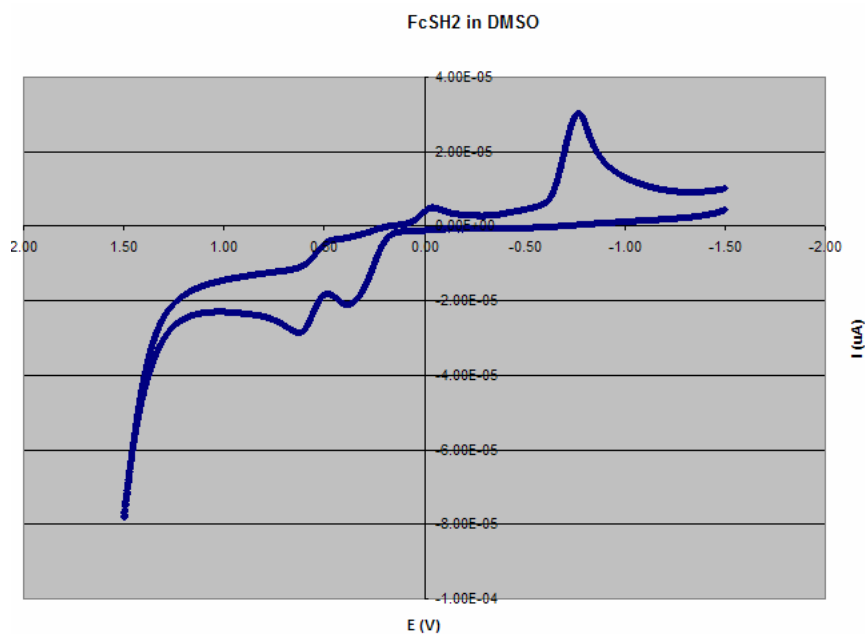


Figure A.67: CV scan of the FcSH2 ligand in DMSO, scan rate 100 mV/sec. Fe^{II} to Fe^{III} oxidation peak is at 627 mV with an irreversible oxidation at 389 mV (most likely due to the thiol groups).

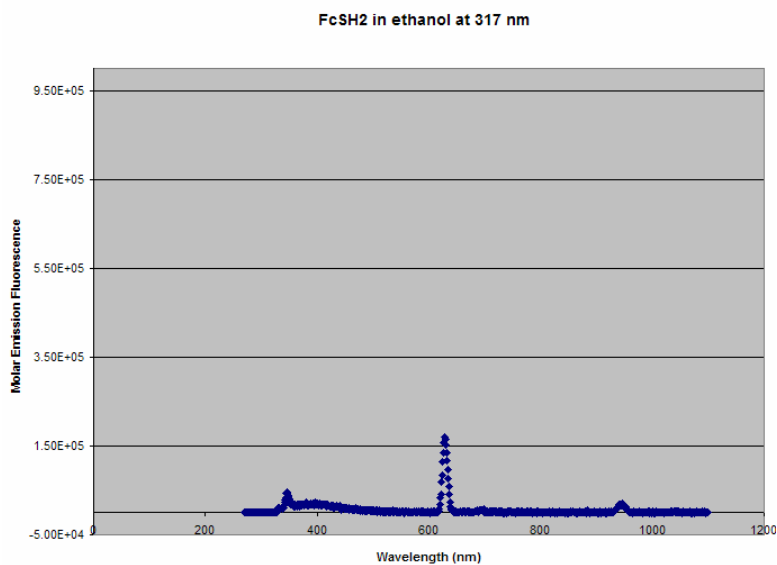


Figure A.68: Emission fluorescence of the FcSH2 ligand in ethanol at 317 nm with peaks at 347, 629 and 947 nm.

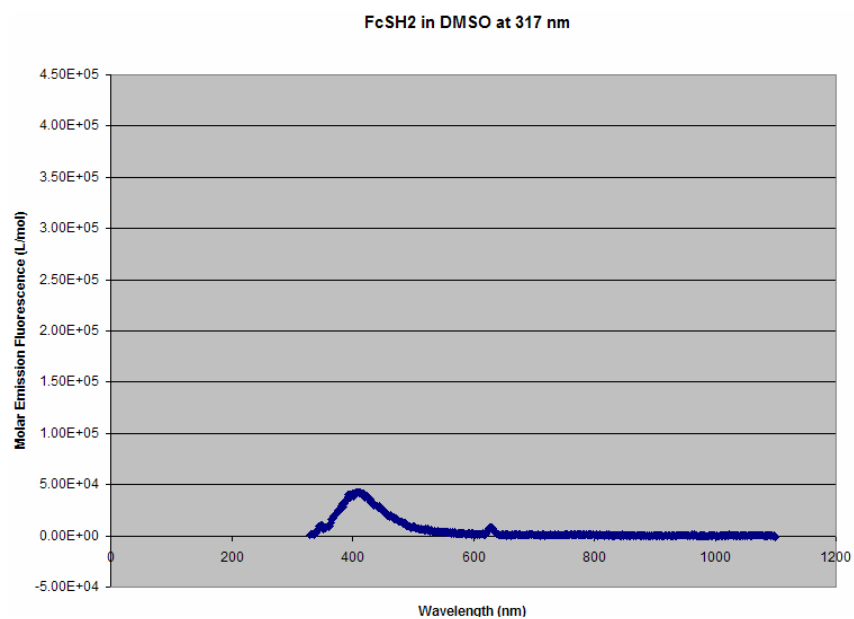


Figure A.69: Emission fluorescence of the FcSH ligand in DMSO at 317 nm with peaks at 413, 628 nm.

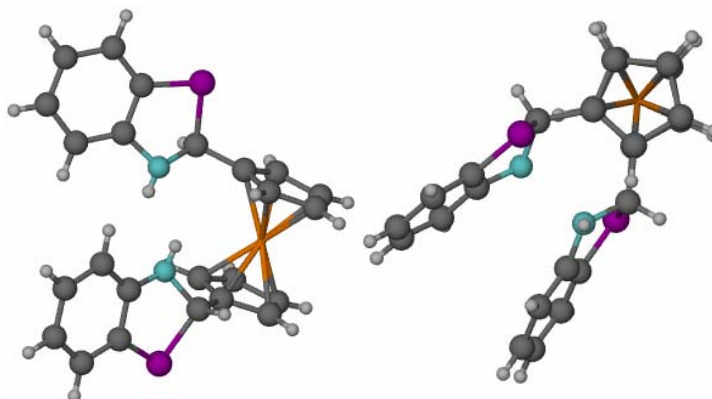


Figure A.70: Crystal structure of the FcSH2 Ligand

Crystal data

$C_{24}H_{18}FeN_2S_2$

$M_r = 454.37$

Triclinic, $P\bar{1}$

$a = 10.0682 (16) \text{ \AA}$

$b = 12.0464 (19) \text{ \AA}$

$c = 18.983 (3) \text{ \AA}$

$\alpha = 71.793 (3)^\circ$

$\beta = 85.700 (3)^\circ$

$\Gamma = 66.279 (3)^\circ$

$V = 1998.9 (6) \text{ \AA}^3$

$Z = 4$

$F_{000} = 936$

$D_x = 1.510 \text{ Mg m}^{-3}$

Mo $K\alpha$ radiation

$\lambda = 0.71073 \text{ \AA}$

Cell parameters from 4139 reflections

$\theta = 2.2\text{--}27.1^\circ$

$\mu = 0.98 \text{ mm}^{-1}$

$T = 173 (2) \text{ K}$

Needle, yellow

$0.55 \times 0.02 \times 0.02 \text{ mm}$

Data collection

Bruker SMART CCD area detector
diffractometer

Monochromator: graphite

$T = 173(2) \text{ K}$

ω scans

Absorption correction: multi-scan

Data were corrected for decay and absorption using
the program SADABS (Sheldrick, G. M. (2003).
SADABS. Version 2.10. University of Göttingen,
Germany).

$T_{\min} = 0.67, T_{\max} = 0.98$

14017 measured reflections

8545 independent reflections

4806 reflections with $I > 2\sigma(I)$

$R_{\text{int}} = 0.055$

$\theta_{\text{max}} = 27.1^\circ$

$\theta_{\text{min}} = 1.1^\circ$

$h = -11 \rightarrow 12$

$k = -10 \rightarrow 15$

$l = -24 \rightarrow 24$

Refinement

Refinement on F^2	Secondary atom site location: difference Fourier map
Least-squares matrix: full	Hydrogen site location: inferred from neighbouring sites
$R[F^2 > 2\sigma(F^2)] = 0.073$	H-atom parameters constrained
$wR(F^2) = 0.206$	$w = 1/[\sigma^2(F_o^2) + (0.1092P)^2]$
$S = 0.99$	where $P = (F_o^2 + 2F_c^2)/3$
8545 reflections	$(\Delta/\sigma)_{\max} < 0.001$
518 parameters	$\Delta\rho_{\max} = 2.91 \text{ e } \text{\AA}^{-3}$
	$\Delta\rho_{\min} = -0.99 \text{ e } \text{\AA}^{-3}$
	Extinction correction: none
Primary atom site location: structure-invariant direct methods	

Refinement of F^2 against ALL reflections. The weighted R-factor wR and goodness of fit S are based on F^2 , conventional R-factors R are based on F , with F set to zero for negative F^2 . The threshold expression of $F^2 > 2\sigma(F^2)$ is used only for calculating R-factors(gt) etc. and is not relevant to the choice of reflections for refinement. R-factors based on F^2 are statistically about twice as large as those based on F , and R-factors based on ALL data will be even larger.

Fractional atomic coordinates and isotropic or equivalent isotropic displacement parameters (\AA^2)

	x	Y	z	$U_{\text{iso}}^*/U_{\text{eq}}$
Fe1A	0.13762 (9)	0.22913 (8)	0.04734 (4)	0.0160 (2)
S1A	0.53720 (16)	-0.15874 (14)	0.16956 (8)	0.0192 (3)
N1A	0.3347 (5)	-0.1116 (4)	0.0724 (3)	0.0192 (11)
C1A	0.3478 (6)	-0.0593 (5)	0.1312 (3)	0.0180 (13)
H1A	0.2794	-0.0736	0.1705	0.022*
S2A	-0.04860 (16)	0.18467 (15)	-0.16269 (8)	0.0198 (3)
N2A	0.1947 (5)	0.0477 (4)	-0.0815 (3)	0.0180 (11)
C2A	0.5309 (6)	-0.2872 (6)	0.1457 (3)	0.0197 (13)
C3A	0.6245 (7)	-0.4141 (6)	0.1699 (3)	0.0239 (14)
H3A	0.7047	-0.4423	0.2038	0.029*
C4A	0.5996 (7)	-0.4993 (6)	0.1440 (3)	0.0283 (15)
H4A	0.6634	-0.5869	0.1603	0.034*
C5A	0.4835 (7)	-0.4595 (6)	0.0950 (4)	0.0254 (15)

H5A	0.4671	-0.5201	0.0786	0.030*
C6A	0.3893 (7)	-0.3301 (6)	0.0689 (3)	0.0264 (15)
H6A	0.3105	-0.3018	0.0341	0.032*
C7A	0.4143 (6)	-0.2452 (6)	0.0952 (3)	0.0168 (12)
C8A	0.0925 (6)	0.1821 (5)	-0.1033 (3)	0.0174 (12)
H8A	0.1422	0.2365	-0.1338	0.021*
C9A	0.0867 (6)	0.0595 (5)	-0.1905 (3)	0.0175 (12)
C10A	0.0815 (7)	0.0209 (6)	-0.2504 (3)	0.0244 (14)
H10A	-0.0034	0.0608	-0.2827	0.029*
C11A	0.2027 (7)	-0.0774 (6)	-0.2630 (4)	0.0272 (15)
H11A	0.2014	-0.1039	-0.3051	0.033*
C12A	0.3250 (7)	-0.1373 (6)	-0.2153 (3)	0.0252 (14)
H12A	0.4071	-0.2041	-0.2252	0.030*
C13A	0.3306 (7)	-0.1016 (6)	-0.1528 (3)	0.0246 (14)
H13A	0.4139	-0.1446	-0.1192	0.029*
C14A	0.2094 (6)	-0.0005 (6)	-0.1412 (3)	0.0199 (13)
C15A	0.3196 (6)	0.0788 (5)	0.1039 (3)	0.0154 (12)
C16A	0.3570 (6)	0.1464 (5)	0.0345 (3)	0.0181 (13)
H16A	0.4010	0.1116	-0.0041	0.022*
C17A	0.3171 (6)	0.2749 (6)	0.0329 (3)	0.0190 (13)
H17A	0.3294	0.3406	-0.0068	0.023*
C18A	0.2556 (6)	0.2870 (6)	0.1013 (3)	0.0206 (13)
H18A	0.2194	0.3625	0.1154	0.025*
C19A	0.2575 (6)	0.1665 (6)	0.1452 (3)	0.0202 (13)
H19A	0.2232	0.1477	0.1937	0.024*
C20A	0.0283 (6)	0.2283 (5)	-0.0388 (3)	0.0165 (12)
C21A	-0.0103 (6)	0.3556 (6)	-0.0379 (3)	0.0205 (13)
H21A	0.0028	0.4224	-0.0763	0.025*
C22A	-0.0723 (6)	0.3642 (6)	0.0314 (3)	0.0227 (14)
H22A	-0.1091	0.4384	0.0468	0.027*
C23A	-0.0694 (6)	0.2431 (6)	0.0731 (3)	0.0211 (13)

H23A	-0.1028	0.2212	0.1215	0.025*
C24A	-0.0075 (6)	0.1600 (6)	0.0290 (3)	0.0196 (13)
H24A	0.0072	0.0728	0.0432	0.023*
Fe1B	0.36504 (9)	0.27441 (8)	0.45847 (5)	0.0162 (2)
S1B	0.08956 (18)	0.32216 (15)	0.67068 (9)	0.0235 (4)
N1B	0.2193 (5)	0.4638 (5)	0.5873 (3)	0.0193 (11)
C1B	0.2423 (6)	0.3284 (5)	0.6117 (3)	0.0163 (12)
H1B	0.3360	0.2762	0.6422	0.020*
S2B	0.42075 (16)	0.65854 (14)	0.32568 (9)	0.0217 (4)
N2B	0.2378 (5)	0.6208 (5)	0.4272 (3)	0.0201 (11)
C2B	0.0782 (6)	0.4579 (6)	0.6921 (3)	0.0197 (13)
C3B	-0.0031 (7)	0.5122 (6)	0.7434 (3)	0.0262 (14)*
H3B	-0.0667	0.4771	0.7717	0.031*
C4B	0.0065 (7)	0.6163 (6)	0.7540 (4)	0.0279 (15)
H4B	-0.0430	0.6484	0.7926	0.033*
C5B	0.0885 (7)	0.6736 (6)	0.7082 (3)	0.0272 (15)
H5B	0.0932	0.7470	0.7148	0.033*
C6B	0.1649 (7)	0.6266 (6)	0.6522 (3)	0.0239 (14)
H6B	0.2207	0.6674	0.6206	0.029*
C7B	0.1573 (6)	0.5187 (5)	0.6438 (3)	0.0171 (12)
C8B	0.3115 (6)	0.5648 (5)	0.3683 (3)	0.0175 (12)
H8B	0.2373	0.5791	0.3306	0.021*
C9B	0.3005 (6)	0.7872 (6)	0.3549 (3)	0.0197 (13)
C10B	0.2939 (7)	0.9114 (5)	0.3339 (3)	0.0228 (14)
H10B	0.3608	0.9346	0.3009	0.027*
C11B	0.1882 (7)	0.9996 (6)	0.3620 (3)	0.0273 (15)
H11B	0.1810	1.0848	0.3472	0.033*
C12B	0.0931 (7)	0.9658 (6)	0.4110 (3)	0.0249 (15)
H12B	0.0207	1.0282	0.4293	0.030*
C13B	0.1014 (6)	0.8404 (6)	0.4344 (3)	0.0240 (14)
H13B	0.0364	0.8171	0.4688	0.029*

C14B	0.2067 (6)	0.7511 (5)	0.4061 (3)	0.0169 (12)
C15B	0.2415 (6)	0.2766 (6)	0.5497 (3)	0.0176 (12)
C16B	0.1506 (6)	0.3365 (6)	0.4830 (3)	0.0187 (13)
H16B	0.0807	0.4220	0.4676	0.022*
C17B	0.1816 (6)	0.2478 (6)	0.4435 (3)	0.0234 (14)
H17B	0.1366	0.2631	0.3972	0.028*
C18B	0.2934 (6)	0.1306 (6)	0.4861 (3)	0.0239 (14)
H18B	0.3357	0.0542	0.4729	0.029*
C19B	0.3296 (6)	0.1485 (6)	0.5512 (3)	0.0196 (13)
H19B	0.4004	0.0861	0.5893	0.024*
C20B	0.4083 (6)	0.4267 (6)	0.3957 (3)	0.0202 (13)
C21B	0.4299 (7)	0.3406 (6)	0.3550 (3)	0.0207 (13)
H21B	0.3806	0.3603	0.3091	0.025*
C22B	0.5380 (6)	0.2194 (6)	0.3946 (3)	0.0225 (14)
H22B	0.5724	0.1443	0.3801	0.027*
C23B	0.5853 (6)	0.2315 (6)	0.4601 (3)	0.0233 (14)
H23B	0.6577	0.1664	0.4966	0.028*
C24B	0.5035 (6)	0.3595 (6)	0.4605 (3)	0.0198 (13)
H24B	0.5114	0.3940	0.4979	0.024*

Atomic displacement parameters (\AA^2)

	U^{11}	U^{22}	U^{33}	U^{12}	U^{13}	U^{23}
Fe1A	0.0125 (4)	0.0151 (5)	0.0186 (5)	-0.0038 (3)	0.0024 (3)	-0.0056 (4)
S1A	0.0175 (7)	0.0189 (8)	0.0187 (8)	-0.0053 (6)	-0.0011 (6)	-0.0046 (6)
N1A	0.014 (2)	0.015 (3)	0.023 (3)	0.000 (2)	0.001 (2)	-0.007 (2)
C1A	0.016 (3)	0.019 (3)	0.018 (3)	-0.006 (2)	0.004 (2)	-0.006 (3)
S2A	0.0154 (7)	0.0221 (8)	0.0198 (8)	-0.0062 (6)	-0.0010 (6)	-0.0052 (6)

N2A	0.019 (3)	0.016 (3)	0.015 (2)	-0.004 (2)	-0.003 (2)	-0.004 (2)
C2A	0.017 (3)	0.022 (3)	0.020 (3)	-0.009 (3)	0.008 (2)	-0.005 (3)
C3A	0.023 (3)	0.020 (3)	0.021 (3)	-0.002 (3)	-0.001 (3)	-0.003 (3)
C4A	0.033 (4)	0.013 (3)	0.029 (4)	0.000 (3)	0.007 (3)	-0.006 (3)
C5A	0.026 (3)	0.016 (3)	0.035 (4)	-0.004 (3)	0.004 (3)	-0.015 (3)
C6A	0.024 (3)	0.030 (4)	0.027 (4)	-0.014 (3)	0.002 (3)	-0.009 (3)
C7A	0.014 (3)	0.021 (3)	0.015 (3)	-0.005 (2)	0.006 (2)	-0.007 (2)
C8A	0.014 (3)	0.021 (3)	0.021 (3)	-0.009 (2)	0.003 (2)	-0.008 (3)
C9A	0.015 (3)	0.016 (3)	0.019 (3)	-0.006 (2)	0.002 (2)	-0.003 (2)
C10A	0.033 (4)	0.028 (4)	0.015 (3)	-0.017 (3)	-0.001 (3)	-0.003 (3)
C11A	0.026 (3)	0.038 (4)	0.028 (4)	-0.017 (3)	0.006 (3)	-0.019 (3)
C12A	0.022 (3)	0.028 (4)	0.032 (4)	-0.010 (3)	0.009 (3)	-0.019 (3)
C13A	0.021 (3)	0.024 (4)	0.025 (3)	-0.007 (3)	0.001 (3)	-0.006 (3)
C14A	0.019 (3)	0.024 (3)	0.015 (3)	-0.010 (3)	0.003 (2)	-0.003 (3)
C15A	0.012 (3)	0.018 (3)	0.014 (3)	-0.003 (2)	0.001 (2)	-0.007 (2)
C16A	0.014 (3)	0.020 (3)	0.017 (3)	-0.003 (2)	0.003 (2)	-0.007 (3)
C17A	0.016 (3)	0.018 (3)	0.024 (3)	-0.007 (2)	0.005 (2)	-0.008 (3)
C18A	0.014 (3)	0.022 (3)	0.025 (3)	-0.004 (2)	0.002 (2)	-0.011 (3)
C19A	0.024 (3)	0.020 (3)	0.018 (3)	-0.007 (3)	0.004 (2)	-0.010 (3)
C20A	0.014 (3)	0.017 (3)	0.019 (3)	-0.008 (2)	0.003 (2)	-0.004 (2)
C21A	0.019 (3)	0.016 (3)	0.023 (3)	-0.005 (3)	-0.002 (2)	-0.005 (3)
C22A	0.017 (3)	0.019 (3)	0.032 (4)	-0.002 (3)	0.000 (3)	-0.013 (3)
C23A	0.012 (3)	0.029 (4)	0.022 (3)	-0.008 (3)	0.005 (2)	-0.008 (3)
C24A	0.017 (3)	0.020 (3)	0.024 (3)	-0.009 (3)	0.002 (2)	-0.008 (3)
Fe1B	0.0146 (4)	0.0153 (5)	0.0187 (5)	-0.0053 (3)	0.0014 (3)	-0.0061 (4)
S1B	0.0278 (9)	0.0267 (9)	0.0237 (8)	-0.0169 (7)	0.0124 (7)	-0.0123 (7)
N1B	0.022 (3)	0.018 (3)	0.018 (3)	-0.005 (2)	0.003 (2)	-0.009 (2)
C1B	0.016 (3)	0.015 (3)	0.019 (3)	-0.006 (2)	0.004 (2)	-0.007 (2)
S2B	0.0206 (8)	0.0165 (8)	0.0256 (8)	-0.0076 (6)	0.0105 (6)	-0.0053 (7)
N2B	0.022 (3)	0.016 (3)	0.019 (3)	-0.006 (2)	0.004 (2)	-0.004 (2)
C2B	0.015 (3)	0.018 (3)	0.022 (3)	-0.002 (2)	-0.002 (2)	-0.005 (3)

C4B	0.027 (4)	0.023 (4)	0.026 (3)	0.000 (3)	0.004 (3)	-0.012 (3)
C5B	0.033 (4)	0.023 (4)	0.024 (3)	-0.008 (3)	-0.001 (3)	-0.009 (3)
C6B	0.020 (3)	0.022 (3)	0.029 (3)	-0.008 (3)	0.000 (3)	-0.007 (3)
C7B	0.016 (3)	0.016 (3)	0.017 (3)	-0.004 (2)	-0.002 (2)	-0.006 (2)
C8B	0.021 (3)	0.020 (3)	0.012 (3)	-0.011 (3)	0.002 (2)	-0.002 (2)
C9B	0.019 (3)	0.017 (3)	0.020 (3)	-0.004 (2)	-0.001 (2)	-0.007 (3)
C10B	0.024 (3)	0.014 (3)	0.028 (3)	-0.013 (3)	-0.009 (3)	0.005 (3)
C11B	0.035 (4)	0.017 (3)	0.024 (3)	-0.003 (3)	-0.006 (3)	-0.005 (3)
C12B	0.020 (3)	0.024 (4)	0.025 (3)	0.002 (3)	-0.004 (3)	-0.014 (3)
C13B	0.015 (3)	0.026 (4)	0.029 (4)	-0.006 (3)	0.003 (3)	-0.009 (3)
C14B	0.014 (3)	0.016 (3)	0.018 (3)	-0.005 (2)	-0.002 (2)	-0.004 (2)
C15B	0.016 (3)	0.023 (3)	0.018 (3)	-0.009 (2)	0.003 (2)	-0.011 (3)
C16B	0.016 (3)	0.021 (3)	0.019 (3)	-0.006 (3)	0.004 (2)	-0.008 (3)
C17B	0.016 (3)	0.031 (4)	0.026 (3)	-0.011 (3)	0.004 (3)	-0.011 (3)
C18B	0.021 (3)	0.025 (4)	0.032 (4)	-0.014 (3)	0.011 (3)	-0.013 (3)
C19B	0.019 (3)	0.021 (3)	0.017 (3)	-0.006 (3)	0.004 (2)	-0.005 (3)
C20B	0.017 (3)	0.022 (3)	0.021 (3)	-0.009 (3)	0.005 (2)	-0.004 (3)
C21B	0.024 (3)	0.018 (3)	0.022 (3)	-0.009 (3)	0.004 (3)	-0.007 (3)
C22B	0.020 (3)	0.018 (3)	0.033 (4)	-0.007 (3)	0.008 (3)	-0.015 (3)
C23B	0.014 (3)	0.018 (3)	0.032 (4)	-0.005 (3)	-0.003 (3)	0.000 (3)
C24B	0.014 (3)	0.025 (3)	0.019 (3)	-0.007 (3)	0.000 (2)	-0.006 (3)

Table 1

Geometric parameters (Å, °)

Fe1A—C21A	2.037 (6)	Fe1B—C21B	2.041 (6)
Fe1A—C20A	2.044 (6)	Fe1B—C20B	2.043 (6)
Fe1A—C24A	2.045 (6)	Fe1B—C24B	2.044 (6)
Fe1A—C15A	2.049 (5)	Fe1B—C18B	2.044 (6)
Fe1A—C19A	2.051 (6)	Fe1B—C19B	2.049 (6)
Fe1A—C22A	2.056 (6)	Fe1B—C22B	2.049 (6)

Fe1A—C23A	2.056 (6)	Fe1B—C16B	2.050 (6)
Fe1A—C16A	2.057 (6)	Fe1B—C17B	2.051 (6)
Fe1A—C18A	2.059 (6)	Fe1B—C15B	2.056 (6)
Fe1A—C17A	2.068 (6)	Fe1B—C23B	2.065 (6)
S1A—C2A	1.768 (6)	S1B—C2B	1.764 (6)
S1A—C1A	1.852 (6)	S1B—C1B	1.846 (6)
N1A—C7A	1.414 (7)	N1B—C7B	1.411 (7)
N1A—C1A	1.478 (7)	N1B—C1B	1.472 (7)
C1A—C15A	1.491 (8)	C1B—C15B	1.495 (8)
C1A—H1A	1.0000	C1B—H1B	1.0000
S2A—C9A	1.774 (6)	S2B—C9B	1.761 (6)
S2A—C8A	1.863 (6)	S2B—C8B	1.853 (6)
N2A—C14A	1.400 (7)	N2B—C14B	1.398 (7)
N2A—C8A	1.469 (7)	N2B—C8B	1.483 (7)
C2A—C3A	1.380 (8)	C2B—C3B	1.376 (8)
C2A—C7A	1.393 (8)	C2B—C7B	1.397 (8)
C3A—C4A	1.377 (9)	C3B—C4B	1.372 (9)
C3A—H3A	0.9500	C3B—H3B	0.9500
C4A—C5A	1.377 (9)	C4B—C5B	1.376 (9)
C4A—H4A	0.9500	C4B—H4B	0.9500
C5A—C6A	1.405 (9)	C5B—C6B	1.394 (9)
C5A—H5A	0.9500	C5B—H5B	0.9500
C6A—C7A	1.379 (8)	C6B—C7B	1.390 (8)
C6A—H6A	0.9500	C6B—H6B	0.9500
C8A—C20A	1.498 (8)	C8B—C20B	1.490 (8)
C8A—H8A	1.0000	C8B—H8B	1.0000
C9A—C10A	1.368 (8)	C9B—C10B	1.397 (8)
C9A—C14A	1.398 (8)	C9B—C14B	1.398 (8)
C10A—C11A	1.385 (9)	C10B—C11B	1.380 (9)
C10A—H10A	0.9500	C10B—H10B	0.9500
C11A—C12A	1.380 (9)	C11B—C12B	1.375 (9)

C11A—H11A	0.9500	C11B—H11B	0.9500
C12A—C13A	1.395 (8)	C12B—C13B	1.404 (9)
C12A—H12A	0.9500	C12B—H12B	0.9500
C13A—C14A	1.397 (8)	C13B—C14B	1.388 (8)
C13A—H13A	0.9500	C13B—H13B	0.9500
C15A—C19A	1.427 (8)	C15B—C16B	1.426 (8)
C15A—C16A	1.429 (8)	C15B—C19B	1.430 (8)
C16A—C17A	1.425 (8)	C16B—C17B	1.413 (8)
C16A—H16A	0.9500	C16B—H16B	0.9500
C17A—C18A	1.420 (8)	C17B—C18B	1.435 (9)
C17A—H17A	0.9500	C17B—H17B	0.9500
C18A—C19A	1.424 (8)	C18B—C19B	1.415 (8)
C18A—H18A	0.9500	C18B—H18B	0.9500
C19A—H19A	0.9500	C19B—H19B	0.9500
C20A—C24A	1.405 (8)	C20B—C21B	1.418 (8)
C20A—C21A	1.428 (8)	C20B—C24B	1.420 (8)
C21A—C22A	1.427 (8)	C21B—C22B	1.429 (8)
C21A—H21A	0.9500	C21B—H21B	0.9500
C22A—C23A	1.416 (9)	C22B—C23B	1.432 (9)
C22A—H22A	0.9500	C22B—H22B	0.9500
C23A—C24A	1.425 (8)	C23B—C24B	1.428 (8)
C23A—H23A	0.9500	C23B—H23B	0.9500
C24A—H24A	0.9500	C24B—H24B	0.9500
C21A—Fe1A—C20A	41.0 (2)	C21B—Fe1B—C20B	40.6 (2)
C21A—Fe1A—C24A	68.2 (2)	C21B—Fe1B—C24B	68.2 (2)
C20A—Fe1A—C24A	40.2 (2)	C20B—Fe1B—C24B	40.7 (2)
C21A—Fe1A—C15A	160.3 (2)	C21B—Fe1B—C18B	122.5 (2)
C20A—Fe1A—C15A	124.2 (2)	C20B—Fe1B—C18B	160.1 (2)
C24A—Fe1A—C15A	108.6 (2)	C24B—Fe1B—C18B	156.5 (2)
C21A—Fe1A—C19A	157.1 (2)	C21B—Fe1B—C19B	159.0 (2)
C20A—Fe1A—C19A	160.6 (2)	C20B—Fe1B—C19B	158.7 (2)

C24A—Fe1A—C19A	124.5 (2)	C24B—Fe1B—C19B	122.6 (2)
C15A—Fe1A—C19A	40.7 (2)	C18B—Fe1B—C19B	40.5 (2)
C21A—Fe1A—C22A	40.8 (2)	C21B—Fe1B—C22B	40.9 (2)
C20A—Fe1A—C22A	68.4 (2)	C20B—Fe1B—C22B	68.8 (2)
C24A—Fe1A—C22A	67.9 (2)	C24B—Fe1B—C22B	68.6 (2)
C15A—Fe1A—C22A	157.8 (2)	C18B—Fe1B—C22B	105.0 (2)
C19A—Fe1A—C22A	121.7 (2)	C19B—Fe1B—C22B	122.3 (2)
C21A—Fe1A—C23A	68.4 (2)	C21B—Fe1B—C16B	122.1 (2)
C20A—Fe1A—C23A	68.3 (2)	C20B—Fe1B—C16B	109.4 (2)
C24A—Fe1A—C23A	40.7 (2)	C24B—Fe1B—C16B	126.6 (2)
C15A—Fe1A—C23A	122.7 (2)	C18B—Fe1B—C16B	68.2 (2)
C19A—Fe1A—C23A	107.7 (2)	C19B—Fe1B—C16B	68.2 (2)
C22A—Fe1A—C23A	40.3 (2)	C22B—Fe1B—C16B	156.1 (2)
C21A—Fe1A—C16A	123.5 (2)	C21B—Fe1B—C17B	106.6 (2)
C20A—Fe1A—C16A	108.4 (2)	C20B—Fe1B—C17B	124.3 (2)
C24A—Fe1A—C16A	123.5 (2)	C24B—Fe1B—C17B	161.9 (2)
C15A—Fe1A—C16A	40.7 (2)	C18B—Fe1B—C17B	41.0 (2)
C19A—Fe1A—C16A	68.1 (2)	C19B—Fe1B—C17B	68.5 (2)
C22A—Fe1A—C16A	159.6 (2)	C22B—Fe1B—C17B	119.7 (2)
C23A—Fe1A—C16A	159.1 (2)	C16B—Fe1B—C17B	40.3 (2)
C21A—Fe1A—C18A	121.3 (2)	C21B—Fe1B—C15B	158.4 (2)
C20A—Fe1A—C18A	157.7 (2)	C20B—Fe1B—C15B	123.5 (2)
C24A—Fe1A—C18A	160.3 (2)	C24B—Fe1B—C15B	109.6 (2)
C15A—Fe1A—C18A	68.4 (2)	C18B—Fe1B—C15B	68.5 (2)
C19A—Fe1A—C18A	40.5 (2)	C19B—Fe1B—C15B	40.8 (2)
C22A—Fe1A—C18A	107.0 (2)	C22B—Fe1B—C15B	160.1 (2)
C23A—Fe1A—C18A	123.2 (2)	C16B—Fe1B—C15B	40.7 (2)
C16A—Fe1A—C18A	67.8 (2)	C17B—Fe1B—C15B	68.5 (2)
C21A—Fe1A—C17A	106.9 (2)	C21B—Fe1B—C23B	68.4 (2)
C20A—Fe1A—C17A	122.6 (2)	C20B—Fe1B—C23B	68.6 (2)
C24A—Fe1A—C17A	158.6 (2)	C24B—Fe1B—C23B	40.7 (2)

C15A—Fe1A—C17A	68.5 (2)	C18B—Fe1B—C23B	119.8 (2)
C19A—Fe1A—C17A	68.1 (2)	C19B—Fe1B—C23B	107.0 (2)
C22A—Fe1A—C17A	123.0 (2)	C22B—Fe1B—C23B	40.8 (2)
C23A—Fe1A—C17A	159.0 (2)	C16B—Fe1B—C23B	162.5 (2)
C16A—Fe1A—C17A	40.4 (2)	C17B—Fe1B—C23B	155.4 (3)
C18A—Fe1A—C17A	40.3 (2)	C15B—Fe1B—C23B	124.9 (2)
C2A—S1A—C1A	89.9 (3)	C2B—S1B—C1B	90.1 (3)
C7A—N1A—C1A	109.9 (4)	C7B—N1B—C1B	110.0 (5)
N1A—C1A—C15A	114.1 (5)	N1B—C1B—C15B	114.3 (5)
N1A—C1A—S1A	103.1 (4)	N1B—C1B—S1B	104.3 (4)
C15A—C1A—S1A	111.5 (4)	C15B—C1B—S1B	109.7 (4)
N1A—C1A—H1A	109.3	N1B—C1B—H1B	109.5
C15A—C1A—H1A	109.3	C15B—C1B—H1B	109.5
S1A—C1A—H1A	109.3	S1B—C1B—H1B	109.5
C9A—S2A—C8A	89.3 (3)	C9B—S2B—C8B	90.5 (3)
C14A—N2A—C8A	109.9 (4)	C14B—N2B—C8B	111.2 (5)
C3A—C2A—C7A	120.8 (6)	C3B—C2B—C7B	119.5 (6)
C3A—C2A—S1A	128.3 (5)	C3B—C2B—S1B	129.3 (5)
C7A—C2A—S1A	111.0 (4)	C7B—C2B—S1B	111.0 (4)
C4A—C3A—C2A	118.8 (6)	C4B—C3B—C2B	120.9 (6)
C4A—C3A—H3A	120.6	C4B—C3B—H3B	119.6
C2A—C3A—H3A	120.6	C2B—C3B—H3B	119.6
C3A—C4A—C5A	121.1 (6)	C3B—C4B—C5B	119.3 (6)
C3A—C4A—H4A	119.5	C3B—C4B—H4B	120.4
C5A—C4A—H4A	119.5	C5B—C4B—H4B	120.4
C4A—C5A—C6A	120.5 (6)	C4B—C5B—C6B	121.5 (6)
C4A—C5A—H5A	119.7	C4B—C5B—H5B	119.2
C6A—C5A—H5A	119.7	C6B—C5B—H5B	119.2
C7A—C6A—C5A	118.2 (6)	C7B—C6B—C5B	118.3 (6)
C7A—C6A—H6A	120.9	C7B—C6B—H6B	120.9
C5A—C6A—H6A	120.9	C5B—C6B—H6B	120.9

C6A—C7A—C2A	120.6 (6)	C6B—C7B—C2B	120.1 (5)
C6A—C7A—N1A	125.6 (5)	C6B—C7B—N1B	125.7 (6)
C2A—C7A—N1A	113.7 (5)	C2B—C7B—N1B	114.1 (5)
N2A—C8A—C20A	113.6 (5)	N2B—C8B—C20B	114.7 (5)
N2A—C8A—S2A	102.6 (4)	N2B—C8B—S2B	103.4 (4)
C20A—C8A—S2A	111.7 (4)	C20B—C8B—S2B	109.7 (4)
N2A—C8A—H8A	109.6	N2B—C8B—H8B	109.6
C20A—C8A—H8A	109.6	C20B—C8B—H8B	109.6
S2A—C8A—H8A	109.6	S2B—C8B—H8B	109.6
C10A—C9A—C14A	121.4 (6)	C10B—C9B—C14B	120.8 (6)
C10A—C9A—S2A	128.4 (5)	C10B—C9B—S2B	127.7 (5)
C14A—C9A—S2A	110.3 (4)	C14B—C9B—S2B	111.4 (4)
C9A—C10A—C11A	118.7 (6)	C11B—C10B—C9B	118.6 (6)
C9A—C10A—H10A	120.7	C11B—C10B—H10B	120.7
C11A—C10A—H10A	120.7	C9B—C10B—H10B	120.7
C12A—C11A—C10A	120.8 (6)	C12B—C11B—C10B	120.9 (6)
C12A—C11A—H11A	119.6	C12B—C11B—H11B	119.5
C10A—C11A—H11A	119.6	C10B—C11B—H11B	119.5
C11A—C12A—C13A	121.3 (6)	C11B—C12B—C13B	121.0 (6)
C11A—C12A—H12A	119.3	C11B—C12B—H12B	119.5
C13A—C12A—H12A	119.3	C13B—C12B—H12B	119.5
C12A—C13A—C14A	117.7 (6)	C14B—C13B—C12B	118.5 (6)
C12A—C13A—H13A	121.2	C14B—C13B—H13B	120.8
C14A—C13A—H13A	121.2	C12B—C13B—H13B	120.8
C13A—C14A—C9A	120.2 (5)	C13B—C14B—C9B	120.0 (6)
C13A—C14A—N2A	125.7 (5)	C13B—C14B—N2B	126.2 (5)
C9A—C14A—N2A	114.1 (5)	C9B—C14B—N2B	113.6 (5)
C19A—C15A—C16A	107.3 (5)	C16B—C15B—C19B	107.2 (5)
C19A—C15A—C1A	125.5 (5)	C16B—C15B—C1B	128.8 (5)
C16A—C15A—C1A	127.2 (5)	C19B—C15B—C1B	123.8 (5)
C19A—C15A—Fe1A	69.7 (3)	C16B—C15B—Fe1B	69.5 (3)

C16A—C15A—Fe1A	69.9 (3)	C19B—C15B—Fe1B	69.4 (3)
C1A—C15A—Fe1A	128.4 (4)	C1B—C15B—Fe1B	129.9 (4)
C17A—C16A—C15A	108.5 (5)	C17B—C16B—C15B	108.9 (5)
C17A—C16A—Fe1A	70.2 (3)	C17B—C16B—Fe1B	69.9 (3)
C15A—C16A—Fe1A	69.3 (3)	C15B—C16B—Fe1B	69.9 (3)
C17A—C16A—H16A	125.8	C17B—C16B—H16B	125.5
C15A—C16A—H16A	125.8	C15B—C16B—H16B	125.5
Fe1A—C16A—H16A	126.3	Fe1B—C16B—H16B	126.3
C18A—C17A—C16A	107.7 (5)	C16B—C17B—C18B	107.5 (5)
C18A—C17A—Fe1A	69.5 (3)	C16B—C17B—Fe1B	69.8 (3)
C16A—C17A—Fe1A	69.4 (3)	C18B—C17B—Fe1B	69.2 (3)
C18A—C17A—H17A	126.2	C16B—C17B—H17B	126.3
C16A—C17A—H17A	126.2	C18B—C17B—H17B	126.3
Fe1A—C17A—H17A	126.5	Fe1B—C17B—H17B	126.3
C17A—C18A—C19A	108.3 (5)	C19B—C18B—C17B	108.1 (6)
C17A—C18A—Fe1A	70.2 (3)	C19B—C18B—Fe1B	70.0 (4)
C19A—C18A—Fe1A	69.4 (3)	C17B—C18B—Fe1B	69.7 (3)
C17A—C18A—H18A	125.9	C19B—C18B—H18B	125.9
C19A—C18A—H18A	125.9	C17B—C18B—H18B	125.9
Fe1A—C18A—H18A	126.1	Fe1B—C18B—H18B	125.9
C18A—C19A—C15A	108.3 (5)	C18B—C19B—C15B	108.3 (5)
C18A—C19A—Fe1A	70.1 (3)	C18B—C19B—Fe1B	69.6 (3)
C15A—C19A—Fe1A	69.6 (3)	C15B—C19B—Fe1B	69.9 (3)
C18A—C19A—H19A	125.9	C18B—C19B—H19B	125.9
C15A—C19A—H19A	125.9	C15B—C19B—H19B	125.9
Fe1A—C19A—H19A	126.1	Fe1B—C19B—H19B	126.3
C24A—C20A—C21A	107.9 (5)	C21B—C20B—C24B	107.7 (5)
C24A—C20A—C8A	128.1 (5)	C21B—C20B—C8B	123.6 (5)
C21A—C20A—C8A	124.0 (5)	C24B—C20B—C8B	128.5 (5)
C24A—C20A—Fe1A	70.0 (3)	C21B—C20B—Fe1B	69.6 (3)
C21A—C20A—Fe1A	69.3 (3)	C24B—C20B—Fe1B	69.7 (3)

C8A—C20A—Fe1A	127.2 (4)	C8B—C20B—Fe1B	130.4 (4)
C22A—C21A—C20A	107.6 (5)	C20B—C21B—C22B	108.6 (5)
C22A—C21A—Fe1A	70.3 (3)	C20B—C21B—Fe1B	69.7 (3)
C20A—C21A—Fe1A	69.8 (3)	C22B—C21B—Fe1B	69.9 (3)
C22A—C21A—H21A	126.2	C20B—C21B—H21B	125.7
C20A—C21A—H21A	126.2	C22B—C21B—H21B	125.7
Fe1A—C21A—H21A	125.3	Fe1B—C21B—H21B	126.3
C23A—C22A—C21A	108.2 (5)	C21B—C22B—C23B	107.6 (5)
C23A—C22A—Fe1A	69.9 (3)	C21B—C22B—Fe1B	69.2 (3)
C21A—C22A—Fe1A	68.9 (3)	C23B—C22B—Fe1B	70.2 (3)
C23A—C22A—H22A	125.9	C21B—C22B—H22B	126.2
C21A—C22A—H22A	125.9	C23B—C22B—H22B	126.2
Fe1A—C22A—H22A	126.9	Fe1B—C22B—H22B	125.9
C22A—C23A—C24A	107.5 (5)	C24B—C23B—C22B	107.4 (5)
C22A—C23A—Fe1A	69.9 (3)	C24B—C23B—Fe1B	68.9 (3)
C24A—C23A—Fe1A	69.2 (3)	C22B—C23B—Fe1B	69.0 (3)
C22A—C23A—H23A	126.2	C24B—C23B—H23B	126.3
C24A—C23A—H23A	126.2	C22B—C23B—H23B	126.3
Fe1A—C23A—H23A	126.2	Fe1B—C23B—H23B	127.3
C20A—C24A—C23A	108.8 (5)	C20B—C24B—C23B	108.7 (5)
C20A—C24A—Fe1A	69.8 (3)	C20B—C24B—Fe1B	69.6 (3)
C23A—C24A—Fe1A	70.1 (3)	C23B—C24B—Fe1B	70.5 (3)
C20A—C24A—H24A	125.6	C20B—C24B—H24B	125.6
C23A—C24A—H24A	125.6	C23B—C24B—H24B	125.6
Fe1A—C24A—H24A	126.0	Fe1B—C24B—H24B	125.9
C7A—N1A—C1A—C15A	157.5 (5)	C7B—N1B—C1B—C15B	153.5 (5)
C7A—N1A—C1A—S1A	36.3 (5)	C7B—N1B—C1B—S1B	33.8 (5)
C2A—S1A—C1A—N1A	-29.1 (4)	C2B—S1B—C1B—N1B	-26.8 (4)
C2A—S1A—C1A—C15A	-152.0 (4)	C2B—S1B—C1B—C15B	-149.6 (4)
C1A—S1A—C2A—C3A	-164.8 (6)	C1B—S1B—C2B—C3B	-171.3 (6)
C1A—S1A—C2A—C7A	16.0 (4)	C1B—S1B—C2B—C7B	14.1 (4)

C7A—C2A—C3A—C4A	-0.9 (9)	C7B—C2B—C3B—C4B	-8.2 (9)
S1A—C2A—C3A—C4A	-180.0 (5)	S1B—C2B—C3B—C4B	177.6 (5)
C2A—C3A—C4A—C5A	-0.1 (10)	C2B—C3B—C4B—C5B	5.9 (9)
C3A—C4A—C5A—C6A	1.3 (10)	C3B—C4B—C5B—C6B	-1.5 (10)
C4A—C5A—C6A—C7A	-1.5 (10)	C4B—C5B—C6B—C7B	-0.5 (9)
C5A—C6A—C7A—C2A	0.6 (9)	C5B—C6B—C7B—C2B	-1.8 (8)
C5A—C6A—C7A—N1A	176.9 (6)	C5B—C6B—C7B—N1B	175.4 (5)
C3A—C2A—C7A—C6A	0.6 (9)	C3B—C2B—C7B—C6B	6.1 (8)
S1A—C2A—C7A—C6A	179.8 (5)	S1B—C2B—C7B—C6B	-178.7 (4)
C3A—C2A—C7A—N1A	-176.1 (5)	C3B—C2B—C7B—N1B	-171.4 (5)
S1A—C2A—C7A—N1A	3.1 (6)	S1B—C2B—C7B—N1B	3.7 (6)
C1A—N1A—C7A—C6A	156.3 (6)	C1B—N1B—C7B—C6B	157.0 (5)
C1A—N1A—C7A—C2A	-27.1 (7)	C1B—N1B—C7B—C2B	-25.6 (7)
C14A—N2A—C8A—C20A	159.0 (5)	C14B—N2B—C8B—C20B	152.5 (5)
C14A—N2A—C8A—S2A	38.3 (5)	C14B—N2B—C8B—S2B	33.0 (5)
C9A—S2A—C8A—N2A	-30.9 (4)	C9B—S2B—C8B—N2B	-24.9 (4)
C9A—S2A—C8A—C20A	-153.0 (4)	C9B—S2B—C8B—C20B	-147.8 (4)
C8A—S2A—C9A—C10A	-162.4 (6)	C8B—S2B—C9B—C10B	-168.9 (5)
C8A—S2A—C9A—C14A	17.4 (5)	C8B—S2B—C9B—C14B	12.4 (4)
C14A—C9A—C10A—C11A	-1.8 (9)	C14B—C9B—C10B—C11B	-3.1 (8)
S2A—C9A—C10A—C11A	178.0 (5)	S2B—C9B—C10B—C11B	178.4 (5)
C9A—C10A—C11A—C12A	1.4 (10)	C9B—C10B—C11B—C12B	1.5 (9)
C10A—C11A—C12A— C13A	0.4 (10)	C10B—C11B—C12B— C13B	0.5 (9)
C11A—C12A—C13A— C14A	-1.9 (10)	C11B—C12B—C13B— C14B	-0.9 (9)
C12A—C13A—C14A—C9A	1.5 (9)	C12B—C13B—C14B—C9B	-0.7 (8)
C12A—C13A—C14A—N2A	179.4 (6)	C12B—C13B—C14B—N2B	174.9 (5)
C10A—C9A—C14A—C13A	0.4 (9)	C10B—C9B—C14B—C13B	2.7 (8)
S2A—C9A—C14A—C13A	-179.5 (5)	S2B—C9B—C14B—C13B	-178.5 (4)
C10A—C9A—C14A—N2A	-177.8 (5)	C10B—C9B—C14B—N2B	-173.4 (5)
S2A—C9A—C14A—N2A	2.4 (7)	S2B—C9B—C14B—N2B	5.4 (6)

C8A—N2A—C14A—C13A	153.8 (6)	C8B—N2B—C14B—C13B	157.8 (5)
C8A—N2A—C14A—C9A	-28.2 (7)	C8B—N2B—C14B—C9B	-26.3 (7)
N1A—C1A—C15A—C19A	148.3 (5)	N1B—C1B—C15B—C16B	-39.3 (8)
S1A—C1A—C15A—C19A	-95.3 (6)	S1B—C1B—C15B—C16B	77.4 (7)
N1A—C1A—C15A—C16A	-35.8 (8)	N1B—C1B—C15B—C19B	146.0 (5)
S1A—C1A—C15A—C16A	80.5 (6)	S1B—C1B—C15B—C19B	-97.3 (6)
N1A—C1A—C15A—Fe1A	57.1 (7)	N1B—C1B—C15B—Fe1B	55.6 (7)
S1A—C1A—C15A—Fe1A	173.5 (3)	S1B—C1B—C15B—Fe1B	172.3 (3)
C21A—Fe1A—C15A— C19A	161.0 (6)	C21B—Fe1B—C15B—C16B	43.7 (8)
C20A—Fe1A—C15A— C19A	-163.5 (3)	C20B—Fe1B—C15B—C16B	80.7 (4)
C24A—Fe1A—C15A— C19A	-121.7 (4)	C24B—Fe1B—C15B—C16B	123.8 (4)
C22A—Fe1A—C15A— C19A	-44.5 (8)	C18B—Fe1B—C15B—C16B	-81.2 (4)
C23A—Fe1A—C15A— C19A	-79.0 (4)	C19B—Fe1B—C15B—C16B	-118.6 (5)
C16A—Fe1A—C15A— C19A	118.2 (5)	C22B—Fe1B—C15B—C16B	-155.3 (6)
C18A—Fe1A—C15A— C19A	37.5 (3)	C17B—Fe1B—C15B—C16B	-37.0 (3)
C17A—Fe1A—C15A— C19A	81.0 (4)	C23B—Fe1B—C15B—C16B	166.6 (3)
C21A—Fe1A—C15A— C16A	42.8 (8)	C21B—Fe1B—C15B—C19B	162.3 (6)
C20A—Fe1A—C15A— C16A	78.3 (4)	C20B—Fe1B—C15B—C19B	-160.7 (3)
C24A—Fe1A—C15A— C16A	120.1 (3)	C24B—Fe1B—C15B—C19B	-117.6 (4)
C19A—Fe1A—C15A— C16A	-118.2 (5)	C18B—Fe1B—C15B—C19B	37.4 (3)
C22A—Fe1A—C15A— C16A	-162.7 (6)	C22B—Fe1B—C15B—C19B	-36.7 (8)
C23A—Fe1A—C15A— C16A	162.8 (3)	C16B—Fe1B—C15B—C19B	118.6 (5)
C18A—Fe1A—C15A— C16A	-80.7 (4)	C17B—Fe1B—C15B—C19B	81.6 (4)

C17A—Fe1A—C15A— C16A	-37.2 (3)	C23B—Fe1B—C15B—C19B	-74.7 (4)
C21A—Fe1A—C15A—C1A	-79.3 (9)	C21B—Fe1B—C15B—C1B	-80.3 (8)
C20A—Fe1A—C15A—C1A	-43.7 (6)	C20B—Fe1B—C15B—C1B	-43.3 (6)
C24A—Fe1A—C15A—C1A	-1.9 (5)	C24B—Fe1B—C15B—C1B	-0.2 (6)
C19A—Fe1A—C15A—C1A	119.7 (6)	C18B—Fe1B—C15B—C1B	154.7 (6)
C22A—Fe1A—C15A—C1A	75.2 (8)	C19B—Fe1B—C15B—C1B	117.4 (7)
C23A—Fe1A—C15A—C1A	40.8 (6)	C22B—Fe1B—C15B—C1B	80.7 (9)
C16A—Fe1A—C15A—C1A	-122.1 (6)	C16B—Fe1B—C15B—C1B	-124.0 (7)
C18A—Fe1A—C15A—C1A	157.3 (6)	C17B—Fe1B—C15B—C1B	-161.0 (6)
C17A—Fe1A—C15A—C1A	-159.3 (5)	C23B—Fe1B—C15B—C1B	42.6 (6)
C19A—C15A—C16A— C17A	-0.5 (6)	C19B—C15B—C16B— C17B	-0.2 (7)
C1A—C15A—C16A—C17A	-176.9 (5)	C1B—C15B—C16B—C17B	-175.6 (6)
Fe1A—C15A—C16A— C17A	59.5 (4)	Fe1B—C15B—C16B—C17B	59.1 (4)
C19A—C15A—C16A— Fe1A	-60.0 (4)	C19B—C15B—C16B—Fe1B	-59.3 (4)
C1A—C15A—C16A—Fe1A	123.6 (6)	C1B—C15B—C16B—Fe1B	125.3 (6)
C21A—Fe1A—C16A— C17A	76.2 (4)	C21B—Fe1B—C16B—C17B	77.4 (4)
C20A—Fe1A—C16A— C17A	118.9 (4)	C20B—Fe1B—C16B—C17B	120.6 (4)
C24A—Fe1A—C16A— C17A	160.8 (3)	C24B—Fe1B—C16B—C17B	162.8 (4)
C15A—Fe1A—C16A— C17A	-119.7 (5)	C18B—Fe1B—C16B—C17B	-38.3 (4)
C19A—Fe1A—C16A— C17A	-81.4 (4)	C19B—Fe1B—C16B—C17B	-82.0 (4)
C22A—Fe1A—C16A— C17A	41.5 (8)	C22B—Fe1B—C16B—C17B	39.3 (7)
C23A—Fe1A—C16A— C17A	-163.8 (6)	C15B—Fe1B—C16B—C17B	-120.1 (5)
C18A—Fe1A—C16A— C17A	-37.5 (3)	C23B—Fe1B—C16B—C17B	-159.3 (7)
C21A—Fe1A—C16A— C15A	-164.1 (3)	C21B—Fe1B—C16B—C15B	-162.5 (3)

C20A—Fe1A—C16A— C15A	-121.3 (3)	C20B—Fe1B—C16B—C15B	-119.3 (4)
C24A—Fe1A—C16A— C15A	-79.5 (4)	C24B—Fe1B—C16B—C15B	-77.1 (4)
C19A—Fe1A—C16A— C15A	38.3 (3)	C18B—Fe1B—C16B—C15B	81.8 (4)
C22A—Fe1A—C16A— C15A	161.2 (6)	C19B—Fe1B—C16B—C15B	38.1 (3)
C23A—Fe1A—C16A— C15A	-44.1 (8)	C22B—Fe1B—C16B—C15B	159.5 (5)
C18A—Fe1A—C16A— C15A	82.2 (4)	C17B—Fe1B—C16B—C15B	120.1 (5)
C17A—Fe1A—C16A— C15A	119.7 (5)	C23B—Fe1B—C16B—C15B	-39.2 (9)
C15A—C16A—C17A— C18A	0.3 (6)	C15B—C16B—C17B— C18B	0.1 (7)
Fe1A—C16A—C17A— C18A	59.2 (4)	Fe1B—C16B—C17B—C18B	59.2 (4)
C15A—C16A—C17A— Fe1A	-59.0 (4)	C15B—C16B—C17B—Fe1B	-59.1 (4)
C21A—Fe1A—C17A— C18A	118.7 (4)	C21B—Fe1B—C17B—C16B	-120.4 (4)
C20A—Fe1A—C17A— C18A	160.7 (3)	C20B—Fe1B—C17B—C16B	-79.4 (4)
C24A—Fe1A—C17A— C18A	-167.9 (6)	C24B—Fe1B—C17B—C16B	-49.9 (9)
C15A—Fe1A—C17A— C18A	-81.6 (4)	C18B—Fe1B—C17B—C16B	118.8 (5)
C19A—Fe1A—C17A— C18A	-37.6 (3)	C19B—Fe1B—C17B—C16B	81.3 (4)
C22A—Fe1A—C17A— C18A	76.9 (4)	C22B—Fe1B—C17B—C16B	-162.8 (3)
C23A—Fe1A—C17A— C18A	44.8 (8)	C15B—Fe1B—C17B—C16B	37.3 (3)
C16A—Fe1A—C17A— C18A	-119.1 (5)	C23B—Fe1B—C17B—C16B	165.3 (5)
C21A—Fe1A—C17A— C16A	-122.2 (3)	C21B—Fe1B—C17B—C18B	120.8 (4)
C20A—Fe1A—C17A— C16A	-80.1 (4)	C20B—Fe1B—C17B—C18B	161.8 (3)

C24A—Fe1A—C17A— C16A	-48.7 (8)	C24B—Fe1B—C17B—C18B	-168.7 (7)
C15A—Fe1A—C17A— C16A	37.5 (3)	C19B—Fe1B—C17B—C18B	-37.5 (3)
C19A—Fe1A—C17A— C16A	81.5 (4)	C22B—Fe1B—C17B—C18B	78.4 (4)
C22A—Fe1A—C17A— C16A	-164.0 (3)	C16B—Fe1B—C17B—C18B	-118.8 (5)
C23A—Fe1A—C17A— C16A	163.9 (6)	C15B—Fe1B—C17B—C18B	-81.5 (4)
C18A—Fe1A—C17A— C16A	119.1 (5)	C23B—Fe1B—C17B—C18B	46.5 (7)
C16A—C17A—C18A— C19A	0.1 (6)	C16B—C17B—C18B— C19B	0.1 (7)
Fe1A—C17A—C18A— C19A	59.2 (4)	Fe1B—C17B—C18B—C19B	59.7 (4)
C16A—C17A—C18A— Fe1A	-59.1 (4)	C16B—C17B—C18B—Fe1B	-59.6 (4)
C21A—Fe1A—C18A— C17A	-79.1 (4)	C21B—Fe1B—C18B—C19B	163.4 (3)
C20A—Fe1A—C18A— C17A	-47.0 (7)	C20B—Fe1B—C18B—C19B	-168.5 (6)
C24A—Fe1A—C18A— C17A	166.9 (6)	C24B—Fe1B—C18B—C19B	52.1 (7)
C15A—Fe1A—C18A— C17A	81.7 (4)	C22B—Fe1B—C18B—C19B	122.6 (4)
C19A—Fe1A—C18A— C17A	119.4 (5)	C16B—Fe1B—C18B—C19B	-81.5 (4)
C22A—Fe1A—C18A— C17A	-121.3 (4)	C17B—Fe1B—C18B—C19B	-119.2 (5)
C23A—Fe1A—C18A— C17A	-162.4 (3)	C15B—Fe1B—C18B—C19B	-37.6 (3)
C16A—Fe1A—C18A— C17A	37.7 (3)	C23B—Fe1B—C18B—C19B	81.2 (4)
C21A—Fe1A—C18A— C19A	161.5 (3)	C21B—Fe1B—C18B—C17B	-77.5 (4)
C20A—Fe1A—C18A— C19A	-166.4 (5)	C20B—Fe1B—C18B—C17B	-49.3 (8)
C24A—Fe1A—C18A— C19A	47.4 (8)	C24B—Fe1B—C18B—C17B	171.2 (5)

C15A—Fe1A—C18A— C19A	-37.7 (3)	C19B—Fe1B—C18B—C17B	119.2 (5)
C22A—Fe1A—C18A— C19A	119.2 (4)	C22B—Fe1B—C18B—C17B	-118.2 (4)
C23A—Fe1A—C18A— C19A	78.1 (4)	C16B—Fe1B—C18B—C17B	37.6 (3)
C16A—Fe1A—C18A— C19A	-81.8 (4)	C15B—Fe1B—C18B—C17B	81.5 (4)
C17A—Fe1A—C18A— C19A	-119.4 (5)	C23B—Fe1B—C18B—C17B	-159.6 (4)
C17A—C18A—C19A— C15A	-0.3 (7)	C17B—C18B—C19B— C15B	-0.2 (7)
Fe1A—C18A—C19A— C15A	59.3 (4)	Fe1B—C18B—C19B—C15B	59.3 (4)
C17A—C18A—C19A— Fe1A	-59.7 (4)	C17B—C18B—C19B—Fe1B	-59.5 (4)
C16A—C15A—C19A— C18A	0.5 (6)	C16B—C15B—C19B— C18B	0.2 (7)
C1A—C15A—C19A—C18A	177.0 (5)	C1B—C15B—C19B—C18B	175.9 (5)
Fe1A—C15A—C19A— C18A	-59.6 (4)	Fe1B—C15B—C19B—C18B	-59.2 (4)
C16A—C15A—C19A— Fe1A	60.1 (4)	C16B—C15B—C19B—Fe1B	59.4 (4)
C1A—C15A—C19A—Fe1A	-123.4 (6)	C1B—C15B—C19B—Fe1B	-124.9 (6)
C21A—Fe1A—C19A— C18A	-44.3 (8)	C21B—Fe1B—C19B—C18B	-42.3 (8)
C20A—Fe1A—C19A— C18A	164.5 (6)	C20B—Fe1B—C19B—C18B	169.2 (6)
C24A—Fe1A—C19A— C18A	-162.4 (3)	C24B—Fe1B—C19B—C18B	-158.1 (4)
C15A—Fe1A—C19A— C18A	119.4 (5)	C22B—Fe1B—C19B—C18B	-74.3 (4)
C22A—Fe1A—C19A— C18A	-78.8 (4)	C16B—Fe1B—C19B—C18B	81.5 (4)
C23A—Fe1A—C19A— C18A	-120.7 (4)	C17B—Fe1B—C19B—C18B	38.0 (4)
C16A—Fe1A—C19A— C18A	81.1 (4)	C15B—Fe1B—C19B—C18B	119.6 (5)
C17A—Fe1A—C19A—	37.4 (3)	C23B—Fe1B—C19B—C18B	-116.3 (4)

C18A

C21A—Fe1A—C19A— C15A	-163.6 (6)	C21B—Fe1B—C19B—C15B	-161.8 (6)
C20A—Fe1A—C19A— C15A	45.1 (8)	C20B—Fe1B—C19B—C15B	49.6 (8)
C24A—Fe1A—C19A— C15A	78.2 (4)	C24B—Fe1B—C19B—C15B	82.4 (4)
C22A—Fe1A—C19A— C15A	161.8 (3)	C18B—Fe1B—C19B—C15B	-119.6 (5)
C23A—Fe1A—C19A— C15A	119.9 (4)	C22B—Fe1B—C19B—C15B	166.1 (3)
C16A—Fe1A—C19A— C15A	-38.3 (3)	C16B—Fe1B—C19B—C15B	-38.0 (3)
C18A—Fe1A—C19A— C15A	-119.4 (5)	C17B—Fe1B—C19B—C15B	-81.5 (4)
C17A—Fe1A—C19A— C15A	-82.0 (4)	C23B—Fe1B—C19B—C15B	124.2 (3)
N2A—C8A—C20A—C24A	-34.3 (8)	N2B—C8B—C20B—C21B	146.8 (6)
S2A—C8A—C20A—C24A	81.2 (7)	S2B—C8B—C20B—C21B	-97.3 (6)
N2A—C8A—C20A—C21A	147.2 (5)	N2B—C8B—C20B—C24B	-39.5 (8)
S2A—C8A—C20A—C21A	-97.3 (6)	S2B—C8B—C20B—C24B	76.4 (7)
N2A—C8A—C20A—Fe1A	58.5 (7)	N2B—C8B—C20B—Fe1B	55.9 (7)
S2A—C8A—C20A—Fe1A	174.0 (3)	S2B—C8B—C20B—Fe1B	171.8 (3)
C21A—Fe1A—C20A— C24A	-119.2 (5)	C24B—Fe1B—C20B—C21B	118.9 (5)
C15A—Fe1A—C20A— C24A	78.2 (4)	C18B—Fe1B—C20B—C21B	-37.7 (8)
C19A—Fe1A—C20A— C24A	44.2 (8)	C19B—Fe1B—C20B—C21B	163.3 (6)
C22A—Fe1A—C20A— C24A	-81.0 (4)	C22B—Fe1B—C20B—C21B	37.5 (4)
C23A—Fe1A—C20A— C24A	-37.5 (3)	C16B—Fe1B—C20B—C21B	-117.1 (4)
C16A—Fe1A—C20A— C24A	120.5 (4)	C17B—Fe1B—C20B—C21B	-74.7 (4)
C18A—Fe1A—C20A— C24A	-163.0 (5)	C15B—Fe1B—C20B—C21B	-160.1 (3)
C17A—Fe1A—C20A—	162.8 (3)	C23B—Fe1B—C20B—C21B	81.4 (4)

C24A

C24A—Fe1A—C20A— C21A	119.2 (5)	C21B—Fe1B—C20B—C24B	-118.9 (5)
C15A—Fe1A—C20A— C21A	-162.6 (3)	C18B—Fe1B—C20B—C24B	-156.5 (6)
C19A—Fe1A—C20A— C21A	163.4 (6)	C19B—Fe1B—C20B—C24B	44.4 (8)
C22A—Fe1A—C20A— C21A	38.2 (4)	C22B—Fe1B—C20B—C24B	-81.4 (4)
C23A—Fe1A—C20A— C21A	81.7 (4)	C16B—Fe1B—C20B—C24B	124.0 (3)
C16A—Fe1A—C20A— C21A	-120.3 (4)	C17B—Fe1B—C20B—C24B	166.4 (3)
C18A—Fe1A—C20A— C21A	-43.9 (7)	C15B—Fe1B—C20B—C24B	81.1 (4)
C17A—Fe1A—C20A— C21A	-78.0 (4)	C23B—Fe1B—C20B—C24B	-37.5 (3)
C21A—Fe1A—C20A—C8A	117.6 (6)	C21B—Fe1B—C20B—C8B	117.3 (7)
C24A—Fe1A—C20A—C8A	-123.2 (7)	C24B—Fe1B—C20B—C8B	-123.8 (7)
C15A—Fe1A—C20A—C8A	-45.0 (6)	C18B—Fe1B—C20B—C8B	79.6 (9)
C19A—Fe1A—C20A—C8A	-79.0 (9)	C19B—Fe1B—C20B—C8B	-79.4 (8)
C22A—Fe1A—C20A—C8A	155.8 (6)	C22B—Fe1B—C20B—C8B	154.8 (6)
C23A—Fe1A—C20A—C8A	-160.7 (6)	C16B—Fe1B—C20B—C8B	0.2 (6)
C16A—Fe1A—C20A—C8A	-2.7 (6)	C17B—Fe1B—C20B—C8B	42.6 (6)
C18A—Fe1A—C20A—C8A	73.8 (8)	C15B—Fe1B—C20B—C8B	-42.8 (6)
C17A—Fe1A—C20A—C8A	39.6 (6)	C23B—Fe1B—C20B—C8B	-161.3 (6)
C24A—C20A—C21A— C22A	-0.9 (6)	C24B—C20B—C21B— C22B	0.3 (7)
C8A—C20A—C21A—C22A	178.0 (5)	C8B—C20B—C21B—C22B	175.1 (5)
Fe1A—C20A—C21A— C22A	-60.4 (4)	Fe1B—C20B—C21B—C22B	-59.2 (4)
C24A—C20A—C21A— Fe1A	59.5 (4)	C24B—C20B—C21B—Fe1B	59.5 (4)
C8A—C20A—C21A—Fe1A	-121.6 (5)	C8B—C20B—C21B—Fe1B	-125.6 (6)
C20A—Fe1A—C21A— C22A	118.3 (5)	C24B—Fe1B—C21B—C20B	-37.9 (3)

C24A—Fe1A—C21A— C22A	81.0 (4)	C18B—Fe1B—C21B—C20B	165.7 (3)
C15A—Fe1A—C21A— C22A	165.6 (6)	C19B—Fe1B—C21B—C20B	-163.1 (6)
C19A—Fe1A—C21A— C22A	-47.6 (8)	C22B—Fe1B—C21B—C20B	-119.8 (5)
C23A—Fe1A—C21A— C22A	37.1 (4)	C16B—Fe1B—C21B—C20B	82.5 (4)
C16A—Fe1A—C21A— C22A	-162.3 (3)	C17B—Fe1B—C21B—C20B	123.7 (4)
C18A—Fe1A—C21A— C22A	-79.6 (4)	C15B—Fe1B—C21B—C20B	50.4 (8)
C17A—Fe1A—C21A— C22A	-121.2 (4)	C23B—Fe1B—C21B—C20B	-81.8 (4)
C24A—Fe1A—C21A— C20A	-37.3 (3)	C20B—Fe1B—C21B—C22B	119.8 (5)
C15A—Fe1A—C21A— C20A	47.2 (8)	C24B—Fe1B—C21B—C22B	81.9 (4)
C19A—Fe1A—C21A— C20A	-165.9 (5)	C18B—Fe1B—C21B—C22B	-74.5 (4)
C22A—Fe1A—C21A— C20A	-118.3 (5)	C19B—Fe1B—C21B—C22B	-43.3 (8)
C23A—Fe1A—C21A— C20A	-81.3 (4)	C16B—Fe1B—C21B—C22B	-157.6 (3)
C16A—Fe1A—C21A— C20A	79.4 (4)	C17B—Fe1B—C21B—C22B	-116.4 (4)
C18A—Fe1A—C21A— C20A	162.1 (3)	C15B—Fe1B—C21B—C22B	170.3 (6)
C17A—Fe1A—C21A— C20A	120.5 (3)	C23B—Fe1B—C21B—C22B	38.0 (4)
C20A—C21A—C22A— C23A	1.0 (7)	C20B—C21B—C22B— C23B	-0.8 (7)
Fe1A—C21A—C22A— C23A	-59.0 (4)	Fe1B—C21B—C22B—C23B	-60.0 (4)
C20A—C21A—C22A— Fe1A	60.0 (4)	C20B—C21B—C22B—Fe1B	59.2 (4)
C21A—Fe1A—C22A— C23A	119.8 (5)	C20B—Fe1B—C22B—C21B	-37.3 (3)
C20A—Fe1A—C22A— C23A	81.5 (4)	C24B—Fe1B—C22B—C21B	-81.1 (4)

C24A—Fe1A—C22A— C23A	38.0 (4)	C18B—Fe1B—C22B—C21B	122.8 (4)
C15A—Fe1A—C22A— C23A	-47.4 (8)	C19B—Fe1B—C22B—C21B	163.1 (3)
C19A—Fe1A—C22A— C23A	-79.9 (4)	C16B—Fe1B—C22B—C21B	52.9 (7)
C16A—Fe1A—C22A— C23A	166.4 (6)	C17B—Fe1B—C22B—C21B	81.0 (4)
C18A—Fe1A—C22A— C23A	-121.7 (4)	C15B—Fe1B—C22B—C21B	-169.4 (6)
C17A—Fe1A—C22A— C23A	-162.9 (3)	C23B—Fe1B—C22B—C21B	-118.7 (5)
C20A—Fe1A—C22A— C21A	-38.4 (3)	C21B—Fe1B—C22B—C23B	118.7 (5)
C24A—Fe1A—C22A— C21A	-81.8 (4)	C20B—Fe1B—C22B—C23B	81.4 (4)
C15A—Fe1A—C22A— C21A	-167.2 (6)	C24B—Fe1B—C22B—C23B	37.6 (3)
C19A—Fe1A—C22A— C21A	160.3 (3)	C18B—Fe1B—C22B—C23B	-118.5 (4)
C23A—Fe1A—C22A— C21A	-119.8 (5)	C19B—Fe1B—C22B—C23B	-78.2 (4)
C16A—Fe1A—C22A— C21A	46.5 (8)	C16B—Fe1B—C22B—C23B	171.6 (5)
C18A—Fe1A—C22A— C21A	118.5 (4)	C17B—Fe1B—C22B—C23B	-160.3 (4)
C17A—Fe1A—C22A— C21A	77.3 (4)	C15B—Fe1B—C22B—C23B	-50.7 (8)
C21A—C22A—C23A— C24A	-0.8 (7)	C21B—C22B—C23B— C24B	1.0 (7)
Fe1A—C22A—C23A— C24A	-59.2 (4)	Fe1B—C22B—C23B—C24B	-58.4 (4)
C21A—C22A—C23A— Fe1A	58.4 (4)	C21B—C22B—C23B—Fe1B	59.4 (4)
C21A—Fe1A—C23A— C22A	-37.6 (3)	C21B—Fe1B—C23B—C24B	81.3 (4)
C20A—Fe1A—C23A— C22A	-81.8 (4)	C20B—Fe1B—C23B—C24B	37.4 (3)
C24A—Fe1A—C23A— C22A	-118.8 (5)	C18B—Fe1B—C23B—C24B	-162.6 (3)

C15A—Fe1A—C23A— C22A	160.7 (3)	C19B—Fe1B—C23B—C24B	-120.5 (4)
C19A—Fe1A—C23A— C22A	118.4 (4)	C22B—Fe1B—C23B—C24B	119.4 (5)
C16A—Fe1A—C23A— C22A	-166.7 (6)	C16B—Fe1B—C23B—C24B	-49.2 (9)
C18A—Fe1A—C23A— C22A	76.5 (4)	C17B—Fe1B—C23B—C24B	164.1 (5)
C17A—Fe1A—C23A— C22A	43.6 (8)	C15B—Fe1B—C23B—C24B	-79.3 (4)
C21A—Fe1A—C23A— C24A	81.3 (4)	C21B—Fe1B—C23B—C22B	-38.1 (4)
C20A—Fe1A—C23A— C24A	37.0 (3)	C20B—Fe1B—C23B—C22B	-82.0 (4)
C15A—Fe1A—C23A— C24A	-80.5 (4)	C24B—Fe1B—C23B—C22B	-119.4 (5)
C19A—Fe1A—C23A— C24A	-122.7 (4)	C18B—Fe1B—C23B—C22B	78.0 (4)
C22A—Fe1A—C23A— C24A	118.8 (5)	C19B—Fe1B—C23B—C22B	120.1 (4)
C16A—Fe1A—C23A— C24A	-47.8 (8)	C16B—Fe1B—C23B—C22B	-168.6 (7)
C18A—Fe1A—C23A— C24A	-164.6 (3)	C17B—Fe1B—C23B—C22B	44.7 (7)
C17A—Fe1A—C23A— C24A	162.4 (6)	C15B—Fe1B—C23B—C22B	161.3 (3)
C21A—C20A—C24A— C23A	0.4 (6)	C21B—C20B—C24B— C23B	0.3 (7)
C8A—C20A—C24A—C23A	-178.4 (5)	C8B—C20B—C24B—C23B	-174.1 (6)
Fe1A—C20A—C24A— C23A	59.5 (4)	Fe1B—C20B—C24B—C23B	59.8 (4)
C21A—C20A—C24A— Fe1A	-59.1 (4)	C21B—C20B—C24B—Fe1B	-59.5 (4)
C8A—C20A—C24A—Fe1A	122.1 (6)	C8B—C20B—C24B—Fe1B	126.0 (6)
C22A—C23A—C24A— C20A	0.3 (7)	C22B—C23B—C24B— C20B	-0.8 (7)
Fe1A—C23A—C24A— C20A	-59.3 (4)	Fe1B—C23B—C24B—C20B	-59.3 (4)
C22A—C23A—C24A—	59.6 (4)	C22B—C23B—C24B—Fe1B	58.5 (4)

Fe1A

C21A—Fe1A—C24A— C20A	38.0 (3)	C21B—Fe1B—C24B—C20B	37.9 (3)
C15A—Fe1A—C24A— C20A	-121.3 (3)	C18B—Fe1B—C24B—C20B	160.1 (5)
C19A—Fe1A—C24A— C20A	-163.6 (3)	C19B—Fe1B—C24B—C20B	-162.5 (3)
C22A—Fe1A—C24A— C20A	82.2 (4)	C22B—Fe1B—C24B—C20B	82.0 (4)
C23A—Fe1A—C24A— C20A	119.9 (5)	C16B—Fe1B—C24B—C20B	-76.7 (4)
C16A—Fe1A—C24A— C20A	-78.6 (4)	C17B—Fe1B—C24B—C20B	-38.7 (9)
C18A—Fe1A—C24A— C20A	160.8 (6)	C15B—Fe1B—C24B—C20B	-119.1 (4)
C17A—Fe1A—C24A— C20A	-42.9 (8)	C23B—Fe1B—C24B—C20B	119.7 (5)
C21A—Fe1A—C24A— C23A	-81.8 (4)	C21B—Fe1B—C24B—C23B	-81.8 (4)
C20A—Fe1A—C24A— C23A	-119.9 (5)	C20B—Fe1B—C24B—C23B	-119.7 (5)
C15A—Fe1A—C24A— C23A	118.9 (4)	C18B—Fe1B—C24B—C23B	40.4 (7)
C19A—Fe1A—C24A— C23A	76.5 (4)	C19B—Fe1B—C24B—C23B	77.8 (4)
C22A—Fe1A—C24A— C23A	-37.7 (4)	C22B—Fe1B—C24B—C23B	-37.7 (4)
C16A—Fe1A—C24A— C23A	161.5 (3)	C16B—Fe1B—C24B—C23B	163.6 (3)
C18A—Fe1A—C24A— C23A	41.0 (8)	C17B—Fe1B—C24B—C23B	-158.4 (7)
C17A—Fe1A—C24A— C23A	-162.7 (6)	C15B—Fe1B—C24B—C23B	121.2 (4)

All esds (except the esd in the dihedral angle between two l.s. planes) are estimated using the full covariance matrix. The cell esds are taken into account individually in the estimation of esds in distances, angles and torsion angles; correlations between esds in cell parameters are only used when they are defined by crystal symmetry. An approximate (isotropic) treatment of cell esds is used for estimating esds involving l.s. planes.

Data collection: *SMART* (Bruker, 1998); cell refinement: *SAINTE* (Bruker, 1998); data reduction: *SAINTE* (Bruker, 1998); program(s) used to solve structure: *SHELXS97* (Sheldrick, 1997); program(s) used to refine structure: *SHELXL97* (Sheldrick, 1997); molecular graphics: *ORTEPIII* (Burnett & Johnson, 1996); software used to prepare material for publication: *CIFTAB* (Sheldrick, 1997).

Color code for FcSH2 crystal structure:

Orange: Fe atom

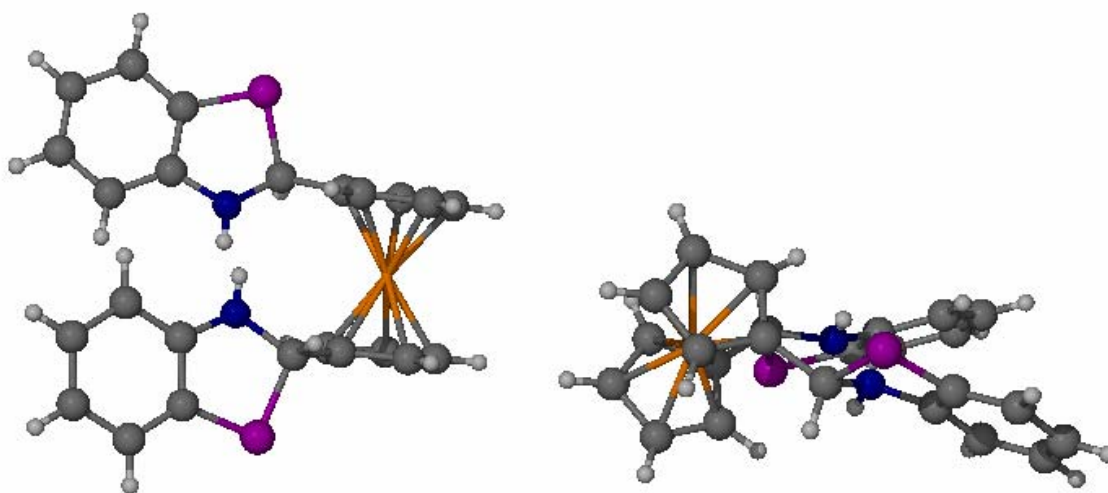
Dark grey: C atom

Light grey: H atom

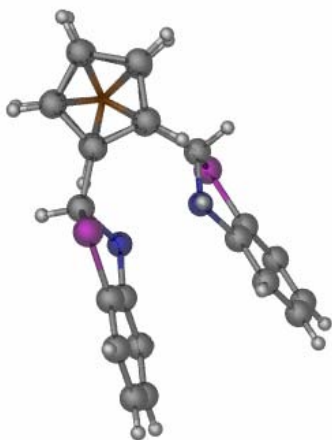
Dark Blue: N atom

Purple: S atom

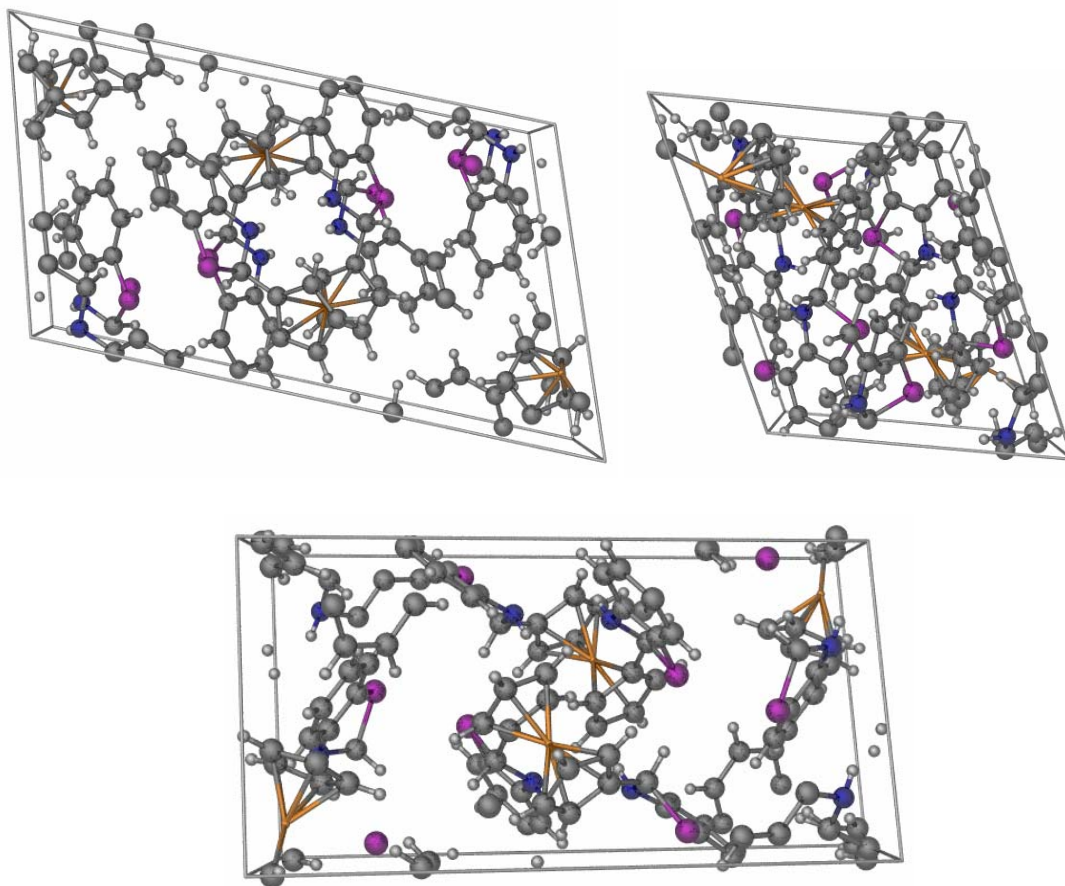
Asymmetric unit structure:



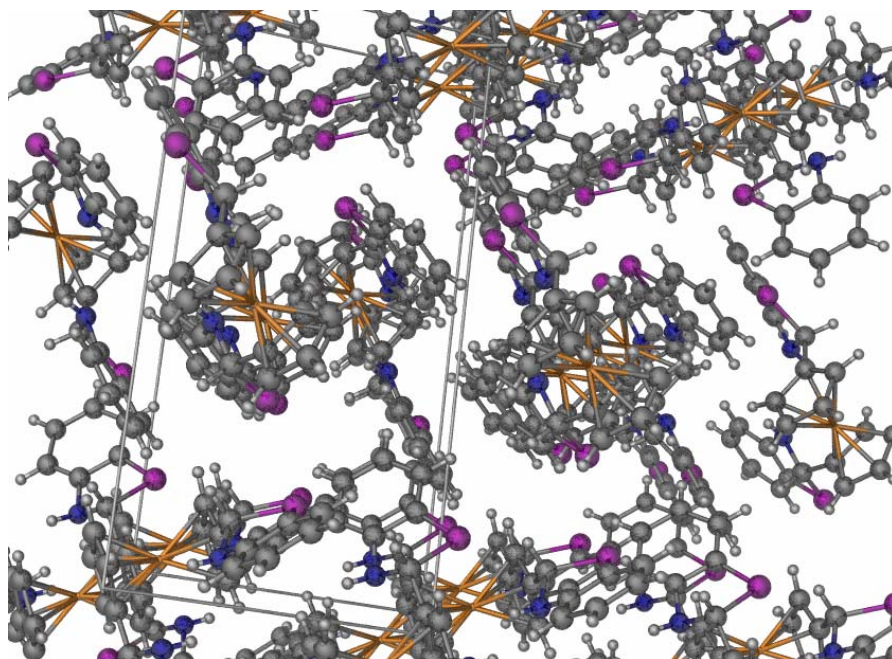
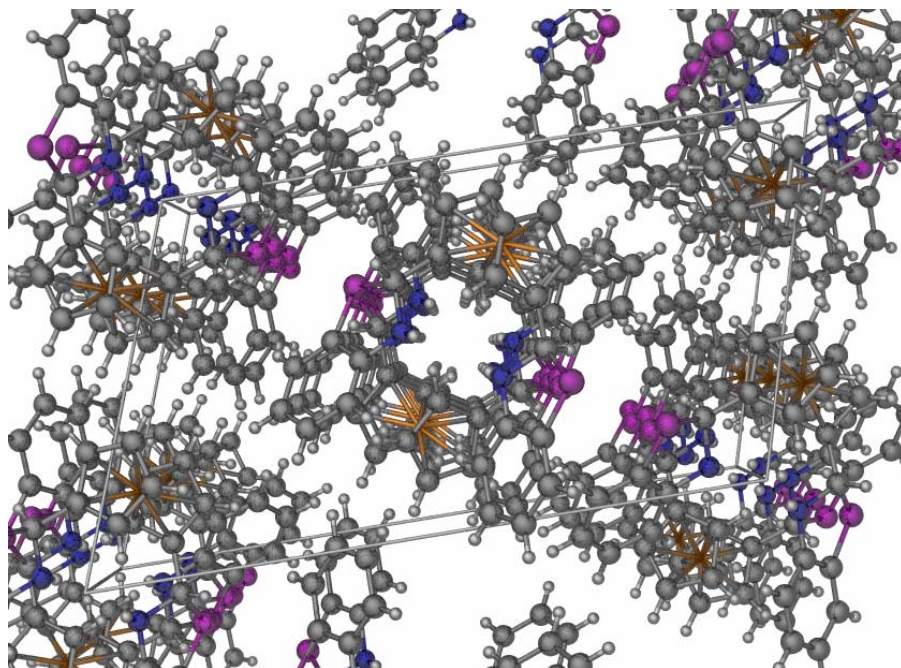
Cp ring overlap:

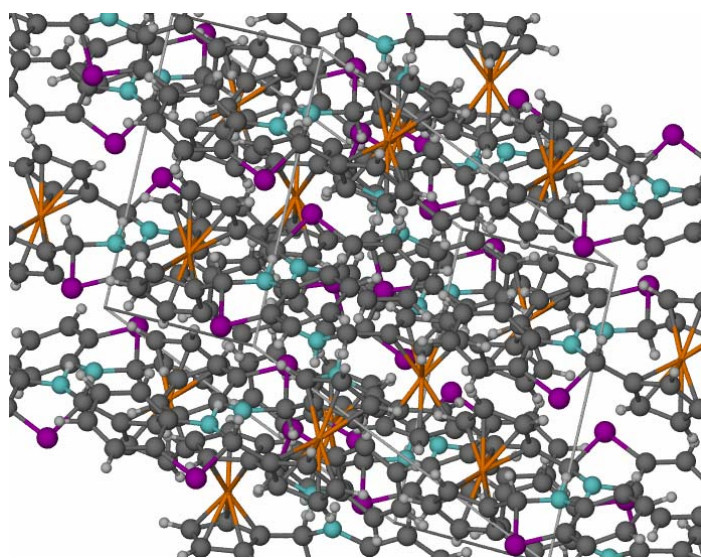
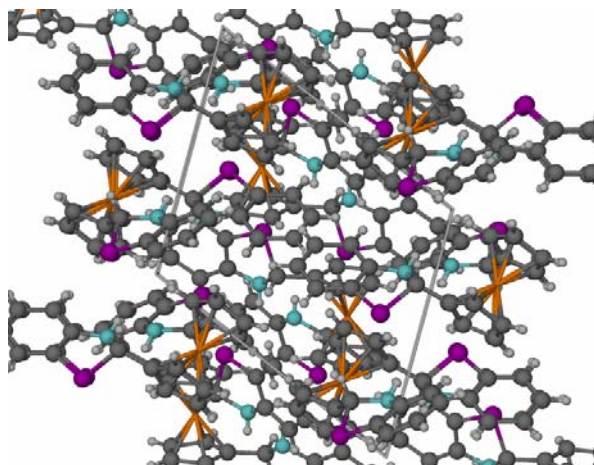
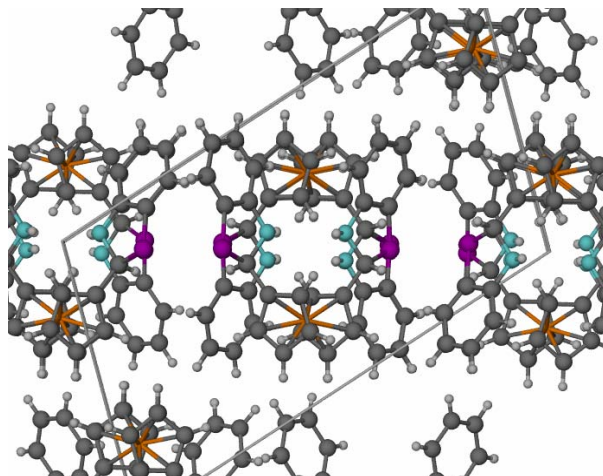


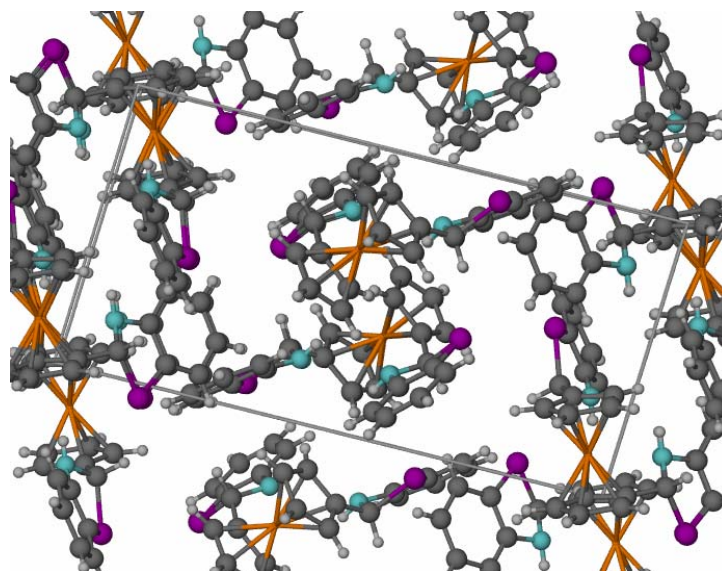
Unit cell:



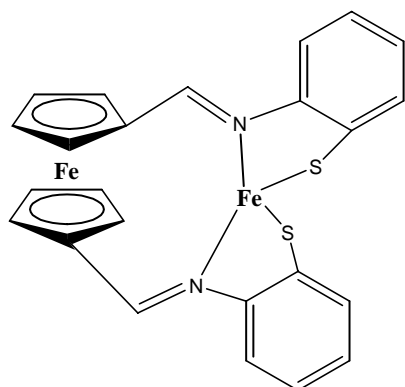
Mass crystal packing:







Compound 22:



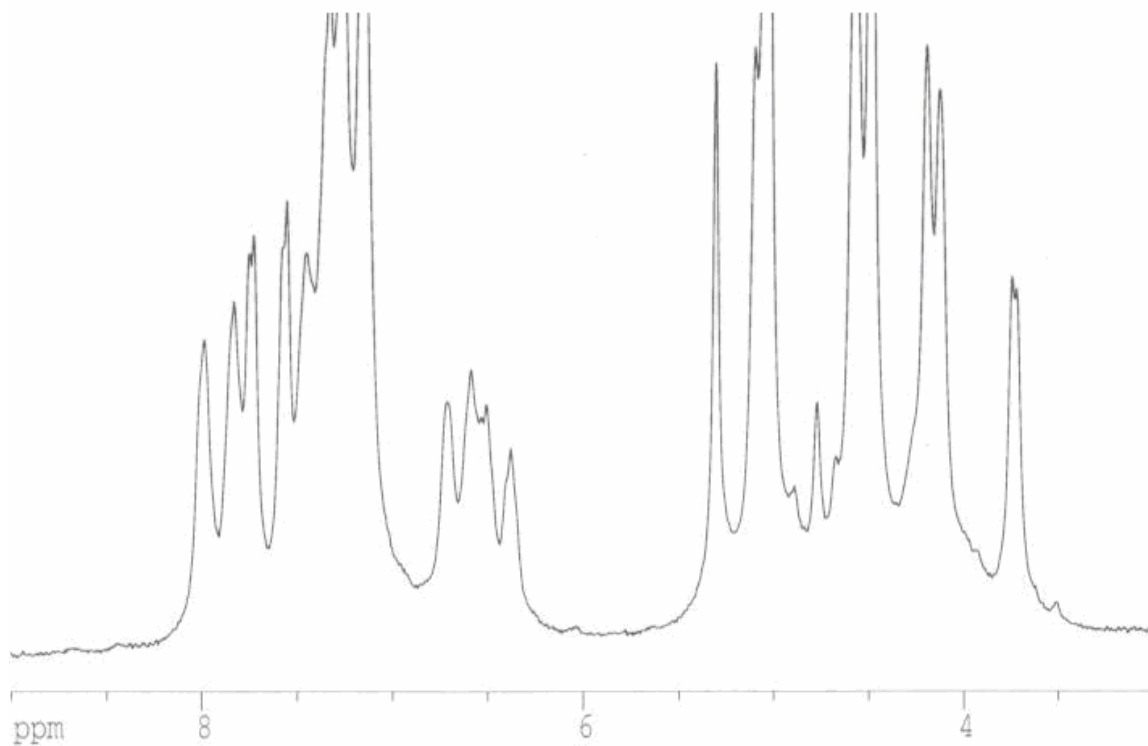


Figure A.71: ^1H NMR spectrum of FcS₂-Fe in CDCl₃: 8.0-7.5 ppm, q, 7.4-7.15 ppm, t, 6.7-6.4 ppm, q, 5.30 ppm, s, 5.09 ppm, d, 4.6-4.5 ppm, d, 4.2-4.10 ppm, d;

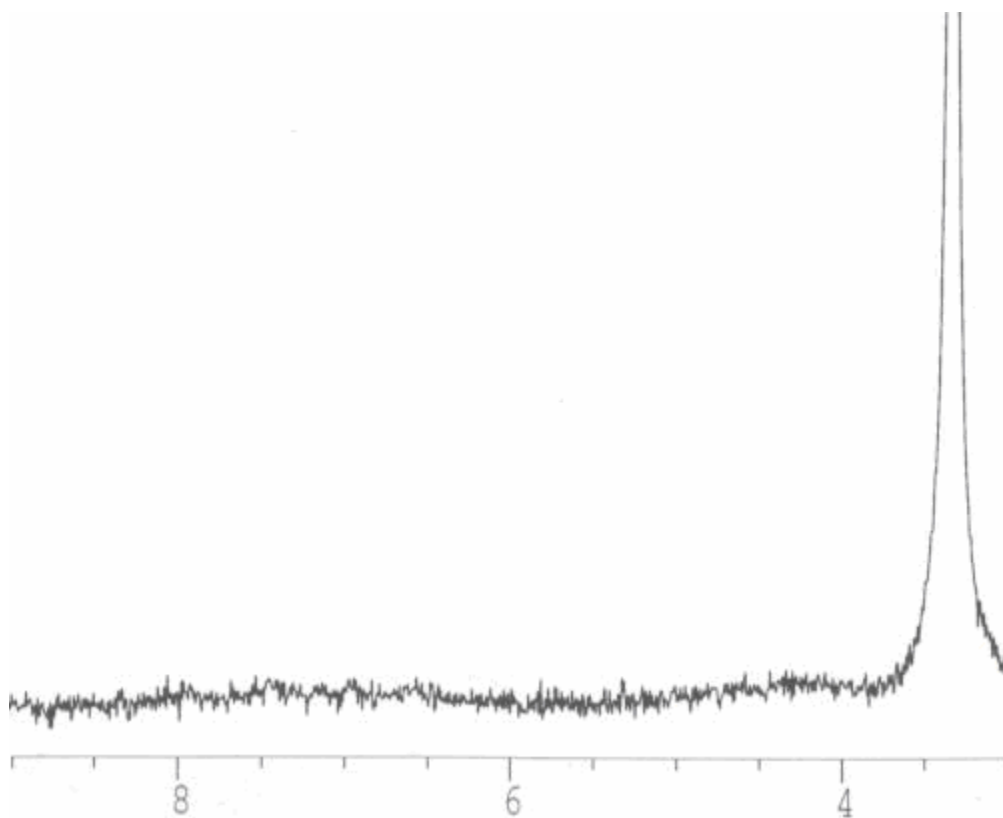


Figure A.72: ^1H NMR spectrum of $\text{FcS}_2\text{-Fe}$ in $d_6\text{-DMSO}$: Broad 8.0 ppm (2H, Cp- $\underline{\text{C}}\text{H}=\text{N}$), Broad 7.3 ppm (2H, phenyl), Broad 7.1 ppm (4H, phenyl), Broad 6.7 ppm (2H, phenyl), Very broad 5-4 ppm (8H, Cp);

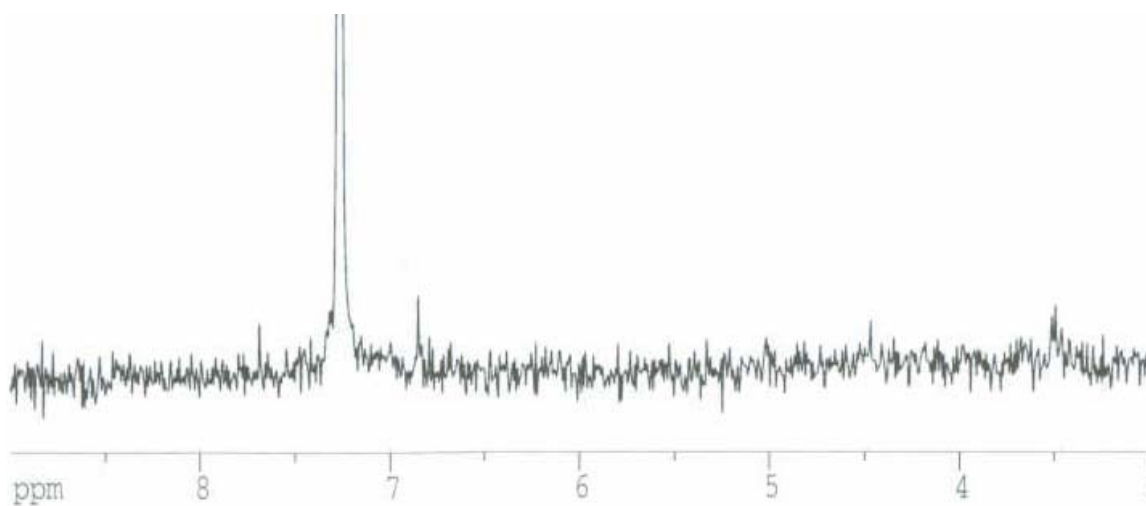


Figure A.73: ^1H NMR spectrum of precipitate from reaction of 22 with $\text{Hg}(\text{CH}_3\text{COO})_2$ in CDCl_3 :

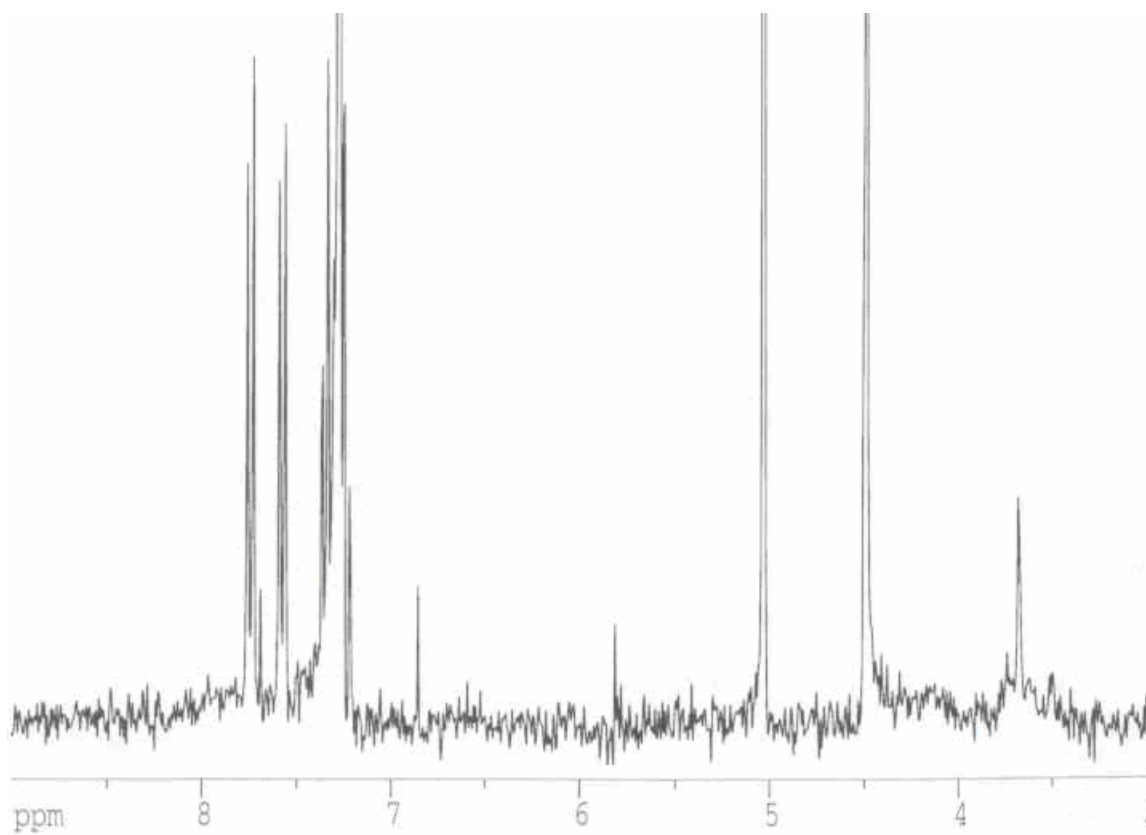


Figure A.74: ^1H NMR spectrum of dried liquid portion from reaction of 22 with $\text{Hg}(\text{CH}_3\text{COO})_2$ in CDCl_3 :

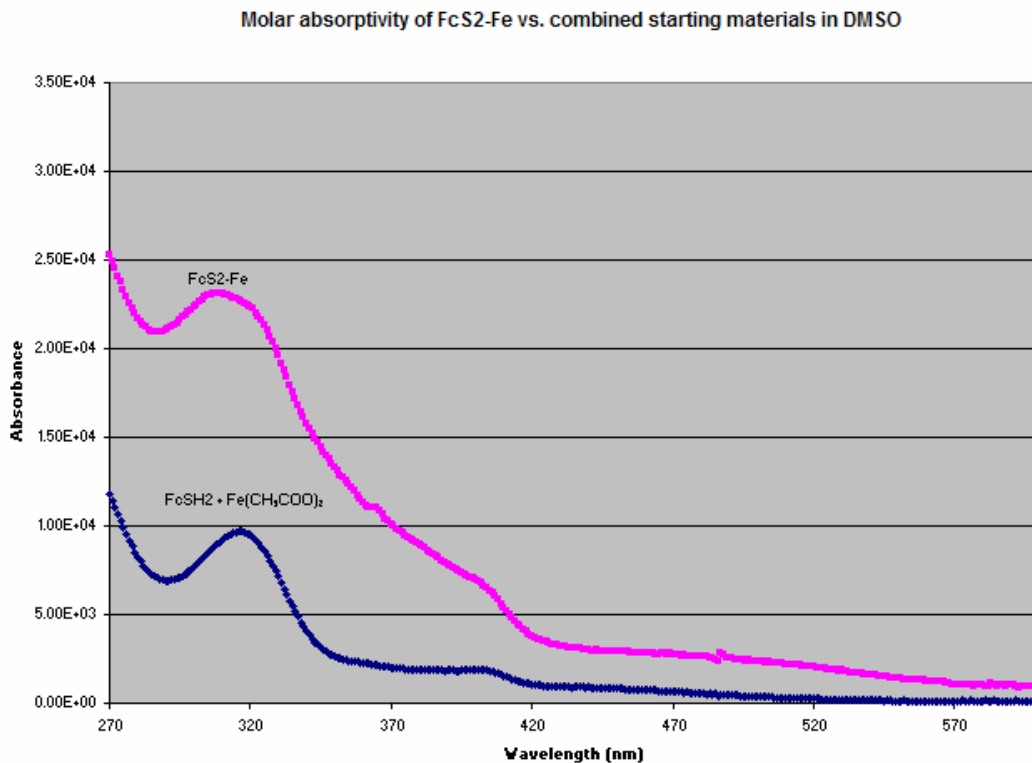


Figure A.75: Comparison between the molar absorptivity (UV-Vis) of FcS2-Fe and the molar absorptivity of the starting materials in DMSO: 308 nm ($12200 \text{ M}^{-1}\text{cm}^{-1}$);

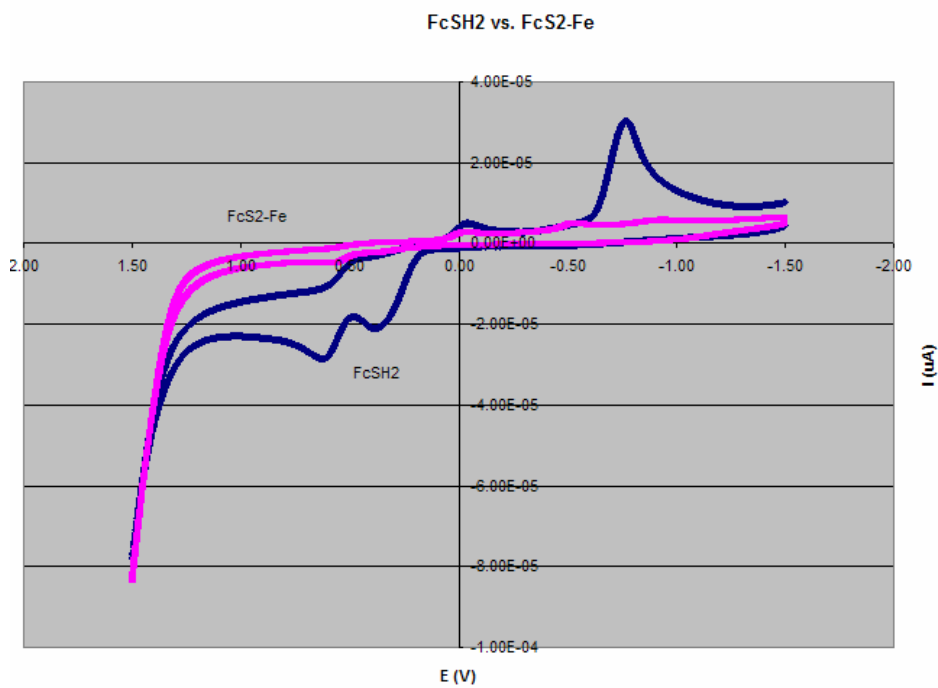


Figure A.76: Comparison between the CV scan of FcS2-Fe and the CV scan of FcSH2 in DMSO, scan rate 100 mV/sec. Fe^{II} to Fe^{III} oxidation peak is at 585 mV.

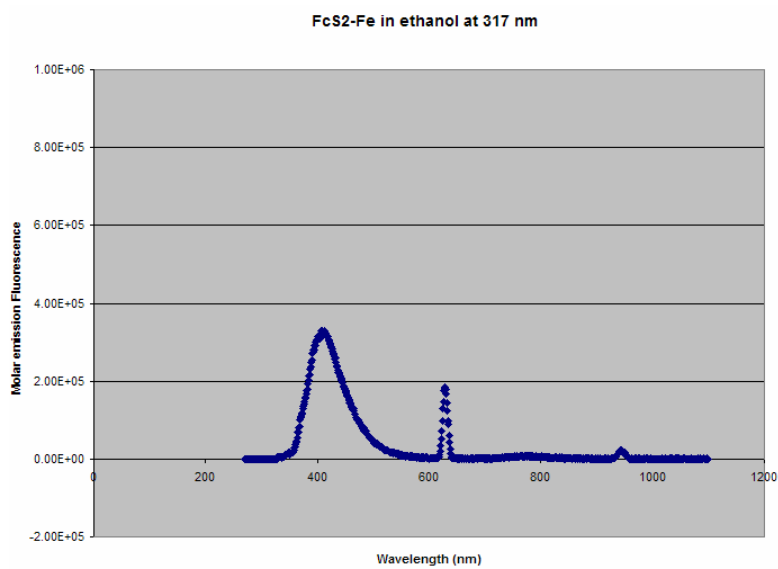


Figure A.77: Emission fluorescence of FcS2-Fe in ethanol at 317 nm with peaks at 412, 628, 942 nm.

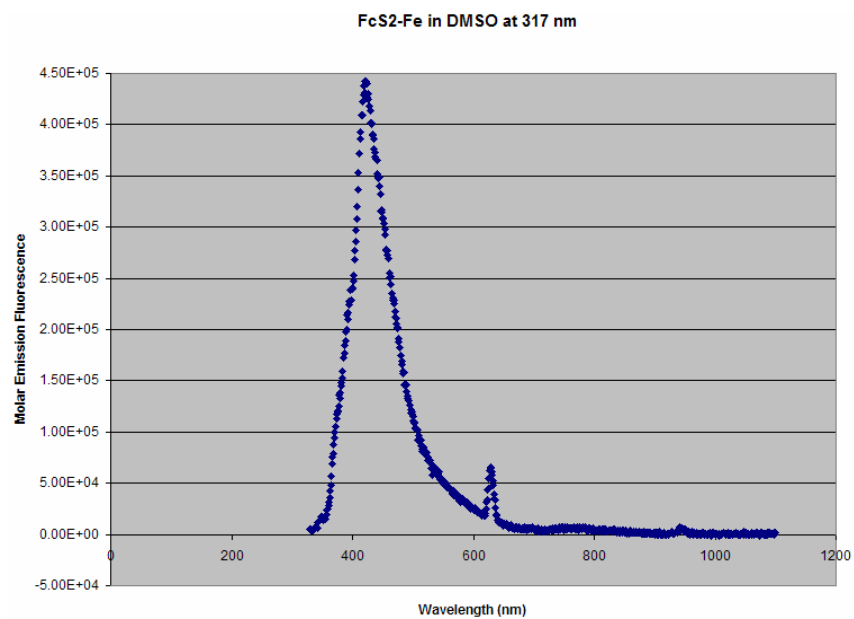


Figure A.78: Emission fluorescence of FcS2-Fe in DMSO at 317 nm with peaks at 422, 628, 942 nm.

Compound 23:

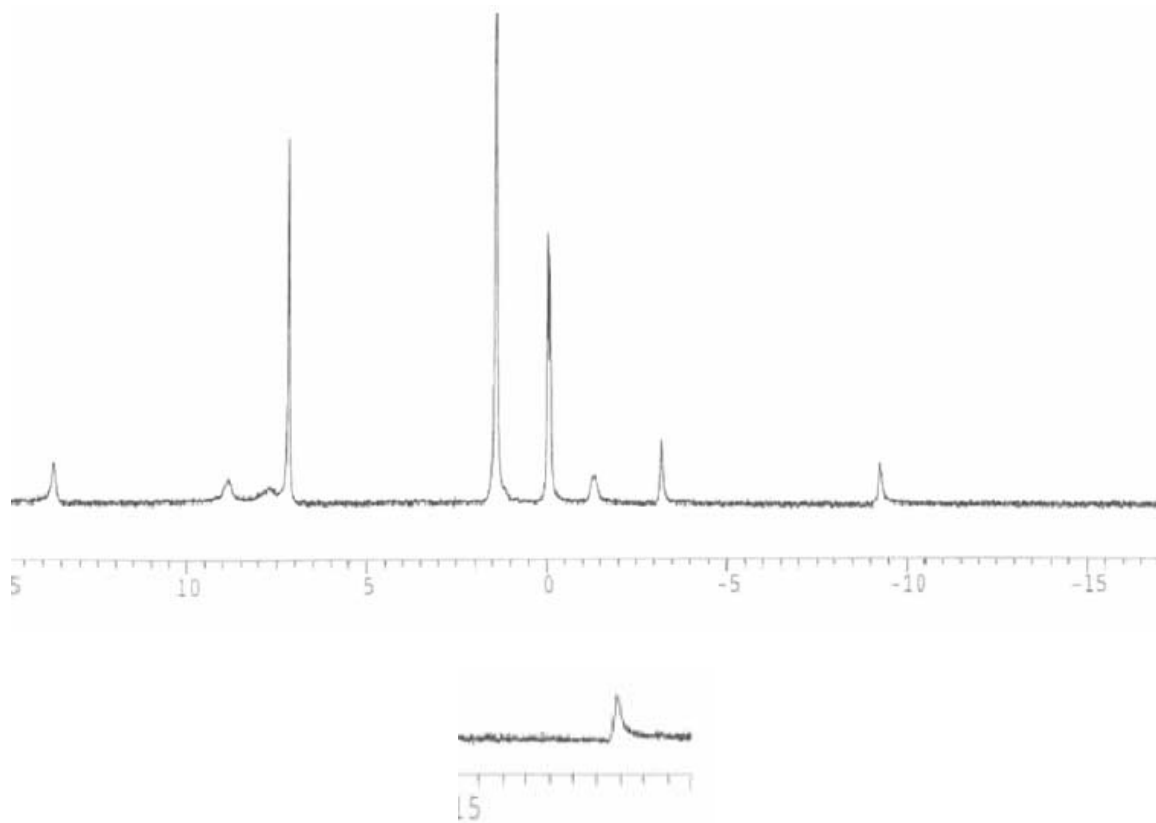
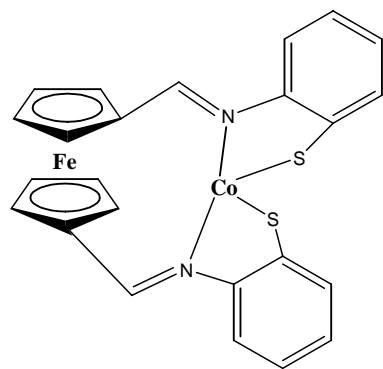


Figure A.79: ^1H NMR spectrum of FcS₂-Co in CDCl₃: 13.81 ppm (s, H), 8.94 ppm (s, H), -1.27 ppm (s, H), -3.11 ppm (s, H), -18.42 ppm (s, H);

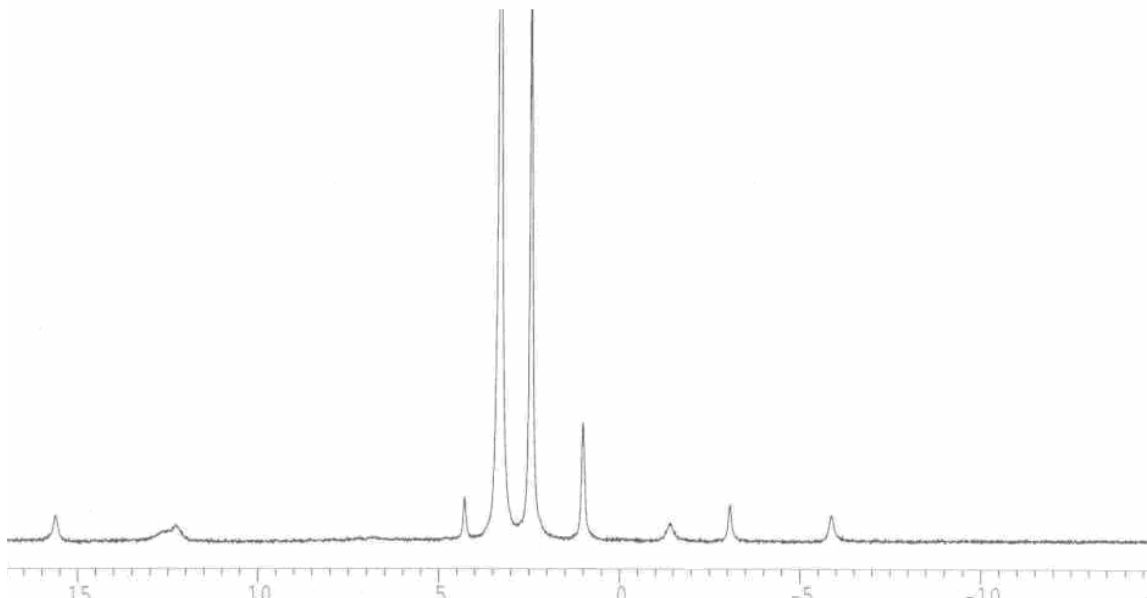


Figure A.80: ^1H NMR spectrum of FcS₂-Co in d₆-DMSO: 15.67 ppm (s, H), 13-12 ppm (broad s, H), 4.35 ppm (s, H), 3.36 ppm (s, H), 1.07 ppm (s, H), -1.5 ppm (s, H), -3.00 ppm (s, H), -5.82 ppm (s, H), -18.65 ppm (s, H);

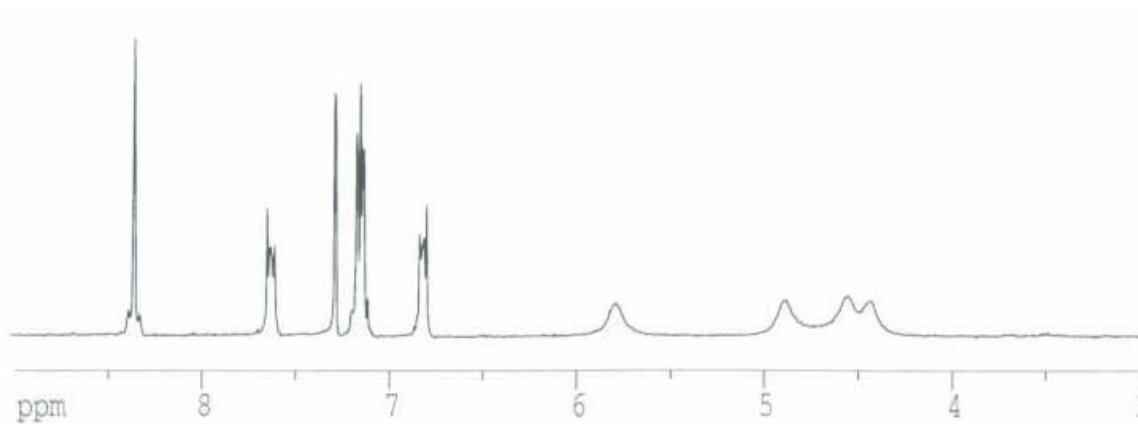


Figure A.81: ^1H NMR spectrum of precipitate from reaction of 23 with $\text{Hg}(\text{CH}_3\text{COO})_2$ in CDCl_3 :

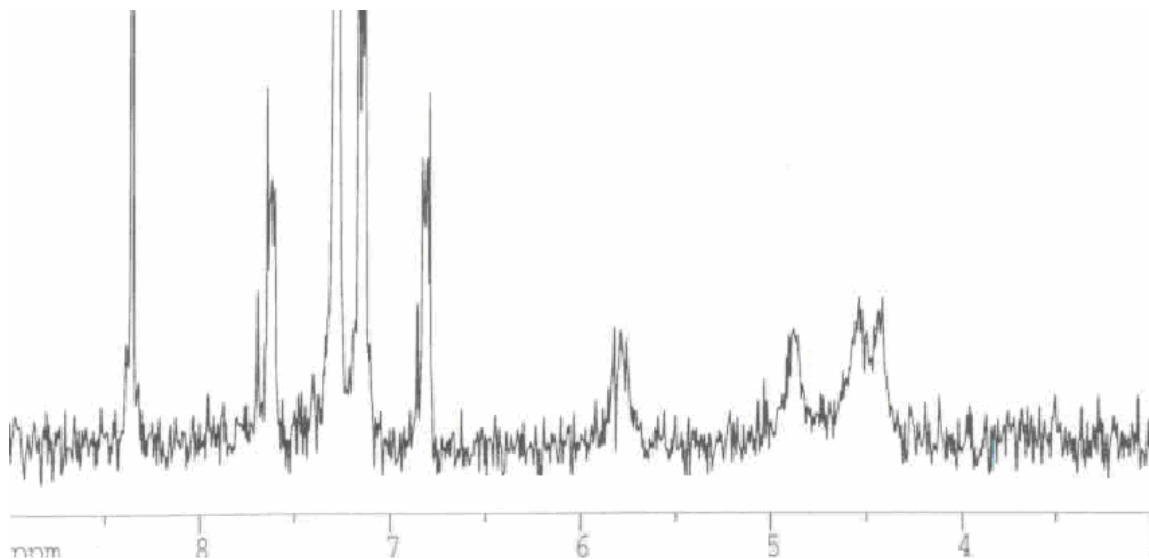


Figure A.82: ^1H NMR spectrum of dried liquid portion from reaction of 23 with $\text{Hg}(\text{CH}_3\text{COO})_2$ in CDCl_3 :

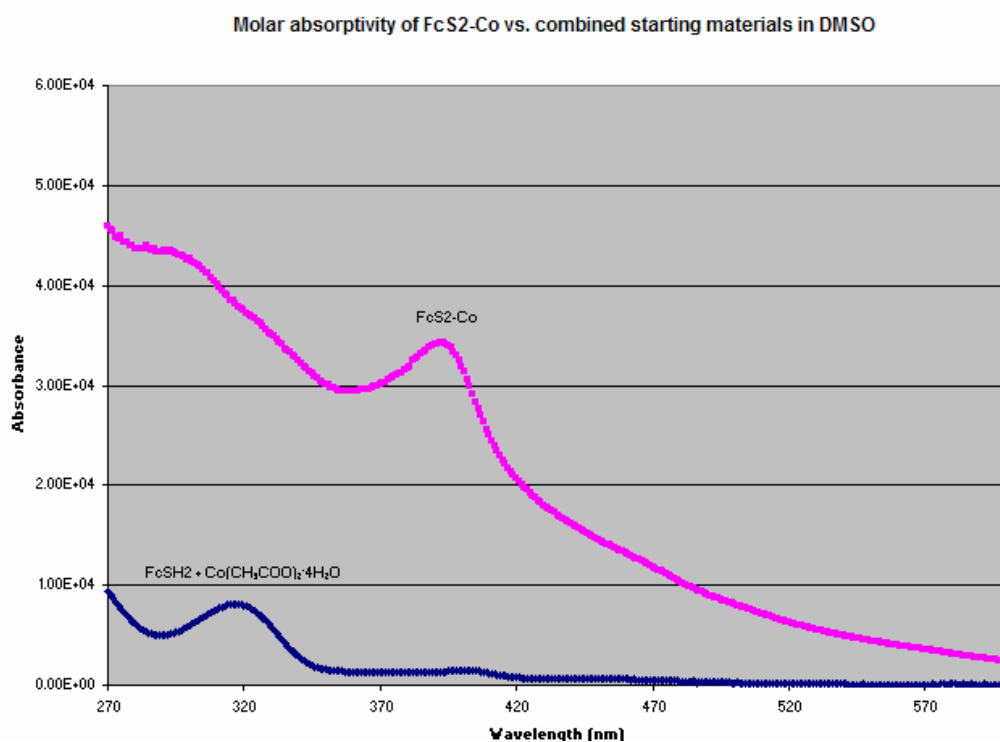


Figure A.83: Comparison between the molar absorptivity (UV-Vis) of FcS2-Co and the molar absorptivity of the starting materials (317, 402 nm peaks) in DMSO: 392 nm ($34300 \text{ M}^{-1}\text{cm}^{-1}$);

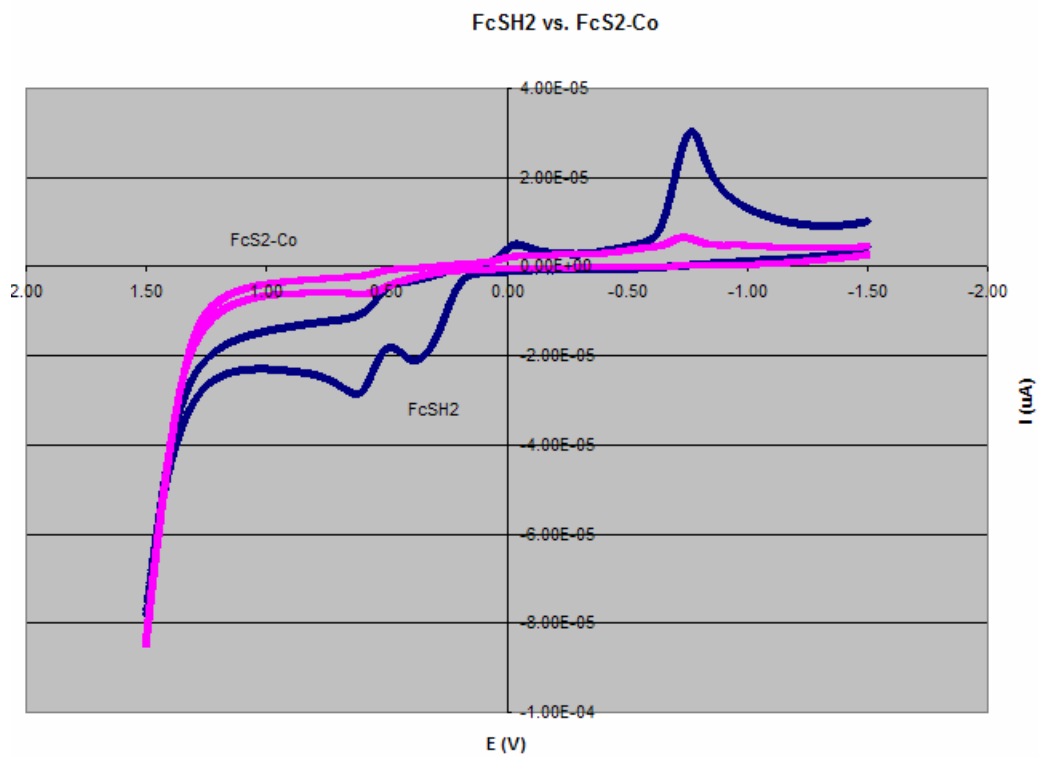


Figure A.84: Comparison between the CV scan of FcS2-Co and the CV scan of FcSH2 in DMSO, scan rate 100 mV/sec. Fe^{II} to Fe^{III} oxidation peak is at 599 mV.

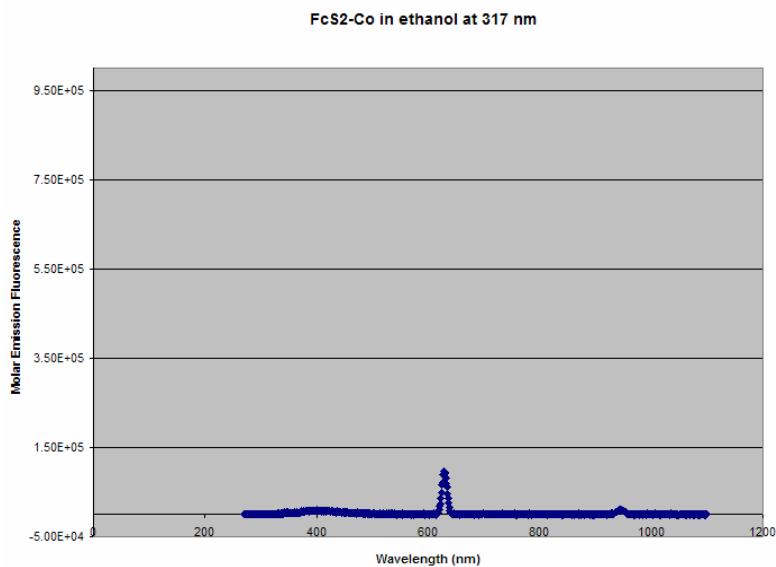


Figure A.85: Emission fluorescence of FcS2-Co in ethanol at 317 nm with peaks at 629, 943 nm.

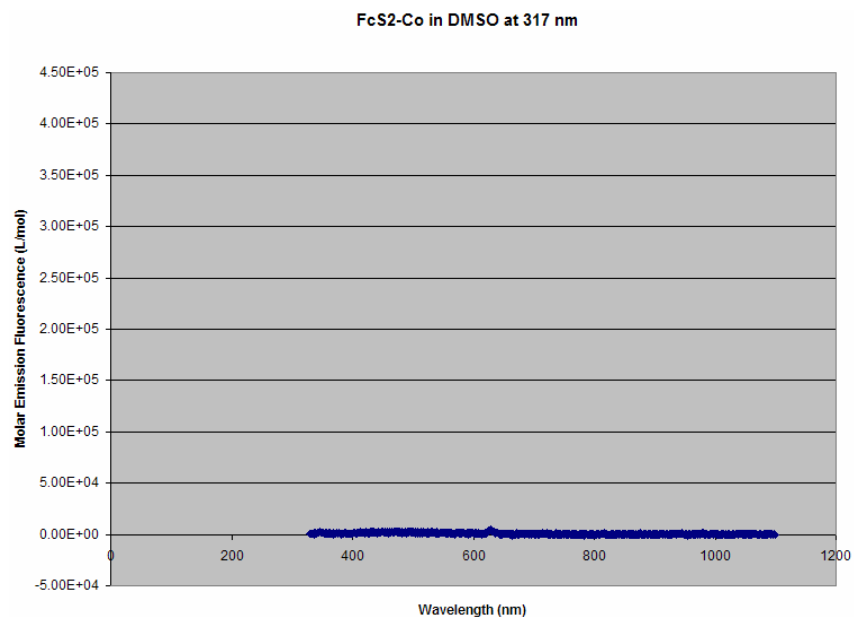


Figure A.86: Emission fluorescence of FcS2-Co in DMSO at 317 nm with a peak at 628 nm.

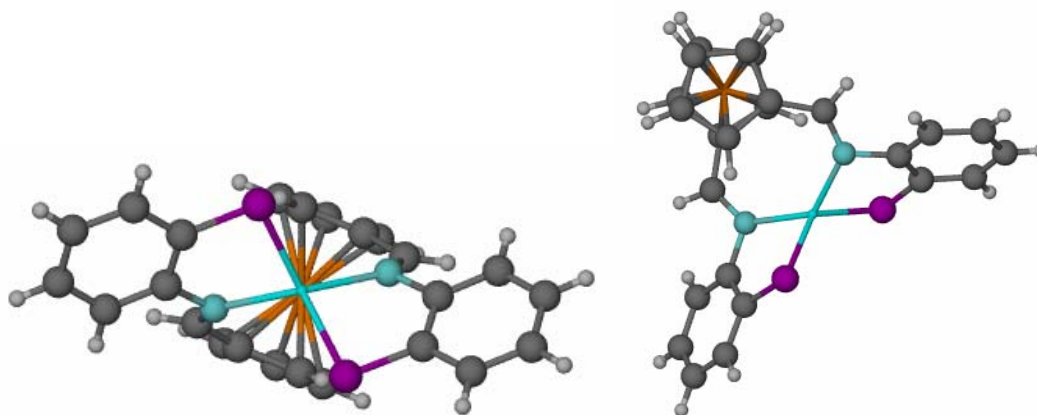


Figure A.87: Crystal Structure of FcS2-Co

Crystal data

$C_{24}H_{18}CoFeN_2S_2$

$M_r = 513.30$

Monoclinic, $P2_1/n$

$a = 7.1861 (6) \text{ \AA}$

$b = 19.2478 (17) \text{ \AA}$

$c = 15.2958 (13) \text{ \AA}$

$\beta = 100.209 (2)^\circ$

$V = 2082.2 (3) \text{ \AA}^3$

$Z = 4$

$F_{000} = 1044$

$D_x = 1.637 \text{ Mg m}^{-3}$

Mo $K\alpha$ radiation

$\lambda = 0.71073 \text{ \AA}$

Cell parameters from 5446 reflections

$\theta = 2.5\text{--}27.0^\circ$

$\mu = 1.71 \text{ mm}^{-1}$

$T = 173 (2) \text{ K}$

Plate, red

$0.35 \times 0.20 \times 0.05 \text{ mm}$

Data collection

Bruker SMART CCD area detector diffractometer	14375 measured reflections
	4577 independent reflections
Monochromator: graphite	3431 reflections with $I > 2\sigma(I)$
	$R_{\text{int}} = 0.043$
$T = 173(2)$ K	$\theta_{\text{max}} = 27.1^\circ$
	$\theta_{\text{min}} = 1.7^\circ$
ω scans	$h = -9 \rightarrow 9$
Absorption correction: multi-scan	
Data were corrected for decay and absorption using the program SADABS (Sheldrick, G. M. (2003). SADABS. Version 2.10. University of Göttingen, Germany).	$k = -24 \rightarrow 24$
$T_{\text{min}} = 0.68, T_{\text{max}} = 0.92$	$l = -17 \rightarrow 19$

Refinement

Refinement on F^2	Secondary atom site location: difference Fourier map
Least-squares matrix: full	Hydrogen site location: inferred from neighbouring sites
$R[F^2 > 2\sigma(F^2)] = 0.044$	H-atom parameters constrained
$wR(F^2) = 0.093$	$w = 1/[\sigma^2(F_o^2) + (0.0327P)^2 + 2.616P]$
$S = 1.09$	where $P = (F_o^2 + 2F_c^2)/3$
4577 reflections	$(\Delta/\sigma)_{\text{max}} = 0.001$
271 parameters	$\Delta\rho_{\text{max}} = 0.62 \text{ e } \text{\AA}^{-3}$
	$\Delta\rho_{\text{min}} = -0.48 \text{ e } \text{\AA}^{-3}$
	Extinction correction: none
Primary atom site location: structure-invariant direct methods	

Refinement of F^2 against ALL reflections. The weighted R-factor wR and goodness of fit S are based on F^2 , conventional R-factors R are based on F , with F set to zero for negative F^2 . The threshold expression of $F^2 > 2\sigma(F^2)$ is used only for calculating R-factors(gt) etc. and is not relevant to the choice of reflections for refinement. R-factors based on F^2 are statistically about twice as large as those based on F , and R-factors based on ALL data will be even larger.

Fractional atomic coordinates and isotropic or equivalent isotropic displacement parameters (\AA^2)

	<i>X</i>	<i>Y</i>	<i>Z</i>	$U_{\text{iso}}^*/U_{\text{eq}}$
Co1	0.93661 (6)	0.24174 (2)	0.75527 (3)	0.02011 (12)

Fe1	0.84250 (7)	0.13857 (2)	0.52705 (3)	0.01970 (13)
S1	1.02932 (12)	0.35331 (5)	0.74637 (6)	0.0244 (2)
N1	0.6859 (4)	0.26979 (13)	0.67490 (18)	0.0184 (6)
C1	0.7963 (5)	0.38566 (17)	0.7209 (2)	0.0204 (7)
S2	0.89176 (12)	0.17910 (5)	0.87517 (6)	0.0237 (2)
N2	1.1473 (4)	0.17158 (14)	0.74107 (18)	0.0206 (6)
C2	0.7593 (5)	0.45641 (17)	0.7266 (2)	0.0262 (8)
H2	0.8611	0.4875	0.7456	0.031*
C3	0.5766 (6)	0.48244 (18)	0.7051 (3)	0.0311 (9)
H3	0.5550	0.5310	0.7083	0.037*
C4	0.4259 (5)	0.43783 (19)	0.6788 (2)	0.0305 (9)
H4	0.3004	0.4553	0.6660	0.037*
C5	0.4600 (5)	0.36716 (17)	0.6714 (2)	0.0236 (7)
H5	0.3572	0.3362	0.6537	0.028*
C6	0.6434 (5)	0.34156 (16)	0.6896 (2)	0.0194 (7)
C7	0.5912 (4)	0.24100 (17)	0.6043 (2)	0.0198 (7)
H7	0.5009	0.2688	0.5671	0.024*
C8	0.6123 (5)	0.16978 (17)	0.5778 (2)	0.0202 (7)
C9	0.5545 (5)	0.14556 (18)	0.4883 (2)	0.0242 (8)
H9	0.4881	0.1719	0.4402	0.029*
C10	0.6132 (5)	0.07594 (18)	0.4844 (2)	0.0246 (8)
H10	0.5952	0.0475	0.4328	0.030*
C11	0.7040 (5)	0.05555 (18)	0.5707 (2)	0.0261 (8)
H11	0.7550	0.0109	0.5867	0.031*
C12	0.7059 (5)	0.11283 (17)	0.6287 (2)	0.0215 (7)
H12	0.7593	0.1136	0.6901	0.026*
C13	1.1214 (5)	0.14360 (17)	0.8939 (2)	0.0210 (7)
C14	1.1991 (5)	0.11336 (18)	0.9747 (2)	0.0254 (8)
H14	1.1253	0.1108	1.0203	0.030*
C15	1.3820 (5)	0.08678 (19)	0.9905 (2)	0.0306 (9)
H15	1.4314	0.0663	1.0463	0.037*

C16	1.4919 (5)	0.09027 (19)	0.9249 (2)	0.0290 (8)
H16	1.6181	0.0734	0.9361	0.035*
C17	1.4176 (5)	0.11833 (18)	0.8428 (2)	0.0249 (8)
H17	1.4923	0.1202	0.7975	0.030*
C18	1.2326 (4)	0.14384 (16)	0.8267 (2)	0.0189 (7)
C19	1.1853 (5)	0.13914 (18)	0.6725 (2)	0.0223 (7)
H19	1.2659	0.0998	0.6834	0.027*
C20	1.1169 (5)	0.15697 (18)	0.5808 (2)	0.0224 (7)
C21	1.0291 (5)	0.21923 (19)	0.5423 (2)	0.0255 (8)
H21	1.0159	0.2615	0.5728	0.031*
C22	0.9655 (5)	0.2065 (2)	0.4507 (2)	0.0298 (8)
H22	0.9016	0.2389	0.4091	0.036*
C23	1.0127 (5)	0.1377 (2)	0.4312 (2)	0.0318 (9)
H23	0.9868	0.1161	0.3746	0.038*
C24	1.1058 (5)	0.1067 (2)	0.5112 (2)	0.0279 (8)
H24	1.1527	0.0605	0.5175	0.033*

Atomic displacement parameters (\AA^2)

	U^{11}	U^{22}	U^{33}	U^{12}	U^{13}	U^{23}
Co1	0.0177 (2)	0.0213 (2)	0.0211 (2)	0.00187 (19)	0.00308 (18)	-0.00099 (19)
Fe1	0.0210 (3)	0.0208 (2)	0.0179 (2)	0.0010 (2)	0.00494 (19)	-0.00080 (19)
S1	0.0185 (4)	0.0250 (5)	0.0291 (5)	-0.0020 (3)	0.0029 (4)	-0.0012 (4)
N1	0.0173 (14)	0.0194 (14)	0.0194 (15)	0.0011 (11)	0.0057 (11)	-0.0009 (11)
C1	0.0203 (17)	0.0251 (17)	0.0174 (17)	-0.0007 (14)	0.0074 (14)	-0.0007 (13)
S2	0.0198 (4)	0.0283 (5)	0.0242 (5)	0.0013 (4)	0.0067 (4)	0.0002 (4)
N2	0.0162 (14)	0.0234 (15)	0.0228 (15)	-0.0002 (12)	0.0050 (12)	-0.0005 (12)
C2	0.030 (2)	0.0180 (17)	0.030 (2)	-0.0012 (15)	0.0051 (16)	-0.0028 (14)

C3	0.040 (2)	0.0182 (18)	0.035 (2)	0.0067 (16)	0.0086 (18)	0.0003 (15)
C4	0.028 (2)	0.029 (2)	0.034 (2)	0.0102 (16)	0.0049 (17)	-0.0020 (16)
C5	0.0222 (18)	0.0237 (18)	0.0256 (19)	0.0035 (14)	0.0059 (15)	-0.0010 (14)
C6	0.0238 (18)	0.0180 (16)	0.0177 (17)	0.0046 (13)	0.0072 (14)	0.0004 (13)
C7	0.0144 (16)	0.0230 (17)	0.0234 (18)	0.0017 (13)	0.0070 (14)	0.0029 (14)
C8	0.0161 (17)	0.0234 (17)	0.0220 (18)	-0.0016 (14)	0.0059 (14)	-0.0020 (14)
C9	0.0227 (19)	0.0250 (18)	0.0240 (19)	-0.0039 (15)	0.0013 (15)	0.0012 (14)
C10	0.027 (2)	0.0251 (18)	0.0214 (19)	-0.0055 (15)	0.0044 (15)	-0.0052 (14)
C11	0.032 (2)	0.0202 (18)	0.026 (2)	-0.0001 (15)	0.0069 (16)	-0.0014 (14)
C12	0.0217 (18)	0.0240 (17)	0.0203 (18)	-0.0005 (14)	0.0080 (14)	-0.0001 (14)
C13	0.0197 (17)	0.0212 (17)	0.0219 (18)	-0.0036 (14)	0.0031 (14)	-0.0033 (14)
C14	0.031 (2)	0.0255 (18)	0.0207 (18)	0.0009 (15)	0.0073 (16)	0.0022 (15)
C15	0.035 (2)	0.030 (2)	0.025 (2)	0.0022 (17)	-0.0017 (17)	0.0044 (16)
C16	0.0218 (19)	0.030 (2)	0.034 (2)	0.0052 (16)	0.0023 (16)	0.0022 (16)
C17	0.0234 (19)	0.0265 (18)	0.0258 (19)	-0.0003 (15)	0.0073 (15)	-0.0040 (15)
C18	0.0183 (17)	0.0183 (16)	0.0195 (17)	-0.0009 (13)	0.0016 (13)	-0.0009 (13)
C19	0.0142 (17)	0.0282 (18)	0.0258 (19)	0.0045 (14)	0.0069 (14)	0.0019 (15)
C20	0.0181 (17)	0.0284 (19)	0.0215 (18)	0.0016 (14)	0.0056 (14)	-0.0017 (14)
C21	0.0201 (18)	0.030 (2)	0.028 (2)	-0.0019 (15)	0.0101 (15)	0.0010 (15)
C22	0.028 (2)	0.039 (2)	0.024 (2)	0.0004 (17)	0.0089 (16)	0.0080 (16)
C23	0.030 (2)	0.048 (2)	0.0200 (19)	0.0018 (18)	0.0102 (16)	-0.0023 (17)
C24	0.0250 (19)	0.037 (2)	0.024 (2)	0.0077 (16)	0.0108 (16)	-0.0018 (15)

Table 1

Geometric parameters (Å, °)

Co1—N1	2.065 (3)	C7—H7	0.9500
Co1—N2	2.069 (3)	C8—C9	1.436 (5)
Co1—S1	2.2596 (10)	C8—C12	1.440 (5)
Co1—S2	2.2651 (10)	C9—C10	1.410 (5)
Fe1—C20	2.029 (3)	C9—H9	0.9500

Fe1—C21	2.038 (3)	C10—C11	1.420 (5)
Fe1—C8	2.039 (3)	C10—H10	0.9500
Fe1—C12	2.041 (3)	C11—C12	1.414 (5)
Fe1—C24	2.044 (3)	C11—H11	0.9500
Fe1—C10	2.052 (3)	C12—H12	0.9500
Fe1—C9	2.054 (3)	C13—C14	1.390 (5)
Fe1—C22	2.055 (4)	C13—C18	1.410 (4)
Fe1—C11	2.055 (3)	C14—C15	1.391 (5)
Fe1—C23	2.069 (3)	C14—H14	0.9500
S1—C1	1.764 (3)	C15—C16	1.385 (5)
N1—C7	1.294 (4)	C15—H15	0.9500
N1—C6	1.441 (4)	C16—C17	1.383 (5)
C1—C2	1.393 (5)	C16—H16	0.9500
C1—C6	1.404 (5)	C17—C18	1.397 (5)
S2—C13	1.762 (3)	C17—H17	0.9500
N2—C19	1.291 (4)	C19—C20	1.442 (5)
N2—C18	1.446 (4)	C19—H19	0.9500
C2—C3	1.389 (5)	C20—C24	1.430 (5)
C2—H2	0.9500	C20—C21	1.431 (5)
C3—C4	1.385 (5)	C21—C22	1.417 (5)
C3—H3	0.9500	C21—H21	0.9500
C4—C5	1.391 (5)	C22—C23	1.411 (5)
C4—H4	0.9500	C22—H22	0.9500
C5—C6	1.388 (5)	C23—C24	1.418 (5)
C5—H5	0.9500	C23—H23	0.9500
C7—C8	1.445 (4)	C24—H24	0.9500
N1—Co1—N2	133.29 (11)	C9—C8—C7	123.3 (3)
N1—Co1—S1	87.20 (8)	C12—C8—C7	129.3 (3)
N2—Co1—S1	112.65 (8)	C9—C8—Fe1	70.02 (19)
N1—Co1—S2	112.76 (8)	C12—C8—Fe1	69.41 (18)
N2—Co1—S2	87.09 (8)	C7—C8—Fe1	121.3 (2)

S1—Co1—S2	129.82 (4)	C10—C9—C8	108.2 (3)
C20—Fe1—C21	41.22 (14)	C10—C9—Fe1	69.9 (2)
C20—Fe1—C8	126.16 (13)	C8—C9—Fe1	68.90 (18)
C21—Fe1—C8	107.08 (14)	C10—C9—H9	125.9
C20—Fe1—C12	107.32 (14)	C8—C9—H9	125.9
C21—Fe1—C12	119.55 (14)	Fe1—C9—H9	126.9
C8—Fe1—C12	41.33 (13)	C9—C10—C11	108.3 (3)
C20—Fe1—C24	41.13 (14)	C9—C10—Fe1	70.0 (2)
C21—Fe1—C24	68.78 (15)	C11—C10—Fe1	69.9 (2)
C8—Fe1—C24	164.64 (14)	C9—C10—H10	125.8
C12—Fe1—C24	126.70 (14)	C11—C10—H10	125.8
C20—Fe1—C10	154.07 (14)	Fe1—C10—H10	125.9
C21—Fe1—C10	163.50 (14)	C12—C11—C10	108.6 (3)
C8—Fe1—C10	68.56 (13)	C12—C11—Fe1	69.27 (19)
C12—Fe1—C10	68.43 (13)	C10—C11—Fe1	69.7 (2)
C24—Fe1—C10	119.59 (15)	C12—C11—H11	125.7
C20—Fe1—C9	164.35 (14)	C10—C11—H11	125.7
C21—Fe1—C9	126.32 (14)	Fe1—C11—H11	127.0
C8—Fe1—C9	41.08 (13)	C11—C12—C8	107.7 (3)
C12—Fe1—C9	68.85 (14)	C11—C12—Fe1	70.35 (19)
C24—Fe1—C9	153.17 (14)	C8—C12—Fe1	69.26 (18)
C10—Fe1—C9	40.15 (13)	C11—C12—H12	126.2
C20—Fe1—C22	68.54 (14)	C8—C12—H12	126.2
C21—Fe1—C22	40.51 (14)	Fe1—C12—H12	125.8
C8—Fe1—C22	119.28 (14)	C14—C13—C18	117.3 (3)
C12—Fe1—C22	154.28 (14)	C14—C13—S2	121.6 (3)
C24—Fe1—C22	67.85 (15)	C18—C13—S2	121.1 (3)
C10—Fe1—C22	126.50 (14)	C13—C14—C15	121.8 (3)
C9—Fe1—C22	107.92 (14)	C13—C14—H14	119.1
C20—Fe1—C11	119.72 (14)	C15—C14—H14	119.1
C21—Fe1—C11	154.40 (14)	C16—C15—C14	119.9 (3)

C8—Fe1—C11	68.48 (13)	C16—C15—H15	120.1
C12—Fe1—C11	40.38 (13)	C14—C15—H15	120.1
C24—Fe1—C11	108.46 (15)	C17—C16—C15	119.9 (3)
C10—Fe1—C11	40.46 (13)	C17—C16—H16	120.0
C9—Fe1—C11	67.88 (14)	C15—C16—H16	120.0
C22—Fe1—C11	163.97 (14)	C16—C17—C18	120.0 (3)
C20—Fe1—C23	68.56 (14)	C16—C17—H17	120.0
C21—Fe1—C23	68.13 (15)	C18—C17—H17	120.0
C8—Fe1—C23	153.35 (14)	C17—C18—C13	121.0 (3)
C12—Fe1—C23	164.19 (15)	C17—C18—N2	121.8 (3)
C24—Fe1—C23	40.34 (14)	C13—C18—N2	117.2 (3)
C10—Fe1—C23	108.19 (14)	N2—C19—C20	126.2 (3)
C9—Fe1—C23	119.24 (15)	N2—C19—H19	116.9
C22—Fe1—C23	40.01 (15)	C20—C19—H19	116.9
C11—Fe1—C23	127.22 (15)	C24—C20—C21	107.3 (3)
C1—S1—Co1	94.03 (12)	C24—C20—C19	121.8 (3)
C7—N1—C6	116.5 (3)	C21—C20—C19	130.4 (3)
C7—N1—Co1	131.2 (2)	C24—C20—Fe1	70.0 (2)
C6—N1—Co1	110.1 (2)	C21—C20—Fe1	69.73 (19)
C2—C1—C6	117.8 (3)	C19—C20—Fe1	119.5 (2)
C2—C1—S1	121.0 (3)	C22—C21—C20	107.7 (3)
C6—C1—S1	121.1 (3)	C22—C21—Fe1	70.4 (2)
C13—S2—Co1	94.27 (11)	C20—C21—Fe1	69.0 (2)
C19—N2—C18	116.1 (3)	C22—C21—H21	126.2
C19—N2—Co1	131.7 (2)	C20—C21—H21	126.2
C18—N2—Co1	110.30 (19)	Fe1—C21—H21	126.0
C3—C2—C1	121.4 (3)	C23—C22—C21	108.9 (3)
C3—C2—H2	119.3	C23—C22—Fe1	70.5 (2)
C1—C2—H2	119.3	C21—C22—Fe1	69.11 (19)
C4—C3—C2	120.2 (3)	C23—C22—H22	125.6
C4—C3—H3	119.9	C21—C22—H22	125.6

C2—C3—H3	119.9	Fe1—C22—H22	126.4
C3—C4—C5	119.3 (3)	C22—C23—C24	107.9 (3)
C3—C4—H4	120.3	C22—C23—Fe1	69.44 (19)
C5—C4—H4	120.3	C24—C23—Fe1	68.88 (19)
C6—C5—C4	120.4 (3)	C22—C23—H23	126.1
C6—C5—H5	119.8	C24—C23—H23	126.1
C4—C5—H5	119.8	Fe1—C23—H23	127.2
C5—C6—C1	120.8 (3)	C23—C24—C20	108.2 (3)
C5—C6—N1	121.9 (3)	C23—C24—Fe1	70.8 (2)
C1—C6—N1	117.3 (3)	C20—C24—Fe1	68.87 (19)
N1—C7—C8	125.1 (3)	C23—C24—H24	125.9
N1—C7—H7	117.5	C20—C24—H24	125.9
C8—C7—H7	117.5	Fe1—C24—H24	126.0
C9—C8—C12	107.2 (3)		
N1—Co1—S1—C1	23.45 (13)	C23—Fe1—C12—C11	-43.5 (6)
N2—Co1—S1—C1	159.79 (13)	C20—Fe1—C12—C8	125.5 (2)
S2—Co1—S1—C1	-94.17 (11)	C21—Fe1—C12—C8	82.3 (2)
N2—Co1—N1—C7	13.4 (4)	C24—Fe1—C12—C8	166.8 (2)
S1—Co1—N1—C7	132.3 (3)	C10—Fe1—C12—C8	-81.6 (2)
S2—Co1—N1—C7	-95.2 (3)	C9—Fe1—C12—C8	-38.37 (19)
N2—Co1—N1—C6	-148.95 (19)	C22—Fe1—C12—C8	49.2 (4)
S1—Co1—N1—C6	-30.03 (19)	C11—Fe1—C12—C8	-118.7 (3)
S2—Co1—N1—C6	102.41 (19)	C23—Fe1—C12—C8	-162.2 (5)
Co1—S1—C1—C2	165.5 (3)	Co1—S2—C13—C14	162.7 (3)
Co1—S1—C1—C6	-18.1 (3)	Co1—S2—C13—C18	-18.3 (3)
N1—Co1—S2—C13	159.72 (13)	C18—C13—C14—C15	2.6 (5)
N2—Co1—S2—C13	23.39 (13)	S2—C13—C14—C15	-178.4 (3)
S1—Co1—S2—C13	-93.97 (12)	C13—C14—C15—C16	0.2 (6)
N1—Co1—N2—C19	14.7 (4)	C14—C15—C16—C17	-1.9 (6)
S1—Co1—N2—C19	-93.9 (3)	C15—C16—C17—C18	0.7 (5)
S2—Co1—N2—C19	133.7 (3)	C16—C17—C18—C13	2.1 (5)

N1—Co1—N2—C18	-148.66 (19)	C16—C17—C18—N2	-178.0 (3)
S1—Co1—N2—C18	102.65 (19)	C14—C13—C18—C17	-3.7 (5)
S2—Co1—N2—C18	-29.69 (19)	S2—C13—C18—C17	177.3 (3)
C6—C1—C2—C3	2.2 (5)	C14—C13—C18—N2	176.4 (3)
S1—C1—C2—C3	178.7 (3)	S2—C13—C18—N2	-2.6 (4)
C1—C2—C3—C4	1.2 (6)	C19—N2—C18—C17	39.3 (4)
C2—C3—C4—C5	-2.2 (6)	Co1—N2—C18—C17	-154.4 (3)
C3—C4—C5—C6	-0.3 (5)	C19—N2—C18—C13	-140.8 (3)
C4—C5—C6—C1	3.8 (5)	Co1—N2—C18—C13	25.5 (3)
C4—C5—C6—N1	-174.2 (3)	C18—N2—C19—C20	180.0 (3)
C2—C1—C6—C5	-4.7 (5)	Co1—N2—C19—C20	17.3 (5)
S1—C1—C6—C5	178.8 (3)	N2—C19—C20—C24	-156.5 (3)
C2—C1—C6—N1	173.5 (3)	N2—C19—C20—C21	14.7 (6)
S1—C1—C6—N1	-3.1 (4)	N2—C19—C20—Fe1	-72.9 (4)
C7—N1—C6—C5	38.8 (4)	C21—Fe1—C20—C24	-118.2 (3)
Co1—N1—C6—C5	-155.9 (3)	C8—Fe1—C20—C24	168.2 (2)
C7—N1—C6—C1	-139.3 (3)	C12—Fe1—C20—C24	126.5 (2)
Co1—N1—C6—C1	25.9 (3)	C10—Fe1—C20—C24	50.3 (4)
C6—N1—C7—C8	-179.8 (3)	C9—Fe1—C20—C24	-160.2 (5)
Co1—N1—C7—C8	18.7 (5)	C22—Fe1—C20—C24	-80.5 (2)
N1—C7—C8—C9	-159.1 (3)	C11—Fe1—C20—C24	84.3 (2)
N1—C7—C8—C12	14.3 (5)	C23—Fe1—C20—C24	-37.3 (2)
N1—C7—C8—Fe1	-73.7 (4)	C8—Fe1—C20—C21	-73.6 (2)
C20—Fe1—C8—C9	167.59 (19)	C12—Fe1—C20—C21	-115.3 (2)
C21—Fe1—C8—C9	126.2 (2)	C24—Fe1—C20—C21	118.2 (3)
C12—Fe1—C8—C9	-118.2 (3)	C10—Fe1—C20—C21	168.5 (3)
C24—Fe1—C8—C9	-161.9 (5)	C9—Fe1—C20—C21	-42.1 (6)
C10—Fe1—C8—C9	-36.95 (19)	C22—Fe1—C20—C21	37.7 (2)
C22—Fe1—C8—C9	83.9 (2)	C11—Fe1—C20—C21	-157.54 (19)
C11—Fe1—C8—C9	-80.6 (2)	C23—Fe1—C20—C21	80.8 (2)
C23—Fe1—C8—C9	51.0 (4)	C21—Fe1—C20—C19	125.8 (4)

C20—Fe1—C8—C12	-74.2 (2)	C8—Fe1—C20—C19	52.2 (3)
C21—Fe1—C8—C12	-115.6 (2)	C12—Fe1—C20—C19	10.5 (3)
C24—Fe1—C8—C12	-43.7 (6)	C24—Fe1—C20—C19	-116.0 (4)
C10—Fe1—C8—C12	81.3 (2)	C10—Fe1—C20—C19	-65.7 (4)
C9—Fe1—C8—C12	118.2 (3)	C9—Fe1—C20—C19	83.8 (6)
C22—Fe1—C8—C12	-157.9 (2)	C22—Fe1—C20—C19	163.5 (3)
C11—Fe1—C8—C12	37.7 (2)	C11—Fe1—C20—C19	-31.7 (3)
C23—Fe1—C8—C12	169.3 (3)	C23—Fe1—C20—C19	-153.3 (3)
C20—Fe1—C8—C7	50.1 (3)	C24—C20—C21—C22	0.2 (4)
C21—Fe1—C8—C7	8.7 (3)	C19—C20—C21—C22	-172.0 (3)
C12—Fe1—C8—C7	124.2 (4)	Fe1—C20—C21—C22	-60.1 (2)
C24—Fe1—C8—C7	80.6 (6)	C24—C20—C21—Fe1	60.2 (2)
C10—Fe1—C8—C7	-154.5 (3)	C19—C20—C21—Fe1	-112.0 (4)
C9—Fe1—C8—C7	-117.5 (3)	C20—Fe1—C21—C22	118.8 (3)
C22—Fe1—C8—C7	-33.6 (3)	C8—Fe1—C21—C22	-115.3 (2)
C11—Fe1—C8—C7	161.9 (3)	C12—Fe1—C21—C22	-158.6 (2)
C23—Fe1—C8—C7	-66.5 (4)	C24—Fe1—C21—C22	80.3 (2)
C12—C8—C9—C10	-0.7 (4)	C10—Fe1—C21—C22	-43.4 (6)
C7—C8—C9—C10	174.0 (3)	C9—Fe1—C21—C22	-74.2 (3)
Fe1—C8—C9—C10	59.0 (2)	C11—Fe1—C21—C22	168.9 (3)
C12—C8—C9—Fe1	-59.7 (2)	C23—Fe1—C21—C22	36.8 (2)
C7—C8—C9—Fe1	114.9 (3)	C8—Fe1—C21—C20	125.9 (2)
C20—Fe1—C9—C10	-159.8 (5)	C12—Fe1—C21—C20	82.7 (2)
C21—Fe1—C9—C10	167.0 (2)	C24—Fe1—C21—C20	-38.5 (2)
C8—Fe1—C9—C10	-119.8 (3)	C10—Fe1—C21—C20	-162.1 (4)
C12—Fe1—C9—C10	-81.2 (2)	C9—Fe1—C21—C20	167.04 (19)
C24—Fe1—C9—C10	49.7 (4)	C22—Fe1—C21—C20	-118.8 (3)
C22—Fe1—C9—C10	125.9 (2)	C11—Fe1—C21—C20	50.1 (4)
C11—Fe1—C9—C10	-37.63 (19)	C23—Fe1—C21—C20	-82.0 (2)
C23—Fe1—C9—C10	83.8 (2)	C20—C21—C22—C23	-0.3 (4)
C20—Fe1—C9—C8	-40.0 (6)	Fe1—C21—C22—C23	-59.5 (3)

C21—Fe1—C9—C8	-73.2 (2)	C20—C21—C22—Fe1	59.2 (2)
C12—Fe1—C9—C8	38.60 (19)	C20—Fe1—C22—C23	81.8 (2)
C24—Fe1—C9—C8	169.5 (3)	C21—Fe1—C22—C23	120.2 (3)
C10—Fe1—C9—C8	119.8 (3)	C8—Fe1—C22—C23	-157.8 (2)
C22—Fe1—C9—C8	-114.3 (2)	C12—Fe1—C22—C23	167.3 (3)
C11—Fe1—C9—C8	82.2 (2)	C24—Fe1—C22—C23	37.3 (2)
C23—Fe1—C9—C8	-156.4 (2)	C10—Fe1—C22—C23	-73.9 (3)
C8—C9—C10—C11	1.1 (4)	C9—Fe1—C22—C23	-114.4 (2)
Fe1—C9—C10—C11	59.6 (2)	C11—Fe1—C22—C23	-42.3 (6)
C8—C9—C10—Fe1	-58.4 (2)	C20—Fe1—C22—C21	-38.4 (2)
C20—Fe1—C10—C9	167.7 (3)	C8—Fe1—C22—C21	82.1 (2)
C21—Fe1—C10—C9	-39.8 (6)	C12—Fe1—C22—C21	47.1 (4)
C8—Fe1—C10—C9	37.8 (2)	C24—Fe1—C22—C21	-82.8 (2)
C12—Fe1—C10—C9	82.4 (2)	C10—Fe1—C22—C21	166.0 (2)
C24—Fe1—C10—C9	-156.7 (2)	C9—Fe1—C22—C21	125.4 (2)
C22—Fe1—C10—C9	-73.5 (2)	C11—Fe1—C22—C21	-162.5 (5)
C11—Fe1—C10—C9	119.3 (3)	C23—Fe1—C22—C21	-120.2 (3)
C23—Fe1—C10—C9	-114.1 (2)	C21—C22—C23—C24	0.3 (4)
C20—Fe1—C10—C11	48.4 (4)	Fe1—C22—C23—C24	-58.3 (2)
C21—Fe1—C10—C11	-159.2 (4)	C21—C22—C23—Fe1	58.6 (2)
C8—Fe1—C10—C11	-81.6 (2)	C20—Fe1—C23—C22	-81.8 (2)
C12—Fe1—C10—C11	-37.0 (2)	C21—Fe1—C23—C22	-37.2 (2)
C24—Fe1—C10—C11	84.0 (2)	C8—Fe1—C23—C22	47.4 (4)
C9—Fe1—C10—C11	-119.3 (3)	C12—Fe1—C23—C22	-159.4 (5)
C22—Fe1—C10—C11	167.1 (2)	C24—Fe1—C23—C22	-119.8 (3)
C23—Fe1—C10—C11	126.6 (2)	C10—Fe1—C23—C22	125.6 (2)
C9—C10—C11—C12	-1.2 (4)	C9—Fe1—C23—C22	83.2 (2)
Fe1—C10—C11—C12	58.5 (2)	C11—Fe1—C23—C22	166.5 (2)
C9—C10—C11—Fe1	-59.6 (2)	C20—Fe1—C23—C24	38.0 (2)
C20—Fe1—C11—C12	81.8 (2)	C21—Fe1—C23—C24	82.5 (2)
C21—Fe1—C11—C12	46.2 (4)	C8—Fe1—C23—C24	167.1 (3)

C8—Fe1—C11—C12	-38.5 (2)	C12—Fe1—C23—C24	-39.7 (6)
C24—Fe1—C11—C12	125.5 (2)	C10—Fe1—C23—C24	-114.6 (2)
C10—Fe1—C11—C12	-120.3 (3)	C9—Fe1—C23—C24	-157.0 (2)
C9—Fe1—C11—C12	-82.9 (2)	C22—Fe1—C23—C24	119.8 (3)
C22—Fe1—C11—C12	-160.7 (5)	C11—Fe1—C23—C24	-73.7 (3)
C23—Fe1—C11—C12	166.4 (2)	C22—C23—C24—C20	-0.2 (4)
C20—Fe1—C11—C10	-157.9 (2)	Fe1—C23—C24—C20	-58.9 (2)
C21—Fe1—C11—C10	166.5 (3)	C22—C23—C24—Fe1	58.6 (2)
C8—Fe1—C11—C10	81.8 (2)	C21—C20—C24—C23	0.1 (4)
C12—Fe1—C11—C10	120.3 (3)	C19—C20—C24—C23	173.1 (3)
C24—Fe1—C11—C10	-114.3 (2)	Fe1—C20—C24—C23	60.1 (2)
C9—Fe1—C11—C10	37.4 (2)	C21—C20—C24—Fe1	-60.0 (2)
C22—Fe1—C11—C10	-40.4 (6)	C19—C20—C24—Fe1	113.0 (3)
C23—Fe1—C11—C10	-73.3 (3)	C20—Fe1—C24—C23	-119.3 (3)
C10—C11—C12—C8	0.7 (4)	C21—Fe1—C24—C23	-80.8 (2)
Fe1—C11—C12—C8	59.4 (2)	C8—Fe1—C24—C23	-157.8 (5)
C10—C11—C12—Fe1	-58.7 (2)	C12—Fe1—C24—C23	167.5 (2)
C9—C8—C12—C11	0.0 (4)	C10—Fe1—C24—C23	83.4 (3)
C7—C8—C12—C11	-174.3 (3)	C9—Fe1—C24—C23	49.0 (4)
Fe1—C8—C12—C11	-60.1 (2)	C22—Fe1—C24—C23	-37.1 (2)
C9—C8—C12—Fe1	60.1 (2)	C11—Fe1—C24—C23	126.3 (2)
C7—C8—C12—Fe1	-114.1 (3)	C21—Fe1—C24—C20	38.5 (2)
C20—Fe1—C12—C11	-115.8 (2)	C8—Fe1—C24—C20	-38.5 (6)
C21—Fe1—C12—C11	-159.0 (2)	C12—Fe1—C24—C20	-73.2 (3)
C8—Fe1—C12—C11	118.7 (3)	C10—Fe1—C24—C20	-157.2 (2)
C24—Fe1—C12—C11	-74.5 (3)	C9—Fe1—C24—C20	168.3 (3)
C10—Fe1—C12—C11	37.0 (2)	C22—Fe1—C24—C20	82.3 (2)
C9—Fe1—C12—C11	80.3 (2)	C11—Fe1—C24—C20	-114.4 (2)
C22—Fe1—C12—C11	167.8 (3)	C23—Fe1—C24—C20	119.3 (3)

All esds (except the esd in the dihedral angle between two l.s. planes) are estimated using the full covariance matrix. The cell esds are taken into account individually in the estimation of esds in distances, angles and torsion angles; correlations between esds in cell parameters are only used when they are defined by crystal symmetry. An approximate (isotropic) treatment of cell esds is used for estimating esds involving l.s. planes.

Data collection: *SMART* (Bruker, 1998); cell refinement: *SAINTE* (Bruker, 1998); data reduction: *SAINTE* (Bruker, 1998); program(s) used to solve structure: *SHELXS97* (Sheldrick, 1997); program(s) used to refine structure: *SHELXL97* (Sheldrick, 1997); molecular graphics: *ORTEPIII* (Burnett & Johnson, 1996); software used to prepare material for publication: *CIFTAB* (Sheldrick, 1997).

Color code for $\text{FeS}_2\text{-Co}$ crystal structure:

Orange: Fe atom

Dark grey: C atom

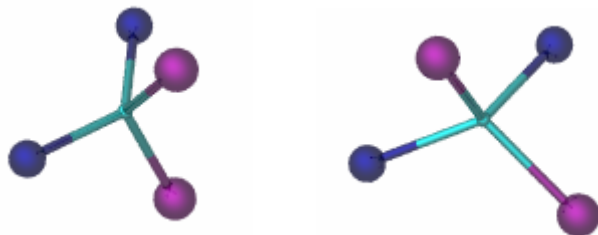
Light grey: H atom

Dark Blue: N atom

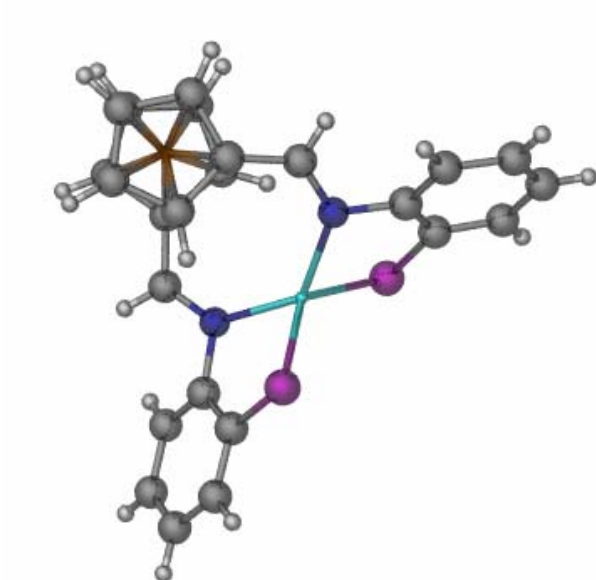
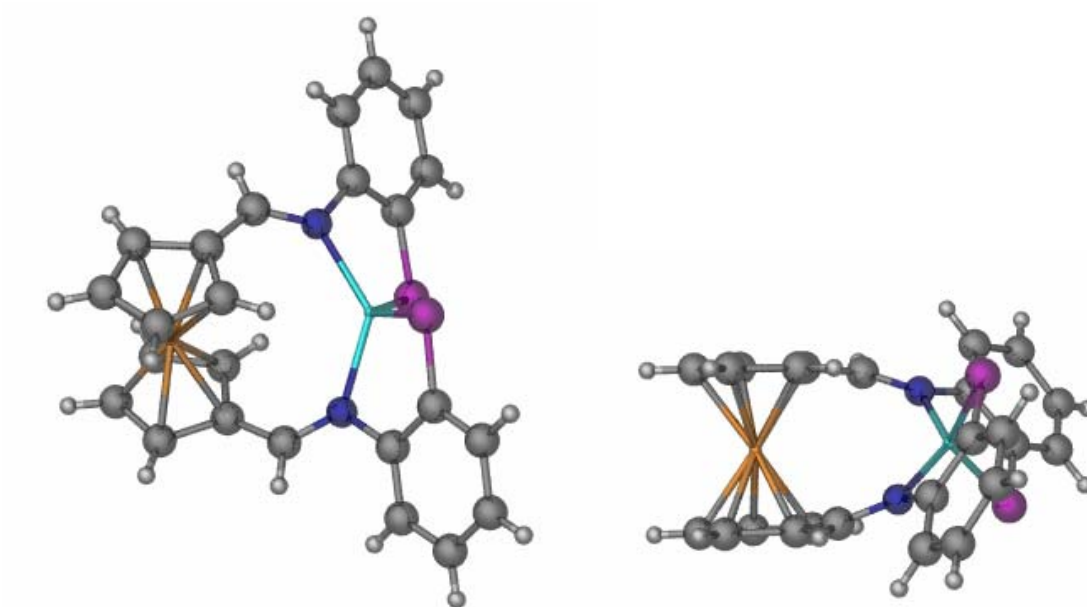
Purple: S atom

Light Blue: Co atom

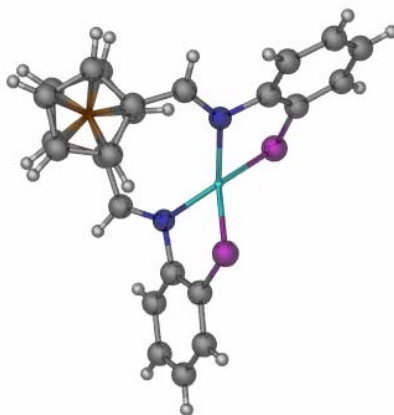
Metal geometry: (tetrahedral)



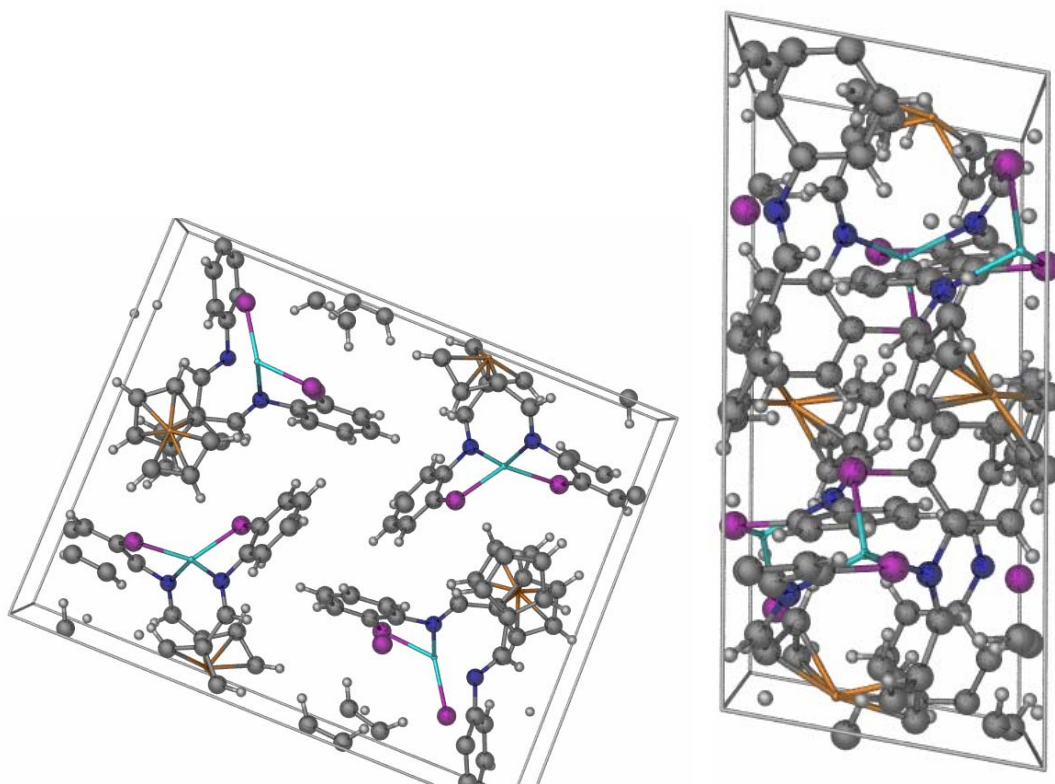
Asymmetric unit structure:

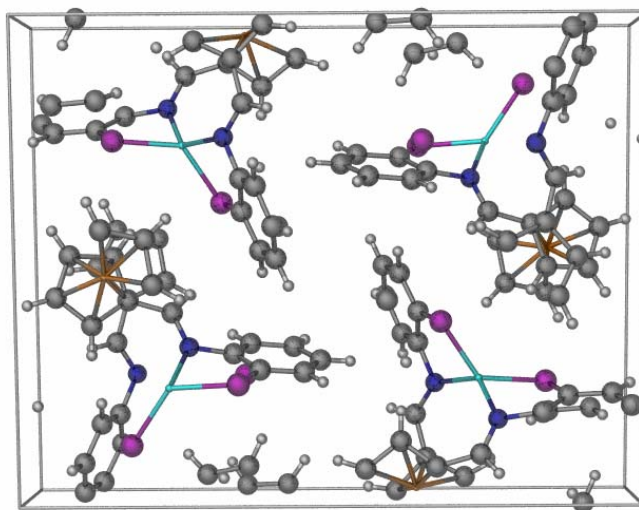


Cp ring overlap:

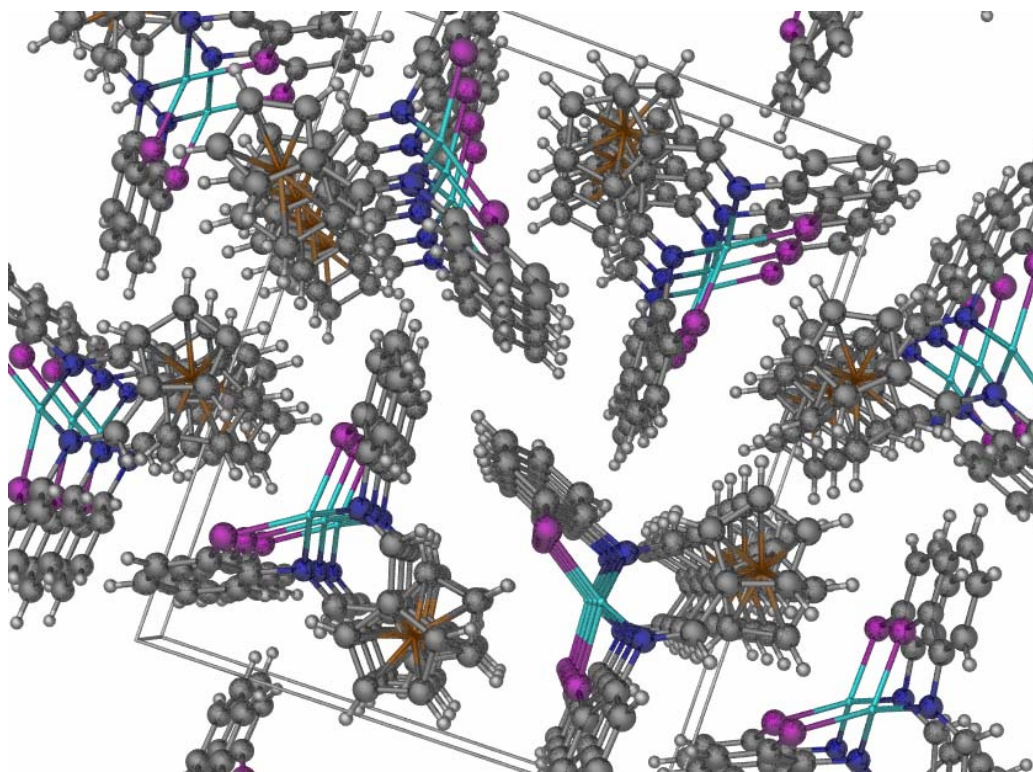


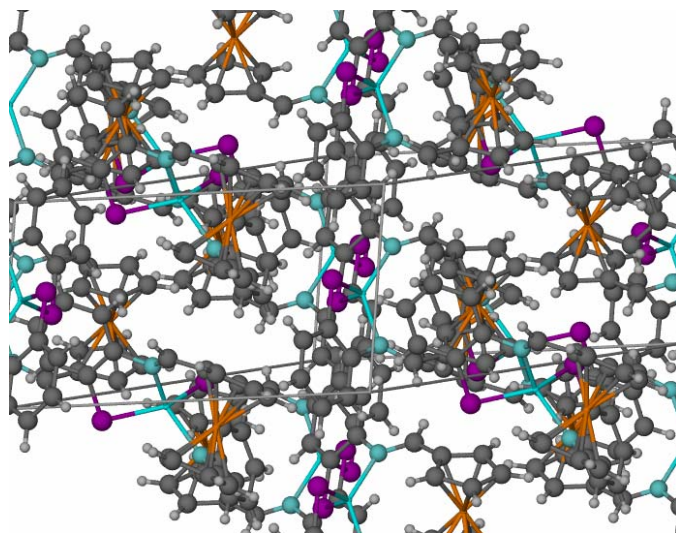
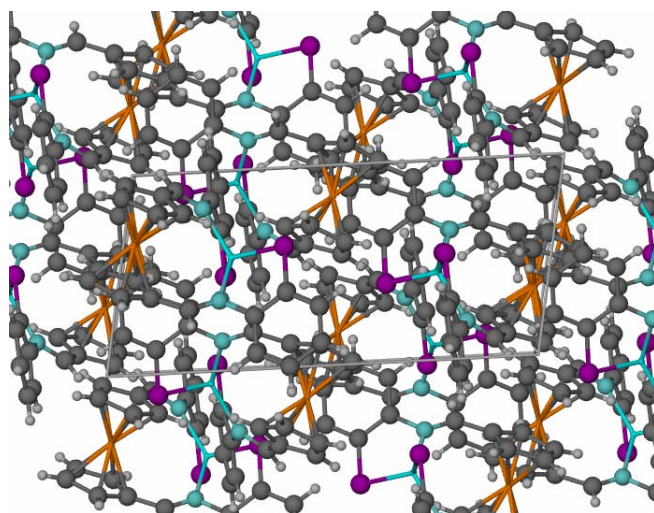
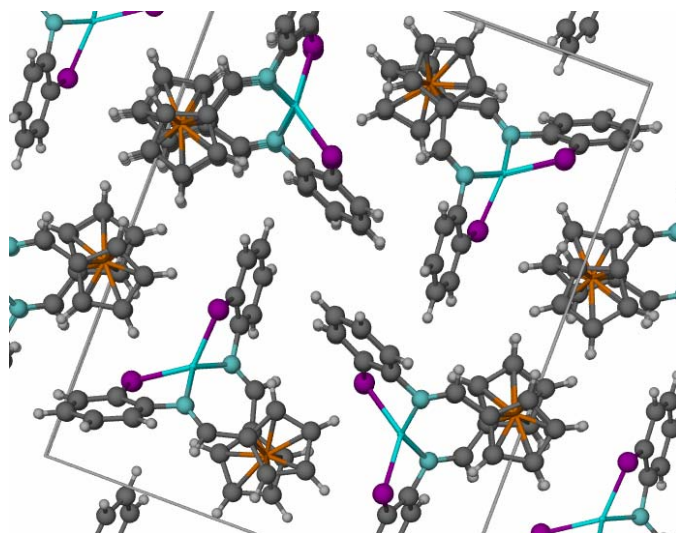
Unit cell:

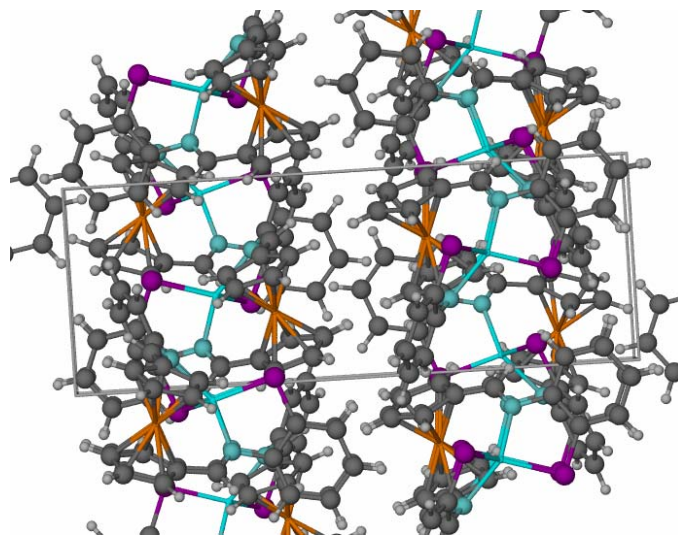




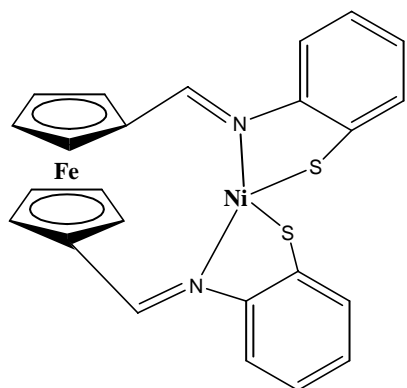
Mass crystal packing:







Compound 24:



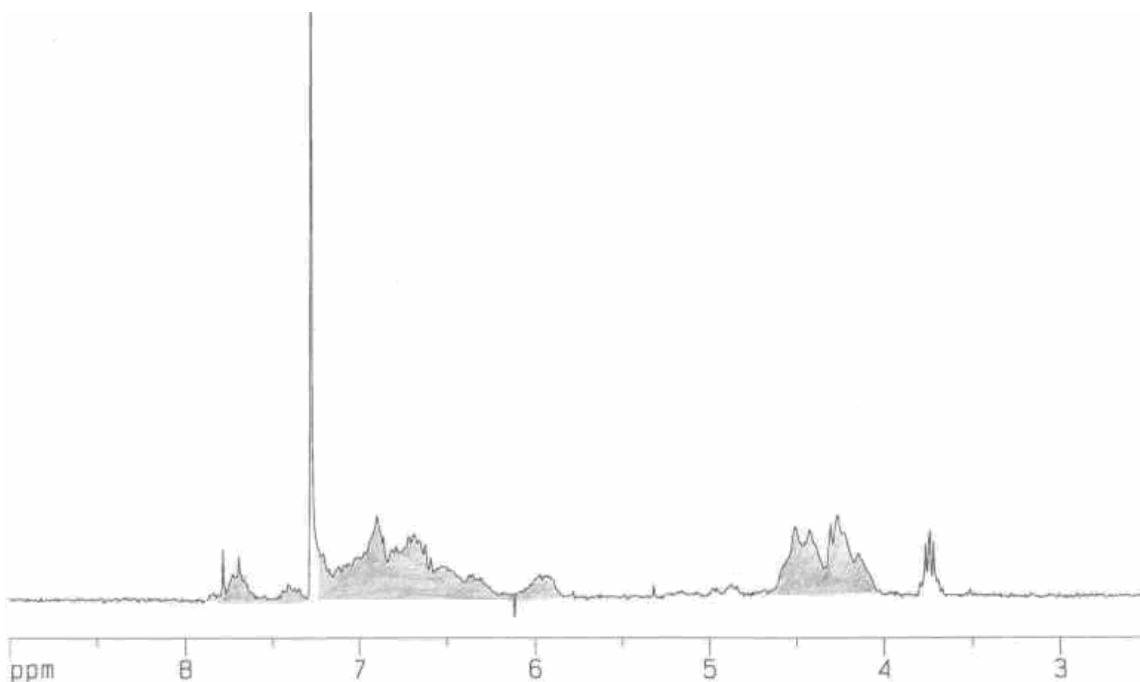


Figure A.88: ^1H NMR spectrum of $\text{FcS}_2\text{-Ni}$ in CDCl_3 : 7.7 ppm (2H, broad s, Cp- $\underline{\text{C}}\text{H}=\text{N}$), 7.2-6.9 ppm (4H, broad m, phenyl), 6.7-6.58 ppm (4H, broad m, phenyl), 4.5-4.41 ppm (4H, broad d, Cp), 4.29-4.14 ppm (4H, broad d, Cp);

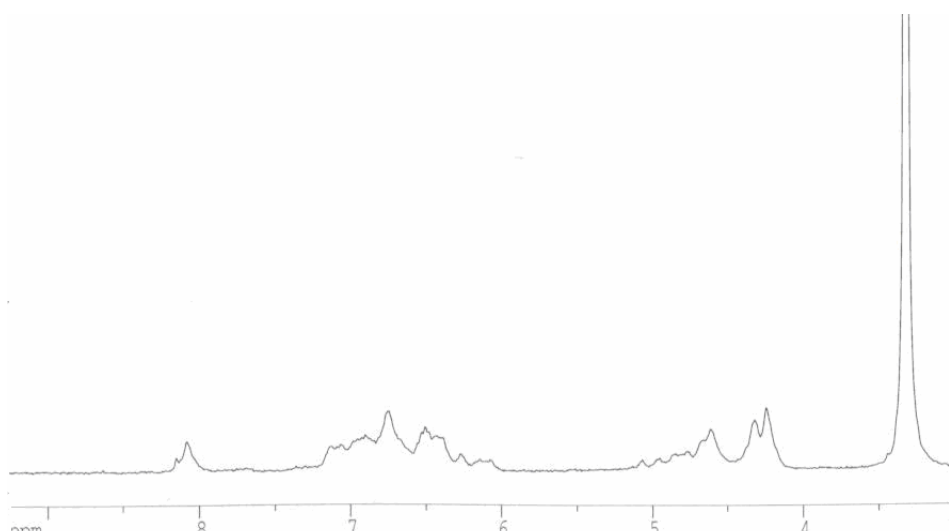


Figure A.89: ^1H NMR spectrum of $\text{FcS}_2\text{-Ni}$ in $d_6\text{-DMSO}$: 8.96 ppm (2H, broad d, Cp- $\underline{\text{C}}\text{H}=\text{N}$), 7.38 ppm (2H, broad d, phenyl), 7.30 ppm (2H, broad d, phenyl), 7.14 ppm (2H, broad m, phenyl), 7.01 ppm (2H, broad m, phenyl), 5.23 ppm (2H, broad d, Cp), 5.17 ppm (2H, broad d, Cp), 4.77 ppm (4H, broad d, Cp);

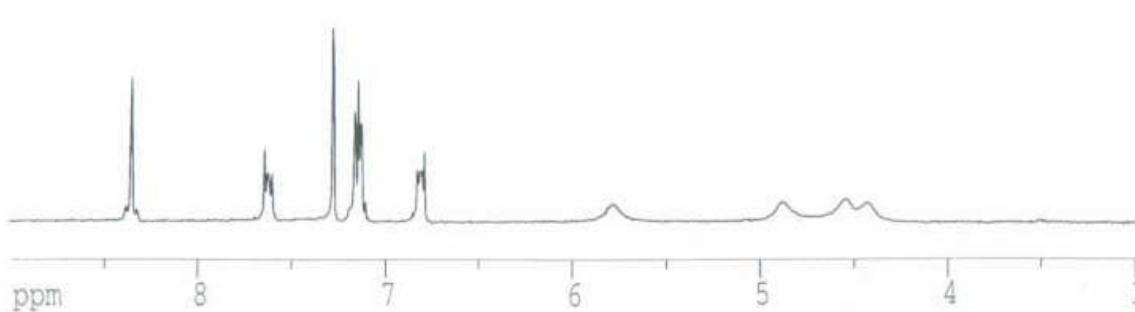


Figure A.90: ^1H NMR spectrum of precipitate from reaction of 24 with $\text{Hg}(\text{CH}_3\text{COO})_2$ in CDCl_3 :

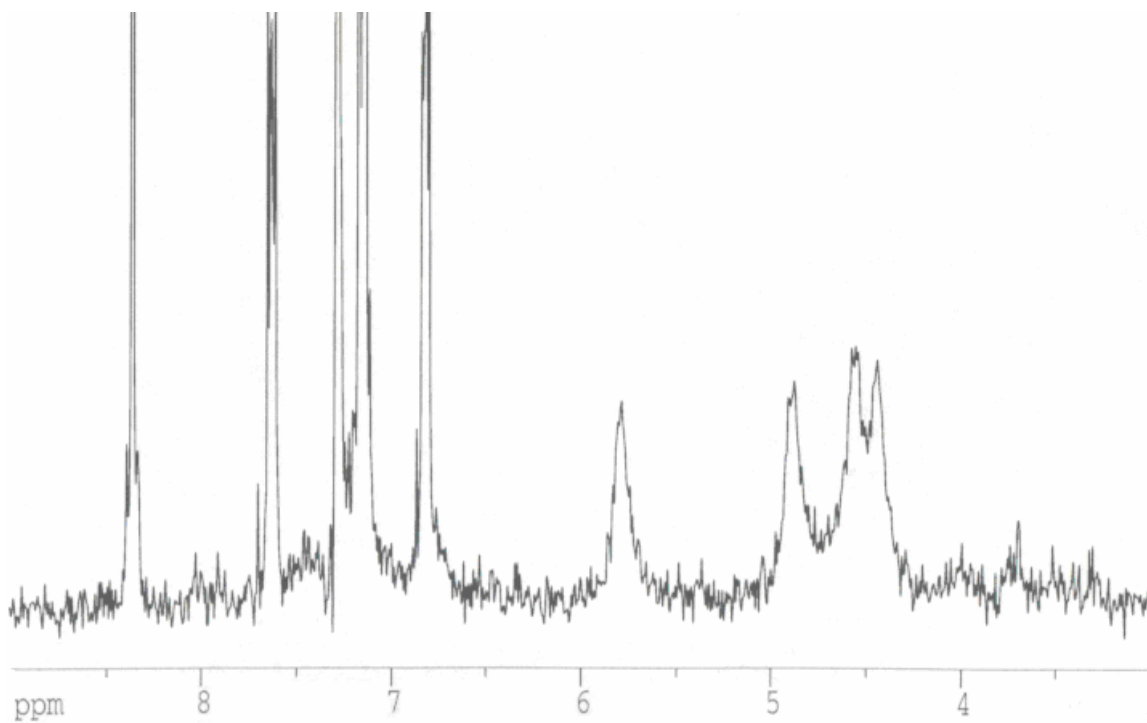


Figure A.91: ^1H NMR spectrum of dried liquid portion from reaction of 24 with $\text{Hg}(\text{CH}_3\text{COO})_2$ in CDCl_3 :

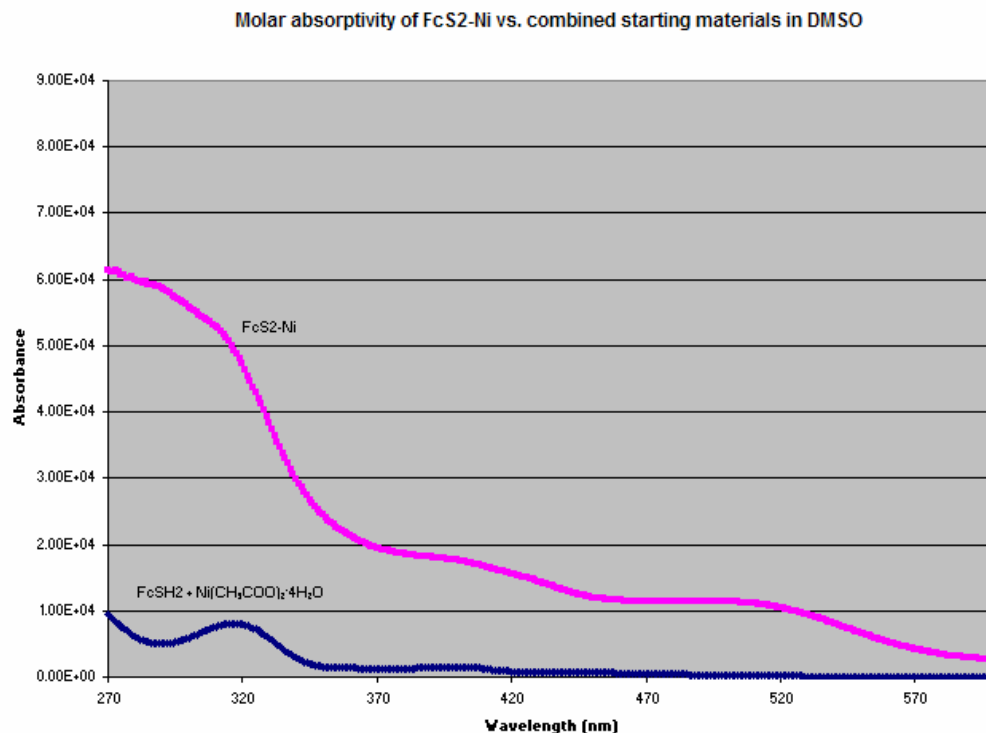


Figure A.92: Comparison between the molar absorptivity (UV-Vis) of FcS2-Ni and the molar absorptivity of the starting materials (317, 402 nm peaks) in DMSO: 495 nm ($11400 \text{ M}^{-1}\text{cm}^{-1}$);

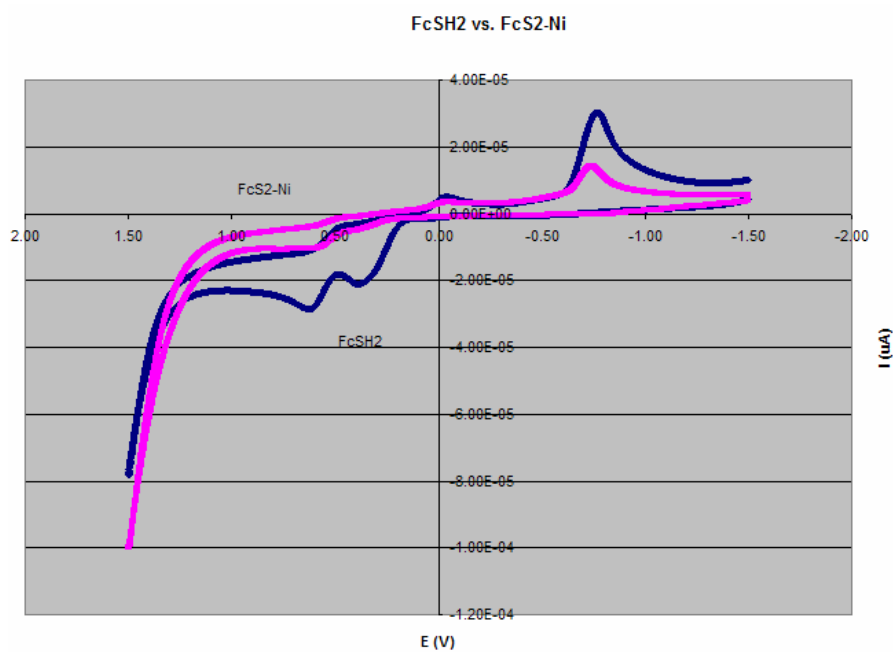


Figure A.93: Comparison between the CV scan of FcS2-Ni and the CV scan of FcSH2 in DMSO, scan rate 100 mV/sec . Fe^{II} to Fe^{III} oxidation peak is at 592 mV .

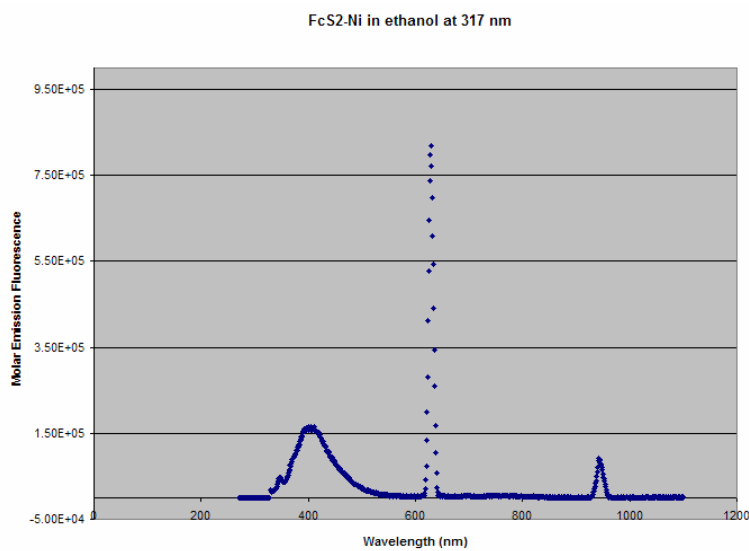
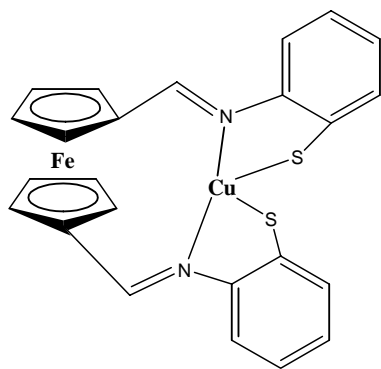


Figure A.94: Emission fluorescence of FcS2-Ni in DMSO at 317 nm with peaks at 347, 404, 629, 942 nm.

Compound 25:



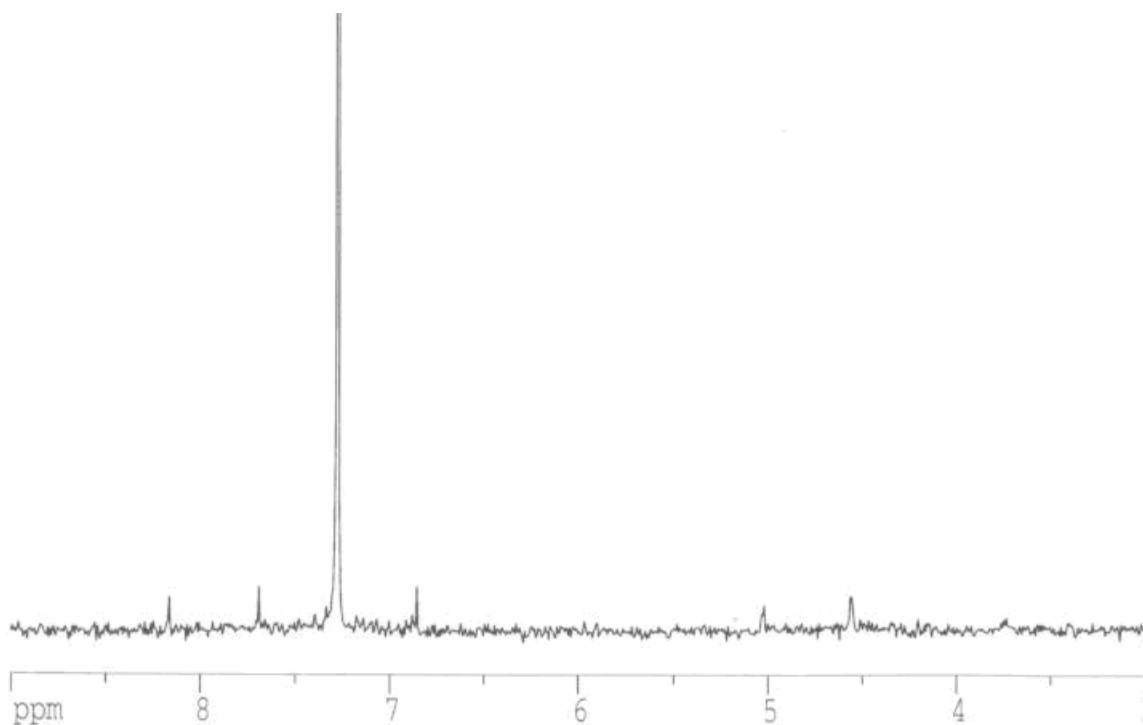


Figure A.95: ^1H NMR spectrum of FcS₂-Cu in CDCl₃: .16 ppm (2H, s, Cp- $\underline{\text{C}}\text{H}=\text{N}$), 7.69 ppm (4H, s, phenyl), 6.85 ppm (4H, s, phenyl), 5.01 ppm (4H, s, Cp), 4.55 ppm (4H, s, Cp);

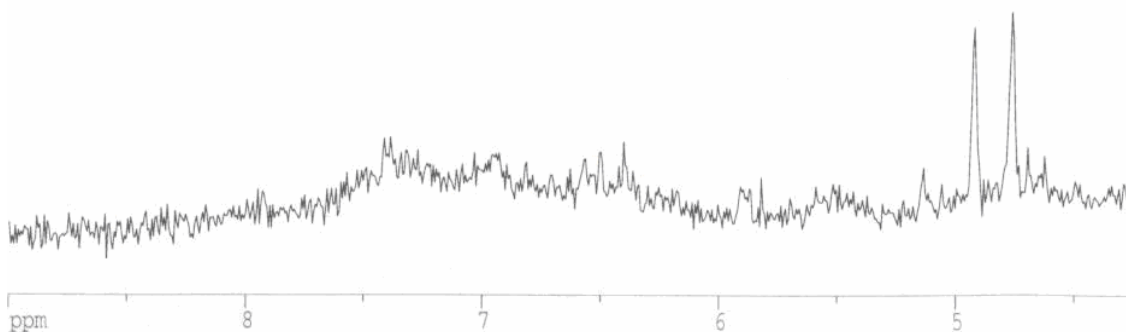


Figure A.96: ^1H NMR spectrum of FcS₂-Cu in d₆-DMSO:): 8.1 ppm (1H, s, Cp- $\underline{\text{C}}\text{H}=\text{N}$), 7.3 ppm (2H, broad d, phenyl), 7.0 ppm (4H, broad s, phenyl), 6.8 ppm (2H, s, phenyl), 4.8 ppm (4H, s, Cp), 4.5 ppm (4H, s, Cp);

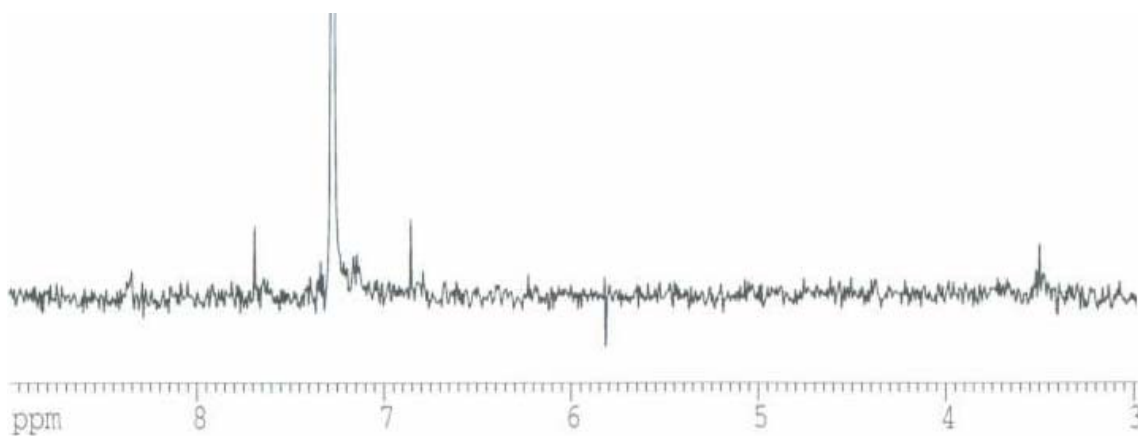


Figure A.97: ^1H NMR spectrum of precipitate from reaction of 25 with $\text{Hg}(\text{CH}_3\text{COO})_2$ in CDCl_3 :

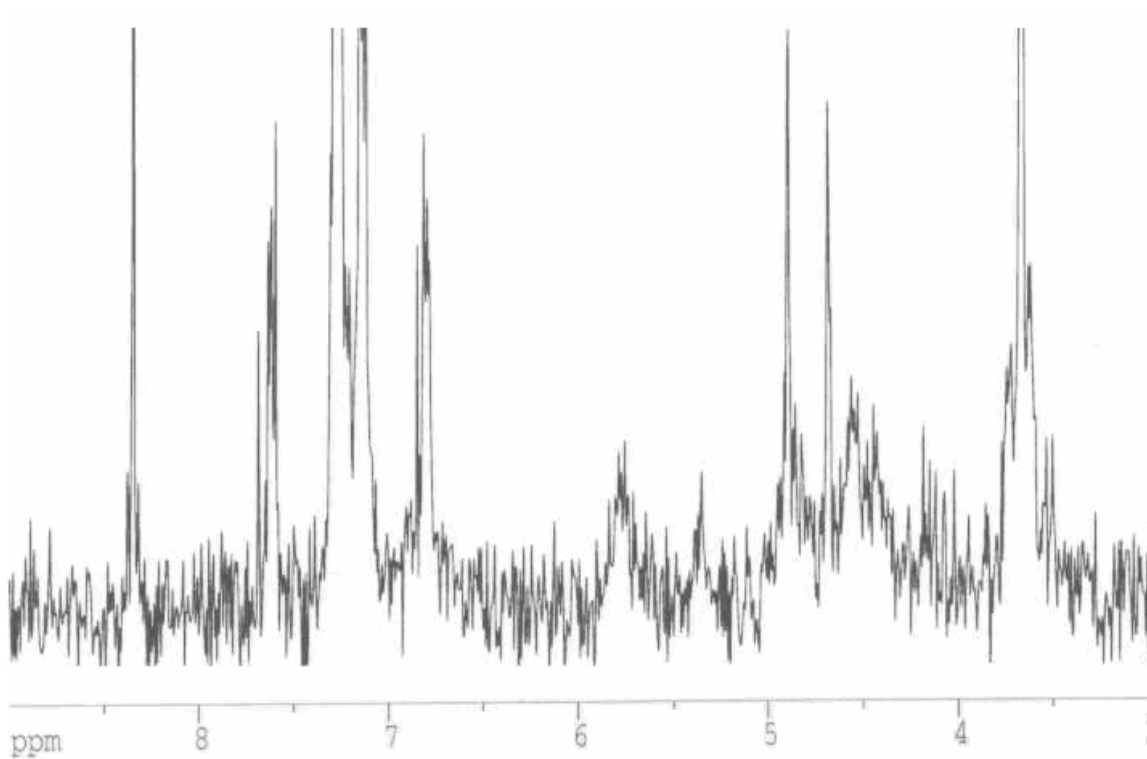


Figure A.98: ^1H NMR spectrum of dried liquid portion from reaction of 25 with $\text{Hg}(\text{CH}_3\text{COO})_2$ in CDCl_3 :

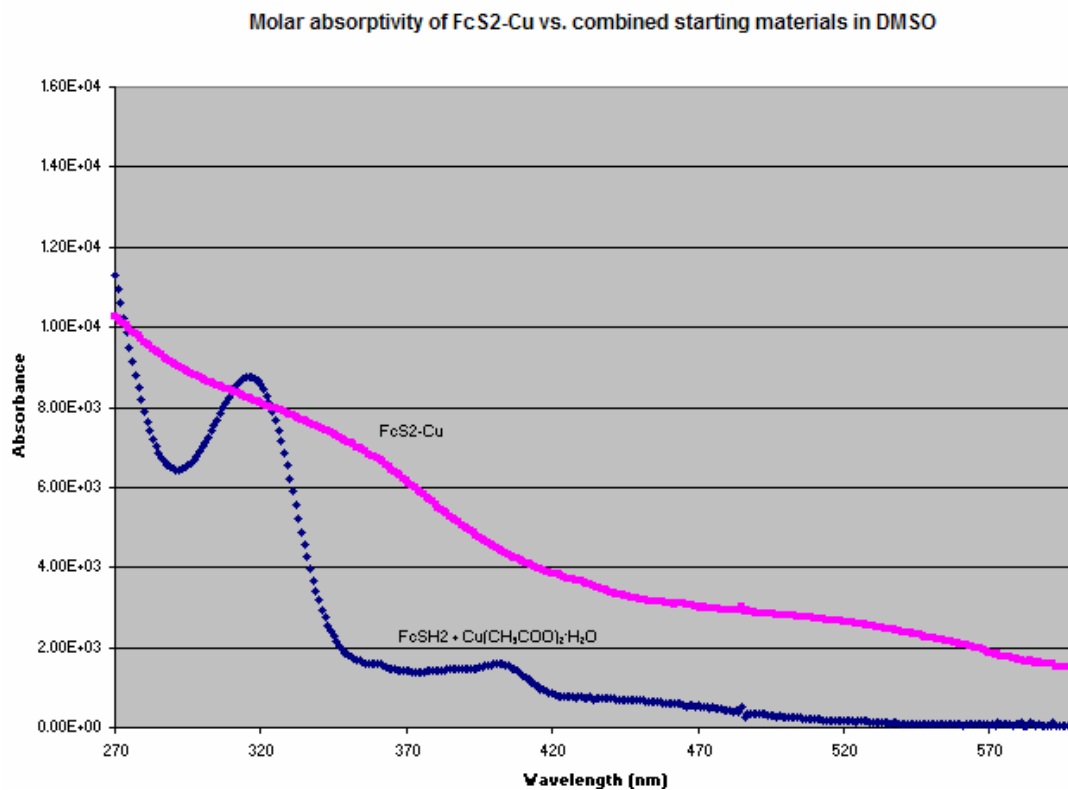


Figure A.99: Comparison between the molar absorptivity (UV-Vis) of Fcs2-Cu and the molar absorptivity of the starting materials (313, 398 nm peaks) in DMSO.

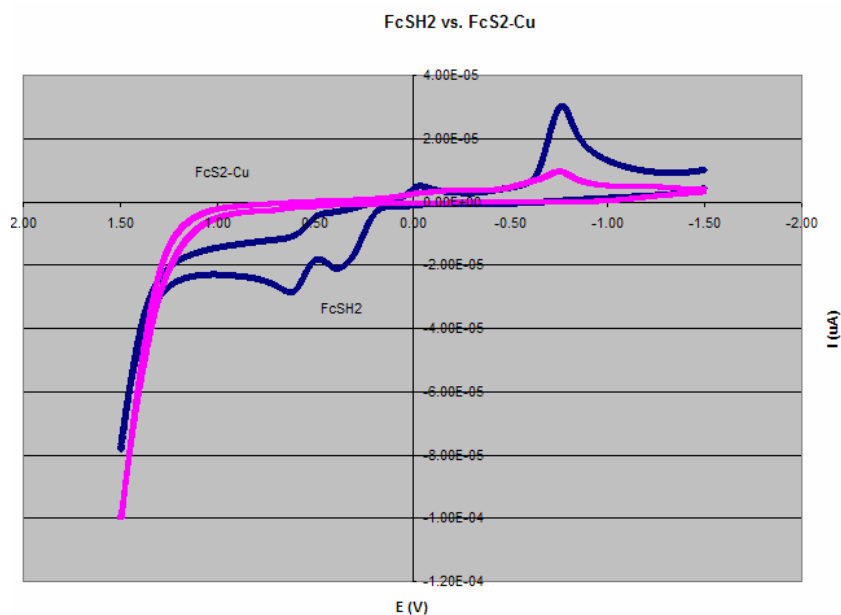


Figure A.100: Comparison between the CV scan of FcS2-Cu and the CV scan of FcSH2 in DMSO, scan rate 100 mV/sec. Fe^{II} to Fe^{III} oxidation does not appear as a peak in the positive direction.

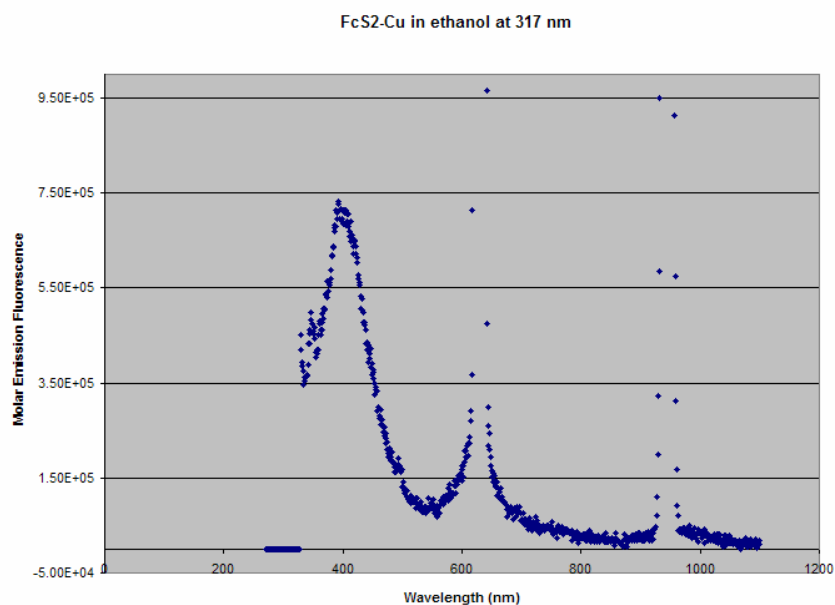


Figure A.101: Emission fluorescence of FcS2-Cu in ethanol at 317 nm with peaks at 393, 629, 943 nm.

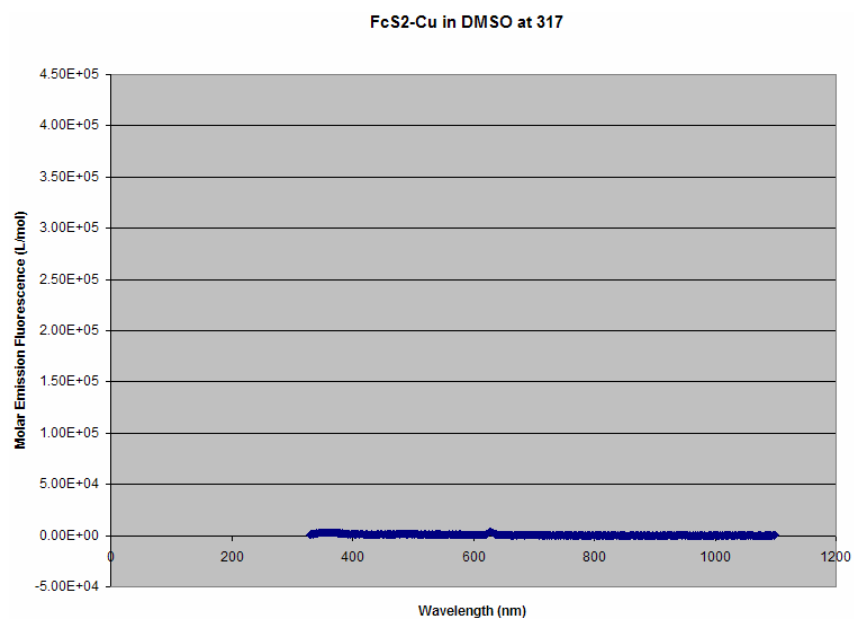


Figure A.102: Emission fluorescence of FcS2-Cu in DMSO at 317 nm with a peak at 629 nm.

Compound 26:

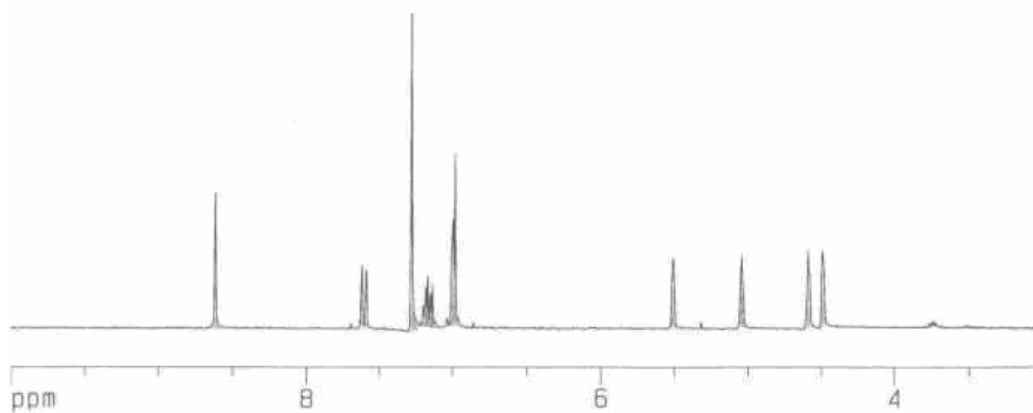
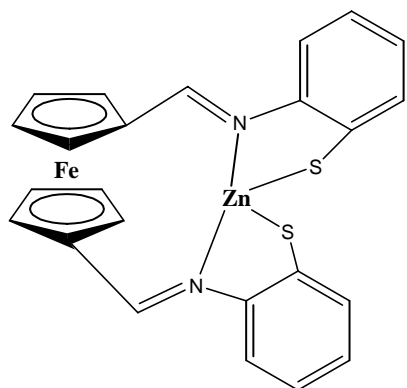


Figure A.103: ^1H NMR spectrum of $\text{FcS}_2\text{-Zn}$ in CDCl_3 : 8.61 ppm (2H, s, Cp- $\text{CH}=\text{N}$), 7.60 ppm (2H, d, phenyl), 7.17-7.12 ppm (2H, t, phenyl), 6.98 ppm (4H, d, phenyl), 5.50 ppm (2H, s, Cp), 5.03 ppm (2H, s, Cp), 4.58 ppm (2H, s, Cp), 4.48 ppm (2H, s, Cp);

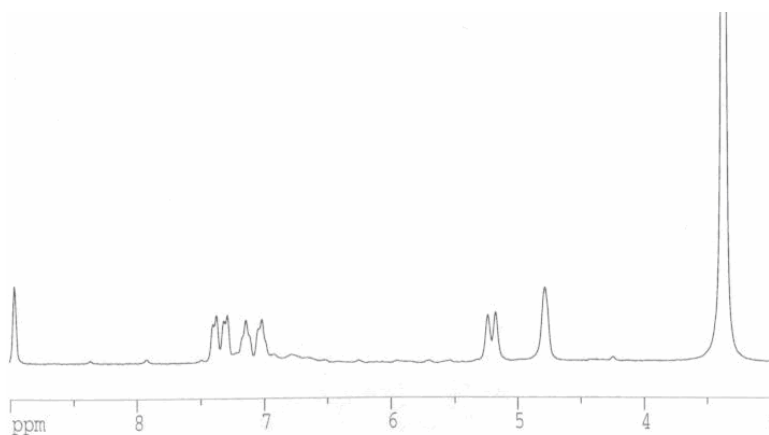


Figure A.104: ^1H NMR spectrum of $\text{FcS}_2\text{-Zn}$ in $d_6\text{-DMSO}$: 8.96 ppm (2H, s, Cp- $\text{CH}=\text{N}$), 7.38 ppm (2H, d, phenyl), 7.30 ppm (2H, d, phenyl), 7.13 ppm (2H, t, phenyl), 7.01 ppm (2H, d, phenyl), 5.22-5.16 ppm (4H, d, Cp), 4.77 ppm (4H, s, Cp);

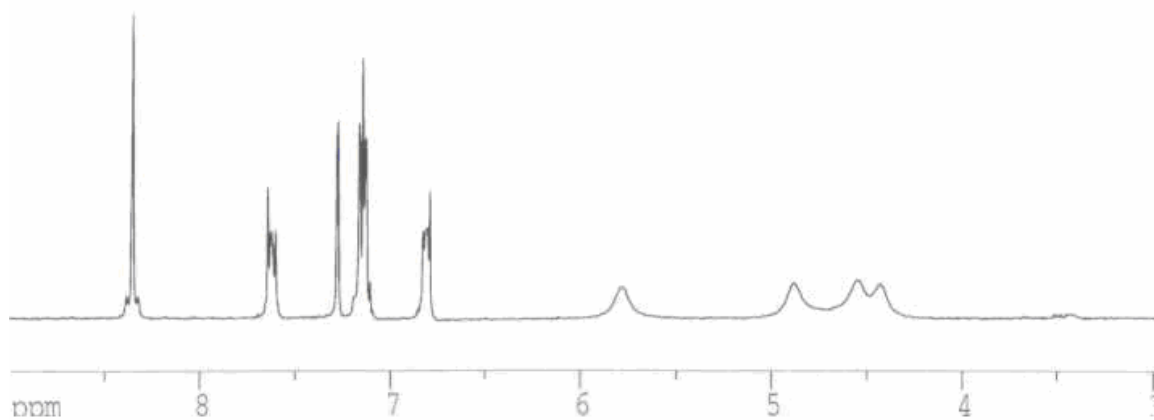


Figure A.105: ^1H NMR spectrum of precipitate from reaction of 26 with $\text{Hg}(\text{CH}_3\text{COO})_2$ in CDCl_3 :

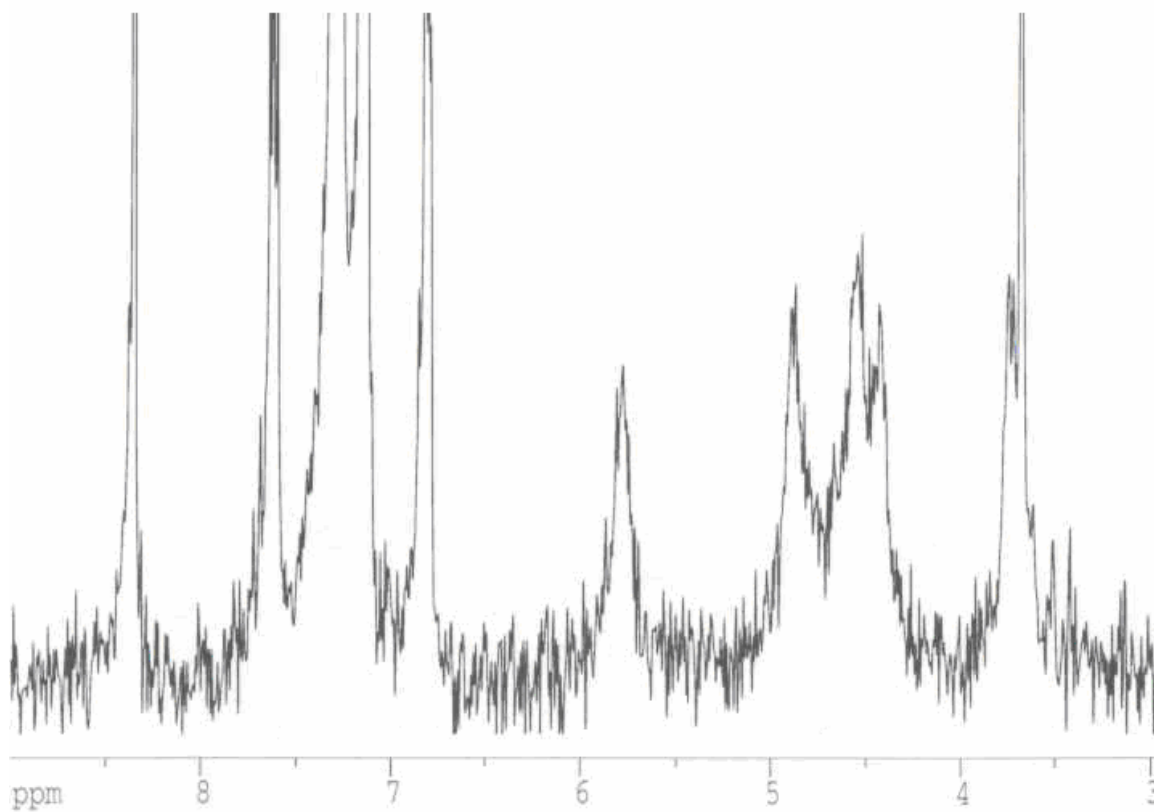


Figure A.106: ^1H NMR spectrum of dried liquid portion from reaction of 26 with $\text{Hg}(\text{CH}_3\text{COO})_2$ in CDCl_3 :

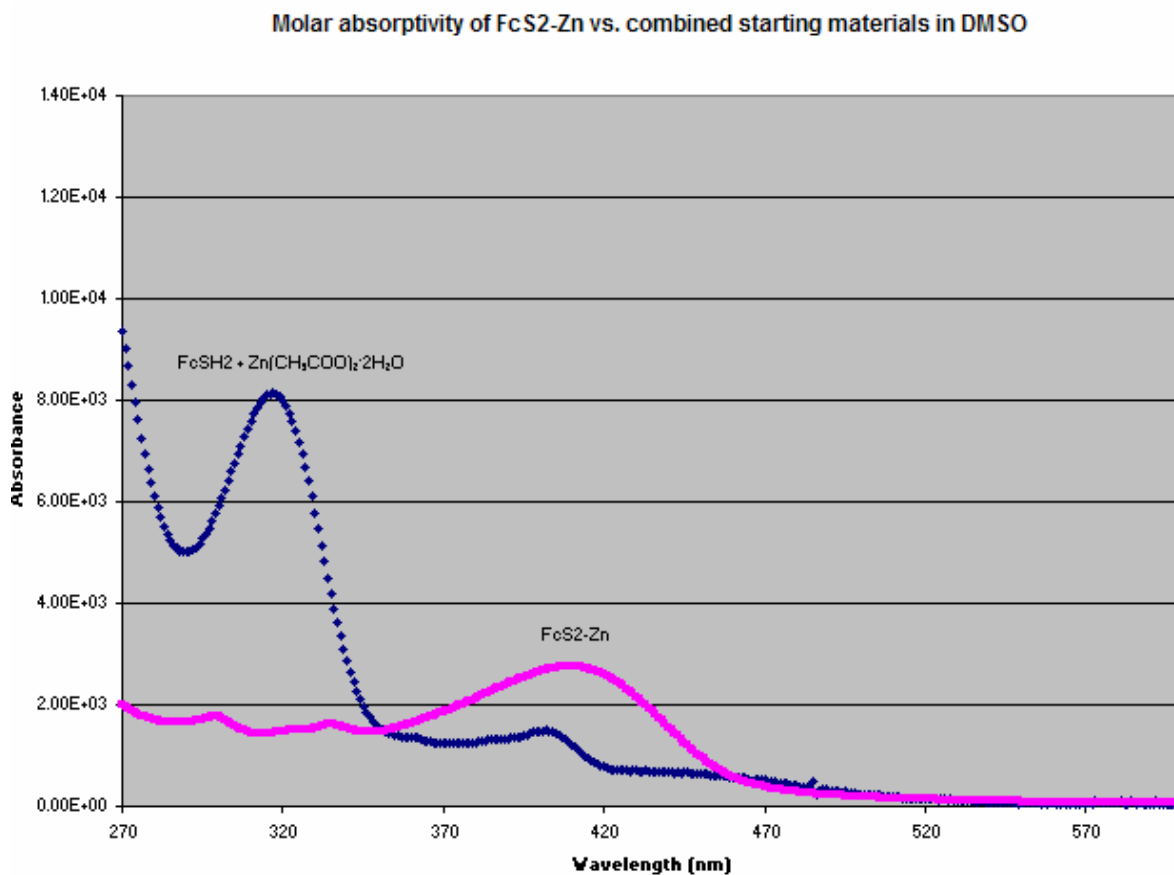


Figure A.107: Comparison between the molar absorptivity (UV-Vis) of FcS2-Zn and the molar absorptivity of the starting materials (317, 402 nm peaks) in DMSO: 299 nm ($1760 \text{ M}^{-1} \text{ cm}^{-1}$), 335 nm ($1600 \text{ M}^{-1} \text{ cm}^{-1}$), 409 nm ($2760 \text{ M}^{-1} \text{ cm}^{-1}$);

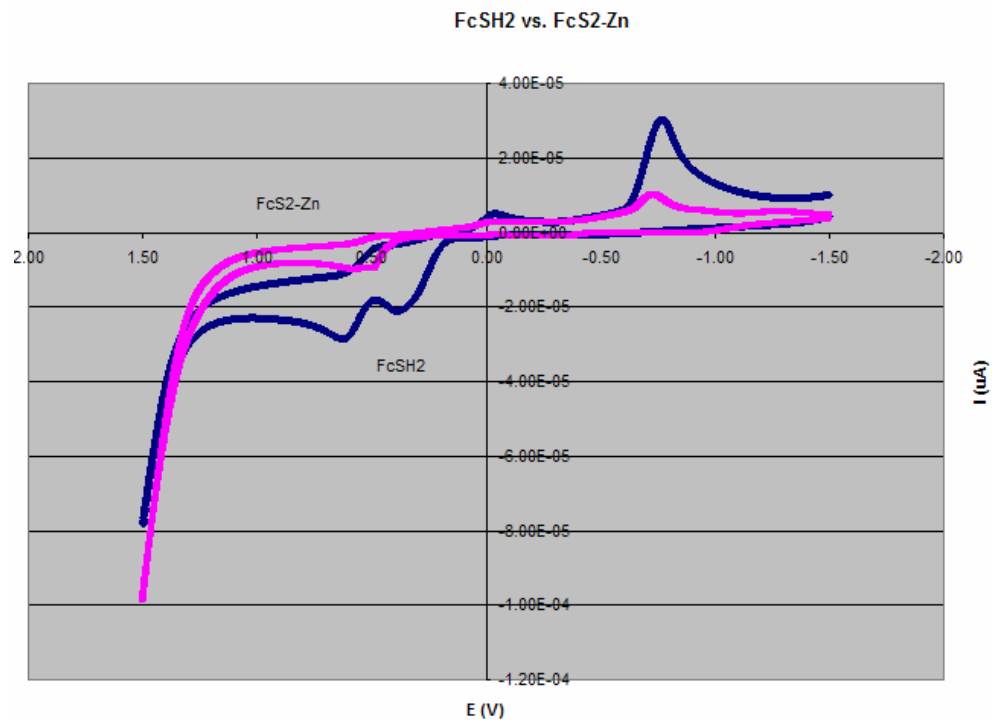


Figure A.108: Comparison between the CV scan of FcS2-Zn and the CV scan of FcSH2 in DMSO, scan rate 100 mV/sec. Fe^{II} to Fe^{III} oxidation peak is at 495 mV.

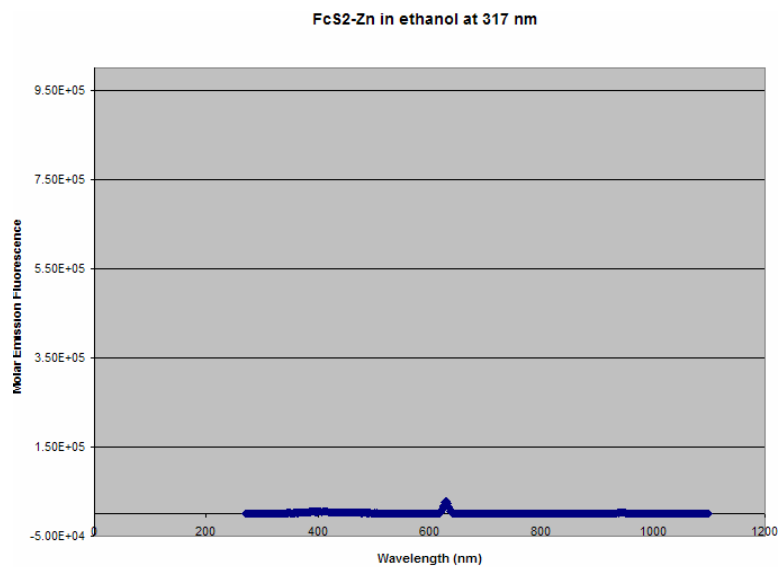


Figure A.109: Emission fluorescence of FcS2-Zn in ethanol at 317 nm with peak at 629 nm.

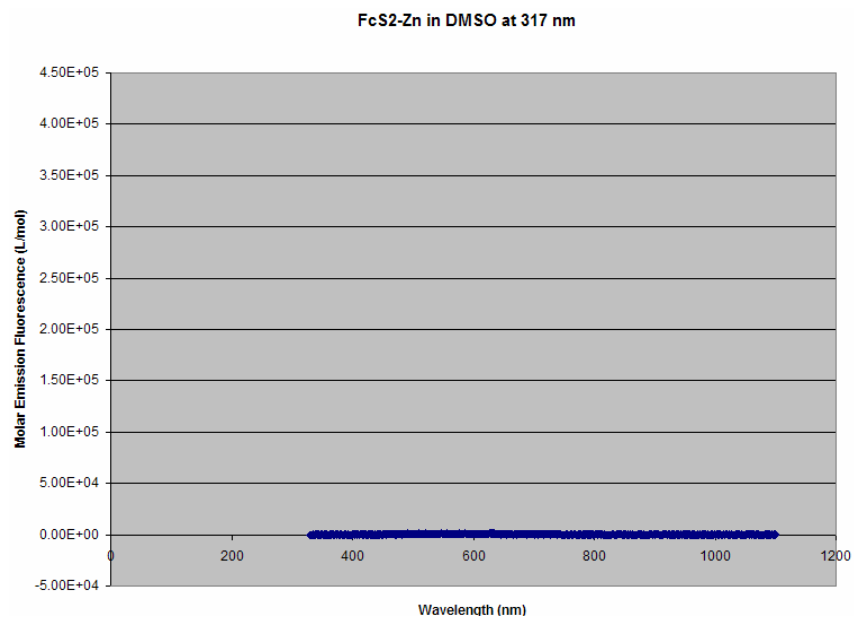


Figure A.110: Emission fluorescence of FcS2-Zn in DMSO at 317 nm with no apparent peaks.

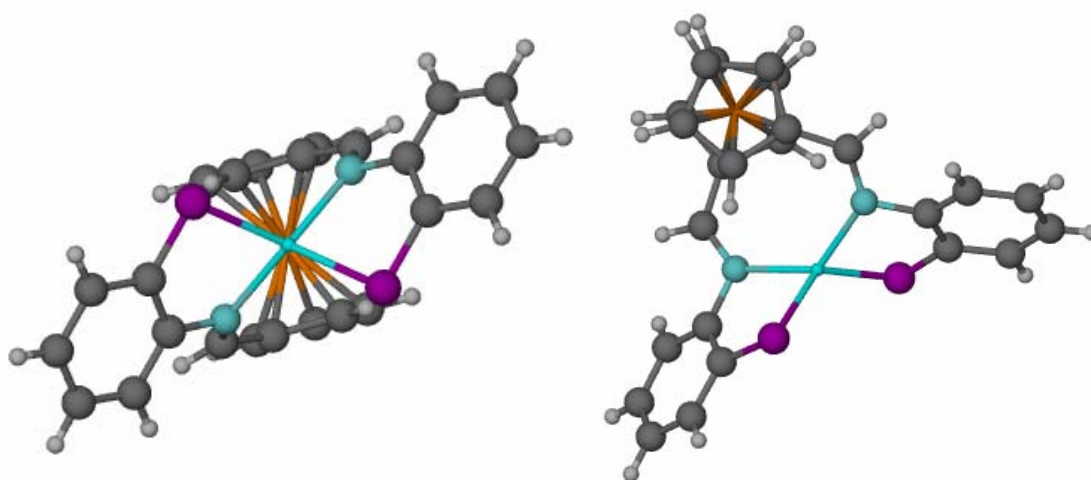


Figure A.111: Crystal Structure of FcS2-Zn

Crystal data

$C_{24}H_{18}FeN_2S_2Zn$

$M_r = 519.74$

Monoclinic, $P2_1/n$

$a = 7.2002 (5) \text{ \AA}$

$b = 19.2667 (12) \text{ \AA}$

$c = 15.2798 (10) \text{ \AA}$

$\beta = 99.7670 (10)^\circ$

$V = 2089.0 (2) \text{ \AA}^3$

$D_x = 1.653 \text{ Mg m}^{-3}$

Mo $K\alpha$ radiation

$\lambda = 0.71073 \text{ \AA}$

Cell parameters from 6068 reflections

$\theta = 2.5\text{--}27.1^\circ$

$\mu = 2.06 \text{ mm}^{-1}$

$T = 173 (2) \text{ K}$

Plate, red

$Z = 4$ $0.35 \times 0.20 \times 0.05$ mm
 $F_{000} = 1056$

Data collection

Bruker SMART CCD area detector diffractometer	14762 measured reflections
	4600 independent reflections
Monochromator: graphite	3688 reflections with $I > 2\sigma(I)$
	$R_{\text{int}} = 0.037$
$T = 173(2)$ K	$\theta_{\text{max}} = 27.1^\circ$
	$\theta_{\text{min}} = 1.7^\circ$
ω scans	$h = -7 \rightarrow 9$
Absorption correction: multi-scan Data were corrected for decay and absorption using the program SADABS (Sheldrick, G. M. (2003). SADABS. Version 2.10. University of Göttingen, Germany).	$k = -24 \rightarrow 24$
$T_{\text{min}} = 0.63, T_{\text{max}} = 0.90$	$l = -19 \rightarrow 19$

Refinement

Refinement on F^2	Secondary atom site location: difference Fourier map
Least-squares matrix: full	Hydrogen site location: inferred from neighbouring sites
$R[F^2 > 2\sigma(F^2)] = 0.032$	H-atom parameters constrained
$wR(F^2) = 0.071$	$w = 1/[\sigma^2(F_o^2) + (0.0285P)^2 + 0.9836P]$
$S = 1.02$	where $P = (F_o^2 + 2F_c^2)/3$
4600 reflections	$(\Delta/\sigma)_{\text{max}} = 0.001$
271 parameters	$\Delta\rho_{\text{max}} = 0.40 \text{ e } \text{Å}^{-3}$
	$\Delta\rho_{\text{min}} = -0.28 \text{ e } \text{Å}^{-3}$
	Extinction correction: none
Primary atom site location: structure-invariant direct methods	

Refinement of F^2 against ALL reflections. The weighted R-factor wR and goodness of fit S are based on F^2 , conventional R-factors R are based on F , with F set to zero for negative F^2 . The threshold expression of $F^2 > 2\sigma(F^2)$ is used only for calculating R-factors(gt) etc. and is not relevant to the choice of reflections for refinement. R-factors based on F^2 are statistically about twice as large as those based on F , and R-factors based on ALL data will be even larger.

Fractional atomic coordinates and isotropic or equivalent isotropic displacement parameters (Å^2)

x	y	Z	$U_{\text{iso}}^*/U_{\text{eq}}$
-----	-----	-----	----------------------------------

Zn1	0.43655 (4)	0.242729 (14)	0.756240 (18)	0.02307 (8)
Fe1	0.34229 (5)	0.139119 (17)	0.52734 (2)	0.02164 (9)
S1	0.39354 (9)	0.17876 (3)	0.87699 (4)	0.02555 (14)
S2	0.52742 (9)	0.35535 (3)	0.74686 (4)	0.02640 (15)
N1	0.6503 (3)	0.17064 (10)	0.74000 (13)	0.0219 (4)
N2	0.1812 (3)	0.27026 (10)	0.67402 (13)	0.0210 (4)
C1	0.6166 (3)	0.15678 (13)	0.57958 (16)	0.0245 (5)
C2	0.6033 (4)	0.10711 (14)	0.50879 (16)	0.0304 (6)
H2	0.6490	0.0608	0.5139	0.036*
C3	0.5107 (4)	0.13904 (15)	0.43029 (17)	0.0332 (6)
H3	0.4831	0.1179	0.3734	0.040*
C4	0.4658 (4)	0.20796 (14)	0.45090 (17)	0.0313 (6)
H4	0.4036	0.2410	0.4100	0.038*
C5	0.5289 (4)	0.21944 (13)	0.54244 (17)	0.0271 (6)
H5	0.5156	0.2612	0.5738	0.032*
C6	0.1115 (3)	0.16999 (12)	0.57840 (15)	0.0210 (5)
C7	0.2057 (3)	0.11398 (12)	0.62955 (16)	0.0233 (5)
H7	0.2584	0.1154	0.6909	0.028*
C8	0.2061 (4)	0.05627 (13)	0.57241 (16)	0.0283 (6)
H8	0.2584	0.0120	0.5890	0.034*
C9	0.1150 (4)	0.07575 (13)	0.48610 (17)	0.0287 (6)
H9	0.0975	0.0469	0.4350	0.034*
C10	0.0550 (3)	0.14530 (12)	0.48926 (16)	0.0244 (5)
H10	-0.0112	0.1712	0.4409	0.029*
C11	0.6850 (3)	0.13830 (13)	0.67102 (16)	0.0246 (5)
H11	0.7632	0.0984	0.6811	0.029*
C12	0.7332 (3)	0.14332 (12)	0.82494 (15)	0.0214 (5)
C13	0.9170 (4)	0.11734 (13)	0.84085 (17)	0.0265 (5)
H13	0.9914	0.1188	0.7951	0.032*
C14	0.9912 (4)	0.08948 (13)	0.92260 (17)	0.0304 (6)

H14	1.1165	0.0721	0.9333	0.037*
C15	0.8819 (4)	0.08697 (14)	0.98872 (17)	0.0316 (6)
H15	0.9316	0.0669	1.0446	0.038*
C16	0.7003 (4)	0.11358 (13)	0.97405 (17)	0.0279 (6)
H16	0.6269	0.1112	1.0201	0.034*
C17	0.6231 (3)	0.14381 (12)	0.89282 (16)	0.0223 (5)
C18	0.0893 (3)	0.24135 (12)	0.60400 (15)	0.0212 (5)
H18	0.0002	0.2690	0.5662	0.025*
C19	0.1413 (3)	0.34199 (12)	0.68877 (15)	0.0211 (5)
C20	-0.0413 (4)	0.36797 (13)	0.67027 (16)	0.0259 (5)
H20	-0.1439	0.3372	0.6525	0.031*
C21	-0.0750 (4)	0.43834 (13)	0.67753 (17)	0.0315 (6)
H21	-0.1998	0.4560	0.6643	0.038*
C22	0.0749 (4)	0.48253 (13)	0.70423 (19)	0.0341 (6)
H22	0.0534	0.5310	0.7073	0.041*
C23	0.2564 (4)	0.45676 (13)	0.72653 (17)	0.0288 (6)
H23	0.3572	0.4879	0.7461	0.035*
C24	0.2940 (3)	0.38599 (12)	0.72076 (15)	0.0218 (5)

Atomic displacement parameters (\AA^2)

	U^{11}	U^{22}	U^{33}	U^{12}	U^{13}	U^{23}
Zn1	0.02383 (16)	0.02132 (15)	0.02320 (15)	0.00271 (12)	0.00151 (12)	-0.00078 (12)
Fe1	0.0251 (2)	0.02098 (17)	0.01881 (17)	0.00102 (14)	0.00376 (14)	-0.00122 (14)
S1	0.0238 (3)	0.0279 (3)	0.0255 (3)	0.0012 (3)	0.0056 (3)	0.0001 (3)
S2	0.0230 (3)	0.0247 (3)	0.0304 (3)	-0.0022 (3)	0.0015 (3)	-0.0015 (3)
N1	0.0216 (11)	0.0231 (10)	0.0207 (10)	0.0006 (9)	0.0025 (8)	-0.0002 (8)
N2	0.0200 (11)	0.0188 (10)	0.0246 (10)	-0.0001 (8)	0.0047 (8)	-0.0010 (8)

C1	0.0205 (13)	0.0306 (13)	0.0230 (13)	0.0028 (10)	0.0057 (10)	-0.0006 (11)
C2	0.0293 (15)	0.0380 (15)	0.0256 (13)	0.0080 (12)	0.0096 (11)	-0.0044 (11)
C3	0.0347 (16)	0.0446 (16)	0.0218 (13)	0.0012 (13)	0.0089 (12)	-0.0035 (12)
C4	0.0304 (15)	0.0384 (15)	0.0262 (14)	-0.0022 (12)	0.0078 (11)	0.0103 (12)
C5	0.0247 (14)	0.0290 (13)	0.0286 (14)	-0.0042 (11)	0.0075 (11)	0.0014 (11)
C6	0.0212 (13)	0.0209 (11)	0.0214 (12)	-0.0038 (10)	0.0052 (10)	-0.0020 (10)
C7	0.0269 (14)	0.0238 (12)	0.0197 (12)	-0.0012 (10)	0.0056 (10)	0.0000 (10)
C8	0.0358 (16)	0.0197 (12)	0.0298 (14)	-0.0015 (11)	0.0069 (12)	-0.0004 (11)
C9	0.0342 (15)	0.0261 (13)	0.0253 (13)	-0.0065 (11)	0.0039 (11)	-0.0065 (11)
C10	0.0251 (14)	0.0242 (12)	0.0223 (12)	-0.0039 (10)	0.0000 (10)	-0.0009 (10)
C11	0.0199 (13)	0.0274 (13)	0.0261 (13)	0.0027 (10)	0.0031 (10)	0.0001 (11)
C12	0.0234 (13)	0.0182 (11)	0.0210 (12)	-0.0032 (10)	-0.0006 (10)	-0.0027 (10)
C13	0.0252 (14)	0.0259 (12)	0.0285 (13)	0.0010 (11)	0.0044 (11)	-0.0009 (11)
C14	0.0261 (14)	0.0286 (13)	0.0345 (15)	0.0054 (11)	-0.0007 (12)	0.0020 (12)
C15	0.0363 (16)	0.0290 (14)	0.0265 (14)	0.0033 (12)	-0.0034 (12)	0.0040 (11)
C16	0.0341 (16)	0.0273 (13)	0.0227 (13)	0.0013 (11)	0.0059 (11)	0.0020 (11)
C17	0.0226 (13)	0.0190 (12)	0.0248 (13)	-0.0030 (10)	0.0030 (10)	-0.0017 (10)
C18	0.0189 (12)	0.0221 (12)	0.0224 (12)	0.0009 (10)	0.0035 (10)	0.0006 (10)
C19	0.0257 (13)	0.0184 (11)	0.0195 (12)	0.0023 (10)	0.0052 (10)	-0.0011 (9)
C20	0.0249 (14)	0.0257 (13)	0.0270 (13)	0.0016 (11)	0.0039 (11)	-0.0008 (11)
C21	0.0298 (15)	0.0300 (14)	0.0347 (15)	0.0103 (12)	0.0052 (12)	-0.0002 (12)
C22	0.0432 (17)	0.0192 (12)	0.0405 (16)	0.0083 (12)	0.0087 (13)	-0.0018 (12)
C23	0.0356 (16)	0.0210 (12)	0.0294 (14)	-0.0008 (11)	0.0043 (12)	-0.0027 (11)
C24	0.0250 (13)	0.0240 (12)	0.0168 (11)	0.0003 (10)	0.0045 (10)	-0.0015 (10)

Table 1

Geometric parameters (Å, °)

Zn1—N2	2.111 (2)	C6—C10	1.435 (3)
Zn1—N1	2.119 (2)	C6—C18	1.446 (3)
Zn1—S2	2.2779 (7)	C7—C8	1.414 (3)

Zn1—S1	2.2831 (7)	C7—H7	0.9500
Fe1—C1	2.030 (3)	C8—C9	1.420 (4)
Fe1—C5	2.037 (3)	C8—H8	0.9500
Fe1—C7	2.040 (2)	C9—C10	1.412 (3)
Fe1—C6	2.041 (2)	C9—H9	0.9500
Fe1—C2	2.043 (3)	C10—H10	0.9500
Fe1—C8	2.053 (2)	C11—H11	0.9500
Fe1—C9	2.053 (3)	C12—C13	1.397 (3)
Fe1—C10	2.055 (3)	C12—C17	1.408 (3)
Fe1—C4	2.065 (3)	C13—C14	1.381 (4)
Fe1—C3	2.068 (3)	C13—H13	0.9500
S1—C17	1.763 (3)	C14—C15	1.382 (4)
S2—C24	1.762 (3)	C14—H14	0.9500
N1—C11	1.285 (3)	C15—C16	1.387 (4)
N1—C12	1.434 (3)	C15—H15	0.9500
N2—C18	1.285 (3)	C16—C17	1.398 (3)
N2—C19	1.437 (3)	C16—H16	0.9500
C1—C5	1.434 (3)	C18—H18	0.9500
C1—C2	1.435 (3)	C19—C20	1.390 (3)
C1—C11	1.445 (3)	C19—C24	1.408 (3)
C2—C3	1.411 (4)	C20—C21	1.385 (3)
C2—H2	0.9500	C20—H20	0.9500
C3—C4	1.415 (4)	C21—C22	1.381 (4)
C3—H3	0.9500	C21—H21	0.9500
C4—C5	1.413 (4)	C22—C23	1.385 (4)
C4—H4	0.9500	C22—H22	0.9500
C5—H5	0.9500	C23—C24	1.396 (3)
C6—C7	1.434 (3)	C23—H23	0.9500
N2—Zn1—N1	132.19 (8)	C3—C4—H4	125.7
N2—Zn1—S2	87.35 (5)	Fe1—C4—H4	127.0
N1—Zn1—S2	113.27 (6)	C4—C5—C1	107.8 (2)

N2—Zn1—S1	113.12 (6)	C4—C5—Fe1	70.95 (15)
N1—Zn1—S1	86.65 (6)	C1—C5—Fe1	69.09 (14)
S2—Zn1—S1	130.15 (3)	C4—C5—H5	126.1
C1—Fe1—C5	41.30 (10)	C1—C5—H5	126.1
C1—Fe1—C7	107.59 (10)	Fe1—C5—H5	125.4
C5—Fe1—C7	119.22 (10)	C7—C6—C10	107.4 (2)
C1—Fe1—C6	127.02 (9)	C7—C6—C18	129.2 (2)
C5—Fe1—C6	107.44 (10)	C10—C6—C18	123.1 (2)
C7—Fe1—C6	41.13 (9)	C7—C6—Fe1	69.43 (14)
C1—Fe1—C2	41.26 (10)	C10—C6—Fe1	70.04 (14)
C5—Fe1—C2	68.92 (11)	C18—C6—Fe1	121.00 (16)
C7—Fe1—C2	127.51 (10)	C8—C7—C6	107.8 (2)
C6—Fe1—C2	165.71 (10)	C8—C7—Fe1	70.26 (14)
C1—Fe1—C8	119.14 (10)	C6—C7—Fe1	69.44 (13)
C5—Fe1—C8	153.69 (10)	C8—C7—H7	126.1
C7—Fe1—C8	40.42 (9)	C6—C7—H7	126.1
C6—Fe1—C8	68.40 (10)	Fe1—C7—H7	125.8
C2—Fe1—C8	108.36 (11)	C7—C8—C9	108.5 (2)
C1—Fe1—C9	153.14 (10)	C7—C8—Fe1	69.33 (14)
C5—Fe1—C9	164.31 (10)	C9—C8—Fe1	69.78 (14)
C7—Fe1—C9	68.35 (10)	C7—C8—H8	125.8
C6—Fe1—C9	68.43 (10)	C9—C8—H8	125.8
C2—Fe1—C9	118.82 (11)	Fe1—C8—H8	126.7
C8—Fe1—C9	40.47 (10)	C10—C9—C8	108.4 (2)
C1—Fe1—C10	165.30 (10)	C10—C9—Fe1	69.98 (14)
C5—Fe1—C10	126.95 (10)	C8—C9—Fe1	69.75 (15)
C7—Fe1—C10	68.75 (10)	C10—C9—H9	125.8
C6—Fe1—C10	41.01 (9)	C8—C9—H9	125.8
C2—Fe1—C10	152.10 (10)	Fe1—C9—H9	126.0
C8—Fe1—C10	67.96 (10)	C9—C10—C6	107.9 (2)
C9—Fe1—C10	40.19 (10)	C9—C10—Fe1	69.83 (15)

C1—Fe1—C4	68.35 (10)	C6—C10—Fe1	68.95 (14)
C5—Fe1—C4	40.28 (10)	C9—C10—H10	126.0
C7—Fe1—C4	153.51 (10)	C6—C10—H10	126.0
C6—Fe1—C4	119.06 (10)	Fe1—C10—H10	126.8
C2—Fe1—C4	67.72 (11)	N1—C11—C1	126.3 (2)
C8—Fe1—C4	164.82 (10)	N1—C11—H11	116.9
C9—Fe1—C4	127.27 (10)	C1—C11—H11	116.9
C10—Fe1—C4	108.18 (10)	C13—C12—C17	120.6 (2)
C1—Fe1—C3	68.43 (10)	C13—C12—N1	121.7 (2)
C5—Fe1—C3	68.05 (11)	C17—C12—N1	117.7 (2)
C7—Fe1—C3	165.00 (10)	C14—C13—C12	120.4 (2)
C6—Fe1—C3	152.71 (10)	C14—C13—H13	119.8
C2—Fe1—C3	40.14 (10)	C12—C13—H13	119.8
C8—Fe1—C3	127.70 (11)	C13—C14—C15	119.6 (2)
C9—Fe1—C3	108.25 (11)	C13—C14—H14	120.2
C10—Fe1—C3	118.77 (10)	C15—C14—H14	120.2
C4—Fe1—C3	40.02 (10)	C14—C15—C16	120.4 (2)
C17—S1—Zn1	93.70 (8)	C14—C15—H15	119.8
C24—S2—Zn1	93.45 (8)	C16—C15—H15	119.8
C11—N1—C12	117.1 (2)	C15—C16—C17	121.3 (2)
C11—N1—Zn1	131.32 (17)	C15—C16—H16	119.4
C12—N1—Zn1	109.50 (14)	C17—C16—H16	119.4
C18—N2—C19	117.3 (2)	C16—C17—C12	117.5 (2)
C18—N2—Zn1	131.28 (16)	C16—C17—S1	120.21 (19)
C19—N2—Zn1	108.98 (14)	C12—C17—S1	122.23 (18)
C5—C1—C2	107.1 (2)	N2—C18—C6	124.9 (2)
C5—C1—C11	130.2 (2)	N2—C18—H18	117.5
C2—C1—C11	122.2 (2)	C6—C18—H18	117.5
C5—C1—Fe1	69.61 (14)	C20—C19—C24	120.6 (2)
C2—C1—Fe1	69.85 (15)	C20—C19—N2	121.4 (2)
C11—C1—Fe1	119.22 (17)	C24—C19—N2	117.9 (2)

C3—C2—C1	108.2 (2)	C21—C20—C19	120.6 (2)
C3—C2—Fe1	70.91 (15)	C21—C20—H20	119.7
C1—C2—Fe1	68.88 (14)	C19—C20—H20	119.7
C3—C2—H2	125.9	C22—C21—C20	119.2 (2)
C1—C2—H2	125.9	C22—C21—H21	120.4
Fe1—C2—H2	125.9	C20—C21—H21	120.4
C2—C3—C4	108.2 (2)	C21—C22—C23	120.6 (2)
C2—C3—Fe1	68.96 (15)	C21—C22—H22	119.7
C4—C3—Fe1	69.88 (14)	C23—C22—H22	119.7
C2—C3—H3	125.9	C22—C23—C24	121.3 (2)
C4—C3—H3	125.9	C22—C23—H23	119.3
Fe1—C3—H3	126.8	C24—C23—H23	119.3
C5—C4—C3	108.7 (2)	C23—C24—C19	117.5 (2)
C5—C4—Fe1	68.77 (14)	C23—C24—S2	120.1 (2)
C3—C4—Fe1	70.10 (15)	C19—C24—S2	122.37 (18)
C5—C4—H4	125.7		
N2—Zn1—S1—C17	158.50 (9)	C9—Fe1—C6—C10	-37.14 (14)
N1—Zn1—S1—C17	23.55 (9)	C4—Fe1—C6—C10	84.54 (16)
S2—Zn1—S1—C17	-94.38 (8)	C3—Fe1—C6—C10	51.0 (3)
N2—Zn1—S2—C24	23.11 (9)	C1—Fe1—C6—C18	50.9 (2)
N1—Zn1—S2—C24	158.50 (9)	C5—Fe1—C6—C18	9.5 (2)
S1—Zn1—S2—C24	-95.26 (8)	C7—Fe1—C6—C18	124.2 (3)
N2—Zn1—N1—C11	14.5 (3)	C2—Fe1—C6—C18	82.4 (5)
S2—Zn1—N1—C11	-94.3 (2)	C8—Fe1—C6—C18	161.9 (2)
S1—Zn1—N1—C11	133.0 (2)	C9—Fe1—C6—C18	-154.4 (2)
N2—Zn1—N1—C12	-148.22 (14)	C10—Fe1—C6—C18	-117.3 (2)
S2—Zn1—N1—C12	103.01 (14)	C4—Fe1—C6—C18	-32.8 (2)
S1—Zn1—N1—C12	-29.67 (14)	C3—Fe1—C6—C18	-66.3 (3)
N1—Zn1—N2—C18	12.7 (3)	C10—C6—C7—C8	-0.1 (3)
S2—Zn1—N2—C18	132.1 (2)	C18—C6—C7—C8	-173.9 (2)
S1—Zn1—N2—C18	-94.9 (2)	Fe1—C6—C7—C8	-60.05 (17)

N1—Zn1—N2—C19	-148.73 (14)	C10—C6—C7—Fe1	59.99 (16)
S2—Zn1—N2—C19	-29.27 (14)	C18—C6—C7—Fe1	-113.8 (3)
S1—Zn1—N2—C19	103.74 (14)	C1—Fe1—C7—C8	-114.56 (16)
C7—Fe1—C1—C5	-114.52 (15)	C5—Fe1—C7—C8	-158.03 (15)
C6—Fe1—C1—C5	-73.16 (17)	C6—Fe1—C7—C8	118.8 (2)
C2—Fe1—C1—C5	118.1 (2)	C2—Fe1—C7—C8	-73.21 (19)
C8—Fe1—C1—C5	-156.99 (14)	C9—Fe1—C7—C8	37.22 (15)
C9—Fe1—C1—C5	168.8 (2)	C10—Fe1—C7—C8	80.54 (16)
C10—Fe1—C1—C5	-41.4 (4)	C4—Fe1—C7—C8	168.8 (2)
C4—Fe1—C1—C5	37.65 (15)	C3—Fe1—C7—C8	-42.4 (5)
C3—Fe1—C1—C5	80.84 (16)	C1—Fe1—C7—C6	126.67 (14)
C5—Fe1—C1—C2	-118.1 (2)	C5—Fe1—C7—C6	83.20 (16)
C7—Fe1—C1—C2	127.39 (15)	C2—Fe1—C7—C6	168.02 (14)
C6—Fe1—C1—C2	168.75 (15)	C8—Fe1—C7—C6	-118.8 (2)
C8—Fe1—C1—C2	84.92 (17)	C9—Fe1—C7—C6	-81.56 (15)
C9—Fe1—C1—C2	50.7 (3)	C10—Fe1—C7—C6	-38.23 (14)
C10—Fe1—C1—C2	-159.5 (4)	C4—Fe1—C7—C6	50.1 (3)
C4—Fe1—C1—C2	-80.44 (16)	C3—Fe1—C7—C6	-161.2 (4)
C3—Fe1—C1—C2	-37.25 (15)	C6—C7—C8—C9	0.6 (3)
C5—Fe1—C1—C11	125.5 (3)	Fe1—C7—C8—C9	-58.98 (18)
C7—Fe1—C1—C11	11.0 (2)	C6—C7—C8—Fe1	59.54 (17)
C6—Fe1—C1—C11	52.3 (2)	C1—Fe1—C8—C7	83.05 (17)
C2—Fe1—C1—C11	-116.4 (3)	C5—Fe1—C8—C7	47.4 (3)
C8—Fe1—C1—C11	-31.5 (2)	C6—Fe1—C8—C7	-38.33 (15)
C9—Fe1—C1—C11	-65.7 (3)	C2—Fe1—C8—C7	126.85 (15)
C10—Fe1—C1—C11	84.1 (4)	C9—Fe1—C8—C7	-120.0 (2)
C4—Fe1—C1—C11	163.1 (2)	C10—Fe1—C8—C7	-82.66 (16)
C3—Fe1—C1—C11	-153.7 (2)	C4—Fe1—C8—C7	-160.7 (4)
C5—C1—C2—C3	0.4 (3)	C3—Fe1—C8—C7	167.25 (15)
C11—C1—C2—C3	172.8 (2)	C1—Fe1—C8—C9	-156.97 (15)
Fe1—C1—C2—C3	60.29 (19)	C5—Fe1—C8—C9	167.4 (2)

C5—C1—C2—Fe1	-59.91 (17)	C7—Fe1—C8—C9	120.0 (2)
C11—C1—C2—Fe1	112.5 (2)	C6—Fe1—C8—C9	81.66 (16)
C1—Fe1—C2—C3	-119.2 (2)	C2—Fe1—C8—C9	-113.17 (16)
C5—Fe1—C2—C3	-80.54 (17)	C10—Fe1—C8—C9	37.32 (15)
C7—Fe1—C2—C3	168.14 (15)	C4—Fe1—C8—C9	-40.7 (5)
C6—Fe1—C2—C3	-158.3 (4)	C3—Fe1—C8—C9	-72.77 (19)
C8—Fe1—C2—C3	127.29 (16)	C7—C8—C9—C10	-0.9 (3)
C9—Fe1—C2—C3	84.37 (18)	Fe1—C8—C9—C10	-59.55 (18)
C10—Fe1—C2—C3	49.9 (3)	C7—C8—C9—Fe1	58.69 (17)
C4—Fe1—C2—C3	-37.06 (16)	C1—Fe1—C9—C10	168.6 (2)
C5—Fe1—C2—C1	38.61 (15)	C5—Fe1—C9—C10	-39.7 (4)
C7—Fe1—C2—C1	-72.71 (18)	C7—Fe1—C9—C10	82.28 (15)
C6—Fe1—C2—C1	-39.1 (5)	C6—Fe1—C9—C10	37.88 (14)
C8—Fe1—C2—C1	-113.56 (15)	C2—Fe1—C9—C10	-155.76 (14)
C9—Fe1—C2—C1	-156.48 (15)	C8—Fe1—C9—C10	119.4 (2)
C10—Fe1—C2—C1	169.04 (19)	C4—Fe1—C9—C10	-72.95 (18)
C4—Fe1—C2—C1	82.09 (16)	C3—Fe1—C9—C10	-113.27 (16)
C3—Fe1—C2—C1	119.2 (2)	C1—Fe1—C9—C8	49.1 (3)
C1—C2—C3—C4	0.0 (3)	C5—Fe1—C9—C8	-159.1 (3)
Fe1—C2—C3—C4	59.02 (19)	C7—Fe1—C9—C8	-37.17 (14)
C1—C2—C3—Fe1	-59.02 (18)	C6—Fe1—C9—C8	-81.57 (16)
C1—Fe1—C3—C2	38.27 (16)	C2—Fe1—C9—C8	84.79 (17)
C5—Fe1—C3—C2	82.90 (17)	C10—Fe1—C9—C8	-119.4 (2)
C7—Fe1—C3—C2	-39.0 (5)	C4—Fe1—C9—C8	167.60 (15)
C6—Fe1—C3—C2	168.5 (2)	C3—Fe1—C9—C8	127.28 (15)
C8—Fe1—C3—C2	-72.6 (2)	C8—C9—C10—C6	0.8 (3)
C9—Fe1—C3—C2	-113.35 (17)	Fe1—C9—C10—C6	-58.59 (17)
C10—Fe1—C3—C2	-155.90 (15)	C8—C9—C10—Fe1	59.40 (18)
C4—Fe1—C3—C2	119.9 (2)	C7—C6—C10—C9	-0.5 (3)
C1—Fe1—C3—C4	-81.59 (17)	C18—C6—C10—C9	173.8 (2)
C5—Fe1—C3—C4	-36.97 (16)	Fe1—C6—C10—C9	59.14 (17)

C7—Fe1—C3—C4	-158.9 (4)	C7—C6—C10—Fe1	-59.60 (16)
C6—Fe1—C3—C4	48.6 (3)	C18—C6—C10—Fe1	114.7 (2)
C2—Fe1—C3—C4	-119.9 (2)	C1—Fe1—C10—C9	-159.4 (4)
C8—Fe1—C3—C4	167.53 (16)	C5—Fe1—C10—C9	167.53 (15)
C9—Fe1—C3—C4	126.79 (16)	C7—Fe1—C10—C9	-81.19 (15)
C10—Fe1—C3—C4	84.23 (18)	C6—Fe1—C10—C9	-119.5 (2)
C2—C3—C4—C5	-0.4 (3)	C2—Fe1—C10—C9	50.2 (3)
Fe1—C3—C4—C5	58.07 (18)	C8—Fe1—C10—C9	-37.57 (14)
C2—C3—C4—Fe1	-58.45 (19)	C4—Fe1—C10—C9	126.79 (15)
C1—Fe1—C4—C5	-38.57 (15)	C3—Fe1—C10—C9	84.46 (17)
C7—Fe1—C4—C5	47.6 (3)	C1—Fe1—C10—C6	-39.8 (4)
C6—Fe1—C4—C5	82.79 (17)	C5—Fe1—C10—C6	-72.94 (17)
C2—Fe1—C4—C5	-83.23 (17)	C7—Fe1—C10—C6	38.34 (13)
C8—Fe1—C4—C5	-161.1 (4)	C2—Fe1—C10—C6	169.8 (2)
C9—Fe1—C4—C5	166.73 (15)	C8—Fe1—C10—C6	81.97 (15)
C10—Fe1—C4—C5	126.23 (15)	C9—Fe1—C10—C6	119.5 (2)
C3—Fe1—C4—C5	-120.4 (2)	C4—Fe1—C10—C6	-113.67 (15)
C1—Fe1—C4—C3	81.82 (17)	C3—Fe1—C10—C6	-156.00 (14)
C5—Fe1—C4—C3	120.4 (2)	C12—N1—C11—C1	-179.9 (2)
C7—Fe1—C4—C3	167.9 (2)	Zn1—N1—C11—C1	18.5 (4)
C6—Fe1—C4—C3	-156.82 (15)	C5—C1—C11—N1	13.4 (4)
C2—Fe1—C4—C3	37.16 (16)	C2—C1—C11—N1	-157.2 (3)
C8—Fe1—C4—C3	-40.7 (5)	Fe1—C1—C11—N1	-73.8 (3)
C9—Fe1—C4—C3	-72.9 (2)	C11—N1—C12—C13	39.9 (3)
C10—Fe1—C4—C3	-113.38 (16)	Zn1—N1—C12—C13	-154.62 (19)
C3—C4—C5—C1	0.6 (3)	C11—N1—C12—C17	-140.5 (2)
Fe1—C4—C5—C1	59.50 (17)	Zn1—N1—C12—C17	25.0 (2)
C3—C4—C5—Fe1	-58.89 (19)	C17—C12—C13—C14	2.3 (4)
C2—C1—C5—C4	-0.6 (3)	N1—C12—C13—C14	-178.1 (2)
C11—C1—C5—C4	-172.2 (3)	C12—C13—C14—C15	0.4 (4)
Fe1—C1—C5—C4	-60.67 (18)	C13—C14—C15—C16	-1.4 (4)

C2—C1—C5—Fe1	60.07 (17)	C14—C15—C16—C17	-0.3 (4)
C11—C1—C5—Fe1	-111.6 (3)	C15—C16—C17—C12	2.9 (4)
C1—Fe1—C5—C4	118.6 (2)	C15—C16—C17—S1	-178.7 (2)
C7—Fe1—C5—C4	-157.84 (15)	C13—C12—C17—C16	-3.9 (3)
C6—Fe1—C5—C4	-114.64 (16)	N1—C12—C17—C16	176.5 (2)
C2—Fe1—C5—C4	80.01 (16)	C13—C12—C17—S1	177.78 (18)
C8—Fe1—C5—C4	169.0 (2)	N1—C12—C17—S1	-1.9 (3)
C9—Fe1—C5—C4	-42.5 (4)	Zn1—S1—C17—C16	162.36 (19)
C10—Fe1—C5—C4	-73.52 (18)	Zn1—S1—C17—C12	-19.4 (2)
C3—Fe1—C5—C4	36.73 (16)	C19—N2—C18—C6	179.8 (2)
C7—Fe1—C5—C1	83.57 (16)	Zn1—N2—C18—C6	19.6 (4)
C6—Fe1—C5—C1	126.77 (14)	C7—C6—C18—N2	13.2 (4)
C2—Fe1—C5—C1	-38.58 (14)	C10—C6—C18—N2	-159.7 (2)
C8—Fe1—C5—C1	50.4 (3)	Fe1—C6—C18—N2	-74.5 (3)
C9—Fe1—C5—C1	-161.1 (3)	C18—N2—C19—C20	39.1 (3)
C10—Fe1—C5—C1	167.89 (14)	Zn1—N2—C19—C20	-156.50 (19)
C4—Fe1—C5—C1	-118.6 (2)	C18—N2—C19—C24	-139.4 (2)
C3—Fe1—C5—C1	-81.86 (16)	Zn1—N2—C19—C24	25.0 (2)
C1—Fe1—C6—C7	-73.26 (17)	C24—C19—C20—C21	4.2 (4)
C5—Fe1—C6—C7	-114.72 (15)	N2—C19—C20—C21	-174.3 (2)
C2—Fe1—C6—C7	-41.8 (5)	C19—C20—C21—C22	-0.6 (4)
C8—Fe1—C6—C7	37.68 (14)	C20—C21—C22—C23	-2.2 (4)
C9—Fe1—C6—C7	81.35 (15)	C21—C22—C23—C24	1.5 (4)
C10—Fe1—C6—C7	118.49 (19)	C22—C23—C24—C19	1.9 (4)
C4—Fe1—C6—C7	-156.97 (14)	C22—C23—C24—S2	178.3 (2)
C3—Fe1—C6—C7	169.5 (2)	C20—C19—C24—C23	-4.7 (3)
C1—Fe1—C6—C10	168.25 (14)	N2—C19—C24—C23	173.8 (2)
C5—Fe1—C6—C10	126.79 (14)	C20—C19—C24—S2	178.96 (18)
C7—Fe1—C6—C10	-118.49 (19)	N2—C19—C24—S2	-2.5 (3)
C2—Fe1—C6—C10	-160.3 (4)	Zn1—S2—C24—C23	165.24 (19)
C8—Fe1—C6—C10	-80.81 (15)	Zn1—S2—C24—C19	-18.5 (2)

All esds (except the esd in the dihedral angle between two l.s. planes) are estimated using the full covariance matrix. The cell esds are taken into account individually in the estimation of esds in distances, angles and torsion angles; correlations between esds in cell parameters are only used when they are defined by crystal symmetry. An approximate (isotropic) treatment of cell esds is used for estimating esds involving l.s. planes.

Data collection: *SMART* (Bruker, 1998); cell refinement: *SAINT* (Bruker, 1998); data reduction: *SAINT* (Bruker, 1998); program(s) used to solve structure: *SHELXS97* (Sheldrick, 1997); program(s) used to refine structure: *SHELXL97* (Sheldrick, 1997); molecular graphics: *ORTEP*III (Burnett & Johnson, 1996); software used to prepare material for publication: *CIFTAB* (Sheldrick, 1997).

Color code for FeS₂-Zn crystal structure:

Orange: Fe atom

Dark grey: C atom

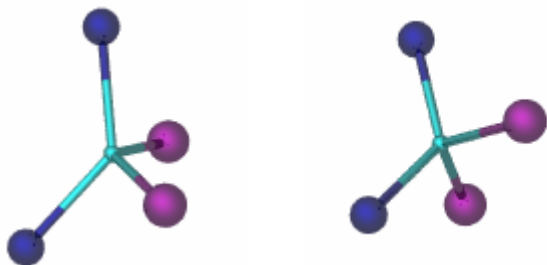
Light grey: H atom

Dark Blue: N atom

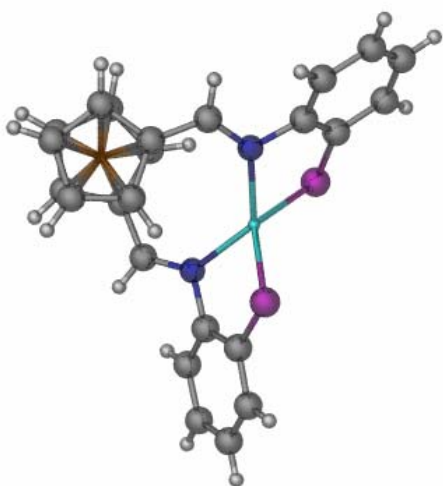
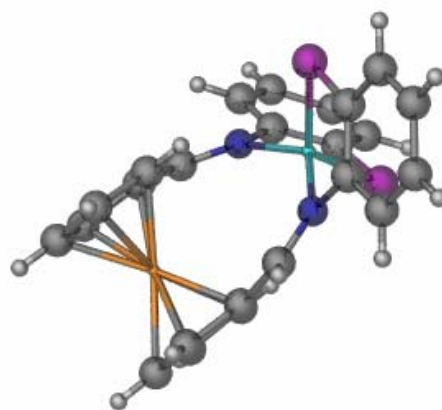
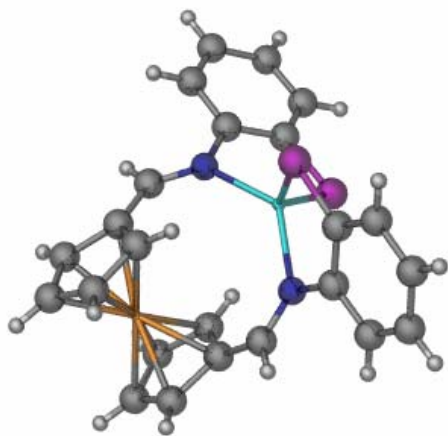
Purple: S atom

Light Blue: Zn atom

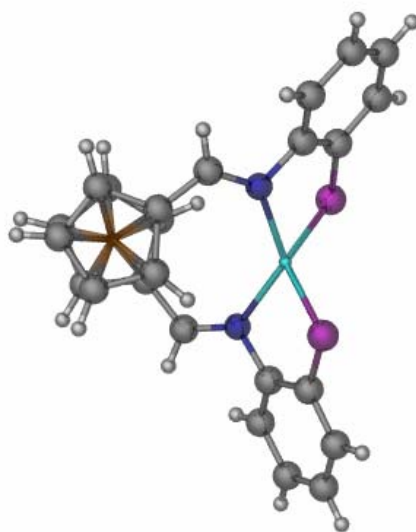
Metal geometry: (tetrahedral)



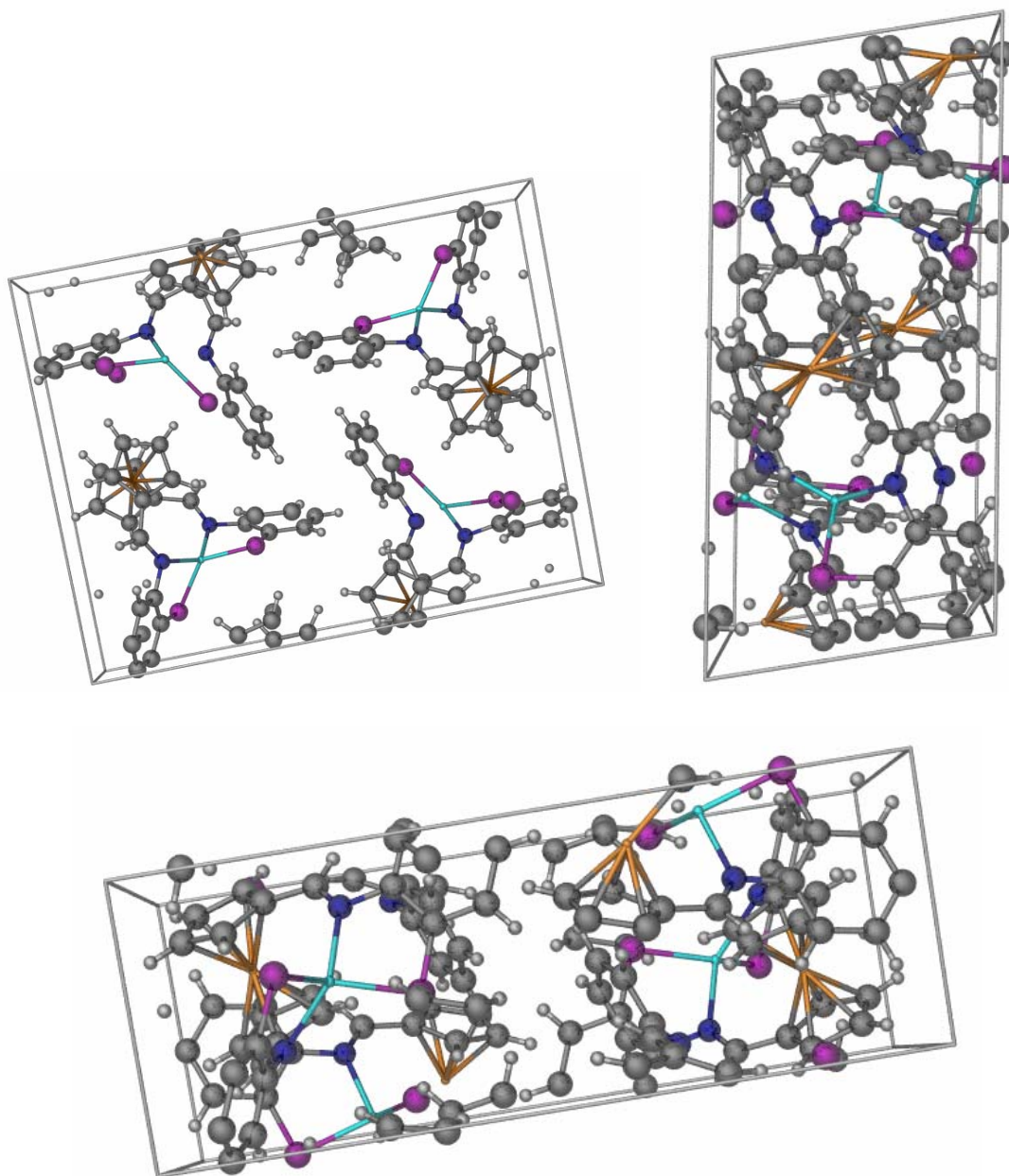
Asymmetric unit structure:



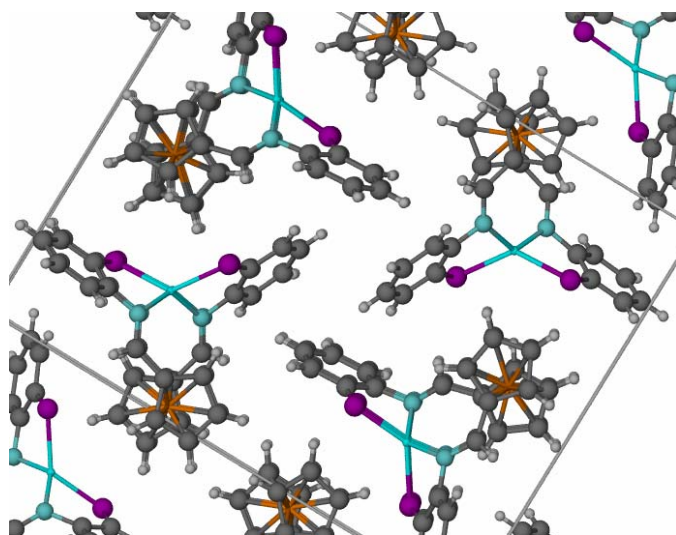
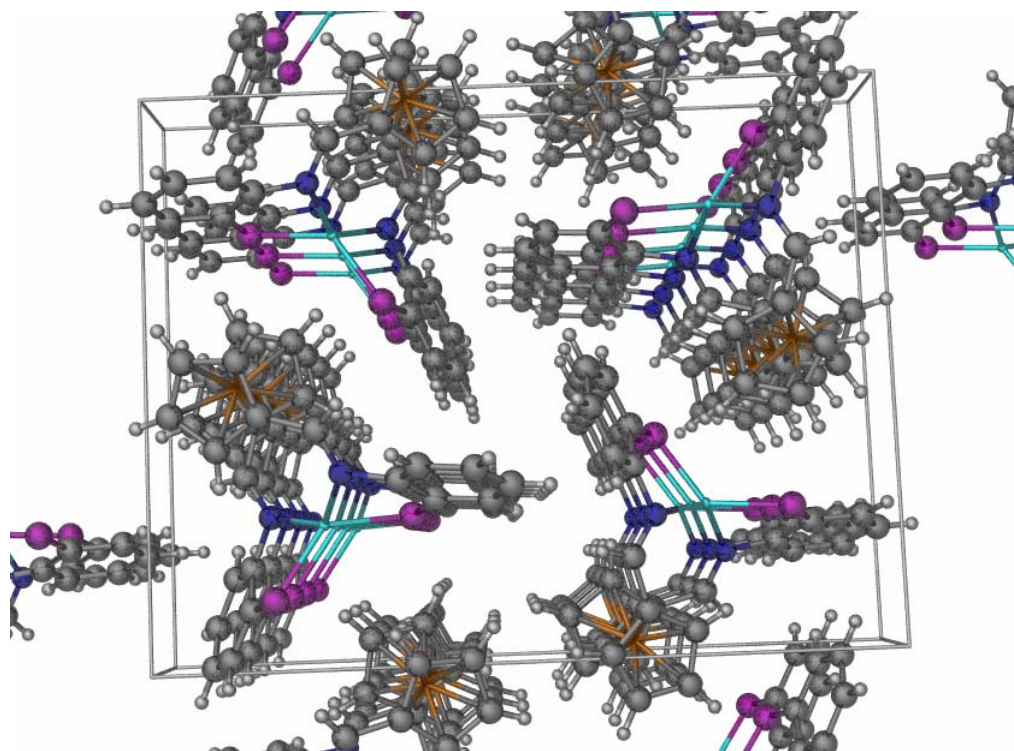
Cp ring overlap:

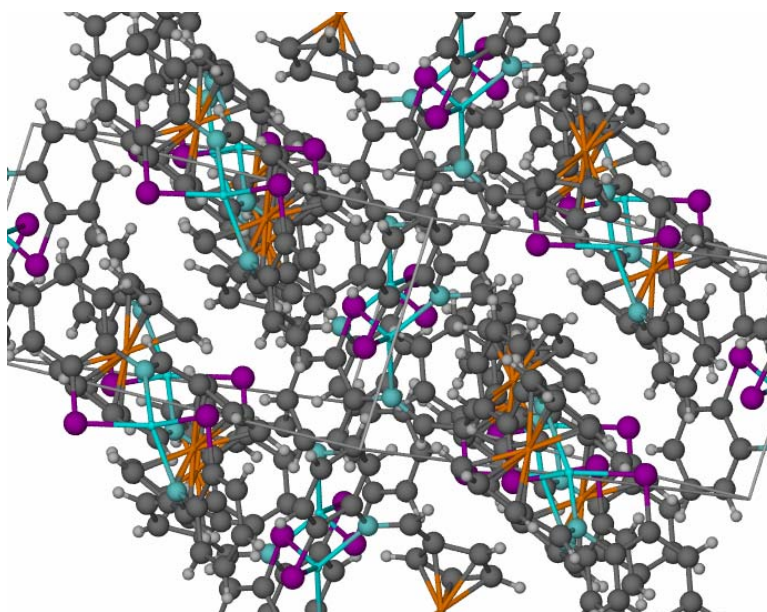
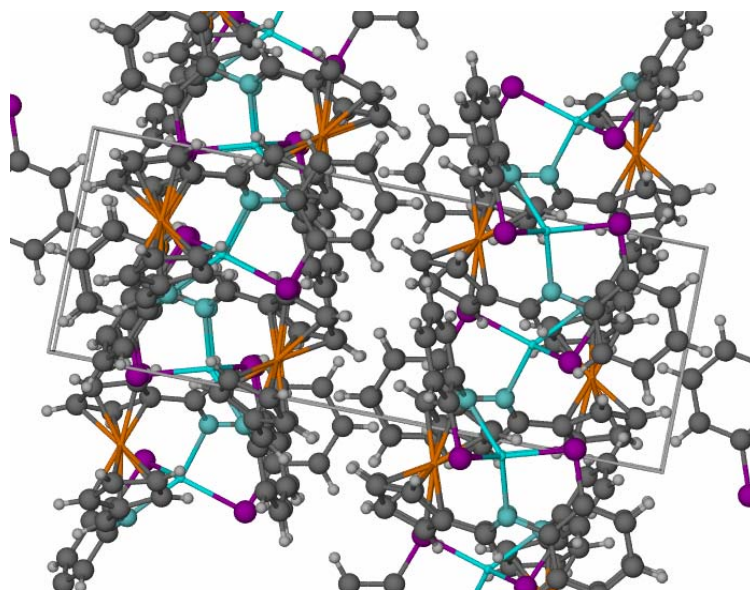


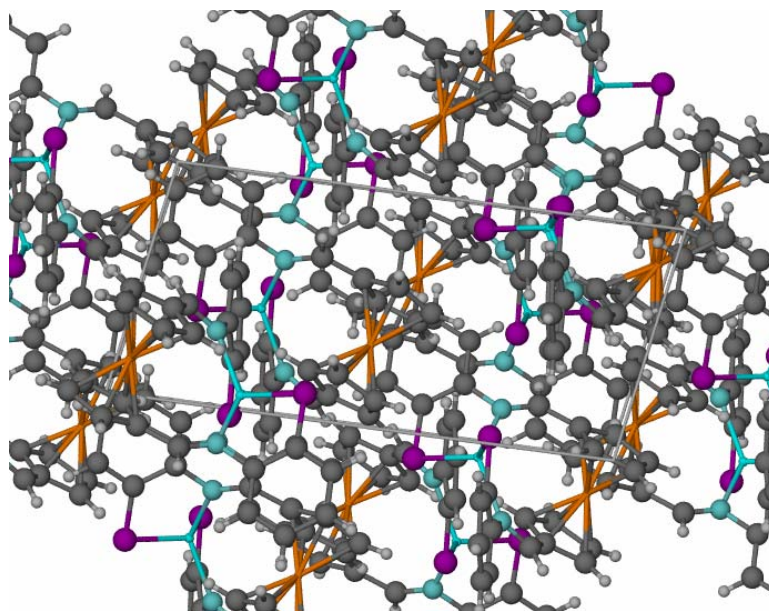
Unit cell:



Mass crystal packing:







Comparison versus [FcS1]₂-Zn from literature:¹

[Zn(fabt) ₂]	Angstroms	Comparison
Zn-S(1)	2.266(2)	0.012 less
Zn-S(2)	2.264(2)	0.019 less
Zn-N(1)	2.089(5)	0.012 less
Zn-N(2)	2.062(5)	0.057 less
N(1)-C(17)	1.298(9)	0.013 more
N2-C(24)	1.290(9)	0.005 more

[Zn(fabt) ₂]	Angle	Comparison
S(1)-Zn-S(2)	123.4(1)	6.75° less
S(1)-Zn-N(1)	88.7(2)	1.35° more
S(1)-Zn-N(2)	128.9(2)	15.63° more
S(2)-Zn-N(1)	121.5(2)	8.38° more
S(2)-Zn-N(2)	89.7(2)	3.05° more
N(1)-Zn-N(2)	106.9(2)	25.29° less

Compound 27:

¹ Kawamoto, T. and Y. Kushi (1992). "Helical Bis[2-(ferrocenylmethyleneamino)benzenethiolato] Metal(II) Complexes (M = Ni, Zn or Pd) and a Related Mercury(II) Complex." *J. Chem. Soc. Dalton Trans.*: 3137-3143.

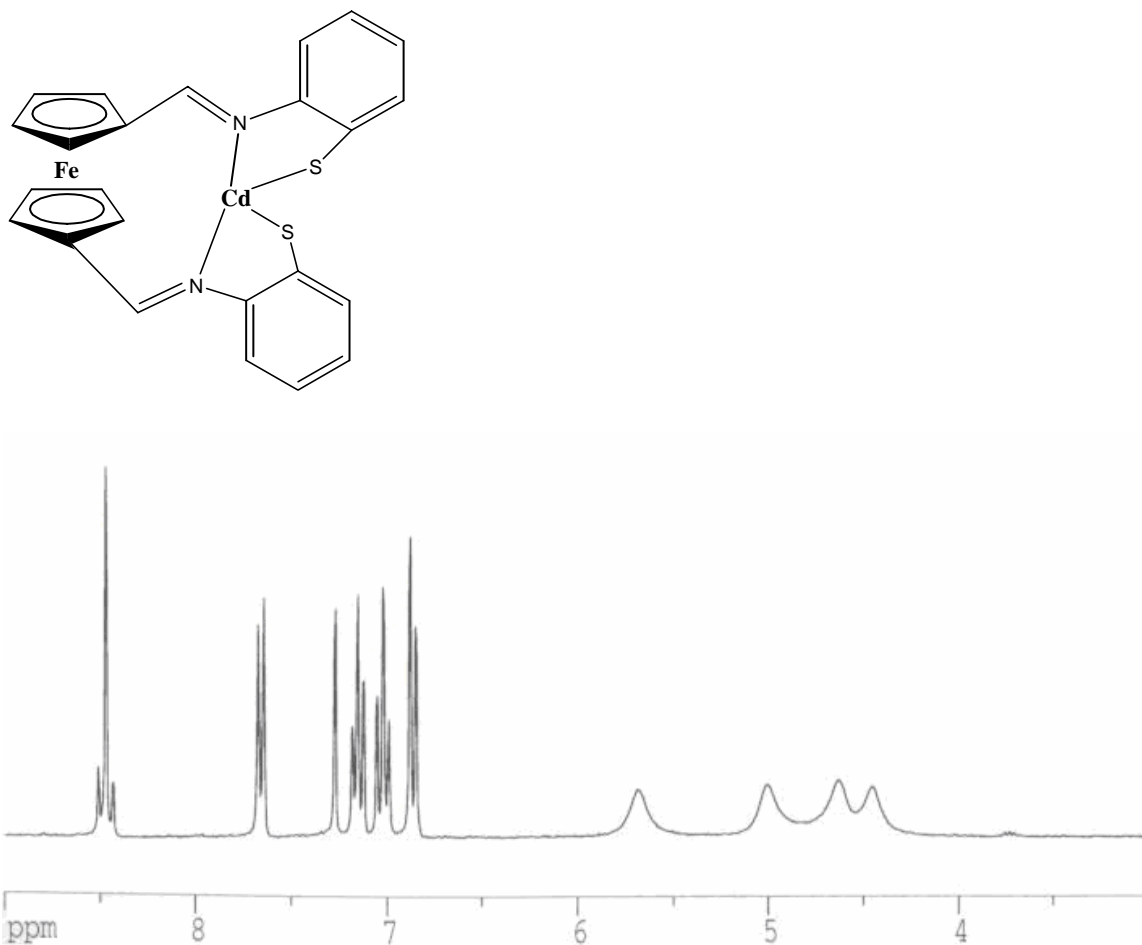


Figure A.112: ¹H NMR spectrum of FcS₂-Cd in CDCl₃: 8.48 ppm (2H, t, Cp-CH=N), 7.66 ppm (2H, d, phenyl), 7.16 ppm (2H, t, phenyl), 7.02 ppm (2H, t, phenyl), 6.86 ppm (2H, d, phenyl), 5.69 ppm (2H, broad s, Cp), 5.01 ppm (2H, broad s, Cp), 4.63 ppm (2H, broad s, Cp), 4.46 ppm (2H, broad s, Cp);

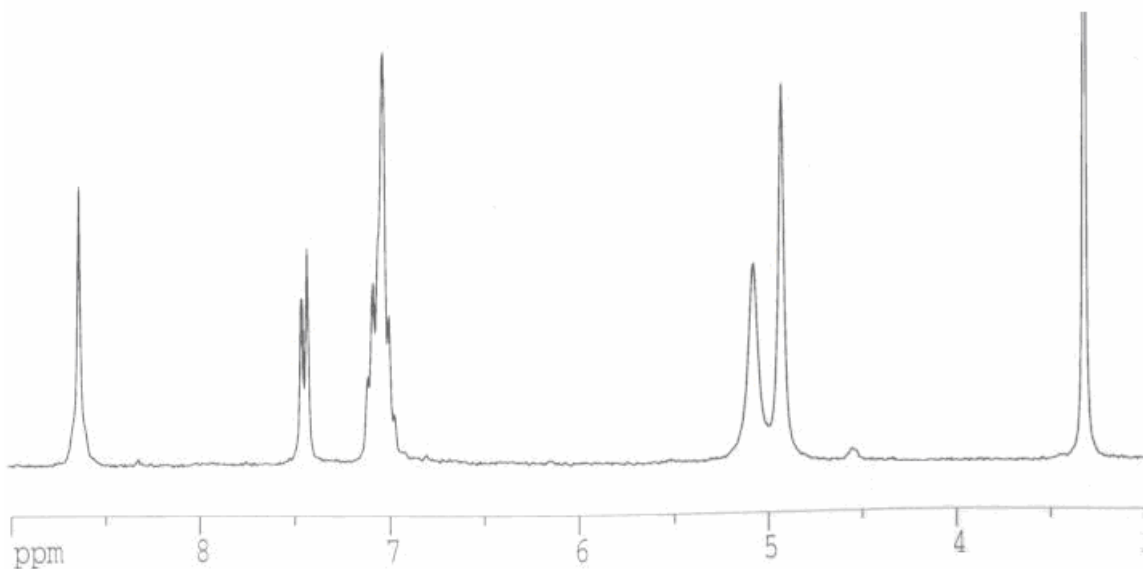


Figure A.113: ^1H NMR spectrum of FcS₂-Cd in d₆-DMSO: 8.63 ppm (2H, s, Cp- $\underline{\text{C}}\text{H}=\text{N}$), 7.42 ppm (2H, d, phenyl), 7.09-6.96 ppm (6H, m, phenyl), 5.06 ppm (4H, broad s, Cp), 4.91 ppm (4H, s, Cp);

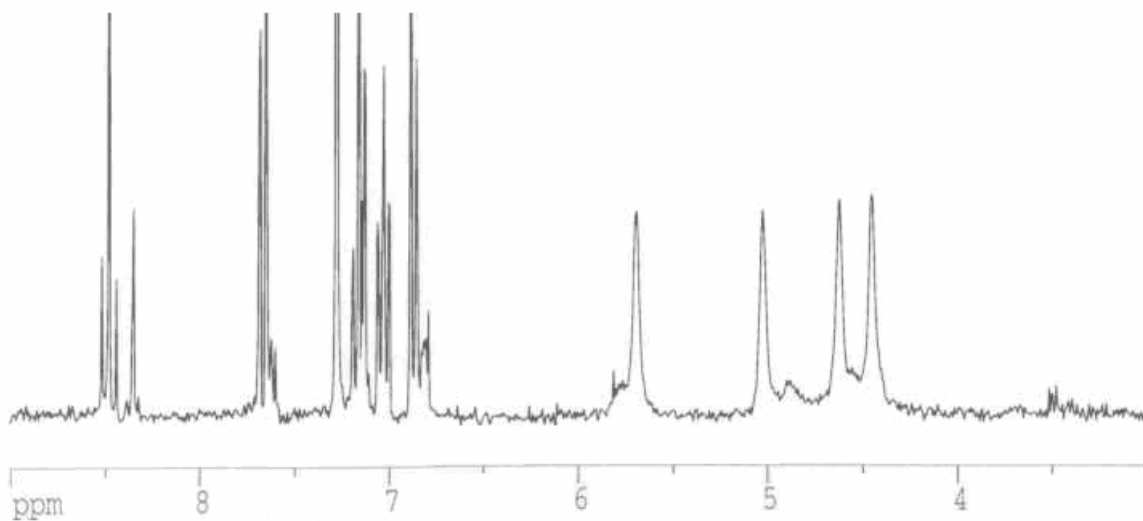


Figure A.114: ^1H NMR spectrum of precipitate from reaction of 27 with $\text{Hg}(\text{CH}_3\text{COO})_2$ in CDCl_3 :

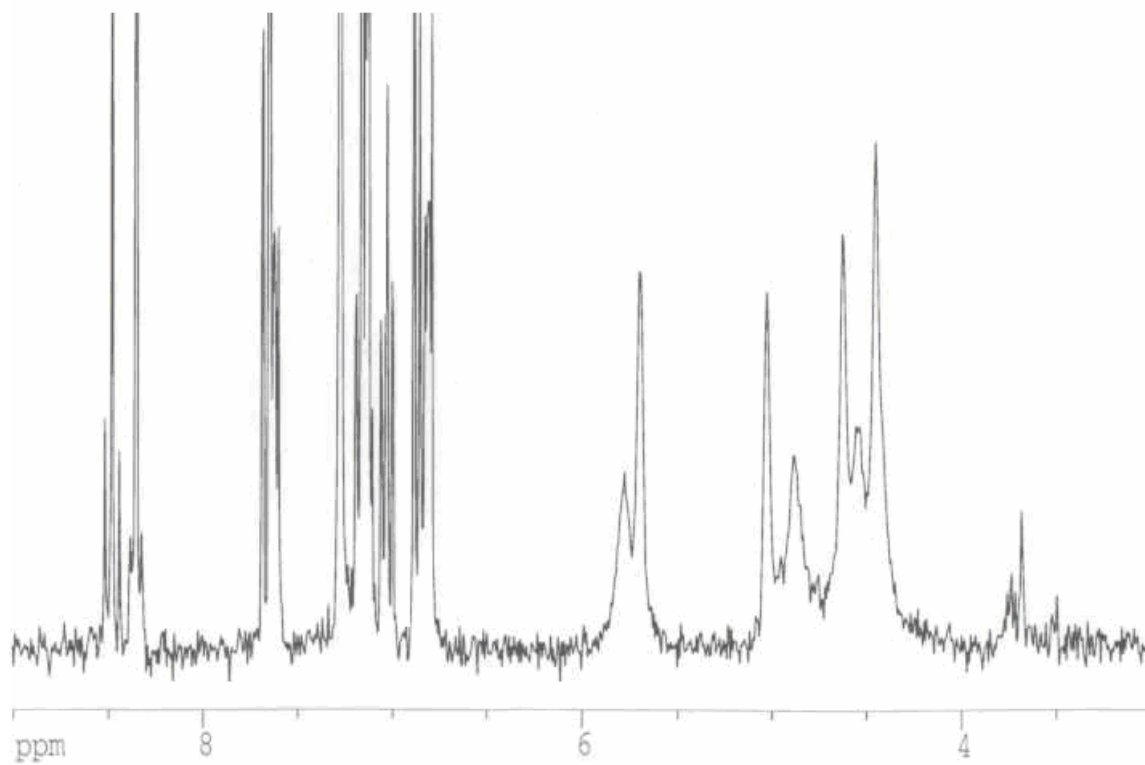


Figure A.115: ^1H NMR spectrum of dried liquid portion from reaction of 27 with $\text{Hg}(\text{CH}_3\text{COO})_2$ in CDCl_3 :

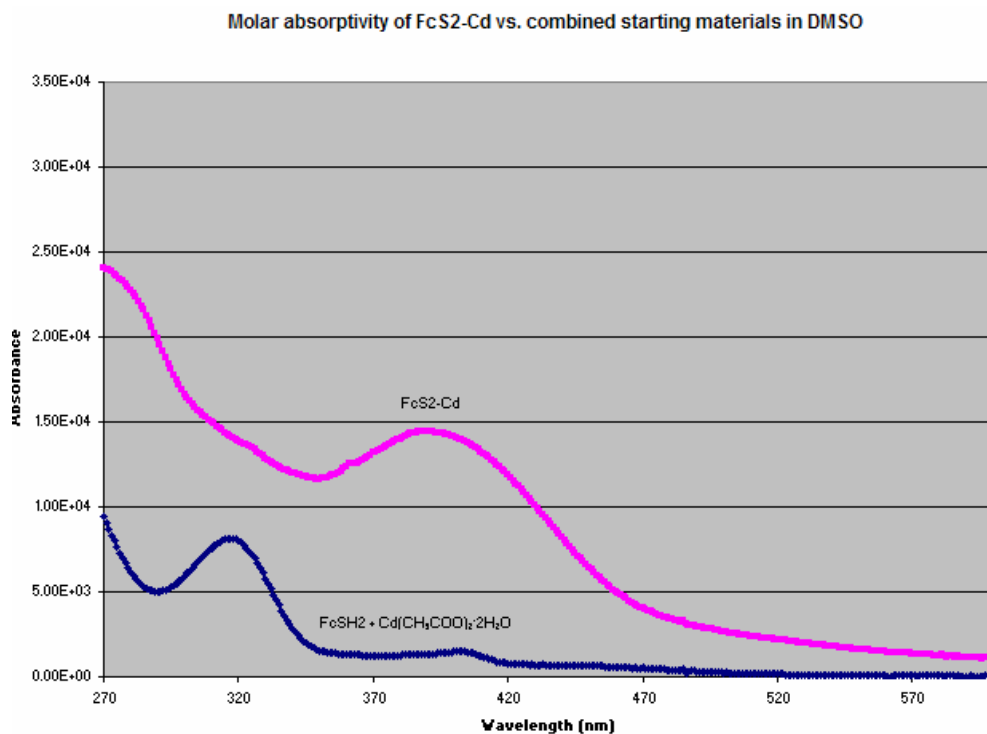


Figure A.116: Comparison between the molar absorptivity (UV-Vis) of FcS2-Cd and the molar absorptivity of the starting materials (317, 402 nm peaks) in DMSO: 392 nm ($14400 \text{ M}^{-1}\text{cm}^{-1}$);

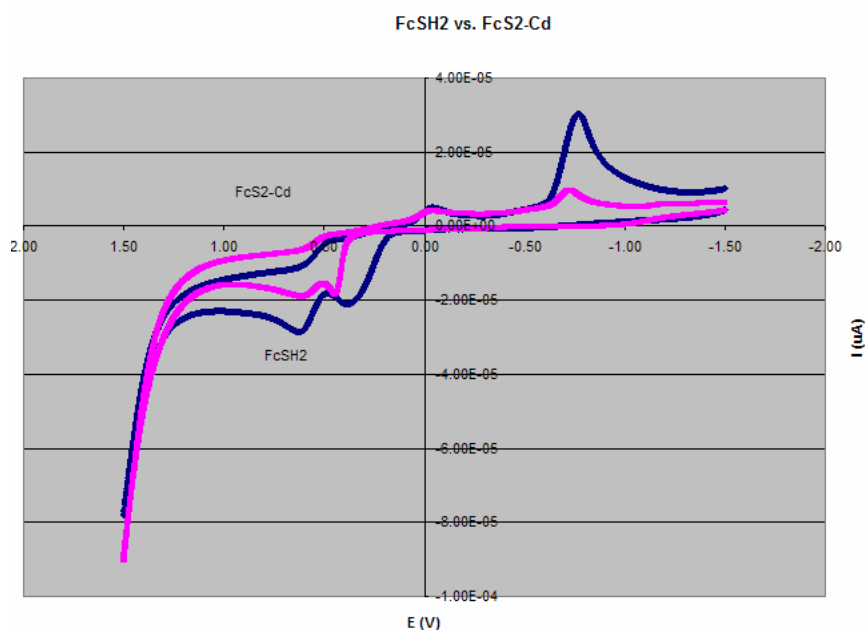


Figure A.117: Comparison between the CV scan of FcS2- Cd and the CV scan of FcSH2 in DMSO, scan rate 100 mV/sec. Fe^{II} to Fe^{III} oxidation peak is at 445 mV.

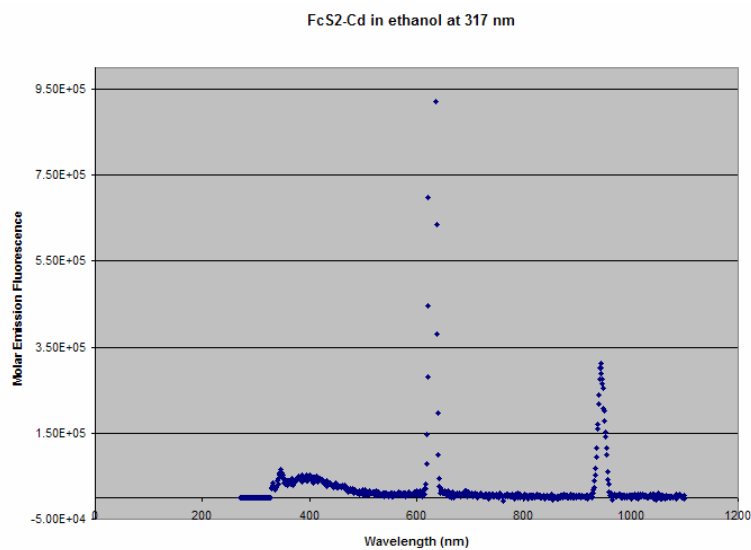


Figure A.118: Emission fluorescence of FcS2-Cd in ethanol at 317 nm with peaks at 347, 394, 629, 943 nm.

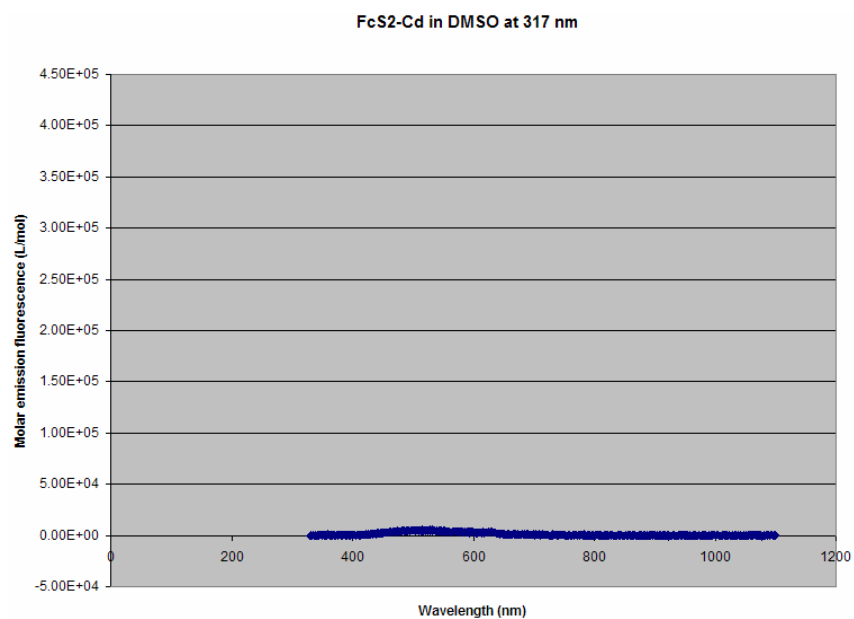


Figure A.119: Emission fluorescence of FcS2-Cd in DMSO at 317 nm with no apparent peaks.

Compound 28:

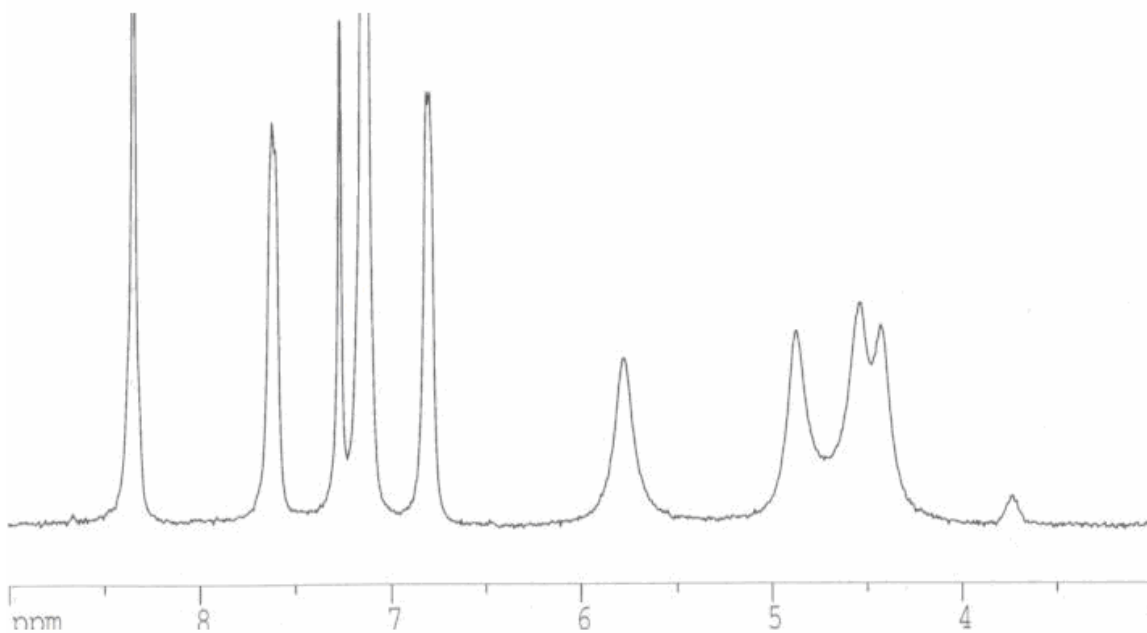
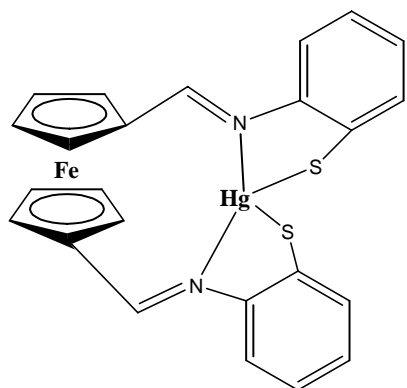


Figure A.120: ^1H NMR spectrum of $\text{FcS}_2\text{-Hg}$ in CDCl_3 : 8.34 ppm (2H, s, Cp- $\underline{\text{C}}\text{H}=\text{N}$), 7.61 ppm (2H, s, phenyl), 7.14 ppm (2H, s, phenyl), 6.80 ppm (2H, s, phenyl), 5.77 ppm (2H, broad s, Cp), 4.80 ppm (2H, broad s, Cp), 4.53 ppm (2H, broad s, Cp), 4.42 ppm (2H, broad s, Cp);

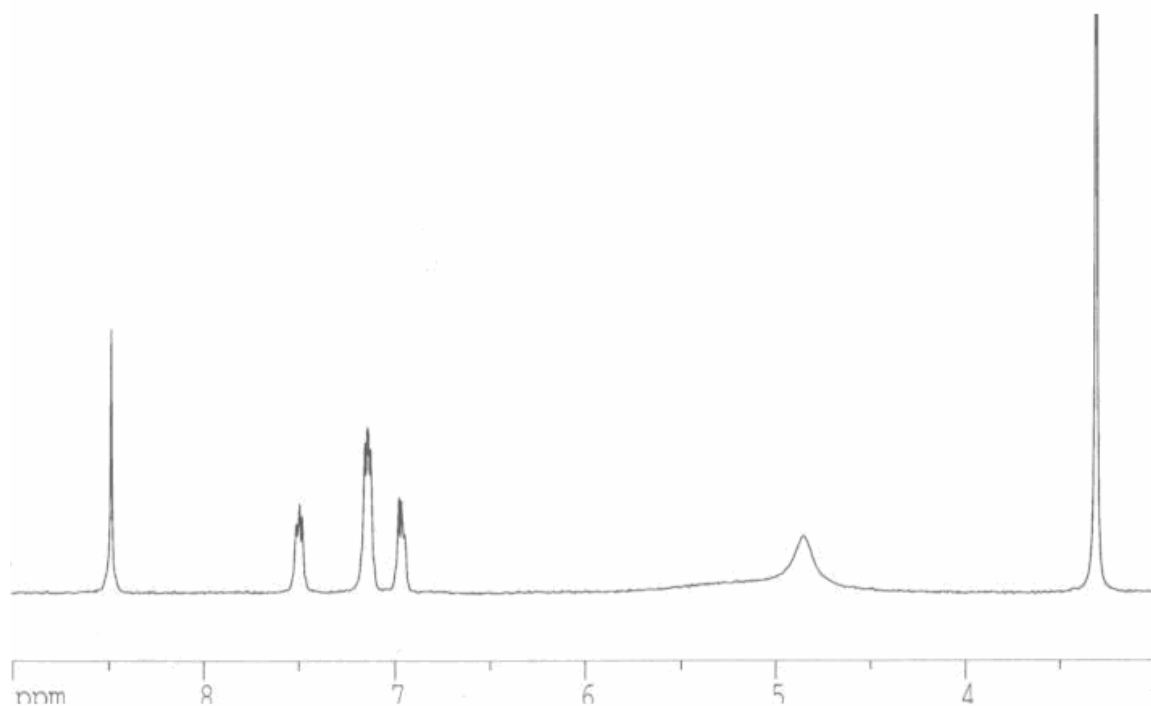


Figure A.121: ^1H NMR spectrum of FcS₂-Hg in d_6 -DMSO: 8.48 ppm (2H, s, Cp- $\underline{\text{C}}\text{H}=\text{N}$), 7.49 ppm (2H, t, phenyl), 7.14 ppm (4H, m, phenyl), 6.97 ppm (2H, t, phenyl), 6.0-5.0 ppm (4H, Cp), 4.85 ppm (4H, very broad s, Cp);

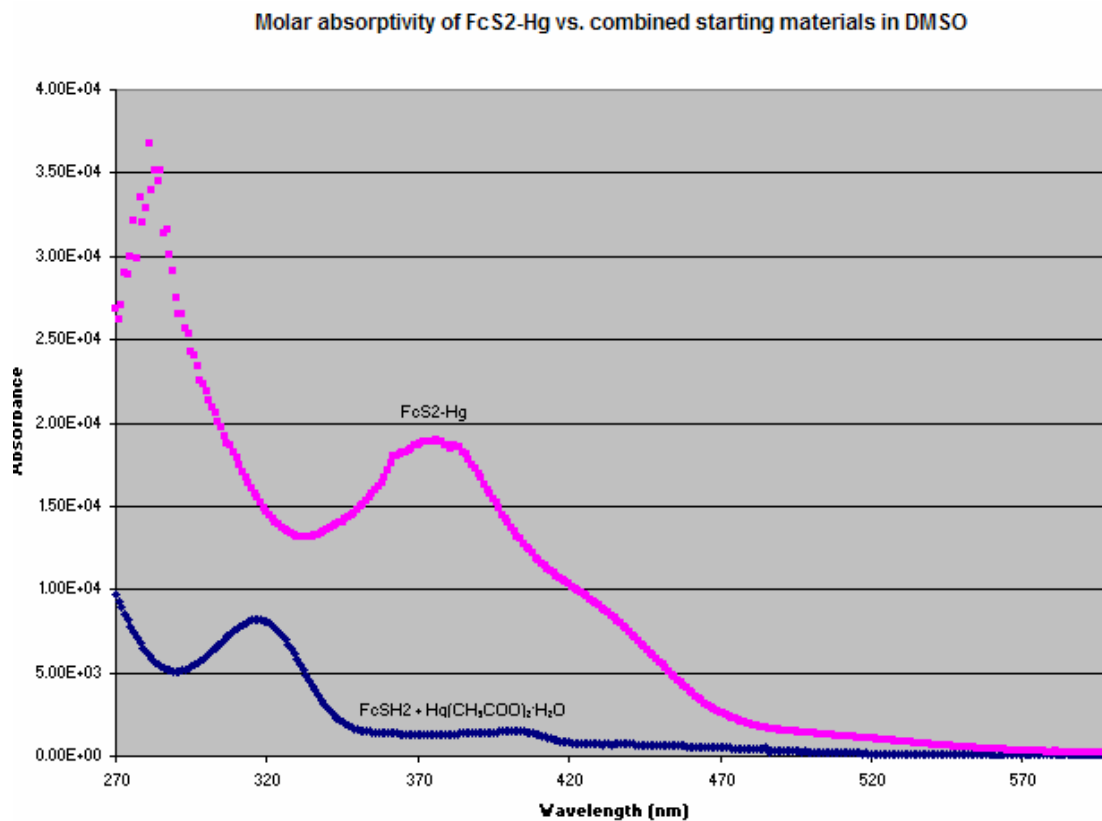


Figure A.122: Comparison between the molar absorptivity (UV-Vis) of FcS2-Hg and the molar absorptivity of the starting materials (317, 398 nm peaks) in DMSO: 285 nm ($35100 \text{ M}^{-1}\text{cm}^{-1}$), 376 nm ($19000 \text{ M}^{-1}\text{cm}^{-1}$);

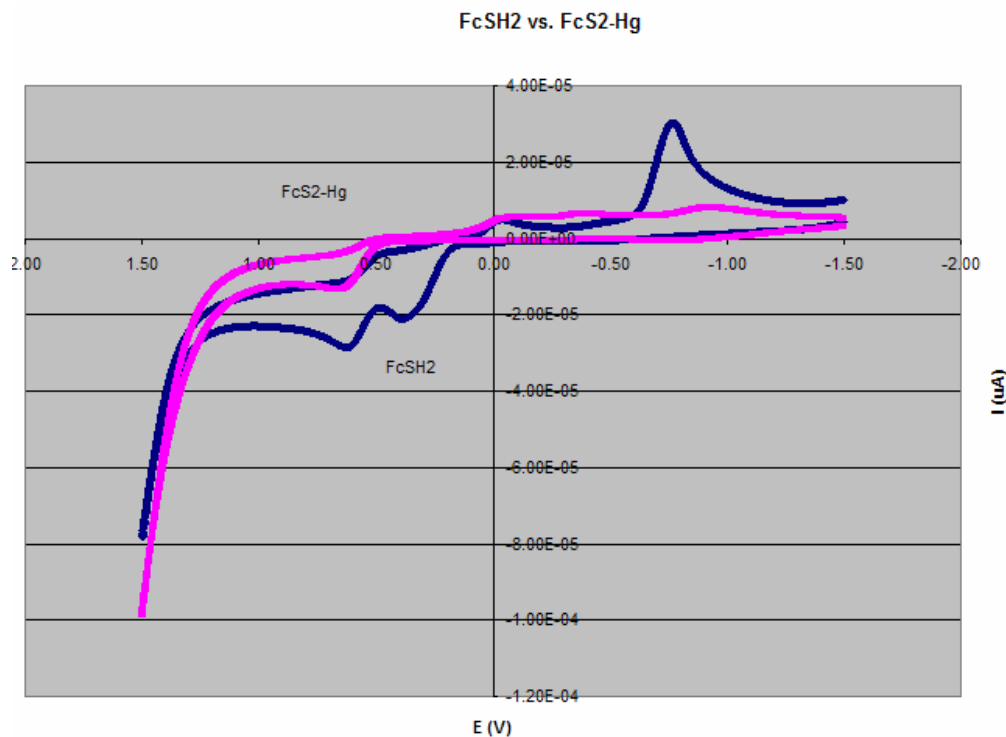


Figure A.123: Comparison between the CV scan of FcS2-Hg and the CV scan of FcSH2 in DMSO, scan rate 100 mV/sec. Fe^{II} to Fe^{III} oxidation peak is at 663 mV.

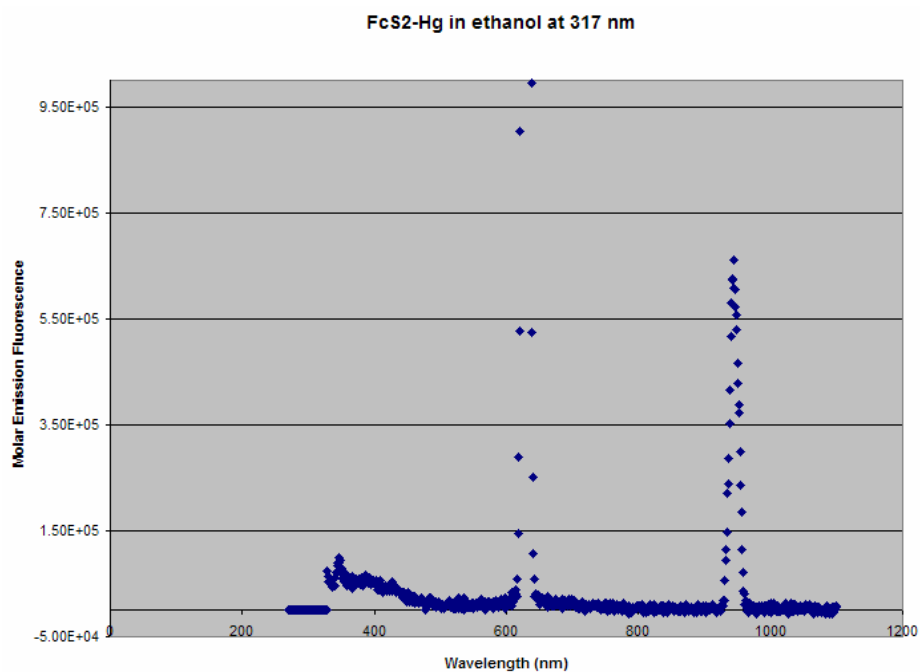


Figure A.124: Emission fluorescence of FcS2-Hg in ethanol at 317 nm with peaks at 346, 629, 944 nm.

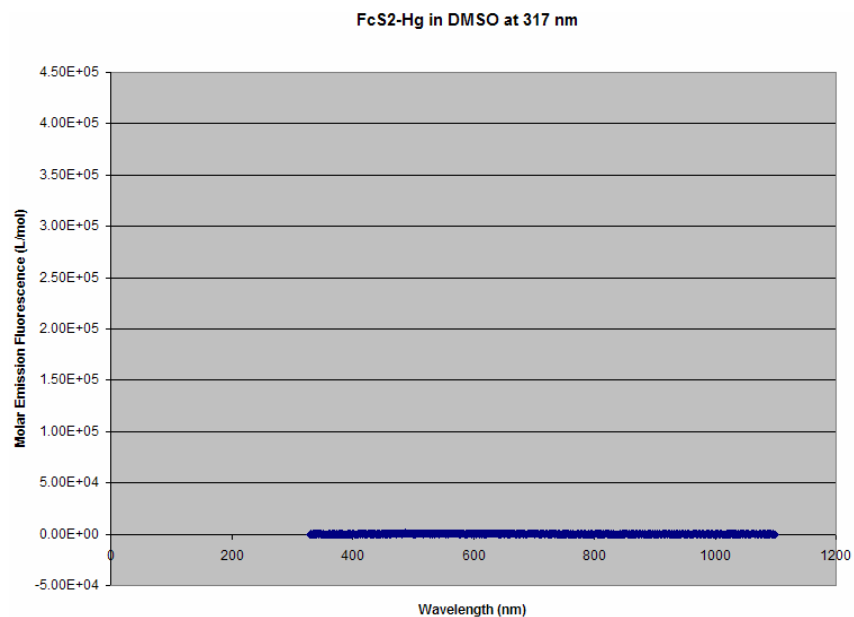


Figure A.125: Emission fluorescence of FcS2-Hg in DMSO at 317 nm with no apparent peaks.

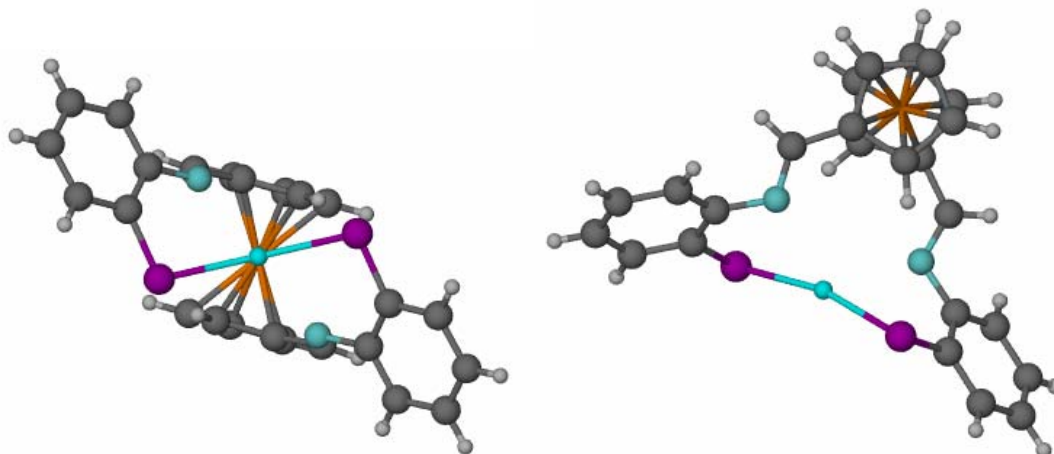


Figure A-126: Crystal Structure of FcS2-Hg

Crystal data

$C_{24}H_{18}FeHgN_2S_2$

$M_r = 654.96$

Orthorhombic, $C222_1$

$a = 7.7926 (4) \text{ \AA}$

$b = 17.5924 (8) \text{ \AA}$

$c = 15.7168 (7) \text{ \AA}$

$V = 2154.62 (18) \text{ \AA}^3$

$Z = 4$

$F_{000} = 1256$

$D_x = 2.019 \text{ Mg m}^{-3}$

Mo $K\alpha$ radiation

$\lambda = 0.71073 \text{ \AA}$

Cell parameters from 5902 reflections

$\theta = 2.3\text{--}27.1^\circ$

$\mu = 8.00 \text{ mm}^{-1}$

$T = 173 (2) \text{ K}$

Plate, red

$0.50 \times 0.15 \times 0.05 \text{ mm}$

Data collection

Bruker SMART CCD area detector diffractometer	7762 measured reflections
	2400 independent reflections
Monochromator: graphite	2261 reflections with $I > 2\sigma(I)$
	$R_{\text{int}} = 0.028$
$T = 173(2)$ K	$\theta_{\text{max}} = 27.1^\circ$
	$\theta_{\text{min}} = 2.3^\circ$
ω scans	$h = -10 \rightarrow 9$
Absorption correction: multi-scan	
Data were corrected for decay and absorption using the program SADABS (Sheldrick, G. M. (2003). SADABS. Version 2.10. University of Göttingen, Germany).	$k = -22 \rightarrow 17$
$T_{\text{min}} = 0.36, T_{\text{max}} = 0.69$	$l = -20 \rightarrow 20$

Refinement

Refinement on F^2	Hydrogen site location: inferred from neighbouring sites
Least-squares matrix: full	H atoms treated by a mixture of independent and constrained refinement
$R[F^2 > 2\sigma(F^2)] = 0.019$	$w = 1/[\sigma^2(F_o^2) + (0.0076P)^2 + 1.6112P]$
$wR(F^2) = 0.039$	where $P = (F_o^2 + 2F_c^2)/3$
$S = 1.09$	$(\Delta/\sigma)_{\text{max}} = 0.001$
2400 reflections	$\Delta\rho_{\text{max}} = 0.99 \text{ e } \text{Å}^{-3}$
138 parameters	$\Delta\rho_{\text{min}} = -0.65 \text{ e } \text{Å}^{-3}$
	Extinction correction: none
	Absolute structure: Flack H D (1983), Acta Cryst. A39, 876-881
Primary atom site location: structure-invariant direct methods	Flack parameter: 0.351 (8)
Secondary atom site location: difference Fourier map	

Refinement of F^2 against ALL reflections. The weighted R-factor wR and goodness of fit S are based on F^2 , conventional R-factors R are based on F , with F set to zero for negative F^2 . The threshold expression of $F^2 > 2\sigma(F^2)$ is used only for calculating R-factors(gt) etc. and is not relevant to the choice of reflections for refinement. R-factors based on F^2 are statistically about twice as large as those based on F , and R-factors based on ALL data will be even larger.

Fractional atomic coordinates and isotropic or equivalent isotropic displacement parameters (Å^2)

x	y	z	$U_{\text{iso}}^*/U_{\text{eq}}$
-----	-----	-----	----------------------------------

Hg1	0.5000	-0.115033 (9)	0.7500	0.02603 (6)
Fe1	0.5000	0.14299 (3)	0.7500	0.02262 (12)
S1	0.4987 (3)	-0.13121 (5)	0.89850 (5)	0.03038 (17)
N1	0.7648 (4)	-0.03050 (17)	0.80936 (19)	0.0242 (7)
C1	0.7388 (4)	0.09527 (17)	0.7479 (6)	0.0251 (6)
C2	0.7521 (5)	0.1761 (2)	0.7586 (7)	0.0336 (13)
H2	0.8048	0.2014	0.8052	0.040*
C3	0.6740 (6)	0.2114 (3)	0.6887 (3)	0.0363 (10)
H3	0.6631	0.2646	0.6799	0.044*
C4	0.6143 (5)	0.1536 (2)	0.6334 (2)	0.0311 (9)
H4	0.5573	0.1617	0.5807	0.037*
C5	0.6530 (5)	0.0819 (2)	0.6691 (2)	0.0252 (8)
H5	0.6268	0.0337	0.6451	0.030*
C6	0.7940 (5)	0.0410 (2)	0.8127 (2)	0.0254 (8)
H6	0.8555	0.0600	0.8604	0.030*
C7	0.8305 (5)	-0.0747 (2)	0.8782 (2)	0.0228 (8)
C8	0.7206 (5)	-0.1249 (2)	0.9210 (2)	0.0227 (8)
C9	0.7881 (5)	-0.1701 (2)	0.9869 (2)	0.0249 (8)
H9	0.7156	-0.2051	1.0156	0.030*
C10	0.9586 (4)	-0.1641 (2)	1.0103 (2)	0.0268 (11)
H10	1.0021	-0.1940	1.0558	0.032*
C11	1.0650 (5)	-0.1149 (3)	0.9677 (2)	0.0353 (10)
H11	1.1824	-0.1112	0.9834	0.042*
C12	1.0015 (11)	-0.07032 (18)	0.90133 (19)	0.0311 (7)
H12	1.0762	-0.0367	0.8719	0.037*

Atomic displacement parameters (\AA^2)

	U^{11}	U^{22}	U^{33}	U^{12}	U^{13}	U^{23}
Hg1	0.02454 (9)	0.02806 (9)	0.02550 (8)	0.000	-0.00370 (16)	0.000
Fe1	0.0283 (3)	0.0204 (3)	0.0192 (3)	0.000	0.0008 (6)	0.000
S1	0.0214 (4)	0.0425 (5)	0.0272 (4)	-0.0031 (11)	0.0008 (9)	0.0093 (3)
N1	0.0218 (17)	0.0265 (18)	0.0244 (15)	-0.0026 (14)	0.0014 (13)	0.0021 (13)
C1	0.0217 (15)	0.0266 (15)	0.0271 (16)	-0.0018 (12)	0.004 (3)	-0.002 (4)
C2	0.0359 (19)	0.0292 (18)	0.036 (4)	-0.0132 (14)	-0.001 (3)	0.006 (3)
C3	0.044 (3)	0.028 (2)	0.037 (2)	-0.006 (2)	0.004 (2)	0.0102 (18)
C4	0.035 (2)	0.036 (2)	0.0221 (18)	0.0019 (19)	0.0033 (16)	0.0053 (17)
C5	0.022 (2)	0.030 (2)	0.0234 (17)	0.0006 (17)	0.0042 (14)	-0.0011 (16)
C6	0.0197 (19)	0.033 (2)	0.0240 (18)	-0.0062 (16)	0.0005 (15)	-0.0013 (16)
C7	0.025 (2)	0.023 (2)	0.0204 (17)	0.0040 (16)	0.0001 (14)	-0.0028 (15)
C8	0.0236 (19)	0.0240 (19)	0.0204 (17)	0.0039 (16)	-0.0008 (14)	-0.0064 (14)
C9	0.033 (2)	0.022 (2)	0.0195 (17)	0.0031 (16)	0.0006 (15)	0.0005 (14)
C10	0.032 (3)	0.0294 (19)	0.0189 (15)	0.0125 (16)	-0.0031 (13)	0.0018 (14)
C11	0.0230 (19)	0.052 (3)	0.0308 (19)	0.0041 (18)	-0.0049 (15)	-0.003 (2)
C12	0.0204 (16)	0.0385 (19)	0.0344 (16)	0.003 (5)	0.001 (4)	0.0034 (13)

Table 1

Geometric parameters (Å, °)

Hg1—S1	2.3512 (7)	C2—C3	1.402 (9)
Hg1—S1 ⁱ	2.3512 (7)	C2—H2	0.9500
Fe1—C1 ⁱ	2.042 (3)	C3—C4	1.416 (6)
Fe1—C1	2.042 (3)	C3—H3	0.9500
Fe1—C4 ⁱ	2.046 (4)	C4—C5	1.413 (6)
Fe1—C4	2.046 (4)	C4—H4	0.9500
Fe1—C5 ⁱ	2.048 (4)	C5—H5	0.9500
Fe1—C5	2.048 (4)	C6—H6	0.9500
Fe1—C3 ⁱ	2.053 (4)	C7—C12	1.384 (9)

Fe1—C3	2.053 (4)	C7—C8	1.402 (5)
Fe1—C2	2.053 (4)	C8—C9	1.408 (5)
Fe1—C2 ⁱ	2.053 (4)	C9—C10	1.383 (5)
S1—C8	1.769 (4)	C9—H9	0.9500
N1—C6	1.279 (5)	C10—C11	1.373 (5)
N1—C7	1.427 (5)	C10—H10	0.9500
C1—C5	1.427 (9)	C11—C12	1.395 (5)
C1—C2	1.436 (5)	C11—H11	0.9500
C1—C6	1.461 (8)	C12—H12	0.9500
S1—Hg1—S1 ⁱ	166.10 (4)	C2—C1—C6	123.0 (6)
C1 ⁱ —Fe1—C1	131.44 (16)	C5—C1—Fe1	69.8 (2)
C1 ⁱ —Fe1—C4 ⁱ	68.1 (3)	C2—C1—Fe1	69.91 (19)
C1—Fe1—C4 ⁱ	116.7 (3)	C6—C1—Fe1	121.7 (4)
C1 ⁱ —Fe1—C4	116.7 (3)	C3—C2—C1	108.4 (6)
C1—Fe1—C4	68.1 (3)	C3—C2—Fe1	70.0 (3)
C4 ⁱ —Fe1—C4	169.5 (2)	C1—C2—Fe1	69.05 (18)
C1 ⁱ —Fe1—C5 ⁱ	40.9 (3)	C3—C2—H2	125.8
C1—Fe1—C5 ⁱ	109.0 (2)	C1—C2—H2	125.8
C4 ⁱ —Fe1—C5 ⁱ	40.38 (15)	Fe1—C2—H2	126.7
C4—Fe1—C5 ⁱ	149.03 (16)	C2—C3—C4	107.8 (4)
C1 ⁱ —Fe1—C5	109.0 (2)	C2—C3—Fe1	70.0 (2)
C1—Fe1—C5	40.9 (3)	C4—C3—Fe1	69.5 (2)
C4 ⁱ —Fe1—C5	149.03 (16)	C2—C3—H3	126.1
C4—Fe1—C5	40.38 (15)	C4—C3—H3	126.1
C5 ⁱ —Fe1—C5	116.7 (2)	Fe1—C3—H3	125.9
C1 ⁱ —Fe1—C3 ⁱ	68.4 (2)	C5—C4—C3	109.1 (3)
C1—Fe1—C3 ⁱ	148.3 (3)	C5—C4—Fe1	69.9 (2)
C4 ⁱ —Fe1—C3 ⁱ	40.40 (17)	C3—C4—Fe1	70.1 (2)
C4—Fe1—C3 ⁱ	130.89 (17)	C5—C4—H4	125.4
C5 ⁱ —Fe1—C3 ⁱ	68.38 (17)	C3—C4—H4	125.4
C5—Fe1—C3 ⁱ	169.61 (16)	Fe1—C4—H4	126.2

C1 ⁱ —Fe1—C3	148.3 (3)	C4—C5—C1	107.3 (3)
C1—Fe1—C3	68.4 (2)	C4—C5—Fe1	69.7 (2)
C4 ⁱ —Fe1—C3	130.89 (17)	C1—C5—Fe1	69.3 (2)
C4—Fe1—C3	40.40 (17)	C4—C5—H5	126.4
C5 ⁱ —Fe1—C3	169.61 (16)	C1—C5—H5	126.4
C5—Fe1—C3	68.38 (17)	Fe1—C5—H5	126.1
C3 ⁱ —Fe1—C3	108.2 (3)	N1—C6—C1	124.1 (4)
C1 ⁱ —Fe1—C2	170.9 (2)	N1—C6—H6	117.9
C1—Fe1—C2	41.05 (13)	C1—C6—H6	117.9
C4 ⁱ —Fe1—C2	109.4 (3)	C12—C7—C8	119.8 (3)
C4—Fe1—C2	67.5 (3)	C12—C7—N1	121.0 (3)
C5 ⁱ —Fe1—C2	131.7 (3)	C8—C7—N1	119.2 (3)
C5—Fe1—C2	68.5 (2)	C7—C8—C9	118.8 (3)
C3 ⁱ —Fe1—C2	115.7 (2)	C7—C8—S1	122.7 (3)
C3—Fe1—C2	39.9 (3)	C9—C8—S1	118.5 (3)
C1 ⁱ —Fe1—C2 ⁱ	41.05 (13)	C10—C9—C8	120.7 (4)
C1—Fe1—C2 ⁱ	170.9 (2)	C10—C9—H9	119.6
C4 ⁱ —Fe1—C2 ⁱ	67.5 (3)	C8—C9—H9	119.6
C4—Fe1—C2 ⁱ	109.4 (3)	C11—C10—C9	119.9 (3)
C5 ⁱ —Fe1—C2 ⁱ	68.5 (2)	C11—C10—H10	120.0
C5—Fe1—C2 ⁱ	131.7 (3)	C9—C10—H10	120.0
C3 ⁱ —Fe1—C2 ⁱ	39.9 (3)	C10—C11—C12	120.3 (5)
C3—Fe1—C2 ⁱ	115.7 (2)	C10—C11—H11	119.8
C2—Fe1—C2 ⁱ	147.0 (2)	C12—C11—H11	119.8
C8—S1—Hg1	100.76 (13)	C7—C12—C11	120.5 (5)
C6—N1—C7	116.1 (3)	C7—C12—H12	119.8
C5—C1—C2	107.4 (5)	C11—C12—H12	119.8
C5—C1—C6	129.5 (3)		
S1 ⁱ —Hg1—S1—C8	95.05 (12)	C2—Fe1—C3—C4	118.9 (4)
C1 ⁱ —Fe1—C1—C5	68.98 (19)	C2 ⁱ —Fe1—C3—C4	-90.1 (4)
C4 ⁱ —Fe1—C1—C5	152.4 (3)	C2—C3—C4—C5	0.7 (5)

C4—Fe1—C1—C5	-37.9 (3)	Fe1—C3—C4—C5	-59.1 (3)
C5 ⁱ —Fe1—C1—C5	109.2 (3)	C2—C3—C4—Fe1	59.8 (3)
C3 ⁱ —Fe1—C1—C5	-171.5 (3)	C1 ⁱ —Fe1—C4—C5	-88.3 (2)
C3—Fe1—C1—C5	-81.5 (3)	C1—Fe1—C4—C5	38.3 (2)
C2—Fe1—C1—C5	-118.3 (5)	C4 ⁱ —Fe1—C4—C5	157.1 (2)
C2 ⁱ —Fe1—C1—C5	37.2 (19)	C5 ⁱ —Fe1—C4—C5	-52.2 (5)
C1 ⁱ —Fe1—C1—C2	-172.7 (5)	C3 ⁱ —Fe1—C4—C5	-172.0 (2)
C4 ⁱ —Fe1—C1—C2	-89.3 (5)	C3—Fe1—C4—C5	120.3 (4)
C4—Fe1—C1—C2	80.4 (5)	C2—Fe1—C4—C5	82.8 (2)
C5 ⁱ —Fe1—C1—C2	-132.5 (4)	C2 ⁱ —Fe1—C4—C5	-132.4 (2)
C5—Fe1—C1—C2	118.3 (5)	C1 ⁱ —Fe1—C4—C3	151.4 (2)
C3 ⁱ —Fe1—C1—C2	-53.2 (6)	C1—Fe1—C4—C3	-82.0 (3)
C3—Fe1—C1—C2	36.8 (4)	C4 ⁱ —Fe1—C4—C3	36.8 (2)
C2 ⁱ —Fe1—C1—C2	155.5 (14)	C5 ⁱ —Fe1—C4—C3	-172.5 (3)
C1 ⁱ —Fe1—C1—C6	-55.7 (3)	C5—Fe1—C4—C3	-120.3 (4)
C4 ⁱ —Fe1—C1—C6	27.8 (5)	C3 ⁱ —Fe1—C4—C3	67.8 (4)
C4—Fe1—C1—C6	-162.5 (5)	C2—Fe1—C4—C3	-37.5 (2)
C5 ⁱ —Fe1—C1—C6	-15.5 (5)	C2 ⁱ —Fe1—C4—C3	107.3 (3)
C5—Fe1—C1—C6	-124.7 (4)	C3—C4—C5—C1	-0.2 (5)
C3 ⁱ —Fe1—C1—C6	63.9 (4)	Fe1—C4—C5—C1	-59.4 (3)
C3—Fe1—C1—C6	153.8 (5)	C3—C4—C5—Fe1	59.3 (3)
C2—Fe1—C1—C6	117.1 (7)	C2—C1—C5—C4	-0.4 (5)
C2 ⁱ —Fe1—C1—C6	-87 (2)	C6—C1—C5—C4	174.7 (4)
C5—C1—C2—C3	0.8 (5)	Fe1—C1—C5—C4	59.7 (3)
C6—C1—C2—C3	-174.6 (4)	C2—C1—C5—Fe1	-60.1 (3)
Fe1—C1—C2—C3	-59.2 (3)	C6—C1—C5—Fe1	115.0 (5)
C5—C1—C2—Fe1	60.0 (3)	C1 ⁱ —Fe1—C5—C4	109.2 (3)
C6—C1—C2—Fe1	-115.5 (5)	C1—Fe1—C5—C4	-118.5 (3)
C1 ⁱ —Fe1—C2—C3	156.8 (17)	C4 ⁱ —Fe1—C5—C4	-172.1 (2)
C1—Fe1—C2—C3	119.9 (6)	C5 ⁱ —Fe1—C5—C4	152.9 (3)
C4 ⁱ —Fe1—C2—C3	-131.4 (3)	C3 ⁱ —Fe1—C5—C4	35.9 (10)

C4—Fe1—C2—C3	37.9 (3)	C3—Fe1—C5—C4	-37.0 (2)
C5 ⁱ —Fe1—C2—C3	-171.2 (3)	C2—Fe1—C5—C4	-80.1 (3)
C5—Fe1—C2—C3	81.6 (4)	C2 ⁱ —Fe1—C5—C4	68.8 (3)
C3 ⁱ —Fe1—C2—C3	-88.0 (5)	C1 ⁱ —Fe1—C5—C1	-132.3 (2)
C2 ⁱ —Fe1—C2—C3	-53.2 (3)	C4 ⁱ —Fe1—C5—C1	-53.6 (4)
C1 ⁱ —Fe1—C2—C1	37 (2)	C4—Fe1—C5—C1	118.5 (3)
C4 ⁱ —Fe1—C2—C1	108.7 (4)	C5 ⁱ —Fe1—C5—C1	-88.5 (2)
C4—Fe1—C2—C1	-82.0 (5)	C3 ⁱ —Fe1—C5—C1	154.4 (9)
C5 ⁱ —Fe1—C2—C1	68.9 (5)	C3—Fe1—C5—C1	81.5 (3)
C5—Fe1—C2—C1	-38.3 (4)	C2—Fe1—C5—C1	38.4 (3)
C3 ⁱ —Fe1—C2—C1	152.1 (4)	C2 ⁱ —Fe1—C5—C1	-172.7 (3)
C3—Fe1—C2—C1	-119.9 (6)	C7—N1—C6—C1	179.3 (4)
C2 ⁱ —Fe1—C2—C1	-173.1 (5)	C5—C1—C6—N1	-3.3 (8)
C1—C2—C3—C4	-0.9 (5)	C2—C1—C6—N1	171.1 (4)
Fe1—C2—C3—C4	-59.5 (3)	Fe1—C1—C6—N1	85.7 (6)
C1—C2—C3—Fe1	58.6 (3)	C6—N1—C7—C12	-53.0 (5)
C1 ⁱ —Fe1—C3—C2	-173.2 (4)	C6—N1—C7—C8	129.0 (4)
C1—Fe1—C3—C2	-37.8 (4)	C12—C7—C8—C9	-0.2 (5)
C4 ⁱ —Fe1—C3—C2	69.4 (4)	N1—C7—C8—C9	177.8 (3)
C4—Fe1—C3—C2	-118.9 (4)	C12—C7—C8—S1	177.3 (3)
C5 ⁱ —Fe1—C3—C2	39.3 (11)	N1—C7—C8—S1	-4.6 (5)
C5—Fe1—C3—C2	-81.9 (4)	Hg1—S1—C8—C7	37.4 (3)
C3 ⁱ —Fe1—C3—C2	108.6 (4)	Hg1—S1—C8—C9	-145.0 (3)
C2 ⁱ —Fe1—C3—C2	151.1 (2)	C7—C8—C9—C10	1.4 (5)
C1 ⁱ —Fe1—C3—C4	-54.3 (5)	S1—C8—C9—C10	-176.3 (3)
C1—Fe1—C3—C4	81.1 (4)	C8—C9—C10—C11	-1.6 (6)
C4 ⁱ —Fe1—C3—C4	-171.7 (2)	C9—C10—C11—C12	0.7 (6)
C5 ⁱ —Fe1—C3—C4	158.1 (9)	C8—C7—C12—C11	-0.7 (5)
C5—Fe1—C3—C4	37.0 (2)	N1—C7—C12—C11	-178.7 (3)
C3 ⁱ —Fe1—C3—C4	-132.5 (3)	C10—C11—C12—C7	0.5 (6)

Symmetry codes: (i) $-x+1, y, -z+3/2$.

All esds (except the esd in the dihedral angle between two l.s. planes) are estimated using the full covariance matrix. The cell esds are taken into account individually in the estimation of esds in distances, angles and torsion angles; correlations between esds in cell parameters are only used when they are defined by crystal symmetry. An approximate (isotropic) treatment of cell esds is used for estimating esds involving l.s. planes.

Data collection: *SMART* (Bruker, 1998); cell refinement: *SAINTE* (Bruker, 1998); data reduction: *SAINTE* (Bruker, 1998); program(s) used to solve structure: *SHELXS97* (Sheldrick, 1997); program(s) used to refine structure: *SHELXL97* (Sheldrick, 1997); molecular graphics: *ORTEPIII* (Burnett & Johnson, 1996); software used to prepare material for publication: *CIFTAB* (Sheldrick, 1997).

Color code for FcS2-Zn crystal structure:

Orange: Fe atom

Dark grey: C atom

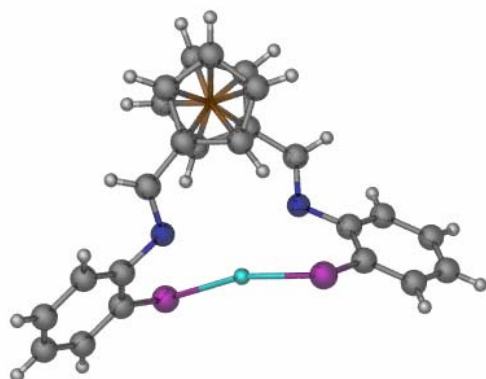
Light grey: H atom

Dark Blue: N atom

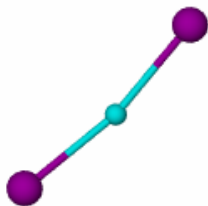
Purple: S atom

Light Blue: Hg atom

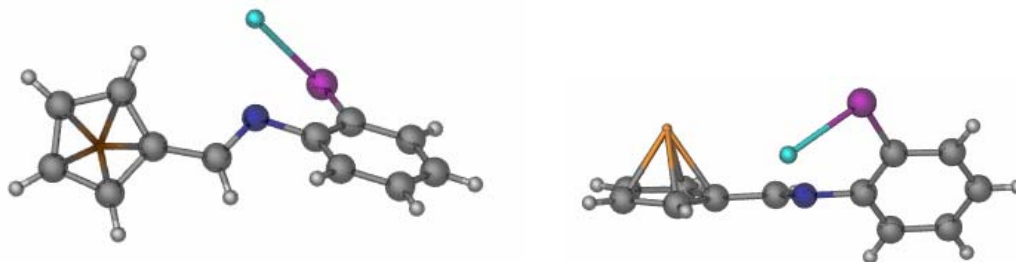
Cp ring overlap:



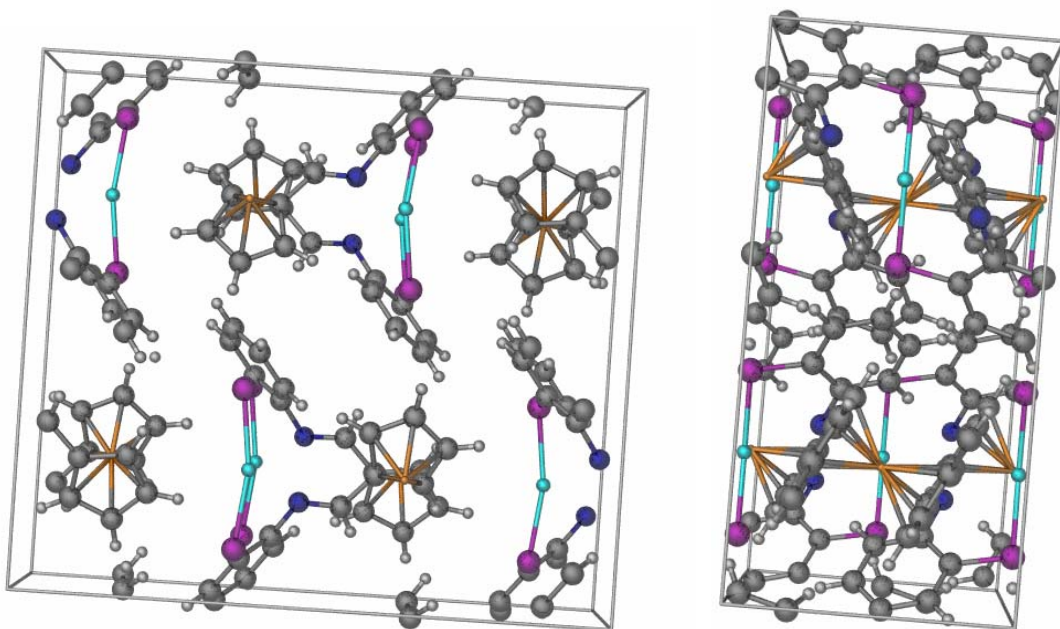
Metal geometry: (bent linear, bond angle of S-Hg-S is 166.10°)

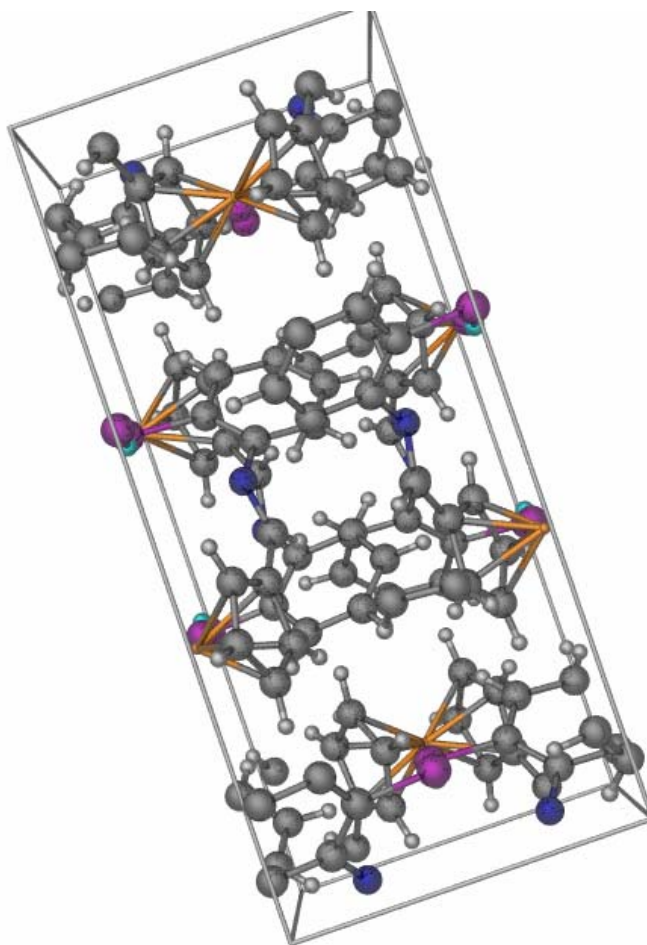


Asymmetric unit structure: (Fe^{II} , Hg^{II} atoms lie on a 2-fold rotation axis)

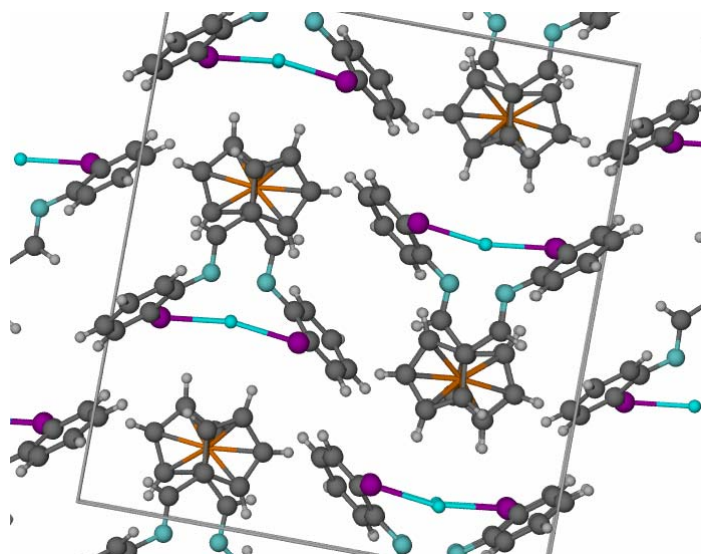
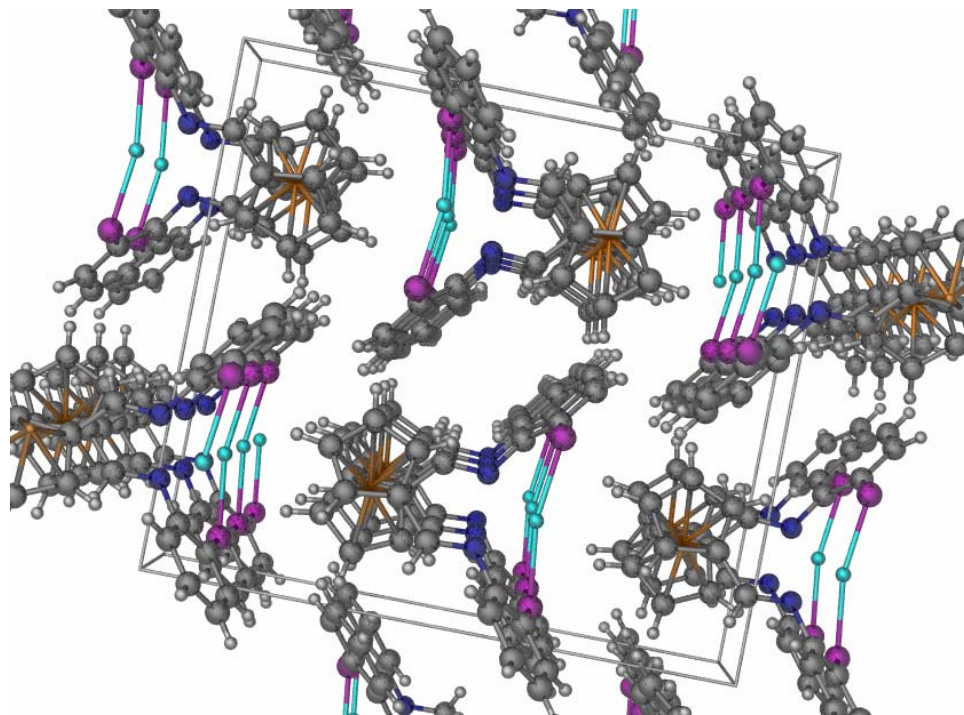


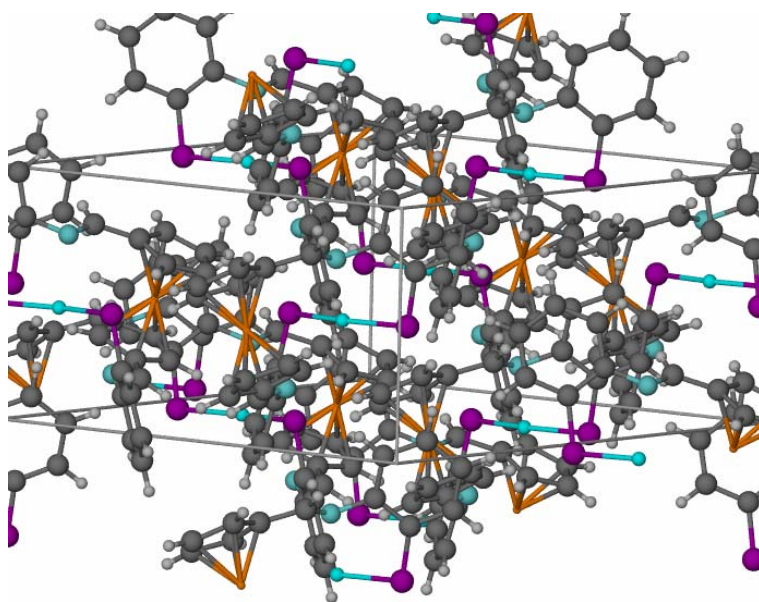
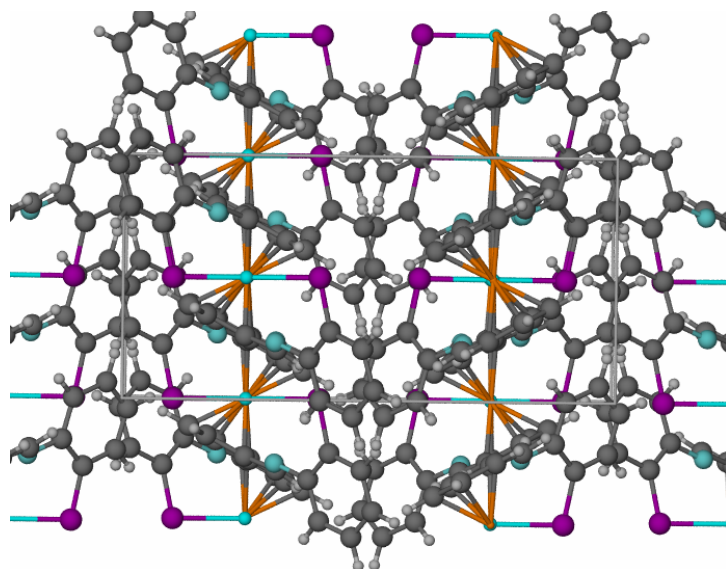
Unit cell:

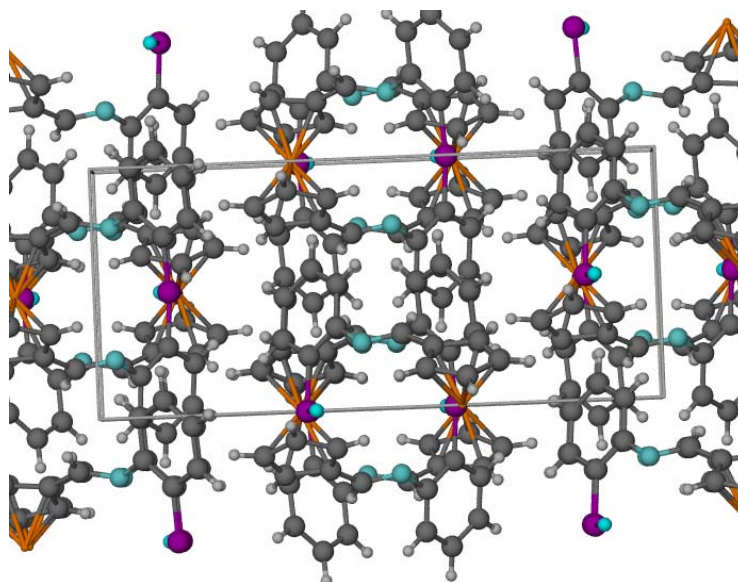




Mass crystal packing:







Comparison versus [FcS1]₂-Hg from literature:²

[Hg(fabt) ₂]	Angstroms	Comparison
Hg-S(1)	2.345(4)	0.006 less
Hg-S(2)	2.329(4)	0.022 less
Hg-N(1)	2.808(13)	0.099 more
Hg-N(2)	2.860(14)	0.151 more
N(1)-C(17)	1.259(20)	0.020 less
N(2)-C(24)	1.231(19)	0.048 less

[Hg(fabt) ₂]	Angle	Comparison
S(1)-Hg-S(2)	174.0(1)	7.90° more
S(1)-Hg-N(1)	73.2(2)	1.01° less
S(1)-Hg-N(2)	111.2(2)	2.69° less
S(2)-Hg-N(1)	108.5(2)	5.39° less
S(2)-Hg-N(2)	72.2(2)	2.01° less
N(1)-Hg-N(2)	131.6(3)	18.19° more

Compound 29:

² Kawamoto, T. and Y. Kushi (1992). "Helical Bis[2-(ferrocenylmethyleneamino)benzenethiolato] Metal(II) Complexes (M = Ni, Zn or Pd) and a Related Mercury(II) Complex." *J. Chem. Soc. Dalton Trans.*: 3137-3143.

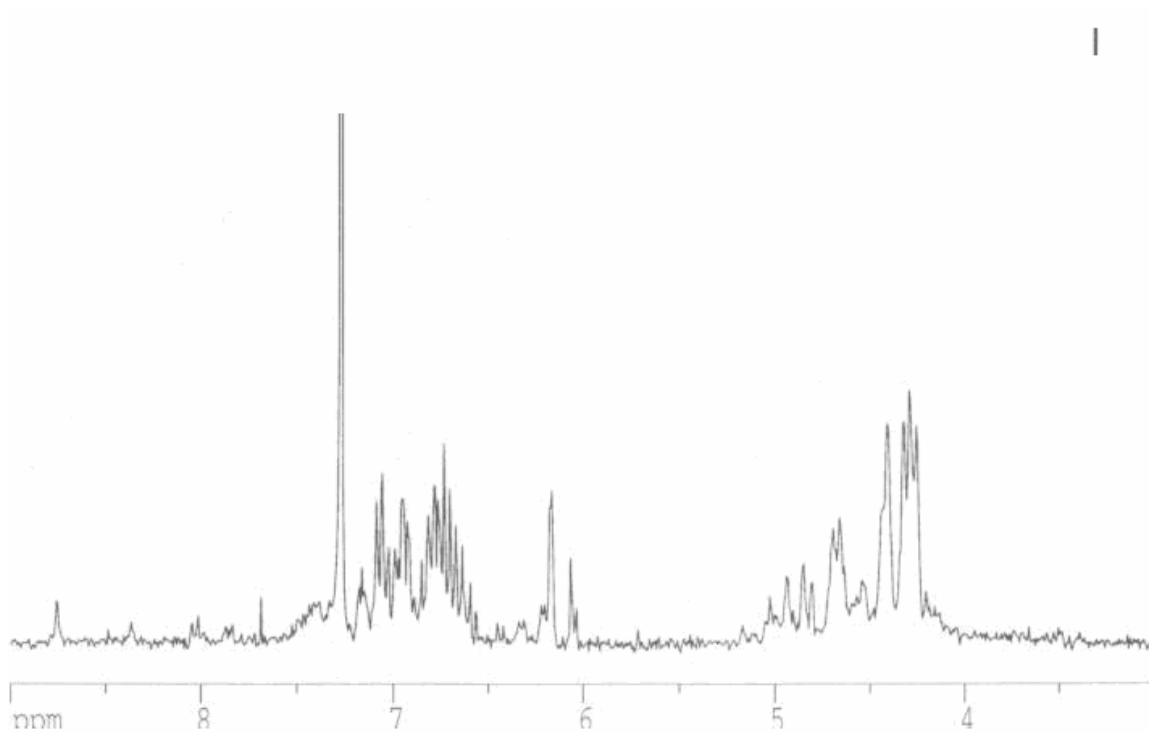
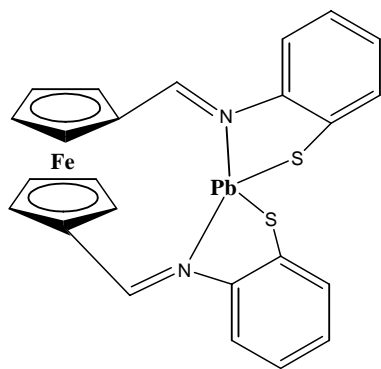


Figure A.127: ^1H NMR spectrum of FcS₂-Pb in CDCl₃: 8.75 ppm (H, s), 7.16-6.93 ppm (H, d), 6.85-6.07 ppm (H, t), 6.57 ppm (H, t), 6.07 ppm (H, m), 4.69 ppm (H, d), 4.41 ppm (H, d), 4.25 ppm (H, t);

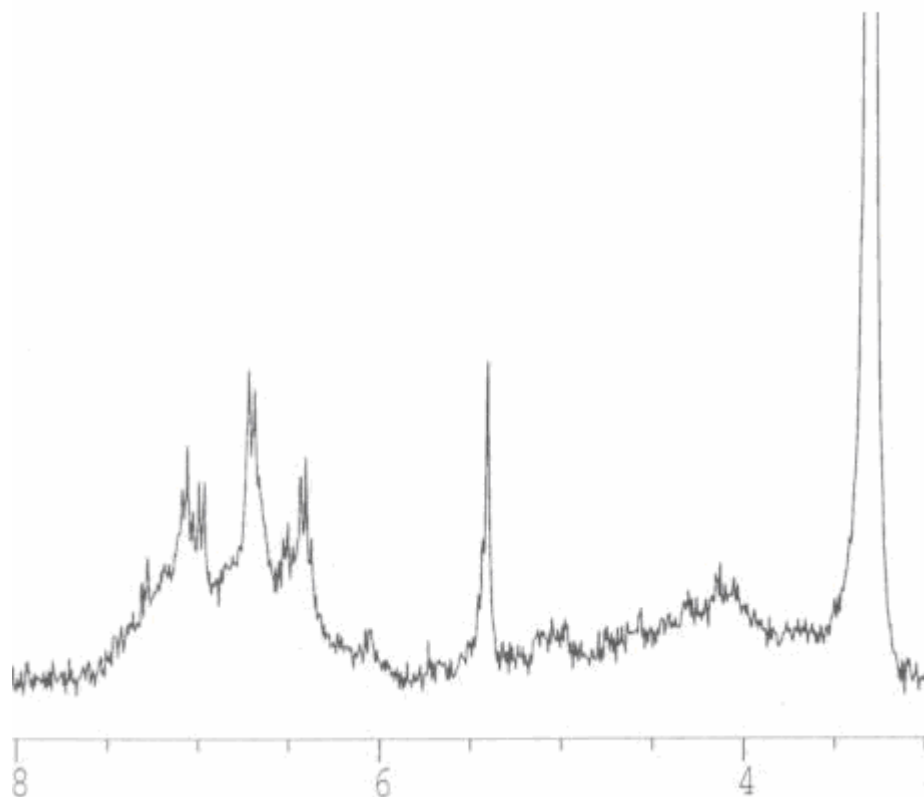


Figure A.128: ^1H NMR spectrum of FcS₂-Pb in d₆-DMSO: 7.07-6.98 ppm (H, d, phenyl), 6.72 ppm (H, d, phenyl), 6.72 ppm (H, d, phenyl), 6.1 ppm (H, d, phenyl), 5.42 ppm (H, s, Cp-CH=N), 5.3-5.0 ppm (H, m, Cp), 4.5-3.8 ppm (H, m, Cp);

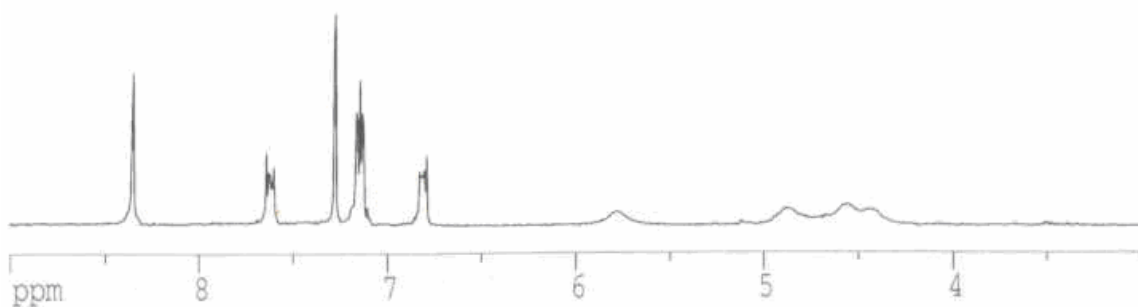


Figure A.129: ^1H NMR spectrum of precipitate from reaction of 29 with $\text{Hg}(\text{CH}_3\text{COO})_2$ in CDCl_3 :

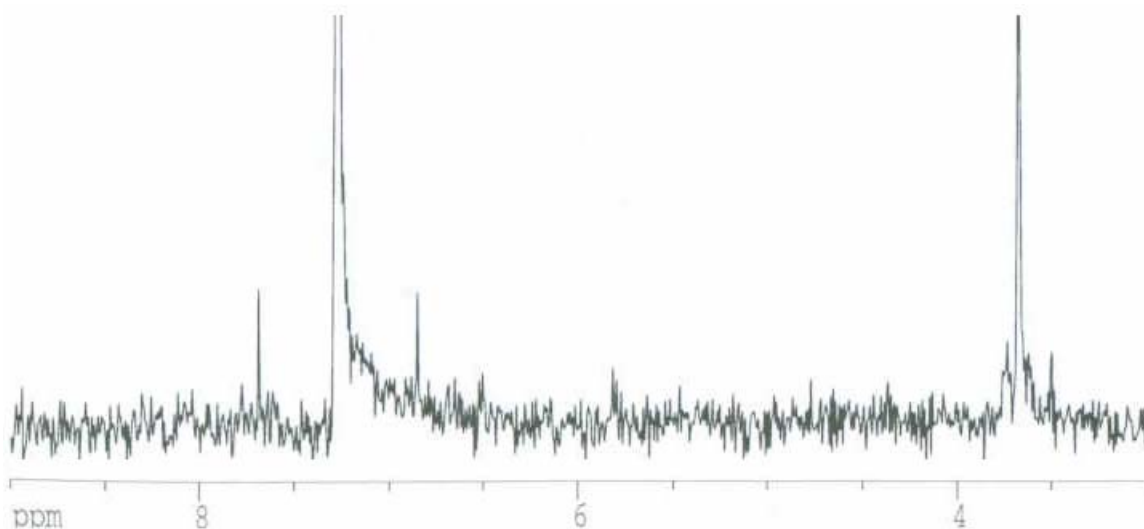


Figure A.130: ^1H NMR spectrum of dried liquid portion from reaction of 29 with $\text{Hg}(\text{CH}_3\text{COO})_2$ in CDCl_3 :

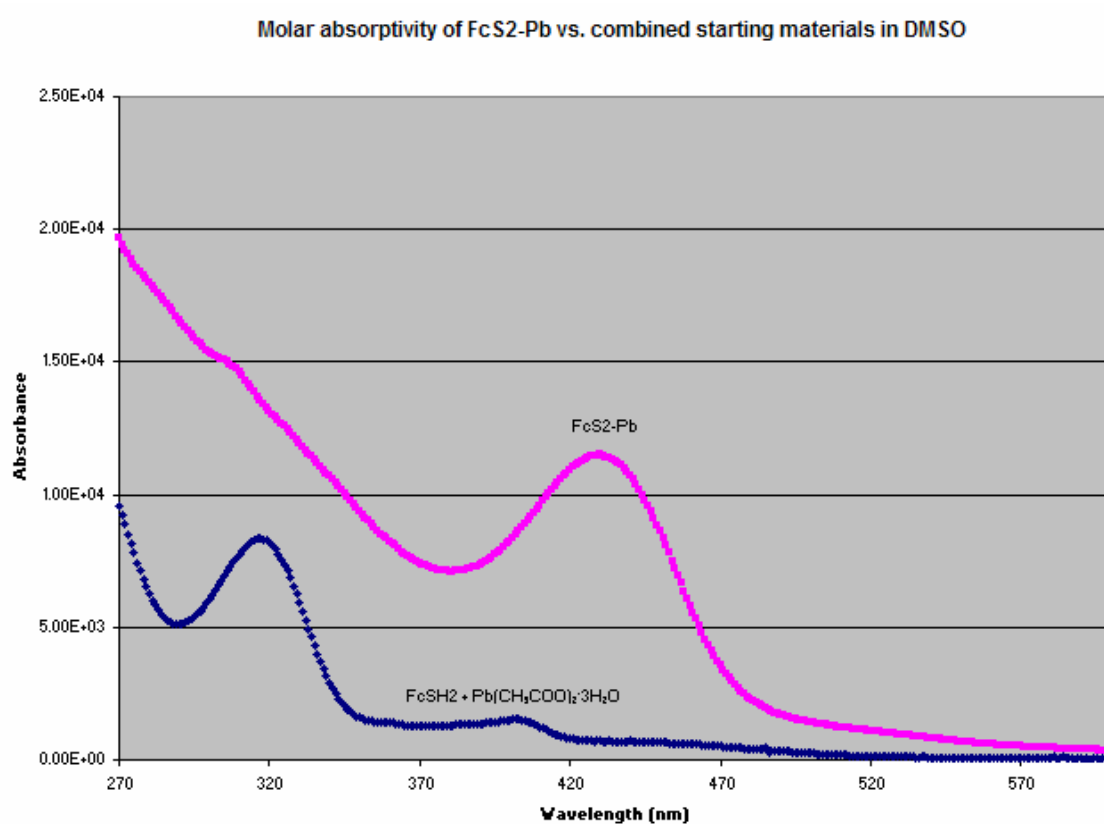


Figure A.131: Comparison between the molar absorptivity (UV-Vis) of FcS2-Pb and the molar absorptivity of the starting materials (317, 403 nm peaks) in DMSO: 430 nm ($11500 \text{ M}^{-1}\text{cm}^{-1}$);

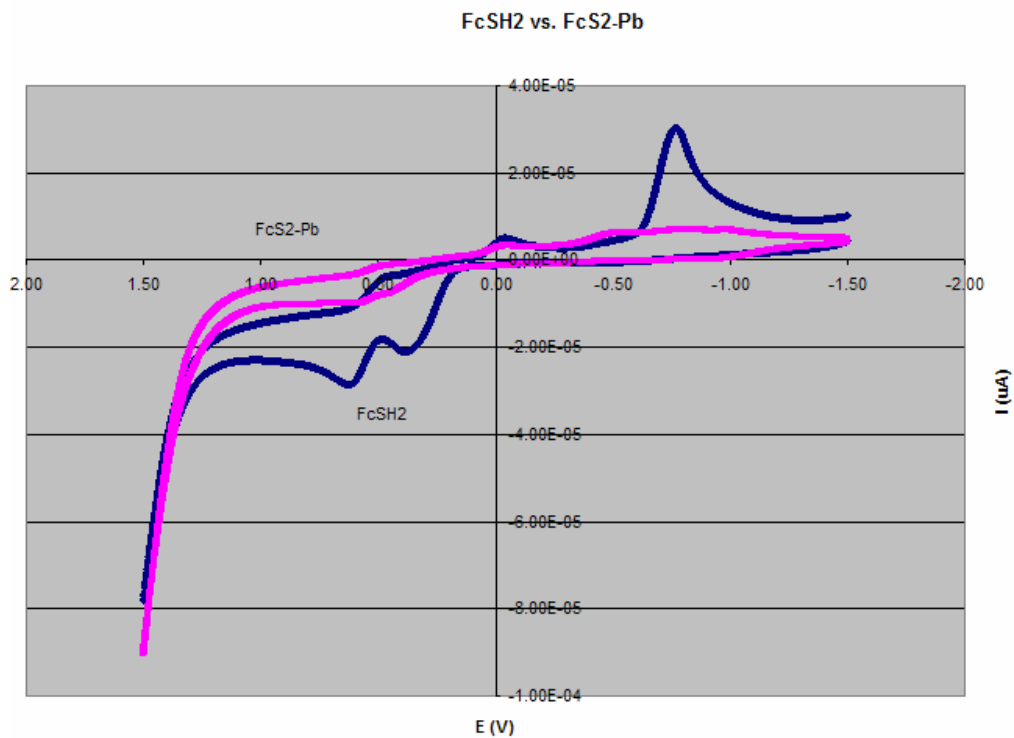


Figure A.132: Comparison between the CV scan of FcS2-Pb and the CV scan of FcSH2 in DMSO, scan rate 100 mV/sec. Fe^{II} to Fe^{III} oxidation peak is at 602 mV.

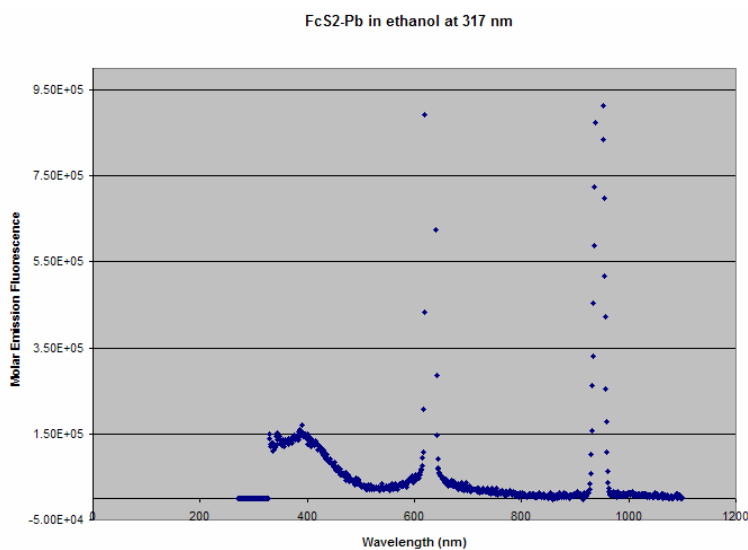


Figure A.133: Emission fluorescence of FcS2-Pb in ethanol at 317 nm with peaks at 390, 629, 943 nm.

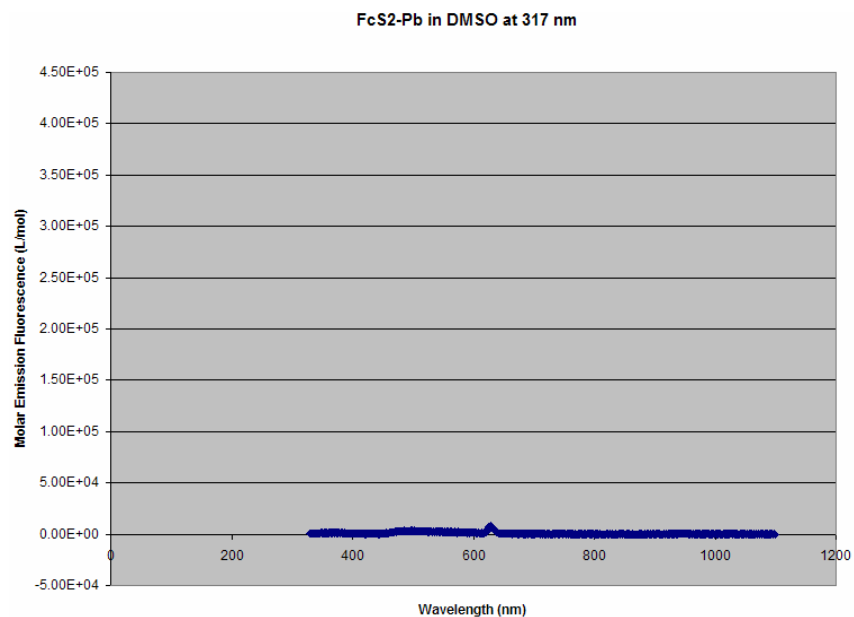


Figure A.134: Emission fluorescence of FcS2-Pb in DMSO at 317 nm with a peak at 629 nm.

Compound 30: [FcSH1]₂-Co

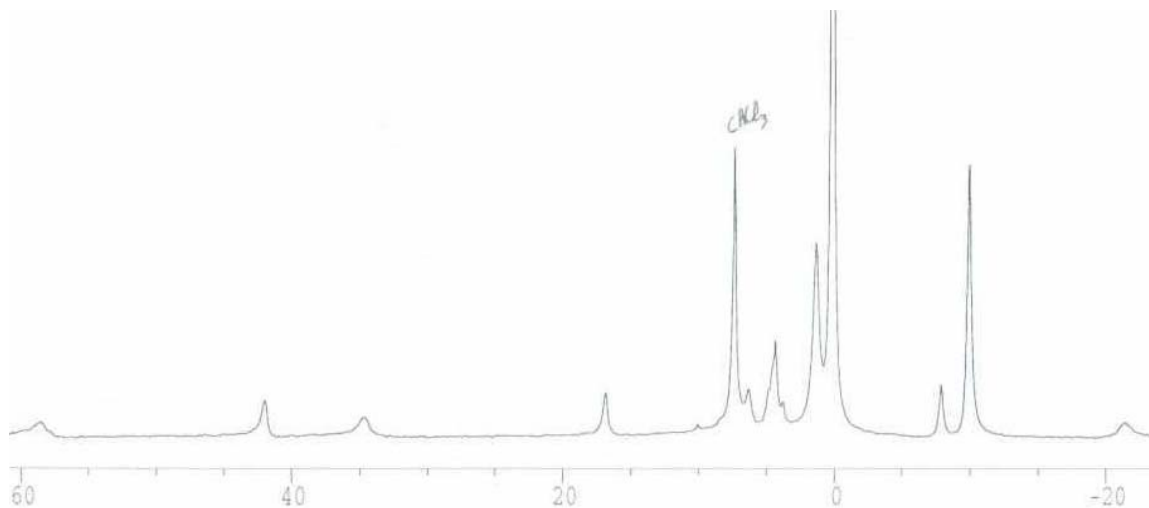


Figure A.135: ¹H NMR spectrum of [FcS1]₂-Co in CDCl₃: 58.48 ppm (1H, broad s), 41.92 ppm (1H, s), 34.59 ppm (1H, broad s), 16.82 ppm (1H, s), 6.25 ppm (1H, s), 4.28 ppm (3H, s), -7.96 ppm (1H, s), -9.99 ppm (5H, s), -21.51 ppm (1H, broad s),

Table 15: FcOH2 mixed metal reaction precipitate measured by X-ray fluorescence:

Description: FcO₂-M , Filter 1, Measurement 1

Sample Name:	Yellow oxo1A	Dilution					
	Chad	Material:	None				
Description:	Magee	Sample Mass (g):	4				
		Element		Norm. No. of Impulses		Concentration	
26	Fe	Iron	2.6805	C	< 15	ng/cm ²	
27	Co	Cobalt	0.03081	C	< 3.0	ng/cm ²	
28	Ni	Nickel	0	C	< 1.0	ng/cm ²	
29	Cu	Copper	0	C	< 1.0	ng/cm ²	
30	Zn	Zinc	0.44675	C	< 1.0	ng/cm ²	
48	Cd	Cadmium	0.01555	C		43	ng/cm ²
80	Hg	Mercury	0.23108	C	< 2.0	ng/cm ²	
82	Pb	Lead	0.06162	C		21	ng/cm ²

Preset Sample Data

Description: FcO₂-M , Filter 1, Measurement 2

Sample Name:	Yellow oxo1B	Dilution					
	Chad	Material:	None				
Description:	Magee	Sample Mass (g):	4				
26	Fe	Iron	3.7753	C		398	ng/cm ²
27	Co	Cobalt	0.02697	C	< 3.0		ng/cm ²
28	Ni	Nickel	0	C	< 1.0		ng/cm ²
29	Cu	Copper	0.41798	C		87	ng/cm ²
30	Zn	Zinc	0.39101	C	< 1.0		ng/cm ²
48	Cd	Cadmium	0.0048	C		13	ng/cm ²
80	Hg	Mercury	0.4854	C	< 2.0		ng/cm ²
82	Pb	Lead	0.22922	C		78	ng/cm ²

Preset Sample Data

Description: FcO₂-M , Filter 2, Measurement 1

Sample Name:	Yellow oxo2A	Dilution					
	Chad	Material:	None				
Description:	Magee	Sample Mass (g):	4				
26	Fe	Iron	2.8937	C	< 15		ng/cm ²
27	Co	Cobalt	0	C	< 3.0		ng/cm ²
28	Ni	Nickel	0	C	< 1.0		ng/cm ²
29	Cu	Copper	0	C	< 1.0		ng/cm ²
30	Zn	Zinc	0.38583	C	< 1.0		ng/cm ²
48	Cd	Cadmium	0.01	C		27	ng/cm ²
80	Hg	Mercury	0	C	< 2.0		ng/cm ²
82	Pb	Lead	0.14468	C		49	ng/cm ²

Preset Sample Data

Description: FcO₂-M , Filter 2, Measurement 2

Sample Name: Yellow
 Name: oxo2B Dilution Material: None
 Chad Sample Mass
 Description: Magee (g): 4

26	Fe	Iron	2.8185	C	< 15	ng/cm ²
27	Co	Cobalt	0.01336	C	< 3.0	ng/cm ²
28	Ni	Nickel	0	C	< 1.0	ng/cm ²
29	Cu	Copper	0	C	< 1.0	ng/cm ²
30	Zn	Zinc	0.32059	C	< 1.0	ng/cm ²
48	Cd	Cadmium	0.01347	C	37	ng/cm ²
80	Hg	Mercury	0	C	< 2.0	ng/cm ²
82	Pb	Lead	0.10686	C	36	ng/cm ²

Preset Sample Data

Description: FcO₂-M , Filter 3, Measurement 1

Sample Name: Yellow
 Name: oxo3A Dilution Material: None
 Chad Sample Mass
 Description: Magee (g): 4

26	Fe	Iron	2.6393	C	< 15	ng/cm ²
27	Co	Cobalt	0	C	< 3.0	ng/cm ²
28	Ni	Nickel	0	C	< 1.0	ng/cm ²
29	Cu	Copper	0	C	< 1.0	ng/cm ²
30	Zn	Zinc	0.49682	C	< 1.0	ng/cm ²
48	Cd	Cadmium	0.00472	C	13	ng/cm ²
80	Hg	Mercury	0	C	< 2.0	ng/cm ²
82	Pb	Lead	0.17078	C	58	ng/cm ²

Preset Sample Data

Description: FcO₂-M , Filter 3, Measurement 2

Sample Name: Yellow
 Name: oxo3B Dilution Material: None
 Chad Sample Mass
 Description: Magee (g): 4

26	Fe	Iron	2.8319	C	< 15	ng/cm ²
27	Co	Cobalt	0.0897	C	23	ng/cm ²
28	Ni	Nickel	0	C	< 1.0	ng/cm ²
29	Cu	Copper	0	C	< 1.0	ng/cm ²
30	Zn	Zinc	0.21784	C	< 1.0	ng/cm ²
48	Cd	Cadmium	0.00869	C	24	ng/cm ²
80	Hg	Mercury	0	C	< 2.0	ng/cm ²
82	Pb	Lead	0.11533	C	39	ng/cm ²

Preset Sample Data

Description: FcO₂-M , Filter 4, Measurement 1

Sample Name: Yellow
 Name: oxo4A Dilution Material: None

Description:	Chad Magee	Sample Mass (g):	4				
26	Fe	Iron	2.7226	C	< 15	ng/cm ²	
27	Co	Cobalt	0	C	< 3.0	ng/cm ²	
28	Ni	Nickel	0	C	< 1.0	ng/cm ²	
29	Cu	Copper	0	C	< 1.0	ng/cm ²	
30	Zn	Zinc	0	C	< 1.0	ng/cm ²	
48	Cd	Cadmium	0.00973	C	27	ng/cm ²	
80	Hg	Mercury	0	C	< 2.0	ng/cm ²	
82	Pb	Lead	0.10022	C	34	ng/cm ²	

Preset Sample Data

Description: FcO₂-M , Filter 4, Measurement 2

Sample Name: Yellow oxo4B
 Dilution Material: None
 Chad Sample Mass

Description:	Magee	Sample Mass (g):	4				
26	Fe	Iron	2.822	C	< 15	ng/cm ²	
27	Co	Cobalt	0.02475	C	< 3.0	ng/cm ²	
28	Ni	Nickel	0	C	< 1.0	ng/cm ²	
29	Cu	Copper	0	C	< 1.0	ng/cm ²	
30	Zn	Zinc	0.70551	C	29.3	ng/cm ²	
48	Cd	Cadmium	0	C	< 0.7	ng/cm ²	
80	Hg	Mercury	1.2006	C	< 2.0	ng/cm ²	
82	Pb	Lead	0.23517	C	80	ng/cm ²	

Table 16: FcSH2 mixed metal reaction precipitate measured by X-ray fluorescence**Description: FcS₂-M , Filter 1, Measurement 1**

Sample Name: Red thio 1A
 Dilution Material: None
 Chad Sample Mass

Description:	Magee	Sample Mass (g):	4				
		Element	Norm. #	of Impulses		Concentration	
26	Fe	Iron	13.152	C	4690	ng/cm ²	
27	Co	Cobalt	0	C	< 3.0	ng/cm ²	
28	Ni	Nickel	0	C	< 1.0	ng/cm ²	
29	Cu	Copper	0	C	< 1.0	ng/cm ²	
30	Zn	Zinc	2.1024	C	380	ng/cm ²	
48	Cd	Cadmium	0.01492	C	41	ng/cm ²	
80	Hg	Mercury	37.371	C	#REF!	ng/cm ²	
82	Pb	Lead	0.3532	C	120	ng/cm ²	

Preset Sample Data

Description: FcS₂-M , Filter 1, Measurement 2

Sample Name: Red thio 1B
 Dilution Material: None
 Chad Sample Mass

Description: Magee (g): 4

26	Fe	Iron	13.131	C	4680	ng/cm ²
27	Co	Cobalt	0.02555	C	< 3.0	ng/cm ²
28	Ni	Nickel	0	C	< 1.0	ng/cm ²
29	Cu	Copper	0.22992	C	37	ng/cm ²
30	Zn	Zinc	1.9543	C	343	ng/cm ²
48	Cd	Cadmium	0	C	< 0.7	ng/cm ²
80	Hg	Mercury	37.131	C	#REF!	ng/cm ²
82	Pb	Lead	0.3321	C	113	ng/cm ²

Preset Sample Data

Description: FcS₂-M , Filter 2, Measurement 1

Sample Red thio Dilution
 Name: 2A Material: None
 Chad Sample Mass
 Description: Magee (g): 4

26	Fe	Iron	27.405	C	11200	ng/cm ²
27	Co	Cobalt	0.08705	C	22	ng/cm ²
28	Ni	Nickel	0	C	< 1.0	ng/cm ²
29	Cu	Copper	0.38304	C	77	ng/cm ²
30	Zn	Zinc	3.2036	C	657	ng/cm ²
48	Cd	Cadmium	0	C	< 0.7	ng/cm ²
80	Hg	Mercury	94.384	C	#REF!	ng/cm ²
82	Pb	Lead	0.81831	C	277	ng/cm ²

Preset Sample Data

Description: FcS₂-M , Filter 2, Measurement 2

Sample Red thio Dilution
 Name: 2B Material: None
 Chad Sample Mass
 Description: Magee (g): 4

26	Fe	Iron	28.112	C	11530	ng/cm ²
27	Co	Cobalt	0.0821	C	20	ng/cm ²
28	Ni	Nickel	0	C	< 1.0	ng/cm ²
29	Cu	Copper	0.37767	C	76	ng/cm ²
30	Zn	Zinc	3.6782	C	776	ng/cm ²
48	Cd	Cadmium	0	C	< 0.7	ng/cm ²
80	Hg	Mercury	100.66	C	#REF!	ng/cm ²
82	Pb	Lead	0.77176	C	262	ng/cm ²

Preset Sample Data

Description: FcS₂-M , Filter 3, Measurement 1

Sample Red thio Dilution
 Name: 3A Material: None
 Chad Sample Mass
 Description: Magee (g): 4

26	Fe	Iron	26.569	C	10820	ng/cm ²
27	Co	Cobalt	0.0737	C	17	ng/cm ²

28	Ni	Nickel	0	C	< 1.0	ng/cm ²
29	Cu	Copper	0.47906	C	103	ng/cm ²
30	Zn	Zinc	2.6532	C	518	ng/cm ²
48	Cd	Cadmium	0	C	< 0.7	ng/cm ²
80	Hg	Mercury	91.629	C	#REF!	ng/cm ²
82	Pb	Lead	0.47906	C	162	ng/cm ²

Preset Sample Data

Description: FcS₂-M , Filter 3, Measurement 2

Sample Red thio Dilution
 Name: 3B Material: None
 Chad Sample Mass
 Description: Magee (g): 4

26	Fe	Iron	27.156	C	11090	ng/cm ²
27	Co	Cobalt	0	C	< 3.0	ng/cm ²
28	Ni	Nickel	0	C	< 1.0	ng/cm ²
29	Cu	Copper	0.27268	C	48	ng/cm ²
30	Zn	Zinc	3.4326	C	714	ng/cm ²
48	Cd	Cadmium	0	C	< 0.7	ng/cm ²
80	Hg	Mercury	94.283	C	#REF!	ng/cm ²
82	Pb	Lead	0.68972	C	234	ng/cm ²

Preset Sample Data

Description: FcS₂-M , Filter 4, Measurement 1

Sample Red thio Dilution
 Name: 4A Material: None
 Chad Sample Mass
 Description: Magee (g): 4

26	Fe	Iron	23.1	C	9240	ng/cm ²
27	Co	Cobalt	0.18247	C	58	ng/cm ²
28	Ni	Nickel	0	C	< 1.0	ng/cm ²
29	Cu	Copper	0.74811	C	174	ng/cm ²
30	Zn	Zinc	3.4121	C	709	ng/cm ²
48	Cd	Cadmium	0	C	< 0.7	ng/cm ²
80	Hg	Mercury	84.208	C	#REF!	ng/cm ²
82	Pb	Lead	0.63863	C	217	ng/cm ²

Preset Sample Data

Description: FcS₂-M , Filter 4, Measurement 2

Sample Red thio Dilution
 Name: 4B Material: None
 Chad Sample Mass
 Description: Magee (g): 4

26	Fe	Iron	26.263	C	10680	ng/cm ²
27	Co	Cobalt	0.04673	C	7.2	ng/cm ²
28	Ni	Nickel	0	C	< 1.0	ng/cm ²
29	Cu	Copper	0	C	< 1.0	ng/cm ²
30	Zn	Zinc	2.2431	C	415	ng/cm ²

48	Cd	Cadmium	0	C	< 0.7	ng/cm ²
80	Hg	Mercury	87.7	C	#REF!	ng/cm ²
82	Pb	Lead	0.43616	C	148	ng/cm ²

VITA

Chad L. Magee was born on March 11, 1973 in Cozad, Nebraska. He graduated Atwood High School in Atwood, Kansas in 1991. After attending KSU for some time where he was dual majoring in both chemistry and nuclear engineering, he decided to concentrate on chemistry at UNK in Kearney Nebraska, where he earned his ACS Certified Bachelor's degree in Chemistry in the Spring of 1998. He worked on an organic research project involving 9-methyl acridine substitution under Dr. Michael Mosher during his time at UNK. Upon graduation, he left Nebraska for the cold weather of South Dakota where he attended USD as a chemistry graduate student in the Master's program. In the fall of 2000, he was awarded his Masters degree in inorganic chemistry from USD for his work with ferrocene mixed-metal polymers under Dr. Andrew Sykes. Shortly after, he was accepted at the University of Missouri-Columbia as a chemistry graduate student.

Upon arrival in Columbia, Chad decided to continue to study inorganic chemistry by joining Dr. Paul Sharp's research group in the summer of 2001. He worked there for one year before switching to Dr. Paul Duval's research group, focusing upon ferrocene chemistry with various metal systems for the purpose of making molecular switches. This interest grew into the discovery of potential new ferrocene sensor systems that were the focus of this research project